ITALIAN PHYSICAL SOCIETY

PROCEEDINGS
OF THE
INTERNATIONAL SCHOOL OF PHYSICS «ENRICO FERMI»

COURSE XXVII

edited by D. SETTE
Director of the Course

VARENNA ON LAKE COMO
VILLA MONASTERO
AUGUST 6 - AUGUST 18 1962

Dispersion and Absorption of Sound by Molecular Processes

1963

ACADEMIC PRESS • NEW YORK AND LONDON

SOCIETÀ ITALIANA DI FISICA

RENDICONTI
DELLA
SCUOLA INTERNAZIONALE DI FISICA «ENRICO FERMI»

XXVII CORSO

a cura di D. SETTE
Direttore del Corso

VARENNA SUL LAGO DI COMO
VILLA MONASTERO
6-18 AGOSTO 1962

Dispersione ed assorbimento del suono nei processi molecolari

1963

ACADEMIC PRESS • NEW YORK AND LONDON

IIA Lib.,
02932

ACADEMIC PRESS INC.
111 Fifth Avenue
New York 3, N. Y.

United Kingdom Edition
Published by
ACADEMIC PRESS INC. (London) Ltd.
Berkeley Square House, London W. 1

Copyright © 1963, by Società Italiana di Fisica

ALL RIGHTS RESERVED

NO PART OF THIS BOOK MAY BE REPRODUCED IN ANY FORM,
BY PHOTOSTAT, MICROFILM, OR ANY OTHER MEANS,
WITHOUT WRITTEN PERMISSION FROM THE PUBLISHERS.

Library of Congress Catalog Card Number: 63-20574

PRINTED IN ITALY

INDICE

Gruppo fotografico dei partecipanti al Corso . . . . fuori testo

D. **Sette** - Introduction . . . . pag. IX

K. F. **Herzfeld** – Theory of fluids . . . . » 1

H. O. **Kneser** – Relaxation thermique dans le gaz . . . . » 40

M. **Greenspan** – Translational dispersion in gases . . . . » 73

J. **Lamb** – Dispersion and absorption of sound by molecular processes: thermal relaxation in liquids . . . . » 101

T. A. **Litovitz** – Ultrasonic relaxation in liquids . . . . » 133

K. **Tamm** – Acoustic relaxation in electrolyte solutions . . . . » 175

W. P. **Mason** – Absorption and dispersion of sound in polymer solutions, polymer liquids, rubbers and solid polymers . . . . » 223

K. F. **Herzfeld** – Theories of relaxation times . . . . » 272

H.-J. **Bauer** – Phenomenological theory of multiple relaxation processes » 325

C. G. **Sluijter** – Rotational relaxation in the sound absorption of hydrogen isotopes . . . . » 338

R. T. **Beyer** – Measurements of ultrasonic velocity and absorption in liquids at high frequencies, at high temperatures and under high hydrostatic pressure . . . . » 340

R. T. **Beyer** – Measurements of ultrasonic velocity and absorption in liquids under high sound intensities . . . . » 351

L. **Liebermann** – Determination of the kinetics of chemical reactions by sound absorption or dispersion . . . . » 363

J. M. STEVELS – The dielectric properties of quartz crystals and fused silica in relation to their imperfections . . . . pag. 368

R. W. B. STEPHENS – Ultrasonic attenuation in liquid metals . . . . . . » 393

A. J. KOVAKS – Recouvrance de volume des verres; comparaison entre les expériences et une théorie phénoménologique . . . . » 401

A. J. KOVACS and J. D. FERRY – Variations des paramètres viscoélastiques du polyacétate de vinyle dans le domaine de sa transition vitreuse » 415

P. G. BORDONI – Relaxation of lattice imperfections in solids . . . . . . » 425

Introduction

D. Sette

Direttore del Corso

The study of interaction between mechanical waves and matter has received much attention in the last 40 years and the use of ultrasonics has developed into a powerful tool for investigating fundamental aspects of the physisc of gases, liquids and solids.

The thermodynamical behaviour of rapidly perturbed systems, molecular and structural properties of fluids, electronic conductivity of metals, paramagnetic properties of solids, structural analysis of defects in solids, nuclear properties, cosmic rays interaction with matter have received major contributions by acoustic investigations.

The present Course of the Fermi School is dedicated to one of the most fruitful applications of sound waves to the study of matter, and which has developed in the last two decades into what is today ultrasonic spectroscopy of fluids.

Fluids are thermodynamical systems whose particles may possess energy in various forms: the molecules may be found in various energetic states. An equilibrium distribution of molecules among allowed states corresponds to a certain equilibrium condition. A variation of thermodynamical variables causes the passage of molecules to a new equilibrium distribution with a mechanism which is of relaxation type: a finite time is required to reach the new equilibrium and during this time there is no equilibrium correspondence between distribution of particles among energy states and independent thermodynamical variables. The relaxation induces therefore dispersion and absorption of sound waves.

Various types of relaxation processes may be found, each corresponding to a different form in which energy may be kept by the molecular systems and characterized by a relaxation time and by the energies of the allowed states. These parameters are related to basic properties of the molecules and to the structure of the fluids; their determination gives valuable information for the study of fluids.

The development of techniques for measuring sound speed and absorption in a wide range of frequencies enables to get, sometimes, full information about a single relaxation process; it is then possible to have clear ideas on the transfer of energy, on the behaviour of molecules and on the intermolecular structure. Often however, the information is only partial, either because the relaxation times are too short or because there is an overlapping of many relaxation processes of different nature which is not possible to resolve in the limits of the accessible range of frequencies. The efforts intended to extend further the high-frequency limit of experiments are at present of great importance.

Many of the problems which we face in the analysis of the behaviour of fluids subjected to sound waves are similar to those found studying sound propagation in other systems, or are related to the behaviour of matter in different conditions such as, for instance, inside the electric field.

This brief presentation of the field of research helps in the illustration of the scheme of the Course on « Sound dispersion and absorption by molecular processes » as it has been organized by the Italian Physical Society.

A first series of lectures given by K. F. HERZFELD of the Catholic University (Washington D.C.) will present those concepts of modern theory of fluids which are needed in the more specific courses.

The propagation in gases will be treated during two series of lectures. Relaxation processes connected to the equilibrium between translational degrees of freedom on one side and rotational or vibrational degrees on the other, will be treated by H. O. KNESER of the I Physikalisches Institut of the Polytechnic of Stuttgart.

The problems, instead, concerning the propagation in gases when the wavelength becomes comparable with the mean free path will be discussed by M. GREENSPAN of the National Bureau of Standards (Washington D.C.) in the lectures on translational relaxation.

Relaxation processes in liquids will be presented by three scientists. J. LAMB of Glasgow University will treat thermal relaxation with special reference to vibrational relaxation, to rotational isomeres and to the case of aqueous solutions of nonelectrolytes. T. A. LITOVITZ of the Catholic University will mainly discuss structural and shear relaxation, while K. TAMM of the Applied Physics Institute of the University of Heidelberg will lecture on relaxation in electrolytic solutions.

W. P. MASON of Bell Telephone Laboratories will give a series of lectures on polymers with special attention to liquid polymers and to solutions of polymers.

As a conclusion and a co-ordination of the various sections in which we have divided the field, we have one more fundamental course on the theories of relaxation times, which will be given by K. F. HERZFELD.

A number of seminars will present either important aspects which could not find an adequate place in preceeding lectures or the status of research in related fields.

They will be given by: H. J. **BAUER** of the I. Physikalisches Institut der Technischen Hochschule of Stuttgart; R. T. **BEYER** of Brown University; P. G. **BORDONI** of Rome University; A. J. **KOVACS** of the Centre de Recherches sur les Macromolecules of Strasbourg; R. W. B. **STEPHENS** of the Imperial College (London) and J. M. **STEVELS** of Philips Research Laboratoires.

I have limited myself to simple indication of title of lectures and names of scientists which will given them: I dit not feel, in fact, that a formal presentation of each one of them was necessary: the large majority of the people present, having already worked in the field, know them very well and appreciate how fondamental has been the contribution to research given by each one of them.

However I can not resist the desire of pointing out the presence of the two persons who started research in this field, respectively in the case of relaxation in gases and relaxation in liquids: professor K. F. **HERZFELD** and Professor H. O. **KNESER**.

We have been particularly fortunate in securing the collaboration of all the above mentioned outstanding scientists. The Italian Physical Society thanks them very much for accepting its cordial invitation. At the same time, the Society is happy of offering to the young researchers present at the Course the unique opportunity of spending two weeks listening to lectures and discussing problems with these scientists who have started and largely developed research in this field.

It is a well founded hope that the common work of these two weeks will result stimulating and fruitful for lecturers and students, will cause further progress of physics and constitute a positive human experience through the enjoyment of old friendships and the constitution of new ones.

SOCIETÀ ITALIANA DI FISICA

SCUOLA INTERNAZIONALE DI FISICA « E. FERMI »

XXVII CORSO - VARENNA SUL LAGO DI COMO - VILLA MONASTERO - 6-18 Agosto 1962

Theory of Fluids.

K. F. HERZFELD
Catholic University of America - Washington D.C.

Introduction.

Under « fluids » it is customary to include both gases and liquids. I intend to discuss on this first day the general theory of fluids. Very much work is being done at present in this field, but it is usually limited to spherically symmetrical molecules (rare gases, and, approximately CX_4); even with this limitation, the formulae are very complicated and not of too much use for our purposes [1-5].

1. – Formal description of molecular distribution in fluids.

The following description is valid for all fluids although in the special case of ideal gases it can be greatly simplified. It can be applied directly only to particles of spherical or quasi spherical symmetry, *i.e.* rare gas atoms or CX_4. We abbreviate the co-ordinates of the s-th particle by x_s, and the volume element $dx_s dy_s dz_s$ by d^3x_s. Similarly the velocity shall be called w_s, and the element in the velocity space d^3w_s. We assume the absence of volume forces but allow internal stresses, connected with surface stresses (tensors).

Our description may then be restricted to the positions of the molecules, or may also include velocities. Such a description shall be a statistical description, either referring to an ensemble of equivalent systems in a heat bath, or to the statistics of the history of a stationary isolated system.

We will call probability functions restricted to position g, those including velocities f. There are then quite a hierarchy of such functions g and f. Let the total number of particles be N, the total volume V, and let us restrict ourselves at first to a discussion of the distribution in space, *i.e.* the g's.

The most detailed statistics is then given by the quantity

$$g_N(x_1, x_2, \ldots, x_N)\, d^3x_1 \ldots d^3x_N \,, \tag{1.1}$$

which is the probability of finding molecule 1 within a given d^3x_1 and molecule N in d^3x_N.

This will, in principle, depend on the boundaries, but in the limit $N=\infty$, $V=\infty$ will be independent of them.

One may now ask less detailed questions: what is the probability of finding molecules 1, 2, ..., $N-1$ in d^3x_1, $d^3x_2 \dots d^3x_{N-1}$ no matter where molecule N is? Obviously

$$g_{N-1}(x_1, \dots x_{N-1}) = \int g_N(x_1, \dots x_N)\, d^3x_N\,. \tag{1.2}$$

The last terms of this series are

$$g_3(x_1, x_2, x_3) = \int g_N(x_1, x_2, \dots x_N)\, d^3x_4 \dots d^3x_N\,, \tag{1.3}$$

$$g_2(x_1, x_2) = \int g_3(x_1, x_2, x_3)\, d^3x_3\,, \tag{1.4}$$

$$g_1(x_1) = \int g_2(x_1, x_2)\, d^3x_2 = \frac{1}{V}\,. \tag{1.5}$$

Classically, kinetic and spatial properties can be separated. At least in equilibrium, which we will treat first, they are uncorrelated (the total distribution function is a product of kinetic and spatial factors) and the kinetic distribution function has the Maxwellian form.

In principle, one can write down the values of g_N in equilibrium: this is of theoretical importance; namely

$$g_N = g_1^N \exp\left[-\frac{E_p}{kT}\right]\Big/\sum g_N\,, \tag{1.6}$$

where E_p is the total interaction energy of the system; if the physical nature of the forces is understood, this can be calculated. Summing up over all possible distributions, one gets the partition function and from it, by well-known expressions all thermodynamic properties of the fluid. One can also get, by going down the hierarchy (1.2) to (1.4), all the other g's, in particular g_2.

As stated, this can be done on principle, if E_p is known for all distributions. In practice, it is an impossible task. The quantity which determines most physical properties is g_2.

By defining

$$\boldsymbol{r} = \boldsymbol{x}_2 - \boldsymbol{x}_1$$

we can write

$$g_2(x_1, x_2) = g_2(\boldsymbol{x}_1, \boldsymbol{x}_1 + \boldsymbol{r})\,.$$

In a fluid and in the absence of external forces, g_2 does not depend on x_1. One can next introduce an expression g by

$$g_2(x_1, x_2) = g_1(x_1)\, g(x_2 | x_1) = g_1(x)\, g(x+r | x) \;,$$

g is called a conditional probability, namely the probability that particle (2) is at $x+r$ under the condition that particle (1) is at x. In the present case, g is a function of r only, and g_1 is a constant. g is closely connected with the so-called autocorrelation function (or convolution) R defined (in one dimension) as

$$R(r) = \int f(x)\, f(x+r)\, \mathrm{d}x \left[\int f^2(x)\, \mathrm{d}x\right]^{-1} , \tag{1.7}$$

where f is a random function with the average value zero (*).

If f varies irregularly, one should expect that if r is small (*i.e.* at two places close by), the sign of $f(x)$ and $f(x+r)$ would usually be the same, and therefore the product will usually be positive, while if r is large, there should be no connection between the signs of $f(x)$ and $f(x+r)$, so that the product should be as often positive as negative, and the contribution to the integral is small. For the particular application considered here, the function $f(x)$ is the momentary density of matter at x (or rather, the deviation from the mean value), and we use the fact that spatial average and time average are identical. One then can prove that

$$R(r) = g(x+r | x) \;. \tag{1.8}$$

The next task is to approximate g_2. There are two extreme cases were g_2 can be written down exactly.

The ideal gas case, where there is *no* correlation between molecules, $R=0$, $g_2 = g_1^2$; and the ideal crystal (point atoms, no heat motion) where g_2 (and R)

(*) As a matter of fact a more careful investigation of the condition under which the above holds is necessary. One cannot define the autocorrelation function for a completely random function but must know something about its distribution.

Assume the function f can, at a given moment, be developed into a Fourier series

$$f(x) = \sum_S a_S \cos 2\pi S \frac{x}{L} + \sum_S b_S \sin 2\pi S \frac{x}{L} \,.$$

Then the coefficients a, b form an infinite number of random parameters. It then follows from the central limit theorem, that at any given place the distribution of f is Gaussian, although the parameters of the Gaussian distribution may vary with x. But this is sufficient to allow the formation of the autocorrelation function. I am grateful to Prof. E. **Batschelet** of the Catholic University for clearing up this matter for me.

in one dimension are a set of δ-functions repeated periodically at the lattice distance (of course, the ideal crystal is not a fluid, but everything said up to now still applies there). Physically, approximate theories of liquids take their starting point from these extremes. The original van-der-Waals theory took the liquid as a condensed gas, the cell theory and others as a slightly disordered crystal. A third, more mathematical approach has been taken by BORN and GREEN on the one hand, by KIRKWOOD and his students on the other, by assuming « closure » of the hierarchy at g_3; *i.e.* the assumption is made that

$$g_3(x_1, x_2, x_3) = g_2(x_1, x_2)\, g_2(x_2, x_3)\, g_2(x_3, x_1)\,. \tag{1.9}$$

No complete physical understanding of the conditions necessary for this equation exists.

One can see that it is obeyed in the case of three hard molecules. If one describes these, as usual, by « spheres of action » of twice the molecular radius, takes molecules 1 and 2 with overlapping spheres and molecule 3 as a point, one sees that the regions inaccessible to 3 (and only these) have either $g_2(x_1, x_3)$ or $g_2(x_2, x_3)$ equal zero. Numerical calculations of thermodynamical properties have given fair agreement with experiment near the critical point; at the higher densities of normal liquids this is doubtful. Anyway, application of (1.9) to (1.4) gives then an integral equation for g_2, for which approximate solutions can be given, which depend on the interaction potential between pairs of molecules.

One has next to calculate the stresses.

These have two components: the first is kinetic and due to momentum transport by the moving molecules just as in ideal gases. The second is due to the forces of interaction.

In this manner one gets, in equilibrium

$$p = \frac{N}{V} kT - \frac{1}{6}\int r \frac{\partial H_{12}}{\partial r}\, g_2(x, x+r)\, \mathrm{d}^3 r\,, \tag{1.10}$$

where H_{12} is the interaction energy between molecules 1 and 2. In nonequilibrium, one has also to take into account the change 1 produced in g_2 by the nonequilibrium condition. KIRKWOOD and his students have done so in a series of papers [6-9].

Approximately, the expressions are

$$\xi_0^2 = \frac{\varrho}{2}\int \Delta H g_2\, \mathrm{d}^3 r_{12}\,, \tag{1.11}$$

where Δ is the Laplace operator $= (\partial^2/\partial x^2) + (\partial^2/\partial y^2) + (\partial^2/\partial z^2)$ and r_{12} refers to the relative positions of particles 1 and 2. Furthermore (also approximately), the shear viscosity is

$$\eta = \frac{\varrho}{30\xi_0}\left(\frac{N}{V}\right)\int r_{12}^2\left(\frac{\mathrm{d}^2H}{\mathrm{d}r_{12}^2}+\frac{4}{r_{12}}\frac{\mathrm{d}H}{\mathrm{d}r_{12}}\right)g_2\,\mathrm{d}^3r_{12}\,, \tag{1.12}$$

the bulk viscosity η'

$$\eta' = \frac{\varrho}{18\xi_0}\frac{N}{V}\int r_{12}^2\left(\frac{\mathrm{d}^2H}{\mathrm{d}r_{12}^2}+\frac{1}{r_{12}}\frac{\mathrm{d}H}{\mathrm{d}r_{12}}\right)g_2\,\mathrm{d}^3r_{12}\,. \tag{1.13}$$

There are additional terms in both (1.12) and (1.13) which are due to momentum transport due to molecular motion, but they are negligible in liquids compared to the terms written here, while they are alone present in ideal gases.

The shear viscosity contains the distribution function g_2 in a very critical way, and g_2 has to be adjusted to give the correct value. In addition, the equation contains a constant ξ, called the constant of the Brownian motion; applying the equation to liquid argon, the experimental data can be represented. Most important for us is the fact that a bulk viscosity, different from zero, for rapid pure compression emerges, which contains the same quantities as η, and which gives for liquid argon a bulk viscosity of the same order of magnitude, but smaller than, η.

GREEN has analyzed the heat motion in the liquid into Debye waves and, with their help defined three quantities analogous to the virial. He finds that the correlation functions of the fluctuations of these quantities determine the stress tensor. In particular, the time correlations of the pressure fluctuations determine the bulk viscosity. Basing on this theory, I have expressed this quantity by the change of compressibility with pressure, a length characteristic of the spatial correlation of pressure fluctuation and a time characteristic of temporal correlations. If one assumes the fluctuations to be due to interference effects of Debye waves, one can connect these two last quantities through the sound velocity and finds for the correlation length, for a bulk viscosity of 0.01 poise, a few Å. I have been unable to connect this theory with Kirkwood's expression [9*a*, *b*].

One might ask whether it is possible to determine g_2 experimentally, and here structure determination by X-ray diffraction immediately comes to mind.

As is well known, this involves the fundamental difficulty, that only intensities, not phases can be measured.

There is an interesting general theorem which tells us what one can conclude as to the structure, if only intensities of the scattered radiation are measured as function of the angle. For the sake of simplicity, let us limit ourselves to a one-dimensional distribution along the x-axis, on which there is distributed the amplitude-scattering power $f(x)$. If this arrangement is then illuminated normally by a plane wave, the scattered amplitude $A(\theta)$ in the direction θ ($\theta =$ angle between incident and scattered ray) is given by

$$(1.14)\qquad A(\theta) = \int f(x) \exp\,[ikx \sin\theta]\,\mathrm{d}x\,.$$

If we write instead of $A(\theta)$, $A(k \sin\theta)$, $k = 2\pi/\lambda$, A is the Fourier-transform of f. Write now the conjugate complex

$$(1.15)\qquad A^*(k \sin\theta) = \int (f^*(x') \exp\,[-\,ikx' \sin\theta]\,\mathrm{d}x'\,,$$

and multiply, then one gets the intensity

$$(1.16)\qquad |A(k \sin\theta)|^2 = \int\!\!\int f(x)\cdot f(x') \exp\,[ik \sin\theta(x - x')]\,\mathrm{d}x\,\mathrm{d}x'\,.$$

Make now a transformation from x, x', to x, $r = x - x'$ then (*)

$$(1.17)\qquad |A|^2 = \int \exp\,[ikr \sin\theta]\,\mathrm{d}r \int f(x)\,f(x + r)\,\mathrm{d}r\,.$$

The latter integral is, however, the correlation function for f.

$$R(r) = \int f(x)\,f(x + r)\,\mathrm{d}x \Big/ \int f^2(x)\,\mathrm{d}x\,.$$

It is assumed in this argument that the borders of the region do not contribute. Then [10]

$$(1.18)\qquad |A(k \sin\theta)|^2 = \int R(r) \exp\,[ikr \sin\theta]\,\mathrm{d}r \cdot \int f(x^2)\,\mathrm{d}x\,,$$

(*) It should be noted that the formula found in the usual literature is

$$\int g(r)\,\frac{\sin\,(kr \sin\theta)}{kr \sin\theta}\,4\pi r^2\,\mathrm{d}r\,.$$

The difference between this and (1.18) arises from the fact that the latter is for one dimension only; the denominator in the expression above arises from integration over an angle.

or, using the expression for the inverse Fourier transform [10]

$$(1.19)\qquad R(r)=\frac{\int|A(k\sin\theta)|^2\exp[-ikr\sin\theta]\,\mathrm{d}(\sin\theta)}{\int|A(k\sin\theta)|^2\,\mathrm{d}(\sin\Theta)}\,.$$

Accordingly, if $|A|^2$ were measured accurately enough, one could get the correlation function. Now this is not enough to get $f(x)$, the distribution; there are more than one distribution which provides the same R. In addition, the measurements are not good enough at present to provide a g_2 of sufficient accuracy; however in view of the recent improvement in crystal X-ray equipment, it ought to be possible to improve the measurements in liquids appreciably.

There is, however, one other catch in the story. In the Fourier transformation (1.14), there is nothing which says that the variable in A, namely $k\sin\theta$, has this particular physical meaning, *i.e.* in the power spectrum $(A(k\sin\theta))^2$ there will follow from (1.15) values of diffracted intensity belonging to $k\sin\theta > k$.

These correspond to scattered waves proportional to

$$\exp[ik\cos\theta]=\exp\left[i\sqrt{k^2-k^2\sin^2\theta}\right],$$

e.i. they will have real (negative) exponents and are therefore « waves » emanating from the scatterer which are heavily damped (although not producing loss); they may be compared to the waves which occur within the Heaviside layer when a radio wave is reflected. These waves, restricted to the immediate neighbourhood of the scatterer, called evanescent waves, are also part of the power spectrum and their $|A|^2$ should be known—but it is not—and included on the right of (1.19) to calculate the correct R.

If the wave length of the radiation used is shorter than the « structure » of the scatterer, the evanescent waves form a negligible part of the power spectrum and R can be calculated fairly well even if they are omitted. If on the other side the incident wave length is long, the evanescent waves form the major part of the power spectrum and no clue to R is given if only the intensities of the real scattered waves are used.

2. – Ideal gases.

I will now leave the general study of fluids and restrict myself to ideal gases. As mentioned before, this appears formally in the assumption that the correlation between different molecules is zero, or as Boltzmann and Planck called it, the assumption of molecular chaos.

For more detailed treatment, see Ref. [11-13].

We now define as the single molecule distribution function a quantity f, abbreviate the volume element $\mathrm{d}x\,\mathrm{d}y\,\mathrm{d}z$ by $\mathrm{d}v$ and the element in velocity space $\mathrm{d}w_1$, $\mathrm{d}w_2\,\mathrm{d}w_3$ by $\mathrm{d}\omega$. Then the number of molecules which are in $\mathrm{d}v$ and have at the same time velocity components within $\mathrm{d}\omega$ is

$$\mathrm{d}^6N = n(x, y, z, t)\, f(x, y, z, w_1, w_2, w_3, t)\,\mathrm{d}v\,\mathrm{d}\omega\,, \tag{2.1}$$

n is the local number density of molecules and in this way of writing, f is normalized as to velocities, *i.e.*

$$\int f\,\mathrm{d}\omega = 1\,.$$

The happenings in the gas are governed by Boltzmann's fundamental equation of gas theory. We simplify this by assuming the absence of body forces.

Then the changes which occur in the distribution are divided into slow changes and rapid changes.

By « changes » we mean changes in the number of moleculse which simultaneously are spatially within $\mathrm{d}v$ and have velocity components within $\mathrm{d}\omega$.

The slow changes occur because molecules move into and out of $\mathrm{d}v$. The flow in the x direction is given by w_1nf, and the excess of outflow over inflow is, by an argument customary in the development of the continuity equation,

$$-w_1\frac{\partial nf}{\partial x} - w_2\frac{\partial nf}{\partial y} - w_3\frac{\partial nf}{\partial z} = -\,\boldsymbol{w}\cdot\operatorname{grad}(nf)\,. \tag{2.2}$$

The rapid changes are due to collision. Originally, when the molecules were thought of as hard spheres, the time of a collision was considered zero. Such a collision did not change the molecule's momentary position, *i.e.* did not affect its belonging to $\mathrm{d}v$, but changed its velocity abruptly, *i.e.* threw it into or out of $\mathrm{d}\omega$.

If we take into account that the intermolecular forces have a finite range, it is not strictly true any more to say that there are parts of the motion where the velocity is constant; but we have to make a practical division, say for example, that the effect of the intermolecular forces is negligible beyond 10^{-7} cm, and then compare the time during which the velocity changes appreciably with the time it does not. At standard conditions, the mean free path is about 10^{-5} cm, so that the collision lasts for about 1 % of the time of free motion. At lower pressure, this fraction diminishes, at higher pressure it increases, so that at higher pressure (nonideal gases) our assumptions are less justified. For long range forces, *e.g.* Coulomb forces, they are not justified at all; this is particularly true for one of their consequences namely that only interaction between pairs need be considered. Therein lies one of the difficulties of plasma dynamics.

The collisions have two effects on d^6N. They throw molecules out of the group, which belonged formerly to $d\omega$, and they throw molecules *in* which before the collision did not belong to $d\omega$. These quantities were called by Boltzmann a and b, so that the fundamental equation of gas theory has now the form

$$\frac{\partial}{\partial t}(nf) = -\boldsymbol{w}_0 \operatorname{grad}(nf) - (a-b)\,, \tag{2.3}$$

and our task is the calculation of the last term. The calculation of a is simple, since *every* collision is considered to throw a molecule out of the group. Consider a target at which one is shooting without aiming; the assumption of noncorrelation means that the bombarding molecules do not aim.

Then the fraction hitting a ring of radius σ and width $d\sigma$ is $2\pi\sigma\,d\sigma$ or, if we want to specify more closely, $\sigma\,d\sigma\,d\varphi$.

We have to sum up over all hitting molecules. $d\omega$ has already been crossed out in (2.3) and we find:

$$a = nf\iiint nf'\,d\omega'\,w_r\,\sigma\,d\sigma\,d\varphi, \tag{2.4}$$

where w_r is the relative speed of the molecules. This expression is quite independent of the forces between the molecules.

This is not so for b. We have to see which molecules in a pair will have after the collision velocity $\boldsymbol{w}$, when before the collision the molecules had velocities $\boldsymbol{w}_{\text{I}}$ and $\boldsymbol{w}'_{\text{I}}$; this involves solving the collision equation. The number of such collisions is

$$n^2\iiint f_{\text{I}}f'_{\text{I}}\,\frac{d\omega_{\text{I}}\,d\omega'_{\text{I}}}{d\omega\,d\omega'}\,d\omega'\,w_r\sigma\,d\sigma\,d\varphi\,. \tag{2.5}$$

The relative speed w_r is not changed by an elastic collision, and the ratio

$$\frac{d\omega_{\text{I}}\,d\omega'_{\text{I}}}{d\omega\,d\omega'}\,,$$

can be shown (by direct calculation, using conservation of energy and linear momentum, or by Liouville's theorem) to be unity. It is intended in (2.5), that $\boldsymbol{w}_{\text{I}}$ and $\boldsymbol{w}'_{\text{I}}$ be expressed with the help of the collision equations, by $\boldsymbol{w}$ and $\boldsymbol{w}'$, the former being the value of the velocity appearing in f (*) (see (2.4)), integration being made over $\boldsymbol{w}'$.

(*) f' is the function f with w' as velocity argument.

We then end up with the following equation

$$\frac{\partial}{\partial t}(nf) + \boldsymbol{w}\cdot\operatorname{grad}(nf) = -n^2\iiint(ff' - f_1 f_1')w_r\,\mathrm{d}\omega'\sigma\,\mathrm{d}\sigma\,\mathrm{d}\varphi\,. \tag{2.6}$$

The following remark has nothing directly to do with the interests of this group, but might be significant.

Boltzmann thought that he had found a mechanical or statistical explanation of the irreversibility which is characteristic of thermal processes in nature.

He constructed the function

$$-H = -\int(\ln f)f\,\mathrm{d}\omega\,,$$

and was convinced that eq. (2.6) leads to the consequence that $-H$ could decrease, so that $-H$ is an analog to entropy (or rather to entropy divided by k). Against this, Zermelo made the « Umkehreinwand » or objection of reversal. He asserted that, if at a given moment one reversed all the molecular velocities, all processes would go exactly backward, so that, if $-H$ increased before reversal, it would decrease after reversal.

The solution has come through the work of EHRENFEST, and much recent work.

Boltzmann's equation is based on the assumption of molecular chaos, or of complete absence of correlation between position and velocity and between different molecules. But if, with ZERMELO, we have two molecules right after a collision A↙ ↘B: and we reverse their velocities so A↗ ↖B, there *is* correlation between the inverted velocities and the relative positions. If the modified motions were this: A↗ ↖B the, overall process would *not* go backwards.

3. – Stresses. General considerations on the solution of the Boltzmann equation.

Before we proceed further with the consideration of the Boltzmann equation, we must investigate the stresses.

Stresses in a continuous medium form a tensor P_{ij}, which, as we shall show, is symmetric.

A stress is characterized by the direction in which the force acts (first index) and the direction of the normal to the surface, on which it acts (second index).

There are normal stresses (indices equal) and shear stresses (indices unequal). *E.g.* P_{33} is a normal stress, the force acting in the z direction on an area normal to it. P_{13} is a shear stress, the force being directed in the x direction along a surface which is normal to z.

In an ideal gas, where at a given moment only a negligible fraction of the molecules exert forces on each other, the origin of the stresses is purely kinetic, namely, due to the transport of linear momentum by the molecules through a surface.

E.g., P_{ij} is produced by the linear momentum nw_i of a molecule, $w_j nf\,\mathrm{d}\omega$; such molecules within the group $\mathrm{d}\omega$ cross a unit area, which is normal to the j-axis, per second. Therefore the total momentum transport is

$$P_{ij} = \int m w_i\, w_j n f\,\mathrm{d}\omega = \varrho \int w_i w_j f\,\mathrm{d}\omega\,, \tag{3.1}$$

with ϱ, the mass density, equal to mn.

It is immediately clear from (3.1) that the stress tensor is symmetric, *i.e.* $P_{ij} = P_{ji}$.

The Boltzmann eq. (2.6) gives the variation of the distribution function nf.

Let Q be any quantity depending on the velocity of a molecule. One can then also ask how the total Q, carried by the molecules within $\mathrm{d}v\,\mathrm{d}\omega$, changes with time. It will change, as does f, by molecules changing their velocities through collision. In the collision of a pair of molecules with original velocities $\boldsymbol{w}$, $\boldsymbol{w}'$, and velocities after collision of $\boldsymbol{w}_\mathrm{I}$ and $\boldsymbol{w}_\mathrm{I}'$ the Q carried by that pair decreases by

$$Q + Q' - Q_\mathrm{I} - Q_\mathrm{I}'\,. \tag{3.2}$$

If one defines the average Q per molecule as

$$\bar{Q} = \int Q f\,\mathrm{d}\omega\,, \tag{3.3}$$

and integrates the equation of change resulting from the preceding considerations over $\mathrm{d}\omega$, one gets

$$\begin{aligned} \frac{\partial n\bar{Q}}{\partial t} + \frac{\partial}{\partial x}\left(n\int Q w_1 f\,\mathrm{d}\omega\right) + \frac{\partial}{\partial y}\, n\int Q w_2 f\,\mathrm{d}\omega + \ldots = \\ = -\frac{n^2}{4}\iiiint (Q + Q' - Q_\mathrm{I} - Q_\mathrm{I}')(ff' - f_\mathrm{I} f_\mathrm{I}')\,\mathrm{d}\omega'\,\mathrm{d}\omega\, w_r \sigma\,\mathrm{d}\sigma\,\mathrm{d}\varphi\,. \end{aligned} \tag{3.4}$$

Here

$$n\int Q w_1 f\,\mathrm{d}\omega\,, \tag{3.5}$$

is the flow in the x direction of the quantity Q per unit time through the unit area normal to x. Equation (3.4) has been developed by Maxwell and was much used by him.

Hilbert [14] has pointed out that there are exactly five quantities which are preserved in a collision: the mass, the three components of linear momentum and, in an elastic collision, the kinetic energy. If any of these is chosen as Q, $Q+Q'-Q_1-Q_1'$ will be zero and therefore the collision integral, *i.e.* the term on the right of eq. (3.4), will be zero, no matter what the distribution function f is. In this way one gets five equations for macroscopic quantities, by having the right side of (3.4) equal zero. These five equations are: the continuity equation, the three components of the equation of motion, and the energy equation. However, the equations of motion (of which M. Greenspan made use in his lectures) are of the type

$$\frac{\partial}{\partial t}\varrho w_1+\frac{\partial}{\partial x}P_{11}+\frac{\partial}{\partial y}P_{12}+\frac{\partial}{\partial z}P_{13}=0\,,$$

and can be of practical use only if the P's themselves are known as functions of the state, just as application of Newton's equation requires that the force be known as function of the co-ordinates. This requires the knowledge of f, *i.e.* the solution of the Boltzmann equation.

Let us first consider equilibrium, in which the left side of (2.6) is identically zero and therefore the right side, the collision integral, must disappear. This means physically that the collisions maintain the equilibrium distribution without the influence of transport.

The solution for this condition is the well-known Maxwell distribution (which shall be designated as f^0), namely

$$f^0=\left(\frac{m}{2\pi kT}\right)^{\frac{3}{2}}\exp\left[-\frac{mw^2}{2kT}\right]. \tag{3.6}$$

This function reduces the quantity

$$ff'-f_1f_1'=\left(\frac{m}{2\pi kT}\right)^3\left[\exp\left[-\frac{m}{2kT}\left(w^2+(w')^2\right)\right]-\exp\left[-\frac{m}{2kT}\left(w_1^2+(w_1')^2\right)\right]\right], \tag{3.7}$$

to zero, as can be seen if the conservation of kinetic energy is considered. In fact, a slightly more general distribution function leads to the same result. This is a Maxwell function superposed on a steady uniform flow. If one defines the average velocity as

$$W=\int wf\,\mathrm{d}\omega\,, \tag{3.8}$$

then this generalized function is

$$(3.9)\qquad f^0 = \left(\frac{m}{2\pi kT}\right)^{\frac{3}{2}} \exp\left[-\frac{m}{2kT}\{(w_1-W_1)^2+(w_2-W_2)^2+(w_3-W_3)^2\}\right] = \left(\frac{m}{2\pi kT}\right)^{\frac{3}{2}} \exp\left[-\frac{m}{2kT}(\boldsymbol{w}-\boldsymbol{W})^2\right].$$

That this function also reduces $ff'-f_If'_I$ to zero can be proved as above, if one also makes use of the conservation of linear momentum in the collision. It is somewhat more complicated to prove that (3.9) is the *only* function for which the right-hand side of (2.6) is zero. We will not give this proof.

Let us now consider a nonstationary or not uniform state (of motion or temperature); we assume that the external co-ordinates or the time enter f, only through W or T (see beginning Section 4).

If we now tried to use a Maxwell distribution, we would find the left side of the Boltzmann equation different from zero (*e.g.* because

$$(3.10)\qquad \frac{df^0}{dx} = \frac{\partial f^0}{\partial W_1}\cdot\frac{\partial W_1}{\partial x} + \frac{\partial f^0}{\partial W_2}\cdot\frac{\partial W_2}{\partial x} + \frac{\partial f^0}{\partial W_3}\cdot\frac{\partial W_3}{\partial x} + \frac{\partial f^0}{\partial T}\cdot\frac{\partial T}{\partial x} \neq 0\Big),$$

while the right side is zero. That means that we cannot satisfy the Boltzmann equation by using simply a Maxwell distribution function with nonuniform, or time-varying macroscopic flow or temperature.

The Boltzmann equation, which we need to solve for the function f, is an integro-differential equation, containing the unknown both under the differential and integral signs. In addition, it is nonlinear, since a product of two f functions appears under the integral. This makes the solution enormously more difficult. To avoid this difficulty, one « linearizes » the equation, which means that one assumes that the deviation of f from the Maxwellian distribution (with variable $\boldsymbol{W}$ and T) is so small, that its square can be neglected *i.e.* one writes,

$$(3.11)\qquad \begin{cases} f = f^0(1+\Phi)\,, \\ ff'-f_If'_I = f^0(1+\Phi)(f^0)'(1+\Phi')-(f^0)_I(1+\Phi_I)(f^0)'_I(1+\Phi'_I), \end{cases}$$

$$(3.12)\qquad = f^0(f^0)'(\Phi+\Phi'-\Phi_I-\Phi'_I)\,.$$

This would not be justified for, *e.g.* shock waves, but is justified in the « acoustical » case, in which the sound amplitude (and therefore the deviation from equilibrium) has the limit zero. The Boltzmann equation is then

$$(3.13)\qquad \frac{\partial}{\partial t}(nf)+\boldsymbol{w}\,\mathrm{grad}\,(nf) = -n^2\iiint f^0(f^0)'[\Phi+\Phi'-\Phi_I-\Phi'_I]\,d\omega'\cdot w_r\sigma\,d\sigma\,d\varphi\,.$$

Assuming now that the gradients and rate changes of the macroscopic parameters are small, even the insertion of f^0 instead of f on the left of (3.13) will give an expression small of the first order (see (3.10)) and the inclusion of Φ would therefore result in terms small of the second order; to be consistent, these will therefore be left out. The gradients, *e.g.* of temperature being small means that

$$\Lambda \frac{1}{T} \operatorname{grad} T \ll 1 ,$$

where Λ is the mean free path.

One gets therefore, for the Boltzmann equation, after dividing by nf_0

$$\text{(3.14)} \qquad \frac{\partial \ln n}{\partial t} + (\boldsymbol{w} \operatorname{grad} \ln n) + \frac{m}{kT}(\boldsymbol{w} - \boldsymbol{W}) \cdot \frac{\partial \boldsymbol{W}}{\partial t} + \frac{m}{2kT}(\boldsymbol{w} - \boldsymbol{W})^2 \frac{\partial \ln T}{\partial t} +$$

$$+ \frac{m}{2kT}(\boldsymbol{w} - \boldsymbol{W})^2 (\boldsymbol{w} \operatorname{grad} \ln T) - \frac{m}{2kT} w \operatorname{grad} (\boldsymbol{w} - \boldsymbol{W})^2 =$$

$$= -n \iiint (f^0)' [\Phi + \Phi' - \Phi_\text{I} - \Phi_\text{I}'] \, \mathrm{d}\omega' w_r \sigma \, \mathrm{d}\sigma \, \mathrm{d}\varphi .$$

E.g. in the stationary case of uniform temperature and density and pure shear flow, the only term remaining on the left is

$$\text{(3.15)} \qquad + \frac{m}{2kT} w_3 \cdot 2(w_1 - W_1) \frac{\partial W_1}{\partial z} = \frac{m}{kT} w_1 w_3 \frac{\partial W_1}{\partial z} ,$$

(transformation to local $W_1 = 0$), in the case of stationary heat conduction (nT = constant)

$$\text{(3.16)} \qquad w_1 \left(-1 + \frac{m}{2kT} w^2 \right) \frac{\partial \ln T}{\partial x} .$$

One more remark should be made about the stresses in a moving medium. One has to distinguish whether the measurement is made from a stationary frame (*e.g.* stagnation pressure) when (3.1) remains unchanged, or from a frame moving with the fluid (static pressure), when

$$P_{ij} = \varrho \int (w_i - W_i)(w_j - W_j) f \, \mathrm{d}\omega ,$$

should be substituted.

4. – Methods for solving the Boltzmann equation.

In the attempt to solve the Boltzmann eq. (3.14) CHAPMAN [15] and ENSKOG [16] make the fundamental assumption that the effect of the gradients, *i.e.* dependence on the co-ordinates (and t), appears only in the macroscopic velocities $\boldsymbol{W}$ and in the temperature. The latter is always defined by

$$\frac{3}{2}kT=\int\frac{m}{2}w^2 f\,\mathrm{d}\omega\,. \tag{4.1}$$

We assume, for the sake of simplicity, that we have a stationary case $\partial/\partial t=0$, and that the gradient of $\boldsymbol{W}$ is in the i-direction and that of T in the j-direction, and that $nT=$ constant. This is no restriction, since, because of the linearity the superposition principle holds. Then (3.14) takes the form, (after transforming again to $\boldsymbol{W}=0$)

$$\left(-1+\frac{m}{2kT}w^2\right)w_j\frac{\partial T}{\partial x_j}+\frac{m}{kT}w_i\left(w_i\frac{\partial W_i}{\partial x_i}+w_k\frac{\partial W_k}{\partial x_i}+w_s\frac{\partial W_s}{\partial x_i}\right)= \tag{4.2}$$
$$=-n\iiint(f^0)'[\Phi+\Phi'-\Phi_{\mathrm{I}}-\Phi'_{\mathrm{I}}]\,\mathrm{d}\omega\,w_r\,\sigma\,\mathrm{d}\sigma\,\mathrm{d}\varphi\,.$$

One now writes

$$\Phi=F^{(1)}\frac{\partial T}{\partial x_j}+F^{(i)}\frac{\partial W_i}{\partial x_i}+F^{(k)}\frac{\partial W_k}{\partial x_i}+F^{(s)}\frac{\partial W_s}{\partial x_i}\,. \tag{4.3}$$

Inserting in (4.2) and identifying coefficients, one gets

$$\left(-1+\frac{m}{2kT}w^2\right)w_j=-n\iiint(f^0)'[F^{(1)}+(F^{(1)})'-F^{(1)}_{\mathrm{I}}-(F^{(1)}_{\mathrm{I}})']\,w_r\,\mathrm{d}\omega\,\sigma\,\mathrm{d}\sigma\,\mathrm{d}\varphi, \tag{4.4}$$

$$\frac{m}{2kT}w_i^2=-n\iiint(f^0)'[F^{(i)}+(F^{(i)})'-F^{(i)}_{\mathrm{I}}-(F^{(i)}_{\mathrm{I}})']\,w_r\,\mathrm{d}\omega\,\sigma\,\mathrm{d}\sigma\,\mathrm{d}\varphi, \tag{4.5}$$

$$\frac{m}{2kT}w_iw_s=-n\iiint(f_0)'[F^{(s)}+(F^{(s)})'-F^{(s)}_{\mathrm{I}}-(F^{(s)}_{\mathrm{I}})']\,w_r\,\mathrm{d}\omega\,\sigma\,\mathrm{d}\sigma\,\mathrm{d}\varphi, \tag{4.6}$$

and the analogous equation for the index k, both k, $s\neq i$.

If then, *e.g.* $F^{(s)}$ is found, one has the corresponding part of the distribution function as

$$f=f^0\left(1+F^{(s)}\frac{\partial W_s}{\partial x_i}\right),$$

and the stress tensor P_{si} is, from (3.1)

$$P_{si}=\varrho\iint w_s w_i f \, d\omega=\varrho\iint w_s w_i f^0\left(1+F^{(s)}\frac{\partial W_s}{\partial x_i}\right)d\omega=\varrho\frac{\partial W_s}{\partial x_i}w_s w_i f^0 F^{(s)}\,d\omega\,,$$

or

$$\eta=\varrho\int w_s w_i F^{(s)} f^0 \, d\omega\,. \tag{4.7}$$

Since, from (4.4) to (4.6), the functions F are inversely proportional to n, η is proportional to $\varrho/n=m$, or independent of the density, as it must be.

The final outcome for the viscosity is as follows:

Call χ the angle by which an incoming molecule is deflected from its original path. Define then an effective cross-section Q (this has nothing to do with the Q of Section 3) for viscosity by

$$Q^{(2)}=\int(1-\cos^2\chi)\sigma\,d\sigma\,d\varphi\,. \tag{4.8}$$

This is dependent on the relative velocity w_r.

Define next the integral

$$Y^{2,s}=\frac{3}{(s+1)!}(\pi r_0^2)^{-1}\int Q^{(2)}\left(\frac{\tilde{m}w^2}{2kT}\right)^{s+1.5}\exp\left[-\frac{\tilde{m}w^2}{2kT}\right]dw\,,$$

where r_0 is an appropriate length and $\tilde{m}$ the effective mass of the relative motion of the colliding molecules. In the following, M will be the corresponding « molecular weight »).

$Y^{2,s}$ is a dimensionless function of T, which is unity for hard spheres. Y depends on the law of interaction because the angle of deflection χ which occurs in $Q^{(2)}$ depends on it.

The coefficient of viscosity for hard spheres is

$$\eta=\frac{5}{16}\frac{\sqrt{kTm\pi}}{\pi r_0^2}=\frac{5}{16}m\sqrt{\frac{kT}{\pi m r_0^2}}=266.93\cdot10^{-7}\frac{\sqrt{MT}}{r_0^2}\,. \tag{4.9}$$

Here, r_0 is the diameter of the hard molecule. In the last part η is in poise and r_0 in angström.

For molecules with a different force law, (4.9) is replaced by

$$\eta=266.93\cdot10^{-7}\frac{\sqrt{MT}}{r_0^2 Y^{2,2}}\,, \tag{4.10}$$

the force law entering only into $Y^{2,2}$, *i.e.* the temperature-dependence of η.

5. – Relaxation times of distribution.

We are going now to change the subject of discussion and will discuss qualitatively the rate at which deviations from equilibrium die out. This subject, which goes back to Maxwell, has recently be clarified particularly by work GRAD [11], SARDI [17) and OFFERHAUS [18].

It is found that one should divide the overall change into three processes, needing for description widely separated time scales.

A) The fastest process is one in which any existing correlation is destroyed, the correlation between molecules and the correlation between position and velocity of a molecule. This needs the time during which a molecule is within the field of force of another or about $r_0/|\overline{w}|$. Here, $|\overline{w}|$ is the average speed of a molecule. Under normal conditions, this is

$$\tau_A = r_0/|\overline{w}| \simeq \frac{10^{-8}}{10^5} \simeq 10^{-13}\,\text{s}, \tag{5.1}$$

the *duration* of a collision.

B) Process B is one which will be discussed in more detail below. In it, the distribution adjusts itself to a nearly Maxwellian one, with locally and temporarily slowly varying temperature and flow speed, *i.e.* the distribution $f^0(1+\Phi)$ previously discussed. This takes a time τ_B which is about

$$\tau_B = \Lambda/|\overline{w}| \simeq 10^{-5}/10^5 = 10^{-10}\,\text{s} \tag{5.2}$$

under standard conditions, or about the time between collisions. For «Maxwellian molecules» Maxwell proved

$$\eta = p\tau_B\,. \tag{5.3}$$

How far this holds in general will be investigated below.

C) Process C is the macroscopic adjustment to true equilibrium. *E.g.* after regular thermal gradients to which the macroscopic laws of heat conduction can be applied have been established by B, heat conduction will, during C lead to uniform temperature. Then

$$\tau_C = \frac{L^2}{\Lambda^2}\,\tau_B \simeq \frac{L^2}{\Lambda|\overline{w}|}\,, \tag{5.4}$$

where L is a macroscopic dimension of the vessel.

Next, this subject will be treated with more modern mathematical methods.

6. – Development into eigenfunctions.

In the following, we sketch the newer mathematical methods used to prove the results given qualitatively in the last Section [11, 18, 19].

I will start with a superficial introduction to the notions of operator calculus. An operator is a rule which tells how to make of any given function (with certain restrictions) any other function, *i.e.*

$$\mathscr{L}f(x) = F(x)\,. \tag{6.1}$$

For example, a differentiation presents an operator; it makes out of $ax \to a$, out of $x^2 \to 2x$, out of $e^{ax} \to ae^{ax}$.

The last exemple is interesting because it shows that it is possible that the new function $F(x)$ is simply the old function multiplied by a constant.

Of course the operator need not be anything as simple as a differentiation, it may be an integration or just a verbal rule. We will limit ourselves to linear operators, defined by

$$\mathscr{L}(u+v) = \mathscr{L}u + \mathscr{L}v\,. \tag{6.2}$$

We next ask the following question: given an operator, are there functions, which operated upon produce the same function multiplied by a constant? For the previous example in which the operator was a differentiation, we have seen that the exponential is such a function. Physical examples are well known, the vibrations of a stretched string, determined by

$$\frac{\mathrm{d}^2u}{\mathrm{d}x^2} = -k^2u\,.$$

For the given boundary conditions (which are to be included in the operator definition) this equation has an infinite set of well-known solutions,

$$u_s = a\sin\frac{\pi s x}{l}\,,$$

for a discrete set of k^2, neamely $(\pi s/l)^2$.

In general, the question is this: what functions exist so that a given operator operating on them reproduces them, multiplied, with a constant, *i.e.*

$$\mathscr{L}\psi = \lambda\psi\,. \tag{6.3}$$

It turns out that this is in general not possible for all values of the λ but only for a discrete set, λ_s, which we call the eigenvalues or characteristic values of the operator. The totality of λ_s we call the spectrum of eigenvalues (in analogy to a coupled system of oscillators). For most of the operators occurring here the spectrum is discrete but infinite, but there may be a continuum also. *E.g.* in the quantum-theoretical problem of the H atom, the negative eigenvalues are discrete, the positive continuous. The function ψ belonging to a certain eigenvalue λ_s is called the eigenfunction ψ_s.

For many operators eigenfunctions belonging to different eigenvalues are orthogonal. Write

$$\mathscr{L}\psi_S = \lambda_S\psi_S \,; \qquad \mathscr{L}\psi_R = \psi_R\lambda_R \,,$$

multiply the first equation with ψ_R, the second with ψ_S, subtract and integrate the result over the permitted range of the independent variable x, possibly with a weight factor (*) $g(x)$,

$$\int(\psi_R\,\mathscr{L}\,\psi_S - \psi_S\,\mathscr{L}\,\psi_R)\,g(x)\,\mathrm{d}x = (\lambda_S - \lambda_R)\int\psi_S\psi_R\,g(x)\,\mathrm{d}x\,. \tag{6.4}$$

Since $\mathscr{L}$ may contain differential or integral operators, one cannot in general, change the order of the factors on the left. But by partial integration and with the proper boundary conditions (either ψ or $\mathrm{d}\psi/\mathrm{d}x$ zero at the boundary) the integral on the left can be shown to be zero. Since the eigenvalues λ are different

$$\int\psi_S\psi_R\,g(x)\,\mathrm{d}x = 0\,. \tag{6.5}$$

which property is called orthogonality.

Since the eq. (6.1) is homogeneous, ψ can be multiplied with any constant. It is convenient to choose this constant so that

$$\int\psi_S^2\,g(x)\,\mathrm{d}x = 1\,; \tag{6.6}$$

then ψ is called normalized (all the integrals over the whole range of x).

Returning now to the collision integrals, let us define an operator G acting on an arbitrary function F of $\boldsymbol{w}$, such that

$$\mathscr{G}F = \iiint(f^0)'\,[F + F' - F_1 - F_1']\,\mathrm{d}\omega' w_r\sigma\,\mathrm{d}\sigma\,\mathrm{d}\varphi\,. \tag{6.7}$$

(*) This g has nothing to do with the distribution functions g of Section **1**.

Furthermore, given an arbitrary function $F(x)$, it is possible to represent it by a series:

$$F(x) = \sum a_s \psi_s$$

provided $F(x)$ obeys the same boundary conditions as the ψ_s (*e.g.*, is zero at the ends of the interval) and is quadratically integrable over the range of x.

This is a linear operator according to the definition (6.2) and it depends on the interaction potential ε_p of a pair of molecules, since the arguments $\boldsymbol{w}_{\mathrm{I}}$ and $\boldsymbol{w}'_{\mathrm{I}}$ of F_{I} and F'_{I} depend on ε_p for given $\boldsymbol{w}$ and $\boldsymbol{w}'$.

Let us now define the eigenfunctions ψ_s and eigenvalues λ_s of the operator $\mathscr{G}$ through:

$$\mathscr{G}\psi_s = \lambda_s \psi_s \,. \tag{6.8}$$

Both the ψ_s and λ_s depend on the interaction potential since $\mathscr{G}$ does. We know, from Section 3, of five eigenfunctions with $\lambda = 0$, namely m, mw_1, mw_2, mw_3 and $mw^2/2$ which obey

$$\mathscr{G}\psi = 0\,,$$

whatever the interaction potential. We will call them ψ_0 and count S from unity beyond that.

Than

$$\mathscr{G}F(\boldsymbol{w}) = \mathscr{G}\left(\sum a_s\psi_s\right) = \sum a_s \mathscr{G}\psi_s = \sum a_s\lambda_s\psi_s \tag{6.9}$$

whatever F is.

If we have to solve the equation

$$\mathscr{G}\Phi = I(\boldsymbol{w}) \tag{6.10}$$

we write

$$\Phi = \sum a_s\psi_s\,, \qquad I = \sum b_s\psi_s \tag{6.11}$$

or

$$\sum a_s\lambda_s\psi_s = \sum b_s\psi_s\,. \tag{6.12}$$

In the case of the particular operator $\mathscr{G}$ we are now using, the proper weight function is the Maxwellian distribution f^0. If we want to determine the coefficients b_s, we therefore multiply in the second eq. (6.11) both sides with $\psi_j f^0$ and integrate over the whole range of $d\omega$

$$\int I\psi_j f^0 d\omega = \sum b_s \int \psi_s \psi_j f^0 d\omega = b_j . \tag{6.13}$$

Similarly, by applying this same procedure to (6.12) we find

$$a_j = \frac{b_j}{\lambda_j} . \tag{6.14}$$

Let us now return to eq. (3.14); and consider as an example a stationary uniform shear (with constant n and T). The function I is then given by (3.15) divided by n and

$$b_s = \frac{1}{n} \frac{\partial W_1}{\partial z} \frac{m}{kT} \int w_1 w_3 \psi_s f^0 dw . \tag{6.15}$$

It should be remembered that $\partial W_1 / \partial z$ is a constant, independent of $\boldsymbol{w}$. Therefore

$$\Phi = \sum \frac{b_s}{\lambda_s} \psi_s = \frac{1}{n} \frac{\partial W_1}{\partial z} \frac{m}{kT} \sum \frac{1}{\lambda_s} \psi_s \int w_1 w_3 \psi_s f^0 dw , \tag{6.16}$$

and therefore (see (3.1))

$$P_{13} = \varrho \int w_1 w_3 f^0 (1 + \Phi) d\omega = \varrho \int w_1 w_3 f^0 d\omega = \tag{6.17}$$

$$= \frac{\partial W_1}{\partial z} \frac{m^2}{kT} \sum \frac{1}{\lambda_s} \left(\int w_1 w_3 \psi_s f^0 d\omega \right)^2 .$$

Since by macroscopic definition

$$P_{13} = \eta \frac{\partial W_1}{\partial z} , \tag{6.18}$$

we have first by proved that P_{13} is of this form, and secondly calculated

$$\eta = \frac{m^2}{kT} \sum \frac{1}{\lambda_s} \left(\int w_1 w_3 f^0 \psi_s d\omega \right) , \tag{6.19}$$

independent of n.

From what has been said earlier (Section 4) only those ψ_s will contribute which are odd in both w_1 and w_3.

Similar calculations may be made for heat conduction.

Next, consider a distribution which deviates slightly from one of the stationary nonequilibrium distributions (*).

If Φ refers to such a stationary distribution, let the momentary distribution be $f^0(1+\Phi+\tilde{\Phi})$.

Then the momentary linearized Boltzmann equation, will be

$$\frac{\partial\tilde{\Phi}}{\partial t}+(\boldsymbol{w}\operatorname{grad}\tilde{\Phi})=-n\,\mathcal{G}\,\tilde{\Phi}\,. \tag{6.20}$$

If we now develop

$$\tilde{\Phi}=\sum c_s(t)\,\psi_s$$

we find

$$\sum_s\frac{\partial c_s(t)}{\partial t}\,\psi_s+\sum c_s(\boldsymbol{w}\operatorname{grad}\psi_s)=-n\sum\lambda_s c_s\psi_s\,. \tag{6.21}$$

The second term on the left concerns slow (transport) changes and will now be neglected. Multiplication of (6.21) with ψ_j and integration over $\boldsymbol{w}$ gives

$$\frac{\partial c_j}{\partial t}=-n\lambda_j c_j\,,\qquad c_j\sim\exp\left[-\frac{t}{\tau_j}\right],\qquad \frac{1}{\tau_j}=n\lambda_j\,, \tag{6.22}$$

τ_j is the relaxation time of the mode j, is inversely proportional to the number density (or the pressure) and to the eigenvalue λ_s. Different low lying modes have different relaxation times, but of the same order of magnitude.

While the theory here presented is mathematically satisfactory it suffers from the fact that actually eigenfunctions and eigenvalues are exactly known only for Maxwellian molecules, molecules which interact with an attractive potential $\sim r^{-4}$, but which do not exist in nature. Here the only eigenfunction of proper symmetry for which b_s is not zero $\psi_2=w_1w_3$ unnormalized, or $(kT/m)w_1w_3$ normalized.

Then the integral in (6.19)

$$\int w_1w_3\psi_2 f^0\,d\omega=\frac{kT}{m}\,,$$

and

$$\eta=\frac{m^2}{kT}\left(\frac{kT}{m^2}\right)\frac{1}{\lambda_2}=nkT\,\frac{1}{n\lambda_2}=p\tau_2\,. \tag{6.23}$$

(*) In the lecture this was done incorrectly.

For other molecular models (other $\mathcal{G}$'s) no exact solution is known. If one develops the real eigenfunctions into a series of Maxwell eigenfunctions ψ^M

(6.24) $$\psi_s = \sum_j h_{sj}\psi_j^M .$$

one finds

(6.25) $$\eta = kT \sum_s h_{s2}^2 \frac{1}{\lambda_s^M} .$$

The operator equation for ψ_s has the form

(6.26) $$\sum_j h_{sj}\Gamma\psi_j^M = \lambda_s \sum h_{sj}\psi_j^M .$$

Multiplication with $\psi_R^M f^0$ and integration leads to

(6.27) $$\sum_j h_{sj} G_{Rj}^M = \lambda_s h_{sR} ,$$

where the matrix element G_{Rj}^M is an abbbreviation for

(6.28) $$\mathcal{G}_{Rj}^M = \int f^0 \psi_R^M \mathcal{G} \psi_j^M \, \mathrm{d}w .$$

On principle the set of linear eqs. (5.30) can be solved giving the λ_s as the roots of the secular determinant

$$(G^M - \lambda) = 0$$

and the values of the coefficient h follow.

However, if one assumes that ψ_j and ψ_j^M are similar, one can conclude that only the h_{jj} and G_{jj}^M have appreciable values.

Then, approximately:

(6.29) $$h_{jj}\mathcal{G}_{jj}^M = \lambda_j h_{jj} ,$$

i.e.

(6.30) $$\tau_j^{-1} = n\mathcal{G}_{jj}^M$$

and (*)

(6.31) $$\eta = p\tau_2 h_{22}^2 \sim p\tau_2$$

(*) According to HIRSCHFELDER *et al.* [13] the inclusion of three terms of the series provides a factor, which varies slowly with the temperature, and for the Lennard-Jones potential, differs from unity less than 0.8%.

since

$$\sum h_{2j}^2 = 1 . \tag{6.32}$$

It is obvious by comparison that the quantity $\mathscr{G}_{2,2}^M$ is proportional to $r_0^2 Y^{2\cdot 2}$ of (4.10).

7. – Interaction between molecules.

I will now change the subject and speak of the nature of the interaction between molecules, since this affects the viscosity and its temperature-dependence.

I might say beforehand, that for the small masses handled in the laboratory, gravitational effects are negligible in comparison with those discussed here. Gravitational effects are long-range effects but have a very small constant factor. If one considers larger and larger amounts of matter, the molecular forces acting on a molecule soon do not increase further, because of their short range, while the gravitational forces do; but it takes amounts of planetary or stellar size to make the two comparable.

Molecular forces have certain characteristics in common. At large distances they are weak but attractive. They increase at first while the distance decreases. On the other hand, at small distances they must be repulsive, and increasingly repulsive the smaller the distance, or matter would collapse. Therefore the general behaviour of the interaction energy H between two uncharged particles is represented by the curve of Fig. 1.

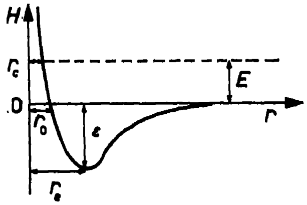

Fig. 1.

That the value of H at infinity has been put equal to zero, is a matter of convenience. r_e is the equilibrium distance, ε the depth of the well and r_0 the turning point of a particle coming in with negligible kinetic energy from infinity. A particle coming in with energy E has its turning point at r_c.

It is of historical interest that this type of curve was first considered by the Italian Jesuit Roger BOSCOVICH in the middle of the 18th century. He was born in Dalmatia, of Slavic country stock, to judge from his name. After joining the Jesuits and making his studies, he taught mathematics at the Collegio Romano and at the University of Pavia. He considered the atoms as dimensionless centres of force, and has in his books several curves equivalent to ours. It is of interest that his curves have several maxima and minima, to take care of the different densities of the various states of aggregation, since the role of kinetic energy was not then known. (Even in the first half of the 19th century, physicists still spoke of the « elastic » tension of vapours.) Boscovich's book appeared in many editions, the first being published in Vienna 1758 [20]. As to the nature of the attractive forces, the first reasonable theories appeared soon after 1912, when Debye proposed the existence of permanent electric dipoles in (some) molecules.

It might be mentioned here that magnetic forces are negligible compared to electric ones, since the ratio to electric fields is about w/c, and the velocity w of the (outer) electrons in atoms and molecules is small compared to c, the velocity of light.

Soon after 1912, it was not known that relatively few molecules have permanent dipoles, and so this interaction energy between permanent dipoles, was evaluated. However molecules rotate due to thermal motion, and some relative positions are attractive, others repulsive; the attractive positions are taken more frequently because of the Maxwell-Boltzmann distribution function. The effective attraction energy turns out to be $\sim 1/T$, disappears therefore at high temperatures, and even at room temperature and for molecules with appreciable permanent dipoles is only a fraction of the total in gases, as Keesom's [21] calculations have shown.

The next steps were taken by DEBYE [22]. If one considers with the former, a magnetic permanent dipole rotating in front of a sphere of soft iron, then one sees that, in case the north pole of the needle points to the sphere, a south pole will be induced there giving attraction. If, next in the rotation, the south pole of the needle points to the sphere, a north pole will be induced, again giving attraction. It follows that the interaction between an existing dipole and an induced dipole is always attractive, independent of rotation and therefore temperature, because and in so far the induced and the inducing dipole are in phase.

But where is the dipole, say in a helium atom? Here, looking at it classically, one can point out that each moving electron in an atom or molecule, together with the nucleus, can be considered as a rotating dipole which will induce in a neighboring molecule another dipole in phase with its own motion. Since the interaction between a dipole and its induced dipole is proportional to the square of the electric field, and since the electric field of a dipole decreases like r^{-3}, the interaction energy is proportional to r^{-6}. This general attraction is now usually called van der Waals attraction. The ideas just discussed were finally translated into quantum-theoretical form by LONDON [23] who reached this result with the help of second-order perturbation calculation.

In quantum theory, there is substituted for the classical rotating dipoles, made up of orbiting electron and nucleus, all the « virtual dipoles » connected with all those possible electronic transitions from the ground state, which are optically allowed, *i.e.* which have a dipole moment connected with it. These virtual transitions then induce in the other molecule a dipole just as the classically assumed real dipoles would. The attractive interaction energy is, therefore, given by $-A/r^6$, where A contains, apart from universal constants, two factors: the first is the sum of the strength of all absorption lines starting from the ground state, divided by their frequencies, squared. This is the sum of the virtual dipole moments squared. The second factor is the polarizability of the particle in which the dipole is induced. CASIMIR [24] has shown that for larger distances — where however, the attraction is already small — r^{-7} should be substituted for r^{-6}, due to the retardation of the electric field, which retardation introduces a phase difference between the original and the induced dipole.

After discussing the physical nature of the attractive forces, we will next treat the repulsive potential and then enumerate the different expressions for the overall potential. The existence of the repulsive potential is necessary to prevent matter from collapsing, in view of the generally existing attraction. When the atoms were thought of as hard spheres, this was no problem. Formally a hard sphere is described by a potential equal to zero beyond r_0, positive infinite for distances smaller than r_0. But when LENARD, by his experiments on the penetration of matter by electrons (around 1895) found that atoms were mainly empty space, and when the Bohr theory held to the same view, a more elaborate theory became necessary. The first attempts at explanation turned out to be wrong. In 1918, BORN and LANDÉ [25] tried to explain the lattice force in sodium chloride type crystals. They imagined the ions—following LANGMUIR and KOSSEL—as cubes, with the nucleus in the center and the eight outer electrons in the corners. The attraction was of course provided in this case mainly by the Coulomb attraction between the excess charges, while as BORN and LANDÉ proved, neutral cubes of the kind described above, arranged side by side, gave repulsive potential energies $\propto r^{-8}$. However this picture proved to be wrong.

According to Earnshaw's theorem, no two charge arrangements, each held rigid within itself, can have relative to each other positions of equilibrium. Physically, the idea is simple. In any arrangement of charges, which is neutral as a whole, there are as many lines of force leaving as are returning. Mathematically this is a consequence of the fact that any spherical harmonic (except the zeroth, which corresponds to an excess charge) integrated over a sphere vanishes. Therefore in any interaction between overall neutral rigid charge arrangements there are as many orientations in which there is attraction as there are orientations in which there is repulsion. According to the statistical Maxwell-Boltzmann formula, the positions of attractions will be chosen preferentially except at very high temperature, where the average interaction is zero (*). That means for the Born-Landé crystal case, that neighbouring cubes should arrange themselves side against corner, which would provide attraction.

No solutions was found until the paper of HEITLER and LONDON [26] in 1927, which explained the universal repulsion at low distance (the « impenetrability » of matter) by a first order perturbation calculation.

It is found to be a typical quantum effect, to which no classical analogue exists, and is bound up with the Pauli exclusion principle, or the fact that the electrons obey Fermi-Dirac instead of classical statistics.

It only arises when the electron clouds of the two particles (atoms, molecules) overlap and is proportional to that overlap. Since the densities of the electron clouds of spherically symmetrical particles (rare-gas atoms) are roughly proportional to $\exp[-r/r']$, the overlap is roughly proportional to $\exp[(r/r'+r/r'')]=\exp[-r/r''']$ which explains the short range and steepness of the repulsive potential. One might try to explain the repulsion due to the overlap electrostatically, by asserting that the overlap of two electron clouds of course produces repulsion. But the electron cloud of B, by penetrating the cloud of A, has also come closer to the nucleus of A (and correspondingly the electron cloud of A to the nucleus of B) and on balance, the electrostatic effect is attractive.

The first attempt at a more physical interpretation of the Heitler-London calculation is due to the late LENZ [27, 28].

Consider the Fermi-Thomas model of a rare gas atom containing N electrons as simple example of a molecule. In it, all the N quantum states of lowest energy are each filled by one electron. If one now brings electrons from the other cloud, belonging to the atom B, into the space already filled by the electrons of atom A, they cannot go into the same quantum states which are already filled by electrons of atom A, because of the Pauli principle. So they must fill higher, originally unfilled states. It is the energy of this « promotion » to higher states which has to be supplied by work when the two atoms approach too closely, which appears as repulsive interaction. One sees that, without the Pauli principle, this would not exist.

A modification of this explanation is due to BERLIN [29]. According to BERLIN, attraction between two atoms results from an accumulation of negative charges between the nuclei, repulsion from a deficit of such charges (as compared with the formal superposition of charge densities of the free atoms). The Pauli exclusion principle forces electrons out of the overlap region, into the space opposite the line joining the molecules.

(*) One might ask whether this contradicts our previous statement, that the attraction between dipole and induced dipole is temperature-independent. It does not, because the existence of an induced dipole implies nonrigidity or more specifically, the presence of nonelectrostatic Hooke's law restoring forces.

We turn now to the interaction formulae which have been proposed.

I) The oldest is the van-der-Waals model, which has been applied to viscosity calculations by SUTHERLAND in 1900, long before quantum mechanics. It is a hard sphere model, with relatively long range, weak atrractive forces. In the viscosity calculations, two constants appear: the molecular diameter r_0, and C, Sutherland's constant, which has the physical meaning that Ck is the attractive potential energy of two molecules in contact.

II) The one most closely connected to theory is the formula of Cunningham

$$H = B \exp\left[-\frac{r}{r_0}\right] - Ar^{-6}\,. \tag{7.1}$$

The first term approximates the theoretically expected repulsion, the second the theoretically expected attraction. It contains 3 constants, B, r_0 and A.

III) The Lennard-Jones expression

$$H = 4\varepsilon\left\{\left(\frac{r_0}{r}\right)^{12} - \left(\frac{r_0}{r}\right)^{6}\right\}. \tag{7.2}$$

It contains the theoretically expected attraction. The repulsion term was originally chosen in deference to the Born-Landé ideas of interaction of high multipoles (the cubes correspond to octupoles). Lennard-Jones originally left the exponent of the repulsion term indetermined, with the only proviso that, because of the greater steepness of the repulsive forces, it had to be appreciably higher than that of the attraction. He settled than on 12 for no physical reason but for the mathematical one that if the two exponents are in the ratio 2:1, the calculations are much simpler.

The Lennard-Jones expression contains only two constants ε, which is the depth of the well, and r_0, which is characterized by the fact, that for $r = r_0$, $H = 0$. Therefore $r = r_0$ is the place at which the H curve cuts the abscissa; it is also the turning point for a molecule approaching with negligible kinetic energy. The equilibrium position (minimum of the well) is at $\sqrt[6]{2}\,r_0$.

IV) The next important formula is that of MORSE.

This is a purely empirical equation, which MORSE originally introduced as an empirical expression to describe the (asymmetrical) potential-energy curve governing the internal vibration of molecules. In its original form, it was

$$H = \varepsilon\{\exp[-2\varkappa(r - r_e)] - 2\exp[-\varkappa(r - r_e)]\}\,. \tag{7.3}$$

It is a three-constant expression, ε being the depth of the well, r_e the equilibrium distance, and $1/\varkappa$ the width of the well. It has the exponential form for the repulsion, but also for the attraction, although less steep ($\varkappa$ instead of $2\varkappa$). The attraction here drops off much faster than for a power law like r^{-6}.

In the discussion, Dr. SETTE pointed out that both for (7.2) and (7.3), the repulsive term is the square of the attractive term (except for a factor 2 in (7.3)), but that in the Lennard-Jones form the latter is chosen according to the theory, in the Morse equation the former.

HIRSCHFELDER and LOVELL [30] have chosen the independent constants in (7.3) differently. They write

$$\varkappa = \frac{C}{\sigma},$$

and

$$r_e = 1 - \ln \frac{C}{2}.$$

If one then chooses reduced lengths r/σ, $r/\sigma = 1$ for $H = 0$, and C has to be used as an additional parameter.

V) AMDUR [31, 32] has investigated the interaction potential for higher kinetic energies by scattering experiments with molecular beams and has found

$$H = Br^{-S}, \tag{7.4}$$

$S = 5.94$ for He, 8.33 for A, 7.22 for N_2, in the range of $(0.1 \div 1)$ eV for H.

On principle, the use of molecular beams for scattering experiments is the most direct way of determining the interaction law between molecules. However the usual beams have a Maxwell distribution of velocities, and one must therefore include a velocity selector, which cuts the intensity too much. In addition, molecular beams have only velocities within the thermal range. Several groups are working at present to get around these difficulties [33, 34].

AMDUR [34] produces a beam of positive ions, which are accelerated to a uniform velocity by a given potential difference, then neutralizes the ions by electrons. This produces strong neutral beams of several volts energy or more. The method cannot be used for very low energies, because of Volta potential differences in the apparatus.

We will finally discuss in how far theory can predict the value of the constants in the expressions for H.

SLATER [35, 36] has calculated long ago the complete interaction expression (7.1) between two helium atoms, the simplest saturated molecules. This expression agrees fairly well with experiments. The constant in the exponential repulsion expression was later calculated by BLEICK [37] for Ne, and this work has been extended recently to A [38].

Recently, the method of molecular orbitals has been applied to the problem. In it, the interaction between the molecules A and B is treated so that they are considered as a complex AB to which all the electrons belong.

One then has to calculate numerically H for a series of distances between A and B. This has been done, as an example, by GRIFFING and WEHNER [39] for the interaction of two helium atoms, considered as a two-nuclei, four-electron complex. The result agrees rather well with Slater's and other newer improved calculations.

It is interesting to see how the van-der-Waals attraction arises in this method. When the two atoms are very far apart, the electrons are completely in (spherically symmetrical) $1s$ states. But when the atoms get closer together, the best electron states are those into which $2p$ states are mixed (more precisely, $2\sigma p$-states). These are directional, and mixed with the s-states, describe polarization, *i.e.* the induced dipoles.

In recent years great interest has arisen in the transport properties of very hot mixed gases, *e.g.* in the heat conduction in the exhaust of jet motors, or in the shock waves important in high-speed aerodynamics, or in the properties of the atmosphere at very high altitudes.

Here, due to the high temperature or to the effect of sunlight, many of our customarily saturated molecules are dissociated or even ionized. It becomes therefore important to know something of the interaction energy of, say, oxygen atoms and oxygen or nitrogen molecules. To determine this experimentally would be rather difficult, so it has to be attempted theoretically.

One can say immediately that in the case of such unsaturated species as an oxygen atom, the main attractive force will not be provided by van-der-Waals type forces (although these will also be present), but by a kind of chemical force. This latter will decrease with distance much faster than the van-der-Waals type, probably, exponentially, so that one should expect that the Morse-formula (7.3) should represent the situation better than (7.1) or (7.2). The problem can be and has been approached by the method of molecular orbitals, but in practice this is limited up to now to very simple particles, since the whole calculation must be made from the beginning for each case.

A semi-empirical method, proposed by MASON and VANDERSLICE (in a number of papers in the *Journal of Chemical Physics* since 1958 [40-42]) is very useful. It uses the valence bond method, in which the binding of two atoms in a molecule is made up of interactions between pairs of electrons, each member of a pair belonging to a different atom. As an example, consider the potential energy curve as function of distance in different excited electrons states of NO. This curve can be gotten from a study of the bands in the optical spectrum in the visible and ultraviolet.

Because one has them for different electronic states, one can decompose the overall interaction curves into components each belonging to a particular electron pair *e.g.* an outer *p*-electron in oxygen and an outer *s*-electron in nitrogen, for all different spin orientations.

If one then wishes to calculate the interaction energy of an oxygen atom with N_2, one makes it up additively out of the previously determined interaction curves of a particular oxygen electron and a particular nitrogen electron.

One extreme case of « chemical » interaction has been calculated recently by KOROBKIN [43].

It concerns the interaction energy of an hydrogen molecule and proton, which approaches the molecule in the midplane normal to the molecular axis. This potential is calculated both for chemical binding (electron sharing or formation of electron orbitals embracing all three nuclei) and for purely electrostatic interaction.

8. – The effect of the form of the interaction potential on the transport properties.

In the previous Section, we have discussed the different expressions for the energy of interaction between particles. We shall now be concerned with the question how these influence the transport properties.

Except for single power laws like (7.4), one can write the viscosity (*) (see (4.10))

$$\eta = 266.9 \cdot 10^{-7} \frac{\sqrt{MT}}{r_0^2 Y^{2,2}} . \tag{8.1}$$

Here, $Y^{2,2}$ is a dimensionless function of a dimensionless quantity for which one can profitable choose

$$\frac{kT}{\varepsilon} .$$

If one writes this $T/(\varepsilon/k)$, one can give ε/k in degrees Kelvin without having to bother with negative powers of 10, as would be if ε were measured in ergs.

The particular force law *only* enters in $Y^{2,2}$, and therefore it is necessary to known η over a wide range of temperatures if one wants to test a law. There exist measurements for argon and air from somewhat below room temperature to about 1800 °K, and N_2 and CO_2 up to 1700 °K, made with the capillary flow method [44]. The limit on accuracy and range is the limit of fabricating the capillary and preventing changes at the high temperature. Other gases have been measured very precisely up to 1500 °K by JOHNSTON [45].

(*) This is only a first order approximation, none the less quite good. At extremely low temperatures (H_2 and He) quantum corrections come in.

For most force laws, the integrals which make up $Y^{2,2}$ (4.7), (4.8) can only be calculated numerically on a computer. A further complication lies in the fact, that to the actual interaction energy H must be added the quasi-potential energy of the centrifugal motion, to get the effective potential energy $(H)_{\mathrm{eff}}$

$$H_{\mathrm{eff}} = H + \frac{1}{2\tilde{m}} \frac{p_\varphi^2}{r^2}, \tag{8.2}$$

where p_φ is the angular momenrum of the relative motion equal to

$$p_\varphi = \tilde{m} w_r^0 \sigma ,$$

where w_r^0 is the relative motion at large distance and σ the distance at which the asymptote of the original motion would pass the scatterer. Under some conditions, the positive quasi-energy of the centrifugal motion may produce a maximum of H_{eff} in the region where H is attractive. Molecules of low energy may collide with and be turned back by this hump without ever getting very near to the scatterer. Molecules which have an energy slightly below that of the maximum will make a number of circuits around the hump (which acts like a circular wall) before flying off again. These « orbiting » molecules make a further complication for the computation. An extensive table of $Y^{2,2}$ for the Lennard-Jones potential (which contains as only independent variable the dimensionless temperature kT/ε) has been calculated by HIRSCHFELDER and his collaborators and can be found in his book [13].

To give an idea of the necessary range of temperature measurement, one has the following values for a number of gases

Gas	He	H_2	N_2	O_2	Cl_2	CO_2	CS_2
ε/k (°K)	6	34	91	113	357	190	490

This means that, if one excludes H_2 and He, kT/ε lies for 300 °K between 0.6 and 3; for 1500 °K, the range is as high as between 3 and 17. In the range between 0.6 and 3, Y varies between 2.15 and 1.04.

As a matter of fact, while η and its temperature variation, *i.e.* Y, permit one to determine the constants fairly accurately provided the force law is assumed, they are not very sensitive to the force law. The Sutherland model gives

$$y = 1 + \frac{C}{T} .$$

If one chooses $C=1.089\varepsilon$ and the two r_0 as differing by a constant factor, the temperature variation of the Lennard-Jones model and the Sutherland model is indistinguishable [46] in the range of kT/ε between 0.75 and 4.

Quite recently, HIRSCHFELDER and LOVELL [30] have calculated tables of $Y^{2,2}$ for the Morse law. This is of course a two-parameter table. No comparison has yet been made of the temperature-dependence of η for the Lennard-Jones and the Morse law. Experimentally, the temperature-dependence of η for the Lennard-Jones expression agrees very well for the experiments of JOHNSTON on Cl_2.

MONCHICK and MASON [47] have published a table of Y for the Stockmayer potential, which is applicable to polar gases and which contains besides the Lennard-Jones expression an angle-dependent term for the interaction of two permanent dipoles. They compare their results with the measurements of the viscosity of steam, the latter being of considerable engineering importance.

AMDUR [48] has calculated the viscosity of some gases at a range of temperatures, using for the lower part of the potential-energy curve the Lennard-Jones formula and for the upper part his expression (5.4). The result is shown in the following table for argon.

T °K	1000	5000	15000
η calculated entirely from (6.2)	5.4	15.4	30.7
η calculated from combination of (6.2) and (6.4)	5.6	18.6	42.

Some years ago, SMILEY [49] has extended the measurements of the heat conductivity of argon up to 3000 °K. Since this is a monoatomic gas, the ratio of thermal conductivity to viscosity is temperature-independent, so that this can be considered as an indirect measurement of viscosity. A shock wave in argon is reflected from the back end of the tube. Between this end and the reflected shock, the gas is at rest at high temperature. The heat conducted from the gas to a resistance thermometer on the back-wall, which thermometer consisted of a thin platinum film, was measured. The evaluation is not simple, since the temperature in the gradient varied all the way from the interior of the gas to the wall, and the conductivity is temperature-dependent. Agreement with the predictions of the Lennard-Jones equation was found to be within 20 % which is about the accuracy of the measurement.

One might ask whether there are any other methods which might distinguish more easily between different force laws besides scattering experiments.

There is first the second virial coefficient.

The Kammerlingh-Onnes equation of state for moderately dense gases can be written

$$\frac{pV}{RT} = 1 + \frac{B}{V} + \frac{C}{V^2} + \dots, \tag{8.3}$$

which for small density is reduced to

$$\frac{pV}{RT} = 1 + \frac{B}{V}. \tag{8.4}$$

Within the same approximation, this can also be written

$$\frac{pV}{RT} = 1 + \frac{B}{RT}p,$$

B is called the second virial coefficient. The form (8.4) is completely independent of the force law, provided the forces have short range. The force law enters only into the temperature-dependence of B, which looks typically as follows (B is in units of volume) (Fig. 2).

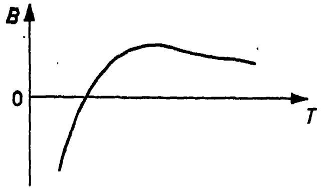

Fig. 2.

The region where B is negative is determined by the attractive forces, the region where it is positive, by the repulsive ones. The temperature where B is zero is called the Boyle-temperature. For hard molecules, B should be constant at high temperature. The fact that in reality the curve there has a slight negative slope is a proof that the molecules are « compressible ». As ZWICKY [50] has first pointed out the repulsive force increases as a continuous function with decreasing r, so that faster molecules can approach closer, and the apparent volume of the molecule decreases at higher T.

Unfortunately, as the curves in Hirschfelder's book [13] show, the situation with $B(T)$ differs not much from that of $\eta(T)$; for a given assumed force law, one can determine the constants, but for different force laws with the « best » constants, the curves differ very little.

There is next thermal diffusion of different isotopes of the same element, since the coefficient of thermal diffusion depends directly on the force law. However, the experiment is so difficult that no results useful for our purpose are available.

Lastly, and perhaps most promisingly, would be a measurement of the compressibility and its variation with pressure in the solid state at low temperature, since this measures directly differential quotients of the interaction energy. The usefulness of such data was already recognized by Lennard-Jones in his early papers. Here again these are not enough modern measurements (of frozen gases!) available. For complicate molecules, one must also take into account the compressibility of the intra-molecular bonds, as MÜLLER [51] has done for the paraffins.

As far as the calculation of relaxation times is concerned, the greatest gap in our understanding of the forces is due to the absence of a theory of the viscosity of nonspherical molecules. In the treatment of the interaction of vibration and translation we will have to assume that when a particle A, say an atom of argon, hits a molecule BC, there will be separate forces between A and B and between A and C. But the present theory of transport phenomena replaces this by the interaction between A and a spherical model BC. The problem is: If I know the potential energy which, exerted by a spherical molecule BC, gives the right viscosity, what separate interactions A-B and A-C together will give the same result?

Connected with this is the other question: For a spherical molecule, the collisions responsible for viscosity are truly elastic, but for a nonspherical, *e.g.* dumbbell molecule they are probably not, but exchange of translational and rotational energy will take place. Exchanges with vibrational energy are too rare in most circumstances to matter.

Many years ago PIDDUCK [52] considered collisions between rough hard spheres, but he was mainly interested in establishing that in the end the rotational degrees of freedom would attain the equipartition energy, and did not calculate viscosity. Another model consisted of spherical molecules with asymmetric mass distribution.

CURTISS [53] has investigated the Boltzmann equation in a general form in which the interaction energy depends also on internal co-ordinates, but has not carried it far enough yet for our purposes.

KIHARA [54] has calculated the equation of state for hard, ellipsoidal molecules or those of the shape of cylinders, capped with a sphere, and endowed with van-der-Waals' attraction. I have (unpublished) tried to see what would happen if one substituted a sphere which had the same average cross-section as the Kihara molecule, used the radius of the sphere as r_0 in the (spherical) Lennard-Jones equation while the radius of the cylinder was used as the r_0 in a Lennard-Jones expression for each atom, and determined the ε by identifying the second virial-T curves in the Kihara and Lennard-Jones calculations.

CURTISS and MUCKENFUSS [55] have calculated recently the viscosity for a gas of Kihara's sphero-cylindrical molecules.

Another rather doubtful attempt at a theory of viscosity of a dumbbell molecule will be reported in the article on relaxation times.

Finally, we will discuss the heat conductivity of polyatomic molecules. The coefficient of heat conductivity will be designated as c.h.c. For monoatomic gases the kinetic theory of gases gives, as first but excellent approximation

$$\text{c.h.c.} = \frac{5}{2}\frac{C_v}{M}\eta = \frac{15}{4}\frac{R}{M}\eta .$$

For polyatomic molecules, with $C_v > \frac{3}{2}R$, the factor $\frac{5}{2}$ has to be changed. Dr. GREENSPAN reported on Eucken's hypothesis. We will call this factor the Eucken number (Eu)

$$\text{c.h.c.} = (Eu)\frac{C_v}{M}\eta . \tag{8.5}$$

The newer investigations of CHAPMAN and MEIXNER [56] look on the molecules in the different states of internal excitation as different chemical species, which diffuse along the temperature gradient. This leads to

$$(Eu) = \frac{1}{C_v}\left(\frac{15}{4}R + \frac{D\varrho}{\eta}C_i\right). \tag{8.6}$$

Here C_i is the internal specific heat and D the diffusion coefficient. (8.6) presupposes, that the cross-section of the excited molecules does not differ from that of the unexcited ones, which might be wrong in the case of high excitation.

$D\varrho/\eta$ is a ratio of several integrals Y, and therefore dependent on both the force law and T, but this dependence is very slight, and the ratio lies mostly between 1.3 and 1.35.

We have finally to consider the effect of slow exchange of internal and external energy on the heat conduction process, which leads to the fact that the diffusing excited molecules are not in equilibrium with their surroundings. This was first done by UBBELOHDE [57] who investigated heat conduction between parallel plates. He introduced a diffusion length, which is the distance a molecule must travel in a uniform gas before equilibrium is established, and found a region on the plates of the thickness of this diffusion length, where a discontinuity in the gradient of the internal energy occurs, just as in normal Poiseuille flow there is a slip region and in normal heat conduction an anomalous region, both of the thickness of a mean free path. He calculated that for normal pressure in CO_2, the effect would only be noticeable if the plates were closer than $\frac{1}{2}$ mm.

MASON and MONCHICK [58] have developed the equations for heat conduction to an approximation one order higher than is usual and discovered a direct influence of the internal relaxation time on the coefficient of heat conductivity, *i.e.* and effect which exists also in large vessels, in addition to Ubbelohde's effect, which is noticeable only in small vessels.

They find for the Eucken number instead of (8.6)

$$(8.7)\qquad (Eu) = \frac{1}{C_v}\left\{\frac{15}{4}R + \frac{D\varrho}{\eta}C_i - \frac{1}{2}\left(\frac{5}{2}-\frac{D\varrho}{\eta}\right)^2 \sum_j \frac{\eta}{p\tau_j}C_j\right\},$$

where C_j is the specific heat and τ_j the relaxation time of the j-th internal degree of freedom. When the relaxation times become infinite (very slow energy exchange) this goes over into (8.6).

O'NEAL and BROKAW [59] have tested (8.7), by measuring the Eucken number directly, in cases (N_2, O_2, CO_2) where contributions by rotational energy are the only internal parts which matter, and have deduced from their results reasonable values of τ.

REFERENCES

[1] J. DE BOER: *Rep. Progr. Phys.*, **12**, 305 (1949).

[2] G. H. A. COLE: *Rep. Progr. Phys.*, **19**, 1 (1956).

[3] G. H. A. COLE: *Adv. in Phys.*, **8**, 225 (1959).

[4] D. MASSIGNON: *Méchanique statistique des fluides* (Paris, 1957).

[5] H. S. GREEN: *Handb. d. Phys.*, **10**, 1 (1960).

[6] J. G. KIRKWOOD, F. P. BUFF and M. GREEN: *Journ. Chem. Phys.*, **17**, 988 (1949)

[7] S. A. RICE and J. G. KIRKWOOD: *Journ. Chem. Phys.*, **31**, 901 (1959).

[8] S. A. RICE: *Journ. Chem. Phys.*, **33**, 1376 (1960).

[9] F. C. COLLINS and H. RAFFEL: *Journ. Chem. Phys.*, **29**, 699 (1958); **30**, 1620 (1959).

[9*a*] M. S. GREEN: *Journ. Chem. Phys.*, **22**, 398 (1954).

[9*b*] K. F. HERZFELD: *Journ. Chem. Phys.*, **28**, 595 (1958).

[10] This is called the Wiener-Khintchine theorem. See J. A. RATCLIFFE: *Rep. Progr. Phys.*, **19**, 188 (1956).

[11] H. GRAD: *Handb. d. Phys.*, **12**, 205 (1959).

[12] L. WALDMANN: *Handb. d. Phys.*, **12**, 295 (1959).

[13] J. O. HIRSCHFELDER, C. W. CURTISS, R. BIRD: *Molecular Theory of Gases and Liquids* (New York, 1954).

[14] D. HILBERT: *Grundzüge einer allgemeinen Theorie der Integral Gleichungen* (Lipsia 1924).

[15] S. CHAPMAN and T. G. COWLING: *The Mathematical Theory of Non-Uniform Gases* (Cambridge, 1952).

[16] D. ENSKOG: *Kinetische Theorie der Vorgänge in mäßig verdünnten Gasen* (Uppsala, 1917).

[17] G. SANDRI (Aeronautical Res. Assoc. of Princeton, Inc.): *Reports to Project Squid.*

[18] M. OFFERHAUS: Report Wisc.-OOR-31, Series 2, November 6, 1961, Theoretical Chemistry Laboratory, University of Wisconsin.

[19] C. S. WANG CHANG and G. E. UHLENBECK: Report M 999, in *Eng. Res. Inst.* (University of Michigan, 1952).

[20] R. G. BOSCOVICH, S. J.: *Theoria philosophiae naturalis redacta ad unicam legem virium in natura existentium*, First ed. (Vienna, 1758); Third ed. (Venice, 1763). Latin-English edition (Chicago, London, 1922).

[21] W. H. Keesom: *Proc. Amst. Acad.*, **15**, 250, 256, 417, 643 (1913); *Phys. Zeits.*, **22**, 129, 643 (1921); **23**, 225 (1922).

[22] P. Debye: *Phys. Zeits.*, **21**, 178 (1920); H. Falkenhagen: *Phys. Zeits.*, **23**, 87 (1922).

[23] R. Eisenschitz and F. London: *Zeits. f. Phys.*, **60**, 491 (1930); F. London: *Zeits. f. Phys. Chem.*, **11**, 222 (1930).

[24] H. B. G. Casimir and D. Polder: *Phys. Rev.*, **73**, 360 (1948).

[25] M. Born and A. Landé: *Berl. Ber.* (1918), p. 1048.

[26] W. Heitler and F. London: *Zeits. f. Phys.*, **44**, 455 (1927).

[27] W. Lenz: *Zeits. f. Phys.*, **77**, 713 (1932).

[28] H. Jensen: *Zeits. f. Phys.*, **77**, 722 (1932).

[29] Th. Berlin: *Journ. Chem. Phys.*, **19**, 208 (1951).

[30] S. E. Lovell and J. O. Hirschfelder: Report dated 20 December 1961, Series 5, Wis.-AF-19, Theoretical Chemistry Lab., University of Wisconsin.

[31] *E.g.*, I. Amdur and E. A. Mason: *Journ. Chem. Phys.*, **22**, 670 (1954).

[32] I. Amdur and J. Ross: Technical Report no. 2, Nonr 1841-23 dated August 1, 1958, MIT and Brown University.

[33] F. A. Morse, R. B. Bernstein and H. U. Hostettler: *Journ. Chem. Phys.*, **36**, 1947 (1962). Unpublished papers by D. Beck, E. F. Greene and J. Ross.

[34] For higher energies, see *e.g.*, I. Amdur, M. S. Longmire and E. A. Mason: *Journ. Chem. Phys.*, **35**, 895 (1961). An example of an application to other molecules is given by R. D. Cloney and J. T. Vanderslice: *Journ. Chem. Phys.*, **36**, 1866 (1962).

[35] J. C. Slater: *Phys. Rev.*, **32**, 349 (1928).

[36] H. Margenau: *Rev. Mod. Phys.*, **11**, 1 (1939).

[37] W. E. Bleick and J. E. Mayer: *Journ. Chem. Phys.*, **2**, 252 (1934).

[38] M. Kunimune: *Progr. Theor. Phys.* (*Japan*), **5**, 412 (1954); *Journ. Chem. Phys.*, **18**, 754 (1950).

[39] V. Griffing and J. F. Wehner: *Journ. Chem. Phys.*, **23**, 1024 (1955).

[40] J. T. Vanderslice, E. A. Mason and E. R. Lippincott: *Journ. Chem. Phys.* **30**, 129 (1959).

[41] J. T. Vanderslice, E. A. Mason and W. G. Marsh: *Journ. Chem. Phys.*, **31**, 738 (1959); **32**, 515 (1960).

[42] J. T. Vanderslice and E. A. Mason: *Rev. Mod. Phys.*, **32**, 417 (1960); *Journ. Chem. Phys.*, **33**, 492 (1960).

[43] I. Korobkin and Z. I. Slawsky: *Journ. Chem. Phys.*, **37**, 226 (1962).

[44] V. Valesco: *Ann. de Phys.*, **20**, 137, 292 (1945).

[45] H. L. Johnston and K. E. Mc Closkey: *Journ. Phys. Chem.*, **44**, 1038 (1940); H. L. Johnston and E. R. Grilly: *Journ. Phys. Chem.*, **46**, 948 (1942).

[46] K. F. Herzfeld and H. M. Smallwood: in *States of Matter*, by H. L. Taylor and S. Glasstone (New York, 1951).

[47] L. Monchick and E. A. Mason: *Journ. Chem. Phys.*, **35**, 1676 (1961).

[48] I. Amdur and J. Ross: ONR Contract Nonr 1841(23); MIT and Brown University, August 1, 1958, Report 2 and 3.

[49] E. F. Smiley: *Ph. D. diss.* (Catholic University of America, 1957).

[50] F. Zwicky: *Phys. Zeits.*, **22**, 449 (1921).

[51] A. Müller: *Proc. Roy. Soc.* (*London*), A **178**, 227 (1941).

[52] F. B. Pidduck: *Proc. Roy. Soc.* (*London*), A **101**, 101 (1922).

[53] C. F. Curtiss: Ser. 2 Wis.-NF 18, Report dated April 6, 1962, Theoretical Chemistry Laboratory University of Wisconsin.

[54] T. Kihara: *Journ. Phys. Soc.* (*Japan*), **6**, 289 (1951), see ref. [13].

[55] C. F. Curtiss and C. Muckenfuss: *Journ. Chem. Phys.*, **26**, 1619 (1957); **29**, 1257 (1958).

[56] J. Meixner: *Zeits. f. Naturfor.*, **8a**, 69 (1953).

[57] A. R. Ubbelohde: *Journ. Chem. Phys.*, **3**, 219, 362 (1935).

[58] E. A. Mason and L. Monchick: *Journ. Chem. Phys.*, **36**, 1622 (1962).

[59] C. O'Neal Jr. and R. S. Brokaw: *Physics of Fluids*, **5**, 567 (1962).

Relaxation thermique dans les gaz.

H. O. Kneser

I. Physikalisches Institut der Technischen Hochschule - Stuttgart

I.

Relaxation acoustique dans les gaz.

1. – La théorie phénoménologique.

On entend par « relaxation »: équilibre non atteint. La thermodynamique classique qui s'appelle plus proprement « thermostatique » n'est valable que dans le cas où un système, lors de changements d'état, passe par des états d'équilibre. D'après la thermodynamique classique, la vitesse du son dans les fluides — mise à part l'influence de la viscosité et de la conduction de chaleur — est

$$c = (K_s \cdot \varrho)^{-\frac{1}{2}}, \tag{1}$$

K_s signifiant la compressibilité adiabatique et ϱ la masse spécifique. Lorsque, pendant une période du son, l'équilibre thermique n'est pas atteint, il faut reviser cette affirmation. En ce cas, ce sont particulièrement les états de transition d'un équilibre à l'autre qui déterminent la propagation du son, c'est-à-dire des processus de relaxation. Nous pouvons les décrire comme des réactions, dont les participants peuvent être des atomes ou des molécules plus ou moins énérgétiques, excités ou non excités, dissociés ou associés, etc.

De là résultent differentes possibilités d'interprétation théorique:

1) Avec la mécanique statistique on calcule les fonctions de changements et de répartition en fonction du temps. Cela devrait fournir en principe une représentation complète du processus de relaxation. C'est Lorenz qui a essayé cette méthode pour la première fois. Chapman et Enskog l'on développée complètement, mais pour les cas les plus simples seulement. Pour tous les problèmes accessibles aux expériences pratiques, la méthode se trouve en face de difficultés insurmontables.

2) Avec la théorie cinétique des réactions: si l'on suppose des réactions élémentaires spéciales, il est possible d'établir des équations cinétiques sous

forme de « rate equations ». De cette façon on peut calculer des fonction décrivant la dépendance de la concentration. Les « rate-constants » ne sont calculables que par la théorie des quantas. De nouveau on rencontra ici des difficultés presque insurmontables.

3) Avec la théorie thermodynamique des processus irréversibles. Ici on rencontra à côté de grandeurs d'états thermiques des coefficients phénoménologiques, par exemple la viscosité, la conduction de la chaleur etc., mais la théorie est incapable d'évaluer leur grandeur.

4) Avec la théorie phénoménologique. Avec cette théorie on ne peut déceler que le type général du phénomène de relaxation. En dépit de cela, nous nous bornons pour l'instant à la phénoménologie, d'autant plus que les autres théories seront traitées plus en détail dans les autres leçons. Naturellement nous ferons usage de la statistique en utilisant ses résultats concernant la chaleur spécifique des gaz etc.

Nous considérons donc le rapport entre la tension et la déformation d'un corps quelconque d'une manière entièrement phénoménologique. Le corps sera soumis à une déformation (ε) soudaine, qui sera annulée après un temps donné. Le changement de la tension (σ) en fonction du temps est donné qualitativement par la Fig. 1. L'équation décrivant cela de la manière la plus simple et applicable dans plusieurs cas est

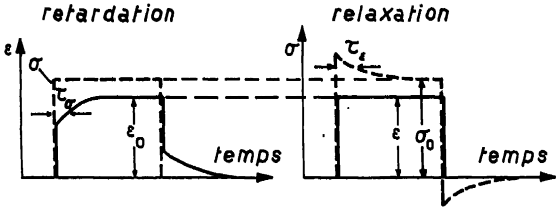

Fig. 1.

(2) $$\dot{\sigma} = \frac{1}{\tau_\varepsilon}(\sigma_0 - \sigma)\,.$$

De plus nous supposerons que pour l'état définitif la règle de Hooke est valable

(3) $$\frac{\sigma_0}{\varepsilon_0} = M_0\,,$$

où le module M_0 représente une vraie constante de la matière. Pour le phénomène inverse, la retardation, on a d'une façon analogue

(4) $$\dot{\varepsilon} = \frac{1}{\tau_\sigma}(\varepsilon_0 - \varepsilon)\,.$$

Nous éliminons ε_0 et σ_0 de (2) et de (4) et obtenons

$$\sigma + \tau_\varepsilon \dot{\sigma} = M_0(\varepsilon + \tau_\sigma \dot{\varepsilon}) . \tag{5}$$

C'est l'équation fondamentale pour le phénomène de relaxation simple.

Dans une onde élastique σ et ε changent périodiquement avec le temps:

$$\sigma(t) = \sigma . \exp[i\omega t] , \qquad \varepsilon(t) = \varepsilon \exp[i\omega t] ,$$

σ et ε étant complexes. Avec ces données l'éq. (5) donne

$$\sigma(1 + i\omega\tau_\varepsilon) = M_0 \varepsilon(1 + i\omega\tau_\sigma) . \tag{6}$$

Pour les fréquences très hautes ($\omega \gg 1/\tau$) on obtient un module différent:

$$M_\infty \equiv \frac{\sigma(\omega \to \infty)}{\varepsilon(\omega \to \infty)} = \frac{\tau_\sigma}{\tau_\varepsilon} M_0 . \tag{7}$$

En général on peut démontrer que M_∞ doit être $> M_0$ et de là que $\tau_\sigma > \tau_\varepsilon$.

Si $M_\infty - M_\sigma \equiv \Delta M$ est $\ll M_0$ la distinction entre les temps de retardation (τ_σ) et de relaxation (τ_ε) sera irrélevante. Pour des fréquences quelconque l'équation (6) donne

$$M(\omega) \equiv \frac{\sigma}{\varepsilon} = M' + iM'' . \tag{8}$$

avec

$$M' = M_0 + \Delta M \frac{\omega^2 \tau_\varepsilon^2}{1 + \omega^2 \tau_\varepsilon^2} \qquad \text{et} \qquad M'' = \Delta M \frac{\omega \tau_\varepsilon}{1 + \omega^2 \tau_\varepsilon^2} , \tag{9}$$

où

$$J(\omega) \equiv \frac{\varepsilon}{\sigma} = J' + iJ'' , \tag{10}$$

avec

$$\left| \begin{array}{l} J' = J_0 - \Delta J \dfrac{\omega^2 \tau_\sigma^2}{1 + \omega^2 \tau_\sigma^2} , \qquad J'' = -\Delta J \dfrac{\omega \tau_\sigma}{1 + \omega^2 \tau_\sigma^2} \\ \text{et} \\ \Delta J = \dfrac{1}{M_0} - \dfrac{1}{M_\infty} . \end{array} \right. \tag{11}$$

$J(\omega) \equiv 1/M(\omega)$ signifie la « compliance ».

On aura une représentation très claire, si on inscrit $M(\omega)$ ou $J(\omega)$ dans le plan des nombres complexes avec ω comme paramètre. Dans les deux cas on obtient un demi-cercle, dont le centre se trouve sur la coordonnée réelle (« Cole-plot ») Dans la Fig. 2 ce cas est représenté sous la forme d'un diagramme de force. On peut y reconnaître en même temps la différence de phase (δ) entre les grandeurs correspondantes qui a un maximum tout près de la fréquence $\omega \approx 1/\tau$. On sait que δ détermine quelle part (ΔW) de l'énergie (W) sera convertie irréversiblement pendant un cycle:

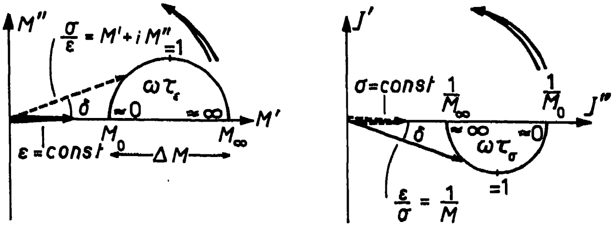

Fig. 2.

$$\frac{\Delta W}{W} = 2\pi \sin\delta\,. \tag{12}$$

La Figure 3 représente cela pour des données différentes.

Dans les fluides la compressibilité K se met à la place de J. Tout comme J, elle dépend de la fréquence comme dans (10) et (11) et nous obtenons

$$K(\omega) = K' + iK''\,, \tag{13}$$

$$K' = K^0 - \Delta K \frac{\omega^2\tau^2}{1+\omega^2\tau^2}\,, \tag{14}$$

$$K'' = -\Delta K \frac{\omega\tau}{1+\omega^2\tau^2}\,, \tag{15}$$

$$\Delta K \equiv K^0 - K^\infty\,. \tag{16}$$

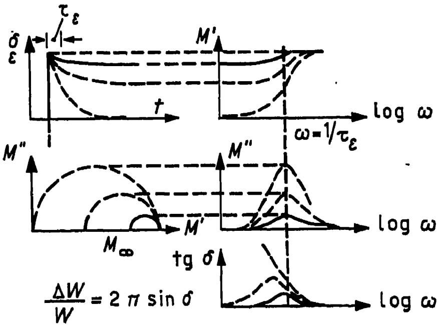

Fig. 3.

Nous considérons maintenant l'influence que la relaxation exerce sur l'onde du son, en introduisant dans la formule (1) pour la vitesse du son ($c \equiv \omega/k$) la compressibilité complexe qu'il faut évaluer en fonction de (13). Il s'ensuit, k complexe,

$$k = k' + ik'' = \omega\sqrt{\varrho}\cdot\sqrt{K'+iK''}\,. \tag{17}$$

De là, on obtient, à l'aide de (14) et (15) la vitesse du son

$$c^2 = c_0^2 \left(1 + \frac{\Delta K_s}{K_s^\infty} \frac{\omega^2 \tau^2}{1 + \omega^2 \tau^2}\right), \tag{18}$$

et pour l'indice d'absorption (μ = coefficient d'absorption par longueur d'onde):

$$\mu = \pi \frac{\Delta K_s}{\sqrt{K_s^0 K_s^\infty}} \cdot \frac{\omega \tau}{1 + \omega^2 \tau^2}. \tag{19}$$

En dérivant les formules (19) et (20) nous avons négligé des expressions de l'ordre de grandeur ($\mu^2/4\pi^2$).

A partir de (14) nous avons simplement écrit τ (sans index) au lieu de τ_σ. Un calcul plus rigoureux [1] montre que dans les fluides:

1) les changements d'état, qui se passent dans une onde sonore, peuvent toujours être traités comme adiabatiques ($\tau \equiv \tau_s$);

2) il faut remplacer τ par $\sqrt{\tau_{ps} \tau_{vs}}$.

D'autre part en comparaison avec (7) nous avons

$$\frac{\tau_s}{\tau_{ps}} = \frac{K_s^\infty}{K_s^0}, \tag{20}$$

et en suivant

$$\tau \to \sqrt{\frac{K_s^\infty}{K_s^0}} \cdot \tau_{ps}. \tag{21}$$

Introduisant (21) en (18) et (19) on obtient avec

$$\frac{\Delta K_s}{K_s^0} = \varepsilon, \tag{22}$$

$$\frac{c^2}{c_0^2} = 1 + \varepsilon \frac{\omega^2 \tau_{ps}^2}{1 + (1 - \varepsilon) \omega^2 \tau_{ps}^2}, \tag{23}$$

$$\mu = \pi \varepsilon \frac{\omega \tau_{ps}}{1 + (1 - \varepsilon) \omega^2 \tau_{ps}^2}. \tag{24}$$

2. – Processus simples de relaxation des gaz.

Maintenant nous appliquerons les considérations de la première leçon aux gaz. Nous parlerons seulement des gaz dont le nombre des molécules ne varie pas, si on change l'état. Les nombres d'occupation des états quantiques doivent assumer un nouvel état d'équilibre après un certain temps de relaxation limité. Ici il s'agit surtout des états de *rotation* et *d'oscillation*, cela veut dire des gaz avec deux ou plusieurs atomes, parce que les états électroniques ne sont occupés qu'aux températures de quelques 1000° (sauf une seule exception).

Les «réactions», qui peuvent se passer dans un des gaz considérés, sont tels que quelques molécules d'un état excité assument un autre état excité. L'expérience montre que ce passage ne se fait qu'après des collisions.

Quest'ce qu'il se passe dans ce gaz, si on dérange soudainement l'équilibre thermique, par exemple en diminuant son volume en poussant un piston dans un cilindre? Les molécules touchant le piston augmentent leur énergie translatoire et la transmettent par quelques collisions aux autres molécules. La répartition de vitesse des degrés de liberté de *translation* correspond à une température élevée après un temps très court (à peu près quelques temps de collision). C'est la température extérieure T_a: La distribution aux degrés de liberté d'oscillation et de rotation ne change pas aussi vite, cela veut dire qu'elle correspond à une température plus basse (*), T_i («température intérieure»).

Pendant le processus de relaxation T_i et T_a s'égalisent davantage jusqu'au moment où ils ont atteint la valeur d'équilibre qui correspond au nouvel état.

Ici il faut distinguer les cas où le processus est isothermique des autres cas, où le processus se deroule d'une manière adiabatique après le premier coup. Dans le premier cas ($T_a = \text{const}$) la pression et le volume restent constants (à cause de $\Delta v = 0$), et l'égalisation se produit avec un temps de relaxation τ_{pi} $(= \tau_{vi})$. Dans le deuxième cas ($S = \text{const}$), le temps de relaxation dépend du type du processus de réaction isobarique ou isochorique. Seulement dans le cas du processus isochorique la pression a son maximum au même temps où le volume a son minimum; dans tous les autres cas, le maximum de pression arrive plus tôt que le minimum du volume, cela veut dire le maximum de densité (Fig. 4).

Pour les trois temps de relaxation différents, on a toujours

$$\tau_{pi} > \tau_{ps} > \tau_{vs} \, .$$

Les changements des états dans une onde de son sont toujours adiabatiques. La pression court au devant de la compression; il y a une différence de phase entre la pression et la compression; dans le diagramme p-V le processus montre

---

(*) Cette définition simple de la température intérieure ne correspond qu'aux «processus simples de relaxation»; dans ce cas T_i peut servir comme variable caractéristique du système au lieu des nombres de réaction. Pour la définition de la température intérieure: J. **Meixner**: *Zeits. Phys.*, **124**, 129 (1947).

une palier limite, cela veut dire qu'on perd de l'énergie qui se transforme irréversiblement en chaleur.

La dissipation d'énergie provoque une absorption du son. Si le temps de la période et le temps qui est nécessaire pour former l'équilibre sont en concordance, l'absorption est la plus forte possible.

On voit qu'une diminution rapide du volume, qui provoque une augmentation extrême de la pression, provoque une compressibilité plus petite qu'une diminution lente. Pour une onde de son à haute fréquence il faut s'attendre une compressibilité plus petite (et une vitesse de son plus grande) que pour une onde à petite fréquence. L'expérience montre que la courbe de dispersion monte dans le même domaine de fréquence, où la courbe d'absorption passe par un maximum.

Utilisant les mêmes symboles qu'en la première section nous introduisons un « nombre de relaxation » ε

$$(25) \qquad \varepsilon = \frac{\Delta K_s}{K_s^0} = 1 - \frac{K_s^\infty}{K_s^0},$$

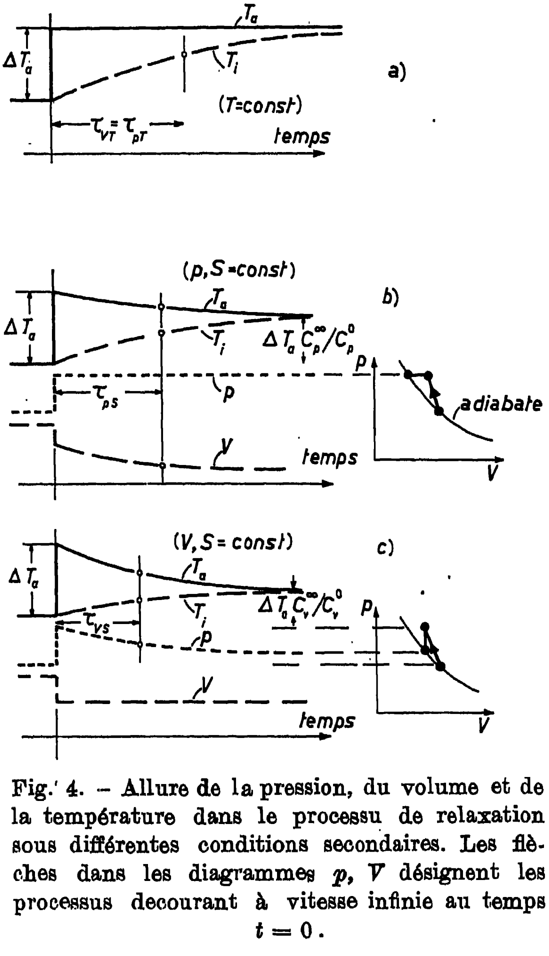

Fig. 4. – Allure de la pression, du volume et de la température dans le processu de relaxation sous différentes conditions secondaires. Les flèches dans les diagrammes p, V désignent les processus decourant à vitesse infinie au temps $t = 0$.

(K_s^∞ et K_s^0 = compressibilité adiabatique pour des processus très rapides et très lents).

Avec $K_s^0 = C_v^0/C_p^0 \cdot p$ et $K_s^\infty = C_v^\infty/C_p^\infty \cdot p$ on obtient

$$(26) \qquad \varepsilon = \frac{C_p - C_v}{C_v^0 \cdot C_p^\infty} \cdot C_i,$$

0 et ∞ ont la même signification que dans (25). C_i est la partie de relaxation de la chaleur moléculaire, cela veut dire ici: la partie des états de rotation ou

d'oscillation:

$$C_i = C_p^0 - C_p^\infty = C_v^0 - C_v^\infty \,. \tag{27}$$

Pour un gaz parfait on peut remplacer $C_p^0 - C_v^0$ par R:

$$\varepsilon = \frac{RC_i}{C_v^0(C_p^0 - C_i)} \,. \tag{28}$$

La partie des états de rotation de la chaleur moléculaire ne peut pas surpasser $(3/2)R$. La partie des états d'oscillation ne peut surpasser $C_i > R$ que pour les molécules qui possèdent plus que 2 atomes; mais dans ce cas la supposition d'un processus simple de relaxation devient douteuse. Avec $C_i < \frac{3}{2}R$, $C_v^0 \geqslant \frac{5}{2}R$ et $C_p^0 \geqslant \frac{7}{2}R$, ε devient

$$\varepsilon < 0.3 \,. \tag{29}$$

Pour les formules de dispersion et d'absorption nous adoptons les notations suivantes:

c = vitesse de phase de l'onde du son,

$c_0 = c(\omega \to 0)$; $c_\infty = c(\omega \to \infty)$,

α = coéfficient d'absorption de l'amplitude,

$\mu = \alpha \cdot \lambda$ = indice d'absorption (sans dimension).

Après un petit calcul dont la manière a été montrée dans la première section on obtient

$$\frac{c_0^2}{c^2} = 1 - \varepsilon \frac{\omega^2 \tau_{ps}^2}{1 + \omega^2 \tau_{ps}^2} \,, \tag{30}$$

$$\mu = \pi\varepsilon \frac{\omega \tau_{ps}}{1 + \omega^2 \tau_{ps}^2 (1 - \varepsilon)} \,. \tag{31}$$

Les formules (30), (31) ne sont valables qu'à la condition $(\mu/2\pi)^2 \ll 1$. D'après l'estimation réalisée en haut, $(\mu/2\pi)^2$ ne peut pas surpasser $8 \cdot 10^{-3}$ dans le cas de relaxation d'excitation des gaz parfaits.

Les mesures aux ondes de son nous donnent des information sur τ_{ps}. L'autre temps de relaxation (τ_{vs}) s'obtient par (20)

$$\frac{\tau_{\;s}}{\tau_{ps}} = \frac{K_s^\infty}{K_s^0} = 1 - \varepsilon \,. \tag{32}$$

3. – Le diagramme f/p et la probabilité de désexcitation Z.

Pour les diagrammes de dispersion et d'absorption on ne choisit pas ln ω comme abscisse, mais lg f/p. Cela s'explique par la considération suivante: Si l'activation et la désactivation ne se produisent que par des collision de deux molécules, les temps de relaxation sont proportionnels au temps moyen entre deux collisions τ_c. Pour un gaz parfait les temps de relaxation sont proportionnels à $1/p$. Dans les formules (30) et (31) les temps de relaxation sont toujours liés à ω. Entre f/p et $\omega\tau$ il n'y a comme différence qu'un facteur constant, qui ne dépend pas de la fréquence et de la pression, mais seulement de la température.

Dans cet article — comme dans plusieurs autres — nous ne donnerons pas les temps de relaxation τ_{xy} eux-même, mais $\tau^0_{xy} \equiv \tau_{xy}/p$, cela veut dire les temps de relaxation à la pression 1. Une courbe d'absorption sur f/p doit avoir un maximum de μ à $(f/p)_{\max}$. D'après, l'éq. (7), μ a un maximum, si

$$\omega = \omega_{\max} = \frac{1}{\sqrt{1-\varepsilon}} \cdot \frac{1}{\tau_{ps}} \tag{33}$$

$$= \frac{1}{\sqrt{1-\varepsilon}} \cdot \frac{1}{\tau_{pt}} \cdot \frac{C_p^0}{C_p^\infty}\,. \tag{34}$$

Avec $\tau_{pt} = \tau^0_{pt}/p$ on obtient

$$\frac{1}{\tau^0_{pt}} = \frac{C_p^\infty}{C_p^0}\, 2\pi \left.\frac{f}{p}\right|_{\max} \cdot \sqrt{1-\varepsilon}\,. \tag{35}$$

Dans les cas pas trop compliqués on peut calculer avec la théorie quantique la probabilité qu'une molécule excitée retourne à l'état fondamental après une collision avec une autre molécule ou le processus inverse. Cela veut dire qu'on peut calculer le nombre Z de collisions qu'une molécule subit avant de changer son énergie d'excitation en énergie de translation et le Z' pour le processus inverse. S'il n'y a qu'un seul état quantique sauf l'état fondamental, on obtient pour Z et Z' l'équation simple suivante:

$$\frac{Z}{Z'} = \frac{c_B}{c_A}\,. \tag{36}$$

c_A et c_B sont les concentration des molécules dans les deux seuls états occupés.

D'après Fig. 4 il semble plausible, que Z et Z' déterminent le temps de relaxation isothermique τ_{pt} $(= \tau_{vt})$, mais les diagrammes d'absorption et de dispersion donnent τ_{ps} ou τ_{vs}.

Pour des réactions bimoléculaires on trouve

$$\frac{\tau_c^0}{\tau_{pt}^0} = \frac{1}{Z} + \frac{1}{Z'} \,. \tag{37}$$

τ_c^0 est le temps moyen entre 2 collisions à une pression 1.

Avec (35), (36) et (37) nous obtenons pour le modèle de deux états:

$$Z = \left(1 + \frac{c_B}{c_A}\right) \frac{1}{\tau_c^0} \frac{C_p^0}{C_p^\infty} \left[2\pi \frac{f}{p} \bigg|_{\max} \cdot \sqrt{1-\varepsilon} \right]^{-1} . \tag{38}$$

Si l'état excité est faiblement occupé, cela veut dire $c_B \ll c_A$, ε est preque toujours $\ll 1$.

S'il y a plus que 2 états comme par exemple à l'oscillateur harmonique, le problème est plus compliqué. Il y a la question s'il n'y a qu'un seul temps de relaxation. LANDAU et TELLER ont donné la réponse: Les états des équilibres d'un gaz d'oscillateurs harmoniques, qui seraient des états d'équilibre pour une autre température extérieure n'ont qu'*un* temps de relaxation pour atteindre l'équilibre. On ne passe que des répartitions d'équilibre des nombres d'occupation, qui appartiennent aux températures différentes. Pour ces processus de relaxation on peut choisir une température intérieure T_i comme paramètre de réaction. Dans l'onde du son il y a aussi seulement un processus de relaxation. La possibilité d'appliquer des probabilités de transition optiques pour l'activation et la désactivation par une collision et de négliger une transition de plusieurs quanta est la condition de cette théorie de Landau et Teller.

Alors (37) se modifie légèrement. Comme différence remarquable il y a un signe négatif

$$\frac{\tau_c^0}{\tau_{pt}^0} = \frac{1}{Z} - \frac{1}{Z'} \,. \tag{37'}$$

$1/Z'$ est la probabilité d'excitation pour le passage de l'état fondamental au premier état excité, $1/Z$ la probabilité de désexcitation. Au lieu de Z et Z' on écrit souvent Z_{10} et Z_{01}.

Avec (35) et (36) on obtient l'éq. (38'); entre (38) et (38') il y a une différence légère:

$$Z_{10} = \left[1 - \exp\left[-\frac{h\nu}{kT}\right]\right] \frac{1}{\tau_c^0} \frac{C_p^0}{C_p^\infty} \left[2\pi \frac{f}{p} \bigg|_{\max} \cdot \sqrt{1-\varepsilon} \right]^{-1} . \tag{38'}$$

RÉFÉRENCES

[1] H. A. LORENTZ: *Arch.*, *Néerl. Phys.*, **16**, 51 (1880).
[2] J. MEIXNER: *Acustica*, **2**, 101 (1952).

II.

L'interprétation qualitative des temps de relaxation.

Dans cet exposé je veux essayer d'établir une connexion simple entre les temps de relaxation de gaz différents. Cela ne veut pas dire, que je développerai une théorie des temps de relaxation. C'est la tâche que le Dr. HERZFELD a résolue d'une manière magnifique. Je ne veux qu'indiquer un point de vue selon lequel les temps de relaxation peuvent être classifiés, et peut-être on sera mis en état d'estimer la valeur des temps de relaxation pour des molécules pour lesquelles la théorie rencontre des difficultés insurmontables.

La vitesse de toutes les réactions dans un gaz est déterminée par le nombre de collisions qu'une molécule subit par seconde. C'est pourquoi la mesure naturelle de temps, par laquelle on doit mesurer le temps de relaxation (τ) n'est pas la seconde, mais le temps moyen entre deux collisions, c'est-à-dire le temps moyen de collision (τ_c). $Z = \tau/\tau_c$ est une quantité caractéristique pour chaque processus de relaxation. Elle dépend exclusivement de la température. Quant à la relaxation mécanique dans les gaz, il s'agit presque toujours de relaxation d'excitation. Alors le temps de relaxation est presque identique au temps pendant lequel une molécule reste dans l'état excité, et Z est le nombre des collisions que la molécule subit pendant ce temps là, ou autrement $1/Z$ est la probabilité avec laquelle une collision fait cesser l'état excité, qui s'appelle la probabilité de désexcitation.

Rappelons alors le principe de l'adiabatisme qui a été introduit dans la théorie des temps de relaxation par LANDAU et TELLER d'une manière ingénieuse. En voici à peu près l'énoncé:

Supposons qu'un mouvement périodique se passe dans une molécule; que, de plus, une force variable dans le temps, mais non périodique, agisse. Le mouvement périodique sera-t-il définitivement distordu, c'est-à-dire l'état quantique sera-t-il changé? Le principe de l'adiabatisme répond à cette question de la manière suivante: L'état quantique ne sera changé que si le changement relatif de la force distordante est grand pendant une période. Dans notre problème, le mouvement périodique peut être une oscillation ou une rotation de la molécule. La force distordante est provoquée par une autre molécule, qui s'approche de la première. Son changement relatif sera grand pendant une période, si la durée du contact des deux partenaires est très courte. Celle-ci sera déterminée approximativement par le quotient diamètre moléculaire (d) divisé par la vitesse moléculaire moyenne (w). Dénotons la durée d'une période par $1/\nu$, donc nous pouvons supposer que la probabilité de désexcitation $1/Z$ est une fonction de la quantité $x = (d/w):(1/\nu)$. De la théorie cinétique des gaz nous prenons la relation $w = \sqrt{3kT/\overline{m}}$ où $\overline{m}$ est la masse réduite des deux partenaires, et nous obtenons

$$x = \frac{d\nu}{\sqrt{3kT/\overline{m}}}.$$

Dans les Fig. 1-3 toutes les valeurs connues de Z pour les gaz diatomiques (excepté ceux de I_2 et Br_2) sont inscrites comme fonctions de x. A Z_{rot} est mis

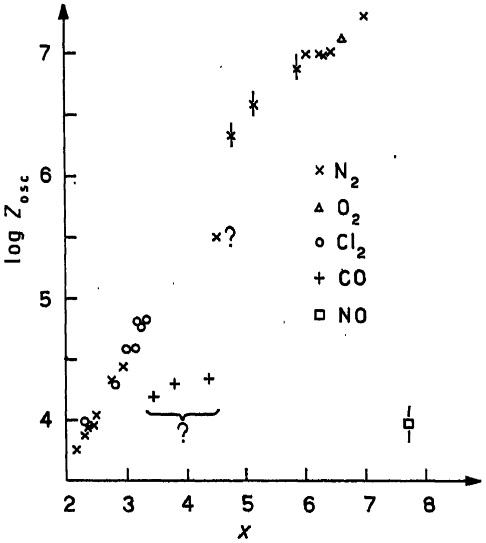

Fig. 1. – Probabilité de transition vibrationnelle en fonction de x.

pour ν, la fréquence de rotation, à Z_{osc} la fréquence d'oscillation. Le résultat n'est pas mauvais compte tenu de l'estimation approximative que nous avons employée. Presque tous les points se groupent autour d'une courbe. Deux points seulement se distinguent, très nettement: ceux correspondant a HCl et NO. Ces molécules se composent de deux atomes différents. Les valeurs de Z sont comparativement trop petites, leur probabilité de désexcitation est beaucoup plus grande que celle de leurs voisines.

Pour cela je veux proposer l'interprétation suivante: Les molécules susnommées sont optiquement actives, c'est-à-dire elles peuvent réémettre aussi leurs quanta de rotation ou d'oscillation comme rayonnement. Ces quanta de lumière parcourent dans le gaz un certain intervalle moyen (l) avec la vitesse de la lumière et sont absorbés par une autre molécule. Si l est petit en comparaison de la longueur des ondes sonores (λ), le processus n'influence pas la propagation du son. Mais si $l > \lambda/2$ ou même $\gg \lambda/2$, il provoque un raccourcissement du temps de relaxation. Cela peut être compris de la manière suivante:

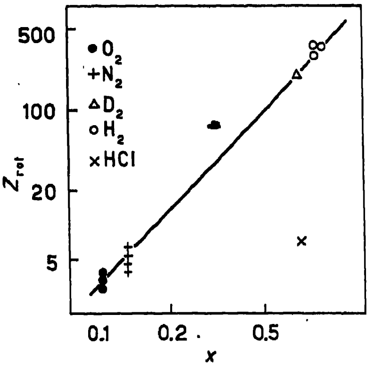

Fig. 2. – Probabilité de transition rotationnelle en fonction de x.

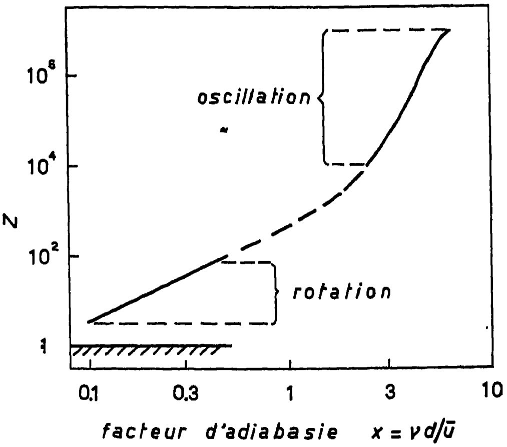

Fig. 3. – Combinaison des Fig. 1 et 2.

En cas de relaxation il n'y a pas d'équilibre thermodynamique dans une onde sonore; cela veut dire que, par exemple au minimum de la température, les états excités sont plus fortement occupés qu'à l'équilibre. Alors, si quelques molécules émettent leur énergie d'excitation sous forme de rayonnement à une distance $l > \lambda/2$, le rapprochement à l'équilibre est accéléré, c'est-à-dire τ et donc Z sont raccourcis.

Ces réflexions ont été discutées il y a quelques années par Lukasik [1]. Il tira la conséquence que des processus de rayonnement n'ont pas d'influence sur le temps de relaxation, parce que la durée naturelle des états de rotation et d'oscillation, c'est-à-dire le temps qui passe jusqu'à ce que la molécule convertisse son quantum d'énergie en rayonnement, est extraordinairement longue. En effet il faudrait que le temps d'établissement de l'équilibre thermique ($\approx \tau_0$) devint égale à la durée naturelle. Même aux pressions les plus petites dans lesquelles on peut encore exécuter des mesures des ondes sonores, τ_0 est déjà plus petit de plusieurs ordres de grandeur que la durée naturelle. Avant que celle-ci finisse, la molécule a subi déjà un nombre extremement élévé de collisions. A cause de cela il est toujours beaucoup plus probable qu'une de ces collisions soit inélastique, c'est-à-dire que l'énergie d'excitation soit transformée de manière purement mécanique en énergie de translation. Voilà l'argumentation de Lukasik.

Il me semble qu'une chose lui a échappé, c'est que l'émission d'un quantum ne doit pas s'effectuer spontanément, mais peut-être aussi provoquée par une collision. En ce cas-là, le temps de relaxation peut être raccourci en effet par l'émission de quanta; à supposer naturellement que la condition établie $l > \lambda/2$, dont on parlait plus haut, soit réalisée. Il nous faudra examiner si la quantité $k \equiv \lambda/2l$ est < 1; seulement dans ce cas une influence de l'émission quantique peut devenir remarquable. Alors l est sans doute inversement proportionnel à la pression; nous mettons en équation $l = 1/\gamma p$. De plus nous posons $\lambda = c/f$, où c signifie la vitesse du son, dont nous négligeons ici, la dépendance de la fréquence, et f la fréquence. Il s'ensuit ainsi:

$$k = \frac{c\gamma}{2f/p}\,. \tag{1}$$

Pour f/p nous substituons la valeur, pour laquelle la relaxation est plus remarquable, c'est-à-dire la valeur pour laquelle on trouve le maximum d'absorption.

Malheureusement nous n'avons que pour deux gaz, pour lesquels les états d'énergie intérieure sont optiquement actifs, des résultats suffisants sur l'absorption acoustique et optique. Pour NO et CO_2. La table I nous donne les valeurs et les positions du maximum de la relaxation d'oscillation ($f/p_{\max}$), de même que la grandeur de $k_{\max}$ pour le processus de relaxation calculée à partir de cette valeur.

TABLE I.

Gaz	c (cm s^{-1})	γ (cm^{-1} atm^{-1})	$f/p_{\max}$ (s^{-1} atm^{-1})	$k_{\max}$
NO	$3.25 \cdot 10^4$	0.6 [2]	$4 \cdot 10^5$ [4]	0.02
CO_2	$2.7 \cdot 10^4$	12.5 [3]	$3.5 \cdot 10^4$ [5]	5

De là, l'influence du rayonnement susmentionné ne devrait pas prédominer chez CO_2, alors qu'il entre en considération pour NO. Ce fait pourrait expliquer le temps de relaxation de NO étonnement court en comparaison avec N_2 et O_2 [6].

Parmi les gaz dont on connait la relaxation de rotation, HCl, l'unique optiquement actif se distingue par un temps de relaxation particulièrement court [7].

Quand nous ne considérons que l'effet des collisions inélastiques et sans radiation (c'est-à-dire $k_{\max} \gg 1$), Z est indépendant de p et par-là aussi de f/p. Alors μ, représenté graphiquement en fonction de $\log f/p$, donne d'après la formule (2) la courbe d'erreur de Gauss symétrique bien connue avec un maximum pour $f/p = f/p_{\max} = 1/A$, une valeur de moitié inférieure pour $f/p =$

$= (2-\sqrt{3})/A$ et une valeur de moitié supérieure pour $f/p = (2+\sqrt{3})/A$, c'est-à-dire avec la demi-largeur logarithmique $\log 3.73/0.27 = 1.14$.

Il en est de même lorsque l'influence de l'émission des quanta prédomine. Cela peut avoir lieu dans le cas où $k_{max} \ll 1$. Là aussi la largeur de moitié logarithmique devrait être 1.14.

Adjonction vol. % He	$c \cdot 10^{-4}$ (m/s)	γ (cm^{-1} atm^{-1})	$f/p_{max} \cdot 10^{-4}$ (s^{-1} atm^{-1})	$\eta \cdot 10^{-4}$ (poise)	k_{max} calculé d'après (1)	demi-largeur logarithmique
0	2.7	12.5	3.5	1.471	5	1.17
58.8	4.13	5.14	27	1.714	3.9	1.21
86.2	6.23	1.72	40	1.908	0.13	1.24
99.0	9.59	0.125	49	1.960	0.012	1.25

Mais si le maximum d'absorption entre dans le domaine de f/p où $k \approx 1$, à cause de la formule (1), Z et par-là A peut avoir une valeur plus grande ($A = A_n$) dans le prolongement de basses fréquences ($k > 1$) que dans le prolongement de haute fréquences ($k < 1$; $A = A_m$), et la demi-largeur sera $\log (3.73/0.27)(A_n/A_m) > 1.14$. Nous pouvons effectivement observer cela dans des mélanges de CO_2-He pour la température ambiante [6].

Avec une adjonction de 99 % He, la demi-largeur logarithmique n'a pas repris sa valeur normale. On pourrait en conclure que l'influence de la radiation — même si elle n'en est pas la seule cause — provoque essentiellement le rétablissement.

RÉFÉRENCES

[1] S. J. Lukasik: *Journ. Acoust. Soc. Am.*, 28, 455 (1956).
[2] S. S. Penner et D. Weber: *Journ. Chem. Phys.*, 21, 649 (1953).
[3] P. E. Martin et E. D. Barker: *Phys. Rev.*, 41, 302 (1932).
[4] H. J. Bauer, H. O. Kneser et E. Sittig: *Journ. Chem. Phys.*, 30, 1119 (1959).
[5] *Handb. d. Phys.*, vol. 11/1, (Berlin, 1961), p. 180.
[6] *Handb. d. Phys.*, vol. 11/1, (Berlin, 1961), p. 177.
[7] M. A. Breazeale et H. O. Kneser: *Journ. Acoust. Soc. Am.*, 32, 885 (1960).

III.

Relaxation oscillatoire et rotatoire.

1. – Introduction.

Le temps de relaxation détermine la position de la montée de la courbe de dispersion et le maximum d'absorption en abscisse ($\ln \omega$ ou $\lg f/p$). Le nombre de relaxation ε donne les dimensions du maximum et de l'augmentation de dispersion.

ε a une dépendance importante de C_i, cela veut dire des parties des degrés de liberté intérieurs de la chaleur moléculaire.

L'énergie intérieure comprend les espèces d'énergie intramoléculaire suivantes:

1) Energie d'oscillation.

2) Energie de rotation.

3) Energie électronique.

Pour toutes ces espèces d'énergie, il faut faire attention à la division en quanta qui n'existe pas pour l'énergie de translation. Des grandes distances des niveaux d'énergie provoquent des grands temps de relaxation, et on sait que les grandes différences d'énergie (comparées avec kT) donnent des petites parties à la chaleur moléculaire, cela veut dire une petite valeur de relaxation ε. On peut comprendre qu'il n'y ait qu'un seul cas spécial (NO), où on pourrait déceler des traces d'une relaxation électronique.

Les quanta de l'énergie de rotation sont presque toujours $< kT$. C'est pourquoi l'on trouve les effets d'absorption et de dispersion de rotation à des valeurs de f/p très élevées mais encore obtenibles. La valeur de relaxation ε est très forte.

Les quanta d'oscillation prennent une position moyenne. C'est pourquoi la relaxation d'oscillation est la mieux connue.

Entre les molécules à deux atomes, ce sont surtout les halogènes qui ont grâce à la grande masse des atomes, des quanta d'oscillation tellement petits qu'on peut observer des effets nets de dispersion et d'absorption à domaines de fréquences bien accessibles par l'expérience.

Les énergies de rotation et d'oscillation ont très souvent un temps de relaxation bien défini. Ces temps de relaxation ont des différences de quelques ordres de grandeurs sous des conditions normales et des domaines d'absorption et de dispersion séparés dont la dépendance de f/p est décrite par les équations dérivées pour la relaxation simple. Le caractère du spectre d'absorption acoustique est toujours le même pour des gaz pas trop compliqués. Un maximum de rotation est superposé à l'accroissement de l'indice d'absorption classique.

Le maximum de rotation a un $\mu_{\max} \approx 0.1$. Aux valeurs de f/p plus petites il y a le maximum d'oscillation. Son $\mu_{\max}$ décroît si la fréquence du maximum décroît. La Fig. 1 montre ces faits à deux températures différentes. Presque toutes les expériences actuelles montrent que les temps de relaxation deviennent plus petits, si l'on augmente la température. Les maxima de relaxation se deplacent vers des valeurs plus élevées de f/p à température croissante.

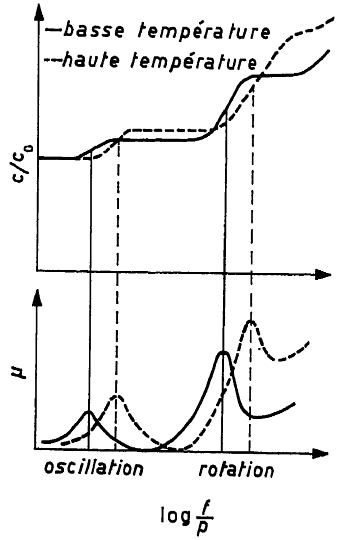

Fig. 1.

On voit que le coefficient de température de l'absorption du son peut avoir des valeurs positives ou négatives.

2. – Relaxation d'oscillation.

2·1. *Gaz à deux atomes.* – Les états quantiques des molécules à deux atomes (oscillateur harmonique) se trouvent à des distances égales $h\nu$; ν est la fréquence fondamentale. On calcule seulement par la « température caractéristique »,

$$\theta = \frac{h\nu}{k}, \tag{1}$$

la partie des oscillations de la chaleur moléculaire en se servant de la formule de Planck et Einstein.

a) Halogènes [1]. Les fréquences fondamentales de toutes les molécules des halogènes sont relativement basses ($\theta = 308$ à $813°$). C'est pourquoi ces gaz montrent une relaxation d'oscillation forte, qui a été examinée surtout par des mesures d'absorption. Si l'on calcule, avec θ la chaleur d'oscillation C_i [2] et l'élévation du maximum d'absorption, on trouve une très bonne concordance avec les valeurs mesurées. Au dessus et au dessous du maximum la courbe d'absorption suit aussi la courbe calculée pour un processus simple de relaxation. C'est une preuve que tous les niveaux d'énergie d'un oscillateur ont un temps de relaxation commun. On peut calculer Z avec $(14')$.

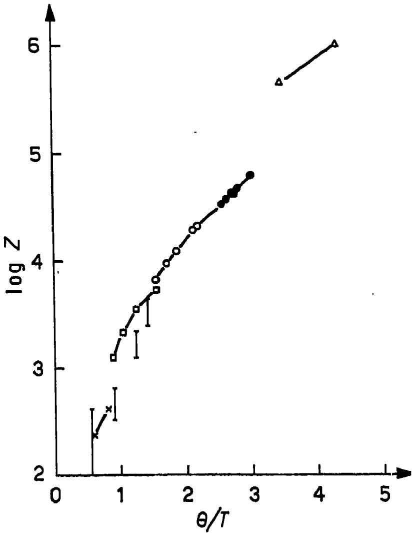

Fig. 2. – △, fluore (Shields, 1962); ○, chlore (Shields, 1960); I, chlore (Smiley, 1954); ●, chlore (Sittig); □, brome (Shields, 1960); × iode (Shields, 1960).

Toutes les valeurs de Z des halogènes (Fig. 2) sont mises en fonction de θ/T, parce que Z est surtout déterminé par θ/T (surtout mais pas seulement).

La combinaison d'un halogène avec l'hydrogène a des quanta d'oscillation beaucoup plus grands à cause de la petite masse de l'atome H. Il n'y a qu'une relaxation d'oscillation aux températures extrêmement hautes et à des fréquences basses. Les mesures de HCl ne montrent qu'une relaxation de rotation.

b) O_2 et N_2. La température caractéristique de ces deux gaz est très haute ($\theta = 2228$ °K et $\theta = 3330$ °K). Une relaxation d'oscillation ne peut exister qu'à des fréquences très basses ou des températures et des pressions très élevées. Des mesures soigneuses existent seulement pour l'oxygène [3].

Le temps de relaxation (τ) du gaz pur à 1 atmosphere et température ambiante est tellement grand, que les méthodes acoustiques ne suffisent pas pour trouver directement la fréquence de relaxation. Mais en ajoutant des gaz convenables, on peut augmenter beaucoup la fréquence de relaxation. On la trouve pour les gaz purs par extrapolation. Pour ces mesures, il est nécessaire d'avoir des gaz extrêmement purs et de déterminer exactement le pourcentage du gaz ajouté.

Pour des additions petites ε ne varie presque pas; c'est seulement τ qui varie. Dans ce cas on applique le diagramme de Cole; on porte la partie imaginaire de la compressibilité adiabatique normalisée en fonction de la partie réelle. La première partie est $(\mu/\pi)(c_0^2/c^2)$, la dernière c_0^2/c^2. La Figure 3 montre le résultat pour O_2 à température ambiante. Tous les points sont près de deux demi-cercles avec les diamètres 0.003 et 0.135. La forme circulaire montre qu'il s'agit de deux processus de relaxation simple. Les diamètres donnent directement les valeurs de relaxation ε. Le petit cercle (c est seulement un peu plus grand que c_0, basses frequences) représente la relaxation d'oscillation; on obtient avec $\theta = 2228$ °K; $C_i = 0.028R$; $\varepsilon = 0.0032$; en concordance avec le diamètre du « Cole-plot ». Le grand cercle représente la relaxation de rotation.

Pour N_2 on vient de faire des mesures sûres [4] à une température de 103 °C malgré la petite valeur de C_i de $0.0046\,R$ et de $\mu_{max} < 10^{-3}$. Ces mesures permettent d'estimer que le maximum se trouve à la valeur extrèmement basse de 1 Hz/atm.

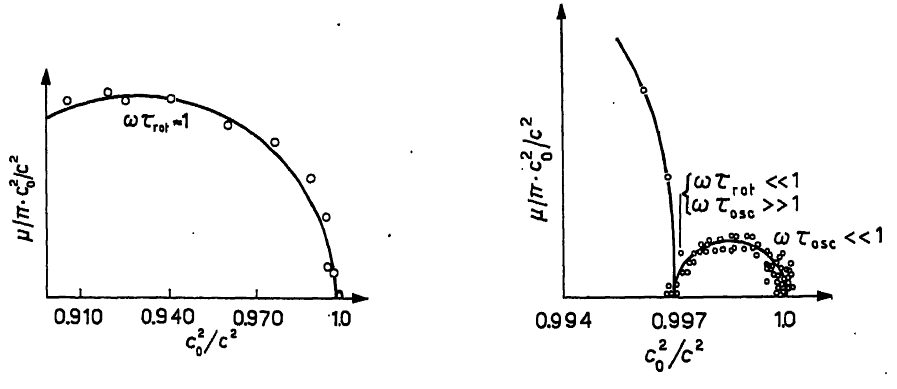

Fig. 3.

Les valeurs de Z obtenues par ces mesures et d'autres mesures se trouvent dans la Fig. 4 en fonction de θ/τ.

c) CO et NO. Pour le CO [5] ($\theta = 3080$ °K) il y a de grandes différences entre les mesures déjà faites dont le nombre est très petit. Les mesures les plus récentes montrent qu'il y a une relaxation d'oscillation avec une fréquence de relaxation f/p_{max} de 73 Hz/atm à une température de 103 °C ($C_i = 0.0033\,R$).

Pour le NO il n'y a pas seulement des états d'oscillation et de rotation qui participent à C_i, mais il y a aussi un état électronique, qui est déjà bien occupé à la température ambiante et qui fournit une partie de C_i. Il faut prévoir trois domaines de relaxation. En effet on réussit à analyser la courbe d'absorption mesurée à 300 °K. On trouve un maximum de μ dont la hauteur ($\mu_{max} = (1.41 \pm 0.05) \cdot 10^{-3}$) est en bonne concordance avec la valeur attendue pour la relaxation

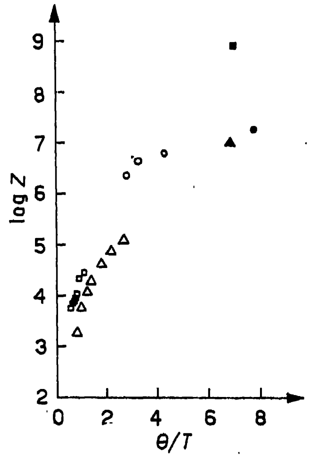

Fig. 4 – N_2: □ BLACKMAN, ○ LUKA IK et YOUNG, ■ HENEDRSON; O_2: △ BLACKMAN, ● KNOTZEL, ▲ HENDERSON.

d'oscillation ($C_i = 0.008\,06$; $\mu_{\max} = 1.359 \cdot 10^{-3}$). On trouve le maximum à une valeur de $f/p = 400$ kHz/atm; cela donne une valeur de Z (2 700 à 300 °K [7]) au moins 20 fois plus grande que les valeurs des molécules pareilles O_2 et N_2. On trouve toutes les valeurs de Z trouvées par des mesures acoustiques pour CO et NO en fonction de θ/T dans la Fig. 5.

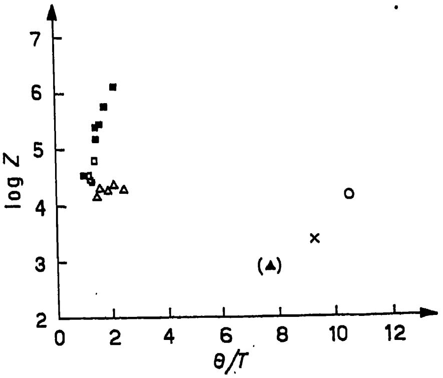

Fig. 5. – CO: △ **Sherrat** et **Griffiths**, ○ **von Itterbeck** et **Mariens**, ▲ **Bender**, ● **Henderson**, ■ **Windsor**, **Davidson** et **Taylor**, □ **Gaidon** et **Hurle**; NO: × **Bauer**.

3. – Relaxation de rotation.

3·1. *Corrélations générales*. – Les quanta de rotation d'une molécule sont presque toujours d'un ordre de grandeur plus petits que les quanta d'oscillation. La Figure 6 montre les valeurs d'énergie du quantum de rotation pour

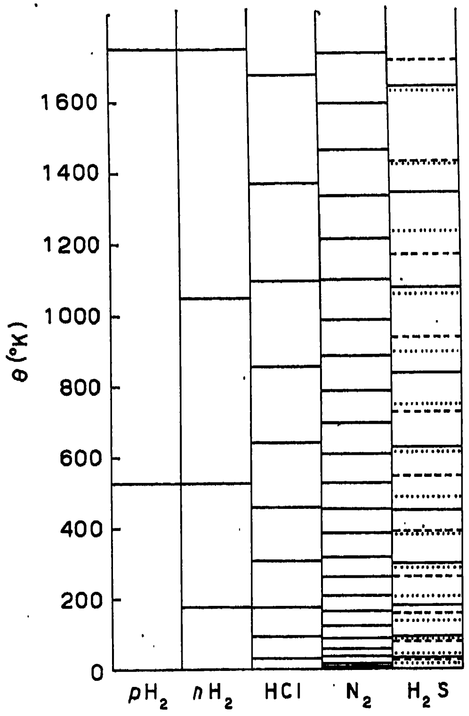

Fig. 6.

quelques gaz données par la température caractéristique

$$\theta = \frac{E_{\mathrm{rot}}}{k}.$$

On voit, qu'un grand nombre d'états de rotation est déjà occupé à la température ambiante. Le para-hydrogène est une exception. Dans tous ces gaz la relaxation de rotation se vérifiera aux valeurs f/p élevées. Les quanta de rotation sont proportionnels à la valeur réciproque du moment d'inertie. C'est pourquoi ils sont relativement grands pour les molécules dont la masse se trouve près du centre de masse. Mais même dans ce cas les relaxations de rotation et d'oscillation n'interfèrent pas car la relaxation d'oscillation se trouve alors aux valeurs f/p extrêmement basses.

Dans le domaine de la dispersion et de l'absorption de rotation on trouve déjà presque toujours les effets classiques, qui suivent la formule de Stokes-Kirchhoff; pour le coefficient d'absorption α on obtient:

$$\alpha_{\mathrm{class}} = \frac{\omega^2}{2\varrho c^3}\left[(\gamma - 1)\frac{\Lambda}{C_p} + \frac{4}{3}\eta\right], \tag{2}$$

avec: c = vitesse du son,

γ = rapport des chaleurs spécifiques C_p/C_v,

Λ = le coefficient de conductibilité calorifique,

η = la viscosité.

La théorie cinétique du gaz donne pour c, Λ et η les équations suivantes:

$$c^2 = \frac{\gamma}{3}\bar{c}^2, \tag{3}$$

$$\frac{\Lambda}{C_p} = \frac{1}{3}\frac{\varrho}{\gamma}\bar{c}^2\tau_c, \tag{4}$$

$$\eta = \tfrac{1}{3}\varrho\bar{c}^2\tau_c; \tag{5}$$

Avec: $\bar{c}$ = vitesse moyenne des molécules,

τ_c = temps moyen entre deux collisions.

L'introduction de (3), (4), (5) dans (2) donne l'équation

$$\alpha_{\mathrm{class}} = \frac{1}{2c}\,\frac{7\gamma - 3}{3\gamma^2}\cdot\omega^2\tau_c. \tag{6}$$

Largement au dessous du maximum de la relaxation de rotation on trouve souvent, que l'absorption totale $\alpha_{\mathrm{exp}} = \alpha_{\mathrm{rot}} + \alpha_{\mathrm{class}}$ est proportionelle à ω^2.

On suppose que la formule d'absorption pour le processus simple de relaxation est valable aussi dans ce domaine. Au moins chaque spectre continu des temps de relaxation donnerait un accroissement en fonction de la fréquence moins forte.

Pour $\omega\sqrt{\tau_{ps}\tau_{pT}} \ll 1$ on obtient:

$$\alpha_{\text{rot}} = \frac{\omega}{2\pi c}\,\frac{\pi\varepsilon}{\sqrt{1-\varepsilon}}\,\omega\sqrt{\tau_{ps}\cdot\tau_{vs}}\,. \tag{7}$$

En utilisant les formules dérivées dans les leçons précédentes on trouve

$$\sqrt{\frac{\tau_{ps}\tau_{vs}}{1-\varepsilon}} = \frac{C_p^\infty}{C_p^0}\,\tau_{p\tau}\,, \tag{8}$$

et

$$\varepsilon = (\gamma-1)\,\frac{C_i}{C_p^\infty}\,. \tag{9}$$

On obtient

$$\alpha_{\text{rot}} = \frac{1}{2c}\,(\gamma-1)\,\frac{C_i}{C_p^0}\,\omega^2\tau_{p'}\,, \tag{10}$$

et par (6) et (7) et (13) de la leçon précédente

$$\frac{\alpha_{\text{exp}}}{\alpha_{\text{class}}} = 1 + \frac{\alpha_{\text{rot}}}{\alpha_{\text{class}}} = 1 + P\left(\frac{1}{Z}+\frac{1}{Z'}\right)^{-1} = 1 + P\cdot\bar{Z}\,, \tag{11}$$

avec

$$P = \frac{3\gamma^2(\gamma-1)C_i}{(7\gamma-3)C_p^0}\,. \tag{12}$$

On peut supposer que les degrés de liberté de rotation sont totalement excités à la température ambiante (sauf p-H_2) et qu' il n'y a aucune excitation des degrés de liberté d'oscillation pour des valeurs de f/p convenables.

Pour des molécules non linéaires, on obtient dans ce cas:

$$\gamma = \frac{6+2}{6}\,; \qquad C_i = \frac{3}{2}R; \qquad C_p^0 = \frac{8}{2}R, \tag{13}$$

pour les molécules lineaires:

$$\gamma = \frac{5+2}{5}\,; \qquad C_i = \frac{2}{2}R; \qquad C_p^0 = \frac{7}{2}R\,. \tag{14}$$

Avec ces valeurs on obtient:

$$(15)\qquad \left\{\begin{array}{ll} P \text{ (non linéaire)} & = 0.105\,, \\ P \text{ (linéaire)} & = 0.099\,. \end{array}\right.$$

Par l'éq. (11), on peut estimer directement $\bar{Z}$ par le rapport de l'absorption mesurée et l'absorption calculée avec les équations classiques [8]. Le $\bar{Z}$ signifie bien le processus de relaxation de rotation, mais il n'a pas du tout la signification physique précise qu'il a dans le cas de la relaxation d'oscillation. C'est aussi valable pour le temps de relaxation, qu'on peut calculer en appliquant (7). Surtout on ne peut pas trouver directement le temps de relaxation du niveau le plus bas de rotation ($\Theta_{\min}$), ce qui est possible pour l'oscillateur harmonique.

3·2. *Para-hydrogène.* – Grâce à ses quanta de rotation très grands, le para-hydrogène est une exception. Seulement les deux premiers niveaux de rotation sont occupés remarquablement avec 16.7 % et 0.26 %.

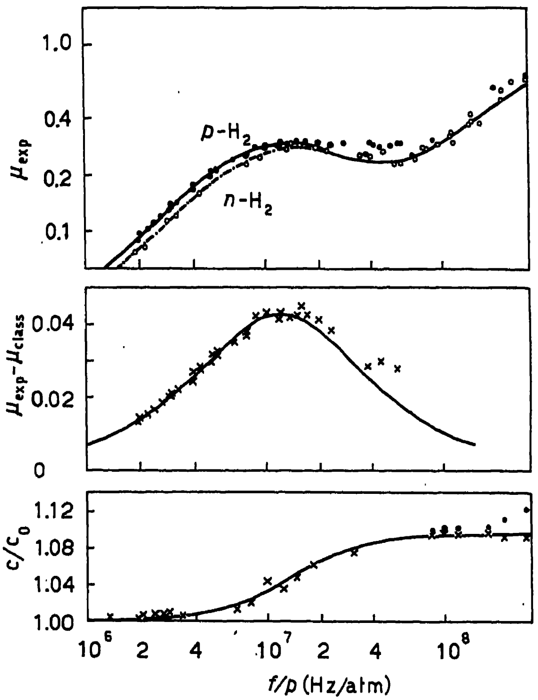

Fig. 7.

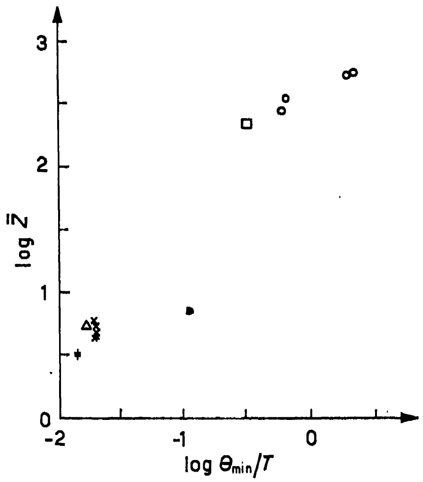

Fig. 8. – ○ n-H_2 (von Itterbeck et Mariens, 1937; Stewart et Stewart, 1952; von Itterbeck et Verhaegen, 1951); □ D_2 (Stewart et Stewart, 1952); ● HCl (Breazeale et Kneser, 1960); × N_2 (Zmuda, 1951; Keller, 1940; Parbrook et Tempest, 1958; Sessler, 1958; Bauer, 1959); + O_2 (Parbrook et Tempest, 1958; Sessler, 1958); △ NO (Bauer, 1959).

Jusqu'à une valeur de f/p de $2 \cdot 10^7$ Hz/atm l'absorption est surtout determinée par la relaxation de rotation. Jusqu'à 10^8 Hz/atm c'est la même chose pour la dispersion. En plus il faut soustraire les parties classiques [9]. Ainsi on obtient des courbes [10] qu'on ne peut pas expliquer par une relaxation simple (Fig. 7). L'analyse donne assez bien deux temps de relaxation: pour le passage 1er/2ème niveau $1.21 \cdot 10^{-8}$ s, pour le passage 2ème/3ème niveau $2.11 \cdot 10^{-8}$ s. Les valeurs de Z correspondantes sont 173 et 301. Au point de vue ordre de grandeur elles sont en bonne concordance avec les valeurs trouvés par la théorie quantique pour la collision de deux molécules de para-hydrogène [11].

La Fig. 8 donne un resumé des résultats expérimentaux.

RÉFÉRENCES

[1] F. Douglas Shields donne: *Journ. Acoust. Soc. Am.*, **32**, 180 (1960) et **34**, 271 (1962). Voir aussi E. Sittig: *Acustica*, **10**, 81 (1960) pour des valeurs extrapolées pour Cl_2; il donne aussi des résultats plus vieux.

[2] En faisant les calculs on trouve aussi l'influence de l'inharmonicité. Cfr. D. R. Stull et G. C. Sinke: *Journ. Am. Chem. Soc.*, **80**, 507 (1958).

[3] H. O. Kneser et V. O. Knudsen: *Ann. d. Phys.*, **21**, 682 (1934); H. et L. Knötzel: *Ann. d. Phys.*, **2**, 393 (1948); J. G. Parker: *Journ. Chem. Phys.*, **34**, 1763 (1961); M. C. Henderson: *Journ. Acoust. Soc. Am.*, **34**, 349 (1962).

[4] M. C. Henderson: *Journ. Acoust. Soc. Am.*, **34**, 349 (1962).

[5] G. G. Sherrat et E. Griffiths: *Proc. Roy. Soc.*, A **147**, 292 (1934); A. van Itterbeck et P. Mariens: *Physica*, **4**, 609 (1937); M. C. Henderson et G. J. Donnelly: *Journ. Acoust. Soc. Am.*, **34**, 779 (1962).

[6] H. J. Bauer, H. O. Kneser et E. Sitting: *Journ. Chem. Phys.*, **20**, 119 (1959).

[7] Cette valeur est en bonne concordance avec la valeur $Z = 3\,000$, trouvée par A. B. Callear (*Disc. Far. Soc.*, **33**, 28 (1962)) d'une façon totalement différente.

[8] C'est K. F. Herzfeld, qui a montré le premier cette possibilité.

[9] La formule classique d'absorption est juste jusqu'à une valeur de f/p de $0.02/\eta$ d'après l'experience. La viscosité dynamique (η) du parahydrogène est $8.4 \cdot 10^{-11}$ atm/Hz.

[10] D'après les mesures de K. Geide: *Thèse* (Göttingen, 1962). La dispersion de rotation de l'hydrogène a été prouvée la première fois par J. E. Rhodes: *Phys. Rev.*, **70**, 91 (1946).

[11] K. Takayanagi: *Proc. Phys. Soc.*, A **70**, 348 (1957).

IV.

Histoire des recherches sur la propagation du son.

Depuis que les hommes connaissent l'éclair et le tonnerre, ils savent que le son se transmet avec une vitesse limitée. Mais ce n'est que le génie de NEWTON qui reconnut le premier dans la vitesse du son un problème de mécanique (1687). Il le résolut avec un succès étonnant: le carré de la vitesse du son dans l'air (et dans tous les autres corps) est égal au quotient de la pression de la masse spécifique. La valeur numérique qui en résultait s'accordait, dans les limites de l'erreur de cette époque-là, avec les expériences. NEWTON ajouta une observation surprenante, que l'on peut facilement vérifier: La vitesse du son dans l'air est égale à celle d'un corps qui tombe en chute libre de la moitié de la hauteur de l'atmosphère homogène et isothermique. Un autre résultat contenu dans la formule de Newton et sur lequel on disputa pendant un siècle encore était beaucoup plus important: La vitesse du son est absolument indépendante de la fréquence et, dans certaines limites, de l'amplitude.

Cela ne changea pas, quand LAPLACE alla plus loin en tenant compte du fait que la compression d'un gaz est liée à l'élévation de sa température. En effet, la théorie de Laplace — qui fit du problème de la propagation du son un problème thermodynamique — était d'une audace extraordinaire. Elle supposa que, dans un espace libre rempli d'un gaz, des différences de température peuvent exister, changeant cent ou mille fois pendant une seconde. Outre cela, la théorie prouva que les différences de température s'équilibrent moins aux basses fréquences qu'aux hautes fréquences.

Naturellement la théorie de Laplace a été complété à certains égards par des auteurs postérieurs:

1) Si la longueur des ondes diminue, les différences de température tendent à s'équilibrer par conduction de chaleur (STOKES).

2) Dans une onde plane, chaque élément de volume d'un gaz est soumis non seulement à une déformation de ressemblance isotrope, mais aussi à une déformation de cisaillement. Celle-ci est toujours ralentie par la viscosité (KIRCHHOFF).

3) L'amplitude augmente, si une onde se propage dans un gaz de densité diminuante — par exemple verticalement dans l'atmosphère (SCHRÖDINGER).

Toutes ces corrections influencent en premier lieu l'absorption du son, et, à une approximation plus élévée seulement, la vitesse du son. Elles forment l'objet de la théorie classique.

Tout d'abord nous partons du point de vue de LAPLACE. Ceci est justifié surtout lorsqu'il s'agit d'ondes de basse fréquence; car toutes les corrections citées plus haut influencent particulièrement les hautes fréquences. La seule exception serait l'influence de la radiation mais elle n'a jamais été prouvée par l'expérience.

LAPLACE avait donc supposé que la pression et la masse spécifique dans l'onde du son sont liées de la même façon avec la température que dans une expérience lente, c'est-à-dire en réalisant l'équilibre thermique. Sa théorie était donc une théorie vraiment thermostatique, opposé à la théorie qu'on appelle aujord'hui un peu lourdement la « théorie thermodynamique des processus irréversibles ».

A notre avis BOLTZMANN était le premier à être sceptique. Il croyait y trouver la cause du fait, qu'on n'obtenait pas toujours pour la vitesse du son la valeur $C_p/C_v=(f+2)/f$ comme le demanderait le théorème d'équipartition, f signifiant le nombre de degrées de liberté des molécules. Serait-il donc possible que la distribution de l'énergie sur les degrés de liberté translatoire et intramoléculaire prenne autant de temps, qu'elle n'aurait pas son plein effet sur l'onde du son? BOLTZMANN essaya donc d'expliquer les anomalies par des processus « thermodynamiques », qui ont été parfaitement expliqués par la suite par la théorie quantique des chaleurs spécifiques. Nous savons aujourd'hui qu'elles sont la cause de l'absorption et de la dispersion moléculaires du son. H. A. LORENZ supposa également, que la théorie thermostatique de Laplace n'aurait qu'une validité limitée. Il déduisit de la théorie cinétique des gaz les équations hydrodynamiques permettant les calculs macroscopiques pour les gaz, et calcula ainsi la vitesse du son. Avec raison il prévit, contrairement à BOLTZMANN, l'influence de l'ajustement de l'équilibre thermique en un temps limité, aux fréquences extrêmement hautes, qu'on croyait à ce temps-là qu'elles ne seraient jamais réalisables.

Enfin RAYLEIGH discuta également le problème et reconnut déjà que une dissipation de l'énergie devait avoir lieu, c'est-à-dire que l'onde du son devait subir une absorption supplémentaire.

Nous laisserons de côté, pour l'instant, les théories et les expériences concernant la propagation du son dans des gaz partiellement dissociés. L'employ des méthodes thermostatiques y paraît d'ailleurs particulièrement douteux car on ne peut guère s'attendre qu'un équilibre de dissociation s'établisse complètement pendant des fractions d'une milliseconde. En dépit de cela, ce problème a été résolu expérimentalement il y a quelques années seulement.

En plus de celà, tous les doutes concernant la théorie thermostatique de Laplace devaient disparaître lorsque les résultats obtenus avec les méthodes de précision modernes pour la mesure de la vitesse du son (c) dans l'air et dans

H_2 confirmèrent exactement la formule de Laplace: ce sont les mesures de **Grüneisen** et de **Merkel**. Dans tout le domaine mesuré la valeur de C_p/C_v diffère de moins de 5 ‰ de la valeur théorique attendue de $\frac{7}{5}$.

Seulement 4 ans plus tard, G. W. **Pierce** publia son interféromètre d'ultrasons. Un énorme nouveau domaine de recherches s'ouvrit. L'idée expérimentale, toute géniale et fructueuse qu'elle était, ne donna d'abord pas des résultats bien convaincant. Ils montraient un maximum étroit de la vitesse du son dans l'air à 50 kHz et un léger accroissement avec la fréquence dans CO_2 (Fig. 1).

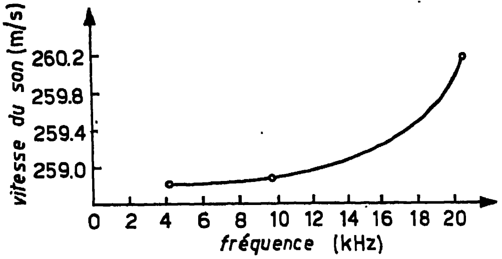

Fig. 1. – Les donnés de Pierce pour la vitesse du son dans CO_2 en fonction de la fréquence, dont **Herzfeld** et **Rice** ont dérivé l'idée de la relaxation acoustique.

Le fait que **Herzfeld** et **Rice** — en 1925 déjà — donnèrent une interprétation juste de ces premiers résultats est particulièrement à relever. Cette interprétation a été depuis confirmée beaucoup de fois. Ils reconnurent la relaxation de la chaleur spécifique du CO_2 comme cause de la dispersion et arrivèrent à estimer correctement l'ordre de grandeur du temps de relaxation.

Permettez-moi d'ajouter quelques souvenirs personnels: en 1927 je suis devenu assistant à l'Institut de Physique de l'Université de Marburg dont le directeur était le Professeur E. **Grüneisen**. Ses mesures très précises de la vitesse du son dans le domaine audible, dont j'ai parlé plus haut, n'avaient donné aucun signe de dispersion même dans l'air. C'est pourquoi il se méfia des résultats de Pierce, et me dit de vérifier ces mesures. Mes expériences avec cette méthode merveilleuse ne montrèrent en effet aucune dispersion dans l'air. Au contraire, l'effet dans du CO_2 était même plus fort que chez Pierce. A ce moment je ne connaissais pas encore la publication de **Herzfeld** et **Rice**. Pour cela je me formais moi-même une théorie très simple, sans m'occuper des phénomènes de transport. En dépit de cela, elle était en accord avec les résultats expérimentaux et l'interprétation qu'il s'agissait ici de la relaxation de la chaleur spécifique d'oscillation (et non pas de la rotation) était confirmée. Mais il y avait des difficultés: justement les mesures dans le domaine de la dispersion la plus forte ne voulaient pas bien réussir. Alors, je ne savais pas encore que le phénomène de relaxation est lié à une dispersion d'énergie. Cela ne fut rectifié que par une publication de P. S. H. **Henry**, qui montre que la formule représentant la courbe d'absorption était déjà contenue dans ma simple théorie. Peu de temps après, A. **Eucken** à Göttingen commença une longue série d'expériences sur la dispersion du son au moyen de l'interféromètre. On lui doit deux conclusions importantes:

1) le temps de relaxation est inversement proportionnel à la pression;

2) le temps de relaxation est extrêmement raccourci par certaines contaminations.

Le dernier fait expliquait la large fluctuation de mes mesures de la dispersion. Le premier fait rendait possible l'obtention d'une courbe de dispersion complète sans changement de fréquence. La variation de la pression faisait justement la même chose. Pour cette raison tous les résultats d'absorption et de dispersion sont exprimés en fonction du quotient f/p. Seulement s'il s'agit de gas décomposants et si des triples collisions ont lieu, l'absorption et la dispersion ne dépendront plus uniquement de f/p.

Jusqu'à ce moment (1932), la technique de la mesure de l'absorption n'avait guère dépassé le stade que NEKLEPAJEFF avait déjà atteint en 1911. Ses expériences faites avec un talent expérimental admirable, avaient donné à ce moment-là, au moins l'ordre de grandeur juste pour l'absorption du son dans l'air. Ce problème a été de nouveau repris par V. O. KNUDSEN à Los Angeles et cela pour donner enfin des résultats sûrs à l'acoustique d'édifice. Sa méthode rendait possible de mesures d'absorption du son très exactes dans le domaine audible et au delà. Il est évident que cette méthode fonctionne d'autant mieux que l'absorption est plus petite, les temps de ralentissement étant plus longs et pouvant être mesurés plus précisément. Avec cela il trouvait un effet très curieux: en étudiant l'absorption d'un son de fréquence constante en fonction de l'état hygrométrique de l'air, il s'en suit un maximum raide.

Moi même j'avais la chance de travailler en ce temps à l'Université de Californie. Il m'était possible d'interpréter cet effet comme relaxation de l'oxygène qui dépend beaucoup de la teneur de la vapeur d'eau, comme EUCKEN l'avait déjà montré dans le CO_2. Si cette interprétation était juste, il fallait que le maximum de l'absorption du son dans de l'oxygène pur fût presque cinq fois plus grand que dans de l'air. KNUDSEN fit cette expérience et le résultat confirma cette hypothèse.

Il ne manquait plus qu'une chose à l'éclaircissement fondamental: est-ce que le phénomène de relaxation est causé seulement par la chaleur d'oscillation ou y-a-t-il aussi une relaxation de la chaleur de rotation, comme H. A. LORENZ l'avait déjà supposé? Le team, qui se réunissait autour de HUBBARD, répondait à cette question. Il avait bien développé l'interféromètre et en donnait une théorie détaillée. Ses élèves H. et L. STEWART pouvaient ainsi atteindre des fréquences si hautes ou des pressions si basses que la relaxation de la chaleur de rotation de l'hydrogène devenait mesurable. Les recherches de GREENSPAN continuaient dans cette direction. Il réussit à construire un appareil très sensible pour mesurer la dispersion et l'absorption, ce qui lui rendait possible de travailler avec des pressions de moins de 1/100 atm. Grâce à cela il était possible pour la première fois de produire des ondes sonores plus longues que le libre parcours. Les problèmes qui s'en suivirent étaient des problèmes de la cinétique des gaz et demandaient un élargissement important de cette théorie (BURNETT, UHLENBECK, WANG CHANG).

Le développement suivant vous est bien connu. Aujourd'hui nous connaissons les temps de relaxation de la chaleur d'oscillation pour environ 20 gaz purs. Les mesures de mélanges de gaz ne sont presque plus comptables. Les temps de relaxation de la chaleur de rotation aussi sont connus en 10 cas. Avec cela nous connaissons des valeurs numériques extraordinairement nombreuses et nouvelles que nous trouvons tout au long de leur interprétation théorique dans le livre fondamental de HERZFELD et LITOVITZ.

RÉFÉRENCE

[1] E. GRÜNEISEN et E. MERKEL: *Ann. d. Phys.*, **6**, 344 (1921).

V.

Les méthodes expérimentales.

Les phénomènes de relaxation ont lieu lors de changements rapides d'état C'est pourquoi on est incliné à les examiner en faisant subir au milieu un seul changement d'état. C'est en effet ce que différents auteurs ont fait, par exemple en comprimant rapidement [1] une substance ou en observant la masse spécifique après une onde de choc [2] ou bien encore en freinant subitement un jet de gaz [3]. Toutes ces méthodes permettent de mesurer des durées de relaxation, en partie avec une précision remarquable. Mais souvent il n'est pas possible par cette méthode de mesurer des quantités de relaxation et ce sont elles seulement qui éclaircissent la nature du phénomène. C'est pourquoi nous allons traiter par la suite des méthodes expérimentales qui se servent des changements d'état périodiques, c'est-à-dire nous nous limiterons aux méthodes de mesures de la vitesse et de l'absorption du son.

Depuis longtemps on a des méthodes très précises pour la mesure de la vitesse du son. Dans le domaine audible on a obtenu, par la méthode des résonateurs cylindriques, une précision meilleure que ±1 ‰ et depuis le développement de l'interféromètre de Pierce, on obtient presque la même précision dans le domaine des ultrasons. Pour l'exploration des phénomènes de relaxation on utilise aujourd'hui particulièrement des mesures d'absorption. Pour obtenir des fréquences basses ou élevées, les méthodes expérimentales ont été perfectionnées pendant les dernières années. Une précision meilleure que ±2 % est obtenue dans quelques cas sans qu'il soit nécessaire de maintenir la température constante de plus que de quelques degrés.

On peut classifier les méthodes expérimentales selon deux points de vue: ou en distinguant les méthodes qui se servent des ondes conduites par exemple dans un tube (A), des méthodes qui utilisent des ondes se propageant librement dans l'espace (B); ou en distinguant les méthodes qui utilisent des interférences des ondes sonores (I) de celles qui les évitent (II). En général les méthodes I sont meilleures pour la mesure de la vitesse du son (comme produit de la longueur d'onde par la fréquence), et les méthodes II se prêtent à la mesure de l'absorption. Les méthodes A sont soumises à une limitation par la fréquence, au dessus de laquelle les ondes cessent d'être planes. Cette fréquence est déterminée par le rapport de la longueur d'onde au diamètre du tube. On comprend que les méthodes utilisant la diffraction de la lumière, très utiles dans le cas des liquides, ne sont pas très utilisables pour les gaz, sauf pour des pressions élevées. Pour toutes les réactions du premier ordre qui peuvent se passer et causer des phénomènes de relaxation dans un gaz, le temps de relaxation est proportionnel à $1/p$. Parce que les formules de dispersion et d'absorption ne contiennent la fréquence qu'en fonction de τ, le même résultat est obtenu ou par une augmentation de la fréquence, ou par une diminution de la pression. C'est-à-dire la puissance d'une méthode est caractérisée par

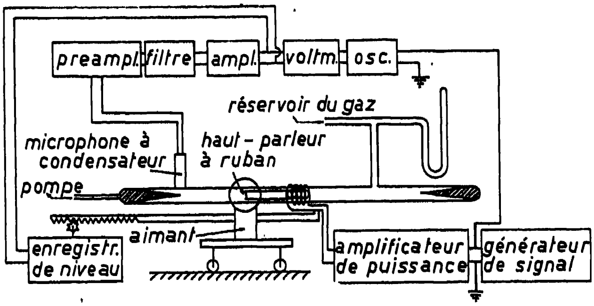

Fig. 1.

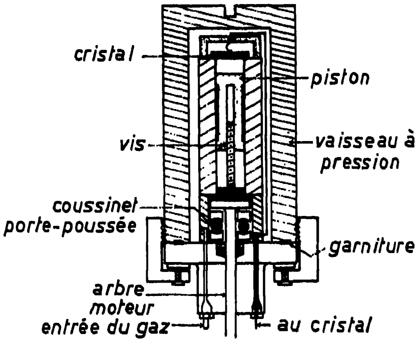

Fig. 2.

Type	Fréquence/ pression (kHz/atm)	Fig.	Auteurs
I-*A*) Résonateur cylindrique	0,06 ÷ 1,7 2 ÷ 200		J. G. Parker: *Journ. Acoust. Soc. Am.*, **34**, 1763 (1961) L. Fritsche: *Acustica*, **10**, 189 (1960); M. Henderson: *Journ. Acoust. Soc. Am.* (1962)
II-*A*) Ondes progressives dans des tubes	20 ÷ 2000	1	F. A. Angona: *Journ. Acoust. Soc. Am.*, **25**, 92 (1953)
I-*B*) Interféromètre	300 ÷ 300 3000 ÷ 10000	2	M. C. Henderson et L. Peselnick: *Journ. Acoust. Soc. Am.*, **29**, 1047 (1957) S. Petralia: *Nuovo Cimento*, **1**, 351 (1955)
II-*B*) Signaux limités; ondes s'amortissant rapidement	500 ÷ 13000 100 ÷ 9000 $10^3 \div 10^8$ $10^3 \div 10^9$	 3 4 5	W. Tempest et H. D. Parbrook: *Acustica*, **7**, 355 (1957) E. Sittig: *Acustica*, **10**, 81 (1960) M. Greenspan: *Journ. Acoust. Soc. Am.*, **25**, 92 (1953) E. Meyer et G. Sessler: *Zeits. f. Phys.*, **149**, 15 (1957)

le quotient de la fréquence et de la pression, pour lesquelles la méthode est capable de fonctionner. Aujourd'hui on dispose d'appareils qui mesurent la propagation de <10 jusqu'à $>10^{10}$ Hz/atm. En comparaison avec les ondes élec-

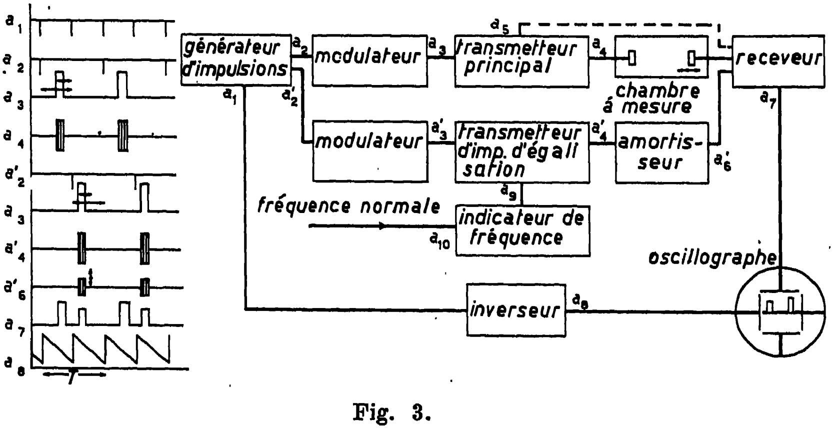

Fig. 3.

tromagnétiques celà correspond au domaine qui s'étend des rayons X aux ondes de l'infrarouge extrême.

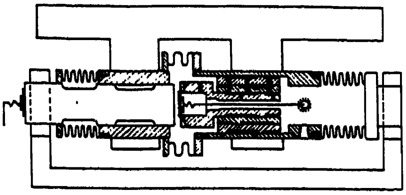

Fig. 4.

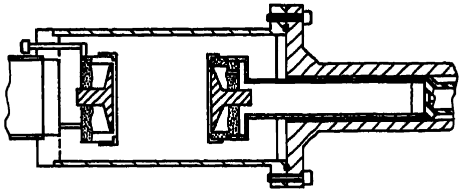

Fig. 5.

Il est impossible de décrire tous les appareils ingénieux construits par des auteurs nombreux. C'est pourquoi nous avons choisi — assez arbitrairement — quelques exemples des quatre types signalés ci-dessus I-*A*, I-*B*, II-*A* et II-*B*. Ils sont énumérés dans la Table I, et illustrés par les Fig. 1-6.

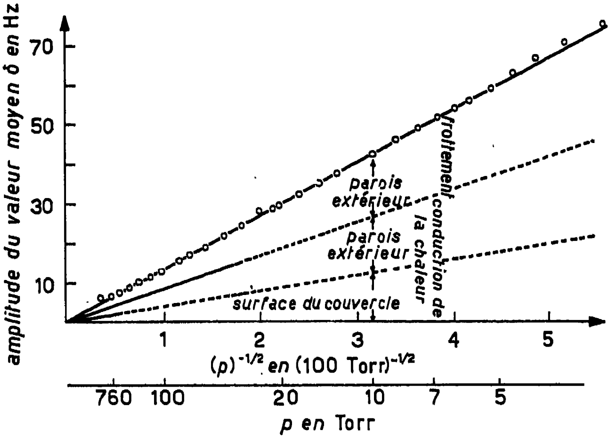

Fig. 6.

Il faut ajouter quelques remarques à deux de ces méthodes:

1) Aux fréquences basses, l'absorption du son est mesuré par la largeur des « peaks » de résonance d'un cylindre rempli de gaz. Cette largeur est déterminée par l'absorption du gaz et par l'amortissement causé par les parois du cylindre. Pour connaître l'absorption du gaz, il faut connaître l'influence des parois. Celle-là peut être calculée à partir de la théorie de Stokes et Kirchoff. FRITSCHE réussit à construire un résonateur cylindrique, qui — rempli d'un gaz non absorbant — produisit des « peaks » de résonance correspondant exactement à la théorie de Stokes et Kirchhoff. (Fig. 6). Depuis ce temps-là nous possédons un instrument de précision pour ce domaine.

2) On aperçoit l'étendue énorme de la méthode de Greenspan, modifiée et adaptée à pressions encore plus basses par **Meyer** et **Sessler**. A moins de 1 mm Hg, l'absorption « classique » devient très grande et il n'y a plus d'interférence. Naturellement le récepteur « Sell », doit être extrêmement sensible et la distance entre lui et l'émetteur devient une fraction de millimètre. Si le libre parcours des molécules devient plus grand que la longueur d'onde on rencontre des problèmes de la théorie cinétique des gaz complètement nouveaux.

RÉFÉRENCES

[1] A. **Carelli** et F. **Cennamo**: *Nuovo Cimento*, **11**, 429 (1954).
[2] H. B. **Palmer** et D. F. **Hornig**: *Journ. Chem. Phys.*, **26**, 8 (1957).
[3] P. W. **Huber** et A. **Kantrowitz**: *Journ. Chem. Phys.*, **15**, 257 (1947).

Translational Dispersion in Gases.

M. GREENSPAN

National Bureau of Standards - Washington

1. – Introduction.

The study of sound propagation in a fluid is essentially a problem in the hydrodynamics of small motions, and if attention is confined to situations in which viscous, thermal and relaxational effects are negligible, then only minor interest attaches to the problem. It is only when circumstances are such that these ordinarily small effects become easily measurable that useful information about the structure of the medium may be gotten from sound-propagation measurements. More commonly, the equilibrium structure of the gaseous medium is sufficiently well known; the measurement then provides a tool for the investigation of the mechanics of a nonuniform gas. In principle, the nonuniformity can be made arbitrarily large (*i.e.*, the space and time gradients of the dynamical variables that specify the motion can be made arbitrarily large) by the establishment of a sufficiently high « ratio of frequency to density ». At the same time the complication of nonlinearity can be avoided by keeping the particle-velocity amplitude small relative to the speed of sound. This separation of the effects of nonuniformity and nonlinearity is not possible in shock-wave experiments, for instance. On the other hand, extreme conditions in the acoustic case give rise to an attenuation of the principal mode which eventually becomes so great as to make it difficult to distinguish among the various modes.

Some semi-quantitative ideas about the propagation of sound in gases result immediately from kinetic-theoretical considerations. To begin with, it is clear that in a gas of smooth, rigid spheres, the speed of sound can depend only on the mean speed of the molecules, provided only that the gas is sufficiently dilute so that practically all of a molecular property is transferred while the molecule is in free flight, and that the mean collision rate is very high relative to the sound frequency. The ordinary Laplace formula for a monatomic gas reflects this; here the speed of sound depends on the molecular mass and the temperature, which together determine the molecular speed. Calculations based on this elementary notion were attempted by WATERSTON, by STEFAN, and by PRESTON. In an addendum to Preston's paper [1], J. C. MAXWELL arrived at the Laplace formula (for a monatomic gas) by this means.

It is now obvious that any dispersion must depend on the ratio of mean collision rate to sound frequency and that the dispersion is small unless this ratio is small. A suitable parameter is therefore one proportional to this ratio (which is inversely proportional to « frequency/pressure » or « frequency/density »). Consider a sound wave at an audio frequency of some kilohertz in a gas near atmospheric temperature and pressure. The mean collision rate is of the order $10^{10}\,s^{-1}$; the medium is very fine-grained and the dispersion negligible. As the sound frequency is steadily increased, it becomes comparable at first to the collision rates of the *slower* molecules, the collision rates being positively correlated with molecular speed. The slower molecules are now not in a position to transfer the acoustic (ordered) momentum coherently, and the burden accordingly shifts to the faster molecules. Since, the sound speed depends, as we have seen, on the thermal speed of the molecules which transport the momentum, it steadily increases with frequency. The effect is negligible unless the frequency is very high, for the average collision rate of even the zero-velocity molecules is $\sqrt{2}/2$ times the mean.

Attenuation can be examined in a similar way, but the arguments are less intuitive and the exercise less instructive.

2. – Nomenclature.

In these lectures, sinusoidal time variation is expressed by the (usually suppressed) factor $\exp[i\omega t]$, so that $\partial/\partial t = i\omega$. For a plane, progressive wave traveling in the $+x$-direction, the space variation is proportional to $\exp[-\Gamma x]$ (so that $\partial/\partial x = -\Gamma$). The propagation constant is

$$\Gamma = \alpha + i\beta = \alpha + i\omega/c = \alpha + i2\pi/\lambda\,, \tag{1}$$

in which α is the amplitude attenuation per unit length, c is the phase speed of propagation, and λ is the wavelength. It is often convenient to use the nondimensional propagation constant

$$k = \Gamma/\beta_0 = c_0\Gamma/\omega\,, \tag{2}$$

in which c_0 is the Laplacian speed of sound.

It will be found that the frequency $f = \omega/2\pi$ enters into the dispersion relations through the nondimensional parameters

$$r = c_0^2\varrho_0/\gamma_0\omega\mu\,, \tag{3}$$

which has the nature of a Reynolds number, and

$$s = c_0^2\varrho_0 c_v/\gamma_0\omega\nu\,, \tag{4}$$

which is a similar number for thermal effects. Here ϱ_0 is the equilibrium density, γ_0 is the zero-frequency specific-heat ratio, c_v is the isometric thermal capacity, μ is the viscosity and ν the thermal conductivity.

For an ideal gas of Maxwellian molecules, we will find

$$r = \frac{2}{5\pi}\frac{f_c}{f}\,, \tag{5}$$

so that r is proportional to the ratio of mean collision rate to frequency, as anticipated (s is related to r). For $f_c = f$, $r = 2/5\pi = 0.126$, approximately.

In accordance with the usual convention, repeated literal indices denote summation. The indices x, y, z, $(= 1, 2, 3)$ are not considered literal.

3. – Theory.

The propagation constant, Γ, of eq. (1) is obtained in the same manner as in a hydrodynamic continuum, namely by combination of the conservation laws with the equation of state. This point of view is usually justified as a consequence of the Boltzmann equation [2].

3·1. *The conservation laws.* – For the present purpose we may limit ourselves to the one-dimensional case with no loss of generality. The laws are: mass,

$$\dot{\varrho} + \varrho(\partial u/\partial x) = 0\,; \tag{6}$$

momentum,

$$\varrho\dot{u} - \partial T_{xx}/\partial x = 0\,; \tag{7}$$

and energy,

$$\varrho\dot{E} - \frac{\partial}{\partial x}(T_{xx}u) + \frac{\partial q}{\partial x} = 0\,. \tag{8}$$

In eq. (6) and (7), which are self-explanatory, ϱ is the density, u the flow velocity, and T_{xx} the normal stress. The dot signifies the total time derivative. In eq. (8) E is the total (intrinsic plus kinetic) energy per unit mass, $T_{xx}u$ is the rate of working of the stress, and q is the total heat flux.

Equation (8) can be rearranged in many ways. For instance, since

$$\frac{\partial}{\partial x}(T_{xx}u) = T_{xx}\frac{\partial u}{\partial x} + u\frac{\partial T_{xx}}{\partial x} = T_{xx}\frac{\partial u}{\partial x} + \varrho u\dot{u}\,,$$

from eq. (7), and $u\dot{u}$ is the rate of change of kinetic energy per unit mass eq. (8) is

$$\varrho\dot{U} - T_{xx}\frac{\partial u}{\partial x} + \frac{\partial q}{\partial x} = 0\,, \tag{9}$$

in which U is the intrinsic energy per unit mass.

The conservation equations may be derived from the Boltzmann equation, but are more general. The stress and heat flux are still unspecified; the main problem is, in fact, to obtain suitable expressions for these in terms of the macroscopic variables.

The equations are now linearized about the equilibrium values ϱ_0, p_0 ($T_{xx} = -p_0$ at equilibrium). To the same approximation the dot is replaced by $\partial/\partial t = i\omega$ (for sinusoidal time-dependence). We have, finally,

$$i\omega\,\delta\varrho + \varrho_0(\partial u/\partial x) = 0\,, \tag{10}$$

$$\frac{\partial}{\partial x}\,\delta T_{xx} - i\omega\varrho_0 u = 0\,, \tag{11}$$

and

$$i\omega\varrho_0\,\delta U + p_0\frac{\partial u}{\partial x} + \partial q/\partial x = 0\,. \tag{12}$$

3·2. *The constitutive relations.*

3·2.1. Equation of state. In the equation of state as here considered we deal not with the stress tensor T_{ij}, but with the hydrostatic pressure $p = -T_{ii}/3$. In the case of a perfect gas, for which the stresses are entirely accounted for by the flux of momentum, the equation of state for the non-uniform condition is the same as that at equilibrium, a consequence of the kinetic-theory definition of temperature adopted here (CHAPMAN and COWLING [2], p. 87). For an imperfect monatomic gas, there is a contribution to pressure proportional to the rate of dilatation (*i.e.* to $\dot{\varrho}/\varrho$), so that a bulk viscosity $\varkappa$, small relative to the ordinary viscosity μ, is involved. Enskog [3] has shown that $\varkappa/\mu$ is of the order (volume of molecules/volume of gas)^2; we therefore regard this $\varkappa$ as zero for the dilute gases with which we are concerned.

The situation is more complicated in polyatomic gases, which exhibit thermal relaxation. Tisza [4] showed that a complex, frequency-dependent, and disposable bulk viscosity can be introduced to give a phenomenological accounting of thermal relaxation. What is of more interest here is that it has been shown [5] that thermal relaxation induces an excess, frequency-dependent pressure. If the state variables are taken as p, ϱ, and the « transitional temperature », then the equation of state is the same as in the equilibrium case; the excess pressure in question is over that corresponding to another temperature, namely that which would obtain if the density change had occurred reversibly. Our kinetic-theoretical temperature is the same as the « transitional temperature » above, and we therefore take the view that the equation of state

$$\varrho = \varrho(p, T)\,, \tag{13}$$

is adequate for even a highly nonuniform, nonsimple gas, provided it is sufficiently dilute. This is not to say that energy is not dissipated during the isotropic compression of a relaxing gas. For instance, in the form of eq. (13) applicable to small motions,

$$\delta\varrho/\varrho_0 = b^T\,\delta p - \alpha^p\theta\,, \tag{14}$$

in which $b^T = (\partial\varrho/\partial p)_T/\varrho_0$ is the isothermal compressibility, $\alpha^p = -(\partial\varrho/\partial T)_p/\varrho_0$ is the isobaric coefficient of thermal expansion, and $\theta = \delta T$, the incremental variables are complex quantities not necessarily in phase for sinusoidal time-dependence.

The above considerations are superfluous in the case of a monatomic gas, but for a relaxing gas we shall generally assume (because there is no other simple choice, and it is anyway plausible) that, for sinusoidal time-dependence, the ordinary thermodynamic identities hold formally if the appropriate quantities are taken as complex. As an example, consider the intrinsic energy U for a gas in which U depends only on T. Then the usual relation $\delta U = c_v\theta$ still holds if thermal relaxation is present; c_v is considered complex and frequency-dependent. In fact, this is the basic notion of the common phenomenological theory of thermal relaxation (Herzfeld and Litovitz [5], p. 58).

More generally

$$U = U(T, \varrho)\,,$$

so that

$$\delta U = c_v\theta + (\partial U/\partial \varrho)_T \,\delta\varrho \,. \tag{15}$$

From the thermodynamic identity (see *e.g.* CONDON and ODISHAW [6])

$$c_p - c_v = \alpha_\varrho^p \left[\frac{p}{\varrho} - \varrho\left(\frac{\partial U}{\partial \varrho}\right)_T\right],$$

there follows, for eq. (15), the form

$$\delta U = c_v\theta + \frac{1}{\varrho_0}\left(\frac{p_0}{\varrho_0} - \frac{c_p - c_v}{\alpha^p}\right)\delta\varrho \,. \tag{16}$$

Equation (16) enables us to eliminate δU in favor of θ in the energy eq. (12); from the result we also eliminate $\delta\varrho$ as gotten from the mass eq. (10). The energy equation then has the simple form

$$i\omega\varrho_0 c_v\theta + \frac{\partial q}{\partial x} + \frac{\varrho_0(c_p - c_v)}{\alpha^p}\frac{\partial u}{\partial x} = 0 \,. \tag{17}$$

In the sequel we will require numerical values of c_0, the zero-frequency limit of the speed of sound. This is readily calculated, for each gas, from an equation of state appropriate to it. It is convenient to use a modified Laplace formula

$$c_0 = (\gamma_0 RT/M)^{\frac{1}{2}}(1 + \delta)\,, \tag{18}$$

in which M is the molecular weight and δ is a correction, calculated from the virial equation of state, which has been tabulated by WOOLLEY and BENEDICT [7]. The necessary force constants are given by HIRSCHFELDER *et al.* [8], for instance.

3.2.2. Stress and heat-flux. The most elementary expressions are

$$T_{xx} = -p + \frac{4}{3}\mu\frac{\partial u}{\partial x}\,, \tag{19}$$

where p is the mean pressure appropriate to the density and temperature, and

$$q = -\nu(\partial T/\partial x)\,. \tag{20}$$

These lead to the « Navier-Stokes » equations and are a second approximation from the Boltzmann equation. However, eq. (20) is just Fourier's law, and eq. (19) is an assimilation of a fluid to a linear, elastic solid. For an isotropic solid

$$T_{ij} = \lambda S_{rr}\delta_{ij} + 2\mu S_{ij}\,, \tag{21}$$

where S_{ij} is the strain, and λ and μ are two elastic moduli. It is supposed that in a fluid T_{ij} differs from $-p\delta_{ij}$ by a quantity which depends on the strain rate, rather than the strain, and has the same form as eq. (21), so that for a fluid

$$T_{ij} = (-p + \lambda\dot{S}_{rr})\delta_{ij} + 2\mu\dot{S}_{ij}\,, \tag{22}$$

where λ and μ are now two viscosities. Contraction of eq. (22) gives

$$T_{ii} = -3p + (3\lambda + 2\mu)\dot{S}_{rr}\,,$$

in which, as before, we take the bulk viscosity $\lambda + 2\mu/3 = 0$, so that eq. (22), with $i, j = 1$, becomes eq. (19). ($\dot{S}_{11} = \partial u/\partial x$, $\dot{S}_{22} = \dot{S}_{33} = 0$.)

Expressions leading to the so-called Burnett equations result from a third approximation to the distribution function obtained from the Boltzmann equation. The forms

$$T_{xx} = -p + \frac{4}{3}\mu\left(\frac{\partial u}{\partial x} + \frac{\mu'}{p}\frac{\partial^2 p}{\partial x^2} - \frac{3}{5}\frac{\nu'}{T}\frac{\partial^2 T}{\partial x^2}\right), \tag{23}$$

and

$$q = -\nu\frac{\partial T}{\partial x} - \frac{\varrho\nu'}{5}(3\nu' - 4\mu')\frac{\partial^2 u}{\partial x^2}\,, \tag{24}$$

are special cases for Maxwellian molecules, of expressions due to WANG CHANG and UHLENBECK [9]. The primes denote kinematic quantities, *i.e.* $\mu' = \mu/\varrho$ and $\nu' = \nu/\varrho c_v$.

The « thirteen-moment » expressions of GRAD [10] are third approximations of another type, in which the stress and heat flux are implicit. The small-motion approximations for sinusoidal time-dependence are

$$\left(1 + \frac{i\omega\mu}{p_0}\right)(T_{xx} + p) = \frac{4}{3}\mu\frac{\partial u}{\partial x} + \frac{8}{15}\frac{\mu}{p_0}\frac{\partial q}{\partial x}\,, \tag{25}$$

and

$$\left(1 + \frac{3}{2}\frac{i\omega\mu}{p_0}\right)q = -\nu\frac{\partial T}{\partial x} + \frac{3}{2}\mu'\frac{\partial}{\partial x}(T_{xx} + p)\,. \tag{26}$$

The above equations are for an ideal monatomic gas and have been recast to exhibit clearly the Maxwell relaxation effect. In fact, μ/p_0 is exactly the viscous, and $3\mu/2p_0$ the thermal, relaxation time for Maxwellian molecules [11]. (μ/p_0 is $\frac{5}{4}$ times the mean collision time.) For small $\omega\mu/p_0$, *i.e.* for large r and s (eq. (3), (4) for an ideal gas), eq. (25), (26) reduce to the Navier-Stokes equations (19), (20).

It should be noted that the convergence of the series assumed in all of the above developments has not been established [12], [13]. See however, GRAD [14].

3'2.3. **The transport numbers.** The viscosity μ and thermal conductivity ν which appear in the expressions for T_{xx} and q are determined by experiment. Nevertheless, it is of value to note that they are related to the mean free path L. For Maxwellian molecules, for instance, if $\bar{v}$ is the mean speed, (KENNARD [11], p. 179)

$$\mu = \frac{5\pi}{32}\varrho\bar{v}L\,,$$

from which eq. (5) for r follows in consideration of $L = \bar{v}/f_c$, $\bar{v}^2 = 8p/\pi\varrho$ (KENNARD [11], p. 50).

For helium, Keesom's empirical formula [15]

$$\mu = 5.023\,T^{0.647}\ \mu\text{poise}\,, \tag{27}$$

is convenient. For other gases we have used Sutherland's formula (*e.g.* CHAPMAN and COWLING [2], p. 224)

$$\frac{\mu}{\mu_0} = \left(\frac{T}{T_0}\right)^{\frac{3}{2}}\frac{T_0+S}{T+S}\,, \tag{28}$$

for interpolation.

Measured values of ν are not as accurate as those of μ, and in any case it is sometimes convenient to have ν expressed in terms of μ and other known properties of the gas in order to exhibit the results as a function of one parameter (r of eq. (3), (5)) only.

In the case of a monatomic gas, $\nu/c_v\mu = \frac{5}{2}$, approximately. Following the elegant (but not rigorous) reasoning of EUCKEN (*e.g.* KENNARD [11], p. 182) for a polyatomic gas, we divide ν and also c_v into two parts, one translational and one internal, so that

$$\nu = (\tfrac{5}{2}c_{vt} + c_{vi})\mu\,. \tag{29}$$

The factors ($\frac{5}{2}$ and 1) differ because the translational energy of a molecule is correlated with its speed but the internal energy is assumed not. The approximations $c_v = 3R/2$, $c_p - c_v = R$, together with eq. (29) give

$$\frac{\nu}{c_v \mu} = \frac{r}{s} = \frac{9\gamma - 5}{4} = 1 + \frac{9}{4}\frac{C_v}{R}. \tag{30}$$

The point here is that in our case any experiment on a polyatomic gas involves thermal relaxation effects, which we take into account by considering c_v (and therefore also $c_p = R + c_v$ and γ) to be a complex function of frequency. The argument which leads to Eucken's formula (eq. (30)) is unchanged, and we see that whatever validity it possesses is retained for a relaxing gas. The thermal conductivity ν is thus complex in this scheme.

3'3. *Plane waves.* – For the plane progressive wave case, we write $-\Gamma$ for $\partial/\partial x$ in the conservation eq. (10), (11), (17) to get

$$i\omega\,\delta\varrho - \varrho_0 \Gamma u = 0\,, \tag{31}$$

$$\Gamma\,\delta T_{xx} + i\omega\varrho_0 u = 0\,, \tag{32}$$

and

$$i\omega\varrho c_v\theta - \Gamma q - [\varrho_0(c_p - c_v)/\alpha_p]\,\Gamma u = 0\,, \tag{33}$$

to which we append the equation of state (14)

$$\delta\varrho/\varrho_0 = b^T\,\delta p - a^p\theta\,. \tag{14}$$

The desired forms for T_{xx} and q (with $\partial/\partial x = -\Gamma$) are inserted, producing a set of four homogeneous equations in δp, $\delta\varrho$, u, and θ; the condition of consistency is the vanishing of the determinant. The result is an equation of the second or higher degree which in effect gives Γ^2 as a function of ω (although we use nondimensional quantities instead) corresponding to two directions of travel of the waves.

In the Navier-Stokes and 13-moment cases, the equation is of the second degree in Γ^2. If the roots are Γ_{I} and Γ_{II}, then for positive-going waves, for instance,

$$V = A_1 \exp[-\Gamma_{\text{I}} x] + A_2 \exp[-\Gamma_{\text{II}} x]\,,$$

where V stands for any one of the four variables δp, $\delta\varrho$, u, θ, and the arbitrary constants are different for the different meanings of V. Of the eight constants, two are independent and can be determined by specification of u and θ (or any pair of V's) at $x=0$, for instance.

In the Burnett case there will be three propagation constants (Γ) and more for higher order approximations. The problem of how to assign the boundary conditions has not been solved (GRAD [14], p. 277).

3·4. *The propagation constant.* – The details are exhibited for the Navier-Stokes case only. The appropriate forms of the constitutive eqs. (19), (20), namely

$$\delta T_{xx} = -\delta p + \tfrac{4}{3}\Gamma\mu u\,, \qquad q = \nu\Gamma\theta\,,$$

when substituted into eqs. (32), (33) yield

$$(i\omega\varrho_0 - \tfrac{4}{3}\Gamma^2\mu)u - \Gamma\delta p = 0\,. \tag{34}$$

and

$$[\varrho_0(c_p - c_v)/\alpha^p]\Gamma u - (i\omega\varrho_0 c_v - \nu\Gamma^2)\theta = 0\,. \tag{35}$$

The condition that eqs. (14), (31), (34), (35) are consistent is [16]

$$\frac{k^4}{\gamma_0^2 s}\left(i - \frac{4}{3}\frac{1}{r}\right) + \frac{k^2}{\gamma_0}\left[\gamma + i\left(\frac{1}{s} + \frac{4}{3}\frac{1}{r}\right)\right] + 1 = 0\,, \tag{36}$$

in which r and s are from eqs. (3), (4). The compressibility b^T of eq. (14) was eliminated using $\varrho_0 b^T = \gamma_0/c_0^2$, so that γ_0 is the zero-frequency specific-heat ratio. As for γ, it is complex and frequency-dependent if relaxation is present, as is also s.

The corresponding Burnett equation, restricted to an ideal gas of Maxwellian molecules, is

$$\begin{aligned} \frac{k^6}{\gamma_0^3 rs}\left[-\frac{4}{3}\frac{i}{r} + \frac{4}{5}(\gamma_0 - 1)\left(-\frac{4}{3}\frac{1}{r^2} + \frac{9}{5}\frac{1}{rs} - \frac{3}{5}\frac{1}{s^2}\right) + \right. \\ \left. + \frac{k^4}{\gamma_0^2}\left\{\frac{i}{s} - \frac{4}{3}\frac{\gamma}{r^2} - \frac{3}{5}\frac{(\gamma-1)}{s^2} + \left[\frac{8}{5}(\gamma - 1) - \frac{4}{3}\right]\frac{1}{rs}\right\} + \right. \\ + \frac{k^2}{\gamma_0}\left[\gamma + i\left(\frac{1}{s} + \frac{4}{3}\frac{1}{r}\right)\right] + 1 = 0\,. \end{aligned} \tag{37}$$

The 13-moment equation is for monatomic gases only, and we defer consideration of it.

3·4.1. **Monatomic gas.** Here $\gamma = \gamma_0$. For purposes of illustration it is sufficient to take $\gamma_0 = \frac{5}{3}$ and $r/s = \nu/c_v\varrho = \frac{5}{2}$. We have:

Navier-Stokes, from eq. (36),

$$k^4 \frac{3}{5}\frac{1}{r}\left(\frac{3}{2}i - \frac{2}{r}\right) + k^2\left(1 + \frac{23}{10}\frac{i}{r}\right) + 1 = 0; \tag{38}$$

Burnett, from eq. (37)

$$k^6 \frac{3}{25}\frac{1}{r^3}\left(-\frac{7}{5}\frac{1}{r} - 6i\right) + k^4 \frac{1}{10}\frac{1}{r}\left(-\frac{97}{5}\frac{1}{r} + 9i\right) + k^2\left(1 + \frac{23}{10}\frac{i}{r}\right) + 1 = 0; \tag{39}$$

and from 13-moment, obtained from eqs. (14), (31), (32), (33), (25), (26).

$$k^4 \frac{9}{10}\frac{1}{r}\left(i - \frac{9}{5}\frac{1}{r}\right) + k^2\left(1 + \frac{24}{5}\frac{i}{r} - \frac{117}{25}\frac{1}{r^2}\right) + 1 + \frac{5}{2}\frac{i}{r} - \frac{3}{2}\frac{1}{r^2} = 0. \tag{40}$$

It is sometimes convenient to use expansions in powers of $1/r$. These are, for the roots which are asymptotic to the Laplace value in each case:

Navier-Stokes,

$$k_{\text{I}} = i + \frac{7}{10}\frac{1}{r} - \frac{141}{200}\frac{i}{r^2} - \frac{1559}{16\cdot 5^3}\frac{1}{r^3} + \dots; \tag{41}$$

Burnett,

$$k_{\text{I}} = i + \frac{7}{10}\frac{1}{r} - \frac{43}{40}\frac{i}{r^2} - \frac{4203}{2000}\frac{1}{r^3} + \dots; \tag{42}$$

13-moment,

$$k_{\text{I}} = i + \frac{7}{10}\frac{1}{r} - \frac{43}{40}\frac{i}{r^2} - \frac{527}{400}\frac{1}{r^3} + \dots. \tag{43}$$

The three solutions agree to the first order; the Burnett and 13-moment solutions agree to the second order.

We see by inspection that in the zero-th approximation the speed is constant and the attenuation is zero; the first approximation introduces the « classical attenuation » (proportional to the square of the frequency) and the second, a dispersion in the speed.

The expansions are not useful except for large r. The situation is most easily studied in the Navier-Stokes case. The solution of eq. (38) is

$$k^2 = \frac{5}{3} r \frac{r + (23/10)i \pm (r^2 - 49/100 + ir)^{\frac{1}{2}}}{4 - 3ir}, \tag{44}$$

in which the root associated with the minus sign corresponds to k_{I} (the « I-wave »). The right-hand side of eq. (44), as a function of $1/r$, has singularities at $1/r = (50i \pm 20\sqrt{6})/49$, so that eq. (41) converges only for $r > 7/10$. The solutions of eqs. (38), (39), (40) are best got numerically, and it is found that the series solutions converge too slowly to be of use unless the dispersion is small [17].

The so-called « II-wave », which corresponds to the plus sign in eq. (44) resembles a diffusive wave ($\alpha = \beta$) such as occurs in the elementary theory of heat conduction.

The solution for the I-wave (Navier-Stokes) is depicted in Fig. 1 (dashed lines). It is seen that for r less than about 6, the speed of the I-wave increases monotonically with decreasing r, and α/β_0 for this wave becomes less than the « classical value » and eventually decreases with decreasing r after a maximum at r about 0.8 ($f_0/f \approx 6$). The speed of the II-wave is always less, and the attenuation more than that of the I-wave. In the limit of low r, the waves are indistinguishable and diffusive ($\alpha = \beta$).

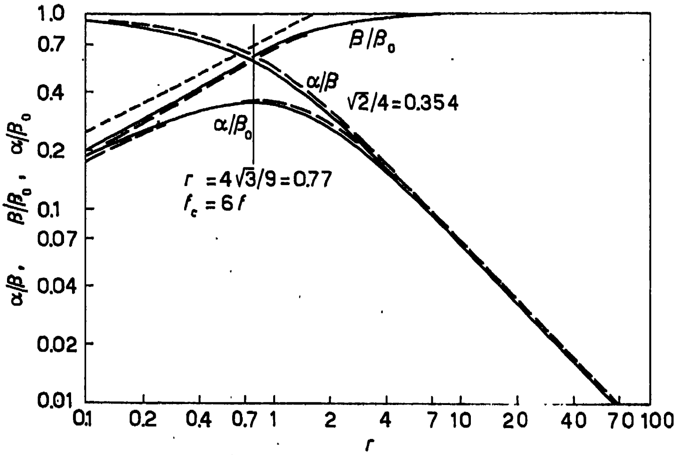

Fig. 1. – Solution of the Navier-Stokes equation for a monatomic gas (I-wave) and for a Becker gas (I-wave and II-wave). The latter represents polyatomic gases within the accuracy of the plot. —— factorized; — — $\gamma = \frac{5}{3}$.

Our equations predict that the speed of sound (I-wave) should be 1 % above its normal value for $r \approx 8$. For He at room temperature this corresponds to about 100 MHz/atm and $f_c/f \approx 61$. The increase is about 10 % for $r = 2.4$ (325 MHz/atm, $f_c/f \approx 19$). The maximum value of α/β_0 is about 0.36. In Kr at 11 MHz and room temperature this amounts to an attenuation of about 10^4 db/cm, or 1 db/μm.

It is sometimes convenient to have an approximate solution for the I-wave of eq. (44). The expression

$$k_I = i\left(1+\frac{7}{5}\frac{i}{r}\right)^{-\frac{1}{2}} \tag{45}$$

furnishes a remarkable fit. The expression for large r is

$$k_I = i + \frac{7}{10}\frac{1}{r} - \frac{147}{200}\frac{i}{r^2} - \frac{1715}{16\cdot 5^3}\frac{1}{r^3} + \dots,$$

which should be compared to eq. (41). The maximum value of α/β_0 from eq. (45) is about 0.35 at $r \approx 0.7$, with $\beta/\beta_0 \approx 0.61$; the corresponding values from eq. (44) are 0.36, 0.8, and 0.61.

Figure 2 shows the I-wave for Navier-Stokes (full line) and Burnett (dashed

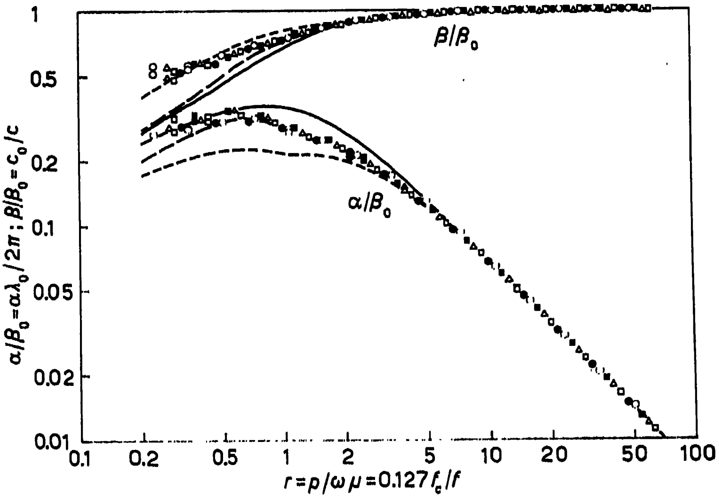

Fig. 2. – Results in five monatomic gases. Full line, NAVIER-STOKES; dashed line, BURNETT; dotted line, super-BURNETT. All I-wave: ○ He; ● Ne; □ A; ■ Kr; △ Xe.

line). The dotted line is for a « super Burnett » solution (fourth order approximation) which we do not discuss here.

The 13-moment solution is not graphed. The attenutation agrees well with the other cases for $r > 6$ or so, but it peaks at r about 2 and falls off rapidly for smaller r. The speed is in good agreement for $r > 1$. However, the shape of the β/β_0 *vs.* r-curve is radically different from that of the other theories; it has an S-shaped transition between a high-and a low-frequency speed, the ratio being about 1.65. This is a most interesting feature of the 13-moment solution, as we shall see later on when we discuss the experimental results.

3'4.2. Polyatomic gas, Becker gas. Solutions to eq. (36), (37) for any polyatomic gas, characterized by a specific value of γ_0, a relation between γ and r obtained from relaxation theory, and a relation between s and r got from experiment or given by the Eucken formula, eq. (30), or some other expression, are easily calculated. However, we turn to a simpler, and perhaps more interesting, attack.

It was discovered by BECKER [18] that the shock-wave equation for the Navier-Stokes case has an explicit solution if $r/s = 4\gamma_0/3$. It turns out that eq. (36) has a particularly simple form for such a «Becker» gas. Furthermore, the diatomic dumb-bell molecule and the rigid nonsymmetrical molecule are good approximations to a Becker gas; the values of $4\gamma_0/3$ are 1.867 and 1.778, respectively, which are close to the corresponding values given by Euken's formula (30), namely 1.900 and 1.750. Even for $\gamma_0 = 9/7$ (diatomic dumb-bell plus vibration) the difference in r/s is only 4.4%.

For a Becker gas affected by relaxation we write $r/s = 4\gamma/3$, following the argument already used in connection with the Eucken relation (30). Equation (36) is now

$$\frac{4}{3}\frac{\gamma}{\gamma_0^2}\frac{k^4}{r}\left(i-\frac{4}{3}\frac{1}{r}\right)+\frac{k^2}{\gamma_0}\left[\gamma+\frac{4}{3}\frac{i}{r}(\gamma+1)\right]+1=0; \tag{46}$$

which factors into [19]

$$\left(\frac{4}{3}\frac{ik^2}{\gamma_0 r}+1\right)\left[\left(1+\frac{4}{3}\frac{i}{r}\right)\frac{\gamma k^2}{\gamma_0}+1\right]=0,$$

so that

$$k_{\text{II}}^2 = \tfrac{3}{4} i\gamma_0 r = is, \tag{47}$$

which is exactly the result of the elementary theory of heat conduction, and

$$k_{\text{I}}^2 = -\frac{\gamma_0}{\gamma}\left(1+\frac{4}{3}\frac{i}{r}\right)^{-1}. \tag{48}$$

We concentrate our attention on the I-wave, and drop the subscript. If relaxation were absent, then we would have $\gamma = \gamma_0$ in eq. (48) and

$$k_i^2 = -\left(1+\frac{4}{3}\frac{i}{r}\right)^{-1}. \tag{49}$$

On the other hand, the theory of relaxation (in which translational effects are ignored) gives

$$k_r^2 = -\gamma_0/\gamma \,. \tag{50}$$

Therefore, from eq. (48)

$$k = -ik_t k_r \,. \tag{51}$$

Equation (51), which provides a simple algorithm for the combination of translational and relaxational effects in a Becker gas, is probably adequate for a real gas. We would expect it to be useful even in cases other than Navier-Stokes. It subsumes the rules

$$\frac{\alpha}{\beta_0} = \frac{\alpha_t}{\beta_0}\frac{\beta_r}{\beta_0} + \frac{\alpha_r}{\beta_0}\frac{\beta_t}{\beta_0}, \tag{52}$$

and

$$\frac{\beta}{\beta_0} = \frac{\beta_t}{\beta_0}\frac{\beta_r}{\beta_0} - \frac{\alpha_t}{\beta_0}\frac{\alpha_r}{\beta_0}. \tag{53}$$

Equation (52) shows that the total attenuation is always less than the sum of the attenuations computed separately. Also,

$$\frac{\alpha}{\beta} = \frac{\alpha_t\beta_r + \alpha_r\beta_t}{\beta_r\beta_t - \alpha_r\alpha_t}, \tag{54}$$

and if $\alpha_r\alpha_t \ll \beta_r\beta_t$ as is usually the case,

$$\frac{\alpha}{\beta} \approx \frac{\alpha_t}{\beta_t} + \frac{\alpha_r}{\beta_r}, \tag{55}$$

so that the attenuations par actual radian phase shift are additive, approximately. When the dispersions are negligible the attenuations themselves add directly. With the same approximation eq. (53) gives

$$c \approx c_t c_r/c_0 \,, \tag{56}$$

and it is easily seen that the separate speed increments add if they are small.

It is easy to examine eq. (49) analytically and gain some insight into the structure of the I-wave solution for a Becker gas. (The approximate solution, eq. (45), for a monatomic gas can be treated in the same way.) Equation (49) is equivalent to

$$(57)\qquad \left(\frac{\alpha, \beta}{\beta_0}\right)^2 = \frac{1}{2}\left[\left(1+\frac{16}{9}\frac{1}{r^2}\right)^{\frac{1}{2}} \mp 1\right]\left(1+\frac{16}{9}\frac{1}{r^2}\right)^{-1},$$

from which it is easily shown that α/β_0 has a maximum value of $\sqrt{2}/4$ (≈ 0.35) at $r = 4\sqrt{3}/9$ (≈ 0.77; $f_c/f \approx 6$). The corresponding value of $\beta_0/\beta = c/c_0$ is 1.63.

In Fig. 1, the solid lines are for the I-wave of a Becker gas. They represent also, within the accuracy of the plot, any Navier-Stokes polyatomic gas which obeys the Eucken relation. The dotted line gives both the real and imaginary parts of k_{II}.

The interpretation of experimental data on polyatomic gases is beset by a difficulty, namely that there is no good *a priori* way to separate the translational and relaxational effects. If the translational effects were known, a reasonable point of view would be to regard the experiment as measuring the relaxational effects. This entails a knowledge of how the effects combine, and as we have already remarked, we cannot at present do better than to apply the rule of eq. (51) even though it is especially appropriate to a Becker gas in the Navier-Stokes case. As for the translational effects, we have to fall back on the experimental results for monatomic gases. As we shall see these are fitted best by the Burnett equation, and we therefore assume that, relaxation aside, eq. (37) evaluated for the appropriate value of γ_0 (with $\gamma = \gamma_0$) is adequate.

In particular we are interested in diatomic gases. Taking $\gamma = \gamma_0 = \frac{7}{5}$, eq. (37) becomes

$$(58)\qquad k^6 \frac{4}{7^3}\frac{1}{rs}\left(-\frac{5^3}{3}\frac{i}{r} - \frac{40}{3}\frac{1}{r^2} + \frac{18}{rs} - \frac{6}{s^2}\right) + k^4 \frac{1}{7^2}\left(25\frac{i}{s} - \frac{140}{3}\frac{1}{r^2} - \frac{52}{3}\frac{1}{rs} - \frac{6}{s^2}\right) +$$
$$+ k^2\left[1 + \frac{5}{7}i\left(\frac{1}{s} + \frac{4}{3}\frac{1}{r}\right)\right] + 1 = 0\,.$$

The expansion for the I-wave is

$$(59)\qquad k = i + \frac{5}{7}\left(\frac{2}{3}\frac{1}{r} + \frac{1}{7}\frac{1}{s}\right) - \frac{i}{7^2}\left(\frac{40}{r^2} + \frac{82}{21}\frac{1}{rs} + \frac{17}{14}\frac{1}{s^2}\right) -$$
$$- \frac{5^2}{7^3}\left(\frac{520}{27}\frac{1}{r^3} + \frac{32}{9}\frac{1}{r^2 s} + \frac{17}{21}\frac{1}{rs^2} + \frac{5^2}{2\cdot 7^3}\frac{1}{s^3}\right) + \dots\,.$$

If the Eucken relation (eq. (30)) $r/s = 19/10$ holds, eq. (59) is

$$(60)\qquad k = i + 0.6701/r - 1.0572\, i/r^2 - 2.1273/r^3 + \dots\,.$$

These expressions are used in the processing of data on gases such as O_2 and N_2 in order to get rotational collision numbers [20].

For the most part, we restrict our further attention to monatomic gases.

3·5. *Another attack.* – The critical step in the methods so far described is the selection of suitable expressions for T_{xx} and q. These have to be obtained by approximation from the highly nonlinear Boltzmann equation even though the conservation equations, into which they are inserted, are later on linearized.

WANG CHANG and UHLENBECK [21] linearize the one-dimensional Boltzmann equation *ab initio* and insert immediately the space- and time-dependence $\exp[-\Gamma x + i\omega t]$. The solution is in the form of an infinite determinant. At each stage of approximation one has a finite determinant and a series expansion in $1/r$. In this way expressions similar to, but not identical with the third-order Navier-Stokes, and fifth-order Burnett, equations for Maxwellian molecules were obtained.

PEKERIS [22] has attempted to circumvent the convergence difficulties associated with expansions in powers of $1/r$ by numerical solution of each finite approximating determinant up to that of order 20. Later, PEKERIS *et al.* [23] continued the work up to order 483. For $r >$ about 0.6, the results are closely the same as for order 225, indicating good convergence for this range.

4. – Experimental methods.

4·1. *General.* – The techniques for measurement of α and c in rarefied gases are in principle the same as those commonly used in denser fluids. Various refinements are usually incorporated in order to overcome the difficulties resulting from the very large attenuations encountered and from the low characteristic impedance of the medium. On account of this latter, a substantial velocity-amplitude at the transducer produces a disappointingly low sound pressure. The upshot is that the received signals are so minute as to raise severe problems with respect to both signal-to-noise ratio and discrimination against electrical and mechanical cross-talk.

The methods divide themselves naturally into pulse-modulated (pulse) and continuous-wave (cw). The advantages of pulse methods include freedom from standing waves and the almost automatic discrimination (in time) against cross-talk. The poor signal-to-noise ratio associated with the necessarily large bandwidth inherent in a pulse system is its main disadvantage. The useful range does not, at present, extend beyond about 50 MHz/atm which is well below the region of appreciable translational dispersion. For this reason we do not consider pulse methods in detail, but it is worth noting that very good measurements have been made by a number of investigators, beginning with PARKER *et al.* [24]. These measurements are valuable not only for the problems they were designed to solve, but also because they provide a desirable check on the cw measurements within the range of overlap.

4.2. *Single-crystal interferometer.* – The ordinary single-crystal interferometer has been widely applied to our problem, with results that in many cases are surprisingly good, considering the inherent limitations of the instrument. To explain these we need to consider briefly the principle of operation.

The instrument may be thought of as a column of gas terminated at one end by a solid reflector, and at the other by a transducer, usually an x-cut quartz thickness expander. One or the other termination is movable to allow the length of the gas column, x, to be varied by accurately known amounts. The input impedance at the electrical terminals of the transducer, at its resonant frequency *in vacuo*, is measured as a function of x. Ordinarily only the magnitude of the impedance is measured; this is conveniently done by measurement of the voltage on the transducer driven from a constant-current (high-impedance) source. Such an arrangement is provided by the ordinary Q-meter circuit, which also provides a simple means of eliminating the effect of the static capacity of the transducer.

To simplify the analysis we consider a case for which the losses in the crystal are nil and the impedance of the reflector is infinite, although these are not necessary assumptions. Then under the supposition that the sound waves in the medium are plane, the input impedance in question is

$$z = Az_0 \operatorname{ctgh} \Gamma x = Az_0 \frac{1 + i \operatorname{tgh} \alpha x \operatorname{tg} \beta x}{\operatorname{tgh} \alpha x + i \operatorname{tg} \beta x}, \tag{61}$$

in which A is a constant and z_0 is the characteristic impedance, also a (complex) constant. The voltage measured on the transducer is proportional to

$$|z| = |Az_0| \left(\frac{1 + \operatorname{tgh}^2 \alpha x \operatorname{tg}^2 \beta x}{\operatorname{tgh}^2 \alpha x + \operatorname{tg}^2 \beta x}\right)^{\frac{1}{2}}. \tag{62}$$

It is easily shown that the graph of $|z|$ *vs.* x is a damped oscillatory curve of which the upper peaks are tangent to the curve $|z| = |Az_0| \operatorname{ctgh} \alpha x$, and the lower, to $|z| = |Az_0| \operatorname{tgh} \alpha x$. The points of tangency are those for which βx is an even or odd multiple of $\pi/2$, respectively.

If αx is so small that $\operatorname{tgh} \alpha x \ll 1$, the curve described has a sharply defined structure from which α and β can be evaluated. But for αx so large that $\operatorname{tgh} \alpha x$ is nearly unity, $|z|$ is nearly constant and eq. (62) gives no information. As eq. (61) shows, it is also of no avail to measure the phase of z under these circumstances.

Thus the utility of the ordinary interferometer is confined to the region of high standing-wave ratio. The implication is twofold; first, the smallest value of r that can be reached is about 20, and the accuracy is poor even at considerably larger values, and second, the transverse modes associated with resonant conditions introduce errors which are difficult to evaluate [25]. The Stewarts' work with hydrogen [26] furnishes a good example of the single-crystal interferometer technique [27].

4·3. *Double-crystal interferometer.* – In the so-called double-crystal interferometer, the shortcomings described above are mostly eliminated, but at the cost of increased complexity. The column of gas is terminated by two transducers, of which one serves as a sender and the other as a receiver. The principle may be illustrated by consideration of one of several possible modes of operation. We suppose the static capacities of the two crystals annulled at the operating frequency by tunable inductors. The sender is driven at the common resonant frequency of the two transducers from a high-impedance source (constant current, I_s) and the receiver is terminated on the electrical end by a high-impedance preamplifier. Then the voltage on the receiver is

$$E_R = Az_0 I_s \operatorname{csech} \Gamma x = \frac{Az_0 I_s}{\sinh \alpha x \cos \beta x + i \cosh \alpha x \sin \beta x}, \tag{63}$$

so that

$$\frac{|E_R|}{|Az_0 I_s|} = (\sinh^2 \alpha x + \sin^2 \beta x)^{-\frac{1}{2}}, \tag{64}$$

and

$$\varphi = \arg \frac{E_R}{Az_0 I_s} = -\operatorname{tg}^{-1} (\operatorname{ctgh} \alpha x \operatorname{tg} \beta x). \tag{65}$$

When αx is small, $|E_R|$ (eq. (64)) undergoes periodic variations as $\sin \beta x$ oscillates between plus and minus one, and the variable part of the phase φ (eq. (65)) shifts rather abruptly between plus and minus $\pi/2$, $\operatorname{ctgh} \alpha x$ being large. However, we make no use of this region of high standing-wave ratio, and thus we avoid the effect of transverse modes. Instead, for a particular value of α, we make the smallest value of x so large that $\sinh \alpha x \gg 1$ and $\operatorname{ctgh} \alpha x \simeq 1$. Then from eqs. (64), (65) $|E_R|$ varies like $\exp[-\alpha x]$ and φ like $-\beta x$. The slope of a graph which gives the logarithm of anything proportional to $|E_R|$ *vs.* x gives α directly, and β is similarly obtained from a plot of φ (relative to I_s) *vs.* x.

The first such instrument to be built and adapted to the present purpose was fitted with quartz crystals and operated at a fixed frequency of 1 MHz [28].

It was superseded by an 11 MHz instrument of greater refinement [29]. The amplitude is presented by a recorder having a logarithmic characteristic and the phase by a conventional recorder; these recorders are driven synchronously with motion of the transmitter crystal.

The amplitude-measuring system is of the single-conversion superheterodyne type, with an intermediate frequency (I.F.) of about 440 kHz. The overall bandwidth, set by a crystal filter at the I.F., is 23 Hz.

The signal at the output, together with a reference signal are both converted to about 4 kHz before phase measurement. The phase of the reference, which ordinarily remains fixed, is instead uniformly advanced at an accurately known rate nearly equal to the rate at which the output phase is advanced by the change in acoustic path length. The errors in the phase meter are now less important, for the meter measures only a small difference between the (variable) reference and the unknown phases [30].

The overall gain from the receiving crystal to the rectifier, which is at the input of the amplitude recorder, can be varied from -10 to $+120$ db. The neutralization can be adjusted so that the total output, in the absence of signal, is about 1.5 db above the noise, which is about $3\cdot10^{-8}$ V referred to the input.

As the pressure is lowered, the useful length of the record reduces to one wavelength at about $r=0.1$ (10^{10} Hz/atm in A). The attenuation does not get larger for smaller r, but the sound pressure levels do; the accuracy rapidly deteriorates and at r about 0.01 the instrument reaches the end of its useful range.

An instrument similar to the above, but equipped with solid dielectric electrostatic transducers, has been used with very considerable success by MEYER and SESSLER [31]. These « Sell » transducers [32] are made by stretching a thin, metallized plastic membrane (say about 10 μm thick) over a metal backplate. The resonant frequency of a typical unit is in the 50 to several hundred kilohertz range, and changes with external pressure and with polarizing voltage. The resonance is very broad and the transducers need to be matched only roughly.

The several instruments of this type which have been built at the III Physikalisches Institut, Göttingen, operate over the range of r from 0.01 to 100 and at frequencies of from 100 to 600 kHz. The data are taken point by point. The amplitude-measuring system has a bandwidth of 100 Hz; a cosine voltmeter (lock-in amplifier) is used for the phase determination.

Our own work at the National Bureau of Standards has been done mostly at 11 MHz, that at the III Institute mostly at 100 or 200 kHz. The question naturally arises as to whether, for a given value of r, it is better to use a high or a low frequency and pressure. The higher the frequency, the shorter is the useful path length and the greater the demands on the accuracy of the screw. On the other hand, in a low-pressure system it is more difficult to maintain gas purity. For a particular laboratory, the best compromise depends on the displacement-measuring and vacuum techniques available.

5. – Results and discussion.

The results of measurements at the National Bureau of Standards [30] on five monatomic gases are shown in Fig. 2. It is seen that all five gases behave in substantially the same way. The frequency in all cases was about 11 MHz. For argon, there are also available data taken at 100 and 200 kHz for $r < 20$ by MEYER and SESSLER [31]. Their results are practically the same.

In the nondispersive range ($r >$ about 10) where the various theories are nearly indistinguishable, the measured values agree with the calculated ones very closely. That is to say, the so-called « classical » theory is verified for monatomic gases.

The Burnett theory appears to be satisfactory for $r >$ about 0.5 to 1. The dotted line in Fig. 2 is for a « super-Burnett » theory [30], [33] calculated by Wang Chang and Uhlenbeck, which we have so far not discussed. The super-Burnett expression corresponds to the fourth approximation to the velocity-distribution function. Experiment indicates it to be far inferior to the Burnett expression; the arguments about convergence of solutions of this type (« normal » solutions) are thus given additional meaning.

The calculation of PEKERIS *et al.* [23] reproduces the data about as well as does Burnett's expression, but for low values of r the two are very different. It should be noted that Pekeris' result represents an approximation of much higher order than does that of Burnett.

We have already noted that the 13-moment expression gives a poor value for α if $r <$ about 6. However, β is not too bad for $r > 1$. For $r < 1$, β/β_0 levels off to about 0.6. This is of particular interest because measurements, not shown in Fig. 2, have actually been carried out down to $r = 0.01$. Such data on argon are given by MEYER and SESSLER [31]. What is found is a leveling off of β/β_0 to about 0.5, and of α/β_0 to about 0.25. This raises the interesting possibility that some modification of the 13-moment solution is possible. However, other considerations are important to any interpretation of the results for low r. For one thing the attenuation of the II-wave in this region is not much more than that of the I-wave, so that it is probable that what is observed is a mixture of (at least) two types of wave. Furthermore, the measurements in the region of low r are made with a total sound path of length comparable to the mean free path. Thus, the propagation is not entirely a collisional process, particularly at very low r. Such processes are discussed in Section 7.

6. – Mixtures.

The subiect of mixtures is somewhat beyond our scope, as the experiments and theory have been carried out in the nondispersive region only. Nevertheless, it is of interest to note the present status. So far, calculations have been made of the necessary corrections to the first two terms of eq. (41) for an ideal gas mixture; to this approximation the speed c will be independent of frequency and the attenuation α proportional to its square.

We study a binary mixture; the mole (or number) fractions are x_1 and x_2 $(x_1+x_2=1)$. The molecular weight of the mixture is

$$M = x_1 M_1 + x_2 M_2 \,, \tag{66}$$

so that on account of unmixing, there is an additional state variable, M, or alternatively, x_1 or x_2. There is also an additional dynamical variable, as we are now concerned with two flow velocities, u_1 and u_2. The velocity u which appears in the conservation equations is the mass velocity given by

$$\varrho u = \varrho_1 u_1 + \varrho_2 u_2 \,, \tag{67}$$

ϱ_1 and ϱ_2 being the partial densities $(\varrho_1+\varrho_2=\varrho)$.

The effect of the unmixing is to change the form of the heat flux q in the energy equation, eq. (33) for example. The stress tensor in the present (second) approximation is unchanged (CHAPMAN and COWLING [2], p. 146). The heat flux ([2], p. 145), as generalized to polyatomic gases by KOHLER [34, 35], to whom the calculation of α is due, is, in one dimension,

$$q = -\nu\frac{\partial T}{\partial x} + p\left[\frac{\gamma_1 x_1}{\gamma_1 - 1}(u_1 - u) + \frac{\gamma_2 x_2}{\gamma_2 - 1}(u_2 - u) + k_T(u_1 - u_2)\right], \tag{68}$$

where k_T is the thermal diffusion ratio. The ratio k_T is of particular interest because it is the only transport coefficient which is very sensitive to the intermolecular force law; for Maxwellian molecules it vanishes.

The ordinary theory, then, needs to be modified only by substitution of eq. (68) for the simple expression $q=-\nu(\partial T/\partial x)$. However, two additional equations are required because of the increased number of variables. One is obtained by splitting the mass equation (such as eq. (6)) into two, one for each component of the mixture. The other is the general diffusion equation (CHAPMAN and COWLING [2], p. 144; KOHLER [35]), which is, for one dimension,

$$u_1 - u_2 = -\frac{D_{12}}{x_1 x_2 p}\left(\frac{\varrho_2}{\varrho}\frac{\partial p_1}{\partial x} - \frac{\varrho_1}{\varrho}\frac{\partial p_2}{\partial x} + \frac{p k_T}{T}\frac{\partial T}{\partial x}\right), \tag{69}$$

in which D_{12} is the coefficient of diffusion, and p_1 and p_2 are the partial pressures x_1p and x_2p. Note that D_{12} relates to the diffusion caused by a concentration gradient, and $k_T D_{12}$ to that caused by a thermal gradient.

The equations are combined as in Section 3·4; the calculations are tedious even for the case $\gamma_1 = \gamma_2 = \gamma$ to which we now restrict ourselves. For the sound speed c_0 we get the expected result,

$$c_0^2 = \gamma(RT/M)\,,$$

where γ is that for the mixture, *i.e.*

$$\gamma = 1 + R/(c_{v,1}x_1 + c_{v,2}x_2)\,. \tag{70}$$

The c's are the molar specific heats. The attenuation is given by

$$\frac{\alpha p_0}{\omega^2} = \frac{2\mu}{3c_0\gamma} + \frac{(\gamma-1)\nu}{2\gamma c_0 c_p} + \frac{x_1 x_2 \varrho_0 D_{12}}{2c_0}\left(\frac{M_2 - M_1}{M} + \frac{\gamma-1}{\gamma}\,\frac{k_T}{x_1 x_2}\right)^2. \tag{71}$$

In eq. (71) the four transport coefficients are for the mixture in question, and must be measured or calculated for each. Otherwise the form is as that for a one-component gas, except for the additional term representing the effect of diffusion. A large effect is to be expected when $M_2 - M_1$ is large, as for instance when one component is helium. For air, the attenuation due to diffusion is only 0.3 % of the total, where as in He-Kr it may account for 60 % of the total.

Holmes and Tempest [36], utilizing a pulse technique [37] have measured α and c_0 in a A-He mixture, and α in the mixtures Ne-He and Kr-He over the entire concentration range and at various pressure. They estimate the accuracy of the measurements at about 2 % and that of the calculations at about 5 %. In all cases the agreement between calculation and experiment is within the maximum possible error of 7 %.

Similar measurements in A-He had been made by Petralia [38] at 3 MHz by interferometer. He obtained the expected variation with concentration, but α was about 50 % high. It is likely that the discrepancy is due to experimental error.

7. – Free-molecule propagation.

We have already seen that one limitation on measurements of Γ in gases at small r is that the length of the sound path is comparable to the mean free path; at least this is so in existing equipment. It is easy to frame an elementary theory for the case of no collisions [39]. (This requires, among other things, that the boundary conditions be stochastic.)

Consider two parallel walls, separated by a gap, h. One wall, the source, has a prescribed axial motion, $u_0(t)$. The thermal velocity $\bar{u}$ at the source has a Maxwellian distribution appropriate to the temperature, and we suppose that the axial component u for each molecule as it is emitted from the source is increased by the amount u_0, small relative to u. At any time t, the velocity of a molecule at the wall (the receiver) is that which existed at the source at time $t - h/u$. If, at the source, $u_0(t) = u_0 \exp[i\omega t]$, then at time t the non-thermal velocity of a molecule at the receiver is $u_0 \exp[i\omega(t - h/u)]$. Supposing the boundary condition to be stochastic, the excess pressure is

$$\delta p = m u_0 \int_0^\infty f_1(u) \exp[i\omega(t - h/u)]\,\mathrm{d}u\,, \tag{72}$$

where $f_1(u)\,\mathrm{d}u$ is the number of molecules approaching the receiver per unit area per unit time with axial velocity in the range u to $u + \mathrm{d}u$. The distribution function [40] in question is (KENNARD [11], p. 64)

$$f_1(u) = \frac{nb}{\sqrt{\pi}}\, u \exp[-b^2 u^2]\,, \tag{73}$$

where n is the number density and $b^2 = 1/2RT$, so that with $nm = \varrho$,

$$\delta p = \varrho u_0 b \pi^{-\frac{1}{2}} \int_0^\infty \exp\left[-b^2 u^2 + i\omega\left(t - \frac{h}{u}\right)\right] u\,\mathrm{d}u\,,$$

which with the substitutions $x = b\omega h$, $v = bu$ becomes, after suppressing the time factor,

$$\delta p = \frac{\varrho u_0}{b\sqrt{\pi}} \int_0^\infty \exp\left[-v^2 - \frac{ix}{v}\right] v\,\mathrm{d}v\,. \tag{74}$$

The form of eq. (74) is independent of the pressure. The integral

$$g(ix) = 2\int_0^\infty \exp\left[-v^2 - \frac{ix}{v}\right] v\,\mathrm{d}v\,; \tag{75}$$

has been extensively studied. A survey is given by ABRAMOWITZ [41]. A series

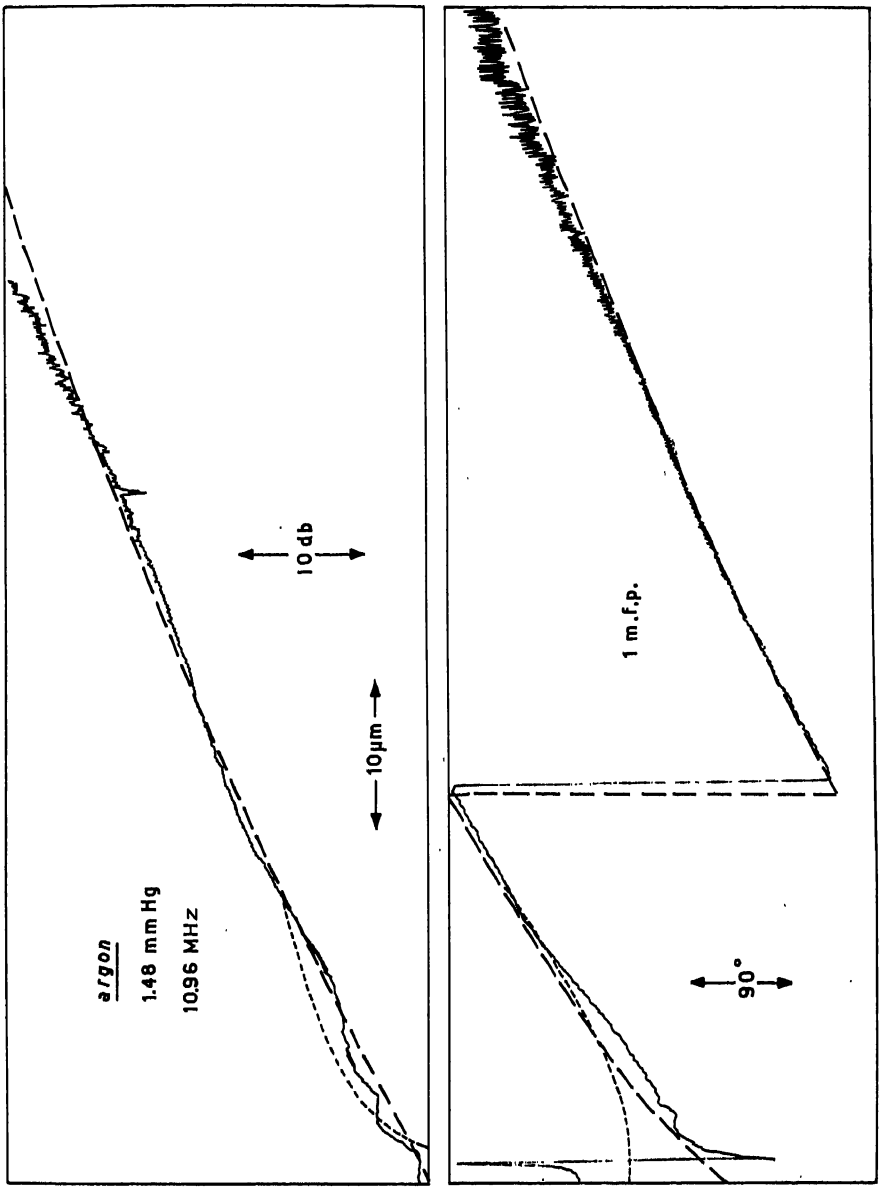

Fig. 3. – Free molecule propagation. See text.

expansion is useful for small x and an asymptotic expression for large x. These are

$$g(ix) = 1 - i\sqrt{\pi}\,x + (\bar{\gamma} - 3 + i\pi + \log x)\,x^2/2 + \dots\,, \tag{76}$$

and

$$g(ix) \sim \frac{2\sqrt{\pi}}{3}\left(\frac{ix}{2}\right)^{\frac{1}{3}} \exp\left[-3\left(\frac{ix}{2}\right)^{\frac{2}{3}}\right]\left[1 + \frac{5}{36}\left(\frac{2}{ix}\right)^{\frac{2}{3}} + \dots\,. \tag{77}$$

In eq. (76) $\bar{\gamma}$ is Euler's constant, 0.577... .

At $h = 0$, the phase velocity is $(2/\gamma\pi)^{\frac{1}{2}}c_0$, and as h increases, the phase velocity ultimately varies as the cube root of (ωh). There is thus no attenuation or phase velocity in the ordinary sense. However, the magnitude and phase of δp as a function of h can be calculated and compared with experiment. Figure 3 shows the results [39] of tests made with an 11 MHz interferometer [29] on argon at $p = 1.48$ mm Hg. The gap h is zero at the left and increases toward the right; the full range of the chart is just over 2 mean free paths. The upper chart shows the amplitude on a logarithmic scale (full range = 4 neper) decreasing upwards. The lower chart is the phase on a linear scale (full range 2π); the abrupt change is a shift of 2π which the recorder makes to get back on scale. The jittery lines are the actual traces, and the dashed lines are computed from eqs. (76), (77). The agreement is remarkably good. The theory is easily modified to allow for specular reflection (but not for the collisions entailed), and the dotted lines are calculated for a reflection coefficient of unity. The results are very little different except near the source.

Many other experiments were made. The agreement for A at 0.5 mm Hg was not as good as at the higher pressure, and at 0.16 mm Hg, was poor. Similar results were obtained in He, N_2, H_2 and air. One would expect better agreement at the lower pressures; on the other hand the accuracy then deteriorates, so that it is hard to evaluate these results.

REFERENCES

[1] S. T. PRESTON: *Phil. Mag.*, **3**, 453 (1877).

[2] For all references herein to the Boltzmann equation, see S. CHAPMAN and T. G. COWLING: *The Mathematical Theory of Non-Uniform Gases* (Cambridge, 1952). Also in paperback (1960).

[3] D. ENSKOG: *Svensk. Acad. Handl.*, **63**, 18 (1922).

[4] L. TISZA: *Phys. Rev.*, **61**, 531 (1942).

[5] K. F. HERZFELD and T. A. LITOVITZ: *Absorption and Dispersion of Ultrasonic Waves* (New York, 1959), p. 156.

[6] E. U. CONDON and H. ODISHAW: *Handbook of Physics* (New York, 1958), p. 54.

[7] H. W. WOOLLEY and W. S. BENEDICT: *Generalized tables of corrections to the thermodynamic properties of non-polar gases*, NACA Technical Note 3272 (1956).

[8] J. O. HIRSCHFELDER, R. B. BIRD and E. L. SPOTZ: *Chem. Revs.*, **44**, 205 (1949).

[9] C. S. WANG CHANG and G. E. UHLENBECK: *On the transport phenomena in rarefied gases*, in *Appl. Phys. Lab.*, Johns Hopkins University CM-433, UMH-3-F (1948).

[10] H. GRAD: *Comm. Pure and Appl. Math.*, **2**, 331 (1949).

[11] E. H. KENNARD: *Kinetic Theory of Gases* (New York, 1938), p. 179, 177.

[12] E. IKENBERRY and C. TRUESDELL: *Journ. Rational Mech. Anal.*, **5**, 1 (1956).

[13] C. TRUESDELL: *Journ. Rational Mech. Anal.*, **5**, 55 (1956).

[14] H. GRAD: *Principles of the kinetic theory of gases*, in *Thermodynamics of Gases*, vol. **12** of Encyclopedia of Physics (Berlin, 1958).

[15] W. H. KEESOM: *Helium* (Amsterdam, 1942).

[16] Equation (36) with $\gamma=\gamma_0$ has been studied exhaustively by C. TRUESDELL: *Journ. Rational Mech. Anal.*, **2**, 643 (1953).

[17] M. GREENSPAN: *Phys. Rev.*, **75**, 197 (1949).

[18] R. BECKER: *Zeits. Phys.*, **8**, 321 (1922).

[19] M. GREENSPAN: *Journ. Acoustical Soc. Am.*, **26**, 70 (1954). This result, but for the nonrelaxing case ($\gamma=\gamma_0$) was discovered and communicated to me in 1951 by D. P. JOHNSON and A. IBERALL (see M. GREESPAN: *Journ. Acoustical Soc. Am.*, **25**, 191 (1953)). It was independently discovered by TRUESDELL [16], p. 718. Our «Becker» gas is the same as Truesdell's «pseudopiezic» fluid.

[20] M. GREENSPAN: *Journ. Acoustical Soc. Am.*, **31**, 155 (1959).

[21] C. S. WANG CHANG and G. E. UHLENBECK: *On the propagation of sound in monatomic gases*, Engg. Research Inst., University of Michigan project M 999, ONR contract N6onr-23222 (Oct. 1952).

[22] C. L. PEKERIS: *Propagation of sound in a rarefied maxwellian gas*, UCLA Inst. of Geophys., ONR contract Nonr-233(18) (Dec. 1953).

[23] PEKERIS, ALTERMAN and FINKELSTEIN: *Propagation of sound in a rarefied gas*, Air Force Cambridge Research Center, Document no. AFCRL- 677 (Jan. 1961).

[24] J. G. PARKER, C. E. ADAMS and R. M. STAVSETH: *Journ. Acoustical Soc. Am.*, **25**, 263 (1953).

[25] P. E. KRASNOOSHKIN: *Phys. Rev.*, **65**, 190 (1944).

[26] J. L. STEWART and E. S. STEWART: *Journ. Acoustical Soc. Am.*, **24**, 194 (1952).

[27] J. L. STEWART and E. S. STEWART: *Journ. Acoustical Soc. Am.*, **24**, 22 (1952).

[28] M. GREENSPAN: *Journ. Acoustical Soc. Am.*, **22**, 568 (1950).

[29] M. GREENSPAN and M. C. THOMPSON Jr.: *Journ. Acoustical Soc. Am.*, **25**, 92 (1953).

[30] M. GREENSPAN: *Journ. Acoustical Soc. Am.*, **28**, 644 (1956).

[31] E. MEYER and G. SESSLER: *Zeits. f. Phys.*, **149**, 15 (1957).

[32] W. KUHL, G. R. SCHODDER and F. K. SCHRÖDER: *Acustica*, **4**, 519 (1954).

[33] C. S. WANG CHANG: Personal communication.

[34] M. KOHLER: *Ann. d. Phys.*, **39**, 209 (1941).

[35] M. KOHLER: *Zeits. f. Phys.*, **127**, 41 (1949).

[36] R. HOLMES and W. TEMPEST: *Proc. Phys. Soc. (London)*, **75**, 898 (1960).

[37] W. TEMPEST and H. D. PARBROOK: *Acustica*, **7**, 354 (1957).

[38] S. Petralia: *Nuovo Cimento*, **11**, 570 (1954).

[39] R. K. Cook, M. Greenspan and M. C. Thompson Jr.: *Journ. Acoustical Soc. Am.*, **25**, 192 (1953).

[40] In a similar analysis, Meyer and Sessler [31] use the distribution function which gives the fraction of molecules *per unit volume* with u in du. I think this is incorrect.

[41] M. Abramowitz: *Journ. Math. and Phys.*, **32**, 188 (1953).

Dispersion and Absorption of Sound by Molecular Processes: Thermal Relaxation in Liquids.

J. Lamb

Department of Electrical Engineering, The University - Glasgow

1. – Introduction.

Propagation of a sound wave through a liquid takes place adiabatically, except at very high frequencies which are outside the range at present available experimentally. Thus, as the pressure in the liquid alternates sinusoidally about the static or ambient pressure at a frequency $f\,(=\omega/2\pi)$, there will, in general, be a corresponding variation in temperature at any point. The exception is water in which, at 4 °C, $\gamma=1$, and the sound wave propagates isothermally: this problem will be discussed later in relation to sound absorption in solutions of nonelectrolytes.

If c is the phase velocity of the wave at a frequency f, then the variations in excess pressure in a plane progressive sound wave can be expressed by

$$p = p_0 \exp[-\alpha x] \exp[j\omega(t - x/c)] \tag{1}$$

where x is the distance measured in the direction of propagation, p_0 is the amplitude of the pressure variations at the source ($x=0$) and α is the amplitude absorption coefficient of the liquid through which the wave is propagated.

In these lectures we shall be concerned primarily with the interpretation of absorption data for pure liquids, binary mixtures and aqueous solutions of nonelectrolytes. Particular attention is given to the ultrasonic relaxation method of studying fast reversible chemical reactions in liquids, in which a sound wave of relatively high frequency is used to perturb sinusoidally an existing molecular equilibrium, specified by a reaction variable, y. y may, for example, represent the degree of reaction or, in the more general sense used by Frenkel [1], the « degree of order ». Examples of such reactions are the equilibrium existing between alternative rotational isomeric configurations of the molecules in the pure liquid or the equilibrium between free water and water molecules forming complexes in solutions of nonelectrolytes.

A further separate topic to be considered is that of vibrational specific heat relaxation in liquids. Extensive studies have been made of the ultrasonic relaxation and its associated dispersion in gases and vapours which arise from the time delay in the redistribution of energy between the vibrational and translational or rotational degrees of freedom of molecules. However, only a few examples of vibrational relaxation in liquids are known, due principally to the fact that the expected region of relaxation falls at frequencies higher than it has yet been possible to attain experimentally. A detailed study will be made of the cases which have been investigated experimentally, but it is convenient to treat this mechanism separately from that of a chemical equilibrium which will be dealt with first.

2. – Basic theory.

2·1. *Thermodynamic relationships.* – Consider a simple fluid system containing a single chemical reaction mechanism or, more generally, a single ordering process. Three independent variables are than required in order to define the state of such a system and these are two thermodynamic variables (for example, p and T) and the ordering parameter, or reaction variable, y, which, for a chemical reaction specified by the stoichiometric formula $\sum_i \nu_i M_i = 0$, can be taken as the degree of reaction. In this case, the change in mole numbers of the i-th constituent due to the reaction is $\mathrm{d}N_i = \nu_i \mathrm{d}y$. We require to relate the measured values of sound absorption, α, and velocity, c, to the parameters of the reaction which is perturbed by the sound wave. The most satisfactory way of tackling this problem is to follow the method outlined by FRENKEL [1] and DE DONDER [2] introducing a parameter, y, which is a measure of the « degree of order », or rather, the degree of reaction for a chemical equilibrium, and the affinity, A, which determines the departure of the system from equilibrium [3]. We then have a change in Gibbs' free energy, given by:

$$-\mathrm{d}G = S\,\mathrm{d}T - V\,\mathrm{d}p + A\,\mathrm{d}y\,. \tag{2}$$

Proceeding from this, it is possible to derive the desired relationships but, for present purposes, these may be obtained in the following less rigorous, though somewhat more straightforward fashion. In either approach, it is essential to make a linear rate hypothesis in the same way as PRIGOGINE [4] and DE GROOT [5]. The system is assumed to be near enough to equilibrium for rates of reaction to be linear functions of the affinities.

Following the procedure of ANDREAE and LAMB [6], ANDREAE, EDMONDS and McKELLAR [7], we expand the adiabatic compressibility, β_S, the isothermal compressibility, β_T, the thermal expansion coefficient, θ, and the specific heat at constant pressure, C_p, in terms of the reaction variable, y:

$$\begin{cases} \beta_S = -\dfrac{1}{V}\left(\dfrac{\partial V}{\partial p}\right)_S = -\dfrac{1}{V}\left(\dfrac{\partial V}{\partial p}\right)_{S,y} - \dfrac{1}{V}\left(\dfrac{\partial V}{\partial y}\right)_{S,p}\cdot\left(\dfrac{\partial y}{\partial p}\right)_S = \beta_{S\infty} + \delta\beta_S\,, \\ \delta\beta_S = -\dfrac{1}{V}\left(\dfrac{\partial V}{\partial y}\right)_{S,p}\left(\dfrac{\partial y}{\partial p}\right)_S\,, \end{cases} \tag{3}$$

$$\begin{cases} \beta_T = -\dfrac{1}{V}\left(\dfrac{\partial V}{\partial p}\right)_T = -\dfrac{1}{V}\left(\dfrac{\partial V}{\partial p}\right)_{T,y} - \dfrac{1}{V}\left(\dfrac{\partial V}{\partial y}\right)_{p,T}\cdot\left(\dfrac{\partial y}{\partial p}\right)_T = \beta_{T\infty} + \delta\beta_T\,, \\ \delta\beta_T = -\dfrac{1}{V}\left(\dfrac{\partial V}{\partial y}\right)_{p,T}\left(\dfrac{\partial y}{\partial p}\right)_T = -\dfrac{\Delta V}{V}\left(\dfrac{\partial y}{\partial p}\right)_T. \end{cases} \tag{4}$$

The volume change of reaction per unit change of y is

$$\Delta V = \left(\frac{\partial V}{\partial y}\right)_{p,T}. \tag{5}$$

$$\begin{cases} C_p = T\left(\dfrac{\partial S}{\partial T}\right)_p = T\left(\dfrac{\partial S}{\partial T}\right)_{p,y} + T\left(\dfrac{\partial S}{\partial y}\right)_{p,T}\cdot\left(\dfrac{\partial y}{\partial T}\right)_p = C_{p\infty} + \delta C_p\,, \\ \delta C_p = T\left(\dfrac{\partial S}{\partial y}\right)_{p,T}\left(\dfrac{\partial y}{\partial T}\right)_p = \Delta H\left(\dfrac{\partial y}{\partial T}\right)_p. \end{cases} \tag{6}$$

The enthalpy change of reaction per unit change of y is

$$\Delta H = T\left(\frac{\partial S}{\partial y}\right)_{p,T} = T\,\Delta S\,, \tag{7}$$

$$\begin{cases} \theta = \dfrac{1}{V}\left(\dfrac{\partial V}{\partial T}\right)_p = \dfrac{1}{V}\left(\dfrac{\partial V}{\partial T}\right)_{p,y} + \dfrac{1}{V}\left(\dfrac{\partial V}{\partial y}\right)_{p,T}\cdot\left(\dfrac{\partial y}{\partial T}\right)_p = \theta_\infty + \delta\theta\,, \\ \delta\theta = \dfrac{1}{V}\left(\dfrac{\partial V}{\partial y}\right)_{p,T}\left(\dfrac{\partial y}{\partial T}\right)_p = \dfrac{\Delta V}{V}\left(\dfrac{\partial y}{\partial T}\right)_p. \end{cases} \tag{8}$$

One of Maxwell's relations requires that:

$$\left(\frac{\partial V}{\partial T}\right)_p = -\left(\frac{\partial S}{\partial p}\right)_T.$$

Hence an alternative expression for θ is:

$$\theta = -\frac{1}{V}\left(\frac{\partial S}{\partial p}\right)_T = -\frac{1}{V}\left(\frac{\partial S}{\partial p}\right)_{T,y} - \frac{1}{V}\left(\frac{\partial S}{\partial y}\right)_{p,T}\left(\frac{\partial y}{\partial p}\right)_T = \theta_\infty + \delta\theta\,, \tag{9}$$

$$\delta\theta = -\frac{1}{V}\left(\frac{\partial S}{\partial y}\right)_{p,T}\left(\frac{\partial y}{\partial p}\right)_T = -\frac{\Delta H}{VT}\left(\frac{\partial y}{\partial p}\right)_T . \tag{10}$$

It follows that

$$\delta C_p = V\frac{\Delta H}{\Delta V}\cdot\delta\theta = \left[\frac{\Delta H}{\Delta V}\right]^2\frac{V}{T}\cdot\delta\beta_T . \tag{11}$$

Now

$$\delta\beta_S = -\frac{1}{V}\left(\frac{\partial V}{\partial y}\right)_{S,p}\left(\frac{\partial y}{\partial p}\right)_S = -\frac{1}{V}\left\{\left(\frac{\partial V}{\partial y}\right)_{p,T} - \left(\frac{\partial V}{\partial S}\right)_{p,y}\left(\frac{\partial S}{\partial y}\right)_{p,T}\right\}\left\{\left(\frac{\partial y}{\partial p}\right)_T + \left(\frac{\partial y}{\partial T}\right)_p\left(\frac{\partial T}{\partial p}\right)_S\right\}.$$

With $(\partial T/\partial p)_S = (T/C_p)(\partial V/\partial T)_p$ and using (11) this yields:

$$\delta\beta_S = VT\,\delta C_p\left\{\frac{\theta_\infty}{C_{p\infty}} - \frac{\Delta V}{V\Delta H}\right\}\left\{\frac{\theta}{C_p} - \frac{\Delta V}{V\Delta H}\right\}. \tag{12}$$

But

$$\theta_\infty - \frac{\Delta V}{V\Delta H}\,C_{p\infty} = (\theta - \delta\theta) - \frac{\delta\theta}{\delta C_p}\,(C_p - \delta C_p) = \theta - \frac{\Delta V}{V\Delta H}\,C_p .$$

Since

$$\frac{\Delta V}{V\Delta H} = \frac{\delta\theta}{\delta C_p}.$$

Now $VT\theta^2 = C_p\beta_S(\gamma-1)$ by standard formula and from eq. (11)

$$\frac{\Delta V}{\Delta H} = \left[\frac{V\,\delta\beta_T}{T\,\delta C_p}\right]^{\frac{1}{2}}.$$

Hence

$$\frac{\delta\beta_S}{\beta_S} = \frac{C_p}{C_{p\infty}}\left\{[\delta\beta_T/\beta_S]^{\frac{1}{2}} - [(\gamma-1)\,\delta C_p/C_p]^{\frac{1}{2}}\right\}^2 . \tag{13}$$

Alternatively from eq. (12) using $VT\theta^2 = C_p\beta_S(\gamma-1)$, we have:

$$\frac{\delta\beta_S}{\beta_S} = \frac{(\gamma-1)\,\delta C_p}{C_{p\infty}}\cdot\left[1 - \frac{\Delta V}{\Delta H}\,\frac{C_p}{V\theta}\right]^2 . \tag{14}$$

2·2. *Kinetic effects.* – Our next task is to relate the relaxation strength $r = \delta\beta_s/\beta_s$, to the sound absorption per wavelength $\mu = \alpha c/f$. In order to do so, it is necessary to consider the time-dependent behaviour of a relaxing system. We postulate a « dynamic » or complex adiabatic compressibility

$$\beta_s^* = \beta_{s\infty} + \frac{\delta\beta_s}{(1 + \tau(\mathrm{d}/\mathrm{d}t))} \, . \tag{15}$$

This is equivalent to assuming that for a small displacement from equilibrium, the kinetic behaviour is determined by

$$\frac{\mathrm{d}y}{\mathrm{d}t} = -(y - y_0)/\tau \, , \tag{16}$$

where y_0 is the equilibrium value of the reaction variable and τ is a relaxation time. Strictly, τ here should be written $\tau_{s,p}$ to signify that it is the relaxation time associated with the adiabatic compressibility [8].

With a sinusoidal perturbation caused by the sound wave of angular frequency ω $(= 2\pi f)$ we have

$$y = \bar{y} + \mathrm{d}y \exp[j\omega t] ; \qquad y_0 = \bar{y}_0 + \mathrm{d}y_0 \exp[j\omega t] \, ,$$

where the use of a bar denotes the average value.

Then from eq. (16)

$$j\omega \, \mathrm{d}y = -\frac{1}{\tau}(\mathrm{d}y - \mathrm{d}y_0) \, ,$$

or

$$\mathrm{d}y = \frac{\mathrm{d}y_0}{(1 + j\omega\tau)} \, .$$

From this, together with eq. (3), we see that the frequency-dependence of the incremental contribution to the adiabatic compressibility will be

$$\delta\beta_{s\omega} = -\frac{1}{V}\left(\frac{\partial V}{\partial y}\right)_{s,p} \cdot \left(\frac{\partial y_0}{\partial p}\right)_s \cdot \frac{1}{(1 + j\omega\tau)} = \frac{\delta\beta_s}{(1 + j\omega\tau)} \, .$$

Hence

$$\left\{\begin{aligned} \beta_s^* &= \beta_{s\infty} + \frac{\delta\beta_s}{1 + j\omega\tau} \, , \quad \text{as in eq. (15)} \, , \\ &= \beta_s - \frac{j\omega\tau\,\delta\beta_s}{1 + j\omega\tau} \, . \end{aligned}\right. \tag{17}$$

We define a complex velocity c^* to represent both the phase velocity c_ω and the absorption α at the angular frequency, ω, and rewrite eq. (1) in the form:

$$p = p_0 \exp[-\alpha x] \exp[j\omega(t - x/c_\omega)] = p_0 \exp[j\omega(t - x/c^*)] . \tag{18}$$

Then

$$\frac{1}{c^*} = (1/c_\omega)(1 - j\alpha c_\omega/\omega) = (1/c_\omega)(1 - j\mu/2\pi) . \tag{19}$$

For $(\mu/2\pi)^2 \ll 1$ we have from the complex form of the Laplace formula for the sound velocity, $(c^*)^2 = (\varrho\beta_S^*)^{-1}$:

$$1/(c^*)^2 = (1/c_\omega)^2(1 - j\mu/\pi) = \varrho\beta_S^* . \tag{20}$$

Substituting for β_S^* from eq. (17) and writing $\tau_1 = \tau(\beta_{S\infty}/\beta_S)^{\frac{1}{2}}$ gives

$$(c/c^*)^2 = \beta_S^*/\beta_S = \frac{\beta_S + \omega^2\tau^2\beta_{S\infty}}{\beta_S(1+\omega^2\tau^2)}\left\{1 - \frac{\delta\beta_S}{(\beta_S\beta_{S\infty})^{\frac{1}{2}}}\cdot\frac{j\omega\tau_1}{(1+\omega^2\tau_1^2)}\right\} = \tag{21}$$
$$\doteq (c/c_\omega)^2(1 - j\mu/\pi) ,$$

c is the limiting value of the phase velocity at low frequencies. Equating real and imaginary parts of eq. (21) gives:

$$\frac{\mu}{\pi} = \frac{\delta\beta_S}{(\beta_S\beta_{S\infty})^{\frac{1}{2}}}\,\frac{\omega\tau_1}{(1+\omega^2\tau_1^2)} . \tag{22}$$

When μ is sufficiently small $\beta_{S\infty} \approx \beta_S$, $C_{p\infty} \approx C_p$, $\tau_1 \simeq \tau$ and eq. (22) combined with eq. (13) yields

$$\frac{\mu}{\pi} \simeq \frac{\delta\beta_S}{\beta_S} = \left\{\left(\frac{\delta\beta_T}{\beta_S}\right)^{\frac{1}{2}} - [(\gamma-1)\,\delta C_p/C_p]^{\frac{1}{2}}\right\}^2 \left[\frac{\omega\tau}{1+\omega^2\tau^2}\right] . \tag{23}$$

Putting $\tau = 1/2\pi\cdot f_c$ gives the frequency-dependent term as $(f/f_c)/(1 + (f/f_c)^2)$ and this attains a maximum value equal to $\frac{1}{2}$ at $f = f_c$. The corresponding maximum value of μ is designated $\mu_{\max}$.

Then

$$\frac{2\mu_{\max}}{\pi} = \left\{\left(\frac{\delta\beta_T}{\beta_S}\right)^{\frac{1}{2}} - [(\gamma-1)\,\delta C_p/C_p]^{\frac{1}{2}}\right\}^2 = \tag{24}$$
$$= \frac{(\gamma-1)\,\delta C_p}{C_p}\left[1 - \frac{\Delta V}{\Delta H}\cdot\frac{C_p}{V\theta}\right]^2 = (\delta\beta_T/\beta_S)\left[1 - \frac{\Delta H}{\Delta V}\,\frac{\theta V}{C_p}\right]^2 .$$

It follows from eq. (23) that we can express the sound absorption in the form:

$$\frac{\alpha}{f^2} = \frac{A}{1 + (f/f_c)^2} + B\,. \tag{25}$$

This equation is convenient for the analysis of experimental results, since for $f \gg f_c$, $\alpha/f^2 \to B$ and if the term B is evaluated, we can subtract this quantity from the measured values of (α/f^2) in order to determine the absorption due to the reaction of interest. In effect, the term B accounts for the absorption due to shear viscosity, heat conduction and those processes having a much smaller relaxation time than the one in question. μ is then given in terms of the remainder by:

$$\mu = \frac{Acf}{1 + (f/f_c)^2} \qquad \text{and} \qquad \mu_{\max} = (\tfrac{1}{2})\, Acf_c\,. \tag{26}$$

The fractional change in sound velocity over the whole relaxation region is given by $\delta c/c \simeq \mu_{\max}/\pi$.

Thus for $\mu_{\max} < 0.03$, as is usually the case, the velocity changes by less than 1 % over the relaxation region whilst (α/f^2) may change by several orders of magnitude. In most cases the dispersion in sound velocity can be neglected and c may be taken as a constant.

Equation (24) relates the measured parameter, $\mu_{\max}$, to the thermodynamic parameters. So far, we have made no important assumptions other than those made in connection with eqs. (20) and (23) $[\mu_{\max}/\pi \ll 1]$ and these can readily be removed if they are not justified.

Unfortunately, the effect of the volume change, ΔV, *opposes* the effect of the enthalpy change, ΔH, and this is one of the major disadvantages of the ultrasonic relaxation method of analysis for fast chemical reactions. Mathematically, this can be seen from the contents of the squared bracket in eqs. (23) or (24) where the thermal part due to ΔH has to be subtracted from the isothermal part due to ΔV. Physically, the adiabatic nature of the sound wave requires that the maxima of pressure and temperature due to the sound wave should be almost coincident in time: an excess temperature shifts the equilibrium in question towards the higher enthalpy state whilst the excess pressure shifts the equilibrium towards a lower volume. ΔH and ΔV will generally have the same sign and, in fact, if it should happen that

$$V0 \cdot \Delta H = C_p \cdot \Delta V,$$

there will be no disturbance of the equilibrium due to the passage of the sound wave!

Rigour is less easily attained in the kinetic analysis. This stage demands more knowledge of the process which is giving rise to the relaxation so that a rate equation can be established. This issue has so far been avoided by leaving the variable, y, undefined.

2.3. *Relationship between relaxation times.* – The complex adiabatic compressibility is given by eq. (17) as

$$\beta_S^* = \beta_{S\infty} + \frac{\delta\beta_S}{1 + j\omega\tau_{p,S}}, \tag{17}$$

where $\tau_{p,S}$ is the relaxation time measured with p and S held constant. Likewise with p and T as independent variables we have:

$$\beta_T^* = \beta_{T\infty} + \frac{\delta\beta_T}{1 + j\omega\tau_{p,T}}, \tag{27}$$

$$\theta^* = \theta_\infty + \frac{\delta\theta}{1 + j\omega\tau_{p,T}}. \tag{28}$$

Hence generalizing eqs. (4) and (9) in complex notation, we have:

$$\delta V^* = -V\left[\beta_{T\infty} + \frac{\delta\beta_T}{1 + j\omega\tau_{p,T}}\right] + V\left[\theta_\infty + \frac{\delta\theta}{1 + j\omega\tau_{p,T}}\right]. \tag{29}$$

$$\delta S^* = -V\left[\theta_\infty + \frac{\delta\theta}{1 + j\omega\tau_{p,T}}\right] + \frac{1}{T}\left[C_{p\infty} + \frac{\delta C_p}{1 + j\omega\tau_{p,T}}\right]. \tag{30}$$

Consider now the relation between p and V at constant T. Using simple time derivatives, we have:

$$V + \tau\delta\dot{V} + V\beta_T\delta p + \tau V\beta_{T\infty}\delta\dot{p} = 0 \qquad (T = \text{constant}).$$

This can be written as:

$$\delta p + \frac{\tau\beta_{T\infty}}{\beta_T}\delta\dot{p} + \frac{\delta V}{V\beta_T} + \frac{\tau}{V\beta_T}\delta\dot{V} = 0 \qquad (T = \text{constant}),$$

which shows that the complex bulk modulus is

$$\frac{1}{\beta_{T\infty}} + \frac{(1/\beta_T)}{1 + j\omega(\tau_{p,T}\beta_{T\infty}/\beta_T)}.$$

However, the relaxation time corresponding to the bulk modulus is $\tau_{V,T}$. Hence

$$\tau_{VT} = \frac{\beta_{T\infty}}{\beta_T}\cdot\tau_{pT}.$$

It can readily be shown that:

$$(31)\qquad \tau_{p,T}=\left(\frac{\beta_T}{\beta_{T\infty}}\right)\tau_{VT}=\left(\frac{C_p}{C_{p\infty}}\right)\tau_{p,S}=\left(\frac{\beta_T C_V}{\beta_{T\infty}C_{V\infty}}\right)\tau_{V,S}=\left(\frac{\theta}{\theta_\infty}\right)\tau_{p,V}=\left(\frac{\theta}{\theta_\infty}\right)\tau_{T,S}\,.$$

Further, it is clear that any ordinary identity between thermodynamic coefficients (*e.g.*, $\beta_T C_V=\beta_S C_p$) subsists between the corresponding « complex » or dynamic coefficients provided that the appropriate relaxation times are used for each coefficient appearing in the identity. Thus

$$\beta_T^* C_V^* = \beta_S^* C_p^* \text{ etc.}$$

In practice, the difference between the various relaxation times depends upon the ratio between equilibrium and instantaneous values of the relaxing parameters and for small relaxation strengths,

$$r=\frac{\delta\beta_S}{\beta_S}=\frac{\beta_S-\beta_{S\infty}}{\beta_S}=1-\frac{\beta_{S\infty}}{\beta_S}\,,$$

these differences can be ignored to a first approximation, and this will be assumed in the following.

2·4. ***Reaction equations in ideal solution.*** – Consider the simple isomeric equilibrium (Fig. 1).

$$(32)\qquad A\underset{k_{21}}{\overset{k_{12}}{\rightleftharpoons}}B\,,$$

for which the rate equation is:

$$(33)\qquad \frac{\mathrm{d}n_B}{\mathrm{d}t}=k_{12}n_A-k_{21}n_B\,,$$

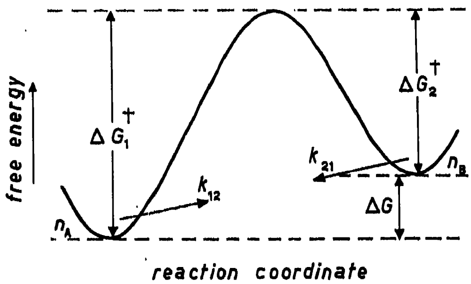

Fig. 1. – Gibbs free energy diagram for a simple isomeric equilibrium $A\underset{k_{21}}{\overset{k_{12}}{\rightleftharpoons}}B$.

n_A and n_B are the populations of the molecular states A and B, k_{12} and k_{21} are the appropriate forward and backward rate constants.

Putting $N=n_A+n_B=$ constant, $K=k_{12}/k_{21}$, $y=n_B/N$, we find

$$(34)\qquad -\frac{\mathrm{d}y}{\mathrm{d}t}=\frac{k_{21}N}{n_A}\cdot\left[y-\frac{K}{1+K}\right],$$

By analogy with eq. (16) this gives

$$\tau^{-1} = \frac{k_{21}N}{n_A} = (k_{12} + k_{21})\,. \tag{35}$$

For a sinusoidal perturbation eq. (34) becomes (cf. the treatment of eq. (16)):

$$\mathrm{d}y = \frac{K}{(1+K)^2}\cdot\frac{\mathrm{d}(\ln K)}{1+j\omega\tau}\,. \tag{36}$$

We have previously expressed the relaxing component of the adiabatic compressibility as:

$$\delta\beta_{S\omega} = -\frac{1}{V}\left(\frac{\partial V}{\partial y}\right)_{S,p}\left(\frac{\partial y_0}{\partial p}\right)_S\cdot\frac{1}{(1+j\omega\tau)} = \frac{\delta\beta_S}{(1+j\omega\tau)}\,. \tag{37}$$

Similarly we can put:

$$\delta\beta_{T,\omega} = -\frac{1}{V}\left(\frac{\partial V}{\partial y}\right)_{p,T}\left(\frac{\partial y_0}{\partial p}\right)_T\cdot\frac{1}{1+j\omega\tau} = \frac{\delta\beta_T}{1+j\omega\tau}\,, \tag{38}$$

$$\delta C_{p\omega} = T\left(\frac{\partial S}{\partial y}\right)_{p,T}\left(\frac{\partial y_0}{\partial T}\right)_p\cdot\frac{1}{1+j\omega\tau} = \frac{\delta C_p}{1+j\omega\tau}\,, \tag{39}$$

$$\delta\theta_\infty = \frac{1}{V}\left(\frac{\partial V}{\partial y}\right)_{p,T}\left(\frac{\partial y_0}{\partial T}\right)_p\cdot\frac{1}{1+j\omega\tau} = \frac{\delta\theta}{1+j\omega\tau}\,. \tag{40}$$

These quantities can be evaluated when the derivatives $(\partial y_0/\partial p)_T$ and $(\partial y_0/\partial T)_p$ are known from eq. (34).

It follows from eq. (36) and the van't Hoff relations that:

$$\left(\frac{\partial y_0}{\partial p}\right)_T = \frac{K}{(1+K)^2}\cdot\left(\frac{\partial \ln K}{\partial p}\right)_T = -\frac{K}{(1+K)^2}\cdot\frac{\Delta V}{RT}\,, \tag{41}$$

$$\left(\frac{\partial y_0}{\partial T}\right)_p = \frac{K}{(1+K)^2}\cdot\left(\frac{\partial \ln K}{\partial T}\right)_p = \frac{K}{(1+K)^2}\cdot\frac{\Delta H}{RT^2}\,. \tag{42}$$

Hence from eqs. (38) and (39):

$$\delta\beta_T = \frac{\Delta V}{V}\cdot\frac{K}{(1+K)^2}\cdot\frac{\Delta V}{RT} = \frac{(\Delta V)^2}{VRT}\cdot\frac{K}{(1+K)^2}\,. \tag{43}$$

$$\delta C_p = \Delta H\cdot\frac{K}{(1+K)^2}\,\frac{\Delta H}{RT^2} = R\left[\frac{\Delta H}{RT}\right]^2\cdot\frac{K}{(1+K)^2}\,. \tag{44}$$

Then from eq. (24):

$$(45)\qquad \frac{2\mu_{\max}}{\pi}=\frac{(\Delta V)^2}{VRT\beta_S}\,\frac{K}{(1+K)^2}\left\{1-\frac{\Delta H}{\Delta V}\cdot\frac{\theta V}{C_p}\right\}^2,$$

$$(46)\qquad =\frac{(\gamma-1)}{C_p}\left\{1-\frac{\Delta V}{\Delta H}\cdot\frac{C_p}{V\theta}\right\}^2\cdot R\left[\frac{\Delta H}{RT}\right]^2\frac{K}{(1+K)^2}\,.$$

If ΔG is the Gibbs free energy difference between the standard isomeric states A and B, then:

$$K=\exp\left[-\Delta G/RT\right]\qquad\text{and}\qquad \Delta G=\Delta H-T\Delta S\,.$$

Further, if $\Delta G>3RT$, say, as is often found to be the case for isomeric equilibria which give rise to ultrasonic relaxation, then within an accuracy of 5 % we can write:

$$(47)\qquad \frac{2\mu_{\max}}{\pi}\simeq\frac{(\gamma-1)}{C_p}\left\{1-\frac{\Delta V}{\Delta H}\cdot\frac{C_p}{V\theta}\right\}^2\cdot R\left(\frac{\Delta H}{RT}\right)^2\exp\left[\Delta S/R\right]\exp\left[-\Delta H/RT\right].$$

The dependence of $\mu_{\max}$ on T is primarily determined by the exponential term in $(-\Delta H/RT)$.

The relaxation time is $\tau=(k_{12}+k_{21})^{-1}$, and for convenience in analysing experimental data plotted against log (f), we define a characteristic frequeny.

$$(48)\qquad f_c=\frac{1}{2\pi\tau}=\frac{1}{2\pi}(k_{12}+k_{21})=\frac{k_{21}}{2\pi}(1+K)\,.$$

With $K\ll 1$: $f_c\simeq k_{21}/2\pi$ and following the theory of rate processes:

$$(49)\qquad f_c\simeq\frac{F_2}{2\pi}\left(\frac{kT}{h}\right)\exp\left[-\Delta H_2^{\dagger}/RT\right],$$

F_2 is a numerical factor representing, in effect, the entropy of activation for the transition 2 → 1. $\Delta H^{\dagger}$ is the activation energy of the backward reaction.

The method employed in this section for an isomeric equilibrium can be extended to other specified reactions. For example, for the equilibrium $A+B\rightleftharpoons AB$, we find

$$\delta\beta_T=\frac{(\Delta V)^2}{VRT}\cdot\frac{K}{4(1+K)^{\frac{3}{2}}}\,,$$

with a similar expression for δC_p.

3. – Analysis of experimental results: rotational isomers.

Ideally one would hope to have available experimental values for the absorption, expressed as (α/f^2), which range from low frequencies well below the relaxation region $(f \ll f_c)$ where $\alpha/f^2 = A + B$ (eq. (25)), to frequencies well above the relaxation region $(f \gg f_c)$ where $\alpha/f^2 = B$, at a given temperature. The measurements would be made at other temperatures covering as wide a range as possible and, provided that the relaxational behaviour can be attributed to a single relaxation time, τ, or characteristic frequency, f_c, we can then obtain values of $\mu_{\max}$ (eq. (26)) and of f_c, the frequency at which μ attains its maximum value, $\mu_{\max}$, as a function of temperature. In practice results are not always available over the complete relaxation region and procedures of extrapolation or estimation have to be employed [9, 10] to determine values of A and B in eq. (25).

Fortunately, experience has shown that the relaxation processes of present interest can be described by a single relaxation time: the exceptions are viscoelastic relaxation mechanisms which lie outside the scope of these lectures.

Additional information is usually available giving the velocity of sound, c, as a function of temperature and this can be expressed:

$$c^2 = \frac{(\gamma - 1)C_p}{T\theta^2}, \tag{50}$$

enabling a value for $(\gamma - 1)$ to be substituted in eq. (24) if required. In cases of relatively large relaxation strength where dispersion cannot be neglected, then it is desirable also to measure the velocity c_ω (eq. (21)) as a function of frequency over the relaxation region.

In order to proceed further in analysing experimental data, one has to introduce a definite assumption about the stoichiometric nature of the reaction in question and this is mainly decided on external evidence. In many cases, variation of the chemical composition in the ultrasonic experiments can lead to identification of the molecular mechanism responsible for the relaxation, as has been demonstrated by the work of YOUNG and PETRAUSKAS [11] and DE GROOT and LAMB [10]. The simplest and most important case is that of a unimolecular reaction in ideal solution. With $K = \exp[-\Delta G/RT]$, we then have from eq. (46) an expression relating the measured quantity $\mu_{\max}$ at each temperature to *three* reaction parameters ΔV, ΔH and ΔG each referred to the « pure constituents ». The only relevant connection between them is the Gibbs-Helmholz equation $\partial(\Delta G/T)/\partial T = -\Delta H/T^2$ and it is clear that further assumptions must be made before information can be obtained about reaction coefficients. The simplest and commonest assumption is that the volume change of reaction ΔV is zero. This is often a very reasonable assumption for isomeric reactions since the kinds of molecular mechanisms which have been studied do not usually involve large changes of size. It carries the immediate simplification that $\delta\theta = \delta\beta_T = 0$ and hence $\mu_{\max}$ can be expressed explicitly in terms of δC_p. Thus from eq. (24) with $\mu_{\max}/\pi \ll 1$:

$$\frac{2\mu_{\max}}{\pi} = \frac{(\gamma-1)}{C_p}\cdot\delta C_p\,, \tag{51}$$

and from eq. (44):

$$\delta C_p = R\left[\frac{\Delta H}{RT}\right]^2 \frac{\exp[-\Delta G/RT]}{[1+\exp[-\Delta G/RT]]^2}\,. \tag{52}$$

Now $\Delta G = \Delta H - T\Delta S$ and, in principle, a fit can be obtained to the combination of eqs. (51) and (52) by an appropriate choice of ΔH and ΔS.

The simplest version of eqs. (51) and (52) comes under the further specialization that the entropy change of the reaction, ΔS, is zero. In this case:

$$\frac{2\mu_{\max}}{\pi} = \frac{(\gamma-1)}{C_p}\cdot R\left[\frac{\Delta H}{RT}\right]^2 \frac{\exp[-\Delta H/RT]}{[1+\exp[-\Delta H/RT]]^2}\,. \tag{53}$$

A plot of δC_p *vs.* $(\Delta H/RT)$ is shown in Fig. 2, from which it is evident that δC_p reaches a maximum at a value $\Delta H/RT = 2.4$. Hence we see immediately from eq. (53) that if $\mu_{\max}\cdot C_p/(\gamma-1)$ decreases with increasing tem-

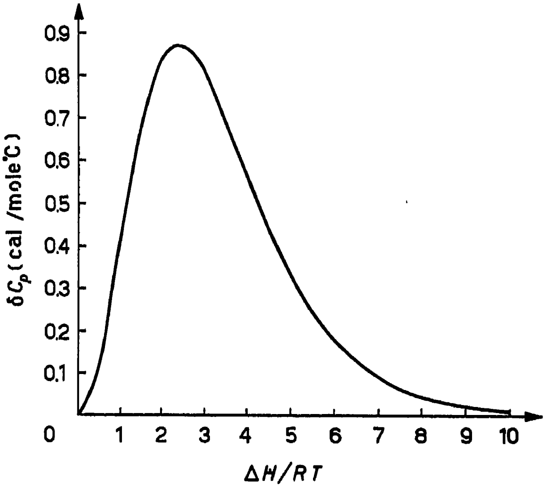

Fig. 2. - The relaxing specific heat for a 2-state equilibrium with $\Delta V = \Delta S = 0$.

$$\delta C_p = R\left[\frac{\Delta H}{RT}\right]^2 \frac{\exp[-\Delta H/RT]}{(1+\exp[-\Delta H/RT])^2}\,.$$

perature, then $\Delta H/RT < 2.4$ whilst, if this quantity increases with increasing temperature, we are reasonably certain that the condition $\Delta H/RT > 3$ will be fulfilled, thus permitting the previous approximation inherent in eqs. (47) and (49) to be used.

The value of the ultrasonic relaxation technique for the study of rotational isomers can be judged from Fig. 2. Taking one third of the maximum value of δC_p we see that δC_p is greater than this figure for values of $\Delta H/RT$ ranging from 0.8 to 5.3, that is, for values of ΔH from 0.48 kcal/mole to 3.18 kcal/mole at 300 °K. The lover value of ΔH corresponds to some 30% of the molecules residing in the state of higher energy whilst the higher value gives a figure of 0.5%. At the maximum of the specific heat curve, approximately 9% of the molecules occupy the position of higher energy. Other methods for studying the behaviour of rotational isomers rely in general on there being at least 10% of the molecules in the state of higher energy so that, for relative population densities from 10% down to below 1%, the ultrasonic relaxation method provides a useful complement to other techniques. Moreover, the energy barrier hindering internal rotation is obtained directly from the observed variation of f_c with temperature in the ultrasonic experiments and it is in this kinetic sense that the ultrasonic relaxation method is particularly valuable as an analytical tool. It should be noted that no relaxation is observed for isomeric reactions in which the alternative configurations are of equal energy ($\Delta H = 0$).

4. – Experimental results: rotational isomers.

The classical example of rotational isomerism is in ethane and its derivatives, where the existence of three stable configurational positions implies that rotation about the C—C bond is restricted. Consider, for example, the case of 1, 1, 2-trichloroethane for which the curves of μ *vs.* frequency are given in Fig. 3. In this molecule there are two ground states of equal energy and one state of higher energy. The previous analysis can be extended readily to include a doubly degenerate ground state, giving a characteristic frequency $f_c = (k_{12} + 2k_{21})/2\pi$ and an incremental specific heat

$$\delta C_p = R\left[\frac{\Delta H}{RT}\right]^2 \frac{K}{(2+K)^2},$$

where $K = (x_2^0/x_1^0)$, x_1^0 and x_2^0 being the equilibrium mole fractions in states 1 and 2 respectively. Substituting for $(\gamma - 1)$ in eq. (53) from eq. (50) we see that, provided $K \ll 2$, the plot of $\log (T_{\mu_{\max}}/c^2)$ *vs.* T^{-1} should be a straight line, the slope of which gives the energy difference ΔH. This plot is shown

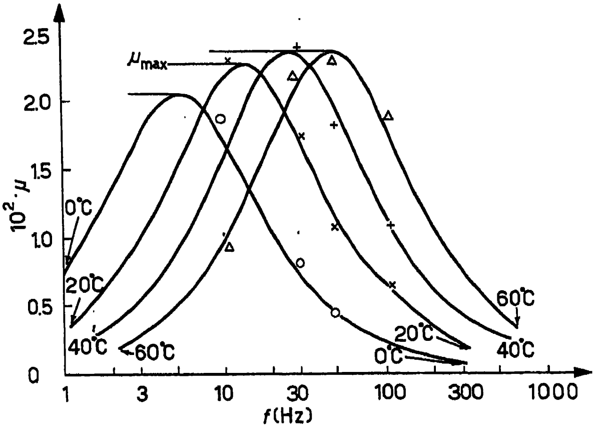

Fig. 3. – Relaxational behaviour for 1, 1, 2-trichloroethane. The curves are theoretical according to eq. (26) and the points are derived from experiment,

$$\mu = \left(\frac{\alpha}{f^2} - B\right) \cdot cf .$$

in Fig. 4, from which we obtain $\Delta H = 2.2$ kcal/mole ($K = 0.025$ at 300 °K). Plotting $\log(f_c/T)$ against T^{-1} in Fig. 5 gives the activation energy of the backward reaction as $\Delta H_2^{\ddagger} = 5.8$ kcal/mole.

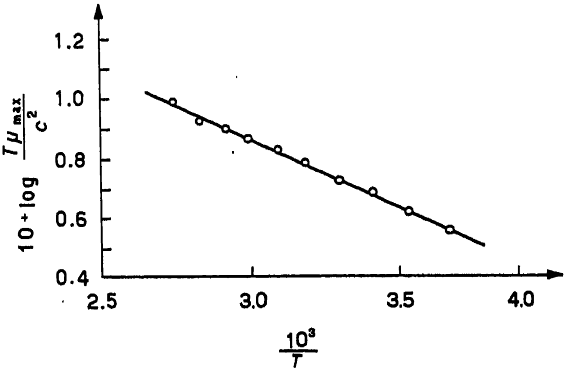

Fig. 4. – Log $(T_{\mu_{max}}/c^2)$ *vs.* T^{-1} for 1, 1, 2-trichloroethane. The value of ΔH obtained from the slope of the line is $\Delta H = 2.2$ kcal/mole.

Similar results have been obtained for other substituted ethanes and a summary of the energy values obtained is given in Table I.

TABLE I. – *Energy values for some substituted ethanes obtained from ultrasonic relaxation studies.*

Liquid	ΔH (kcal/mole)	$\Delta H_2^\dagger$ (reverse) (kcal/mole)	$\Delta H_1^\dagger$ (forward) (kcal/mole)
1, 1, 2-trichloroethane	2.2	5.8	8.0
1, 1, 2-tribromoethane	1.6	6.4	8.0
1-bromopropane	1.3	3.6	4.9
1, 2-dichloropropane	1.1	4.7	5.8
1, 2-dibromopropane	0.9	4.9	5.8
sym-tetrabromoethane	0.9	4.3	5.2
2-methylbutane	0.9	4.7	5.6
2, 3-dimethylbutane	1.0	2.8	3.8
2-methylpentane	0.9	3.9	4.8
3-methylpentane	0.9	4.1	5.0

Another class of rotational isomers investigated by DE GROOT and LAMB [10] is the unsaturated aldehydes in which partial conjugation of the C_1C_2 bond plays a role in stabilising the planar configurations of the molecule shown below for acrolein

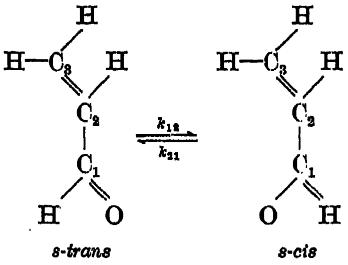

The characteristic frequency for acrolein is 176 MHz at 25 °C.

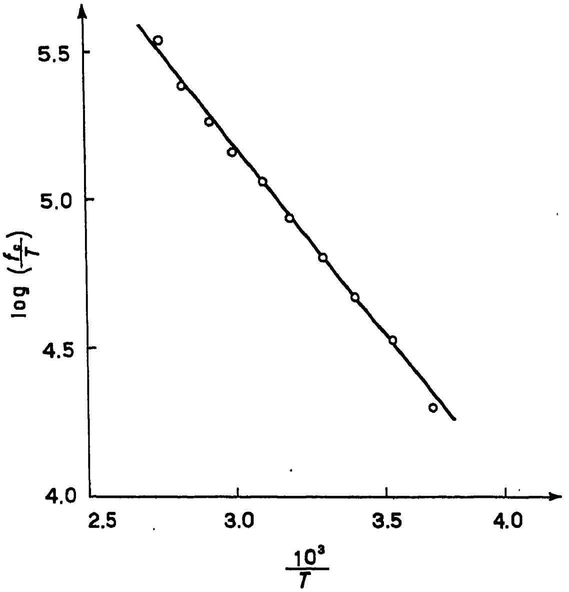

Fig. 5. – Log (f_c/T) *vs.* T^{-1} for 1, 1, 2-trichloroethane. The activation energy of the backward reaction obtained from the slope of this line is $\Delta H_2^\dagger = 5.8$ kcal/mole.

Replacement of the H-atom on C_3 by a methyl group as in crotonaldehyde increases the conjugation of the C_1C_2 bond and leads to a decrease in f_c to 30 MHz at the same temperature. Further substitutions of this group by a benzene ring again increases the conjugation and in cinnamaldehyde, $f_c = 16$ MHz at 25 °C. On the other hand, substitution of a CH_3 group in methacrolein has little effect on the conjugation since the positive charge separation within the molecule resides on the C_3 atom; $f_c = 174$ MHz at 25 °C. Energy values for these liquids are given in Table II and the original paper should be consulted for further information on these and related compounds.

TABLE II. – *Energy values for five unsaturated aldehydes*

	ΔH (kcal/mole)	$\Delta H_2^\ddagger$ (kcal/mole)	$\Delta H_1^\ddagger$ (kcal/mole)
Acrolein	2.1	5.0	7.1
Crotonaldehyde	1.9	5.5	7.4
Cinnamaldehyde	1.5	5.6	7.1
Methacrolein	3.1	5.3	8.4
Furacrolein	1.2	5.1	6.3

5. – Studies of aqueous solutions of nonelectrolytes [7].

In the case of aqueous solutions, the equilibrium which is perturbed by the sound wave and which gives rise to relaxational behaviour can be that between molecular complexes AB and the component parts A and B into which the complex dissociates with a production of enthalpy, ΔH, per mole of complexes dissociated:

$$A + B \rightleftharpoons AB(+\Delta H)\,.$$

ANDREAE *et al.* [7] have made a detailed study of ultrasonic relaxation for a large number of solutions of nonelectrolytes (principally amines) in water, following on the work of SCHNEIDER [12] and BARFIELD and SCHNEIDER [13]. These latter authors have shown that ultrasonic absorption measurements on aqueous solutions of simple amines and alcohols can be interpreted in terms of hydrogen bonding between water and solute molecules.

In all the aqueous solutions studied, there is a certain mole fraction of solute in water at which the sound absorption is a maximum: this is designated the peak sound absorption concentration (P.S.A.C.). Some of the solutions examined also exhibit critical solution behaviour which is a further cause of ultrasonic relaxation, although it has been found possible to separate out on a frequency basis the relaxation due to hydrogen bonding reactions and those arising from critical solution phenomena.

ANDREAE and his collaboratores have given the following rough ultrasonic picture of a nonelectrolyte dissolved in water:

1) The critical solution behaviour gives rise to ultrasonic relaxation with a characteristic frequency below 10 MHz around room temperature, while the formation of hydrogen bond complexes is correlated with characteristic frequencies of ultrasonic relaxation which are above 20 MHz.

2) Solute-water hydrogen bonding occurs between hydrogen atoms or protons of the water molecules and lone pair electrons on the solute.

3) As the concentration of the solute is increased from zero, there is a rapid breakdown of the water structure appearing as a sharp rise in the sound velocity (*i.e.*, a fall in compressibility), despite the fact that the added solute molecule is *more* compressible than water. It appears likely that each solute molecule prevents a number of water molecules around it from maintaining hydrogen bonded contact with the highly oriented water structure nearby. These « free » water molecules then pack more closely around the solute molecule, thereby decreasing the overall compressibility.

4) With further increasing concentration of the solute, the equilibrium between free water molecules and water in complexes begins to give rise to ultrasonic absorption which increases to a maximum at the peak sound absorption concentration. It then falls again as the amount of water available becomes the limiting factor.

5) The equilibrium between solute, water and solute-water complexes is biassed towards the complex. The equilibrium ratio of mole fractions of complex to the product of mole fractions of uncomplexed solute and water is 10 or more. The rate of dissociation is slower than the rate of association ($10^9\ s^{-1}$). The relatively high value of the latter is attributed to the mobility of the water molecules and to the accessibility of water protons.

6) Owing to the high rate of association, water molecules can be expected to associate with the solute, one molecule at a time, a complex containing many water molecules being built up in this way. A simple model of such a mechanism gives a fair representation of the shape of the experimental curves.

7) The thermal expansion coefficient, θ, is approximately zero for water owing to the normal expansion due to temperature rise being counterbalanced by the breakdown of the water to a more dense, more closely packed structure from the open, hexagonal structure, characteristic of ice. When the solute molecules are added to water, the water structure is broken down by the solute and so θ gradually increases to a value appropriate to a more « normal » liquid. If it be supposed that the observed ultrasonic relaxation in these solutions is predominantly thermal, that is, that the enthalpy change, ΔH, outweighs the effect due to volume change, ΔV (or $V\theta\,\Delta H > C_p\cdot\Delta V$), then $\mu_{\max}$ is proportional to $(\gamma-1)$ or to θ^2 and it is not surprising to find that the peak

sound absorption concentration is always higher than the concentration at which the sound velocity goes through a peak itself. This explanation is consistent with the observed results and means that the strength of the ultrasonic relaxation is governed by the enthalpy change, ΔH, or hydrogen bond energy, rather than by the volume change, ΔV. The breakdown of the water structure represented by the peak in sound velocity occurs before θ is large enough to allow the sound absorption to reach a maximum.

Analysis of the observed relaxation processes found by ANDREAE and his collaborators for a number of aqueous solutions of nonelectrolytes has been shown to reveal a high frequency relaxation with a characteristic frequency above 20 MHz for a wide range of solutions. Results for each solution have been analysed in terms of eq. (25) and the characteristic frequencies are plotted in Fig. 6: the solute concentration in each case was close to the P.S.A.C. value.

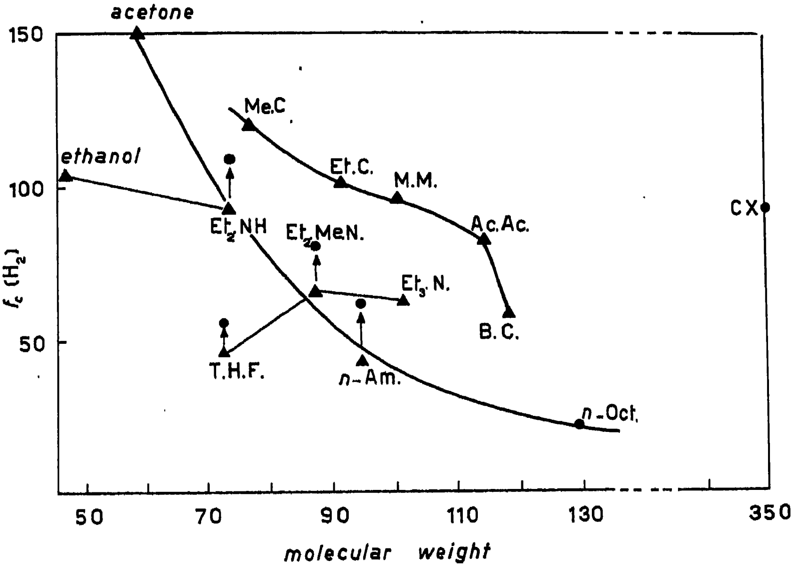

Fig. 6. – Characteristic frequencies in aqueous solutions of acetone, acetonyl acetone (AcAc), *n*-amylamine (*n*-Am), *n*-octylamine (*n*-Oct), diethylamine (Et_2NH), methyldiethylamine (Et_2MeN), triethylamine (Et_3N) N-methylmorpholine (MM), butyl cellosolve (B. C), ethyl cellosolve (Et. C), methyl cellosolve (Me C), tetrahydrofuran (THF), and « Carbowax » 350, $[(CX)=CH_3O(CH_2CH_2O)_7H]$. Triangles are for points near 0 °C and circles for points near 25 °C.

Qualitative conclusions drawn from Fig. 6 are that the characteristic frequency increases with the number of hydrogen bonding centres (N- and O-atoms) and decreases with molecular weight if the number of hydrogen bonding centres is kept constant. If we suppose that the relaxation process is the formation of complexes between solute and water, then the higher the oxygen + nitrogen to carbon ratio in the molecule the larger is the proportion of the molecule available to water molecules as hydrogen bonding sites and the faster is the process of complex formation with a higher value of f_c.

In some way, the concentration at which the peak sound absorption occurs must represent the optimum solute to water ratio for sound absorption. It has been found that the P.S.A.C. is empirically related to the size or molecular weight, M_A, of the solute by

$$\text{Log}_{10}\left\{\frac{1-PSAC}{PSAC}\right\} = M_A/58 + 0.41 - 0.65(n_{\text{OH}} + n_{\text{N}}) - 0.8n_0\,, \tag{54}$$

where n_{N} = number of N-atoms in the solute molecule;

n_{O} = number of O-atoms minus the number, n_{OH}, in OH groups.

This relationship is shown in Fig. 7.

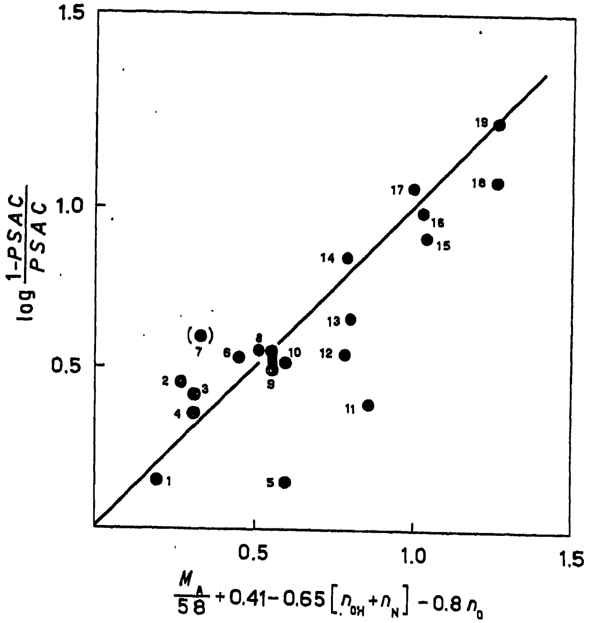

Fig. 7. – Dependence of peak sound absorption concentration on molecular weight for 1) « Carbowax 350 », 2) methyl cellosolve, 3) methanol, 4) diethylene triamine, 5) acetone, 6) triethylene tetramine, 7) dioxan, 8) ethyl cellosolve, 9) ethanol at 0 °C (higher point) and 25 °C (lower point), 10) tetraethylene pentamine, 11) tetrahydrofuran, 12) acetonyl acetone, 13) isopropanol, 14) n-propanol, 15) tert-butanol, 16) diethylamine, 17) butyl cellosolve, 18) methyldiethylamine, 19) n-amylamine. M_A = molecular weight of solute. n_{OH}, n_{N} and n_{O} are numbers of OH groups, nitrogen and oxygen atoms per molecule respectively.

Various models have been put forward to account for the observed behaviour in these systems and these can be described as follows:

Model I

$$A + B \underset{k_b}{\overset{k_f}{\rightleftharpoons}} AB\,. \tag{55}$$

One molecule of water (B) combines with one molecule of solute (A) to form one complex and maximum sound absorption is to be expected for equal mole fractions of A and B: P.S.A.C. $= 0.5$.

We define the mole fraction, x, of solute and z of complex such that when the total number of solute and water molecules, including those in complexes, is unity, x is the *total* number of solute molecules and z is the number of AB complexes. The number of unassociated solute molecules is therefore $(x - z)$ and of unassociated molecules $(1 - x - z)$.

Assuming unimolecular dissociation, the rate equation is

$$\frac{\mathrm{d}z}{\mathrm{d}t} = k_f(x - z)(1 - x - z) - k_b z = k_b(x - z)(1 - x - z)\cdot \\ \cdot\left\{K - \frac{z}{(x - z)(1 - x - z)}\right\}. \tag{56}$$

The equilibrium constant K is defined as the ratio k_f/k_b of the forward and backward rate constants.

With a sinusoidal perturbation caused by a sound wave of frequency $f(= \omega/2\pi)$, let $\mathrm{d}z$ and $\mathrm{d}K$ be the amplitudes of the fluctuations in z and K. Then replacing the time differential by $j\omega$, we have:

$$j\omega\,\mathrm{d}z = k_b(x - z)(1 - x - z)\left\{\mathrm{d}K - \frac{1 + K(1 - 2z)}{(x - z)(1 - x - z)}\cdot\mathrm{d}z\right\}, \tag{57}$$

$$\mathrm{d}z = \frac{z\,\mathrm{d}(\ln K)}{1 + K(1 - 2z)}\cdot\frac{1}{(1 + j\omega\tau)}, \tag{58}$$

$$\tau^{-1} = k_b + (1 - 2z)k_f\,. \tag{59}$$

We identify z with the reaction variable y of eqs. (4) and (6) and use the van't Hoff relation

$$\left[\frac{\partial(\ln K)}{\partial p}\right]_T = -\,(\Delta V/RT)\,.$$

If, following SCHNEIDER [12] we assume that propagation in these aqueous solutions is isothermal, we obtain from the previous equations:

$$(60)\qquad 2\mu_{\max}/\pi = \delta\beta_T/\beta_s = -(1/\beta_s V)\Delta V(-\Delta V/RT)(\partial z/\partial \ln K) = \\ = \frac{(\Delta V)^2}{\beta_s VRT}\cdot\frac{z}{1+K(1-2z)}\,.$$

Since at equilibrium $K = z/(x-z)(1-x-z)$, it follows that

$$(61)\qquad z = \frac{1+K}{2K}\{1-[1-4x(1-x)K^2/(1+K)^2]^{\frac{1}{2}}\} = \frac{1+K}{2K}(1-q)\,,\ \text{say.}$$

Hence since

$$(62)\qquad \beta_s = 1/\varrho c^2: \qquad \mu_{\max} = \frac{\pi}{4}\cdot\frac{\varrho C^2}{VRT}(\Delta V)^2\,\frac{(1-q)}{Kq}\,.$$

The term $(1-q)/q$ reaches a maximum with concentration at $x = $ P.S.A.C. $= 0.5$, that is, for direct association of *one* solute molecule with *one* water molecule. However, in all the systems studied the P.S.A.C. is less than 0.5 (Fig. 8), indicating a greater activity of the solute, A, than of the water, B. A further refinement of the simple model (55) is the following:

Model II:

$$(63)\qquad A + B_m \underset{k_b}{\overset{k_f}{\rightleftharpoons}} AB_m\,.$$

This model assumes that m water molecules combine in a single step with one solute molecule. The theory for model I is applicable if the variables x and z are transformed to

$$x_m = \frac{x}{x+(1-x)/m} \qquad \text{and} \qquad z_m = \frac{z}{x+(1-x)/m}\,.$$

We then obtain the peak sound absorption at $x_m = 0.5$ or

$$PSAC = x = 1/(1+m)\,.$$

In this model, therefore, $m = (1 - PSAC)/PSAC$ is both the number of water molecules in a complex and also the optimum water to solute ratio discussed for model I.

We obtain:

$$(64)\qquad \mu_{\max} = \frac{\pi}{4}\,\frac{\varrho c^2}{V_m RT}(\Delta V_m)^2\,\frac{(1-q_m)}{K_m q_m}\,,$$

(65) $$V_m = (\partial V/\partial z_m)_{p,T}\,,$$

(66) $$q_m^2 = 1 - 4x_m(1 - x_m)K_m^2/(1 + K_m)^2\,,$$

and

(67) $$K_m = z_m/(x_m - z_m)(1 - x_m - z_m)\,.$$

The theory enables a match to be made of the position of the experimental absorption peak by adjusting the value of m, of the height of the peak by adjusting ΔV_m, and of the mean width of the peak by adjusting K_m. This has been done in Fig. 8 for acetone-water and for three amine-water systems. In the model used, the molar volume, V_m, is given by

$$V_m = M = x_m M_A + (1 - x_m)(m M_B)\,,$$

where M_A and M_B are the molecular weights of solute and water and M is that of the solution.

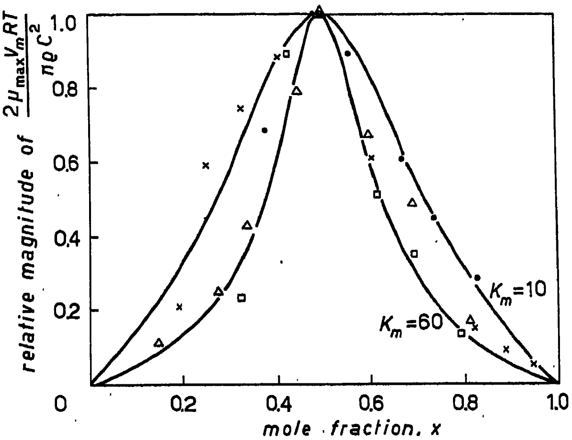

Fig. 8. – Relative values of μ_{max} *vs.* concentration. The curves are calculated on the basis of model II. $A + B_m \rightleftharpoons AB_m$, with $K_m = 10$ and 60. The experimental points are fitted to the theory by selecting the value of m for each solution: acetone, 0 °C, $m = 1.5$ (triangles); diethylamine, 0 °C, $m = 9$ (squares); methyldiethylamine 0 °C, $m = 11.5$ (solid circles); n-amylamine 5 °C, $m = 19$ (crosses).

Now ΔV_m has been determined on the assumption that the thermal term in eqs. (13) and (24) is negligible compared with the isothermal term involving $\delta\beta_T$: we denote this assumed value of ΔV_m by ΔV_m^{is}. We could also proceed by assuming that the thermal term in these equations is dominant, that is, that the enthalpy change denoted ΔH_m^{th} is obtained on the assumption that the volume change of reaction is negligible. It then follows from eq. (24) that the same value of μ_{max} is produced by ΔH_m^{th} (volume change negligible) *or* ΔV_m^{is} (enthalpy change negligible) if $V\theta\Delta H_m^{th} = C_p\cdot\Delta V_m^{is}$. Numerical values of m, K_m, ΔV_m^{is} and ΔH_m^{th} are listed in Table III.

The values of ΔH_m^{th} given in Table III are comparable with estimates given in the literature [14, 15] for hydrogen-bond energies and this is a strong indication that the process is *not* isothermal.

The association of a cluster of water molecules (B_m) with one solute molecule (A) in a single step as assumed in Model II is an unlikely occurrence solutions is isothermal, we obtain from the previous equations:

(60) $$2\mu_{\max}/\pi = \delta\beta_T/\beta_S = -(1/\beta_S V)\,\Delta V(-\Delta V/RT)(\partial z/\partial \ln K) = \frac{(\Delta V)^2}{\beta_S VRT}\cdot\frac{z}{1+K(1-2z)}\,.$$

Since at equilibrium $K = z/(x-z)(1-x-z)$, it follows that

(61) $$z = \frac{1+K}{2K}\{1-[1-4x(1-x)K^2/(1+K)^2]^{\frac{1}{2}}\} = \frac{1+K}{2K}(1-q)\,,\ \text{say}.$$

Hence since

(62) $$\beta_S = 1/\varrho c^2: \qquad \mu_{\max} = \frac{\pi}{4}\cdot\frac{\varrho C^2}{VRT}(\Delta V)^2\,\frac{(1-q)}{Kq}\,.$$

The term $(1-q)/q$ reaches a maximum with concentration at $x =$ $=$ P.S.A.C. $= 0.5$, that is, for direct association of *one* solute molecule with *one* water molecule. However, in all the systems studied the P.S.A.C. is less than 0.5 (Fig. 8), indicating a greater activity of the solute, A, than of the water, B. A further refinement of the simple model (55) is the following:

Model II:

(63) $$A + B_m \underset{k_b}{\overset{k_f}{\rightleftharpoons}} AB_m\,.$$

This model assumes that m water molecules combine in a single step with one solute molecule. The theory for model I is applicable if the variables x and z are transformed to

$$x_m = \frac{x}{x+(1-x)/m} \qquad \text{and} \qquad z_m = \frac{z}{x+(1-x)/m}\,.$$

We then obtain the peak sound absorption at $x_m = 0.5$ or

$$PSAC = x = 1/(1+m)\,.$$

In this model, therefore, $m = (1-PSAC)/PSAC$ is both the number of water molecules in a complex and also the optimum water to solute ratio discussed for model I.

We obtain:

(64) $$\mu_{\max} = \frac{\pi}{4}\,\frac{\varrho c^2}{V_m RT}(\Delta V_m)^2\,\frac{(1-q_m)}{K_m q_m}\,,$$

$$V_m = (\partial V/\partial z_m)_{p,T}\,, \tag{65}$$

$$q_m^2 = 1 - 4x_m(1 - x_m)K_m^2/(1 + K_m)^2\,, \tag{66}$$

and

$$K_m = z_m/(x_m - z_m)(1 - x_m - z_m)\,. \tag{67}$$

The theory enables a match to be made of the position of the experimental absorption peak by adjusting the value of m, of the height of the peak by adjusting ΔV_m, and of the mean width of the peak by adjusting K_m. This has been done in Fig. 8 for acetone-water and for three amine-water systems. In the model used, the molar volume, V_m, is given by

$$V_m = M = x_m M_A + (1 - x_m)(mM_B)\,,$$

where M_A and M_B are the molecular weights of solute and water and M is that of the solution.

Now ΔV_m has been determined on the assumption that the thermal term in eqs. (13) and (24) is negligible compared with the isothermal term involving δ/β_T: we denote this assumed value of ΔV_m by ΔV_m^{is}. We could also proceed by assuming that the thermal term in these equations is dominant, that is, that the enthalpy change denoted ΔH_m^{th} is obtained on the assumption that the volume change of reaction is negligible. It then follows from eq. (24) that the same value of $\mu_{\max}$ is produced by ΔH_m^{th} (volume change negligible) *or* ΔV_m^{is} (enthalpy change negligible) if $V\theta\Delta H_m^{th} = C_p\cdot\Delta V_m^{is}$. Numerical values of m, K_m, ΔV_m^{is} and ΔH_m^{th} are listed in Table III.

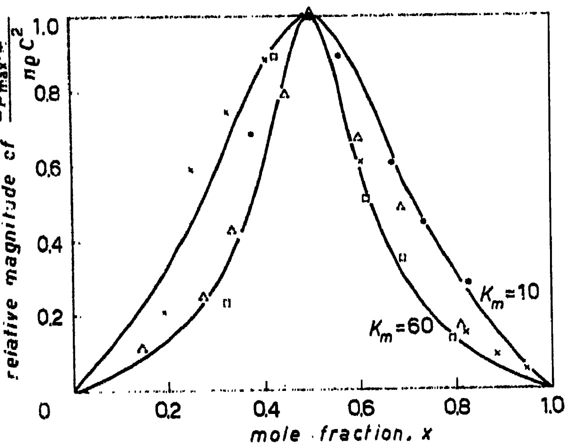

Fig. 8. — Relative values of $\mu_{\max}$ *vs.* concentration. The curves are calculated on the basis of model II. $A + B_m \rightleftharpoons AB_m$, with $K_m = 10$ and 60. The experimental points are fitted to the theory by selecting the value of m for each solution: acetone, 0 °C, $m = 1.5$ (triangles); diethylamine, 0 °C, $m = 9$ (squares); methyldiethylamine 0 °C, $m = 11.5$ (solid circles); n-amylamine 5 °C, $m = 19$ (crosses).

The values of ΔH_m^{th} given in Table III are comparable with estimates given in the literature [14, 15] for hydrogen-bond energies and this is a strong indication that the process is *not* isothermal.

The association of a cluster of water molecules (B_m) with one solute molecule (A) in a single step as assumed in Model II is an unlikely occurrence even though it appears to explain the relatively low P.S.A.C. found with most of the systems. More likely, the water molecules will associate with a solute

TABLE III. – *Summary of calculations for aqueous solutions based on the model.* $A+B_m \rightleftharpoons AB_m$:

T (°C)	Acetone 0 °C	Diethyl-amine 0 °C	Methyl-diethylamine 0 °C	n-amylamine 5 °C
P.S.A.C. mole fraction	0.4	0.1	0.08	0.05
$2\mu_{\max} VRT/\pi\varrho c^2$	0.301	1.54	2.02	0.648
$C_p/V\theta$ (kcal/cm³)	0.7	0.3	0.3	0.15
$m=(1-PSAC)/PSAC$	1.5	9	11.5	19
$2\mu_{\max} V_m RT/\pi\varrho c^2$	3.77	7.72	12.7	6.48
ΔV_m^{is} (cm³/mole)	9.2	14.3	13.5	9.6
ΔH_m^{th} (kcal/mole)	6.4	4.3	4	1.4

ΔV_m^{is} is the volume change of reaction calculated on the assumption of negligible enthalpy of reaction (isothermal); $l \gg \theta V \Delta H/C_p \Delta V$.

ΔH_m^{th} is the enthalpy change of reaction calculated on the assumption of negligible volume change of reaction (thermal); $l \ll \theta V \Delta H/C_p \Delta V$.

molecule one by one to build up a complex containing several water molecules and ANDREAE and his colleagues [7] have made further calculations based on the following models

— *Model III*

$$A+B \rightleftharpoons AB;$$

$$AB+B \rightleftharpoons AB_2 \ldots AB_{m-1}+B \rightleftharpoons AB_m .$$

They assume a forward rate constant k_f independent of m and an equili-

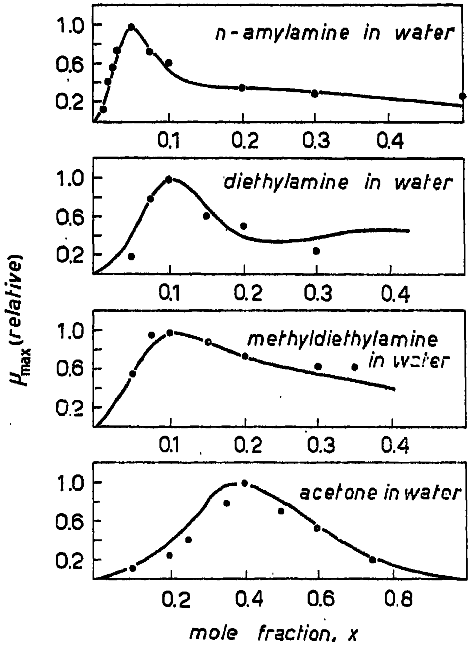

Fig. 9. – Theoretical curves for Model III:

$$A+B \rightleftharpoons AB;$$

$$AB+B \rightleftharpoons AB_2 \ldots AB_{m-1}+B \rightleftharpoons AB_m ,$$

with experimental points for aqueous solutions: n-amylamine, 5 °C, $\varphi=0.7$, $K_1=5\,000$; diethylamine, 0 °C, $\varphi=0.23$, $K_1=10^6$; methyldiethylamine, 0 °C, $\varphi=0.13$, $K_1=640$; acetone, 0 °C, $\varphi=0.6$, $K_1=80$.

brium constant $K_m = \exp[-\Delta G_m/RT]$ where the free energy ΔG_m is taken to be equal to $\Delta G_1 \exp[-(m-1)\varphi]$. ΔG_1 is the free energy change in the first reaction and φ is an adjustable parameter which determines the penetration of the influence of the primary bond between the solute and the first water molecule through the complex to the more distant water molecules. φ and the equilibrium constant K_1 alone determine the shape of the μ_{max} curve.

Experimental values of μ_{max} for solutions of acetone and three amines in water are compared in Fig. 9 with theoretical predictions based on this model.

Although some success has been achieved with the above models in explaining the peak in the absorption *vs.* concentration curves for the aqueous solutions of nonelectrolytes, none of these has any direct connection with the sharp peak in sound velocity which is observed at very low concentrations. A single model which would explain *both* the absorption and the velocity of sound peaks is the ultimate objective of theoretical derivations. Since the absorption peak for acetone-water solutions is close to 0.5 mole fraction, this is the simplest system to consider. The peak actually occurs at 0.4 mole fraction and, to this extent, the following model is expected to be in error. Consider therefore,

Model IV

$$A + B \rightleftharpoons AB; \qquad B \rightleftharpoons B^* . \tag{69}$$

Since the addition of a small amount of solute increases the velocity of sound, it is necessary to suppose that the solute molecule causes some of the water molecules to change to a less compressible form. In the above model it is postulated that water molecules can exist in two forms, bound B^*, and free B, and that ordinary water is composed of a mixture of the two forms.

Since the system acetone-water has a P.S.A.C. approaching 0.5, the formation of complexes is roughly described by a simple $A+B \rightleftharpoons AB$ equilibrium. The water structure is idealized by an equilibrium $B \rightleftharpoons B^*$, where B is free water and B^* is bound water. It is assumed that the characteristic frequency associated with the water equilibrium is much higher than that which is observed experimentally and attributed to the formation of AB complexes. It is also postulated that the equilibrium constant K_{Bx} for the water equilibrium at concentration x varies with concentration according to

$$K_{Bx} = K_{B0}(1-x)^u .$$

The value of u determines the rate of rise of sound velocity with concentration at low concentrations.

Details of the working of this model are involved and, for present purpose, it suffices to show in Fig. 10 a comparison between measured values of absorption and velocity and theoretical calculations based on the above model for acetone-water. It should be emphasized that a P.S.A.C. of 0.5 mole fraction is assumed in the model, whilst the value found for this solution is 0.4. Clearly,

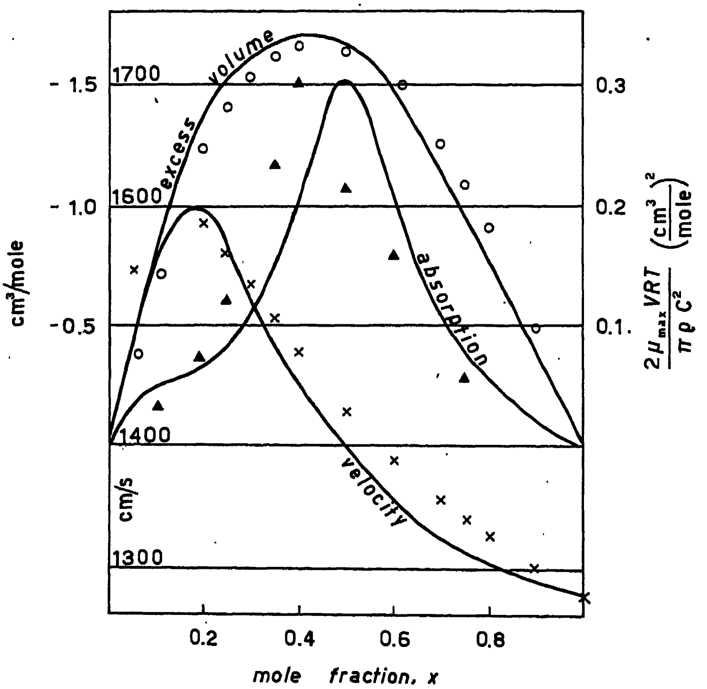

Fig. 10. – Experimental points for sound absorption and velocity for acetone-water solutions compared with theoretical curves based on Model IV:

$$A+B \rightleftharpoons AB; \qquad B \rightleftharpoons B^*.$$

a combination of Models III and IV would be expected to give better agreement with experimental results.

The peak in sound velocity at low concentrations is attributed to the breakdown of the water structure whilst the peak in the absorption at higher concentrations is attributed to the formation of complexes.

6. – Vibrational specific-heat relaxation in liquids.

Extensive studies have been made of the ultrasonic relaxation and its associated dispersion in gases and vapours which arise from the time-delay in the redistribution of energy between the vibrational and translational or rotational degrees of freedom of the molecules.

Physically, the time-delay in establishing the equilibrium is due to the fact that many collisions are required for a molecule to lose one quantum of vibrational energy. The energy is coupled into the molecule via the mode of lowest vibrational frequency and then spreads rapidly to the other vibrational modes.

Only a few examples of vibrational specific heat relaxation have been observed in liquids, due to the fact that the expected region of relaxation generally falls at frequencies higher than it has yet been possible to reach experimentally.

The redistribution of energy between vibrational and translational degrees of freedom of the molecules is initiated by temperature changes and does not involve a change in volume at constant pressure and temperature. Hence, putting $\Delta V = 0$ in eq. (14), we have

$$r = \frac{\delta\beta_S}{\beta_S} = \frac{(\gamma - 1)\,\delta C_p}{C_{p\infty}} = \frac{(\gamma - 1)\,\delta C}{(C_p - \delta C)}\,, \tag{70}$$

where δC is the appropriate amount of vibrational specific heat which is involved in the ultrasonic relaxation.

In the majority of cases, this will be the total vibrational specific heat, C_{vib}, the relaxation of which will be associated with a single relaxation time, τ, or characteristic frequency, f_0.

Certain notable examples exhibit double dispersion in which different vibrational modes have associated with them different relaxation times. In sulphur dioxide, for example, the pronounced relaxation centred about a frequency of 23 MHz at temperatures between 0 °C and 50 °C is associated with the time-delay in deactivation of only two out of the three vibrational modes. The mode which does not participate is that of lowest wave number (lowest quantum energy) which is presumed to be responsible for a relaxation at higher frequencies of the order of 1500 MHz.

The observed relaxation in this liquid [16] is shown in Fig. 11, each curve being plotted according to eq. (25).

$$\frac{\alpha}{f^2} = \frac{A}{1 + (f/f_c)^2} + B\,. \tag{25}$$

Davies and Lamb [3] have shown that provided $r = \delta\beta_S/\beta_S < 0.4$, then to within an accuracy of 1 % we can write

$$\frac{2\mu_{\max}}{\pi} = \frac{r}{(1 - r)^{\frac{1}{2}}}\,. \tag{71}$$

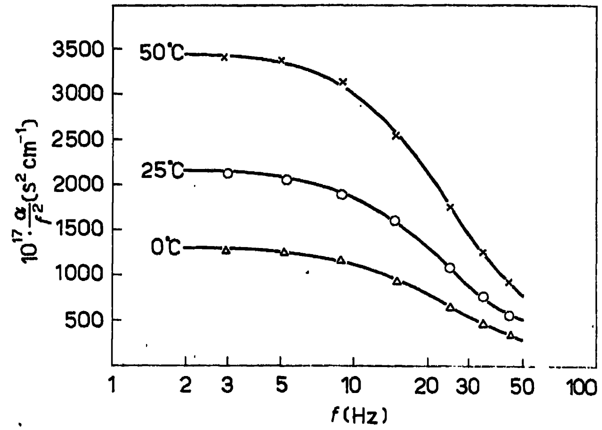

Fig. 11. – Vibrational specific heat relaxation in sulphur dioxide. The curves are calculated according to eq. (25) and the points are experimental.

However, in cases where the velocity dispersion cannot be neglected, μ_{max} is not given simply by $\frac{1}{2}Acf_c$ as was assumed in Sections 2·2 and 2·4, since the velocity of sound at the frequency for which μ attains its maximum value is not equal to the value c at low frequencies. In such cases, BASS and LAMB [16, 17] have shown that the relaxation strength, r, is calculated from the experimentally derived quantities, A, B and f_c, by the relationship

$$r = Acf_c/\pi - \tfrac{1}{4}[1-2B/A](Acf_c/\pi)^2 + \dots \tag{72}$$

Having obtained a value for r from experiment in this way, substitution in eq. (70) gives the experimentally derived value of the relaxing specific heat δC_1 (expt.) and this is compared with the sum of the vibrational specific heats for the two modest of highest wave number for three temperatures in Table IV.

TABLE IV. – *Experimental and theoretical values for the relaxing specific heat for sulphur dioxide.*

T (°C)	δC_1 (expt.) (cal·mole/°C)	δC_2 (theor.) (cal·mole/°C)	% difference $(\delta C_1 - \delta C_2)/\delta C_2$
0	0.291	0.259	+12
25	0.383	0.373	+3
50	0.461	0.502	−8

δC_2 (theor.) is the sum of the vibration specific heats for the 2 modes of highest wave number.

It is concluded that the observed relaxation (Fig. 11) for sulphur dioxide can be attributed to the relaxation of the two vibrational modes of highest wave number. The third mode of lowest wave number contributes a specific heat of 1.289 cal·mole/°C at 50 °C and is presumed to relax at much higher frequencies. The derived value for the quantity B in eq. (25) is consistent with this hypothesis and the second relaxation is calculated to have a characteristic frequency of about 1500 MHz, which is outside the range experimentally obtainable.

In carbon disulphide [18] the observed relaxation centred about 78 MHz at 25 °C and 31 MHz at -63 °C is due to the total specific heat of the three vibrational modes. The curves of Fig. 12 are calculated in accordance with eq. (25). Values of $\mu_{\max}$ (expt.) obtained from experiment are compared with values calculated from the relaxation of the total vibrational specific heat in Table V and agreement is very good indeed.

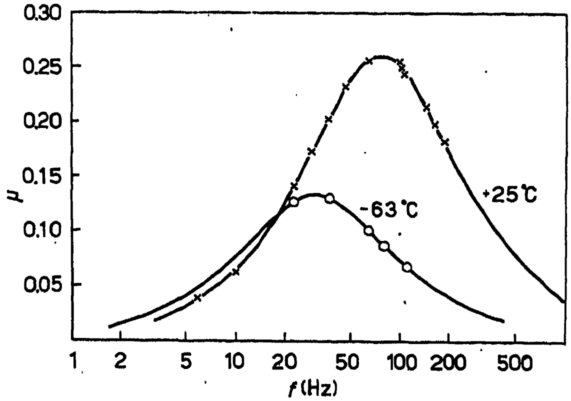

Fig. 12. – Vibrational specific heat relaxation in carbon disulphide. The curves are theoretical and the points experimental.

TABLE V. – *Experimental and theoretical values for $\mu_{\max}$ for carbon disulphide.*

T (°C)	f_c (MHz)	$\mu_{\max}$ (expt.)	δC_{vib} (cal·mole/°C)	$\mu_{\max}$ (calc.)
25	78	0.262	3.933	0.260
-63	31	0.134	2.683	0.133

Similarly, in liquid carbon dioxide the observed relaxation strength is adequately described in terms of a relaxation of the total vibrational specific heat associated with a single relaxation time [17]. A comparison of calculated and experimental values for the relaxation strength of carbon dioxide is given in Table VI.

The principle uncertainty in comparing the above figures is in the reliability of the additional thermal data required in the calculations and agreement with experiment is considered to be satisfactory.

TABLE VI. – *Calculated and experimental values for the relaxation strength of carbon dioxide.*

T (°C)	0	0	25	25	30	35
p (atm.)	70	37.5	97	69	86	103
C_{vib} (cal·mole/°C)	1.440	1.640	1.921	1.921	1.977	2.029
r (theor.)	0.1026	0.1100	0.1308	0.1363	0.1375	0.1397
r (expt.)	0.1088	0.1163	0.1379	0.1454	0.1428	...
$\Delta r/r$ (% difference)	+6.0	+5.8	+5.3	+6.6	+3.8	—

Measurements of ultrasonic absorption in sulphur hexafluoride, nitrous oxide, cyclopropane and methyl chloride are all consistent with the assumption that the observed nonclassical absorption is entirely due to the vibrational specific heat relaxation and that the total vibrational specific heat relaxes with a single relaxation time.

The other notable case of a double relaxation is in methylene chloride [19]. Measurements of ultrasonic absorption in this liquid at frequencies between 7.5 and 210 MHz confirm previous results obtained in the vapour by SETTE BUSALA and HUBBARD [20], from which it was concluded that the relaxation of the vibrational specific heat takes place in two parts. In the frequency range over which measurements were made in the liquid there is a single relaxation of specific heat equal in magnitude to the vibrational specific heat less the contribution of the lowest frequency mode of vibration. The characteristic frequency at 25 °C is 170 MHz.

In conclusion, it can be said that the relaxation of vibrational specific heat in liquids follows the pattern established for gases and vapours and that, in general, the total vibrational specific heat relaxes with a single relaxation time. In certain cases, particularly where relatively large differences occur between the energy quanta of the individual vibrational modes, double relaxation and dispersion is observed but, for all liquids investigated, it has been found possible to specify exactly which vibrational modes are operative over the relaxation region.

Detailed comparisons of the dependence of relaxation time on density from gas to liquid have been made by MADIGOSKY and LITOVITZ [21], using their own measurements over a range of density from 400 to 600 amagat at 25 °C and 50.2 °C for carbon dioxide and the data of HENDERSON and his collaborators [22, 23] and of BASS and LAMB [17] at densities up to about 400 amagat. For densities up to about 400 amagat the relaxation time is inversely proportional to the density, indicating that, in this range, the number of binary collisions required to excite the internal vibrations does not vary with density. However, above about 450 amagat in density, deviations from the simple law are observed. On the basis that only binary collisions are important, Madigosky and Litovitz find that the Eyring-Hirschfelder cell model of a liquid accounts well for the dependence on density of the characteristic frequency but gives values of mean free path which are too large. These authors propose that, for mean free path calculations, a cell model must not incorporate fixed walls, as in the Eyring-Hirschfelder model, but rather moving or free walls. The mowing wall cell model gives a value of mean free path between collisions, which is exactly one-half the value obtained from the fixed wall cell model and, with this modification, good agreement was found for both carbon dioxide and sulphur dioxide.

* * *

During the years whilst I have worked on problems of ultrasonic relaxation effects in liquids my thinking on these topics has been greatly influenced by the numerous discussions which I have had with Dr. J. H. ANDREAE and, in former years, with Dr. R. O. DAVIES. To both of these friends, I wish to express my sincere appreciation of the benefit which I have received from their most stimulating collaboration: each in turn has been responsible for many of the ideas which I have discussed here.

The material described in Section 5 is entirely the work of Drs. ANDREAE, EDMONDS and McKELLAR, and I wish to thank them for their kindness in making their results available to me in advance of publication. I believe this work to be an outstanding contribution to the use of ultrasonic relaxation methods in the study of fast chemical reactions and it is for this reason that I have sought to give a brief description of it at the expense of other material which might otherwise have been included. I am also grateful to the Director of Research, Dyestuffs Division, Messrs. Imperial Chemical Industries Ltd., for permission to describe this work carried out by the above Authors in the I.C.I. Laboratories.

Finally, I should like to record the valuable contribution which Dr. M. S. DE GROOT made to the study of rotational isomers by ultrasonic relaxation methods. The work outlined in Section 4 was the result of a fruitful collaboration with Dr. DE GROOT over a period of some three years and the success of this was largely due to his untiring effort and boundless enthusiasm.

REFERENCES

[1] J. FRENKEL: *Kinetic Theory of Liquids* (Oxford, 1946).
[2] T. L. DE DONDER: *Affinity* (Stanford, Cal., 1936).
[3] R. O. DAVIES and J. LAMB: *Quart. Rev. Chem. Soc. (London)*, **11**, **134** (**1957**).
[4] I. PRIGOGINE: *Etude Thermodynamique des Phénomènes Irreversibles* (Paris, 1947).
[5] S. R. DE GROOT: *Thermodynamics of Irreversible Processes* (Amsterdam, 1951).
[6] J. H. ANDREAE and J. LAMB: *Proc. Phys. Soc.*, **B 69**, **814** (**1956**).

[7] J. H. Andreae, P. Edmonds and J. F. McKellar: *Journ. Chem. Phys.*, (submitted for publication): *Nature*, **195**, 778, 865 (1962).

[8] R. O. Davies and J. Lamb: *Proc. Phys. Soc.*, B **69**, 293 (1956).

[9] J. Lamb and J. M. M. Pinkerton: *Proc. Roy. Soc.*, A **199**, 114 (1949).

[10] M. S. de Groot and J. Lamb: *Proc. Roy. Soc.*, A **242**, 36 (1957).

[11] J. M. Young and A. A. Petrauskas: *Journ. Chem. Phys.*, **25**, 943 (1956).

[12] W. G. Schneider: *Coll. Intern. Centre Nat. Recherche Sci.*, (Paris (77), 1959), p. 529.

[13] R. N. Barfield and W. G. Schneider: *Journ. Chem. Phys.*, **31**, 488 (1959).

[14] L. Pauling: *The Nature of the Chemical Bond* (New. York, 1960).

[15] G. C. Pimental and A. L. McClellan: *The Hydrogen Bond* (New York, 1960).

[16] R. Bass and J. Lamb: *Proc. Roy. Soc.*, A **243**, 94 (1957).

[17] R. Bass and J. Lamb: *Proc. Roy. Soc.*, A **247**, 168 (1958).

[18] J. H. Andreae, E. L. Heasell and J. Lamb: *Proc. Phys. Soc.*, B **69**, 625 (1956).

[19] J. H. Andreae: *Proc. Phys. Soc.*, B **70**, 71 (1957).

[20] D. Sette, A. Busala and J. G. Hubbard: *Journ. Chem. Phys.*, **23**, 787 (1955).

[21] W. M. Madigosky and T. A. Litovitz: *Journ. Chem. Phys.*, **34**, 489 (1961).

[22] M. C. Henderson and L. Peselnick: *Journ. Acoust. Soc. Am.*, **29**, 1074 (1957).

[23] M. C. Henderson and J. Z. Klose: *Journ. Acoust. Soc. Am.*, **31**, 29 (1959).

Ultrasonic Relaxation in Liquids.

T. A. LITOVITZ

Catholic University - Washington, D. C.

I. – Vibrational Relaxation.

1. – Introduction.

LAMB and co-workers [1] have shown that if one uses the measured values of relaxation time the magnitude of the relaxation loss in CS_2, for example, can be very well accounted for by assuming that just as in the gas all the vibrational modes relax with one relaxation time. This work firmly established the existence of vibrational relaxation in liquids. However, the rather interesting problem arises as to what is in liquids the mechanism of energy transfer from internal or vibrational to translational degrees of freedom.

The basic question is whether or not the mechanism is the same as in a gas.

The theory of vibrational relaxation in gases has been successfully developed by SCHWARTZ and HERZFELD [2*a*, 2*b*]. They assume that the transfer of energy between vibrational and translational degrees of freedom is due to binary collisions and derive an expression for the probability of energy transfer per collision (P). LITOVITZ [3] suggested that this concept of binary collisions can account for the vibrational relaxation times in dense gases and liquids if proper attention is given to the finite size of the molecule. One assumes that the collision efficiency P^* is the same in the liquid as in the gas except for a factor which is related to the effect of attractive forces on P^*. In addition, a cell model is used to calculate the mean free path in the liquid.

2. – Comparison of data to gas kinetic theory predictions.

The time it takes the internal degrees of freedom (the vibrational model in the case of CO_2) to return from an excited state to equilibrium with the external degrees of freedom is called the «relaxation time», τ. This thermal relaxation time in the case of binary collisions may be expressed by

$$\tau = (\tilde{N} P^*)^{-1}, \tag{1}$$

where $\tau = (2\pi f_r)^{-1}$, $\tilde{N}$ is the number of collisions per second, and P^* the total probability that a collision is effective in producing a vibrational energy transfer to translational energy (or transition probability).

For the number of collisions per second we may use

$$\tilde{N} = \bar{v}/L_f, \tag{2}$$

where L_f is the mean free path and $\bar{v}$ is the average velocity of the molecules.

When considering the gas kinetic theory one can use the results of the Sutherland model which gives

$$L_f = \left[\sqrt{2}\pi\sigma^2 \varrho \left(1 + \frac{C}{T}\right)\right]^{-1}, \tag{3}$$

and

$$\bar{v} = \left(\frac{8RT}{\pi M}\right)^{\frac{1}{2}}, \tag{4}$$

where σ is the hard-sphere molecular diameter, ϱ the molecular density, and C is the Sutherland constant. If one assumes that the collision efficiency P^* is independent of density (this is reasonable since for low density it should only depend on the mechanics of the collision involved and not on surroundings), then by eqs. (1)–(4) we see that gas kinetic theory predicts that

$$\frac{f_r}{\varrho} = \text{constant}. \tag{5}$$

HENDERSON and PESELNICK [4] have measured the relaxation frequency in gaseous CO_2 at 50.2 °C up to 440 amagat, from which they conclude that f_r/ϱ is constant at a value of 30.9 kHz/a.u. over the entire range of densities. The amagat unit (a.u.) is defined as the ratio of the density to the density at standard conditions. MADIGOSKY and LITOVITZ [5] have made measurements up to much higher densities.

Figure 1 shows the relaxation frequencies at 50.2°C plotted against the density expressed in amagat. At this temperature the CO_2 remains a gas over the entire density range covered. Included in the graph are the values reported by HENDERSON and PESELNICK [4]. The critical density occurs at 237 a.u. The straight line is that of HENDERSON and PESELNICK $f_r/\varrho =$ $= 39.9$ kHz/a.u.

The data of MADIGOSKY and LITOVITZ [5] indicate that there is a large de-

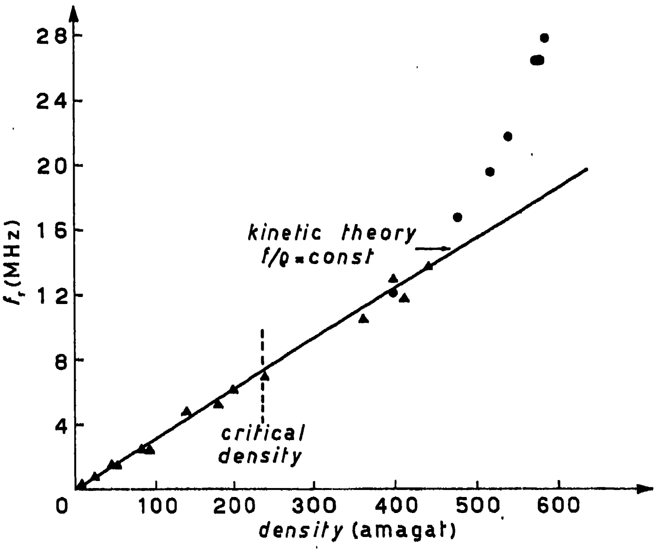

Fig. 1. – Relaxation frequency *vs*. density in gaseous CO_2 at 50.2 °C. (Taken from ref. [5]). ● Madigosky and Litovitz; ▲ Henderson and Peselnick.

parture from the gas kinetic theory (f_r/ϱ = const) in the high-density region above 400 a.u. Furthermore, this departure is in the same direction and of the same general shape as that obtained by Litovitz, Carnevale, and Kendall [6] for liquid CO_2.

In Fig. 2 we see the same type of deviation from the gas kinetic theory

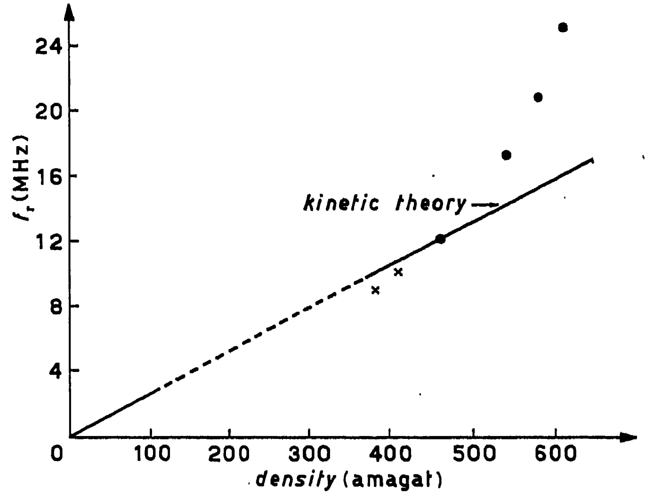

Fig. 2. – Rrlaxation frequency *vs* density in liquid CO_2 at 25 °C. (Taken from ref. [5]). ● Madigosky and Litovitz; ▲ Bass and Lamb.

in the liquid state. The discontinuity in the density that occurs when liquidfying the gas is from 120 to 380 a.u. The straight line $f_r/\varrho = 26.35$ kHz/a.u. is the gas value reported by Shields [7] for CO_2 at 25 °C.

3. – Evaluation of collision times in the liquid and dense gas.

If one assumes that only binary collisions and not the co-operative action of molecules are important, then eq. (1) holds for the liquid and dense gas as well as for the normal gas state. It is in the evaluation of $\tilde{N}$ for the liquid or dense gas that we encounter difficulty. One approach is to use a modified cell model for the liquid state which allows a direct calculation of the mean free path.

3·1. *Use of the cell model to calculate L_f.* – A rigid-sphere model of the liquid state has been proposed by Eyring and Hirschfelder [8]. For short intervals of time the thermal motions of a molecule of diameter σ are assumed to be confined within a shell-like arrangement of nearest neighbors. Assuming that all molecules occupy the lattice points of a cubic cell the center molecule or « wanderer » is free to move a distance of $2(V/N)^{\frac{1}{3}} - 2\sigma$, where V is the volume, N the number of molecules in that volume, σ the diameter of the rigid-sphere molecule, and $(V/N)^{\frac{1}{3}} = (1/\varrho)^{\frac{1}{3}}$ the mean distance between molecular centers. The mean free path for the fixed-wall cell model is given by

$$L_f = 2\left[\left(\frac{1}{\varrho}\right)^{\frac{1}{3}} - \sigma\right]. \tag{6}$$

Combining eq. (6) with eqs. (1) and (2), we have

$$\tau = \left(\frac{2}{\bar{v}p^*}\right)\left[\left(\frac{1}{\varrho}\right)^{\frac{1}{3}} - \sigma\right]. \tag{7}$$

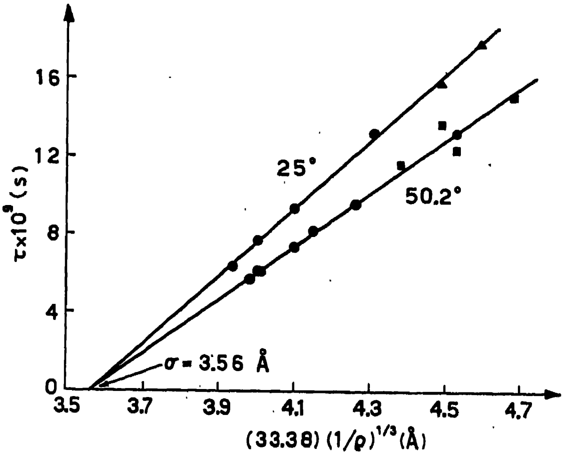

Fig. 3. – Plot of relaxation time in CO_2 *vs.* mean distance between molecular centers; $\tau = ((1/e)^{\frac{1}{3}} - \sigma)/\bar{v}P^*$. (Taken from ref. (5)). ● Madigosky and Litovitz; ▲ Bass and Lamb; ■ Henderson and Peselnick.

If the collision probability P^* is independent of pressure, a plot of τ *vs.* $(1/\varrho)^{\frac{1}{3}}$ should result in a straight line.

Figure 3 shows the experimental data for carbon dioxide plotted in the above manner. Two important observations can be made.

1) The data fit the straight lines extremely well; hence, eq. (7) does predict the correct pressure-dependence in CO_2 for both high-density gas and in the liquid state just as it did for CS_2.

2) The abscissa intercept is a direct measurement of the molecular diameter σ. Furthermore, since both lines have the same intercept, this value is identical for the liquid and highly compressed gas at the two temperatures measured.

TABLE I. – *Comparison of collision efficiencies of the liquid and gas with the dilute gas.*

	T (°C)	σ cell model (Å)	Sutherland (Å)	P^*_{gas}	$\left(\dfrac{P^*_{\text{gas}}}{P^*_{\text{liq}}}\right)_{\text{exp}}$	$1+\dfrac{C}{T}$	$\exp\left[\dfrac{\varepsilon}{(KT)}\right]$	$(P^*_{\text{liq}})_{\text{calc}}$	$(P^*_{\text{liq}})_{\text{exp}}$
CO_2	25	3.56±0.02 (^{i})	3.54 (^{a})	1.75 (^{b,c})	1.1	1.67	1.89	1.55 (^{b})	1.54 (^{b})
CO_2	50.2	3.56±0.02 (^{i})	3.54	2.08 (^{d})	1.1	1.62	1.80	1.87	1.88
CS_2	25	4.32 (^{e})	4.13 (^{f})	10.9 (^{g})	2.5	2.53	5.14	5.4	4.4 (^{h})

(*a*) Calculated by eq. (8).

(*b*) All values should be multiplied by 10^{-4} s^{-1}.

(*c*) Ref. [7].

(*d*) Ref. [4].

(*e*) Ref. [3].

(*f*) Calculated by eq. (8) and viscosity data of *Handbook of Chemistry and Physics* (Cleveland, Ohio, 1949), p. 1763.

(*g*) F. A. ANGONA: *Journ. Acoust. Soc. Am.*, 25, 1116 (1954).

(*h*) Application of the modified cell model using 4.32 [see Ref. [2]] to the liquid data of J. H. ANDREAE, E. L. HEASELL and J. LAMB: *Proc. Phys. Soc. London*, B 69, 625 (1956).

(*i*) W. MADIGOSKY and T. LITOVITZ: *Journ. Chem. Phys.*, 34, 489 (1961).

Not only does the molecular diameter agree in the liquid and gas but it also agrees with that predicted by the kinetic theory hard-sphere Sutherland equation for viscosity (see Table I). From kinetic theory one has that

$$\eta = 0.499\, m\varrho\bar{v}L_f \tag{8}$$

or

$$\eta = \frac{0.499\cdot 2\,(\pi m k T)^{\frac{1}{2}}}{\pi^2\sigma^2(1+C/T)}, \tag{9}$$

where η is the viscosity, m the mass per molecule, $\bar{v}$ the average velocity, and C Sutherland's constant. Both Sutherland's constant and the molecular diameter may be calculated by use of eq. (8) and a knowledge of the viscosity at two different temperatures.

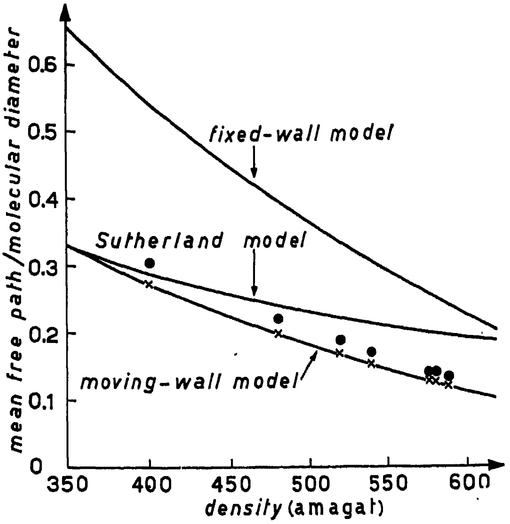

Fig. 4. – Comparison of the mean free path divided by the molecular diameter as a function of density predicted by kinetic theory, fixed-wall cell model, and modified cell model. Included are data assuming $P^*_{\text{liq}}=P^*_{\text{gas}}$ and the same data corrected for $P^*_{\text{liq}}\neq P^*_{\text{gas}}$. (Taken from ref. [5]): ● experimental points using $P^*_{\text{liq}}=P^*_{\text{gas}}$; × experimental points corrected for $P^*_{\text{liq}}/P^*_{\text{gas}}>1.0$.

In Fig. 4 are plotted several curves of the mean free path L_f divided by the molecular diameter σ as a function of the amagat density. The upper is determined from the cell model eq. (6), and the middle is determined from gas kinetic theory (Sutherland model). The two sets of points are experimental values of L_f/σ obtained from acoustic data by assuming $P^*_{\text{liq}}=P^*_{\text{gas}}$ and correcting for the fact that attractive forces play no role in the liquid and thus $P^*_{\text{liq}}/P^*_{\text{gas}}>1.0$ (see Section 4).

One finds that even though the cell model predicts a density-dependence in agreement with experimental values, the magnitude of $(L_f/\sigma)_{\text{cell}}$ is larger than $(L_f/\sigma)_{\text{acoustic data}}$. The Sutherland model though giving better agreement in magnitude does not give the proper density-dependence of L_f/σ. The fact that the fixed-wall cell model predicts so accurately the pressure-dependence of the relaxation time causes one to look for a modification of the cell model rather than propose an entirely new model.

3'2. *Modification of the cell model for movable walls.* – MADIGOSKY and LITOVITZ [5] suggest that a description of the liquid state in terms of fixed-wall cells is somewhat unrealistic. A better approximation would be that of a wandering molecule trapped in not fixed, but moving, walls. Each nearest molecule that makes up the cubic cell is itself a « wanderer » which is in turn trapped within a mowing-wall cage made up of its nearest neighbors.

These ideas are clarified by MADIGOSKY and LITOVITZ by considering the one-dimensional array of molecules shown in Fig. 5. If we fix our attention on any one molecule, then the average length the molecule will travel before suffering a collision (the mean free path) is given by

$$L_f=\sum_{j=1}^{\infty}p_j l_j\,, \tag{10}$$

where l_j is the j-th distance a particle moves and p_j is the probability that the given molecule will move the distance l_j. A few of the different possibilities are shown in Fig. 5.

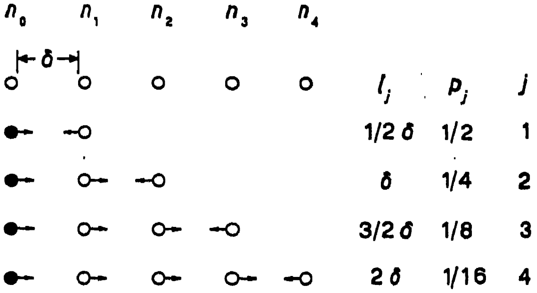

Fig. 5. – First four possible motions of a linear array of free molecules. In each case the distance moved is given by l_j and the probability of moving that distance l_j is given by p_j. (Taken from ref. [5]).

By evaluating all the possibilities eq. (9) becomes

$$L_f = \delta\,, \tag{11}$$

where δ is the average distance between molecular centers. This may be extended to a three-dimensional model by replacing by $(V/N)^{\frac{1}{3}}$ the average distance between molecular centers in a cubic lattice. Hence the mean free path in three dimensions is given by

$$L_f = \left[\left(\frac{1}{\varrho}\right)^{\frac{1}{3}} - \sigma\right]. \tag{12}$$

Thus

$$\tau = \left[\left(\frac{1}{\varrho}\right)^{\frac{1}{3}} - \sigma\right]\Big/\bar{v}P^*\,, \tag{13}$$

where $(1/\varrho) = (V/N)$. Thus the moving-wall model gives a value of L_f which is one-half the value obtained from the fixed-wall cell model. It does, however, yield the same molecular diameter, σ, and pressure-dependence of relaxation frequency as the fixed-wall cell model discussed above.

The lowest curve in Fig. 4 is that of L_f/σ, calculated from eq. (12). The 10% agreement between eq. (12) and the « circled » experimental points is satisfactory considering the assumption made ($P^*_{\text{gas}} = P^*_{\text{liq}}$) in calculating the experimental values of L_f/σ. Actually, it is shown below that P^*_{liq} should not be equal to P^*_{gas} because attractive forces have much less effect in the liquid than in the dilute gas. Taking the results below into consideration gives the excellent agreement shown by the « corrected » values of $(L_f/\sigma)_{\text{exp}}$.

One interesting result is that the Sutherland model mean free path is close to the cell model value over a surprisingly large range of moderate densities. For CO_2 these two theories predict values of L_f which agree within 5% over a range of densities from 150 to 350 amagat. This accounts for the results of HENDERSON and PESELNICK [4] who found that the kinetic theory mean free path gave good results up to approximately twice the critical density. As one continues to go up in pressure, the gas kinetic-theory value based on the Sutherland model is no longer appropriate and one must go over to the cell-model theory. The cell model, of course, breaks down at low densities when a given molecule is no longer effectively trapped in a cage.

4. – Comparison of transition probabilities in the liquid and dense gas versus the dilute gas.

The modified cell model correctly predicts the pressure-dependence of the relaxation time and gives an acceptable value of the mean free path in the liquid. It also enables us to make a calculation of the transition probability in the liquid or dense gas. Using eq. (13) the transition probability, P^*, may be calculated from the average velocity and the slope of the lines in Fig. 3. Values obtained in this manner are compared with the appropriate gas transition probabilities in Table I. The gas transition probabilities were calculated from ultrasonic data, the viscosity relation

$$\eta = 1.271\, p t_c \tag{14}$$

and

$$P^* = t_c/\tau\,, \tag{15}$$

where $t_c = 1/N$ is the time between collisions, η the viscosity in poise and p the pressure in dyne per cm². A similar comparison is listed for CS_2. For CO_2 the transition probabilities P^*_{gas} and P^*_{liq} agree within 10%; however, in CS_2 the agreement is not good. In both CS_2 and CO_2 the transition probabilities P^*_{gas} are larger than P^*_{liq}.

LITOVITZ [3] has suggested that the attractive forces probably do not play a role in determining P^*_{liq}, and therefore this could account for the difference between P^*_{gas} and P^*_{liq}. SCHWARTZ and HERZFELD [2a] have calculated the following expression for P^* in the gas state:

$$P^* = (1.294)\left(\frac{r_c}{r_0}\right)^2 (Z_0\, Z_{\text{osc}}\, Z'_{\text{tr}})^{-1}\, \frac{\exp[\varepsilon/kT]}{1 + C/T}\,, \tag{16}$$

with the abbreviations

$$Z_{\text{osc}} = \frac{M_B M_C (M_A + M_B + M_C)}{(M_B^2 + M_C^2) M_A} \left(\frac{1}{\pi^2}\right)\left(\frac{\theta'}{\theta}\right),$$

and

$$Z'_{\text{tr}} = \pi^2 \left(\frac{\theta}{\theta'}\right)^2 \left(\frac{3}{2\pi}\right)^{\frac{1}{2}} \left(\frac{T}{\theta'}\right)^{\frac{1}{6}} \cdot \exp\left[\frac{3}{2}\left(\frac{\theta'}{T}\right)^{\frac{1}{3}} - \left(\frac{\theta}{2T}\right)\right.\,,$$

where C is Sutherland's constant, r_c is the distance of closest approach, r_0 is the zero of the Lennard-Jones potential well, ε is depth of the Lennard-Jones potential well, $\theta = h\nu/k$, $\theta' = 0.915\,3M\theta^2 l^2$, the M's are molecular weights of the triatomic molecule, l is the characteristic length of the vibrator which is around 0.2 Å, and Z_0 is a geometrical factor approximately equal to three.

If the thermal relaxation mechanism is the same in the liquid as in the gas, then eq. (16) is applicable in the liquid state except that the factors $(1+C/T)^{-1}$ and $\exp[\varepsilon/kT]$ are not needed. The Sutherland correction factor $(1+C/T)^{-1}$ accounts for the long-range attractive forces which cause collisions between slow-moving molecules that otherwise would not have collided. The factor $\exp[\varepsilon/(kT)]$ accounts for the increased effective collision velocity arising from the presence of attractive forces. These factors are not effective in the liquid state since molecules are too close for these attractive forces to play a role. Thus one should write

$$P^*_{\text{liq}} = P^*_{\text{gas}} \frac{1 + C/T}{\exp[(\varepsilon/kT)]}, \tag{17}$$

where P^*_{liq} should be the same as the value of P^* for dense gas. If this assumption is correct, one can calculate the expected P^*_{liq} or $P^*_{\text{dense gas}}$ if the value of P^*_{gas} is shown. The calculated liquid values are listed in Table I. Excellent agreement is found between $(P^*_{\text{liq}})_{\text{calc}}$ and $(P^*_{\text{liq}})_{\text{exp}}$ for both CO_2 and CS_2. The effect of the attractive forces in CO_2 is only 10 % while in CS_2 it is over 100 %. Application of this correction to the data for CO_2 resulted in the excellent agreement between experimental and modified-cell-model mean free paths shown in Fig. 4.

5. – Effect of impurity on vibrational relaxation in liquids.

In Section 4 we saw that the density-dependence of the vibrational relaxation time gave strong evidence that the mechanism of energy transfer in liquids is a binary collision quite similar to that which occurs in dilute gases. A further comparison of this mechanism in gases and liquids can be made if one studies the effect of impurities. In this way energy transfer by collision between unlike molecules can be compared in the liquid and gas state.

If one considers a mixture of two substances, one of molecules type A and the other of molecules type B, the number of deactivations per second of this mixture is

$$\frac{1}{\tau_m} = \left[\frac{(1-x)}{\tau_{AA}}\right] + \frac{x}{\tau_{AB}}, \tag{18}$$

where τ_m is the relaxation time of the mixture related to the relaxation frequency by $\tau_m = (2\pi f_m)^{-1}$, τ_{AA} is the relaxation time of the pure A substance, and τ_{AB} is the relaxation time of an excited A molecule in pure B, x and $(1-x)$ are the molar fractions of B and A, respectively. This equation, rewritten as a function of the relaxation frequency, becomes

$$\left(\frac{f_s}{f_{AA}} - 1\right)\frac{1}{\chi} = \frac{f_{AB}}{f_{AA}}, \tag{19}$$

where f_s is the measured relaxation frequency of the mixture for a concentration χ, f_{AA} is the relaxation frequency of the pure A substance, and f_{AB} is the relaxation frequency of an excited A in a pure B. The ratio f_{AA}/f_{AB} is a measure of the effectiveness of an AB-type collision compared to an AA-type collision in transferring energy. This equation shows that f_s is linear with concentration and has been verified for gases by FRICKE and KNUDSEN [9]. The data of SLIE and LITOVITZ [10] in Fig. 6 for the liquid CS_2-alcohol mixtures show that the deactivation equation (19) also holds for liquids. It should be emphasized that eqs. (18) and (19) are applicable only if *binary collisions* are responsible for the relaxation process. The fact that f_s in the liquid state varies linearly with the impurity concentration is further evidence that the vibrational relaxation process in liquids is a binary collision process.

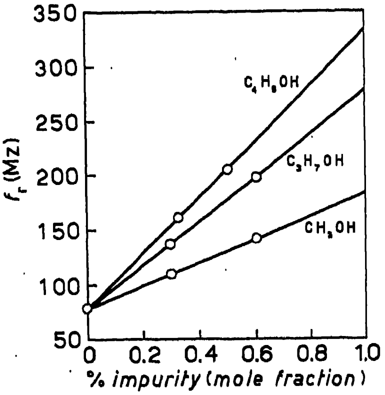

Fig. 6. – Relaxation frequency *vs.* impurity concentration in carbon disulfide. (Taken from ref. [10]).

6. – Comparison of f_{AA}/f_{AB} for liquid and gas state.

Whenever vibrational energy is exchanged between molecules by binary collisions the ultrasonic relaxation frequency is related to the probability of de-exciting a vibrational state P by the following equation:

$$f_r = P\tilde{N}, \tag{20}$$

where $\tilde{N}$ is the number of collisions per second. For like and unlike collisions this equation becomes $f_{AA} = P_{AA}\tilde{N}_{AA}$ and $f_{AB} = P_{AB}\tilde{N}_{AB}$, respectively. The discussions in Sections 1 to 4 indicate that the relaxation process for the AA collisions is the same in liquid and gas. If the AB mechanism is similar in liquid and gas, then the relative effectiveness of an AB to an AA collision should be the same in the liquid and gas. That is to say,

$$\left(\frac{P_{AB}}{P_{AA}}\right)_{gas} \Big/ \left(\frac{P_{AB}}{P_{AA}}\right)_{liq} = 1 .$$

The parameters obtained from the sonic data are f_{AB} and f_{AA}. We have

$$\frac{(f_{AB}/f_{AA})_{gas}}{(f_{AB}/f_{AA})_{liq}} = \frac{(P_{AB}\tilde{N}_{AB}/P_{AA}\tilde{N}_{AA})_{gas}}{(P_{AB}\tilde{N}_{AB}/P_{AA}\tilde{N}_{AA})_{liq}} . \tag{21}$$

The quantity $\tilde{N}_{AB}$ is difficult to calculate for the liquid so we shall assume that $\tilde{N}_{AB}/\tilde{N}_{AA}$ is the same for liquid and gas. Thus

$$\left(\frac{f_{AB}}{f_{AA}}\right)_{gas}\left(\frac{f_{AA}}{f_{AB}}\right)_{liq} = \left(\frac{P_{AB}}{P_{AA}}\right)_{gas}\left(\frac{P_{AA}}{P_{AB}}\right)_{liq} . \tag{22}$$

If this assumption is valid, then

$$(f_{AB}/f_{AA})_{gas}(f_{AA}/f_{AB})_{liq} = 1$$

if the energy transfer process is the same in liquid and gas.

Table II gives a comparison of relaxation frequencies for liquid and gaseous mixturer found by Slie and Litovitz [10].

Table II. – *Collision effectiveness of unlike molecules at 25 °C in liquid and gaseous* CS_2.

Impurities	$(f_{AB}/f_{AA})_{liq}$ (a)	$(f_{AB}/f_{AA})_{gas}$ (b)	$(f_{AB}/f_{AA})_{liq}/(f_{AB}/f_{AA})_{gas}$
CH_3OH	137	131	1.05
C_3H_7OH	255	230	1.11
C_4H_9OH	319	287	1.11

(a) Data taken from ref. [10].
(b) Data taken from ref. [9].

The values of the collision efficiency at 25 °C for both the liquid and gas are given in Table II. The ratio $(f_{AB}/f_{AA})_{liq}/(f_{AB}/f_{AA})_{gas}$ varies from 1.05 to 1.11. The error in the liquid measurement at this temperature is about 5 %, but the combined error for both the liquid and gas data is certainly greater than 5 %. Therefore, it is concluded that $(f_{AB}/f_{AA})_{liq}$ is equal to $(f_{AB}/f_{AA})_{gas}$ within experimental error. This result indicates that the ratio of collision efficiencies

P_{AB}/P_{AA} for liquid and gas is the same in both states. Therefore the same type of binary collision must occur for the AB collision in both liquid and gas states.

7. – Isomeric relaxation.

The discussion by **Lamb** in earlier lectures showed that the process of thermal relaxation is not limited to the transfer of energy between translation and vibrational degrees of freedom. Whenever a molecule has two or more isomeric states differing in energy isomeric relaxation will occur.

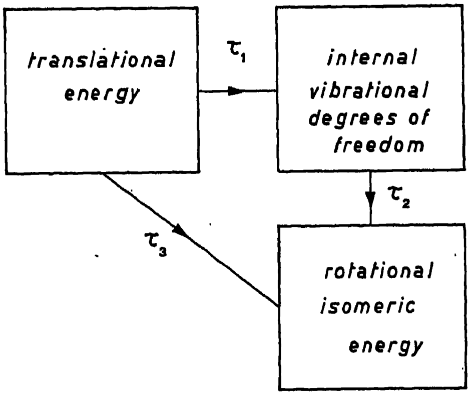
translational energy
τ_1
internal vibrational degrees of freedom
τ_2
τ_3
rotational isomeric energy

Fig. 7. – Box diagram showing possible routes by which energy can be transferred into isomeric degrees of freedom.

Ultrasonic studies have been very useful in yielding such information as the energy difference between the isomeric states and energy barrier impeding the transition between the states. Actually, the ultrasonic absorption is sensitive to the presence of less than 1 % of one of the isomeric forms.

The problem arises as to what determines the relaxation time for isomeric transitions. As shown in Fig. 7, one can conceive of at least two possible routes for the transfer of energy.

1) The energy can be transferred directly from the translational energy of the system by a collision process. In this case the relaxation time would be sensitive to the type and number of collisions. Thus, for example, raising the pressure and squeezing molecules closer together should shorten the relaxation time as in CS_2.

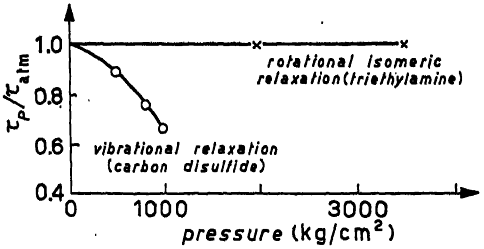

Fig. 8. – Vibrational and isomeric relaxation times *vs.* pressure. (Data taken from T. **Litovitz** and E. **Carnevale**: *Journ. Acoust. Soc. Am.*, **30**, 134 (1958)).

2) A second possible source of energy is through coupling with other internal degrees of freedom of the molecule—such as vibrational modes. Of course, collisions excite the vibrational modes, but these times are usually quite short compared to rotational isomeric relaxation times. This second mechanism of energy transfer

should be independent of the number of collisions per second and thus of the pressure also.

In Fig. 8, we see the experimental answer to the question as to which route the energy takes. The liquid exhibiting vibrational relaxation has had its relaxation time shortened by 40 % at 1000 atoms, while the liquid exhibiting isomeric relaxation has a relaxation time independent of pressure or density or number of collisions. It thus appears that the energy for isomeric transition comes from within the molecule and is independent of environment.

II. – Structural and Shear Relaxation.

1. – Introduction.

The liquid structure lacks long-range order; in addition the short-range order which does exist is imperfect. When the temperature is changed both the extent of the short-range order and the amount of imperfection, that is to say the presence of holes, will change. For example, as the temperature of a liquid is raised the range of the order decreases and the completeness of the short-range order decreases. At every pressure and temperature a degree of order, which describes the geometric state, is associated with a liquid. Any variation of this degree of order requires energy to be added to or taken from the substance because of the change in potential energy associated with the change of structure. This leads to a specific heat of a liquid, $C_{v,\text{liq}}$ which is greater than that of an amorphus solid. The difference is caused by the structural contribution to the specific heat.

An increase in temperature causes more holes to appear in the liquid. This effect contributes to the thermal expansion coefficient, β. An increase in pressure causes a decrease in the number of holes in the liquid and increases the short-range order which leads to a structural contribution to the compressibility, K.

If one wishes to measure the structural contributions to the properties of a liquid one must perform an experiment in which the time scale of the experiment is small compared with the time necessary for the structural rearrangement described above. As a liquid is cooled the rate of any molecular diffusion process necessary to accomplish structural change will be much larger than the time scale of a normal experiment, say the order of thirty minutes. In this region the liquid is said to become a glass. Below this temperature the degree of order will appear fixed and will not vary with either temperature or pressure during any reasonable length of time. Because of this inability of the structure to change with either pressure or temperature at temperatures below the glass transition, the structural degrees of freedom are said to be frozen out, thus the structural contributions to the specific heat, thermal expansion coefficient and compressibility, $C_{p,r}$, β_r and K_r respectively, are absent in the glassy state. Instead these quantities have magnitudes characteristic of crystal.

The differences in the values of C_p, β and K found in the liquid and glass are those parts of the respective parameters which have been frozen out. These relationships may be expressed as

$$C_{p,\text{liq}} = C_{p,r} + C_{p,\text{glass}}\,, \tag{23}$$

$$\beta_{\text{liq}} = \beta_r + \beta_{\text{glass}}\,, \tag{24}$$

$$K_{\text{liq}} = K_r + K_{\text{glass}}\,. \tag{25}$$

These equations show that by measuring quantities in both the liquid and glass states the structural contributions to the thermodynamic properties of a liquid can be obtained. Comparisons of measurements above and below the glass transition temperature show that as much as one-half of $C_{p,\text{liq}}$, β_{liq}, and K_{liq} are due to structural rearrangements.

One does not need to study the substances in the glassy state to investigate the structural relaxation properties. By drastically reducing the time scale of an experiment one can measure certain glasslike proprties of a liquid at temperatures higher than the normal glass transition temperature. It is very difficult to decrease the time scale of an experiment measuring either specific heat or volume expansion to less than several minutes. However, by using sonic and ultrasonic waves one can measure sound velocity and thus compressibility or elasticity from very long times for static measurements down to times as short as a hundredth of a microsecond or less. Using these short times one can make a pseudo glass transition occur at temperatures above the normal glass transition. This pseudo glass transition occurs when the period of the ultrasonic wave is shorter than the relaxation time associated with structural changes. Using these high-frequency ultrasonic waves one can measure the shear rigidity and compressibility of the noncrystalline liquid lattice and compare these properties with the values found in normal solids. The low- and high-frequency parameters are related by the expressions

$$C_{p0} = C_{p,r} + C_{p,\infty}\,, \tag{26}$$

$$\beta_0 = \beta_r + \beta_\infty\,, \tag{27}$$

$$K_{T,0} = K_{T,r} + K_{T,\infty}\,, \tag{28}$$

corresponding to eqs. (23) through (25).

Many liquids crystallize before forming a glass and therefore in most liquids the structural properties cannot be obtained by using the glass transition. For this type of liquid the ultrasonic measurements are of unusual interest for they allow us to obtain information about structural relaxation which could not otherwise be obtained. In fact information about structural relaxation processes is obtained in liquids in which the time scale of the measurement of the period of the wave is still long compared with structural rearrangement time. For example, in many liquids the volume or structural viscosity can be quite easily measured even though the structural relaxation time is of the order of 10^{-11} s or less.

2. – Dynamic elastic moduli of liquids.

In the following section we consider thos visco-elastic equations which relate the measured quantities, absorption and velocity, with the physically interesting parameters such as compressibility, moduli and relaxation times.

In a viscoelastic medium, one can relate the compressional part of stress, P, and strains by the compressional modulus K and the shear part of stress P_{ij} and strain S_{ij} by the shear modulus G. For the former one has

$$P = -Ks \tag{29}$$

and for the latter

$$P'_{ij} = GS'_{ij} . \tag{30}$$

If the applied stress varies with the time these equations are incomplete, one must turn to the general thermodynamic theory of relaxation where a more general stress-strain relationship for fluids has been derived by COLEMAN and NOLL. This theory gives, as a generalization of eq. (29) for pure compressonal deformation,

$$p + \tau_v \frac{\partial p}{\partial t} = -\left(K_0 s + K_\infty \tau_v \frac{\partial s}{\partial t}\right), \tag{31}$$

where K_0 is the static compressional modulus; and τ_v the structural relaxation time at constant volume. This is related to the constant pressure relaxation time, τ_p, by $\tau_p = (K_\infty/K_0)\tau_v$. It is often useful to use compressibility instead of moduli. The compressibility of a liquid is made up of two terms

$$K_0 = K_\infty + K_r ,$$

where K_∞ is the compressibility at high frequency and K_r is the increase resulting from the presence of structural rearrangement. The moduli are related to the compressibilities by the following equations:

$$K_0 = \frac{1}{\varkappa_0}, \qquad K_\infty = \frac{1}{\varkappa_\infty}, \qquad K_r = \frac{\varkappa_\infty - \varkappa_0}{\varkappa_\infty \varkappa_0}. \tag{32}$$

If one applies a sinusoidal pressure to the liquid, one obtains a complex modulus of compression.

$$K = -\frac{p}{s} = K_0 + \frac{K_r \omega^2 \tau_v^2}{1 + \omega^2 \tau_v^2} + i \frac{K_r \omega \tau_v}{1 + \omega^2 \tau_v^2}, \tag{33}$$

where $K_r = K_\infty - K_0$, and K_r is the relaxational modulus. A similar expression can be written for the compressibility

$$K = K_0 - K_r \frac{\omega^2 \tau_p^2}{1 + \omega^2 \tau_p^2} - iK_r \frac{\omega \tau_p}{1 + \omega^2 \tau_p^2}. \tag{34}$$

Rewriting eq. (33) one gets

$$P = K(-S) = [\mathrm{Re}\, K + i\omega\, \eta_v(\omega)](-S). \tag{35}$$

$\mathrm{Re}\, K$ is the real part of the modulus K, and $\eta_v(\omega) = K_r \tau_v / (1 + \omega^2 \tau_v^2)$. At low frequencies the volume viscosity, from eq. (35), is

$$\eta_v = K_r \tau_v. \tag{36}$$

Similar to (31), one has, for the shear stress, assuming a zero static shear modulus,

$$P'_{ij} + \tau_s \frac{\partial P'_{ij}}{\partial t} = G_\infty \tau_s \frac{\partial s_{ij}}{\partial t}, \tag{37}$$

where τ_s is the shear relaxation time and G_∞ is the high-frequency shear rigidity. When considering a sinusoidal applied stress

$$P'_{ij} = \frac{G_\infty \tau_s i\omega}{1 + \omega^2 \tau_s^2} G'_{ij} + \frac{G_\infty \omega^2 \tau_s^2}{1 + \omega^2 \tau_s^2} s'_{ij}. \tag{38}$$

The last term is in phase with the deformation s', so that the liquid has a rigidity which in the limit $\omega\tau_v > 1$ is equal to G_∞.

The complex shear modulus can be written

$$(39)\qquad \begin{cases} G = \dfrac{P'_{ij}}{s'_{ij}} = \dfrac{G_\infty \omega^2 \tau_s^2}{1+\omega^2\tau_s^2} + \dfrac{i\omega G_\infty \tau_s}{1+\omega^2\tau_s^2} \\ \quad = G' + iG'' \\ \quad = G' + i\omega\eta_s\,, \end{cases}$$

where G' and G'' are the real and imaginary part of shear modulus respectively, and $G_\infty\tau_s/(1+|\omega|^2\tau_s^2)$ is the frequency-dependent shear viscosity which at low frequencies reduces to $\eta_s = G_\infty \tau_s$.

2·1. *Longitudinal waves.* – The velocity of propagation, v, of an acoustic wave in a viscoelastic medium where both K and G are different from zero is given by

$$(40)\qquad V^2 = \frac{K + \frac{4}{3}G}{\varrho}\,.$$

Thus, an acoustic wave travelling in an elastic medium has a velocity which is determined by a linear combination of the compressional and shear moduli. It is convenient here to define a complex «longitudinal» modulus, M

$$(41)\qquad \begin{cases} M = M' + iM''\,, \\ \quad = K + \frac{4}{3}G\,. \end{cases}$$

Solving for M' and M'' in terms of α the absorption coefficient and V one finds when (as is usual) $(\alpha V/w)^2$ is small compared with 1 these equations can be simplified to

$$(42)\qquad M' = \varrho v^2\,,$$

$$(43)\qquad M'' = \frac{2\varrho V^2 \alpha}{\omega}\,.$$

Combining eqs. (33), (39), (43) yields an expression for the absorption per wave length

$$(44)\qquad \alpha\lambda = \pi \left[\frac{\dfrac{K_r \omega\tau_v}{1+\omega^2\tau_v^2} + \dfrac{\frac{4}{3}G_\infty \omega\tau_s}{1+\omega^2\tau_s^2}}{K_0 + \dfrac{K_r\omega^2\tau_v^2}{1+\omega^2\tau_v^2} + \dfrac{\frac{4}{3}G_\infty\omega^2\tau_s^2}{1+\omega^2\tau_s^2}} \right]\,.$$

Inserting eqs. (33), (38), and (40), the velocity squared of a liquid may be written as

$$V^2 = \frac{1}{\varrho}\left(K_0 + \frac{K_r \omega^2 \tau_v^2}{1+\omega^2\tau_v^2} + \frac{\frac{4}{3} G_\infty \omega^2 \tau_s^2}{1+\omega^2\tau_s^2}\right). \tag{45}$$

At low frequencies this expression becomes

$$V_0^2 = \frac{K_0}{\varrho}, \tag{46}$$

and at high frequencies it takes the form

$$V_\infty^2 = \frac{1}{\varrho}\left(K_0 + K_r + \frac{4}{3} G_\infty\right). \tag{47}$$

At low frequencies $\alpha\lambda$ has the form

$$\alpha\lambda = \frac{\pi\omega}{K_0}\left(K_r \tau_v + \frac{4}{3} G_\infty \tau_s\right) = \frac{\pi\omega}{K_0}\left(\eta_v + \frac{4}{3}\eta_s\right), \tag{48}$$

which is equivalent to the result derived from the classical hydrodynamic equations when generalized to include a volume viscosity.

2·2. *Shear waves.* – Due to high attenuation, the absorption α_s and velocity V_s of shear waves cannot be directly measured in a liquid. However, the real and imaginary parts of the complex shear impedance can be calculated from measurement of the reflection coefficient of a shear wave when reflected from a solid-liquid boundary.

The complex shear impendance, Z_s, of a liquid is given by

$$Z_s = \varrho V_s = R_s = iX_s = \varrho\left(\frac{1}{V_s} + \frac{\alpha}{i\omega}\right)^{-1} = \sqrt{\varrho G' + iG''}, \tag{49}$$

where R_s is the real part and X_s the imaginary part of the impedance and G_c is the complex shear modulus.

By equating real and imaginary parts on both sides and solving, one finds

$$R_s^2 = \varrho \frac{G'}{2}\left\{\left[1 + \left(\frac{G''}{G'}\right)^2\right]^{\frac{1}{2}} + 1\right\}, \tag{50}$$

$$X_s^2 = \varrho \frac{G'}{2}\left\{\left[1 + \left(\frac{G''}{G'}\right)^2\right]^{\frac{1}{2}} - 1\right\}. \tag{51}$$

Solving for G' and G'' one finds

$$G' = \frac{R_s^2 - X_s^2}{\varrho}, \tag{52}$$

and

$$G'' = \frac{(2R_s)(X_s)}{\varrho}. \tag{53}$$

Assuming single relaxation time theory, the measurable quantities, X_s and R_s, can be related to the parameters of the liquid by substituting the relaxation expression for G' and G'', as obtained from eq. (39) into eqs. (50) and (51). Thus

$$\frac{R_s^2}{\varrho} = \frac{G_\infty \omega^2 \tau_s^2}{2(1+\omega^2\tau_s^2)} \left\{ \left[1 + \frac{1}{\omega^2\tau_s^2} \right]^{\frac{1}{2}} + 1 \right\}, \tag{54}$$

$$\frac{X_s^2}{\varrho} = \frac{G_\infty \omega^2 \tau_s^2}{2(1+\omega^2\tau_s^2)} \left\{ \left[1 + \frac{1}{\omega^2\tau_s^2} \right]^{\frac{1}{2}} - 1 \right\}. \tag{55}$$

We see that for $\omega\tau_s \gg 1$, $R_s^2/\varrho = G_\infty$; thus, measurements of R_s in this frequency region allow a direct calculation of the limiting shear modulus of the liquid. At lower frequencies both R_s and X_s must be known to calculate G' and G''.

2.3. *Distribution of relaxation times.* – If a distribution of relaxation times exists for either the compressional or shear relaxation processes or for both, then eq. (33) can be written

$$K(\omega) = K_0 + K_r \int_0^\infty \frac{k(\tau/\tau_i')i\omega\tau}{1+i\omega t}\, \mathrm{d}\left(\frac{\tau}{\tau_v'}\right), \tag{56}$$

where

$$\int_0^\infty k\left(\frac{\tau}{\tau_v'}\right) \mathrm{d}\left(\frac{\tau}{\tau_v'}\right) = 1\,, \tag{57}$$

where $K_r k(\tau_v)\,\mathrm{d}(\tau/\tau_v)$ is the contribution to the high-frequency compressional modulus, K, of those molecules having individual relaxation times in a range $\mathrm{d}\tau$ near τ; τ_v' represents some fixed value of τ_v. $K(\omega)$ is the value of K at any frequency ω.

Separating into real and imaginary parts one has

$$K' = K_0 + K_r \int_0^\infty \frac{k(\tau/\tau'_v)\omega^2\tau^2}{1+\omega^2\tau^2}\, \mathrm{d}\left(\frac{\tau}{\tau'_v}\right), \tag{58}$$

and

$$K'' = K_r \int_0^\infty \frac{k(\tau/\tau'_v)\omega\tau}{1+\omega^2\tau^2}\, \mathrm{d}\left(\frac{\tau}{\tau'_v}\right). \tag{59}$$

For a distribution of relaxation times the volume viscosity, η_v, is given by the following expression

$$\eta_v = K_r \int_0^\infty \tau k\left(\frac{\tau}{\tau'_v}\right) \mathrm{d}\left(\frac{\tau}{\tau'_v}\right). \tag{60}$$

The real and imaginary parts of the shear modulus can be written in a like manner when a distribution of times exists, by substituting G', 0, G_∞, τ'_s, and η_s for K', K_0, K_r, τ'_v and η_v in eqs. (58), (59), (60).

3. – Volume viscosity.

3'1. *Use of ultrasonic data to calculate volume viscosity.* – The observed absorption coefficient α_{obs} (in frequency regions where no dispersion exists) can be written in terms of both the shear viscosity η_s and the volume viscosity η_v. This relation may be obtained from eq. (48) in the form

$$\alpha_{\text{obs}} = \frac{2\pi^2 f^2}{\varrho V^3}\left(\frac{4}{3}\eta_s + \eta_v\right). \tag{61}$$

Or, if $\eta_v = 0$, one gets the shear viscous loss predicted by STOKES:

$$\alpha_{\text{shear}} = \frac{8\pi^2 f^2}{3\varrho V^3}\,\eta_s, \tag{62}$$

where f is the frequency of the ultrasonic wave. One sees that the total absorption is simply a sum of the two viscous effects.

The difference between the calculated value of α_{shear} and the observed absorption coefficient α_{obs} is usually referred to as the «excess» absorption, that is to say, all absorption in excess of that due to shear viscosity. The values of α_{shear} are easily calculated. Then, using experimental values for α_{obs}, η_v can be calculated from

$$\eta_v = \frac{4}{3}\eta_s\left(\frac{\alpha_{\text{obs}} - \alpha_{\text{shear}}}{\alpha_{\text{shear}}}\right). \tag{63}$$

The results of ultrasonic studies indicate that most liquids exhibit a volume viscosity. Unlike the shear viscosity, there are many different mechanisms of volume viscosity, such as vibrational relaxation discussed above. However, below we shall consider only that contribution to η_v caused by structural relaxation.

The concept here is that the molecules of the liquid, when under an acoustic pressure, will «flow» into lattice positions of closer packing, filling up holes in the liquid. The «flow» or structural rearrangement process takes a finite time, and thus the volume changes are out of phase, the result is absorption, and a volume viscosity which appears closely related to the shear.

The word «flow» is perhaps the clue to why the shear and compressional viscosities appear so closely related. Eyring's theory of shear viscous flow involved a translational «jump» of a molecule from one lattice site to another in a direction of shear flow. The structural or compressional rearrangement process also appears to involve a «jump» of one or more molecules from one site to another. This time, however the «jump» is in the direction of closer packing. In both the shear and compressional processes molecules change their lattice positions, and it is therefore not surprising the same bonds must be broken in both processes and thus the activation energies are closely related.

It is apparent from Table II that a structural volume viscosity exists in many different types of liquids. η_v was first studied in most detail in the hydrogen-bonded liquids and it was at first thought that the relatively strong intermolecular bonding was significant in causing η_v. However it can be seen that in both monatomic liquids such as mercury and the nonassociated organic liquid CS_2, η_v persists with a magnitude still roughly equal to η_s. CS_2 is rather interesting because here the structural η_v could be discovered only at high frequencies where the overwhelming vibrational contribution (at low frequencies) to η_v is over 1000 times larger than the structural contribution given in Table II.

Until recently there has not been sufficient data to judge whether in monatomic liquids a structural viscosity exists. The data by ZARZYNSKI and STEPHENS on the molten metals has changed this picture considerably demonstrating that a structural viscosity does indeed exist in these hydrogen-bonded alcohols. Another striking fact is that in both the long chain polymer polyisobutylene (M.W. 3 000 or more) and in the monatomic molten metal gallium $\eta_v = \eta_s$. One can only conclude that no matter what the type of liquid there remains a close relationship between the shear and structural viscous mechanisms.

3·2. *Temperature and pressure-dependence of volume viscosity.* – In all liquids η_v decreases with increasing temperature. The temperature-dependence of η_v is usually very close to that found for η_s. In Table III is given the ratio

TABLE III. – *Comparison of ratio of η_v/η_s in for several types of liquids.*

	$\eta\ /\eta_s$	Ref.
	Hydrogen-bonded liquids	
Butanediol 1, 3	1.01	(a)
Glycerol	1.03	(a)
n-propanol	1.02	(b)
Water	2.52	(c)
	Weakly and onassociated liquids	
Zinc chloride	0.78	[17]
i-butyl bromide	0.44	[13]
Carbon disulfide	1.50	[10]
	Molten metals	
Mercury	1.2	(d)
Bismuth	4.2	(d)
	Polymeric liquids	
Polyisobutylene	0.95	[12]
Hydrocarbon oil	1.33	(e)
	Molten salts	
Lithium nitrate	2.03	[14]
Silver nitrate	5.3	[14]
Sodium nitrate	20.8	[14]
Lithium chloride	26.6	[15]

(*a*) R. MEISTER *et al.*: *Journ. Appl. Phys.*, 31, 854 (1960).
(*b*) J. R. PELLAM and J. K. GALT: *Journ. Chem. Phys.*, 14, 608 (1946).
(*c*) F. E. FOX and G. O. ROCK: *Phys. Rev.*, 70, 68 (1946).
(*d*) J. ZARZNSKI and R. STEPHENS: to be published.
(*e*) See ref. [19].

η_v/η_s for several types of liquids. In the hydrogen-bonded liquids such as water and ethanediol the ratio η_v/η_s is 3 or less and the ratio changes by only about 10% over a temperature range of 60 °C. In the molten nitrates those liquids such as $LiNO_3$ in which η_v/η_s is less than 3 also exhibit changes in this ratio

TABLE IV. – *Temperature-dependence of* η_v/η_s.

	T (°C)	η_v/η_s		T (°C)	η_v/η_s
Water (a)	0 20 60	3.11 2.9 2.72	Lithium nitrate [15]	262 324 379	1.80 2.10 1.97
Lithium chloride [15]	641 680 705	19.6 26.6 26.6	Mercury (b)	25 128 204	1.2 1.4 1.3

(a) See ref. (c) Table III.
(b) See ref. (d) Table III.

TABLE V. – *Pressure-dependence* (a) *of* η_v/η_s.

	P_{atm}	η_v	η_v/η_s		P_{atm}	η	η_v/η_s
Water	1 1000 2000	2.15 2.02 2.03	2.68 2.33 2.33	Ethyl alcohol	1 1000 2000	1.42 1.88 2.18	1.4 1.2 0.95
Methyl alcohol	1 1000 2000	0.84 1.0 1.2	1.62 1.31 1.19				

(a) T. A. LITOVITZ and E. H. CARNEVALE: *Journ. Appl. Phys.*, **26**, 816 (1955).

of less than 10% over temperature ranges of 1000° C and greater η_v/η_s for KNO_3, $AgNO_3$ and $NaNO_3$ varies more with temperature. It appears that the higher the ratio η_v/η_s the greater is the difference in the temperature-dependence of η_v and η_s. This is borne out when one considers the molten chlorides. Lithium chloride has one of the highest ratios of η_v/η_s and exhibits a considerably greater temperature variation than in lithium nitrate. In all the molten chlorides η_v is less temperature-dependent than η_s. The η_v of the molten metals behaves just as that for water in that the ratio η_v/η_s is remarkably constant over the measured temperature range.

These results indicate that the activation enthalpy for shear and structural flow are close in value for many types of liquids.

The volume viscosity has been measured as a function of pressure for water and several alcohols. Some typical data are listed in Table V. With the exception of water η_v increases with increasing pressure, as does η_s. This increase is to be expected due to the diminished mobility of the molecules as they become closer packed at higher densities. In general η_v is slightly less pressure-dependent than η_s, the values of η_v/η_s dropping with increased pressure.

3·3. *Coexistence of structural and nonstructural processes.* – The mechanism of ultrasonic absorption characteristic of the nonassociated liquids is the thermal type due to either vibrational or rotational isomeric relaxation. This absorption has not been detected in the associated liquids. It is probable that the reason for this is that the efficiency of collisions transferring energy from the external to internal degrees of freedom depends upon the intermolecular bonding; *i.e.* the low degree of intermolecular bonding in the nonassociated liquids may result in a comparatively longer relaxation time and larger vibrational loss. If this bonding of the associated liquids does account for the apparently good coupling between external and internal degrees of freedom and the consequent short thermal relaxation time of these liquids, then by investigating a weakly associated liquid, the ultrasonic properties typical of associated and nonassociated liquids should be found to coexist. CLARK and LITOVITZ [13] have considered this problem in their study of isobutyl bromide.

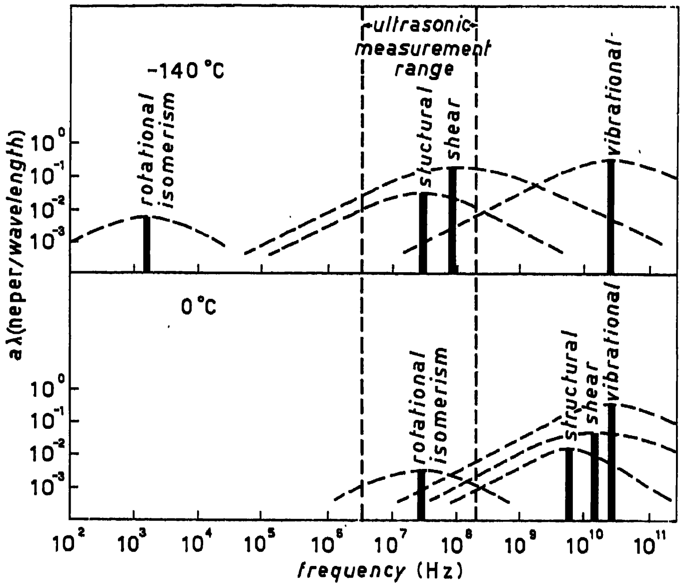

Fig. 9. – Absorption « spectrogram » for liquid isobutyl bromide. (Data from ref. [13]).

Isobutyl bromide is also interesting from the standpoint of its molecular configuration. In a rotation about a C—C bond, the CH_2Br portion of the molecule may have any of three equilibrium positions, two positions having identical energy and the third differing from this. Hence in addition to the mechanisms discussed above, one would expect the total absorption to contain a contribution due to this rotational isomerism. CLARK and LITOVITZ show that four different mechanisms, shear, structural, vibrational and rotational isomeric relaxations are present. The relative importance of the different mechanisms is demonstrated in Fig. 9 where a spectrogram of the loss is plotted. The solid bars represent the maximum value of the loss per wave length $\alpha\lambda_m$ for the four losses; the dotted lines give the absorption per wave length, $\alpha\lambda$ as a function of frequency. Note that although the magnitude of the absorption due to the vibrational mechanism is the largest above 1 GHz, its contribution to the absorption at frequencies below 50 MHz is quite small. At 0 °C and 100 MHz, this contribution is about equal to that of the rotational mechanism, and at —140 °C and 100 MHz, although its magnitude has not changed significantly, its contribution is much less than that of the shear and structural mechanism. At this temperature, the losses due to the structural and shear mechanisms are by far the most important for the frequencies used.

3'4. *Relation of volume viscosity to entropy and volume changes upon fusion.*

– Experimental work on the alcohols and molten salts [14], [15], has yielded a second interesting relationship. It was found that this family of molten salts ($LiNO_3$ excepted) satisfied a simple relationship between the entropies of fusions and the corresponding ratio of viscosities. The general equation expressing this is

$$\ln\frac{\eta_v}{\eta_s} = A - B\frac{\Delta S_f}{R}\,. \tag{64}$$

The corresponding equations are plotted in Fig. 10. HIGGS and LITOVITZ have also shown that the linear relationship expressed by eq. (64) likewise holds for the primary alcohols.

It was found that the value of A is common to all three families of molten salts. Thus the ratio of bulk to shear viscosities for all three families would be identical in the limit as the entropy-changes upon fusion would go to zero. It can be surmised at present that the intercept is likely to be indicative of the common type of bonding (predominantly ionic) for these fused salts. A more satisfactory answer awaits further investigation.

The deviation of $LiNO_3$ is very interesting and can be empirically accounted for as follows: $NaNO_3$, $AgNO_3$, and KNO_3 are known to undergo phase transitions in the solid state prior to melting. X-ray [16] studies of these transitions show that they involve extensive randomization of the orientation and even the onset of rotation of the NO_3 ions, so much so, that no further large increase of orientational randomization of this ion would be ex-

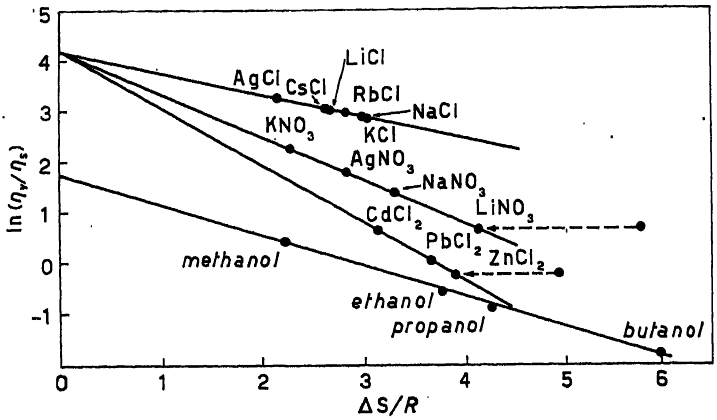

Fig. 10. – Logarithm of η_v/η_s plotted as a function of the entropy of fusion. (After ref. [15]).

pected at the melting point. However, $LiNO_3$ awaits the melting process before this NO_3 ion randomization takes place and its entropy of fusion is, therefore, greater than for the other nitrates. The entropy of fusion of these salts can have contributions both from randomization of the internal structure of the polyatomic molecule, as well as from randomization of the crystalline lattice structure. One would expect that in a liquid the structural relaxation process associated with bulk flow would involve only randomization of the liquid lattice and therefore if the difference between shear and volume relaxation is at all related to the entropy of fusion it should be concerned only with that part of S_F owing to lattice randomization.

One can subtract from S_F for $LiNO_3$ that part, S_T, which is due to orientational randomization which appears in KNO_3 in a solid state transition ($S_T = 3.2$ a.u.). When the $\ln(\eta_v/\eta_s)$ for $LiNO_3$ is plotted using this empirically corrected S_F, then the departure of the $LiNO_3$ point from a straight line is within experimental error. As can be seen in Fig. 5 $ZnCl_2$ also departs from the family of curves. An explanation of this departure similar to the $LiNO_3$ has been given by GRUBER [17].

The relation of η_v/η_s to the entropy of fusion indicates that the structural relaxation flow occurring in liquids is not simply a process where a hole might exist but rather it is a co-operative phenomenon. In this latter case for flow to occur a group of molecules (say 5 ÷ 50) in some quasi-crystalline lattice order, must « melt » or become randomized in their structure. During this time of randomization molecules can change their positions and then revert to a new crystalline order which would have different numbers of holes.

Since it has been argued above that η_v of the ionic liquids has the same origin as the η_v of the hydrogen-bonded liquids such as the alcohols it is reassuring to find that η_v/η_s is related to S_F in the alcohols as well as in the ionic liquids. It is, however, interesting to note that in the alcohols it appears that only about 0.24 S_F is involved, whereas in the ionic liquids this was as high as 0.7 S_F. This difference could be related to the complexity of the structure of the alcohol molecules when compared with that of the ionic salts. For example, the entropy of fusion of the alcohols no doubt involves randomization of the internal structure such as the freeing of rotation about the C—C bonds. This would lead to entropy contribution to fusion which would not be connected with the liquid lattice structure. Thus, for the same reason as in the case of $LiNO_3$ above, only a fraction of the total entropy of fusion is involved in the lattice structural relaxation process.

4. – Velocity dispersion and absorption due to shear and structural relaxation.

We now turn attention to data in the dispersion region, considering first the sound velocity.

The longitudinal velocity data plotted *vs.* frequency are shown in Fig. 11, for two typical associated liquids. It can be seen that considerable dispersion is present. The data indicate relaxational behavior, but unfortunately the experimentally available frequency range does not generally allow a measurement of both the limiting low and high frequencies at any given temperature. The values of V and V_0 shown in Fig. 11 were obtained by calculation from the extrapolated values of M and M_0 from the higher and lower temperatures, respectively. Since the measured properties of the liquids depend

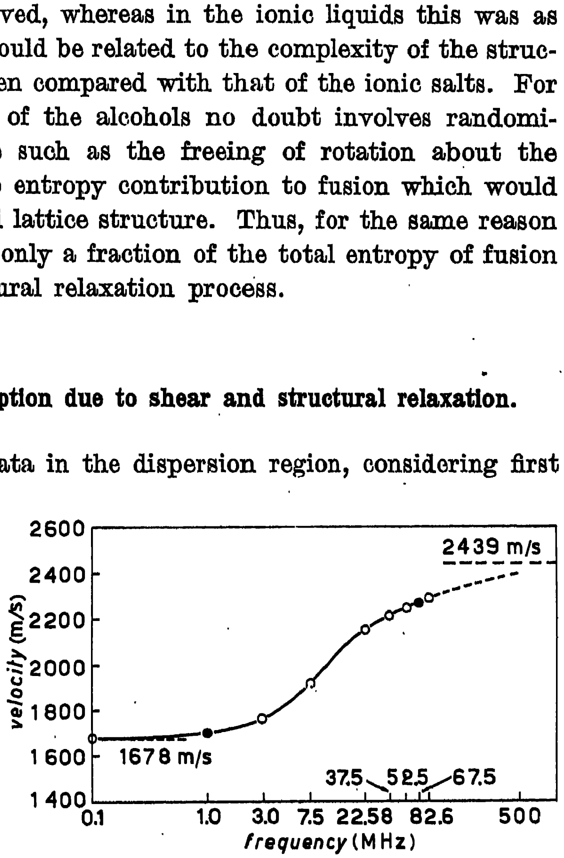

Fig. 11. – Longitudinal velocity as a function of frequency; butanediol 1, 3; temperature —32.4 °C. (Taken from ref. [22]).

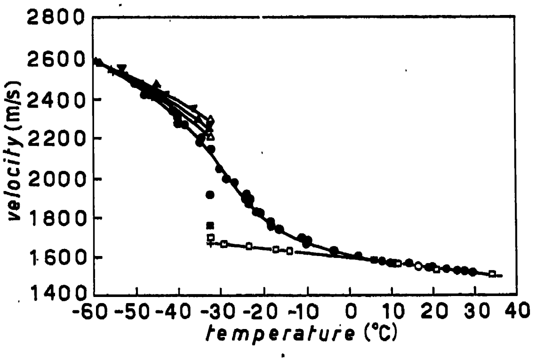

Fig. 12. – Longitudinal velocity *vs.* temperature at various frequencies: butanediol 1, 3. (Taken from ref. [22]). + 0.1 Hz; □ 1 Hz; ■ 3Hz; ○ 7.5 Hz; ● 22.58 Hz; × 34.5 Hz; ▲ 52.5 Hz; ▼ 67.6 Hz; △ 82.8 Hz.

on the product $\omega\tau$ one can change either ω or τ to study the dispersion properties. Changing the temperature, changes τ. The ultrasonic longitudinal velocities measured as a function of temperature at various frequencies are found in Fig. 12. They show a similar behavior in that low- and high-frequency limiting velocities V_0 and V_∞, respectively, are reached. This is shown by the absence of dispersion at low and high temperatures. The magnitude of the dispersion $(V_\infty - V_0)/V_0$ varies between 15 and 60%, for most liquids measured. This can be seen in Table VI-(*a*).

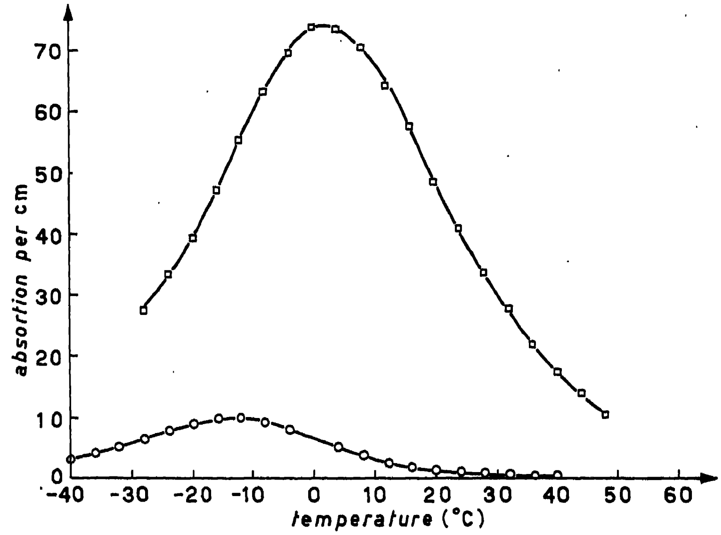

Fig. 13. – Absorption *vs.* temperature at two frequencies: hexanetriol 1, 2, 6: ○ 3 Hz; □ 22 Hz. (Taken from ref. [22]).

The measurement of absorption associated with the longitudinal wave is plotted in Fig. 13, as a function of temperature and at various frequencies. All the curves show a similar behavior exhibiting a bell shape typical of a relaxation process. As the temperature is lowered, the absorption coefficient exhibits a maximum, the magnitude and position of which depends upon the ultrasonic frequency used. The higher frequencies have a correspondingly higher maximum value. The peaks of the curves shift toward lower temperatures at lower frequencies. This, of course, indicates that the relaxation time increases as the temperature is lowered (or as the viscosity is increased) In Table VI-*a* the values of the ratio $\alpha_{\text{obs}}/\alpha_{\text{Stokes}}$ in the nondispersion region are tabulated. The values are independent of temperature (in the nondispersion region) and lie between 1.5 and 3.5. These results are typical of associated liquids and indicate the presence of the structural relaxation in addition to

TABLE VI-*a*). – *Velocity dispersion data in associated liquids.*

	T (°C)	$\alpha/\alpha_{\text{Stokes}}$ (a)	v_0 (m/s)	v_∞ (m/s)	$\dfrac{v_\infty - v_0}{v_0}$
Butanediol 1, 3	— 32.2	1.76	1695	2331	0.375
2-methyl-pentanediol 2, 4	— 26.0	3.38	1460	1865	0.280
Hexanetriol 1, 2, 6	— 10.5	1.65	1820	2740	0.515
Glycerol (b)	— 14.0	1.78	1990	3150	0.59
Propanediol 1, 2 (c)	— 37.8	2.08	1650	2360	0.43
n-propanol (d)	—130.0	1.77	1860	2160	0.15
Diphenyl pentachloride (e)	34.5	3.28	1310	1690	0.29

(*a*) The values of $\alpha/\alpha_{\text{Stokes}}$ listed are those measured in the nondispersion region.
(*b*) R. Piccinelli and T. Litovitz: *Journ. Acoust. Soc. Am.*, **29**, 1009 (1957).
(*c*) R. Meister: private communication.
(*d*) T. Lyon and T. Litovitz: *Journ. Appl. Phys.*, **27**, 179 (1956).
(*e*) T. Litovitz, T. Lyon and L. Peselnick: *Journ. Acoust. Soc. Am.*, **4**, 566 (1954).

the shear viscosity effects. Thus, one can conclude that the dispersion measured is due to both shear and structural relaxation effects.

5. – High-frequency limiting moduli of liquids.

5·1. *Magnitudes.* – At high frequencies or long relaxation times ($\omega\tau > 1$) the complex shear and compressional moduli of a liquid become frequency-independent. Under these conditions one measures the solidlike behavior of a liquid. These so-called «limiting» moduli are of considerable interest since they are a direct measure of the elasticity of the amorphous liquid lattice with flow properties removed.

In Table VI-*b*) these high-frequency moduli are listed for comparison with the low-frequency values ($\omega\tau < 1$).

It can be seen that M_∞ varies from about 1.3 to 3.0 times M_0 (or K_s). The measured values of K_r/K_∞ vary between 0.25 and 0.43.

The ratio K_r/K_∞ is equal to the ratio $\varkappa_r/\varkappa_0$ where $\varkappa_r$ is the relaxational part of the normal liquid compressibility, K_0. The data indicate that about 30 % of the total normal compressibility of these liquids is due to structural relaxation effects.

It is of interest to compare these values with the values of $\varkappa_r/\varkappa_0$ found by measuring the isothermal compressibility above and below the glass transition temperature. The results in Table VII obtained by assuming $\varkappa_r = \varkappa_{\text{liq}} - \varkappa_{\text{glass}}$ indicate that $\varkappa_r/\varkappa_0$ lies between 20 and 75 %. This is in reasonable agreement with the ultrasonic values found using velocity-dispersion data. This agree-

TABLE VI-*b*). – *Comparison of the magnitude of elastic moduli in liquids with various solids* (Units are dyn/ $cm^2 \cdot 10^{-10}$).

	T (°C)	K_0	M	K	K_r	K_r/K	G	G/K
a) Hydro-carbon liquids								
Polyisobutylene (*g*)	+25	—	—	2.68	—	—	0.58	0.1
MVI (*k*)	−10	2.2	4.3	3.2	1.05	.33	0.78	—
b) Weakly or nonassociated liquids								
Molten zinc chloride(*c*)	325	2.50	4.68	3.3	.85	.26	1.0	.3
Isobutyl bromide (*d*)	−100	3.03	6.42	3.45	.42	.12	2.24	.6
c) Associated liquids								
Butanediol 1, 3 (*e*)	−32.2	2.93	6.17	4.53	1.59	0.35	1.23	0.2
Hexanetriol 1, 2, 6 (*f*)	−10.5	3.71	9.53	6.46	2.75	0.43	2.31	0.3
Glycerol (*a*)	−14.0	5.40	12.79	8.79	3.75	0.37	3.00	0.3
Propanediol (*b*) 1, 2	−37.8	3.14	6.16	4.65	1.51	0.32	1.13	0.2
d) Solids								
Fused quartz (*h*)	+25	—	—	27.3	—	—	31.2	0.84
Nickel (*i*)	+25	—	—	371	—	—	73.5	0.20
Sodium chloride (*i*)	+25	—	—	48.5	—	—	12.5	0.25
Organic glasses (*l*)	—	—	—	—	—	—	1.50	—

(*a*) R. PICCINELLI and T. LITOVITZ: *Journ. Acoust. Soc. Am.*, **29**, 1009 (1957).
(*b*) See footnote (*c*), Table II. R. MEISTER: unpublished data.
(*c*) Ref. [17].
(*d*) Ref. [13].
(*e*) Ref. [22].
(*f*) Ref. [22].
(*g*) W. P. MASON, W. O. BAKER, H. J. MCSKIMMIN and J. H. HEISS: *Phys. Rev.*, **75**, 936 (1949).
(*h*) H. J. MCSKIMMIN: *Journ. Appl. Phys.*, **24**, 988 (1953).
(*i*) C. D. HODGMAN: *Handbook of Chemistry and Physics* (Cleveland, Ohio, 1956), 36th ed.
(*k*) See reference [18].
(*l*) S. CRAWFORD: *Proc. Phys. Soc. London*, B **69**, 1312 (1956).

TABLE VII. — *Comparison of glass and liquid values of isothermal compressibility* (*).

	T (°K)	$\varkappa_{\text{glass}}$ ($\cdot 10^{12}$ cm²/dyn)	$\varkappa_{\text{liq}}$ ($\cdot 10^{12}$ cm²/dyn)	$\varkappa_{\text{rel}}/\varkappa_{\text{liq}}$
Glucose	300	9.3	15.4	0.40
Selenium	300	24.4	30.2	0.19
Rubber	200÷320	27	64	0.58
Polystyrene	350	23	98	0.76

(*) Data taken from R. DAVIS and G. O. JONES: *Proc. Roy. Soc.*, A **217**, 26 (1953).

ment is in accord with the concept that high-frequency ultrasonic waves measure the glasslike properties of the liquid.

In Table VI-*b*) values of G_∞ found in the hydrogen-bonded liquids are compared with a polymeric liquid (polyisobutylene) and an organic glass (sucrose octa-acetate), and some hydrocarbon oils. It can be seen that no order-of-magnitude difference exists in the values of G_∞.

However, as shown by BARLOW and LAMB [18] the magnitude of G_∞ is definitely lower in the hydrocarbon and polymeric liquids than in the highly associated liquids. They suggest that the difference is due to the weaker van der Waals forces present in the hydrocarbons compared with the relatively stronger hydrogen bonding present in most of the associated liquids listed.

HERZFELD and LITOVITZ [2*b*] have pointed out that in many of the hydrogen-bonded liquids $K_r = \frac{4}{3} G_\infty$. BARLOW and LAMB have shown this to hold also for the hydrocarbon oils.

Because K_∞ and G_∞ are often called the « solidlike » moduli of the liquids it is of interest to compare values found in the organic liquids with those for amorphous and crystalline solids. The organic liquid values run about 1/10th the values found for fused quartz and sodium chloride and less than 1/20th the values of G_∞ found in nickel.

The values of K_∞ found in the organic liquids are roughly the same as the K_∞ found for the polymer polyisobutylene. However, K_∞ for the organic liquids runs about 1/10th of that of fused quartz and sodium chloride and 1/100th the value found for nickel. After comparing the ratio G_∞/K_∞ for the organic liquids and the solids, it can be seen that even though the values of G_∞ and K_∞ vary by factors of 10 or 100 from organic liquid to crystalline solid, the ratio G_∞/K_∞ remains constant to within a factor of about three.

5·2. *Temperature-dependence of limiting elastic moduli.* – The limiting shear, compressional, and longitudinal moduli are tabulated in Table VIII as a func-

TABLE VIII. – *Temperature-dependence of limiting elastic moduli.*
(Moduli in dyn/cm$^2 \cdot 10^{-10}$; T in °C).

	M_0	G_∞	K_∞
		Associated liquids	
Butanediol 1, 3	$2.61 - 0.010\ T$	$0.962 - 0.00847T$	$3.85 - 0.02098T$
Hexanetriol 1, 2, 6	$3.61 - 0.0094T$	$2.23 - 0.0075T$	$6.28 - 0.018T$
Glycerol	$48.91 - 0.0122T$	$2.75 - 0.0183T$	$8.30 - 0.035T$
		Nonassociated liquids	
(Molten) zinc chloride	—	$69T \exp[14\,790/RT]$	$49T \exp[15\,280/RT]$
Isobutyl chloride	$1.11 - 0.0192T$	$1.76 \cdot 10^5 T \exp[745/T]$	$0.32 \cdot 10^5 T \exp[745/T]$

tion of temperature. In most liquids the moduli decrease with increasing temperature. However, rather marked differences in temperature-dependence can be noted when one compares the behavior of the associated, weakly associated, and hydrocarbon liquids.

The hydrocarbon oils exhibited no measurable change in the relaxational moduli G_∞, and K_r, with temperature. This is in marked contrast to both the hydrogen-bonded liquids and the nonassociated chlorides listed in Table VIII. TASKOPRULU, BARLOW, and LAMB [19] suggest that this is related to the type of lattice bonding. They propose that the van der Waals bonding existing in these liquids not only slightly lowers the magnitude of K_r and G but makes them far less temperature-dependent.

Over the temperature range measured the moduli of all the associated liquids listed decrease linearly with increasing temperature. This decrease emphasizes the difference between the rubber or « entropy » modulus (which is proportional to temperature) found in polymers and the « energy » modulus found here in associated liquids. It also indicates that the Tobolsky-Leaderman-Ferry [20] reduction formula can not hold for the associated liquids.

In the two nonassociated liquids listed the temperature-dependence of K_0 is similar to that found in the associated liquids decreasing linearly with increasing temperatures. However consideration of the temperature-variations of K_r and G_∞ show a striking departure. They both decrease exponentially with increasing temperature.

Comparison of the magnitude of K_r and G_∞ showed that they were usually close in value to K_r often equal to about $\frac{4}{3}G_\infty$. Also in all the liquids listed in Tables VII and VIII the temperature-variation of G_∞ was found to be the same as that for K_r. This is true for such diverse substances as the hydrocarbon oils, hydrogen-bonded organic liquids and the molten zinc chloride. This is one of the contributing factors in making the ratio η_v/η_s so temperature-independent in most liquids.

The theories of Hirai and Eyring [21] predict the temperature-dependence of G_∞ and K_r. MEISTER *et al.* [22] applied these theories to the data on glycerol. Plotted in Fig. 14 are their results found using expressions as directly obtained from this theory, which are

$$G = \frac{kT}{v_0} \exp\left[\frac{\varepsilon_h}{kT}\right], \tag{65}$$

$$K = K_0^2 \frac{(v_h/kT) \exp[-\varepsilon_h/kT]}{(1-K)(v_h/kT) \exp[-\varepsilon_h/kT]}, \tag{66}$$

where ε_h is equal to the energy necessary to create a hole in the liquid, v_h is the volume of a hole, k is the Boltzman's constant, v_0 is the volume the liquid would have without holes. In Fig. 14-*a* the values predicted by eqs. (65) and (66) are plotted and compared with the experimental values obtained for glycerol. On considering the data for G_∞, it can be seen that the Eyring and Hiray theory gives reasonably close agreement with the experimental values at temperature above 0 °C. However, at the lower temperatures there is considerable disagreement between the theoretical and experimental data. It can be seen that at −70° the theoretical value exceeds the experimental one by a factor of three.

When considering data for K_r in Fig. 14-*b* it can be seen that the theory gives the right order of magnitude but the wrong temperature-dependence.

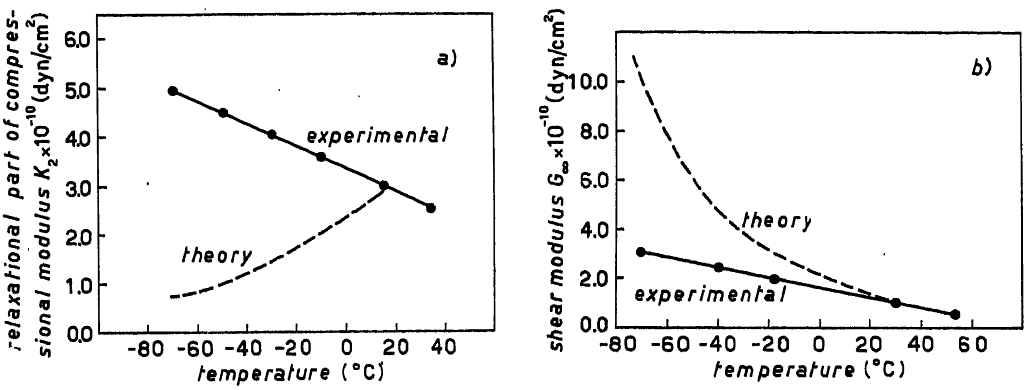

Fig. 14. – Comparison of Eyring and Hirai theory with the data for K_2 and G_∞. (Taken from ref. [22]).

It is apparent that the Hirai and Eyring theory for shear and structural relaxation in associated liquids is inadequate to account for the data on the relaxational part of the elastic moduli which have been found here. This conclusion extends to all the associated liquids and even hydrocarbon oils which have been measured because in every case G_∞ has varied with temperature in a linear manner (or not at all) and K_r has decreased with temperature whereas the Hirai and Eyring theory predicts an increase.

Isobutyl bromide however represents a striking success for Hirai and Eyring's calculation of G_∞. In this liquid G_∞ is found by CLARK and LITOVITZ to be given by

$$G_\infty = 1.76T\cdot 10^5 \exp\,[745/T]\,\frac{\text{dyn}}{\text{cm}^2}\,°\text{K}. \tag{67}$$

Comparing this with eq. (65) one finds $\varepsilon_h = 1490$ cal/mol. It has been shown that the energy to create a mol of holes is about $\frac{1}{6}$ to $\frac{1}{8}$ of the molar heat of vaporization of the liquid, for the organic liquids. For isobutyl bromide, the heat of vaporization E_{vap} can be determined using Trouton's rule, determining the constant with the help of the measured E_{vap} of isobutyl chloride. The ratio of E_h (found above) to the experimentally found value of E_{vap} is

$$\frac{\varepsilon_h}{E_{\text{vap}}} = \frac{1.49}{8.04} = \frac{1}{5.4}\,.$$

The agreement of this ratio to the predicted value is excellent. The same good agreement is found for zinc chloride.

5'3. *Comparison of liquid and solid moduli.* – Changing the temperature of a solid changes only the interatomic spacings; however, when one changes the temperature of a liquid both the interatomic spacing and the degree of short-range order of the liquid change. It is reasonable to expect that the elastic constants of a lattice whose order is changing with temperature would be more temperature-dependent than that lattice where only interatomic spacings change. This point is convincingly demonstrated by consideration of the temperature-dependence of the compressibility over a large temperature range.

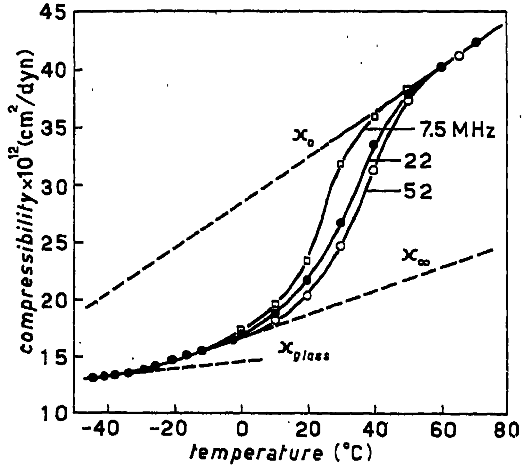

Fig. 15. – Adiabatic compressibility *vs.* temperature in Arochlor. ((After T. LITOVITZ, T. LYON and L. PESELNICK: *Journ. Acoust. Soc. Am.*, **26**, 566 (1954)).

In Fig. 15 $\varkappa$ is plotted as a function of temperature for Arochlor (byphenil pentachloride).. At high temperatures, $\varkappa$ is frequency-independent and decreases with decreasing temperature. As the temperature of the liquid is lowered the relaxation time increases until it is of the order of the time duration of a normal experiment, perhaps 30 minutes, and the liquid exhibits a glass transition. For the ultrasonic measurement this transition occurs in the temperature region where the structural relaxation time is of the order of the period of the ultrasonic wave. For the frequencies used in Fig. 15, the temperature of this transition is about 60 °C above the normal glass transition temperature. As the temperature of the liquid is lowered, the adiabatic compressibility at a given frequency drops rather sharply and levels off at a somewhat lower value, which is again independent of frequency. This lower value is the high-frequency compressibility of the liquid, $\varkappa_{\infty}$. The value of $\varkappa$ is determined purely by the elastic behavior of the liquid lattice. When measuring $\varkappa_{\infty}$, no liquid flow takes place during a sonic compression. The structural contributions to the compressibility have been removed.

It is of interest to compare the temperature-dependence of $\varkappa_{\infty}$ and $\varkappa_0$ in Arochlor. It can be seen that the temperature-dependence of $\varkappa_{\infty}$, the glasslike compressibility, is about the same as that for the liquid compressibility. One normally expects glass or solidlike compressibilities to be less temperature-dependent than the liquid values.

The explanation of this lies in the fact that we have not gone through a glass transition in the usual sense at 20 °C. The liquid behaves like a glass to the sound wave for a given measurement because of the short time-duration of the wave. However, when one changes the external temperature this is a long-time experiment, in changing the liquid structure. Lowering the liquid temperature in the normal times necessary to lower a bath temperature allows increases in the amount of order, decreases in the number of holes, and increases in the number of nearest neighbors. The ultrasonic wave «sees» the order present at the external temperature. When one changes the temperature of a crystal or glass, these effects do not occur. The degree of order in a solid is very much less temperature-dependent than in a liquid.

Thus we must conclude that the changes in lattice structure which occur in our pseudo-glass causes the relatively large temperature effects noted in the high-frequency compressibility measurement. To prove this, one simply lowers the temperature until the time for structural rearrangement of the lattice is longer than the time necessary to change the temperature, *i.e.*, below the normal T_g. Below this temperature the elastic constants should take on a solidlike temperature-dependence, typical of the glass state. This should occur at the ordinary glass-transition temperature, where the time for structural rearrangement becomes longer than normal cooling times. In Fig. 15 one sees that the only change in going through the glass transition is that the slope decreases and becomes more typical of the glass state. The value of $(1/\varkappa)(\partial\varkappa/\partial T)_{\text{glass}}$ is less than one-half the liquid value.

6. – Relaxational behaviour of moduli.

When considering the shear and compressional relaxation behavior of liquids it is found in almost every liquid that a distribution of relaxation times exists. Satisfactory results were obtained on the associated liquids with two types of distribution functions:

a) A symmetrical Gaussian distribution of relaxation times given by

$$g\left(\frac{\tau}{\tau'_s}\right)=\frac{b}{(\pi)^{\frac{1}{2}}}\,\frac{\tau'_s}{\tau}\exp\left[-b\ln\left(\frac{\tau}{\tau'_s}\right)^2\right]\qquad 0<\tau<\infty. \tag{68}$$

This function is logarithmically symmetric and exhibits a maximum at $\tau=\tau'_s$. The width of the distribution is determined by b.

b) An asymmetrical distribution of relaxation times due to Cole-Davidson, where

$$g\left(\frac{\tau}{\tau'_s}\right)=\left(\frac{\tau'_s}{\tau}\right)\left(\sin\beta\,\frac{\tau'_s}{\tau}\right)\left(\frac{\tau}{\tau'_s}\Big/\left(1-\frac{\tau}{\tau'_s}\right)\right)^{\beta},$$

β and τ'_s are parameters which determine the width and position of the maximum, respectively. This function has maximum value at $\tau=\tau'_s$. τ'_s is the longest relaxation present, and β determines the width of the curve.

The theoretical functions which best represent the shear data are given in Table IX. In the case of glycerol, butanediol and 2-metyl pentanediol, the symmetrical Gaussian distribution of relaxation times is found. In using this symmetrical distribution, the constant b which determines the broadness of the reduced curve is calculated using the constants in Table IX. It can be seen

TABLE IX. – *Distribution of mechanical relaxation times.*

Liquid	Shear distribution	Volume distribution	τ_v/τ_s	Ref.
Butanediol 1, 3	Gaussian $b=0.79$	Cole-Davidson $=0.49$	0.79	(^{a})
2-methyl pentanediol	Gaussian $b=0.60$	Cole-Davidson $=0.60$	2.38	(^{a})
Glycerol	Gaussian $b=0.42$	Cole-Davidson $=0.60$	0.81	(^{a})
Hexanetriol 1, 2, 6	Cole-Davidson $=0.32$ (and a single time)	Cole-Davidson $=0.24$	4.60	(^{a})
i-butyl chloride	Cole-Davidson $=0.45$	—	--	(^{b})
Zinc chloride	Single time	Single time	1.05	(^{c})

(*a*) See ref. [22].
(*b*) See ref. [13].
(*c*) See ref. [17] (G. GRUBER and T. LITOVITZ).

in Fig. 16 (solid line) that the assumption of this distribution of relaxation times gives and excellent fit to the data.

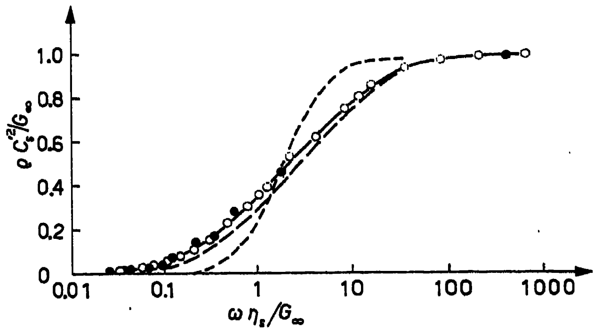

Fig. 16. – Plot of $(\rho C_s'^2/G_\infty)$ vs $\cdot\omega\eta_s/G_\infty$, for butanediol 1, 3, solid line is that obtained using the distribution function listed in Table IX. Short dashed line is predictions of single relaxation time. o 55 Hz, ● 25 Hz. (Taken from ref. [22]).

The shear data on isobutyl bromide demonstrate that even though the temperature-dependence of the modulus is unusual, a distribution of relaxation times exists just as in the strongly associated liquids. This distribution is asymmetric and is fitted by the Davidson-Cole function.

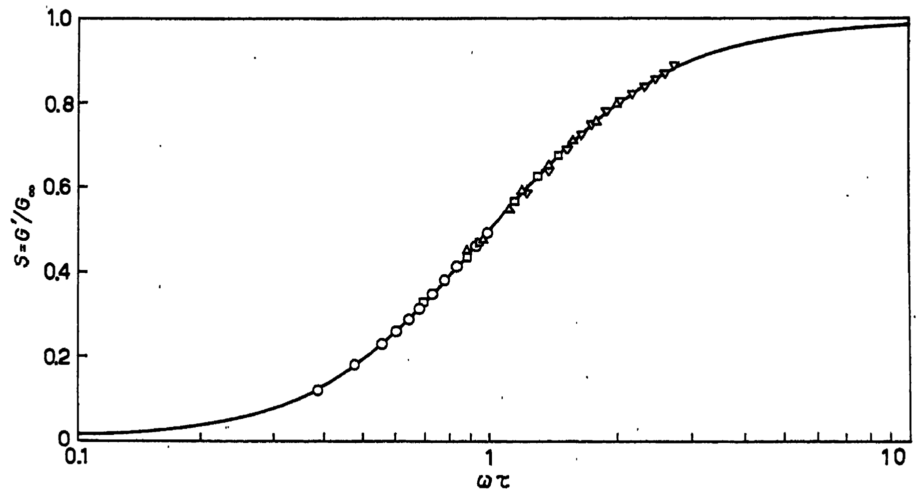

Fig. 17. – Plot of reduced real part of shear modulus *vs.* $\omega\tau$ for zinc chloride: o 43 Hz; □ 63 Hz; △ 86 Hz; ▽ 118 Hz. (Taken from ref. [17]).

The only truly nonassociated liquid in which shear relaxation has been detected is molten zinc chloride by Gruber. The data are shown in Fig. 17

where the reduced real part of the shear modulus is plotted. The rather remarkable result here is that the data can be accounted for using a single relaxation time. This is the only liquid measured (including polymers) which exhibits a single shear relaxation time.

The reduced relaxational part of the compressional modulus has been calculated and the results are plotted in Fig. 18 as a function of $\omega(\tau_v)_{av}$ for typical associated liquids. The average relaxation time is obtained using the relation $(\tau_v)_{av} = \eta_v/K_2$, where the value τ_v is evaluated by using eq. (67) and data on the ratio of $\alpha/\alpha_{\text{Stokes}}$ in the classical region. It can be seen that the single relaxation theory is inadequate to describe the results.

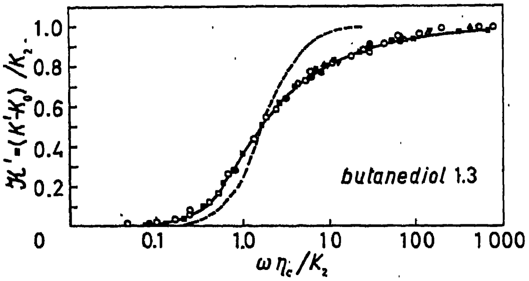

Fig. 18.

It is found that by choosing a distribution function this compressional reduction is adequately represented. In each liquid the reduced compressional modulus is logarithmically asymmetric about its inflection point. Because of this a Cole-Davidson distribution function was chosen to represent the distribution of times. The parameter β is tabulated in Table IX.

In each case there is reasonably good agreement between the shape of the experimental and theoretical curves when the β's listed are used.

The ratio of τ_v/τ_s is also tabulated in Table IX. Because a distribution of times exists the only meaningful comparison is between the average value of shear and compressional relaxation times.

In three of the liquids listed the type of distribution for shear and compressional relaxation differs considerably. However the magnitude of τ_v is still close to τ_s. In two of the liquids they differ by less than 25%. In no case does τ_v differ from τ_s by more than a factor of 5.

In all the liquids the temperature-dependence of τ_v was found to be the same as for τ_s. Combining this with the fact $(1/K_2)(\partial K_2/\partial T) = (1/G_\infty)(\partial G_\infty/\partial T)$ one sees why the ratio η_v/η_s has been found relatively independent of temperature.

A question still unanswered is why there is a difference in the distribution function even when the two processes are so obviously intimately related.

The data in the nonassociated liquid on molten zinc chloride [17] show that the compressional relaxation process is decribed by a single relaxation time just as the case for shear process. In addition the value of τ_v was found to equal τ_s within experimental error.

The data of TASKOPRULU, BARLOW, and LAMB [19] on a hydrocarbon oil show that a double distribution of times exists. Their results indicate that for one process at least τ_s is over 10 times τ_v. Here again despite the marked differences in relaxation spectrum the compressional and shear relaxations show a close relationship as indicated by the same temperature-dependence of τ_v and τ_s and the fact that $K_2 \simeq \frac{4}{3} G_\infty$.

7. – Cooperative effects in shear and structural processes.

7·1. *Shear viscous processes.* – EYRING [25] has proposed a rate theory of shear viscosity which has been very successful in explaining the data in many liquids. The rate process for the flow of liquids consists of the exchange of the position between a hole and its adjacent molecule, and the fluidity is proportional to the probability for a molecule to be adjacent to a hole and to the rate with which it jumps into the hole. This is a nonco-operative theory in the sense that one calculates the probability that an individual molecule attains sufficient energy to jump and that the neighbors do not take part in the process. A major success of this theory is that it leads to a viscosity proportional to $\exp[E/RT]$ where E is the activation energy for shear flow. This is the Arrhenius form which has long been observed to hold in many liquids. However some liquids do exhibit a shear viscosity which does not change exponentially with temperature, particularly at low temperatures. For example the Eyring theory fails completely for supercooled liquids within 100 °C of the glass transition temperature. To fit the data in these liquids one must assume an unreasonably large and highly temperature-dependent activation energy.

To overcome this problem, FOX and FLORY [26] emphasize the concept that the mobility at these temperatures depends on a free volume, V_f. In this approach the probability of a jump is determined not by the rate at which a molecule can overcome an energy barrier but rather by the probability that sufficient free volume exists in the region of the molecule so that it has space to move. This concept is embodied in the expression of Williams, Landel, and Ferry [27] which fits very well the shear viscosity and shear relaxation time data at the low temperature where the Eyring theory fails.

BUECHE [28] has theoretically derived this same relation by considering fluctuations of the local free volume. He assumes that a certain minimum local free volume must be exceeded before a jump can occur. The jump rate is then related to the probability that this critical free volume will be attained. Bueche's theory emphasizes that molecules cannot move as individuals when the mobility is limited by the free volume. When one molecule moves or jumps many others must co-operate to allow such a movement. Thus co-operative effects become a significant factor in determining the low-temperature mobility of molecules. Therefore, the non-Arrenhius behavior of shear viscosity and shear relaxation time is evidence that co-operative effects play a role in the shear flow process in many liquids.

The W.L.F. equation breaks down at temperatures about 100 °C above the glass transition temperature. This is in accord with the concept that co-operative effects are far less significant at high temperatures and that the mobility is no longer simply volume-limited.

7·2. *Volume viscous processes.* – Experimental results on measurements of the volume or structural viscosity, η_v, of many liquids has yielded additional evidence that the structural relaxation process has co-operative aspects similar to that found in the shear flow process. For example, the fact that the volume and shear viscosities and relaxation times have been found to have similar temperature-dependences, indicates that any co-operative argument applied to the shear process is equally applicable to the structural or volume process.

Furthermore the result that the ratio η_v/η_s is simply related to the entropy of fusion is consistent with a co-operative model.

The explanation which has been offered for this relationship assumes that a quasi-crystalline lattice exists which must « melt » or become randomized for structural flow to occur. While the structure is randomized molecules can change their positions and then revert to a new « quasi-crystalline » order. Because of the co-operative nature of the melting process, the above results imply co-operative behavior is involved in the viscous flow processes.

Therefore the non-Arrhenius behavior of shear viscosity and shear relaxation time is evidence that co-operative effects play a role in the shear flow process in many liquids.

McDuffie and Litovitz [29] have proposed the following reasoning to explain the distribution of relaxation times in shear and structural relaxation.

1) Regions of short-range order exist in the liquid which are continually breaking up and reforming.

2) The break-up of this structure is co-operative and does not follow a simple rate process; that is the degree of order of a given structure decreases nonexponentially in time.

3) This co-operative nonexponential behavior is the origin of the observed distribution of shear and structural relaxation times in the liquid.

Fundamental to any simple relaxation theory is the assumption that the degree of order decays exponentially. If however the ability of one molecule to jump or re-align itself depends on the condition of its neighbours, then nonexponential decay would occur. For example if a molecule was part of a « group » whose break-up is co-operative, it should be easier for a part of the group to break up after the first part has randomized.

7·3. *Viscous relaxation in the Arrenhius region.* – In almost every liquid the mechanical relaxation effects have been measured in the non-Arrhenius region where the W.L.F. expression holds. In every one of these liquids a distribution of mechanical relaxation times has been observed. If the explanation for the non-Arrhenius behavior of the viscous processes is correctly given by the assumption of co-operative motion of groups of molecules, and if the origin of the distribution of structural relaxation times is related to the co-operative nature of the process measured in the Arrenhius region this should exhibit a single relaxation time. This is just what has been found. The ultrasonic relaxation measurements on molten zinc chloride have been made in the region where $\ln \eta$ varies as $1/T$ and a single relaxation time has been observed both for shear and structural relaxation processes.

This is again in accord with the concept that because of the large free volume at high temperature the molecular mobility is determined by a simple non-co-operative, thermally activated, rate process.

REFERENCES

[1] E. Heasall and J. Lamb: *Proc. Roy. Soc.* (*London*), **B 69**, 869 (1956).
[2a] R. Schwartz and K. F. Herzfeld: *Journ. Chem. Phys.*, **22**, 767 (1954).
[2b] K. F. Herzfeld and T. A. Litovitz: *Absorption and Dispersion of Ultrasonic Waves* (New York, 1959).
[3] T. Litovitz: *Journ. Acoust. Soc. Am.*, **26**, 469 (1956).
[4] M. C. Henderson and L. Peselnick: *Journ. Acoust. Soc. Am.*, **31**, 29 (1958).
[5] W. Madigosky and T. A. Litovitz: *Journ. Chem. Phys.*, **34**, 489 (1961).
[6] T. Litovitz, E. Carnevale and P. Kendall: *Journ. Acoust. Soc. Am.*, **26**, 465 (1956).
[7] F. D. Shields: *Journ. Acoust. Soc. Am.*, **29**, 450 (1956).
[8] J. O. Hirschfelder, C. F. Curtiss and R. B. Bird: *Molecular Theory of Gases and Liquids* (New York, 1954).
[9] V. O. Knudsen and E. Frick: *Journ. Acoust. Soc. Am.*, **12**, 255 (1940).
[10] W. Slie and T. A. Litovitz: *Journ. Acoust. Soc. Am.*, **33**, 1412 (1961).
[11] B. Coleman and W. Noll: *Rev. Mod. Phys.*, **33**, 239 (1961).
[12] W. P. Mason, W. O. Baker, H. J. McSkimin and J. H. Heiss: *Phys. Rev.*, **75**, 936 (1949).
[13] A. Clark and T. A. Litovitz: *Journ. Acoust. Soc. of Am.*, **32**, 1221 (1960).
[14] R. Higgs and T. A. Litovitz: *Journ. Acoust. Soc. of Am.*, **32**, 1108 (1960).
[15] G. Marchessault and T. A. Litovitz: *Journ. Acoust. Soc. of Am.*, **34**, 616 (1962).
[16] W. J. Davis, S. E. Rogers and A. R. Ubbelohde: *Proc. Roy. Soc.* (*London*), **A 220**, 14 (1953).
[17] G. Gruber: *Ph. D. Dissertation* (Washington, 1962).
[18] A. J. Barlow and J. Lamb: *Proc. Roy. Soc.* (*London*), **A 258**, 52 (1959).

[19] N. Taskoprulu, A. Barlow and J. Lamb: *Journ. Acoust. Soc. of Am.*, **33**, 278 (1961).
[20] J. D. Ferry: *Viscoelastic Properties of Polymers* (New York, 1961).
[21] N. Hirai and H. Eyring: *Journ. Appl. Phys.*, **29**, 810 (1958).
[22] R. Meister, C. Marhoeffer, R. Sciamanda, L. Cotter and T. Litovitz: *Journ. Appl. Phys.*, **31**, 854 (1960).
[23] P. Debye: *Polar Molecules* (New York; 1929).
[24] W. Kauzmann: *Rev. Mod. Phys.*, **14**, 12 (1942).
[25] H. Eyring: *Journ. Chem. Phys.*, **4**, 283 (1936).
[26] T. Fox and T. Flory: *Journ. Am. Chem. Soc.*, **70**, 2384 (1948).
[27] M. Williams, R. Landel and J. Ferry: *Journ. Am. Chem. Soc.*, **77**, 3701 (1955).
[28] F. Bueche: *Journ. Chem. Phys.*, **30**, 748 (1959).
[29] G. McDuffie and T. Litovitz: *Journ. Chem. Phys.*, **37**, 1699 (1962).

Acoustic Relaxation in Electrolyte Solutions.

K. Tamm

Institut für Angewandte Physik - Heidelberg

1. – Introduction.

The sound absorption in aqueous solutions of some electrolytes, including sea water, exceeds that of the solvent considerably. The frequency-dependence of the absorption (Fig. 1) shows that the absorption is given by the superposition of that of the solvent plus a relaxation absorption which is caused by the electrolyte.

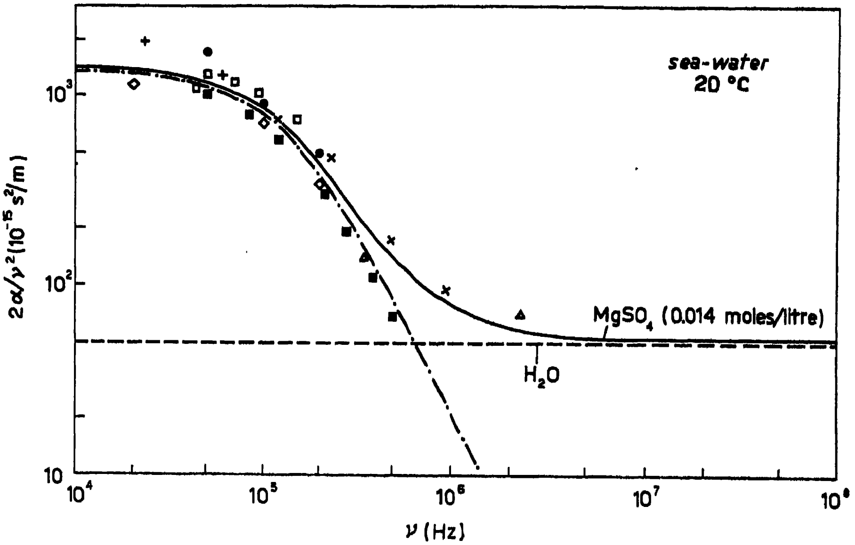

Fig. 1. – Frequency-dependence of total sound absorption per frequency squared ($2\alpha/\nu^2$) in sea water compared with 0.014 m MgSO$_4$-solution.

Systematic investigations have shown that the number of observed relax-

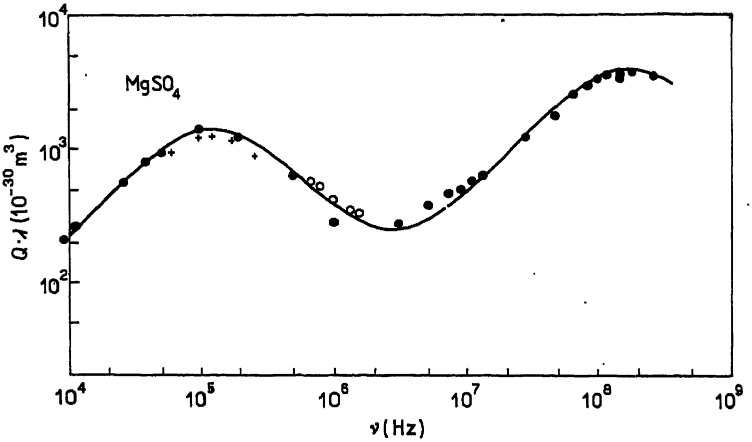

Fig. 2. – Frequency-dependence of sound absorption volume $(Q\lambda)_m$ of in acqueous MgSO$_4$-solution.

ation processes—which correspond to maxima of $\alpha\lambda$ *vs.* frequency ν (see Fig. 2)—depends on the type and the valency of both ion partners. While nearly all the « weak » electrolytes show one relaxation maximum, the number of relaxation maxima varies for strong electrolytes. Strong 1-1 valent electrolytes show either no electrolyte absorption or a small negative one (Fig. 3).

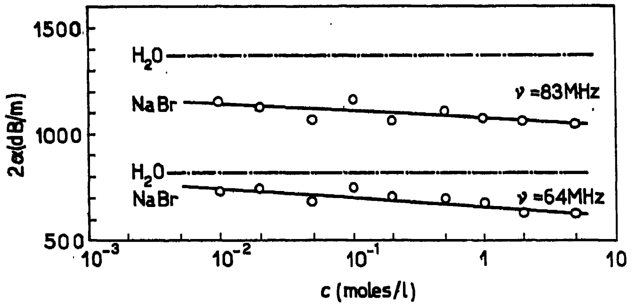

Fig. 3. – Concentration-dependence of total absorption coefficient in NaBr-solutions.

This may be explained by the influence of the ions on the structure of the solvent. Apparently the ions partially destroy the icelike configuration of the water molecules. In contrast, strong 1-2 electrolytes show a relaxation maximum at high frequencies (approximately at 100 MHz), and for strong 2-2 electrolytes there exists an additional one at lower frequencies (Fig. 4). For example MgSO$_4$ has a maximum at 140 kHz which exists neither in Na$_2$SO$_4$ nor in MgCl$_2$. From these facts it may be concluded that the absorption is not caused by the interaction between the ions and the solvent but that there is a specific interaction between different ion partners. This was first supposed by LIEBERMANN [1], who discussed a simple dissociation reaction. Investigations of KURTZE, EIGEN and TAMM [2] have shown that the assumption of a simple dissociation can be shown to hold only for weak electrolytes. For strong electrolytes, especially for 2-2 and higher-valent ones, apparently a step-wise dissociation with at least two steps exists. This may be concluded from the existence of at least two relaxation maxima which have a similar dependence on the electrolyte concentration.

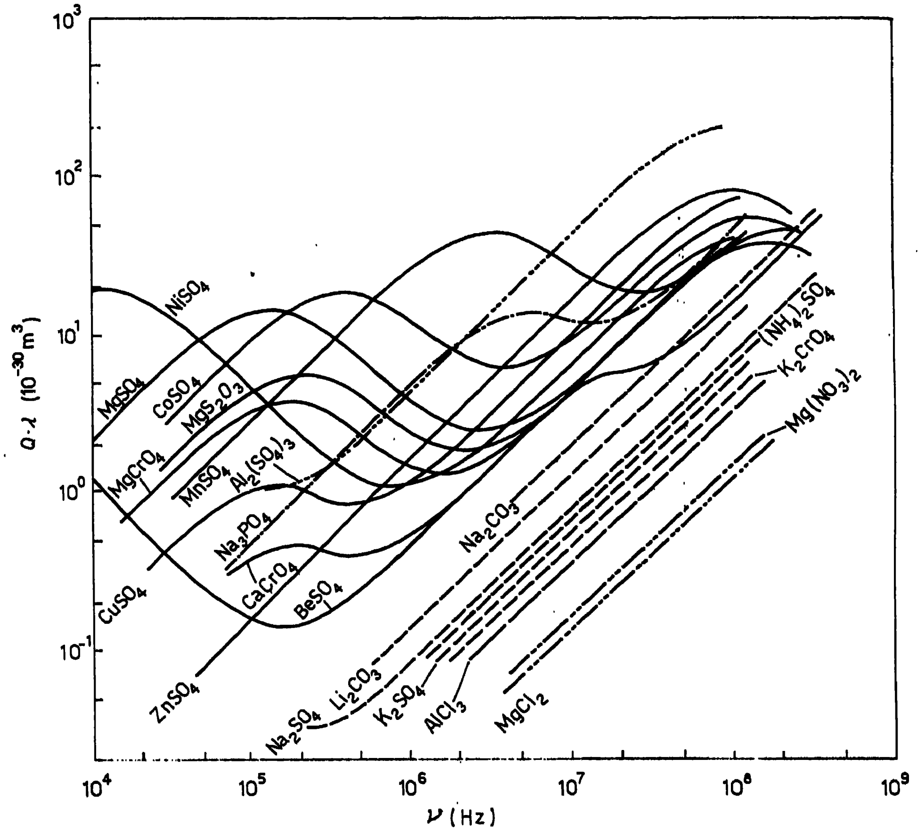

Fig. 4. – Survey on sound-absorption volume ($Q\lambda$) *vs.* frequency of different electrolytes in aqueous solutions (20 °C, small concentrations): – – – 1-2; –·–·– 1-3; ——— 2-2; –·–··– 2-1; — — 3-1; –·····–·– 3-2.

The step-wise dissociation may be interpreted as a step-wise separation of the ions from each other by inserting one, two or more water molecules between them. The first steps are distinctly different from each other and from the following ones with respect to configuration, activation energy and other data. They therefore cause discrete relaxation processes with different time-constants which in 2-2 electrolytes are apparently identical with the two relaxation maxima observed (Fig. 4). It is easy to understand that the specific qualities of the ions may only affect the binding (and the absorption) if the ions are very near together or in direct contact. The lower of the two maxima observed (the relaxation frequency of which varies strongly with the type of the cation) may be ascribed to the first step of dissociation, in which ions in direct contact go over to a complex with one water molecule inserted between them. The fact that the relaxation frequency depends only slightly on the anion is probably caused by the fact that the anions of the electrolytes investigated have similar qualities—they all are salts of the oxygen acids. The insertion of a second water molecule (and further ones) is not affected by the specific qualities of the ion partners, only the electrostatic charge is important:

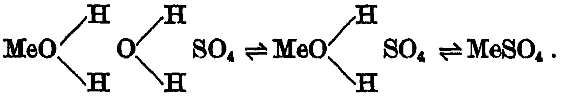

$$\mathrm{MeO}{<}^{\mathrm{H}}_{\mathrm{H}}\ \mathrm{O}{<}^{\mathrm{H}}_{\mathrm{H}}\ \mathrm{SO_4} \rightleftharpoons \mathrm{MeO}{<}^{\mathrm{H}}_{\mathrm{H}}\ \mathrm{SO_4} \rightleftharpoons \mathrm{MeSO_4}\,.$$

Therefore, within a group of electrolytes of the same valence there should be no essential differences in the frequency of the corresponding relaxation maximum. Indeed, all 2-2 electrolytes show the « higher » relaxation maximum at about 100 MHz, which may be ascribed, therefore, to the second step of dissociation (Fig. 4).

The following steps of dissociation caused by insertion of further water molecules do not differ very much from each other. They are included in the ionic atmosphere (ion cloud) interaction which, therefore, has a broad frequency spectrum and is connected with a flat maximum of the absorption per wave length *vs.* frequency curve which differs considerably from that of a discrete relaxation process. In agreement with this an absorption is found for all electrolytes for very high frequencies (>100 MHz) which, of course, depends on the valency of the electrolyte. Unfortunately, the dependence on frequency cannot be tested experimentally since the experimental limit of the frequency range of the measurements is about 300 MHz.

This interpretation of the relaxation phenomena in electrolytes is very plausible since a great number of the existing experimental results can be explained under certain reasonable assumptions by means of a corresponding theory of multi-step dissociation. The theory which gives numerical results being in good agreement with the experiments will be represented in the following sections.

It can be shown that other relaxation processes which might also be considered to be the cause of the measured relaxation maxima do not have the proper behaviour with respect to relaxation frequency and strength. For example the relaxation corresponding to the transfer of energy between the different (translation, rotation and oscillation) degrees of freedom (which is well-known from the investigations in gases by KNESER [3], HERZFELD [4] and others) may be excluded since the relaxation frequency should not, as observed, shift with concentration.

2. – Theory of acoustic relaxation in electrolyte solutions.

It is very well known that when a chemical equilibrium between reactants and reaction products is disturbed by the pressure and temperature variations of a sound wave, the return to equilibrium is retarded because of the finite reaction rate and that this retardation is the cause of an acoustic relaxation. It is the aim of the theory given here to derive relations between the kinetic and thermodynamic parameters of the reactions existing in electrolyte solutions and the measured acoustical relaxation data, *i.e.* frequency-dependence and absolute value of absorption and dispersion. Since such a theory is very similar to the well-known theory of excited states, only the essential differences in the suppositions will be given here and followed through the calculations. The usual statements of chemical kinetics will be used.

2'1. *Calculation of the relaxation times.*

2'1.1. One-step systems. At first the specific interaction of two ions A^+ and B^- in the form of a simple binary dissociation equilibrium will be handled, *i.e.*

$$\underset{(1)}{A^+ + B^-} \underset{k_{21}}{\overset{k_{12}}{\rightleftharpoons}} \underset{(2)}{AB} . \tag{1}$$

The numbers of associates breaking up or recombining per unit time (of momentary concentration c_{AB}) are given by the rate-constants of decomposition k_{21} and recombination k_{12}:

$$-\left(\frac{dc_{AB}}{dt}\right)_{dec} = k_{21}c_{AB}\,; \qquad \left(\frac{dc_{AB}}{dt}\right)_{rec} = k_{12}c_A c_B .$$

The time variation $\dot{c}_{AB}$ is, therefore, a nonlinear function of the concentrations, given by

$$\dot{c}_{AB} = k_{12}c_A c_B - k_{21}c_{AB} . \tag{2}$$

For equilibrium the time variation (2) will be zero, resulting in the well known mass-action equilibrium equation

$$\frac{\bar{c}_A \bar{c}_B}{\bar{c}_{AB}} = \frac{k_{21}}{k_{12}} = K , \tag{3}$$

where $\bar{c}_i$ are the equilibrium concentrations. By subtracting (3) from (2) we get:

$$\dot{c}_{AB} = k_{12}(c_A c_B - \bar{c}_A \bar{c}_B) - k_{21}(c_{AB} - \bar{c}_{AB}) .$$

If the deviations of the concentrations from equilibrium are small ($\delta c_i = c_i - \bar{c}_i \ll \bar{c}$), this relation can be linearized provided the rate constants k_{12} and k_{21} are independent of concentration:

$$\dot{c}_{AB} \approx k_{12}\,\bar{c}_A\,\delta c_B + k_{12}\,\bar{c}_B\,\delta c_A - k_{21}\,\delta c_{AB} \tag{4}$$

so that with $\delta c_A = \delta c_B = -\,\delta c_{AB}$

$$\frac{\partial c_{AB}}{\partial t} \approx -\,[k_{12}(\bar{c}_A + \bar{c}_B) + k_{21}]\,\delta c_{AB} = -\,\frac{\delta c_{AB}}{\tau} . \tag{5}$$

We thus obtain a differential equation for the return to equilibrium with time, the solution of which is an exponential function with time constant τ. The time constant (and, therefore, also the relaxation frequency $\omega_m = 1/\tau$) depends on the equilibrium concentrations since

$$\frac{1}{\tau} = k_{21} + k_{12}(\bar{c}_A + \bar{c}_B) . \tag{6}$$

Equation (6) can be applied only to reactions in solutions with very low ion concentrations, that is, to processes for which only the interaction between two reacting ion partners has to be considered.

The behaviour of $NH_4 \cdot OH$ in aqueous solution *i.e.* of a weak electrolyte may be considered as an example. The experiments (Fig. 5) indicate a strictly linear dependence of the relaxation frequency on ion concentration if one supposes this ion concentration to be proportional to the square root of the electrolyte concentration c, as may be expected from the mass-action law (3).

In order to extend the consideration to higher ion concentrations, the interaction of the ions with other ions in the ionic atmosphere has to be taken into account. In equilibrium this can be done by inserting the activity coefficients f_i or their product Π^f. The mass-action law can then be written as

$$\frac{\bar{c}_A \bar{c}_B}{\bar{c}_{AB}} \cdot \frac{f_A f_B}{f_{AB}} = \frac{\bar{\alpha}^2 c}{1-\bar{\alpha}}\,\Pi^f = K , \tag{7}$$

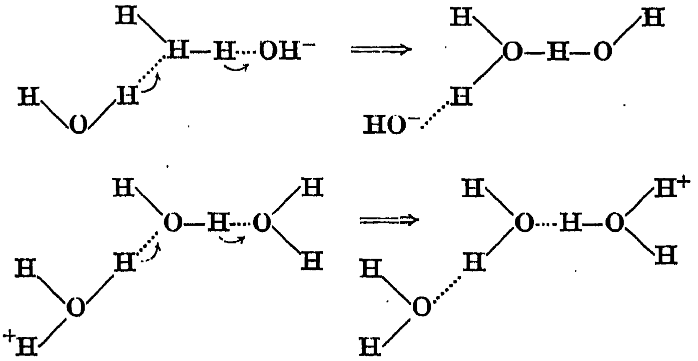

Fig. 5. – Diffusion mechanism of hydroxyl-ions and protons.

where $\bar\alpha = c_A/c$ is the degree of dissociation and K is the equilibrium constant, which is independent of concentration. Thus K/Π' replaces k_{21}/k_{12} in eq. (3). It can be shown that for all reactions, for which the return to equilibrium of the general interionic interaction (*e.g.* for the ionic atmosphere in the sense of Debye and Hückel [5]) is fast when compared with the reaction step considered, the reaction may be represented further by eq. (2). Here k_{21} remains practically constant while $k_{12} = k^0_{12}\Pi'$ may be presented as a product with the concentration-dependence of Π' (k^0_{12} is a constant).

In this case the concentration-dependence of the activity product Π' has to be taken into account when linearizing eq. (2) by including a term

$$\bar c_A \bar c_B \,\delta\Pi' = \bar c_A \bar c_B \sum_i \frac{\partial \Pi'}{\partial c_i}\,\delta c_i = \bar\alpha^2 c \left(\frac{\partial \Pi'}{\partial \alpha}\right)_0 \delta c_{AB}\,.$$

Then instead of (6) one obtains

$$(8)\qquad \frac{1}{\tau} = k_{12} + k'_{12} \quad \text{where} \quad k'_{12} = k^0_{12}\Pi'\left[\bar c_A\left(1 + \frac{\partial \ln \Pi'}{\partial \ln \bar c_B}\right) + \bar c_B\left(1 + \frac{\partial \ln \Pi'}{\partial \ln \bar c_A}\right)\right].$$

(Since AB is practically neutral with respect to charge: $f_{AB} \approx 1$ and $\Pi' \approx f_A \cdot f_B$).

Unfortunately, eq. (8) which takes the activation coefficients into account is limited in application because of the assumption, (which was used in its derivation) that the return to equilibrium in the ionic atmosphere is fast when compared with the reaction-rate in the chemical reaction. This assumption is not fulfilled for one-step reactions according to scheme (1). The reason for this is the fact that both the rate of the return to equilibrium of the ionic atmosphere as well as that of the chemical reaction are given by the collision frequency of the ion partners, which is determined by diffusion. Equation (8) is, therefore, valid only in cases for which the simple eq. (5) is valid too. Its value lies in the possibility of extending it to the case of multi-step relaxation processes.

2·1.2. Two-step relaxation processes. As mentioned above, the recombination and the dissociation of two ions in aqueous solutions are multi-step processes in which, besides the two ion partners, the water molecules of the co-ordination spheres participate. This must be taken into account by extending the reaction-scheme (1) to the form (9) which includes (according to the experimental results) two equilibria of specific ion interaction which depend on each other:

$$(9)\qquad A^+_{aq} + B^-_{aq} \underset{k_{21}}{\overset{k_{12}}{\rightleftharpoons}} [A^+_{aq}]\cdot[B^-_{aq}] \underset{k_{32}}{\overset{k_{23}}{\rightleftharpoons}} [AB]_{aq}\,.$$

1 Free ions
2 complex of hydrated ions
3 aquo-complex

The step 1-2 means the formation of an intermediate complex where both partners are in a hydrated state. The aquo-complex in which one or more H_2O molecules of the inner co-ordination sphere of A^+ are replaced by the ion B^- is formed out of this state. The kinetic equations for the process (9) may be written as follows

$$(10)\qquad \begin{cases} \dot c_1 = \dot c_A = \dot c_B = -k_{12}c_A c_B + k_{21}c_2 \\ \dot c_2 = k_{12}c_A c_B - (k_{21}+k_{23})c_2 + k_{32}c_3 \\ \dot c_3 = k_{23}c_2 - k_{32}c_3\,, \end{cases}$$

if it can be assumed that the equilibrium of the ionic-atmosphere distribution will reestablish much faster than that of the reaction 1-2, so that

$$k_{12} = k^0_{12}\cdot\Pi^f \approx k^0_{12} f_A f_B\,.$$

Assuming that the deviations $\delta c_i = x_i$ from the equilibrium concentrations are small, the system of eqs. (10) can be linearized. With

$$\delta c_1 = \delta c_A = \delta c_B = x_1\,,\qquad \delta c_2 = x_2\,,\qquad \delta c_3 = x_3$$

we obtain from (10)

$$(11)\qquad \begin{cases} \dot x_1 = -k'_{12}x_1 + k_{21}x_2\,, \\ \dot x_2 = k'_{12}x_1 - (k_{21}+k_{23})x_2 + k_{32}x_3\,, \\ \dot x_3 = \phantom{-k'_{12}x_1 - (k_{21}+)}k_{23}\,x_2 - k_{32}x_3\,. \end{cases}$$

In this system the deviations x_i of the concentrations of the different states i are not independent of each other. Therefore, in general the relaxation times τ_j of the system are no longer equal to those (τ_i), which can be calculated for the different steps (if these are treated as « isolated »). The τ_j are given rather by the eigenvalues ($-1/\tau_j$) of the system of eqs. (11) which may be transferred by an affine transformation to a system (12) of independent equations,

$$\dot{y}_j = -\frac{1}{\tau_j} y_j; \qquad j = \mathrm{I, II, III}, \tag{12}$$

each of which refers to only one variable y_j and its derivative with respect to time $\dot{y}_j$. The normal variables y_j are such linear combinations of the concentration deviations x_i which are independent of each other during deviations from the equilibrium.

The affine transformation may be written in form of matrix-products

$$\boldsymbol{y} = \boldsymbol{M}\boldsymbol{x}; \qquad \boldsymbol{x} = \boldsymbol{M}^{-1}\boldsymbol{y}. \tag{13}$$

The transformation matrix $\boldsymbol{M}$ is given by

$$\boldsymbol{M} = \begin{pmatrix} k'_{12}/(k'_{12} - 1/\tau_{\mathrm{I}}) & 1 & k_{32}/(k_{32} - 1/\tau_{\mathrm{I}}) \\ k'_{12}/(k'_{12} - 1/\tau_{\mathrm{II}}) & 1 & k_{32}/(k_{32} - 1/\tau_{\mathrm{II}}) \\ 1 & 1 & 1 \end{pmatrix}. \tag{14}$$

Its inverse $\boldsymbol{M}^{-1}$ is determined by the condition $\boldsymbol{M}\cdot\boldsymbol{M}^{-1} = \boldsymbol{E}$, where $\boldsymbol{E}$ is the unit matrix. For the system (11) the eigenvalues $\lambda_j = -1/\tau_j$ result as solutions of the characteristic equation $|\lambda\boldsymbol{E} - \boldsymbol{K}| = 0$; where $\boldsymbol{K}$ is the matrix of the coefficients of eq. (11):

$$\left\{\begin{aligned} \lambda_{\mathrm{I,II}} &= -1/\tau_{\mathrm{I,II}} = \tfrac{1}{2}\left[\Sigma k \pm \sqrt{(\Sigma k)^2 - 4(\Pi k)}\right] \\ \lambda_{\mathrm{III}} &= -1/\tau_{\mathrm{III}} = 0 \end{aligned}\right. \tag{15}$$

with

$$\Sigma k = k'_{12} + k_{21} + k_{23} + k_{32},$$

$$\Pi k = k'_{12}(k_{23} + k_{32}) + k_{21}k_{32}.$$

These relatively complicated expressions (15) may be simplified considerably with the condition $\tau_{\mathrm{I}} \ll \tau_{\mathrm{II}}$, which in many cases is fulfilled, since the experimental relaxation times mostly differ by a larger factor. The case

$$k'_{12},\ k_{21} \gg k_{23},\ k_{32} \tag{16}$$

is of special interest. Physically this assumption means that the equilibrium of the first step A+B $\rightleftharpoons$ (AB) adjusts very quickly, while the equilibrium of the next step follows only slowly.

With the condition $x_1 + x_2 + x_3 = 0$ (which means constant electrolyte concentration and $\lambda_{\text{III}} = 0$), the eqs. (13) and (14) can be simplified. Since (12) shows that multiplication of y_j by a constant factor does not alter the system, the following variables may be used if (16) is valid

$$(17)\quad \left\{\begin{aligned} y_{\text{I}} &= -\frac{k'_{12}}{k'_{12}+k_{21}}\,x_1 + \frac{k_{21}}{k'_{12}+k_{21}}\,x_2\,; \\ y_{\text{II}} &= -(x_1+x_2) = +x^3\,; \\ y_{\text{III}} &= 0\,, \end{aligned}\right. \qquad (18)\quad \left\{\begin{aligned} x_1 &= -y_{\text{I}} - \frac{k_{21}}{k'_{12}+k_{21}}\,y_{\text{II}}\,; \\ x_2 &= +y^{\text{I}} - \frac{k'_{12}}{k'_{12}+k_{21}}\,y_{\text{II}}\,; \\ x_3 &= +y_{\text{II}}\,. \end{aligned}\right.$$

Under the condition (16) the eigenvalues of the characteristic equation are given by

$$(19)\quad \left\{\begin{aligned} \frac{1}{\tau_{\text{I}}} &= k_{21} + k'_{12}\,, \\ \frac{1}{\tau_{\text{II}}} &= k_{32} + k'_{23} \qquad \text{with } k'_{23} = \frac{k'_{12}}{k'_{12}+k_{21}}\cdot k_{23}\,. \end{aligned}\right.$$

τ_{I} describes the relaxation of the step 1-2, which consists in the fast readjustment of the partial-equilibrium $\text{A}^+ + \text{B}^- \rightleftharpoons$ (AB). Because of its slow transition rate in the step 2-3 the concentration of state 3 is very little influenced by fast variations of the concentrations in the states 1 and 2.

On the other hand, the second relaxation process (with the time constant τ_{II}) is not given simply by the equilibrium of step 2-3 but by an equalizing process between state 3 on one side and the equilibrium of 2 and 1 on the other side.

2·1.3. **Multi-step relaxation phenomena.** If more than two relaxation steps co-exist, τ_j can be given explicitely only for special cases. Such a case occurs when the different relaxation times form a discrete sequence $\tau_{\text{I}} \ll \tau_{\text{II}} \ll \dots \ll \tau_n$, *i.e.* if each step is much faster than the following one. The relaxation spectrum may then be calculated successively.

The relaxation times τ_{I} and τ_{II} are identical with those calculated for a two-step process, since the concentration of the other states *e.g.* $(AB)_4$ etc. is nearly unaltered by variations in states 1,2, and 3. For calculation of τ_{III} the equilibrium between state 4 and the states 1, 2, 3 together has to be considered.

We obtain:

$$(20)\qquad \frac{1}{\tau_{III}} = k_{43} + k'_{34}; \qquad \text{where} \qquad k'_{34} = \frac{k'_{23}}{k'_{23} + k_{32}}\, k_{34} = \frac{1}{1 + k_{32}/k'_{23}}\, k_{34}\,.$$

It may be mentioned that a calculation in explicit form is possible also in the case of nearly equal rate constants of the first two steps

$$k'_{12},\ k_{21},\ k_{23},\ k_{32} \gg k_{34},\ k_{43}\,.$$

For these two steps the general solutions according to eq. (13) have to be used, while for the « slow » step the expression (20) remains valid. Besides k_{43} and k_{34} eq. (20) comprises only equilibrium quantities of the steps 1-2 and 3-4. τ_{III} is independent of the special reaction mechanism of these steps.

2'1.4. **Relaxation of the ion-distribution.** Complicated systems may also be treated according to the method given above provided certain assumptions are fulfilled. The dissociation process of an electrolyte in fact consists of a series of many steps, because state « 1 » includes a great number of different configurations of the two ions with different strength of electrostatic interaction between them. This means the first step $1 \rightleftharpoons 2$ in the reaction-scheme cannot be described by one discrete relaxation time. For this step, therefore, a continuous spectrum of relaxation times exists which, as will be shown later, corresponds to the continuous distribution of the possible distances (*). However, the insertion of an ion into the co-ordination sphere of the other ion does mean a sequence of discrete elementary steps (steps $2 \rightleftharpoons 3 \rightleftharpoons 4$), the time constants of which differ characteristically from that of the preceding steps.

The « encounter-complex » « 2 » is part of the ionic atmosphere. The establishment of the equlibrium of the ionic atmosphere (represented by the distribution function F) may be treated according to DEBYE, FALKENHAGEN and ONSAGER [6] as a diffusion problem. In the case of the readjustment of a small disturbance $F_{(s,\, t=0)}$ we obtain

$$(21)\qquad \delta F(s, t) = \delta F(s, 0) \cdot \frac{1}{2}\operatorname{erfc}\left[\sqrt{t/\theta} - \frac{s}{2\sqrt{t/\theta}}\right],$$

(*) This is valid since in liquids there is no crystallike remote order of the ions.

where

$$\theta \quad = \text{a time period} \qquad = \frac{\varrho_A \varrho_B}{\varrho_A + \varrho_B} \frac{1}{kT/R_0^2},$$

$$\varrho_i \quad = \text{friction coefficient}$$

$$R_0 \quad = \text{radius of ionic atmosphere} = \left[\frac{4\pi e_0^2}{\varepsilon kT} \sum z_i^2 n_i\right]^{-\frac{1}{2}},$$

$$\operatorname{erfc}\ (Z) = \text{error function of } Z \qquad = \frac{2}{\sqrt{\pi}} \int_z^\infty \exp\left[-x^2\right] \mathrm{d}x\,.$$

Relation (21) differs considerably from that of a single discrete step where

$$\delta c(t) = \delta c_0 \cdot \exp\left[-t/\tau\right].$$

The single relaxation time τ is replaced by a continuous sequence of time constants $\lambda\theta$ between 0 and θ.

The quantity

$$\varrho(\lambda) = \frac{1}{\lambda}\left[\frac{\cos(s\lambda^*)}{\sqrt{2}\lambda^*} + \frac{\sqrt{s}}{2}\sin(s\lambda^*)\right], \tag{22}$$

where

$$\lambda^* = \left(\frac{1-\lambda}{\lambda}\right)^{\frac{1}{2}}, \qquad s = r/R_0,$$

is a distribution function that determines the weight of the relaxation processes co-ordinated to the time constants $\lambda\theta$ within the relaxation spectrum.

The theoretical solution for the relaxation of the ion distribution given above is valid for very dilute solutions (under the assumption of point charges). The theoretical treatment of a nonstationary ionic atmosphere for high concentration is a difficult problem which has not been solved so far. However for the examples which will be treated later on, the approximation given above can be used. The specific steps of the (chemical) reaction are so slow that they may be treated separately, taking the influence of the ionic atmosphere into account by using the activity coefficients.

For sufficiently week electrolytes, however, the diffusion-determined recombination may also be treated like a discrete bimolecular reaction since the interaction within the ionic atmosphere remains negligibly small.

2·2. *Calculation of the molecular sound absorption (relaxation strength).* – In a sound wave, the finite rate of chemical reaction causes (time-dependent) deviations of the concentrations from the equilibrium appropriate to the instantaneous pressure, *i.e.* a phase-shift exists between pressure and volume. This means that the part of the compressibility which corresponds to the chemical transition becomes complex, its imaginary portion determining the sound absorption.

The calculation may be reduced if the following assumptions are fulfilled:

a) The deviations of the inner parameters from equilibrium are small ($\delta c_i \ll \bar{c}_i$) so that the equations can be linearized. This is valid for small sound intensities.

b) The contributions of independent relaxation processes are additive. This is valid if *a*) is fulfilled.

c) The variations in the solvent (structure relaxation) are sufficiently fast and may be regarded as being in equilibrium with the external parameters (*e.g.* pressure) in the frequency range under consideration. This can be tested by absorption measurements in the solvent.

d) The chemical relaxation processes may be regarded as proceeding under constant external conditions (T, p). This is approximately fulfilled if the mole fraction of the solved electrolyte is small when compared to the solvent, because under this condition reaction-enthalpy and reaction-volume don't influence temperature and pressure in the sound field. For the same reason the thermodynamic conditions under which the solution is compressed in the sound wave do not influence τ, *i.e.* $\tau_{T,p} \approx \tau_{S,p}$, $\tau_{T,v} \approx \tau_{S,v}$.

2'2.1. **One-step relaxation processes.** With the assumption that the contribution $\bar{\varkappa}_S^{\text{ch}}$ of the adiabatic chemical reaction (for equilibrium) to the compressibility is much smaller than the instantaneous compressibility $\varkappa_S^\infty$ of the solution (*) [this assumption is fulfilled if assumption *a*) in Section 2'2 is fulfilled], the corresponding absorption per wave length is given approximately by eq. (23).

$$\bar{\varkappa}_S^{\text{ch}} \ll \varkappa_S^\infty\,; \qquad \mu^{\text{ch}} \approx 2\pi \frac{\omega\tau}{1+\omega^2\tau^2}\,\frac{\bar{\varkappa}_S^{\text{ch}}}{\varkappa_S^\infty}\,. \tag{23}$$

Thus the absorption volume $Q\lambda$ (absorption cross-section Q times wavelenghth λ)

(*) $\varkappa_S^\infty$ is the compressibility of the solution at frequencies higher than $1/\tau^{\text{ch}}$ but lower than the reciprocal of other (smaller) relaxation times (*e.g.* structural relaxation).

is, for a given concentration c,

$$(Q\lambda)^{ch} = \frac{\mu^{ch}}{c} \approx 2\pi \frac{\omega\tau}{1+\omega^2\tau^2} \frac{\bar{\varkappa}_S^{ch}}{c\cdot\varkappa_S^{\infty}}. \tag{23a}$$

For $\omega = \omega_m = 1/\tau$ we obtain a maximum value

$$\mu_m^{ch} \approx \pi \frac{\bar{\varkappa}^{ch}}{\varkappa_S^{\infty}} \quad \text{or} \quad (Q\lambda)_m^{ch} \approx \pi \frac{\bar{\varkappa}_S^{ch}}{c\cdot\varkappa_S^{\infty}}, \tag{24}$$

where instead of $\tau \approx \tau_S = \sqrt{\tau_{S,v}\cdot\tau_{S,p}}$ with the same approximation ($\bar{\varkappa}_S^{ch} \ll \varkappa_S^{\infty}$); $\tau \approx \tau_T = \sqrt{\tau_{T,v}\cdot\tau_{T,p}}$ may be written.

The equilibrium value of the chemical portion of the compressibility may be derived from thermodynamic relations

$$\bar{\varkappa}_S^{ch} = -\frac{1}{V}\left(\frac{\partial V}{\partial\bar{\alpha}}\right)_{S,p}\cdot\left(\frac{\partial\bar{\alpha}}{\partial p}\right)_S, \tag{25}$$

where $\bar{\alpha}$ is the degree of dissociation for equilibrium (*). The first factor is given by the difference ΔV_S of the partial volumes of the two states (for adiabatic reactions); *i.e.*

$$\frac{1}{V}\left(\frac{\partial V}{\partial\bar{\alpha}}\right)_{S,p} = c\cdot\Delta V_S. \tag{26}$$

The second factor, the variation of equilibrium with pressure, also depends on ΔV_S as follows:

$$\left(\frac{\partial\bar{\alpha}}{\partial p}\right)_S = \frac{c_p^{\infty}}{\bar{c}_p}\Gamma^*\frac{\Delta V_S}{RT}. \tag{27}$$

In eq. (27) the factor Γ^* accounts for the number of individual reactions, and varies with the type of the reaction. For a single step dissociation it is given by

$$\Gamma^* = \frac{\Gamma}{1+\Gamma(\partial\ln\Pi'/\partial\alpha)_c} \quad \text{where} \quad \Gamma = \frac{\alpha(1-\alpha)}{2-\alpha}. \tag{28}$$

Γ depends only on the degree of dissociation and has a maximum for $\alpha = 0.59$. The denominator of the expression for Γ^* accounts for the variation of the

---

(*) The bar is omitted further on, when confusion is not to be expected.

activity coefficients with concentration and is very small for concentrations between 0.1 and 1*m*.

The factor $c_p^\infty/\bar{c}_p$ in (27) has to be introduced because the differentiation should be carried out for constant entropy instead of constant temperature.

We obtain, therefore,

$$\bar{\varkappa}_S^{\text{ch}} = c\Gamma^* \frac{(\Delta V_S)^2}{RT} \frac{c_p^\infty}{\bar{c}_p}, \tag{29}$$

where

$$\Delta V^s = \left(\Delta V - \Delta H \frac{\theta_p^\infty}{\varrho c_p^\infty}\right) \approx \Delta V. \tag{30}$$

ΔV_S is the difference of the partial volumes (for adiabatic reactions) which is given by the differences of the partial molar volumes (reaction volumes) and enthalpies (reaction enthalpies). $\theta_p^\infty \approx \bar{\theta}_p$ is the coefficient of thermal expansion for the whole system for a constant degree of dissociation. For aqueous solutions (because water has a maximum density at 4 °C) the factor $\theta_p^\infty/\varrho c_p^\infty$ is very small ($= 0.21$ cm^3/kcal at 20 °C) and the enthalpy term may be neglected in (30) (*).

Since $c_p^\infty \approx \bar{c}_p$ for electrolytes in aqueous solutions,

$$\bar{\varkappa}_S^{\text{ch}} \approx \bar{\varkappa}_T^{\text{ch}} \approx c\Gamma^* \frac{(\Delta V)^2}{RT}. \tag{31}$$

2'2.2. Multi-step relaxation processes. If a multi-step reaction has discrete relaxation times we obtain for the absorption spectrum the sum

$$\mu = \sum_{j=1}^{n} \frac{\mu_{mj}}{2} \frac{\omega\tau_j}{1 + \omega^2\tau_j^2}, \tag{32}$$

each component j of which may be calculated in a way similar to the single-reaction case. Since the relaxation times τ_j are already known from Section 2'1.2, only an outline of the calculation of μ_{mj} will be given here.

The variations δN_i of the concentrations (caused by the reaction) are connected with a variation δV of the volume V:

$$\delta V = \delta N_1 \cdot V_1 + \delta N_2 \cdot V_2 + \delta N_3 \cdot V_3 \qquad \text{with} \qquad V_1 = V_A + V_B \tag{33}$$

(*) In non-aqueous solutions, however, as well as in other liquids and gases the enthalpy term mostly dominates.

where N_i is the number of moles of the component i within the volume V, and V_i is the partial volume of this component.

Instead of the number of the moles N_i the concentration per unit volume $c_i = N_i/V$ is often introduced. It is advantageous here, however, not to refer to the volume V in which the quantity N of the dissolved moles are contained and which depends on the degree of dissociation, but to a constant quantity, *e.g.* to the mass M_W of the solvent within the volume V or to the volume V_0 of the solvent before the electrolyte was dissolved. With these concentrations c_i^0 we get (*)

$$c_i^0 = N_i/V_0 = c_i V/V_0 ; \qquad \frac{\delta V}{V_0} = \sum \delta c_i^0 V_i .$$

By transforming the deviations δc_i^0 into the normal variables δc_j^0 using eq. (17), we get

$$\frac{\delta V}{V_0} = \delta c_{\mathrm{I}}^0 (V_2 - V_1) + \delta c_{\mathrm{II}}^0 \left[(V_3 - V_2) + \frac{k_{21}}{k'_{12} + k_{21}} (V_2 - V_1) \right] . \tag{34}$$

Introducing the difference of the partial volumes which are attached to the reaction step 2-1 and 3-2, *i.e.*

$$(V_2 - V_1) = \Delta V_{21} ; \qquad (V_3 - V_2) = \Delta V_{32} = -\Delta V_{23} \tag{35}$$

we get (with the approximation given above) the differential volumes ΔV associated with the normal variables δc_j^0

$$\begin{cases} \Delta V_{\mathrm{I}} = -\Delta V_{12} \qquad \text{and} \\ \Delta V_{\mathrm{II}} = -\Delta V_{23} - \dfrac{k_{21}}{k'_{12} + k_{21}} \Delta V_{12} . \end{cases} \tag{36}$$

Considering the differential volume, process I simply corresponds to step 1-2 (with the approximations given above). However, since process II corresponds to a transition between state 3 and the equilibrium between 1 and 2 it does not consist only of step 2-3 but also contains a contribution of step 1-2.

For the additional compressibility of the solution caused by the processes I and II, which here are the only ones of interest, we obtain:

$$\bar{\varkappa}_{\mathrm{I}} + \bar{\varkappa}_{\mathrm{II}} = -\left(\frac{1}{V} \frac{\partial V}{\partial p} - \frac{1}{V} \frac{\partial V}{\partial p} \right)_{\infty} = \Delta V_{\mathrm{I}} \frac{V_0}{V} \frac{\partial c_{\mathrm{I}}^0}{\partial p} + \Delta V_{\mathrm{II}} \frac{V_0}{V} \frac{\partial c_{\mathrm{II}}^0}{\partial p} , \tag{37}$$

(*) $\sum \delta c_i = 0$ but $\sum \delta c_i^0 \neq 0$.

with two corresponding relaxation maxima

$$\mu_{mj} = \pi \frac{\bar{\varkappa}_j}{\varkappa_S^\infty}, \qquad j = \mathrm{I}, \mathrm{II}. \tag{38}$$

The differential volumes ΔV_I and ΔV_II are known from eq. (36). For the calculation of the expressions $\partial c_j^0/\partial p$ it is convenient to transform the normal variables δc_j^0 into the concentration deviations δc_i^0, since the dependence on pressure of the latter may be reduced to the differences ΔV_{12} and ΔV_{23} of the partial volumes.

For this reduction we replace the concentration c_i^0 by especially defined degrees of dissociation and transformation and introduce corresponding equilibrium constants. (The quantities K_{12}, K_{12}/Π^f and $K_{1\Sigma}/\Pi_f$ differ from the usual ones by a factor V/V_0, which is unimportant when compared with Π^f):

— for step 1-2: degree of dissociation α_{12}

$$\alpha_{12} = \frac{c_1^0}{c^0 - c_3^0}; \qquad \frac{K_{12}}{\Pi^f} = \frac{k_{21}}{k_{12}} = \frac{(c_1^0)^2}{c_2^0} = \frac{\alpha_{12}^2(c_1^0 + c_2^0)}{1 - \alpha_{12}}. \tag{39 a}$$

— for step 2-3: degree of transformation α_{23}

$$\alpha_{23} = \frac{c_2^0}{c^0 - c_1^0}; \qquad K_{23} = \frac{k_{32}}{k_{23}} = \frac{c_2^0}{c_3^0} = \frac{\alpha_{23}}{1 - \alpha_{23}}. \tag{39 b}$$

— for step 1-(2, 3): total degree of dissociation α

$$\alpha = \frac{c_1^0}{c^0}; \qquad \frac{K_{1\Sigma}}{\Pi^f} = \frac{K_{23}K_{12}/\Pi^f}{1 + K_{23}} = \frac{(c_1^0)^2}{c_2^0 + c_3^0} = \frac{\alpha^2 c^0}{1 - \alpha}. \tag{39 c}$$

If we now differentiate α_{12}, α_{23}, and α with respect to the corresponding equilibrium parameters given in (39), we have reduced $\partial c_j^0/\partial p$ to derivatives of these equilibrium parameters with respect to pressure *i.e.* to well-known thermodynamic relations

$$\left\{\begin{aligned} \frac{\partial \ln K_{12}/\Pi^f}{\partial p} &= -\frac{\Delta V_{12}}{RT} - \sum \frac{\partial \ln \Pi^f}{\partial c_i^0}\frac{\partial c_i^0}{\partial p}, \\ \frac{\partial \ln K_{23}}{\partial p} &= -\frac{\Delta V_{23}}{RT}, \\ \frac{\partial \ln K_{1\Sigma}/\Pi^f}{\partial p} &= -\frac{\Delta V_{12}}{RT} - \sum \frac{\partial \ln \Pi^f}{\partial c_i^0}\frac{\partial c_i^0}{\partial p} - \frac{1}{1 + K_{23}}\frac{\Delta V_{23}}{RT}, \end{aligned}\right. \tag{40}$$

(where ΔV_{12} and Π^f depend on concentration).

The calculation of $\partial c_j^0/\partial p$ yields the same combination of ΔV_{12} and ΔV_{23} as was found for ΔV_{I} and ΔV_{II}. We, therefore, obtain—as was to be expected—their values squared in the compressibilities of processes I and II:

$$
(41)\quad\left\{
\begin{aligned}
&\bar{\varkappa}_{\mathrm{I}} = c\Gamma_{\mathrm{I}}^{*}\frac{(\Delta V_{\mathrm{I}})^2}{RT}\,; \qquad \bar{\varkappa}_{\mathrm{II}} = c\Gamma_{\mathrm{II}}^{*}\frac{(\Delta V_{\mathrm{II}})^2}{RT}\,,\\
&\text{where}\\
&\Gamma_{\mathrm{I}}^{*} = \frac{\alpha}{\alpha_{12}}\frac{\Gamma_{\mathrm{I}}}{1+\Gamma_{\mathrm{I}}(\partial \ln \Pi^f/\partial\alpha_{12})_{p,c}}\,; \qquad \Gamma_{\mathrm{I}} = \frac{\alpha_{12}(1-\alpha_{12})}{2-\alpha_{12}}\,,\\
&\Gamma_{\mathrm{II}}^{*} = \frac{\Gamma_{\mathrm{II}}}{1+\Gamma_{\mathrm{II}}(\partial \ln \Pi^f/\partial\alpha)_{p,c}}\,\frac{1+k'_{12}/k_{21}}{1+K_{23}}\,; \qquad \Gamma_{\mathrm{II}} = \Gamma = \frac{\alpha(1-\alpha)}{2-\alpha}\,.
\end{aligned}
\right.
$$

The factors Γ_{I}, Γ_{II} are analogous to Γ of the single-step reaction; in Γ_{I}, however, α is replaced by α_{12}. Some deviations occur for Γ_{I}^{*} and Γ_{II}^{*}. The factor α/α_{12} in Γ_{I}^{*} accounts for the fact that only a part of the total number of ions participates in the reaction 1-2. The second factor in Γ_{II}^{*} accounts for the simultaneous variation in the equilibrium 1-2.

The system of equations can easily be extended to multi-step reactions, if the simple rule of formation for Γ_j^{*} is used.

$$
c\Gamma_i^{*} = \frac{(c'_1 + c_2 + \ldots + c_{n-1})c_n^0}{c'_1 + c_2 + \ldots + c_{n-1} + c_n} \qquad \text{where} \qquad \frac{1}{c'_1} = \frac{2}{c_1} + \left(\frac{\partial \ln \Pi^f}{\partial c_1}\right).
$$

For the 3-step system [see scheme (63)] we obtain the 3 contributions to the compressibility (according to the 3 relaxation times τ_{I}, τ_{II}, τ_{III})

$$
(42)\quad\left\{
\begin{aligned}
&\varkappa_j = c\Gamma_j^{*}\frac{(\Delta V_j)^2}{RT}\,,\\
&\text{where}\\
&\Gamma_{\mathrm{I}}^{*} = \frac{\alpha}{\alpha_{12}}\frac{\Gamma_{\mathrm{I}}}{1+\Gamma_{\mathrm{I}}(\partial \ln \Pi^f/\partial\alpha_{12})}\,; \qquad \Gamma_{\mathrm{I}} = \frac{\alpha_{12}(1-\alpha_{12})}{2-\alpha_{12}}\,,\\
&\Gamma_{\mathrm{II}}^{*} = \frac{\alpha}{\alpha_{123}}\frac{\Gamma_{\mathrm{II}}}{1+\Gamma_{\mathrm{II}}(\partial \ln \Pi^f/\partial\alpha_{123})}\,\frac{1+k'_{12}/k_{21}}{1+K_{23}}\,; \qquad \Gamma_{\mathrm{II}} = \frac{\alpha_{123}(1-\alpha_{123})}{2-\alpha_{123}}\,,\\
&\Gamma_{\mathrm{III}}^{*} = \frac{\Gamma_{\mathrm{III}}}{1+\Gamma_{\mathrm{III}}(\partial \ln \Pi^f/\partial\alpha)}\,\frac{1+k'_{12}/k_{21}(1+1/K_{23})}{1+K_{34}(1+K_{23})}\,; \qquad \Gamma_{\mathrm{III}} = \frac{\alpha(1-\alpha)}{2-\alpha}\,,
\end{aligned}
\right.
$$

$$(42)\quad\left\{\begin{aligned}&\text{and}\\ &\Delta V_{\mathrm{I}} = V_2 - V_1; && \alpha_{12} = c_1/(c_1+c_2)\,,\\ &\Delta V_{\mathrm{II}} = (V_3-V_2) + \frac{k_{21}}{k'_{12}+k_{21}}(V_2-V_1); && \alpha_{123} = c_1/(c_1+c_2+c_3)\,,\\ &\Delta V_{\mathrm{III}} = (V_3-V_4) + \frac{k_{32}}{k'_{21}+k_{32}}\Delta V_{\mathrm{II}}; && \alpha \equiv \alpha_{1234} = c_1/(c_1+c_2+c_3+c_4) = c_1/c.\end{aligned}\right.$$

For an example discussed later the degrees of dissociation α_{12}, α_{123}, and α ar of equal order of magnitude and

$$(43)\qquad \left(\frac{\partial \ln \Pi'}{\partial \alpha}\right) = \left(\frac{\partial \ln \Pi'}{\partial \alpha_{12}}\right) = \left(\frac{\partial \ln \Pi'}{\partial \alpha_{123}}\right).$$

The last factor of Γ^*, containing the rate and the equilibrium constants, does not alter considerably the dependence on concentration. Γ^*_{I}, Γ^*_{II} and Γ^*_{III}, therefore, show a similar behaviour with respect to concentration.

2'2.3. *Influence of the ionic atmosphere.* – The expressions (41) and (42) are valid only if the assumptions given above are fulfilled, *i.e.* in the case of relatively weak electrolytes (where the effects of the ionic atmosphere may be neglected) and in the case of strong electrolytes for the slow processes II and III only. If the diffusion is also to be included, the interaction between the kinetics of the ionic atmosphere and chemical kinetics has to be considered. On the other hand, a calculation of the relaxation of the ionic atmosphere is possible in a relatively simple form only for the case of complete dissociation, *i.e.* without consideration of chemical reactions.

According to HALL [7] we obtain for the absorption per wave-length (somewhat different from LEONTOVIC [8]):

$$(44)\qquad \mu = -\frac{u}{u_0}\frac{K_r}{K_0}\,\sigma(\omega\theta)\,,$$

where

$$K_r = \frac{kTK^3}{24\pi}\cdot\left(\frac{V\partial \ln K^2}{\partial V}\right)_T\left(\frac{V\partial \ln K^2}{\partial V}\right)_a,$$

is the relaxing part, and

$$K_0 = \frac{1}{\varkappa_0} = -V\left(\frac{\partial p}{\partial V}\right)_a,$$

the static part of the modulus for adiabatic compression. The ratio of the sound velocities $u_{(\omega)}/u_{(\omega=0)}$ is approximately unity. The frequency term has the form already mentioned (see Fig. 6)

$$\sigma(\omega\theta)=\frac{(\varepsilon^2-1)^{\frac{1}{2}}}{\varepsilon(\varepsilon+1)}\,,\qquad \text{where}\qquad \varepsilon=\left[\frac{(1+\omega^2\theta^2)^{\frac{1}{2}}+1}{2}\right]^{\frac{1}{2}}. \tag{45}$$

For the case of chemical equilibrium, a relaxation process with a continuous spectrum has to be expected for the quickest step 1-2. The evaluation of formula (44) (see Table I), according to HALL, shows that for concentrations $c < 0.1$ m the contribution to the absorption is very small and has its maximum at very high frequencies.

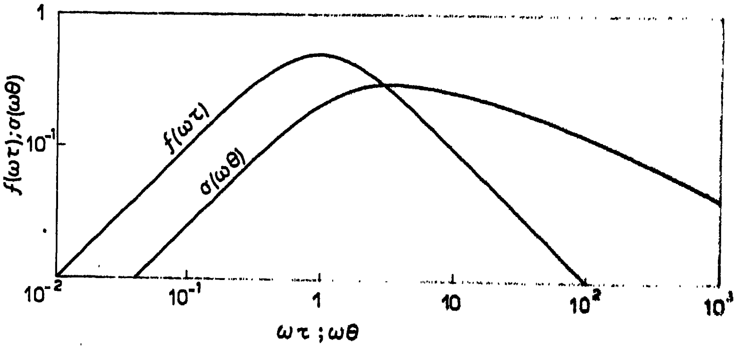

Fig. 6. – Frequency-dependence of absorption volume of the ionic atmosphere relaxation compared with a single-step-relaxation process.

TABLE I. – *Evaluation of 1-step dissociation theory for different equilibrium constants.*

c mol/l	f	$K=3\cdot10^{-3}$ mol/l			$7\cdot10^{-3}$ mol/l			$2\cdot10^{-2}$ mol/l			10^{-1} mol/l		
		ΔV cm³/mol	$(Q\lambda)_m$ 10^{-30} m³	$1/\tau k_{21}$	ΔV cm³/mol	$(Q\lambda)_m$ 10^{-30} m³	$1/\tau k_{21}$	ΔV cm³/mol	$(Q\lambda)_m$ 10^{-30} m³	$1/\tau k_{21}$	ΔV cm³/mol	$(Q\lambda)_m$ 10^{-30} m³	$1/\tau k_{21}$
10^{-3}	0.70	−4	9	1.37	−4	5	1.13	7	4	1.04	15	5	1.01
10^{-2}	0.38	−4	13	2.67	−4	12	1.42	7	15	1.10	14	13	1.02
10^{-1}	0.15	−4	10	5.66	−4	15	1.70	6	16	1.14	12	15	1.02
1	0.05	−2	2	9.9	−2	4	1.69	2	2	1.12	5	3	1.02

2·3. *Discussion of the theoretical results.* – The expressions for the relaxation times and the corresponding $(Q\lambda)_m$ values seem to be a little complicated. They will be discussed, therefore, in terms of a 2-step dissociation.

Process I (which is much quicker than II according to the assumption $\tau_I \ll \tau_{II}$) includes the dissociation equilibrium of step 1-2 (K_{12}), where concentration c_3 is not influenced. It shows the behaviour of a simple binary dissociation process.

Process II includes the total equilibrium. While the reaction 2-3 proceeds only slowly, the equilibrium of step 1-2 follows practically instantaneously. The relaxation time τ_{II} reduces with increasing concentration from $1/k_{32}$ to $1/(k_{32}+k_{23})$ within the concentration range for which $k'_{12} \approx k_{21}$. If $k_{32} \gg k_{23}$, then τ_{II} is independent of concentration. The dependence of the corresponding compressibility on concentration is complicated, since ΔV_I, as well as ΔV_{II}, depend on concentration; the first, because of the ionic interaction, and the second, because of the term $k_{21}/(k'_{12}+k_{21})$.

Now let us proceed to discuss the following cases:

— *Case* 1:

$$(46) \qquad c_3 \ll c_2,\, c_1; \qquad K_{23} \gg 1; \qquad k'_{12} \ll k_{21}K_{23}\,.$$

For the limiting case $c_3 \to 0$: $\alpha_{23}=1$; $\alpha_{12}=\alpha$, there exists a one-step binary dissociation equilibrium; $\varkappa_I$ becomes identical to eq. (7), and $\varkappa_{II}$ becomes equal to zero.

If c_3 is small (but not zero), for $k'_{12} < k_{21}$ the compressibility $\varkappa_{II}$ will have the same dependence on concentration as $\varkappa_I$; however, the maximum will be somewhat smaller. τ_{II} is constant. This case is appropriate for many systems.

— *Case* 2:

$$(47) \qquad c_2 \ll c_3,\, c_1; \qquad K_{23} \ll 1; \qquad k'_{12} \ll k_{21}\,.$$

For the limiting case $c_2 \to 0$: $\alpha_{23}=0$; $\alpha_{12}=1$, there also exists a one-step binary dissociation equilibrium (between c_1 and c_3): $\varkappa_{II}$ becomes identical to (7), $\varkappa_I$ becomes 0. $\Delta V_{II} \to \Delta V_{12}$, τ_{II} depends on the concentration. This case corresponds to the case of a stationary intermediate state:

$$(47a) \qquad \vec{k} = \frac{k'_{12}k_{23}}{k_{21}+k_{23}}\,; \qquad \overleftarrow{k} = \frac{k_{32}k_{21}}{k_{21}+k_{23}}\,,$$

and with (16), *i.e.*, for $k_{21} \gg k_{23}$

$$(47b) \qquad \vec{k} = k_{23}\frac{k'_{12}}{k_{21}}\,; \qquad \overleftarrow{k} = k_{32}\,, \quad i.e. \quad \frac{1}{\tau_{II}} = k_{32} + \frac{k'_{12}}{k_{21}}k_{23}\,.$$

For protolytic reactions often $k_{21} \ll k_{23}$

$$(47c)\qquad \vec{k} = k'_{12}; \qquad \overleftarrow{k} = k_{21}\frac{k_{32}}{k_{23}}, \quad \text{i.e.} \quad \frac{1}{\tau_{II}} = k'_{12} + k_{21}\frac{k_{32}}{k_{23}},$$

which means another case of stationary concentration of the intermediate state.

— *Case* 3:

$$(48)\qquad c_1 \ll c_2, c_3; \qquad k'_{12} \gg k_{21}, (k_{21}K_{22}).$$

For the limiting case of $c_1 \to 0$: $\alpha_{12} = 0$; $\alpha = 0$, there exists a one-step equilibrium with a quasi-monomolecular transition. The activity coefficients are omitted. $\varkappa_I \to 0$; and only $\varkappa_{II}$ remains finite

$$(48a)\qquad \varkappa_{II} = \alpha_{23}(1 - \alpha_{23})c\frac{(\Delta V_{23})^2}{RT},$$

eq. (48*a*) is the relation for a monomolecular process. Besides

$$(48b)\qquad \frac{1}{\tau_{II}} = k_{32} + k_{23}.$$

i.e., $1/\tau_{II}$ will be independent of concentration.

If V_{23} is small or vanishes, there is a special consequence of eq. (36): two relaxation maxima should be expected. ΔV_{II} may vanish if ΔV_{12} and ΔV_{23}, have different signs and cancel each other.

3. – Experimental results and theoretical interpretation.

In the following sections the theory given above will be tested by its application to different systems of electrolytic solutions. Also, with the help of the theory some new insights into the structure of electrolyte solutions can be obtained and some data, already known, can be determined more accurately.

3·1. *Diffusion-determined* 1-*step reactions in weak electrolytes.* – It has already been mentioned that for weak electrolytes only the presumptions of the «1-step reaction» theory may be fulfilled, since the influence of the ionic atmosphere may be neglected as long as the concentrations are not too high. The system phenol (PH)-ammonia (NH_3), for which experimental results (Fig. 7) were given by EIGEN and MAASS [9], may be chosen as an example.

The reaction has the form:

(49)
$$P^- + NH_4^+ \underset{k_{21}}{\overset{k_{12}}{\rightleftharpoons}} PH + NH_3$$

where

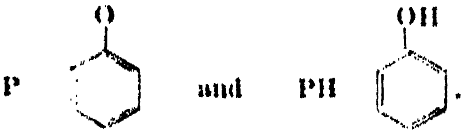

When the ions have come together by diffusion, they may react by a proton transition. The equilibrium:

(50)
$$\frac{[P^-][NH_4^+]}{[PH][NH_3]} = \frac{\alpha^2}{(1-\alpha)^2} = \frac{K}{f'^2}$$

is determined by the equilibrium constant $K = f'^2 \cdot (K_1/K_2) = 0.19$, which is a quotient of the two constants, K_1 and K_2, of the two well-known equilibria:

(51)
$$\frac{[P^-][H^+]}{[PH]} = K_1 = 1.05 \cdot 10^{-10} \, ;$$

$$\frac{[NH_3][H^+]}{[NH_4^+]} = K_2 = 5.6 \cdot 10^{-10} .$$

The given quantities refer to $c = 0.05$ m. The degree of dissociation amounts to $\alpha = 0.30$ for small concentrations. For higher concentrations ($c = 0.1$ m) f' only decreases from 1 to 0.8.

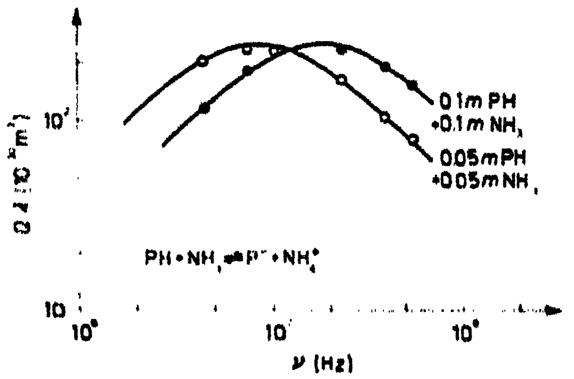

Fig. 7. — Frequency-dependence of $(Q\lambda)_m$ for the system phenol-ammonia.

For the relaxation time we obtain

(52)
$$\left\{\begin{aligned} 1/\tau &= (c_{P^-} + c_{NH_4^+})k_{12} + (c_{PH} + c_{NH_3})k_{21} \\ &= [(1-\alpha)k_{12} + \alpha k_{21}]2c \, . \end{aligned}\right.$$

From the dependence of concentration (Fig. 7), by using the equilibrium constant, we obtain

$$k_{12} = 1.3 \cdot 10^9 \ \mathrm{m^{-1}\,s^{-1}}; \qquad k_{21} = 1.8 \cdot 10^9 \ \mathrm{m^{-1}\,s^{-1}} .$$

These values are somewhat smaller than that for pure diffusion. This difference corresponds to the retardation to be expected by the proton transition.

By means of the factor $\Gamma = (1-\alpha)\alpha/2$ we are able to calculate from the experimental $(Q\lambda)_m$ values:

$$\Delta V = -22 \text{ cm}^3/\text{mol} .$$

3'2. *Ion reactions including protons and hydroxyl ions.* – If one of the ion partners of the electrolyte is identical with one of the ion partners of the solvent, an exchange occurs. For small concentrations (because of the buffer effect of the solvent) one obtains changed dependences on concentration. If one ion is a proton or a hydroxyl ion, (*i.e.* in aqueous solutions of acids and bases) special effects arise. These effects are a consequence of the anomalous mobility of these ions in water, which is caused by the shift of the hydrogen bonds. A transition of a proton from a H_3O^+ ion to a neighbouring water molecule (where it forms a new H_3O^+ ion) means a shift of the proton by a distance equal to the diameter of a water molecule (see Fig. 7). A transition of a proton out of a water molecule to an OH^- ion (forming there another water molecule) is equivalent to the motion of a hydroxyl ion in the other direction.

By means of this mechanism a proton or a hydroxyl ion may easily penetrate the co-ordination sphere of the other ion partner, *i.e.*, the ion partners may react with a high reaction rate if they have once formed an encounter complex. For small ion concentrations the diffusion will be the slowest step in the formation reaction and, therefore, will determine the recombination rate $\vec{k}$.

A very instructive example of this type of process, according to EIGEN [10], is given by ammonium hydroxyde in aqueous solution:

$$NH_4^+ + OH^- \rightleftharpoons NH_3(+)H_2O . \tag{53}$$

Without the buffer effect for very small concentrations the equilibrium of the reaction is given by

$$\frac{\alpha^2 c}{1-\alpha}\Pi^f = \frac{[NH_4^+][OH^-]}{[NH_3\cdot H_2O]}\Pi^f = K , \tag{54}$$

where $K = 1.5\cdot 10^{-5}$ m for 25 °C is relatively accurately known through measurements by ROTH [11]. It follows that the degree of dissociation is so small ($\alpha = 4\cdot 10^{-3}$ for $c = 1$ m) that $\Pi^f \approx 1$. The reaction, therefore, may be treated as a 1-step reaction according to eqs. (6), (28) and (29):

Since $\alpha \approx \sqrt{K/c} \ll 1$, we may expect for the factor Γ^*

$$\Gamma^* \approx \Gamma = \frac{\alpha(1-\alpha)}{2-\alpha} \approx \frac{\alpha}{2} \approx \frac{1}{2}\sqrt{K/c}\,. \tag{55}$$

Therefore, $(Q\lambda)_m$ decreases as the inverse ot the square root of the concentration. The experimental results (Fig. 8) show very accurately this dependence on concentration. From the absolute values of the absorption we obtain

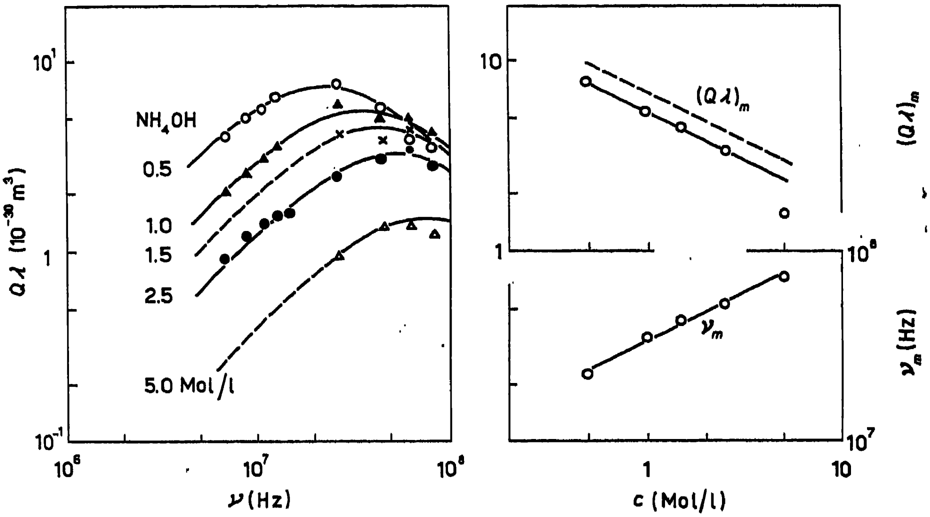

Fig. 8. – Left: frequency-dependence of $(Q\lambda)$ of ammonia in aqueous solution for various concentrations; right: concentration-dependence of $(Q\lambda)_m$ and relaxation frequency ν_m (derived from Fig. 8, left).

a volume difference $|\Delta V| \approx (28 \pm 2)$ cm³/mole (*), which depends very little on concentration. The relaxation frequencies taken from the experiments show an increase with $\sqrt{c}$, corresponding to the theory which predicts

$$\omega_m = \frac{1}{\tau} \approx k_{21} + k_{12}\cdot 2\alpha c \approx k_{21} + k_{12} 2\sqrt{Kc}\,. \tag{56}$$

From the slope of the straight line given by ω_m *vs.* $\sqrt{Kc}$ we obtain

$$k_{12} \approx 3 \cdot 10^{10}\ \text{liter/mol s}\,.$$

(*) $\Delta V = V_{\mathrm{NH}_4^+} - V_{\mathrm{OH}^-} - V_{\mathrm{NH}_3} - V_{\mathrm{H}_2\mathrm{O}} = 15 - 2 - 23 - 18 = -28$ cm³/mol.

This value agrees well with those calculations arrived at by the Debye formula for diffusion to a critical radius of 3, ÷, 5 Å and confirms the assumption that the rate of recombination k_{12} is determined by diffusion. The dissociation rate k_{21} cannot be taken from the diagram because it is too small; it may be calculated from k_{12} by using K:

$$k_{21} = Kk_{12} \approx 5\cdot 10^{5}\ \mathrm{s}^{-1}\,.$$

This value is larger than the dissociation rate in pure water, which is $3\cdot 10^{-5}\ \mathrm{s}^{-1}$ according to EIGEN and DE MAYER [72]. The existence of $NH_3\cdot H_2O$ complexes and a reaction following the path III (Fig. 9), therefore, seems to be proved. Without this complex the reaction would have to follow the path I/II, which would include the dissociation of water and would be slower. These conclusions were confirmed by CARNEVALE and LITOVITZ [12] through measurements of the pressure-dependence of the absorption in 0.1 normal ammonium hydrate solution up to pressures of 2 000 kg/cm². They were able to show that the relaxation frequency increases proportionally to the degree of dissociation α. The latter may be calculated with respect to its dependence on pressure by making use of the relation $\alpha \approx \sqrt{K/\Pi^f c}$ from the thermodynamic relation $\partial \ln K/\partial p = -\Delta V_0/RT$. Since for small degrees of dissociation

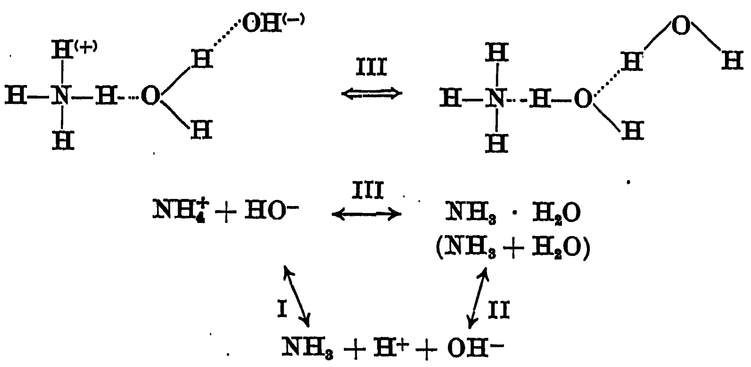

Fig. 9. – Scheme of the dissociation of ammonia in aqueous solution (path III is rate-determining).

$$\alpha \ll 1; \qquad \nu_m \approx \frac{1}{\pi}\,{}^{0}k_{12}\Pi^{f}\alpha c\,, \tag{57}$$

it may be concluded from this experimental result that the product ${}^{0}k_{12}\Pi^{f} = k_{12}$ is nearly independent of pressure. This holds for ${}^{0}k_{12}$ too, because (as known)

Π^f does not vary considerably with pressure. However, the decay rate k_{21} increases strongly with pressure (since $k_{21}=k^0_{12}\Pi^f\cdot\alpha^2c$).

One must expect other results when there is *sulfuric acid* in aqueous solutions. Sulphuric acid is completely dissociated in the first step ($H_2SO_4 \rightleftharpoons\; \leftrightharpoons H^+ + HSO_4^-$). The second step,

$$\text{(58)}\qquad HSO_4^- \rightleftharpoons H^+ + SO_4^{--}\,,$$

therefore, will take place in a H^+-ion concentration equal to $(1+\alpha)c$ (*). The factor Γ is given according to EIGEN [13] by

$$\text{(59)}\qquad \Gamma=\frac{\alpha(1-\alpha)(1+\alpha)}{2-(1-\alpha)^2}\,;\qquad K/\Pi^f=\frac{\alpha(1+\alpha)}{1-\alpha}\,c\,.$$

Its maximum ($\Gamma\approx 0.2$) occurs for $\Pi^f\approx 0.5\ldots 1$ for concentrations $c\approx\approx 0.6\,K/\Pi^f\approx 10^{-2}$ m (since $K_{HSO_4^-}\approx 10^{-2}$ m). In a range around this concentration (where the measurements were also made), only a small dependence of the $(Q\lambda)_m$ values on concentration may be expected because $\Delta V\approx 23$ cm^3/mole, too, does not depend very much on concentration.

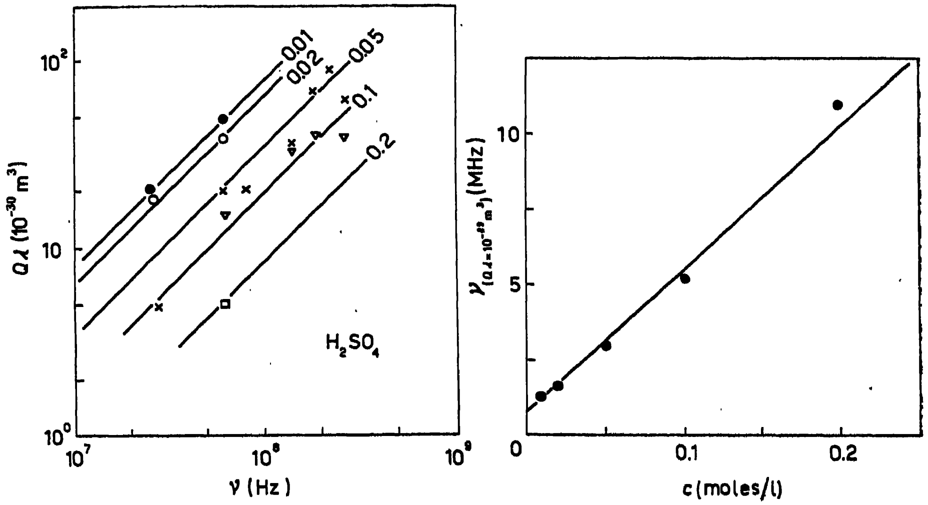

Fig. 10. – Left: frequency-dependence of $(Q\lambda)$ of sulphuric acid for different concentrations; right: concentration-dependence of the frequency $\nu_{Q\lambda=\text{const}}\sim\nu_m$:

Unfortunately the measurements (Fig. 10) do not include the relaxation

---

(*) This is valid for electrolyte concentrations which are not too small because of the dissociation equilibrium of water.

maxima. If the $(Q\lambda)_m$-values were assumed to be independent of concentration, the observed shift of the absorption curves can only be caused by a shift of the relaxation frequency [14]. The shift was found to be proportional to the concentration. This finding is in good agreement with the theory which predicts for $\Pi^f \approx 1$

$$2\pi\nu_m \approx \overleftarrow{k} + \overrightarrow{k}(1 + 2\alpha)c \,. \tag{60}$$

By means of the above $(Q\lambda)_m$ calculations and of the results of the diagram, we obtain $\overleftarrow{k} \approx 3\cdot10^9\ \text{s}^{-1}$ (from the intersection with the ordinate) and $\overrightarrow{k} \approx 10^{11}\ \text{m}^{-1}\ \text{s}^{-1}$ (from the slope). Their quotient, the equilibrium constant $K = 1.5\cdot10^{-2}$ m, agrees well with conductivity measurements. From eq. (60) one obtains the relaxation frequency $\nu_m \approx 5\cdot10^8$ c/s. From the order of magnitude of the recombination rate $\overrightarrow{k} = 10^{11}\ \text{m}^{-1}\ \text{s}^{-1}$, it may be concluded that here (as in ammonium hydroxyde) the « collision frequency » of encounters by diffusion determines the rate. It can be derived from molecular theory that an activation energy of 2 ... 3 kcal/mole may be ascribed to the formation of an encounter-complex. The fact that this value is much lower than the value of — 5.2 kcal/mole, which was measured by DAVIES, JONES and MONK [14], for the dissociation-enthalpy of HSO_4^- is a confirmation of the assumption that another process participates in the reaction. The equilibrium is of the type given by condition (48) and $\overleftarrow{k} = k_{32}/k_{23}\cdot k_{21}$. A similar behaviour may be expected for the dissociation of other oxygen acids such as $HS_2O_3^-$, $HCrO_4^-$ etc.

The reaction discussed here should also exist in solutions of salts composed of the mentioned acids and strong bases (*e.g.* for Na_2SO_4, Li_2SO_4 etc.), since a certain percentage of free H^+-ions in water is used for forming HSO_4^--ions. Because of the low concentration of these ions, the corresponding relaxation may be masked completely by the relaxation of other reactions (*e.g.* $NaSO_4^- \rightleftharpoons Na^+ + SO_4^{--}$).

3'3. *Stepwise dissociation of higher-valent electrolytes.*

3'3.1. Attempt of interpretation by a one-step dissociation. After the first attempt of LIEBERMANN [1] to interpret the acoustic relaxation in seawater, many other authors have tried to explain the experimental results for 2-2 electrolytes by means of a one-step ion association of the BJERRUM type [18]. This theory sufficiently explains a number of experimental results (such as the influences of ionic atmosphere, electrolyte surrounding, pressure etc.) for small concentrations. However, it is not successful for high concentrations and does not explain the existence of two coupled relaxation processes (Table I).

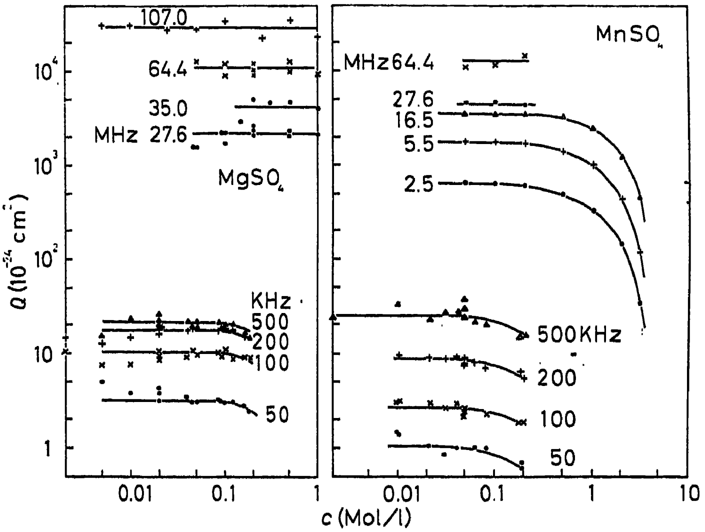

Fig. 11. – Concentration-dependence of absorption cross-section Q of $MgSO_4$ and and $MnSO_4$ in aqueous solutions for different frequencies (measurements in $MnSO_4$ for 2.5, 5.5, 16,5 MHz at 25 °C; all other ones at 20 °C).

It turns out that the dependence of the absorption on concentration (see Fig. 11) gives a particularly good criterion for the validity of a theory; here it excludes the one-step mechanism, as it may be seen from Table I and Fig. 12. Table I shows the result of the evaluation of the theory of one-step dissociation (eqs. (6), (23), and (31)) by using the activity coefficients given by ROBINSON and STOKES [19] and by assuming different equilibrium constants K between $7 \cdot 10^{-3}$ and 10^{-1} m. The ΔV-values were chosen to fit the $(Q\lambda)_m$ values as well as possible. From Fig. 12 we see that the dependence of the measured relaxation frequencies on concentration is reproduced only for $K > 2 \cdot 10^{-2}$ m. The ΔV values will be of the right order of magnitude ($\Delta V_{exp} = -20 \ldots -10$ cm^3/mole) also for $K > 2 \cdot 10^{-2}$, *i.e.* for equilibrium constants much larger than that value $K = 6 \cdot 10^{-3}$ m assumed by Bies. The latter would yield ΔV-values much too small.

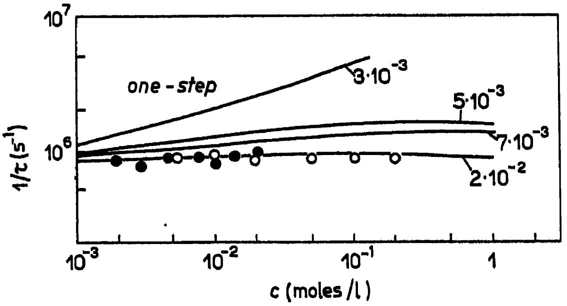

Fig. 12. – Concentration-dependence of the relaxation frequency of a 1-step dissociation for different equilibrium constants (—— theory, × ○ experimental values).

The deviations from the values given by Davies are omitted if a multi-step equilibrium is assumed.

3'3.2. **Interpretation of measurements in 2-2electrolytes by means of multi-step mechanisms.** One might first try to ascribe the higher absorption maximum to a relaxation of the ionic atmosphere. An evaluation according to HALL (Table II), however, yields $(Q\lambda)_m$-values which are lower than the experimental $(Q\lambda)_m$-values by some orders of magnitude. Neither can the differences found between $MgSO_4$ and $MgCl_2$ be explained this way, since in the ionic atmosphere the electric charge only should be essential. Therefore, a specific ion interaction seems to be responsible for the higher maximum too. Only the small absorption in $MgCl_2$ and in other strong electrolytes is in approximate agreement with the calculation by HALL and may be attributed to the ionic atmosphere.

TABLE II. – *Evaluation of ionic atmosphere relaxation theory (according to* HALL).

c mol/l	Calculated for ionic atmosphere		Measured for 100 MHz $(Q\lambda)$ 10^{-30} m^3	
	τ 10^{-9} s	$(Q\lambda)_m$ 10^{-30} m^3		
10^{-3}	30	0.07	—	—
10^{-2}	4.6	0.2	$MgSO_4$	$MgCl_2$
10^{-1}	0.96	0.7	50	1

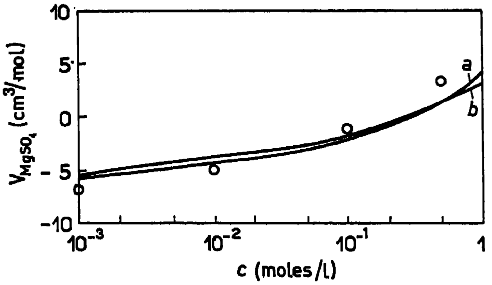

Fig. 13. – Concentration-dependence of the apparent partial molar volume of $MgSO_4$ in aqueous solution.

As an example, the theory of the multi-step dissociation may be applied now to an $MgSO_4$ solution. The underlying assumption $(k_{12}, k_{21} \gg k_{23}, k_{32})$ is fulfilled, since the two relaxation times differ considerably. For evaluation of the theory the volume differences ΔV_{12} and ΔV_{23} were chosen in a way such that a close approximation to the measured values $(Q\lambda)_m$ was obtained. Since the dependence of ΔV_{12} on concentration is given by the dependence of the (experimental) partial volume of $MgSO_4$ on concentration (see Fig. 13), only the concentration-independent values ΔV_{12}^{0} and ΔV_{23} may be chosen freely. Adaption to the measured values is only possible if ΔV_{12} and ΔV_{23} have the same sign, *i.e.* $\Delta V_{II} > \Delta V_{I}$. Because of the experimental result $(Q\lambda)_{mI} > 3(Q\lambda)_{mII}$, we get $K_{23} > 5$.

The total equilibrium constant K, which stands for the equilibrium between the ions, on the one hand, and the sum of all association complexes, on the other hand, has been chosen as a parameter and has been altered between $3 \cdot 10^{-3}$ and $2 \cdot 10^{-2}$ m (see Table III).

The results of the evaluation of the theory are shown in Fig. 14. While the lower relaxation frequency ($\sim 1/\tau_{II}$) remains constant in agreement with the experiment, the higher one ($1/\tau_{I}$) will increase with concentration; the slope depends on K. (The secound result is, so far, unconfirmed experimentally.)

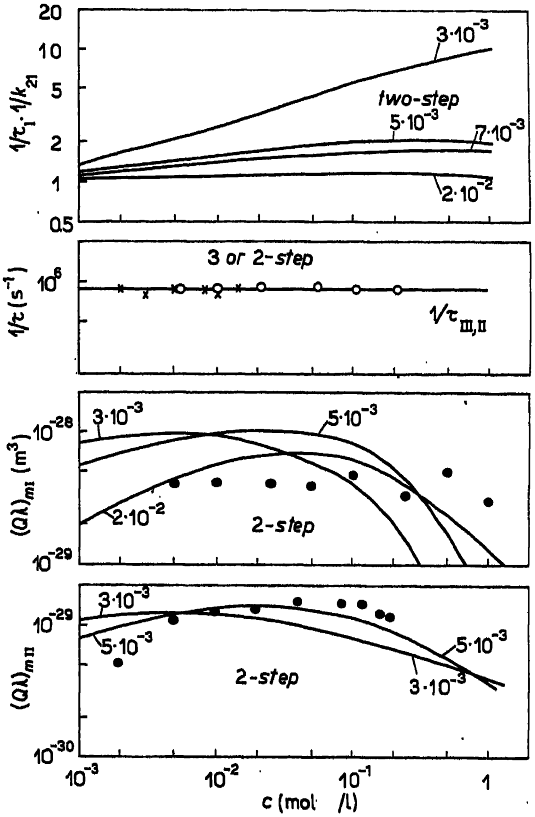

Fig. 14. – Concentration-dependence of $(Q\lambda)_m$-values and relaxation-frequencies for the two relaxation processes of a 2-step dissociation (● experimental results, —— theoretical results).

The calculated $(Q\lambda)_m$-curve fits, in general, the experimental values if the equilibrium constants are chosen correspondingly: $K \approx 10^{-2}$ m, $K_{23} \approx 5 \ldots 10$. (New measurements by SIEGERT [20] in

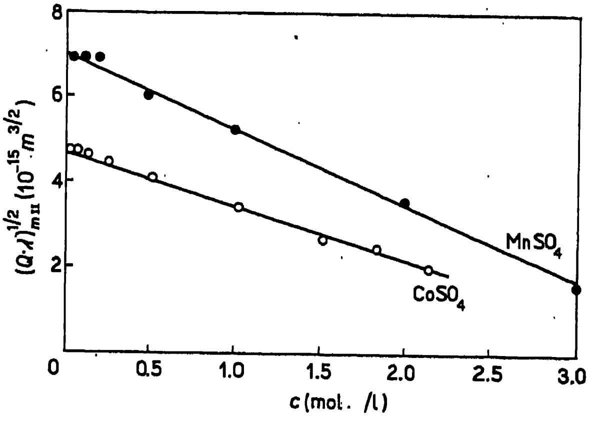

Fig. 15. – Concentration-dependence of $(Q\lambda)_m$ of $MnSO_4$ and $CoSO_4$ in aqueous solutions for high concentrations.

TABLE III. – *Evaluation of 2-step dissociation theory for different parameter series.*

Parameter-series	K (10^{-3} mol/l)	K_{23}	K_{12} (10^{-3} mol/l)	ΔV^0_{12} (cm³/mol)	ΔV_{23} (cm³/mol)	k_{21} (10^8 s^{-1})	k_{32} (10^5 s^{-1})
(*a*)	5	9	4.5	-12	-3	2	8
(*b*)	20	9	18	-15	-5	10	8

c (mol/l)	(*a*) (*b*)	f	$\dfrac{\partial \ln \Pi f}{\partial \ln \alpha}$	$1+\dfrac{k'_{12}}{k_{21}}$	$\Gamma^*_{\rm I}$	$\Gamma^*_{\rm II}$	$\Delta V^0_{12}-\Delta V_{12}$ exp (cm³/mol)	$\Delta V_{\rm I}$ (cm³/mol)	$\Delta V_{\rm II}$ (cm³/mol)	$(Q\cdot\lambda)_{m\rm I}$ (10^{-30} m³)	$(Q\cdot\lambda)_{m\rm II}$ (10^{-30} m³)	$1/\tau_{\rm I}$ (10^8 s^{-1})	$1/\tau_{\rm II}$ (10^5 s^{-1})
10^{-3}	0.90	0.78	-0.20	1.20	0.084	0.010	0	-12	-13	56	8.0	2.4	8.1
	0.98	0.72	-0.34	1.04	0.019	0.002	0	-15	-19	20	3.4	1.0	8.0
10^{-2}	0.71	0.54	-0.57	1.59	0.183	0.029	-1	-11	-9.9	103	13.0	3.2	8.3
	0.93	0.41	-0.70	1.10	0.064	0.007	-1	-14	-18	59	11.0	1.1	8.1
10^{-1}	0.55	0.27	-0.79	1.98	0.224	0.044	-3	-9	-7.6	85	11.7	4.0	8.4
	0.89	0.17	-0.90	1.14	0.097	0.011	-3	-12	-16	65	13.2	1.1	8.1
1	0.52	0.10	-0.97	1.96	0.244	0.048	-10	-2	-4.0	5	3.8	3.9	8.4
	0.88	0.06	-1.10	1.12	0.108	0.013	-10	-5	-10	13	6.1	1.1	8.1

$CoSO_4$ and **KRÄMER** [44] in $MnSO_4$ at higher concentrations (Fig. 15) show a steeper decrease of $(Q\lambda)_{m\rm II}$ values at concentrations around 1 m, where, of course, the assumptions of the theory are no longer valid.)

With the above equilibrium constants we obtain for 0.1 m a concentration $c_3 \approx 2\cdot 10^{-3}$ m of the «inner co-ordination sphere complex». This value is in good agreement with that value $c_{\rm AB}$, which had been derived from the one-step dissociation model using $K = 0.1$ m. The fact that the two models yield the same value for the concentration of the closest complex is a good confirmation for the prediction of the theory that for a description of the slowest process a precise knowledge of the faster processes is not necessary. Especially ion cloud interaction (ionic atmosphere interaction) and «loose-association steps» need not be treated separately from each other. This, of course, also holds for the calculation of the relaxation frequency. Therefore, from Fig. 14 the rate constants of the dissociation of the closest complex can be determined very accurately

$$k_{\rm diss} = 7.5\cdot 10^5\ {\rm s}^{-1}\,.$$

TABLE IV. – *Parameters for evaluation of 2- and 3- step dissociation theory, given in Fig.* 12, 13, 14, *and* 16.

Steps	K (10^{-3} mol/l)	K_{23}	K_{34}	K_{12} (10^{-3} mol/l)	ΔV^0_{12} (cm³/mol)	ΔV_{23} (cm³/mol)	ΔV_{34} (cm³/mol)	k^0_{12} (1/mols)	k_{32} (s^{-1})	k_{43} (s^{-1})
2	3	9	—	3.3	−12	−5	—	$10\cdot10^8$	$8\cdot10^5$	—
2	5	9	—	5.5	−12	−3	—	$10\cdot10^8$	$8\cdot10^5$	—
2	20	9	—	22	−15	−5	—	$10\cdot10^8$	$8\cdot10^5$	—
3	7	0.5	7.5	24	0	−14/10	−3	$4\cdot10^{10}$	$10\cdot10^8$	$8\cdot10^5$
3	20	1	9	40	0	−18	−3	$4\cdot10^{10}$	$10\cdot10^8$	—

The deviations in $(Q\lambda)_m$ existing at higher concentrations do not vanish even if the relaxation of the ionic atmosphere is included. A satisfactory agreement between theory and experiment can only be obtained by assuming a 3-step mechanism. This seems to be very realistic since, in the case of the interaction between two ions, discrete steps should be observed up to distances of 2 or 3 water molecules. However, the assumption k'_{12}, $k_{21} \gg k_{23}$, k_{32} no longer will be valid for the transition between very loosely bound complexes. The calculation has to be carried out without the use of the corresponding simplification. The result is in better agreement with the experimental values (Fig. 16). The best agreement is obtained with the values of Table IV, *i.e.* for $K = 7 \ldots 20 \cdot 10^{-3}$ m, $K_{23} \approx 1$, $K_{34} \approx 5 \ldots 10$ and the volume differences given there.

Strictly speaking, instead of the activity coefficients the time-dependent interaction of the ionic atmosphere has to be taken into account. The ad-

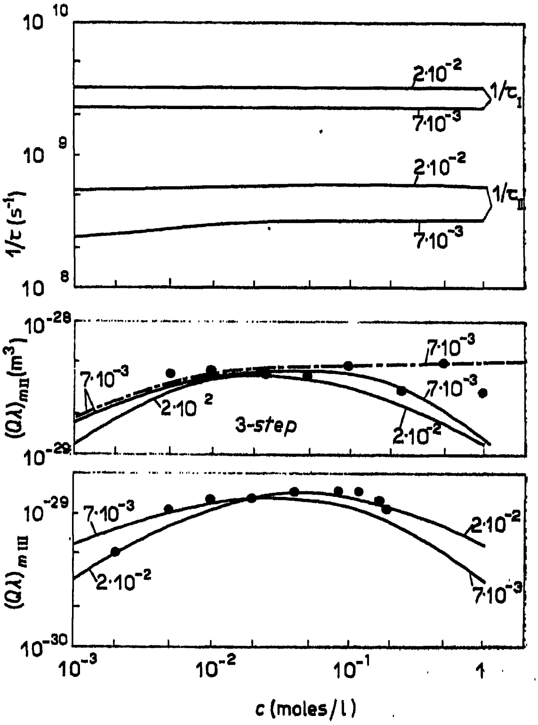

Fig. 16. – Concentration-dependence of $(Q\lambda)_m$-values and relaxation-frequencies for the 3-step dissociation (—— theory, ● experimental values).

vantage of such a complicated calculation, however, is not very great since at the present time the result cannot be checked experimentally for high frequencies.

For $CoSO_4$ solutions SIEGERT [20] found a considerably smaller equilibrium constant $K_{23} = k_{32}/k_{23} = 3 \dots 4$. Therefore, the second term of $1/\tau_{II} = k_{32} + k_{23} \cdot k'_{12}/(k'_{12} + k_{21})$ can no longer be neglected (as in the case of $MgSO_4$) and the relaxation frequency should increase with concentration from k_{32} to $(k_{32} + k_{23})$, *i.e.* by the factor $(1 + K_{23})$. This, indeed, has been observed.

8·3.3. Interpretation for 1-2 electrolytes. It may be supposed that 1-2 electrolytes form complexes similar to those of the 2-2 valent ones, *i.e.*, that water molecules in the co-ordination spheres of the cation are replaced by SO_4^{--} ions. Because of the smaller electric charge of the 1-2 valent metal-ions even for ion radii of the same size (for $Na^+ \approx 0.7$ Å)), smaller binding energies and, therefore, higher relaxation frequencies of the «lower» relaxation have to be expected. This expectation is confirmed by a remarkably large absorption for higher frequency (Fig. 4); *e.g.* in $0.5 \dots 1$ m Na_2SO_4 solutions $(Q\lambda) = 30 \cdot 10^{-30}\ m^3$ is reached for 300 MHz and seems to increase further.

The increase of the rate constants k_{34} and k_{43} causes the relaxation frequency τ_{III} to come closer to τ_{II}, resulting in a nonseparable superposition of the steps 2-3 and 3-4. Therefore from the experimental results it cannot be determined whether state 4 is considerably populated. If this superposition is treated as a single dissociation step (the concentration of the metal-ions being $(1+\alpha)\, c$, that of the anions αc), the equilibrium is given by

$$\frac{[Me^+][R^{--}]}{[MeR^-]}\Pi^f = \frac{(1+\alpha)\alpha}{1-\alpha}\, c\Pi^f = K_D\,. \tag{62}$$

A very rough estimate made by EIGEN and WICKE [21] using $\alpha \approx 0.4$ for $c = 0.5$ m, which is near to the optimal concentration, yields $K_D = 0{,}2$ m. With $\Gamma \approx 0.2$, which depends only little on concentration, and with $\Delta V = 5 \dots 10\ cm^3/mol$, a constant value $(Q\lambda)_m = 25 \dots 100 \cdot 10^{-30}\ m^3$ is found. This fits the experimental result. For concentrations near to the optimum one (optimum with respect to absorption), the two terms of the reaction rate $(\overleftarrow{k} + \overrightarrow{k} \cdot 2\alpha c)$ become nearly equal. By using this relation and the experimental values of the relaxation frequency, $\overleftarrow{k} = 2 \cdot 10^9\ s^{-1}$ is obtained. For higher concentrations the diffusion $(1 \leftrightarrow 2)$ should determine the rate of the process since the transition 2-3 is very fast. For smaller concentrations, however, the dissociation $(3 \rightarrow 2)$ determines the rate. The relaxation frequency, therefore, should increase with concentration, which agrees with the experimental results.

It may be mentioned that a similar process should not occur in 2-1 electrolytes, *e.g.* $MgCl_2$, because a substitution of water molecules in the co-ordination sphere by Cl^- ions is not possible and no complexes will be formed. The experimental results confirm this conclusion. $MgCl_2$ shows only a small absorption for high frequencies, which apparently is due to ionic-atmosphere relaxation.

3'3.4 Influence of the surrounding electrolyte. By means of the conception given here nearly all experimental results can be interpreted quantitatively.

Addition of other electrolytes causes a variation of both relaxation processes according to the shift of the equilibrium. If one of the ions of the added electrolyte ($MgCl_2$, $NaSO_4$) is identical to one of the electrolyte ($MgSO_4$) in the solution, the number of associates and therefore the absorption is increased. If the added ions (*e.g.* Cl^- in NaCl) form complexes with the ions of the electrolyte solution, the number of associates and therewith the special relaxation, which was investigated, will decrease. The reduction of the relaxation of $MgSO_4$, when NaCl is added, shows that $NaSO_4^-$ complexes are formed. Other electrolytes will affect the relaxation processes only by their influence on the ionic atmosphere.

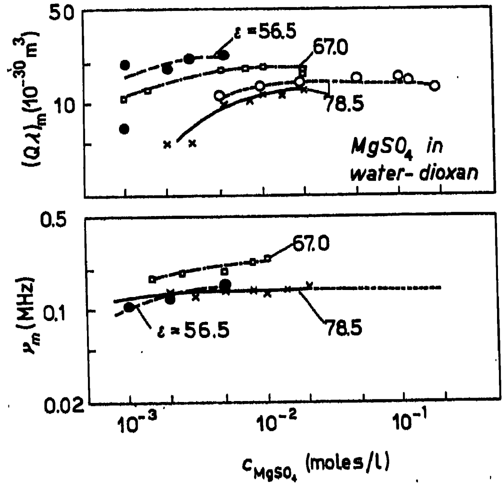

Fig. 17. – Concentration-dependence of $(Q\lambda)_m$ and ν_m of $MgSO_4$ in water-dioxan mixtures of different dielectric constants.

The influence of the *addition of acids* may be explained in a similar way. On the other hand it is very probable that the rapid increase of absorption with the *addition of bases*, which occurs just below the limit of solubility of $Mg(OH)_2$, has to be ascribed to the formation of higher hydroxo-complexes.

The influence of the *addition of other non-dissociating solvents* in most cases can be understood as an effect of a variation of the dielectric constant. In water-dioxan mixtures according to BIES [16] and WILSON [15] the relaxation time of the lower maximum in $MgSO_4$ depends on concentration (Fig. 17). This may be explained by relation (17). In aqueous solutions the equilibrium constant is $K_{23} = k_{32}/k_{23} \approx 5 \dots 10$ so that the shift of the relaxation frequency with increasing concentration by the factor $(1+K_{23})$ is small and can scarcely be measured. As is known from other investigations in analogous systems, k_{32} and k_{21} increase with decreasing dielectric constant. Therefore, $1/K_{23} = k_{23}/k_{32}$ increases and the variation of $1/\tau_{II}$ with concentration increases as well. Since

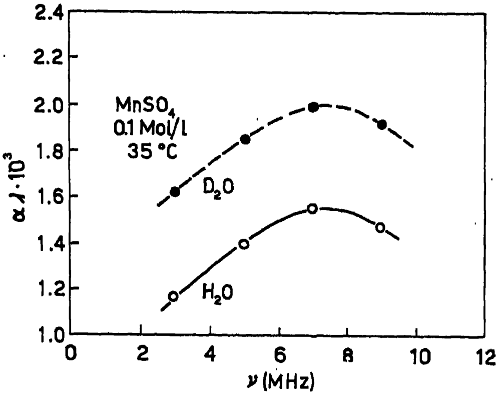

Fig. 18. – Frequency-dependence of ($\alpha\lambda$) of a 0.1 m $MnSO_4$ in H_2O and D_2O-solution.

$1/\tau_{II}$ starts (for increasing concentration) with the value k_{32} (which decreases with decreasing c) the curves for different dielectric constants may intersect. The experimental results show that the $(Q\lambda)_m$-values also vary with the dielectric constant. For a one-step dissociation only a parallel shift of the curves should occur. The observed increase of $(Q\lambda)_m$ may be explained (for a multistep equilibrium) by a variation of the denominator $(1+K_{23})$ in $(Q\lambda)_{mII}$. KURTZE's and TAMM's measurements in water-alcohol mixtures yielded similar results. However, there may be additional influences because the alcohols tend to associate.

Replacing the solvent water by heavy water causes (according to measurements in $MnSO_4$ (Fig. 18) by SMITHSON and LITOVITZ [22]) an increasing absorption while the relaxation frequency remains unaltered. This would be expected since the relaxation frequency is determined by the rate of dissociation of the sulfato complex. The $(Q\lambda)_m$ value, on the other hand, should be altered because ΔV as well as K are altered by the interaction of the ions and the solvent.

The activation energy derived from the *dependence of relaxation time on temperature* (Fig. 19) corresponds in size and variation to the dissociation rate constants.

8'4. *Kinetic behavior of different* 2-2 *electrolytes.* – The considerations presented here yield a mechanism of at least two discrete steps for the establishment

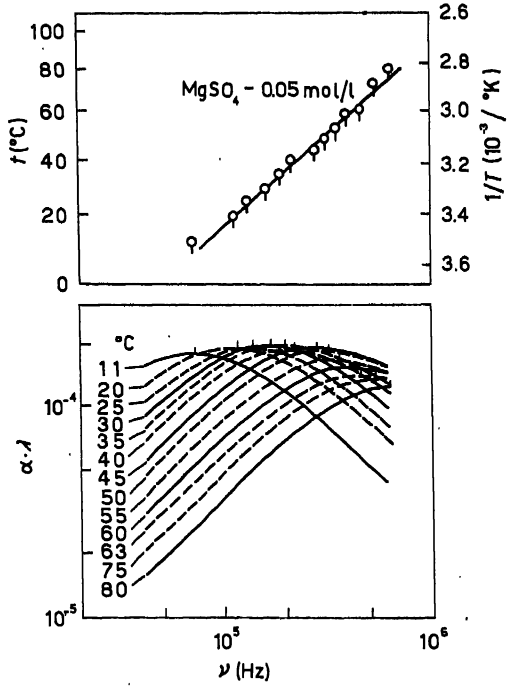

Fig. 19. – Temperature-dependence of relaxation frequency in $MgSO_4$-solution (determination of activation energy).

of the complex equilibrium in sulphates of bi-valent metals. If the relaxation within the ionic atmosphere is taken into account by step 1-2 the following scheme may be proposed:

(63) 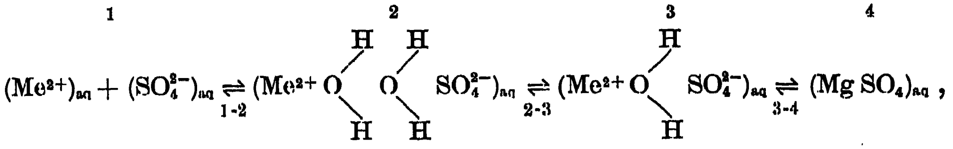

$$\overset{1}{(Me^{2+})_{aq} + (SO_4^{2-})_{aq}} \underset{1\text{-}2}{\rightleftharpoons} \overset{2}{(Me^{2+}\,\overset{H}{\underset{H}{O}}\;\overset{H}{\underset{H}{O}}\;SO_4^{2-})_{aq}} \underset{2\text{-}3}{\rightleftharpoons} \overset{3}{(Me^{2+}\,\overset{H}{\underset{H}{O}}\;SO_4^{2-})_{aq}} \underset{3\text{-}4}{\rightleftharpoons} \overset{4}{(Mg\,SO_4)_{aq}}\,,$$

1 and 2 are states of the ionic atmosphere. The equilibrium 1-2, therefore, does not include any specific influence of the different ions and may be described by the electrostatic Coulomb interaction by using a macroscopic dielectric constant. The step 2-3 depends slightly, the step 3-4 much more on the individual qualities of the ions involved. As already mentioned it has to be assumed that in the « closest » state « 4 » metal-ion and ligand are direct neighbours, *i.e.* not separated by water molecules. However, there is still an interaction with the remaining water molecules of the co-ordination spheres. The state « 4 », therefore, is an aquo-complex.

This statement is substantiated by the strong dependence of the lower relaxation frequency—which is determined by the dissociation rate of the last step (here k_{43})—on the character of the cation. As may be seen from Table V $1/\tau_{II}$ varies for the sulphates from Be^{++} to Mn^{++} by more than 4 orders of magnitude. In this table the ion radii (according to BASOLO and PEARSON [23]) are also listed. The relatively strong dependence of both the relaxation frequency and the dissociation rate on the radius of the unhydrated cation (0.32 Å for Be^{++}, 0.70 Å for Mg^{++}) is evident. The dissociation for $BeSO_4$ proceeds a thousand times slower than for the Mg-salts; and for these another hundred times slower than for the Ca-salts. Another indication that step 3-4 is a substitution of a water molecule of the inner co-ordination sphere by an SO_4^{--}-ion is given by the behaviour of the rate constant k_{34}. Since the equilibrium constants K_{34}—which can be determined almost exactly from the absolute values $(Q\lambda)_m$—vary only slightly for different 2-2 electrolytes, the k_{34} values show the same characteristic variation as the k_{43} values. This is typical for a substitution reaction. On the other hand, (according to new investigations) k_{43} is, for a given metal-ion, nearly independent of the binding of the cation. The binding is weak for SO_4^{--} (as for H_2O) but can be very strong as for the chelates (*e.g.* in phosphate complexes). Deviations from this behaviour were found only for the Be^{2+} and Al^{3+} (see below).

In contrast to k_{34}, the k_{43} values depend strongly on the nature of the ligand, *i.e.* on the strength of the complex. The stability of the complex is manifested only in the rate of dissociation as indicated for $MgSO_4$, MgS_2O_3 and $MgCrO_4$. The strong dependence of the k_{34} and k_{43} values on the radius

TABLE V. – *Rate constants of ligand-water substitution in the inner co-ordination sphere of 2-valent metal ions.*

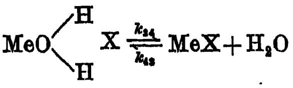

$$\mathrm{MeO}\begin{matrix}\diagup\mathrm{H}\\ \diagdown\mathrm{H}\end{matrix}\,\mathrm{X}\ \underset{k_{43}}{\overset{k_{34}}{\rightleftharpoons}}\ \mathrm{MeX}+\mathrm{H_2O}$$

Reaction	k_{43} (s^{-1})	k_{34} (s^{-1})	$r_{Me^{2+}}$ (Å)
$Be^{2+}+SO_4^{-2}$	$1.3\cdot10^{3}$	$1\cdot10^{2}$	0.35
$Mg^{2+}+SO_4^{-2}$	$8\cdot10^{5}$	$1\cdot10^{5}$	0.78
$Mg^{2+}+S_2O_3^{-2}$	$1.5\cdot10^{6}$	$1\cdot10^{5}$	0.78
$Mg^{2+}+CrO_4^{-2}$	$1.5\cdot10^{6}$	$1\cdot10^{5}$	0.78
$Ca^{2+}+CrO_4^{-2}$	$2\cdot10^{8}$	$2\cdot10^{7}$	0.99
$Mn^{2+}+SO_4^{-2}$	$2\cdot10^{7}$	$4\cdot10^{6}$	0.91
$Fe^{2+}+SO_4^{-2}$	$6\cdot10^{6}$	$1\cdot10^{6}$	0.83
$Co^{2+}+SO_4^{-2}$	$2.5\cdot10^{6}$	$2\cdot10^{5}$	0.82
$Ni^{2+}+SO_4^{-2}$	$1\cdot10^{5}$	$1.5\cdot10^{4}$	0.78
$Cu^{2+}+SO_4^{-2}$	$2\cdot10^{8}$	$<10^{7}$	0.72
$Zn^{2+}+SO_4^{-2}$	$<10^{8}$	$<10^{7}$	0.83

of the cation has already been discussed for the alkaline earths. Some of the transition metals, Co^{++}, Fe^{++}, and Mn^{++} fit relatively well in the sequence of the ions with their electron shells filled. Ni^{++}, Cu^{++} and Zn^{++}, however do not fit in the sequence. Though Ni^{++} and Cu^{++} have nearly the same ion radius as Mg^{++}, Ni^{++} reacts ten times slower, Cu^{++} by some orders of magnitude faster than Mg^{++}. These deviations may be caused by a special electron configuration of these ions. For Ni^{++} (d^8 electron system) a crystal field stabilization of the transition state has been predicted [23]. It retards the reaction when compared with that of a symmetric configuration of the electric charge for the case of the filled-up electron shells of the alkaline-earth ions. This sort of stabilization does not exist for the d^7, d^6 or d^5 electron system of Co^{++}, Fe^{++}, and Mn^{++}.

For Cu^{++} a planar structure of the aquo-complex esists, in which only four H_2O molecules (in an equatorial plane) are bound strongly, while the two remaining ligands (arranged along the axis) are more easily exchanged. This explains both the high reaction rate and the very high relaxation frequency, respectively (*).

It was already mentioned that for some metal ions (*e.g.* Be^{++}) the k_{34} values do depend on the nature of the ligand. It has to be assumed that for Be^{++}, Al^{3+}, and especially Fe^{3+} the substitution of H_2O is so slow that the hydro-

---

(*) The relaxation effect in $CuSO_4$ at about 10 kHz very probably corresponds to a hydrolysis (proton transition between HSO_4^- and $CuOH^+$).

lysis of H_2O determines the decay rate. The hydrolysis depends on the basicity of the ligand. Since the exchange of H_2O molecules in the co-ordination sphere of the hydroxo compound (*e.g.* $FeOH^{2+}$) may proceed relatively fast, the hydrolysis may become the rate-determining process for the substitution. This was observed for Fe^{3+}-compounds [25].

EIGEN, KURTZE, TAMM [2*a*] discussed also an intermediate hydrolysis mechanism of the form

(64)
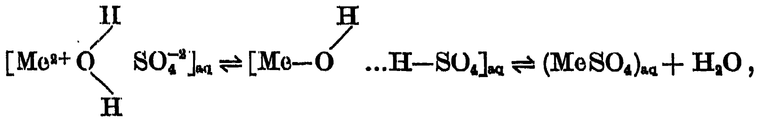

$$[Me^{2+}O(H)(H)\ SO_4^{-2}]_{aq} \rightleftharpoons [Me{-}O(H)\ ...H{-}SO_4]_{aq} \rightleftharpoons (MeSO_4)_{aq} + H_2O\,,$$

for simple dissociation. It is clear, however, that the hydrolysis determines the rate only for very small ions such as Be^{++}, Al^{3+}, Fe^{3+}; it is of low influence for Mg^{++}. In these cases the anomalous values of the rate constants are thus explained.

Contrary to the very characteristic variations of the relaxation times of the lower maximum, only small differences were found for the higher maximum. This was to be expected for the transitions 1-2 and 2-3, because of the small deviations of the radii of the hydrated metals. For instance for Be^{2+} the distance (of the charge center from the surface of the SO_4^{--} ion) is $(2\div 3)$ Å for state « 3 » [0.3 Å in state 4] and for Mg^{2+} only 0.35 Å more. The order of magnitude, 10^{-9} s, of the rate constant of the higher maximum indicates a transition 2-3. The rate constants k_{32} and k_{23} of this transition, which are determined by the activation energy for the decay of the co-ordination sphere or the energy of separation against the electrostatic force, should be approximately of this size.

From the theory of diffusion-determined reactions (according to DEBYE [26] and EIGEN [10]) the values $k_{12}^0 = 4\cdot 10^{10}\ m^{-1}\ s^{-1}$ and $k_{21} \approx 10^9\ s^{-1}$ can be calculated as well as a reaction rate $> 10^{-9}\ s^{-1}$ for step 1-2 which is still higher than that of step 2-3.

4. – Summary.

Sound absorption and dispersion measurements have been made for many electrolytes. For some electrolytes especially ammonium hydroxide, sulfuric acid, the acetates, the sulfates and a great number of organic compounds (showing protolytic reactions), a very extended series of measurements was made. Theoretical investigations have been concentrated on these systems.

The sound absorption in electrolyte solutions can be explained by relaxation processes. Assumptions with respect to the nature of these relaxation processes may be tested by means of experiments upon the dependence of the absorption on frequency, concentration, temperature, pressure, dielectric constant and addition of other electrolytes. This is a relatively complicated task because of the very complex behaviour of the electrolyte solutions, which is a result of the interaction of the ions with each other and with the solvent.

For some electrolytes, expecially those mentioned above, the interpretation was very successful. It could be stated that all the relaxation effects in the frequency range up to some hundred MHz are due to specific interaction of the ions of the electrolyte solved. For weak electrolytes (as ammonium hydroxide) the relaxation is caused by a simple dissociation. For stronger electrolytes, especially 2-2 valent ones, a multi-step dissociation of the aquo-complexes occurs, which includes transitions between different sorts of intermediate hydrate complexes. The so-called lower relaxation maximum in 2-2 valent electrolytes is due to a very specific transition from an outer sphere ion complex to an inner sphere ion complex (where the ions are very close together) *i.e.* by the substitution of an inner co-ordination sphere water-molecule by SO_4^{--}. In solutions of the sulfates of mono-valent metals (Na_2SO_4) similar complexes have to be assumed. The higher relaxation maximum is due to a transition between an outer sphere complex and an encounter complex. The nonspecific interaction within the ionic atmosphere causes an absorption at very high frequencies in all electrolytic solutions.

The results of the interpretation have partly proven the conceptions commonly used in chemistry. Besides, they have initiated some new considerations. While from static measurements only equilibrium quantities can be obtained, from acoustic measurements the reaction rates may also be derived. The thermodynamic equilibrium is thus spread out along the frequency axis and the different sorts of ion interaction can be separated this way. In particular the determination of the rate constant k_{43} of the decay of the inner sphere complex from the relaxation frequency of the lower maximum has brought additional knowledge on complex stability. On the other hand the value k_{34}, which can be calculated from k_{43} by means of the equilibrium constant and which is characteristic for the electron configuration, determines the complex formation.

It is possible to get from sound absorption and dispersion measurements some knowledge about time constants for equilibria with high reaction rates. This may often be used in the future and may be of advantage especially for the chemical kinetics. The acoustical methods need to be improved with respect to accuracy and frequency range, *i.e.* to frequencies above 300 MHz and below 200 kHz for this purpose.

APPENDIX

5. – Experimental methods.

The characteristic parameters of relaxation processes (*i.e.* relaxation frequency and amount of absorption or total change of phase-velocity) may be determined in principle by dispersion as well as by absorption measurements. In consequence of the very small dispersion step in electrolytes, dispersion measurements within reasonable efforts will be successful only in some special cases. On the other hand the absorption coefficient is also small, especially at low frequencies. Hence it follows that extremely high accuracy is required for such measurements, and in an even higher degree for low electrolyte concentrations. On the other hand measurements in a wide range of concentrations are necessary for a satisfactory interpretation of the experimental results. Moreover the different locations of the relaxation frequencies of different electrolytes demand measurements in a wide frequency range. This is impossible by only one measuring method, but there exist appropriate methods for each section of the frequency range.

5·1. *Dispersion measurements.* – In practice the measurement of dispersion in electrolyte solutions is only possible by reducing the measurement to a direct comparison of two sound velocities which are nearly equal. Fox and MARION [27] compare the sound velocities in a solution at two frequencies: one at the lower end and the other at the upper end of the relaxation range. For this purpose two frequencies, exactly harmonic to each other, are emitted simultaneously into the media and the slowly increasing shift of the phase planes of the two progressive waves is detected by an electroacustic transducer (Fig. 20).

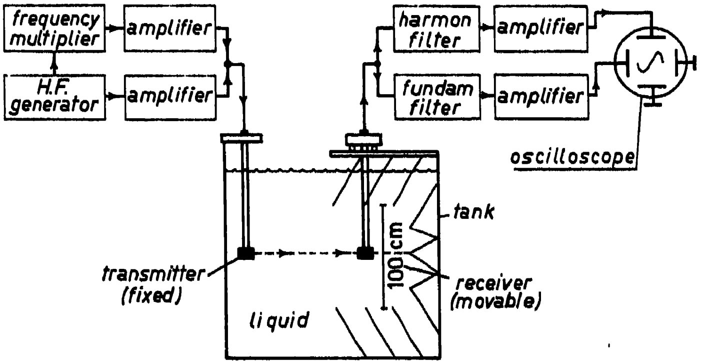

Fig. 20. – Equipment for dispersion measurements - phase comparison between two harmonic frequencies (0.1...1 MHz).

Carstensen [28] succeded in performing comparison measurements in progressive waves down to about 100 kHz by dividing the constant distance between transmitter and receiver by a movable diaphragm into two variable

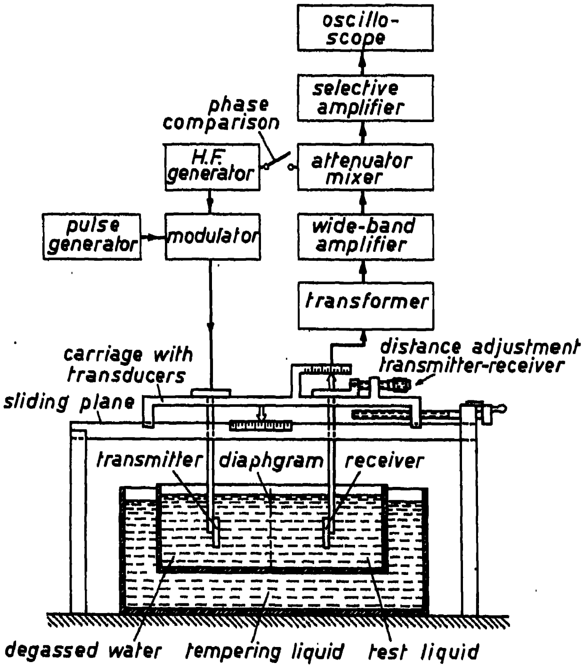

Fig. 21. – Equipment for dispersion and absorption measurements, —— method of continuous substitution (0.1...10 MHz).

pathlengths, one in the solution and one in the solvent (Fig. 21). When moving the diaphragm, the difference of the sound velocities may be derived directly from the phase between transmitter and receiver-voltage.

5·2. *Absorption measurements.* – Whereas for absorption measurements at high frequencies (> 3 MHz) the standard propagation methods (stationary progressive waves with optical measurement of intensity by Debye-Sears-effect, pulse methods with electro-acoustical receivers) may be used, the low absorption below this limiting frequency requires resonance and reverberation methods. For measuring the electrolyte absorption it is not essential to get the absolute value of absorption but only to get exactly the difference between the absorption of the electrolyte solution and that of the pure solvent. Because of the small differences such comparison measurements have to be done under exactly the same conditions for each, *e.g.* in immediate succession using the same apparatus. By taking the difference of the absorption the additional energy losses due to walls and other parts of the apparatus may be eliminated.

5·2.1. **Resonance method.** This method is especially appropriate for low frequencies (5 ... 50 kHz). The electrolyte absorption may be derived either from the half-width or the decay time of only one vibration mode of the liquid volume within the resonators. The energy losses due to deformation of the vessel and friction within the liquid-vessel boundary layer determine the accuracy of measurements. These losses may be reduced by use of resonating vessels with walls made from materials of low internal loss factors, *i.e.* aluminium, glass or quartz. Especially small losses occur at the boundary layer if eigenvibrations of radial symmetry are excited in spherical resonators (Fig. 22).

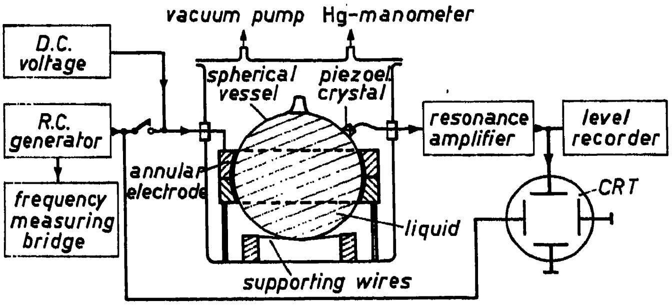

Fig. 22. – Equipment for absorption measurements, —— resonance method (4 ... 50 kHz).

After switching off a frequency band excitation, only these low damped eigenvibrations survive during reverberation (see LEONARD [32], WILSON [29], and MOEN [30]). By using single frequencies these modes can be excited preferably from the beginning (see TAMM and NAAKE [31]). For reduction of the radiation damping, the measuring vessel is placed in another vessel which is evacuated to some mm Hg for the measurement. Excitation and detection of the vibrations are mainly made through the wall of the vessel from outside by piezoelectric transducers. NAAKE and TAMM used a ring-shaped electrode for electrostatic excitation of eigenvibrations of radial symmetry. Measurements at high pressures were carried out by FISHER [6] in thick-walled stainless steel tubes which are completely filled with the liquid under test and carefully set free from air films.

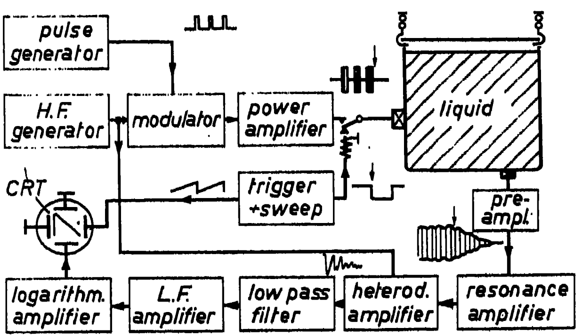

Fig. 23. — Equipment for absorption measurements —— reverberation method (0.05 ... 1 MHz).

5·2.2. **Reverberation method.** In the frequency range beyond 50 kHz, the eigenfrequencies in a liquid-filled resonator are very close together, if the resonator has the minimum dimensions required by sufficiently small wall losses. In this case individual eigenvibrations cannot be excited separately.

Skudrzyk and Meyer [33] and later also Mulders [34] and Tamm [31] passed therefore over to a reverberation method (Fig. 23). They simultaneously excite a large number of eigenvibrations in a narrow frequency band using r.f.-pulses or a band of white noise. To get exponential reverberation curves — (that means all eigenvibrations have the same decay constant) — resonators of low symmetry have to be used in which each eigenvibration is coupled with different angles of incidence on the wall.

5'2.3. Propagation methods. At frequencies higher than 1 MHz the absorption in water and electrolyte solutions becomes so large that it may be measured by the decay of intensity in a progressive sound beam along a very limited path-length. If the cross-section of the beam is very large in comparison to the wavelength the short range field (in which the sound beam is nearly parallel) extends over the whole measuring path. To determine the decay of the sound energy usually receivers are used which integrate over the cross-section of the beam, *i.e.* a receiving quartz of at least the diameter of the transmitting quartz or a broad light beam (in optical methods) or a sufficiently extended radiation-pressure meter.

In principle, for measuring the absorption, the comparison of two sound intensities at two different distances from the transmitter is sufficient. To eliminate fluctuations, however, measuring methods are very often preferred which allow a continuous registration of intensity or better of the logarithm of the intensity as the distance between transmitter and receiver is varied linearly with time.

The optical intensity measurement, using the Debye-Sears effect (Fig. 24), involves an integration of the sound intensity, if the measurements are restricted to small sound intensities for which a linear relation between sound intensity

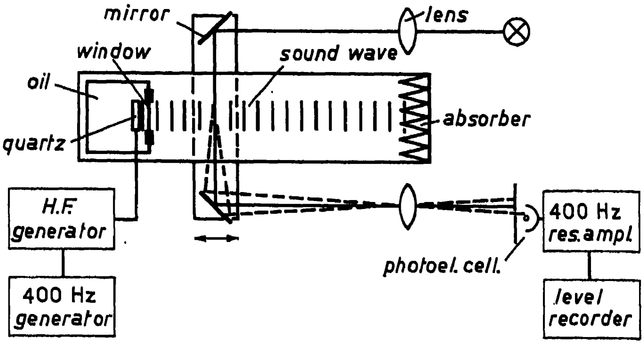

Fig. 24. – Equipment for absorption measurements in progressive waves —— optical intensity measurement (20 ... 100 MHz).

and light intensity exists. This is valid for the first order of the diffraction spectrum as long as the light intensity of the second order is comparatively small. The intensity of the diffracted light can be measured directly photographically and analysed by photometric methods. But it is common to use a photoelectric cell and to record the voltage by electro-mechanical devices. This method is applied especially in the frequency range (3 ÷ 100) MHz. At lower frequencies the isolation of the first diffraction order of the light is more difficult than at higher frequencies. This method is limited by the increase of the sound intensity necessary to get sufficient light in the first order.

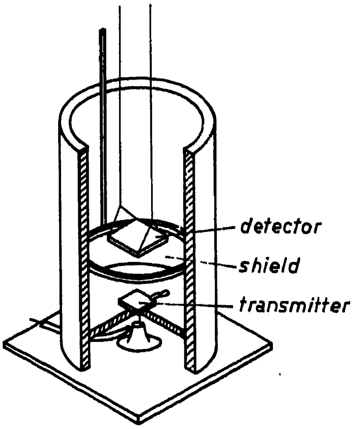

Fig. 25. - Apparatus for absorption measurements in progressive waves —— radiation pressure method (3... 100 MHz).

Measurements by means of the *sound radiation pressure* have been repeatedly applied to determine the absorption (Fig. 25) for example by VAN ITTERBECK and VERHAEGEN [35], HSU [36], and by SMITH and BEYER [37]. These measurements are connected with relatively great mechanical difficulties and require high sound intensities.

The use of *electro-acoustical receivers* (*e.g.* quartz plates) demands (because of the influence of the phases to the integration of the sound pressure) nearly plane wavefronts and accurate adjustment of the receiver surface.

This method is important at higher frequencies, where the optical method fails. Electric cross-talk can be made ineffective by using pulses. Pulse methods have been applied by PELLAM and GALT [38] and by LITOVITZ [39]. To get the pulses separated for short pathlengths in the liquid (high absorption) delay lines are inserted into the sound path. It is possible to use only one

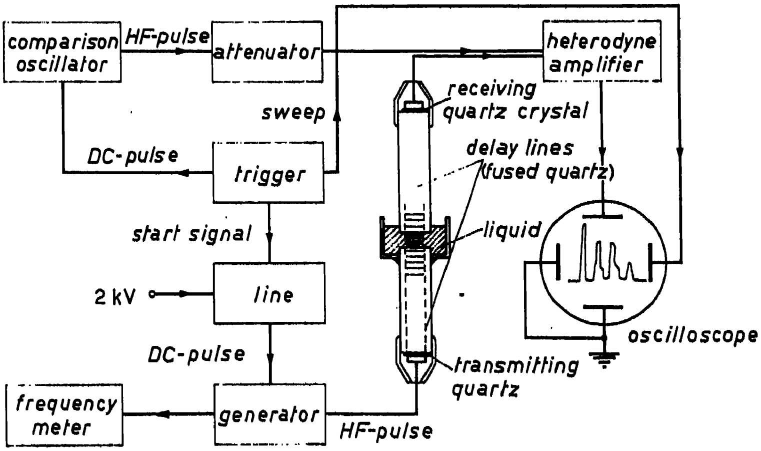

Fig. 26. - Equipment for apbsorption measurements in progressive waves —— delayed ulse method (100 ÷ 300 MHz).

transducer quartz as receiver and transmitter, if the sound pulse which passed the liquid is reflected at the end of an additional delay line. This method (Fig. 26, 27) is suitable for measurements up to the highest frequencies thus far generated in liquids, *i.e.* up to about 500 MHz (see Rapuano [40]).

At still higher frequencies the excitation of the required harmonics in quartz crystals is very difficult. Recently Bömmel and Dransfeld [42] and Jacobsen [43] using a method proposed by Baransky [41] succeeded in avoiding these difficulties by exciting (up to 20000 MHz) a cylindrical rod of crystalline quartz from one end by immersing it in the field of an electromagnetic resonator.

The upper frequency limit is determined only by the magnitude of the attenuation in the quartz crystal which, however, is very small. Up to now measurements in aqueous solutions have been performed only at frequencies below 300 MHz [2]. At higher frequencies the sound intensity decreases so rapidly with distance (because of the steep increase of the absorption with frequency), that the measurements will be very difficult.

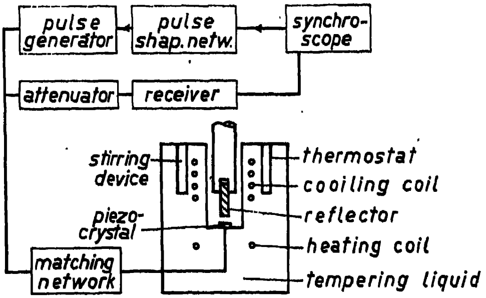

Fig. 27. – Equipment for absorption measurements in progressive waves —— delayed echo method (10 ÷ 50 MHz).

For the frequency range around 1 MHz the method of continuous substitution of Carstensen [28] is especially appropriate for measuring also the relatively small electrolyte absorptions. Krämer [44] and Siegert [20] have improved the accuracy by using a reference liquid (NaCl solution) with the same sound velocity as the liquid to be investigated and by avoiding disturbing reflections and increasing the stability of the electronic equipment. In this way they were able to extend the frequency range to lower frequencies (200 kHz).

5·3. *Accuracy of measurements.* – The accuracy of the measurements is relatively high at higher frequencies; in any case an error of at least 5 % of the absolute value of the absorption of water has to be expected. At lower frequencies the accuracy decreases considerably and the experimental error will rise at 100 kHz to 100 % of the absoprtion value of pure water. Since the electrolyte absorption is obtained from the difference of two experimental values the relative accuracy decreases with decreasing electrolyte absorption, *i.e.* with decreasing concentrations. Therefore the relative error of the absorption cross-section Q and of $(Q\lambda)$ does not depend only on its absolute value but also on the concentration at which it was measured. It other words: absorption cross-sections derived from small absolute values of the absorption mostly have large relative errors. This must be considered when discussing experimental results.

REFERENCES

[1] L. Liebermann: *Phys. Rev.*, **76**, 1520 (1949); *Journ. Acoust. Soc. Am.*, **20**, 868 (1949).

[2] *a*) M. Eigen, G. Kurtze and K. Tamm: *Zeits. Elektrochem., Ber. Bunsenges. phys. Chem.*, **57**, 103 (1953); *b*) G. Kurtze and K: Tamm: *Acustica*, **3**, 33 (1953); *c*) K. Tamm, G. Kurtze and R. Kaiser: *Acustica*, **4**, 380 (1954); *d*) K. Tamm: *Encycl. Phys.*, **11/1**, 202 (1961); *e*) M. Eigen and K. Tamm: *Zeits. Elektrochem., Ber. Bunsen. Phys. Chem.*, **66**, 93 (1962).

[3] H. O. Kneser: *Encycl. Phys.*, **11/1**, 129 (1961).

[4] K. F. Herzfeld and T. A. Litovitz: *Absorption and Dispersion of Ultrasonic Wawes* (New York and London, 1959).

[5] P. Debye and E. Hückel: *Phys. Zeits.*, **24**, 185 (1923).

[6] H. Falkenhagen: *Elektrolyte* (Leipzig, 1953).

[7] L. H. Hall: *Journ. Acoust. Soc. Am.*, **24**, 704 (1952).

[8] M. Leontovic: *Žurn. Èxsp. Teor. Fiz. USSR*, **8**, 40 1938).

[9] M. Eigen and G. Maass: private' communication (1962).

[10] M. Eigen: *Zeits. Phys. Chem.*, *N. F.* **1**, 176 (1954).

[11] Landolt-Börnstein: *Phys. Chem. Tab.*, EG III (1936), 2816 (after measurements of W. A. Roth).

[12] E. H. Carnevale and T. A. Litovitz: *Journ. Acoust. Soc. Am.*, **30**, 610 (1958).

[13] M. Eigen: *Zeits. Elektrochem., Ber. Bunsenges. phys. Chem.*, **64**, 115 (1960)

[14] C. W. Davies, H. W. Jones and C. B. Monk: *Trans. Farad. Soc.*, **48**, 921 (1952).

[15] O. B. Wilson: *Phys. Rev.*, **81**, 657 (1951).

[16] D. A. Bies: *Journ. Chem. Phys.*, **23**, 428 (1955).

[17] F. H. Fischer: *Journ. Acoust. Soc. Am.*, **30**, 441 (1958).

[18] N. Bjerrum: *Dansk. Mat. Fys. Medd.*, **7**, 9 (1926).

[19] R. A. Robinson and R. M. Stokes: *Electrolyte Solutions* (London, 1959).

[20] H. Siegert: *Acustica*, **13**, 48 (1963).

[21] M. Eigen and E. Wicke: *Zeits. Elektrochem., Ber. Bunsenges. phys. Chem.*, **57**, 319 (1953).

[22] J. R. Smithson and T. A. Litovitz: *Journ. Acoust. Soc. Am.*, **28**, 462 (1956).

[23] F. Basolo and R. G. Pearson: *Mechanisms of Inorganic Reactions* (New York, 1958).

[24] M. Eigen, G. Maaß and G. Schwarz: in press.

[25] H. Wendt: *Dissertation* (Göttingen, 1960).

[26] P. Debye: *Trans. Elektrochem. Soc.*, **82**, 265 (1952).

[27] F. E. Fox and Th. M. Marion: *Journ. Acoust. Soc. Am.*, **25**, 661 (1953).

[28] E. L. Carstensen: *Journ. Acoust. Soc. Am.*, **26**, 858 (1954); **26**, 862 (1954).

[29] R. W. Leonard: *Journ. Acoust. Soc. Am.*, **20**, 224 (1948); R. W. Leonard, P. C. Combs and L. R. Skidmore: *Journ. Acoust. Soc. Am.*, **21**, 63 (1949).

[30] O. B. Wilson and R. W. Leonard: *Journ. Acoust. Soc. Am.*, **26**, 223 (1954); O. B. Wilson: *Phys. Rev.*, **81**, 657 (1951).

[31] K. Tamm: *Nachr. Akad. Wiss. Göttingen, Math.-Phys. Kl.*, **10**, 81 (1952); G. Kurtze: *Nachr. Akad. Wiss. Göttingen, Math.-Phys. Kl.*, **9**, 57 (1952).

[32] C. J. Moen: *Journ. Acoust. Soc. Am.*, **23**, 62 (1951).

[33] E. Skudrzyk: *Öst. Ing.-Arch.*, **4**, 408 (1950).

[34] C. E. MULDERS: *Appl. Sci. Res.*, B **1**, 341 (1949); *Dissertation* (Delft 1950).
[35] A. v. ITTERBECK and L. VERHAEGEN: *Coll. Ultrason. Trill.* (Brussels, 1951), p. 220.
[36] E. HSU TSUNG-YUEH: *Journ. Acoust. Soc. Am.*, **17**, 127 (1945).
[37] M. C. SMITH and R. T. BEYER: *Journ. Acoust. Soc. Am.*, **18**, 424 (1946).
[38] J. R. PELLAM and J. K. GALT: *Journ. Acoust. Soc. Am.*, **18**, 251 (1946).
[39] T. A. LITOVITZ: *Journ. Acoust. Soc. Am.*, **23**, 75 (1951).
[40] R. A. RAPUANO: *Phys. Rev.*, **72**, 78 (1947).
[41] K. N. BARANSKI: *Dokl. Akad. Nauk. SSSR.*, **114**, 517 (1957); *Sov. Res. Phys. (Engl. transl.)*, **2**, 237 (1957).
[42] H. E. BÖMMEL and K. DRANSFELD: *Phys. Rev. Lett.*, **1**, 234 (1958); **2**, 298 (1959); **3**, 85 (1959).
[43] E. H. JACOBSON: *Phys. Rev. Lett.*, **2**, 249 (1959); *Journ. Acoust. Soc. Am.*, **32**, 949 (1960).
[44] W. KRÄMER: *Diplomarbeit* (Göttingen 1961).

Absorption and Dispersion of Sound in Polymer Solutions, Polymer Liquids, Rubbers and Solid Polymers.

W. P. MASON

Bell Telephone Laboratories, Incorporated - Murray Hill, N. J.

1. – Introduction.

The mechanical properties of polymers are of conbsiderable interest in a large number of applications. In the form of solid polymers they are widely used in household furniture and as electrical insulation in a large number of applications. Less tightly bonded polymers form rubbers which are widely used in automobile tires, shock insulators, hoses, etc., while liquid polymers are of interest in lubricating oils, damping fluids and for other purposes. The relaxations associated with the motion of complete polymer chains or segments of such chains produce considerable attenuation for sound waves transmitted through such media. Besides being of interest for the fundamental understanding of such transmission—the primary subject for the present course—they have many applications in the damping of unwanted modes of vibration.

The predominant characteristic of polymer molecules is the thread-like character caused by the joining of a large number of repeating elements by the carbon bonds of the central part of the chain. This thread-like character allows the molecule to take up a large number of forms such as those shown by Fig. 1. The form of the molecule is continually changing due to the thermal agitation and all treatments of the characteristics are based on the statistical properties of the chain and how these are altered by the application of stresses and temperature changes. Furthermore, the properties change materially with the degree of cross-linking between adjacent chains, and on whether adjacent segments of neighboring chains can form regions of closely bonded molecules in the form of crystals. The wide divergence in the mechanical behavior of the various forms of polymer materials depends primarily on the nature of such cross-linking or bonding.

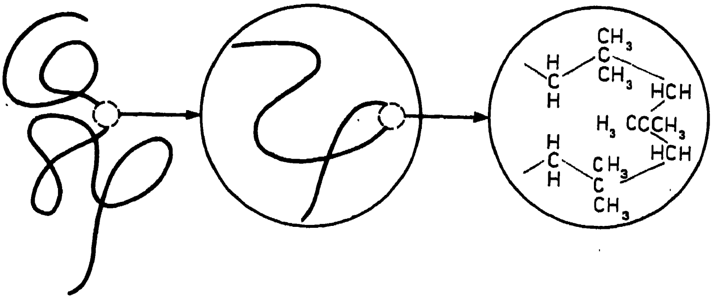

Fig. 1. – Thread-like character of polymer chain (after J. D. Ferry).

If there is no cross-linking, the polymer chain can move as a whole or various parts can move separately without reference to the whole motion. Alfrey [1] has described these relationships, viewed over progressively larger ranges, as «kinks, curls, and convolutions». Figure 1, first illustrated by Ferry [2], shows in qualitative form these types of motions for a polyisobutylene chain. Such free motion is usually obtained only for molecules in dilute solutions as discussed in Section 5. As the concentration increases, adjacent molecules make contact and this limits the types of motion that can take place. For long chain molecules in concentrated solutions, or in polymer liquids, there is a wide range of frequencies over which the properties are very similar to rubbers which are polymer chains joined together at irregular intervals by cross-linked bonds. The type of motion possible here is a motion of segments of the chain in the order of 100 polymer units. However, if one goes to very low frequencies, *i.e.*, the long time application of a stress, whole polymer chains can eventually move and there is a difference in the mechanical behavior of polymer liquids and rubbers.

On the other hand if one goes to high frequencies, *i.e.*, a very short time application of a force, one finally reaches a state where the shortest complete segment can no longer respond in the time of a cycle and the material approximates the glassy state, observed at lower temperatures and smaller frequencies, for which the elastic stiffness approximates that of a solid polymer. Even here, however, there is evidence from the hysteresis type response—see Section 6—that one or more monomers are still able to follow the motion of the applied stress.

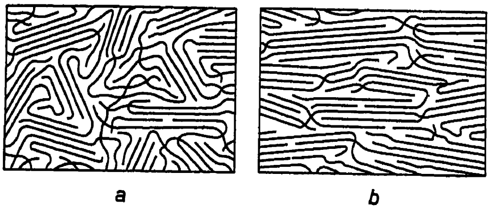

Fig. 2. – Crystalline form of polyethylene (after Treloar).

There are a large number of linear polymers for which this whole range of properties can be observed with only small changes between different types of chains. Table I shows the chemical formula for a number of these chains and their descriptive names.

All of these chains can exist as linear chains in dilute solutions of solvents. For more concentrated conditions some of them like polyethylene tend to form crystallites as shown in Fig. 2. Here adjacent chains are oriented parallel to

TABLE I.

Chemical formula	
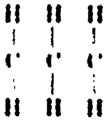	Polyethylene (paraffin for short lengths)
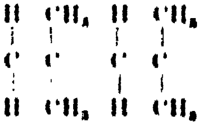	Polyisobutylene (basis of butyl rubber)
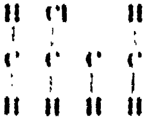	Polychloroprene (neoprene)
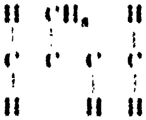	Polyisoprene (natural rubber-guttapercha)
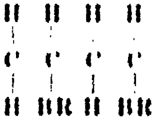	Polystyrene (BR = benzene ring of 6 carbon atoms in the form of a hexagon)
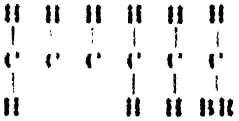	Butadiene-styrene interpolymer: (GR-S) rubber
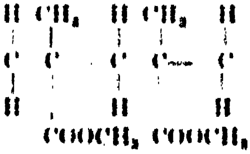	Polymethyl methacrylate (lucite)

each other and regions exist in the structure for which fundamental atomic bonds forms between adjacent atoms. These crystalline regions are separated by amorphous regions for which the chains bear no necessary relations to each other. The mechanical properties are determined mostly by the amorphous regions.

2. – Methods for measuring velocities, absorptions and mechanical impedances.

The techniques used to measure the properties of polymer solutions, liquids rubbers and solids are rather special to the polymer field and will be described briefly. Although there are many types of devices possible [3], the present discussion is limited to the most widely used devices and the ones which enable the properties of polymers to be measured at very high-frequencies.

The transmission of plane acoustic waves, which forms the basis for most of the measurements described previously, can be carried out in polymer solids. Both shear and longitudinal waves have been employed and the data of the next section shows measurements on polyethylene which have been obtained by pulse methods. The quantities measured are the attenuation and the velocity of wave propagation, whereas the desired quantities, for a theoretical interpretation, are the real and imaginary parts of the stiffness. Since the wave propagation equation is of the form

$$E^* \frac{\partial^2 \mu}{\partial x^2} = \varrho \frac{\partial^2 u}{\partial t^2}; \qquad E^* = E_1 + jE_2, \tag{1}$$

the solution becomes

$$u = C \exp[(A + jB)x] \exp[j\omega t], \tag{2}$$

where

$$(E_1 + jE_2)(A + jB)^2 = -\omega^2 \varrho . \tag{3}$$

Solving for E_1, E_2 and their ratio, we have

$$E_1 = \frac{(B^2 - A^2)\omega^2 \varrho}{(A^2 + B^2)^2}; \qquad E_2 = \frac{2AB\omega^2 \varrho}{(A^2 + B^2)^2}; \qquad \frac{E_2}{E_1} = \operatorname{tg}\theta = Q^{-1} = \frac{2AB}{B^2 - A^2}. \tag{4}$$

The attenuation A is expressed in nepers/cm, (1 neper = 8.68 db), while the phase velocity V is determined by the ratio of $\omega = 2\pi f$ to the phase constant B, which is expressed in radians per cm. For plane longitudinal and shear waves, the appropriate stiffness values are

$$E = (\lambda + 2\mu) \text{ (long.)} ; \qquad E = \mu \text{ (shear)} , \tag{5}$$

where λ and μ are the two Lamé elastic moduli. The ratio of the imaginary to real part of the stiffness values determines the phase angle θ and the internal friction factor Q^{-1} according to eq. (4). If the ratio of B to A is 10 or greater, which is usually the case for most measurements carried out with plane waves, the formulae can be simplified to

$$E_1 = \frac{\omega^2}{B^2}\varrho = V^2\varrho ; \qquad \frac{E_2}{E_1} = \mathrm{tg}\,\theta = Q^{-1} = \frac{2AV}{\omega} . \tag{6}$$

The imaginary part of the stiffness is often written in the form

$$E_2 = \omega\eta , \tag{7}$$

where η is the equivalent viscosity of the substance.

For many polymer solutions, liquids, rubbers and even solids, the attenuation constant A is often so high that direct attenuation and velocity measurements are not feasible. One can still obtain measurements of the elastic moduli by using the impedance of the medium which is defined as the ratio of stress to particle velocity at the interface between the transducer and the medium. The stress is determined from the equation

$$T = E^* \frac{\partial u}{\partial x} = CE^*(A + jB) \exp\left[(A + jB)x\right] \exp\left[j\omega t\right] . \tag{8}$$

The particle velocity, which is the time derivative of the displacement u is

$$\dot{u} = \frac{\partial}{\partial t}(u) = j\omega C \exp\left[(A + jB)x\right] \exp\left[j\omega t\right] . \tag{9}$$

Hence their ratio determines the characteristic impedance

$$Z_0 = \frac{T}{\dot{u}} = \frac{E^*(A + jB)}{j\omega} = R + jX , \tag{10}$$

where R is the real part (resistance) of the characteristic impedance Z_0 and X the imaginary or reactive part. Multiplying both sides of (10) by $(A+jB)$ and employing the relations of eq. (3)

$$(R + jX)(A + jB) = j\omega\varrho . \tag{11}$$

Hence a measurement of either the characteristic impedance or the propagation constant can determine the real and imaginary parts of the stiffness characteristic. In particular if we solve for the values in terms of the impedance values

$$E_1 = \frac{(R^2 - X^2)}{\varrho}; \qquad E_2 = \omega\eta = \frac{2RX}{\varrho}. \tag{12}$$

For light liquids vibrating in shear, the stiffness constant $\mu = E_1$ is usually zero and hence the reactance equals the resistance. The viscosity η is then determined by

$$\eta = \frac{2RX}{\omega\varrho} = \frac{2R^2}{\omega\varrho}. \tag{13}$$

There are two general methods for measuring the characteristic impedance of a highly damped liquid. One involves the change in amplitude and phase of a wave reflected from an interface between a solid such as fused silica and the liquid or solid to be measured. Figure 3 shows such a device [4] for shear waves. This device operates by reflecting a shear wave at a small angle of incidence from a polished surface of a fused silica rod. By using a particle displacement parallel to the polished surface, only a shear wave is reflected. By loading the surface with a liquid or solution whose viscosity and shear stiffness are to be measured, a change in amplitude and a change in phase occur in the reflections. To measure this change, an identical unit, labeled

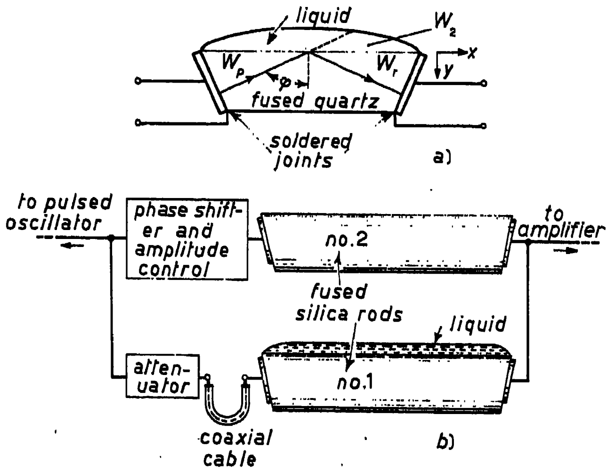

Fig. 3. – Shear reflectance method for measuring shear impedance.

number 2, is used in parallel but without a liquid loading. The complete unit is placed in a temperature-controlled cell. A phase shifter and an amplitude control are used to cause cancellation of the two parallel pulses and a fairly accurate measurement of the change of phase and amplitude is obtainable. This device operates in the frequency range from 1 MHz to about 100 MHz.

Still higher frequencies as well as measurements for longitudinal waves can be obtained by using a rod whose end is dipped into the solution. The change of phase or amplitude is smaller than for the device of Fig. 3, but by using a number of successive reflections from the interface, a measurable change occurs. This type of device can be used to frequencies as high as 1000 MHz.

The other type of a device employs the loading put on by a shear wave in a liquid to change the frequency and the resonant resistance of a mechanical resonator such as the torsional crystal [5] shown by Fig. 4. This crystal was attached to a vacuum tube socket as shown by Fig. 4. A purely torsional mode is generated in the crystal and this launches a shear wave in the cylindrical medium. If the distance that the wave propagates into the medium is small—as is usually the case—a shear wave in a cylindrical medium will have the same characteristic impedance as a plane shear wave shown by eq. (10). The method for measuring the characteristic impedance of the liquid is to first measure the resonant resistance and the resonant frequency of the crystal in a vacuum. The liquid or solution to be measured is then introduced in the cylinder surrounding the crystal. The temperature of the liquid can be controlled by circulating water or other temperature-control liquid in the jacket surrounding the measuring chamber.

One method of determining the effect of the liquid—which is applicable to light liquids—is to measure the change in the resonant resistance ΔR and the change Δf in the resonant frequency. From the equivalent circuit of the crystal it has been shown [5] that ΔR and Δf are given by

$$(14)\qquad \left\{\begin{aligned} \Delta R &= \frac{r}{2\pi f_R^2 C_0 I}\left[a^3+\frac{a^4}{l}\right] R = K_1 R\,, \\ \Delta f &= -\left(\frac{a^3+a^4/l}{2I}\right) X = -K_2 X\,, \end{aligned}\right.$$

where r is the ratio of capacitances of the torsional crystal, f_R the vacuum frequency of resonance, C_0 the static capacitance of the crystal, $I=\pi\varrho_0 a^4/2$ is the moment of inertia of the crystal and a the radius and l the length of the crystal. An alternate and more exact way of determining K_1 and K_2 is to use liquids of known density and viscosity to evaluate the changes in resistance and frequency. By using an impedance bridge and measuring the impedances at a number of frequencies, the use of the torsional crystal can be extended to much higher viscosities, and **Philippoff** [6] and collaborators

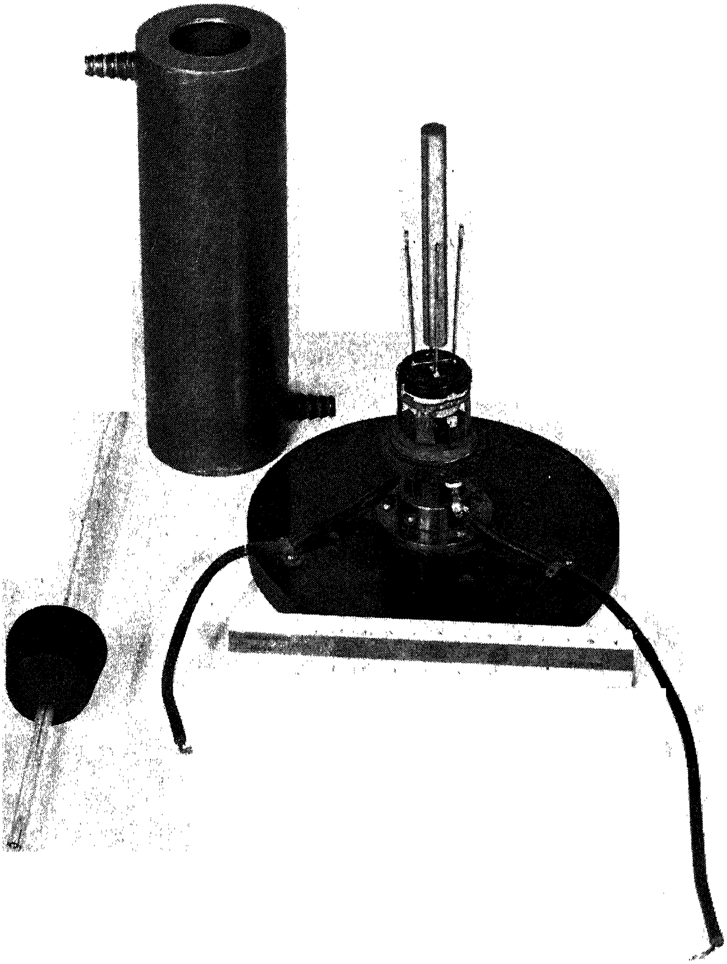

Fig. 4. – Torsional crystal method for measuring shear impedance.

describe the use of the crystal to measure liquids having viscosities as high as 50 poises.

Torsional crystals have been used in the frequency range from 20 kHz to 150 kHz. A similar device for much lower frequencies is the torsional pendulum method of Sittel, Rouse and Bailey [7], shown by Fig. 5. A much lower frequency is obtained by using a massive bob, containing the chamber to be filled by the liquid, on the end of a torsional rod. Frequencies in the order of 200 to 2000 Hz have been used. In this device, the lower bob is set into motion by a magnetic driving system which is then cut off. The frequency of oscillation is measured by a counter system and the rate of dying down is measured by a mirror system. The constants of the system, evacuated, are first determined and then the changes caused by filling the lower bob are determined. From these the mechanical resistance and reactance of the liquid can be determined from formulae similar to eq. (14). The constants K_1 and K_2 are usually evaluated by means of known liquids.

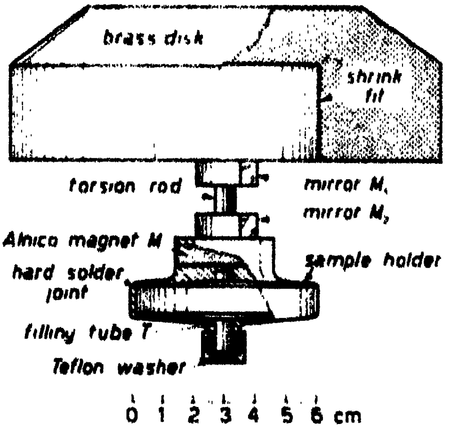

Fig. 5. — Torsional pendulum of Sittel, Rouse and Bailey.

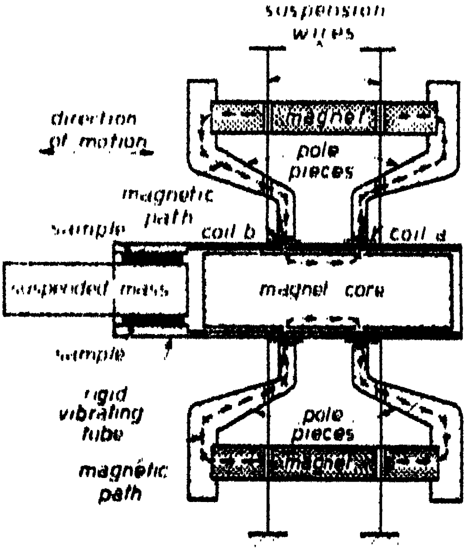

Fig. 6. — Fitzgerald-Ferry transducer.

Most of these systems are valid for single frequencies and to change the frequency, one has to make some changes in the system. A continuous range of frequency can be employed by using the transducers of FITZGERALD and FERRY [8], shown by Fig. 6. Here a rigid tube supported by eight wires is driven by coil *a* and the resulting motion is determined by the voltage picked up by coil *b*. Since this is a moving-coil type of transducer, no eddy currents are generated and the simplified transducer equation [9] can be employed. The sample to be measured, here shown as a rubber specimen, is inserted between a fixed mass and the moving tube, and the impedance is determined by the change in the impedance of the transducer. The fixed electrical impedance is balanced out in one arm of the bridge, and the mechanical impedance of the load is determined from the ratio and phase angle of the driving current i_a to the pick-up voltage V_b:

This device has been used to measure the mechanical impedance of concentrated polymer solutions, rubbers and even solid polymers. The sensitivity is not as great as that for the resonant devices which have been used to measure dilute polymer solutions. By making measurements over wide temperature ranges and employing the reduction formulae discussed in Section 5, measurements have been obtained over the whole range from the glass phase to the rubber phase. However, to completely determine the high-frequency range, for which the reduction formulae are not applicable, requires measurements at the high frequencies of interest.

3. – Typical stiffness and resistance curves.

Using these and other methods of measurements, the real and imaginary stiffnesses (or effective viscosities) have been determined for a large number of polymer materials. Since the greatest freedom of motion is present for dilute polymer solutions, the first curves are for this situation. Figure 7(*a*) and 7(*b*) show measurements [7] of the shear modulus and the effective viscosity of three different chain lengths of polystyrene dissolved in toluene. The measured points are indicated while the solid lines zhow calculations using the Rouse theory discussed in Section 5. The concentrations of the polymer chains are so low that they are essentially isolated. The frequency range co-

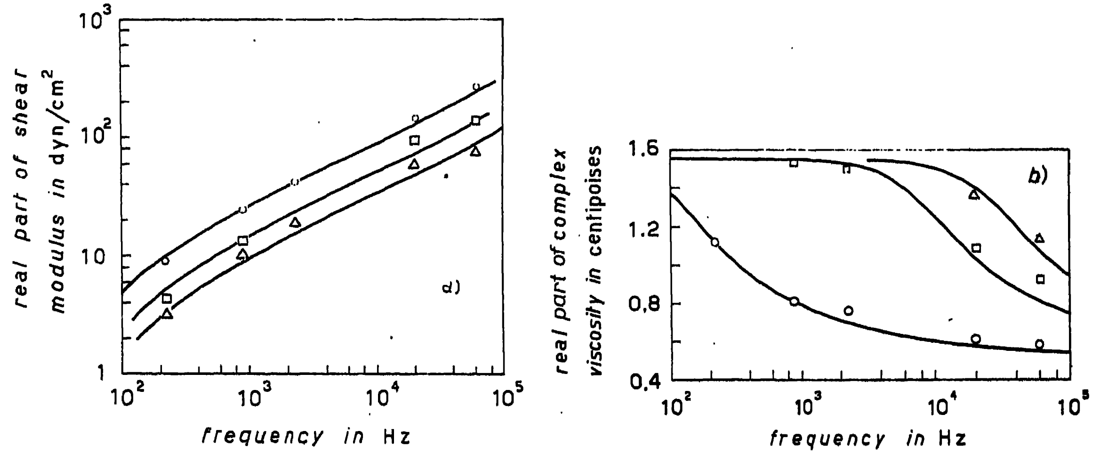

Fig. 7. – Shear stiffness and viscosity of polystyrene in toluene for several concentrations. Solid lines show calculations from Rouse's formula (after Sittel, Rouse and Bailey); *a*) polystyrene (molecular weight $= 6.2 \cdot 10^6$) in toluene at 30.3 °C: △ concentration 0.101 g/ml, relative viscosity 2.31; □ concentration 0.144 g/ml, relative viscosity 3.12; ○ concentration 0.222 g/ml, relative viscosity 1.48; *b*) polystyrene in toluene at 30.3 °C: △ molecular weight 253 000, concentration 1.48 g/ml, relative viscosity 2.99; □ molecular weight 520 000, concentration 0.89 g/ml, relative viscosity 3.00; ○ molecular weight 6 200 000 concentration 0.144 g/ml, relative viscosity 3.12.

vered is from 200 Hz to 60 kHz. The effect of introducing the polymer into the solution is to raise the static viscosity by the factor (relative viscosity) shown on Fig. 7(*a*) and 7(*b*). The bottom Fig. 7(*b*) shows three different molecular weights and three different concentrations adjusted to give nearly the same static viscosity. The highest molecular weight solution falls off more rapidly with frequency and approaches the viscosity of the solvent at very high frequencies.

Figure 8 shows the effect of different solvents on the shear stiffness of essentially the same chain length of polyisobutylene. The highest-frequency shear wave measurements [10] have been made on two solutions of different molecular weight polyisobutylene chains dissolved in cyclohexane. As shown by the solid lines of Fig. 9, the Rouse theory fits the measured points well up to 150 kHz, but appears to diverge from it for the 14 MHz measurements. These measurements are for a concentration of 1 g of polymer material for 100 cm^3 of solvent.

When the concentration gets larger, the stiffness and viscosity of the solution become greater. Figure 10 shows measurements [11, *a*] of polyisobutylene in a decalin solution. The concentrations range from 5% to 22%. The measurements were taken from 0.005 Hz to 100 Hz and temperature ranges from 5 °C to 35 °C. All the measurements are made to lie on single curves by employing the reduction formulae discussed in Section 5.

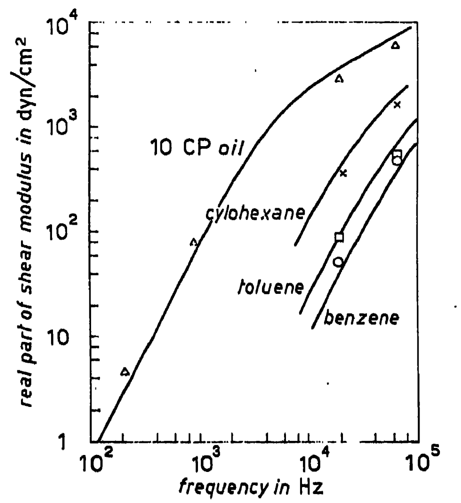

Fig. 8. – Shear stiffness of low molecular weight polyisobutylene in several solutions as a function of frequency. Solid lines show theoretical results from Rouse's formula (after SITTEL, ROUSE and BAILEY): ● solvent benzene, molecular weight 127000, concentration 1.20 g/100 ml, relative viscosity 1.71; □ solvent toluene, molecular weight 165000, concentration 1.24 g/100 ml, relative viscosity 2.05; △ solvent cyclohexane, molecular weight 143000, concentration 1.19 g/100 ml, relative viscosity 2.60; ▵ solvent oil ($\eta =$ .10 poise), molecular weight 136000, concentration 1.21 g/100 ml, relative viscosity 2.08.

A number of measurements of the shear properties of polymer liquids have been made with the results shown by Fig. 11, 12 and 13. Figure 11, circles and triangles, shows the measured shear stiffness and viscosity of a short polymer chain polyisobutylene liquid [12] measured over the complete frequency range from 200 Hz to 30 MHz. Two relaxation ranges, with stiffnesses around 10^7 dyn/cm^2 and 10^9 dyn/cm^2 are beginning to appear. This is accentuated by

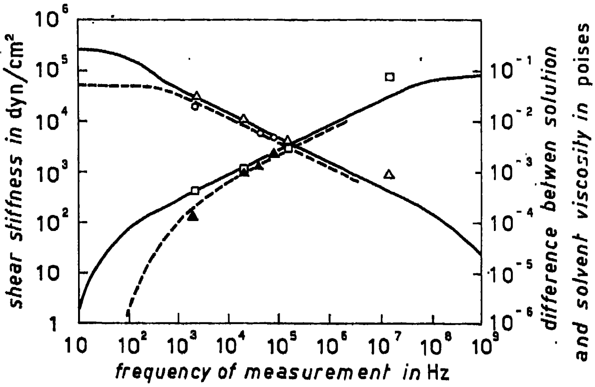

Fig. 9. – Measurements of shear stiffness and difference between solution and solvent viscosity for 1% $80X$ and $120X$ solutions as a function of the frequency, $80X = 1.18\cdot10^6$ M.W. $120X = 3.9\cdot10^6$ M.W. $120X$ solution: —— theoretical value, △ measured viscosity $\eta - \eta_s$, □ measured shear stiffness; $80X$ solution: – – – theoretical value, ○ measured viscosity $\eta - \eta_s$, ▲ measured shear stiffness.

the much longer polymer chain length measurements [13] made by a large number of techniques and shown in Fig. 12. These measurements were co-

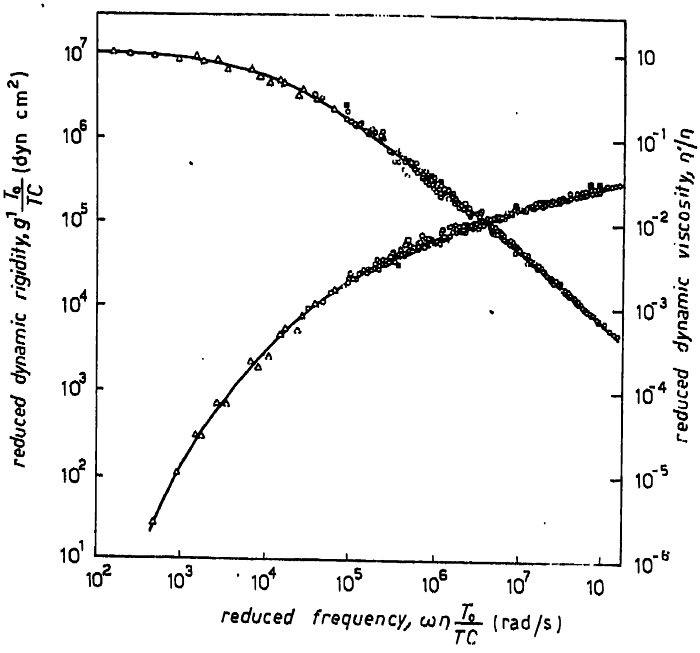

Fig. 10. – Reduced dynamic viscosity and shear elasticity for polyisobutylene in decalin (after PADDEN and DEWITT): ○ rheometer; △ torsion pendulum; □ FERRY: [11, *b*].

ordinated by the Bureau of Standards who supplied samples to a large number of investigators. The result shows clearly the two relaxation regions which extend over many decades of frequency. Figure 13 shows measurements [14] of a number of polyisobutylene liquids of molecular weight from 3100 to 8300 in the high frequency range and efforts made to fit the data by a reduction formula. Up to stiffnesses of about 10^7 dyn/cm², the formulae hold well, but about this stiffness a divergence occurs.

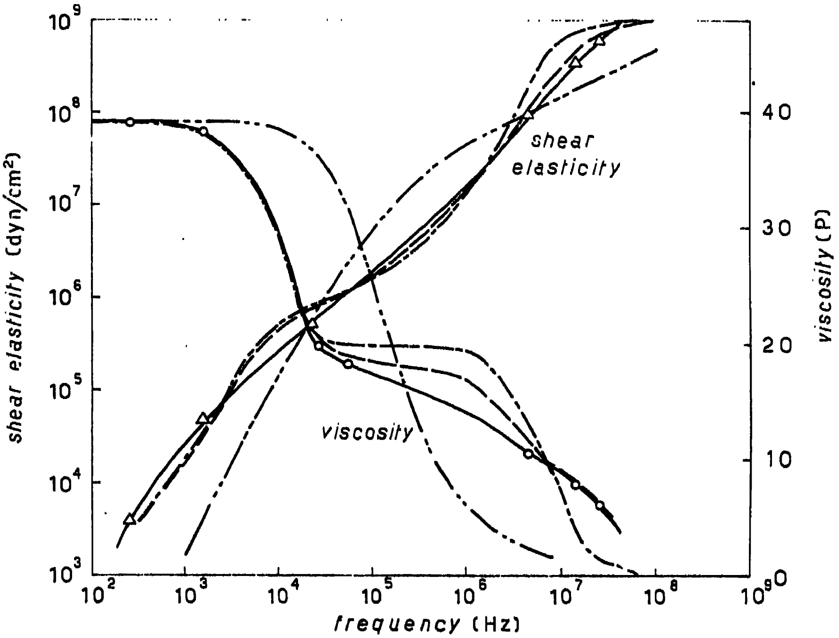

Fig. 11. – Measurements for 1660 molecular weight polyisobutylene liquid: —·—·— calculated from network; – – – calculated with hysteresis component in μ_s; —··—··— Rouse-Bueche-Zimm theory.

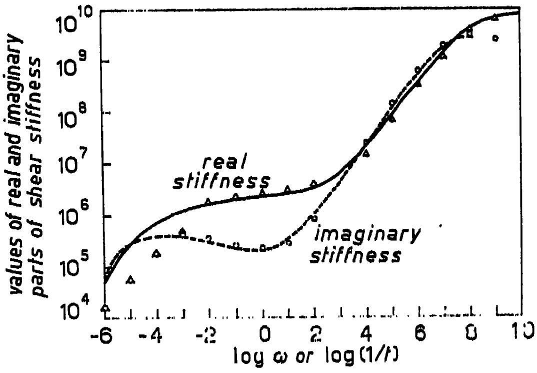

Fig. 12. – Real and imaginary stiffness components of bureau of standards poly-isobutylene of $1.5 \cdot 10^6$ M.W., $\eta_0 = 6.16 \cdot 10^{10}$ poise, $T = 25$ °C (after MARVIN). Triangles and circles represent calculated real and imaginary stiffness from network of Fig. 28.

All the measurements reported so far are for shear waves, and for polymers in solution. This is because the compressional modulus of the solvent is affected very little by the introduction of a small amount of polymer chains, and shear waves are required for any chemical interpretation. Longitudinal waves can give additional information for polymer liquids since they can determine the compressional viscosity effects when their measurements are compared with those for shear waves for the same liquids. Figure 14 shows measurements [14] of the attenuation per wavelength and the velocity dispersion of the same set of polymer liquids given on Fig. 13, plotted as a product of the frequency times a viscosity. This method was an early form of a reduction formula. These measurements show that the attenuation is not in the form of a simple relaxation shown by the dot-dash line of Fig. 14(*a*) and moreover is not symmetrical with respect to the low and high frequency ranges. For high frequencies the attenuation per wavelength appears to approach a constant value independent of the frequency. This type of loss indicates a hysteresis type of mechanism in which a constant loss per herz occurs. A possible mechanism for this effect is discussed in Section 6. Rubber materials have been measured by a variety of techniques including the transducer technique

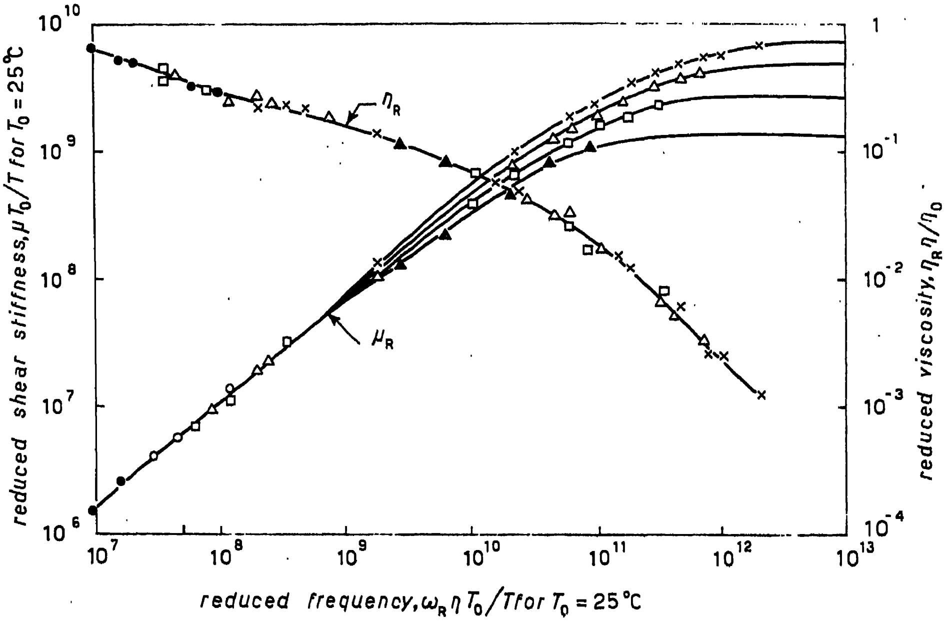

Fig. 13. – Reduced shear stiffness and viscosity for polyisobutylene for molecular weights from 8100 to 8300: × 15 °C; △ 25 °C; □ 35 °C; ⊙ 45 °C; ▲ 50 °C; ● 55 °C

of Fig. 6, and the vibrating tuning fork technique of Rorden and Grieco [15] and Hopkins [16]. Figure 15 shows a contour map [17] of the properties of the shear stiffness E_1 and the ratio of the imaginary part E_2 to E_1 plotted as

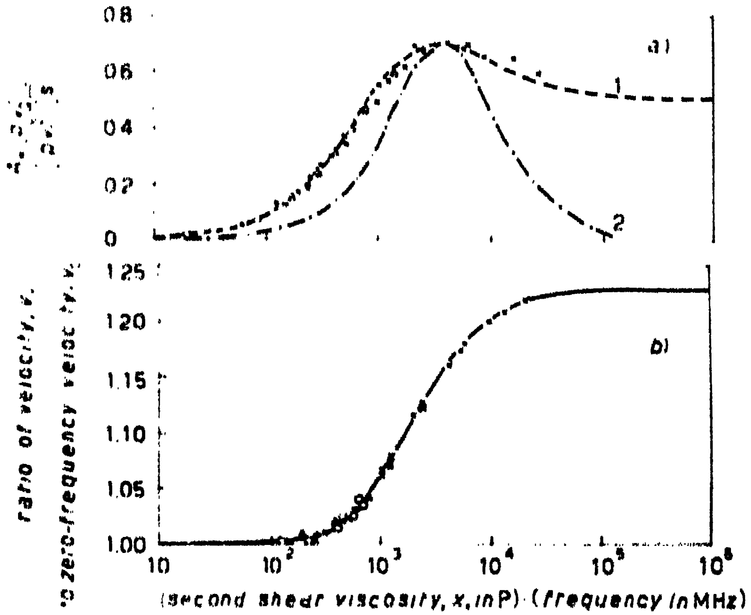

Fig. 14. *a*) Attenuation per wave length and velocity dispersion of three polyisobutylene polymer liquids (after Mason, Baker, McSkimin and Heiss): · polymer *d*; △ polymer *e*; ○ polymer *b*; *b*) attenuation per wave length and velocity dispersion of three polyisobutylene polymer liquids (after Mason, Baker, McSkimin and Heiss): · polymer *d*; △ polymer *e*; ○ polymer *b*.

a function of both frequency and temperature. For a given frequency as the temperature decreases the stiffness goes from a rubbery region where the stiffness is in the order of 10^7 dyn/cm^2 to the «glassy» region where the stiffness is above 10^{10} dyn/cm^2. At the highest frequency of 10^8 Hz the material is always in the high modulus region. As discussed in the later sections, this is because the smallest regular segment of the chain can no longer move about in the time of a cycle of the impressed stress wave, and appears to be frozen in position. The lower curve shows that the internal friction $E_2/E_1 = Q^{-1}$ reaches a maximum when the rate of change of the elastic modulus E_1 is greatest with respect to either temperature or frequency. This is consistent with a relaxation process. It will be noted by comparing Fig. 12 and Fig. 15 that above a certain frequency, the mechanical properties of long chain liquids and of rubbers are quite comparable. As indicated in later sections, this appears to be due to the fact that restricted polymer segments of approximately the same length are operative in both the long chain liquids and in the rubbers. However, if the period of stress application is made long enough, the long chain liquid approaches the action of a very viscous liquid whereas the rubber always has a stiffness no matter how long the application of a stress. This is due to the cross-linking which does not occur in the liquid.

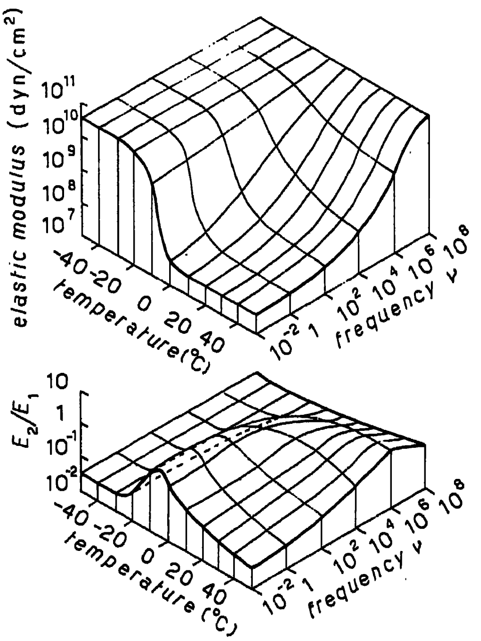

Fig. 15. – Contour map of real and imaginary components of the shear stiffness of Buna rubber (after A. W. NOLLE).

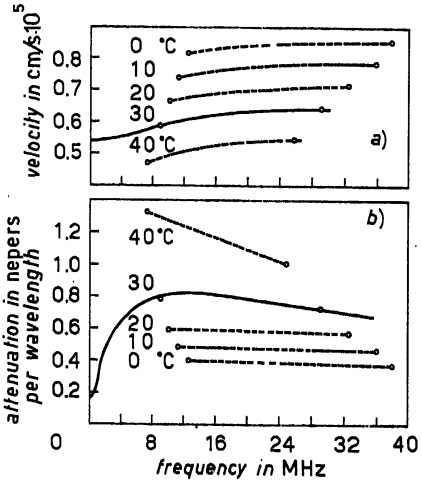

Fig. 16. – Shear velocity (*a*) and shear attenuation (*b*) for polyethylene as a function of the frequency (after MC SKIMIN).

Some of the less cross-linked polymer solids show relaxations which appear to be associated with the motions of the shortest segment lengths. Figures 16(*a*) and 16(*b*) show measurements [18] of the shear modulus and attenuation per

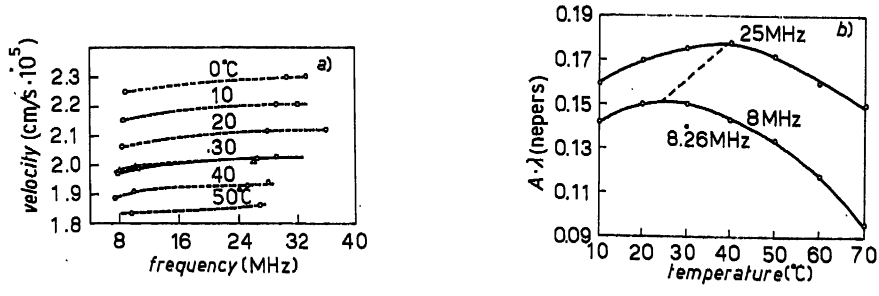

Fig. 17. – Longitudinal velocity (*a*) and longitudinal attenuation (*b*) for polyethylene as a function of the frequency and temperature (after MC SKIMIN).

wave length of polyethylene of « equilibrium » crystallinity and average molecular weight corresponding to an intrinsic viscosity in xylene $[\eta]$ of 0.89 at 85 °C. These measurements can be fitted by a single relaxation mechanism having a relaxation frequency of 8 MHz for a temperature of 30 °C. The corresponding longitudinal measurements are shown by Fig. 17(*a*) and 17(*b*). If we compare the two sets of measurements it appears that most of the loss is accounted for by the shear relaxation, but that a compressional viscosity about $\frac{1}{4}$ that of the shear viscosity is indicated.

4. – Phenomenological interpretation.

All the measured stiffnesses and viscosities given in Fig. 7 to 17 show an increase of stiffness and a decrease in the effective viscosity as the frequency increases. This behavior is characteristic of a series of relaxation effects which are caused in polymers by an inhibition of the motion of different segments of the polymer chain which are not able to follow the increased rapidity of stress alternation.

These changes can be reproduced in phenomenological form by means of models which consist of combinations of dash pots and springs or the equivalent electrical circuits employing combinations of resistances and capacitances. Two different forms are possible depending on whether these elements are all in series or all in parallel. In the present section the equivalent electrical representation is considered the fundamental one since it is easier to interpret it in terms of the networks theory discussed in Section 5. However, the equivalent dash pot and spring models are also shown.

The simplest and most widely used model was originally due to MAXWELL [9] who devised it to consider the relaxation time associated with a change in shape of a volume of gas or liquid. He conceived the idea that if a change of shape (shearing displacement) occurred instantaneously, this change would be opposed by elastic forces. In the course of a very short time the molecules or chains in a polymer will move so that all the elastic stresses are relieved and the conditions are restored to the original state before the change in shape. Maxwell's model, which applies quite well for the shear stiffness properties of simple liquids and short chain polymers, is shown by Fig. 18. The left side of the figure shows the single relaxation circuit while the circuit on the right shows the multiple element model which is usually required for most materials.

For sinusoidal vibrations, the relation between the stress T_{12} and the strain S_{12} can be written in the form

$$T_{12} = \left(\frac{j\omega\eta}{1 + j(\omega\eta/\mu)}\right) S_{12} = \left(\frac{j\omega\eta}{1 + j\omega/\omega_0}\right) S_{12} = \frac{\eta \dot{S}_{12}}{(1 + j\omega/\omega_0)}, \tag{15}$$

where $f_0 = \omega_0/2\pi$ is the relaxation frequency given by

$$f_0 = \frac{\mu}{2\pi\eta} = \frac{1}{2\pi t_0} \,. \tag{16}$$

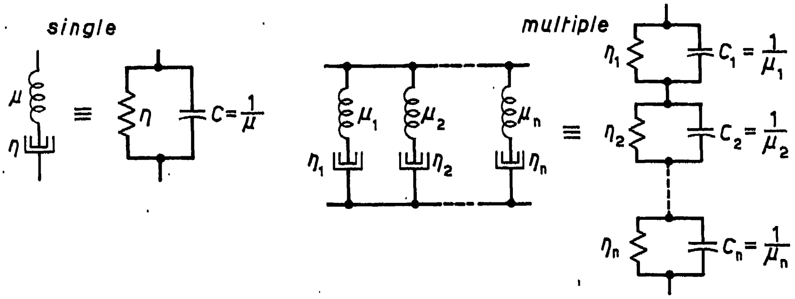

Fig. 18. – Maxwell model, multiple Maxwell model and equivalent electrical circuits.

t_0, the Maxwellian relaxation time, is equal to $t_0 = 1/\omega_0 = \eta/\mu$. If the relaxation time is much shorter than the time of application of the stress, as it is in most light liquids, the ratio between the stress and the time rate of change of the strain is the shear viscosity η.

The multiple relaxation model will have a sum of terms of the form of (15). If we separate out the real and imaginary parts, the stress-strain rate equation can be written in the form

$$T_{12} = \left(\eta_A + \frac{j\mu_A}{\omega}\right)\dot{S}_{12} \quad \text{where} \quad \eta_A = \sum_{i=1}^{n} \frac{\mu_i \tau_i}{1 + \omega^2 \tau_i}; \qquad \mu_A = \sum_{i=1}^{n} \frac{\mu_i \omega^2 \tau_i^2}{1 + \omega^2 \tau_i^2}, \tag{17}$$

where $\tau_i = \eta_i/\mu_i$. From these equations it is evident that the effective value of η_A will decrease as the frequency increases, while the effective stiffness μ_A will increase up to a value

$$(\mu_A)_{\text{Max}} = \sum \mu_i \,. \tag{18}$$

At low frequencies, since $\mu_i \tau_i = \eta_i$, then the static viscosity will be the sum of all the viscosities associated with the relaxation mechanisms. The effective value η_A decreases as the frequency increases.

When polymer chains are immersed in a solvent of low viscosity, the relaxation time of the solvent is so low that its shear stiffness can be neglected. This corresponds to an equivalent circuit of Fig. 18(*b*) for which the first relaxation element has only a viscosity term, which is designated η_s, the solvent viscosity. The frequency variable term η_A then represents the difference between the measured viscosity η_0 and η_s so that

$$(19) \qquad \eta_A = \eta_0 - \eta_s = \sum_{i=2}^{\infty} \frac{\mu_i \tau_i}{1+\omega^2\tau_i^2}; \qquad \mu_A = \sum_{i=2}^{\infty} \frac{\mu_i \omega^2 \tau_i^2}{1+\omega^2\tau_i^2}.$$

This is the form of the impedance of the network model discussed in the next section.

When one wishes to fit measured curves in order to obtain the relaxation frequency distribution, there are several methods that have been employed. If the distribution is not too broad, usable results are sometimes obtained by assuming [20] a series of activation energies differing by a definite factor and assigning a series of constants μ_i to match the values of μ_A or $\eta_0 - \eta_s$ at the resulting relaxation times τ_i. It is only necessary to match one or the other component, for by the Kronig-Kramers equations [21] there is a relation between the matched one and the unmatched one. This is obvious from the form of eq. (19), for if we determine a series of relaxation times τ_1 and shear stiffnesses μ_i to fit the μ_A curve, then the same set of constants determine the $\eta_0 - \eta_s$ function. In fact, ZIMM [22] has suggested that a measurement of the real component—which is more easily measured then the reactive component—is all that is necessary since the reactive component is thereby determined.

There are a number of methods [23] for determining the distributions of relaxation times from the form of the measured shear stiffness or viscosity, but since the relaxation spectra for all cases considered here are obtainable from the network method discussed in Section 5, the reader is referred to other references [23] for the details of the calculations.

The alternate representation due to VOIGT considers a series of elements in parallel as shown in electrical equivalent form in Fig. 19(*a*) and as a series

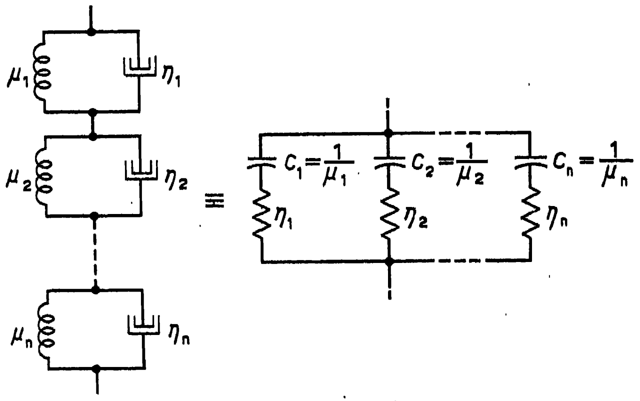

a) b)

Fig. 19. – Multiple Voigt model and equivalent electrical circuit.

of dash pots and springs by Fig. 19(*b*). The Voigt representation is particularly useful when we are dealing with the complex compliance, *i.e.*, the ratio of the strain rate to the applied stress. Since all the measurements given previously are expressed in terms of the complex stiffness, this model will not be discussed further.

Finally, it should be mentioned that a large number of viscoelastic measurements are made by suddenly applying a fixed value of stress, and observing the time rate of deformation of the material. This function is known as the creep function. An alternate method is to apply a constant fixed deformation and measure how the stress relaxes as a function of time. These methods are particularly useful when the response time of the polymer material involves very long times. As discussed in a number of references [23] there are integral relations between the moduli determined by these methods, and the ones determined by sinusoidal stress variations. Since these methods are not discussed here, the reader is referred to the above references for a discussion of the relations.

5. – Atomic interpretation of motion of polymer chains.

5'1. *Chain lengths and mean square separation of chain ends.* – The elasticity exhibited by long chain polymers in the form of single molecules depends principally on the configurations that such molecules can take when acted upon by both stresses and thermal agitation. The statistical treatment of a single molecule is a problem that has not been completely solved. The solutions that have been given involve the representation of a molecule by an idealized mathematical abstraction. Furthermore, the solutions obtained can be carried to various stages of approximation only the first of which is considered here. Hence, the strains considered have to be kept small. Higher approximations have been discussed in a number of references [24] and are required if large strains are to be considered.

The problem of the calculation of the statistical properties is essentially the same for linear polymers irrespective of the details of the structure. One of the simplest chains to consider is the paraffin or polyethylene molecule $(CH_2)_n$. It is usually assumed that each carbon-carbon bond permits free rotation about a carbon atom as shown by Fig. 20(*a*). Hence, the bond C_2—C_3 can be considered to rotate about the C_1—C_2 axis, while C_3—C_4 can rotate about the C_2—C_3 axis, etc. Under the effect of thermal agitation, which causes the bonds to move around at an increasing rate as the temperature increases, the chain will in general assume the kinked form shown by Fig. 20(*b*). The actual configuration will be subject to continued fluctuation due to the effects of thermal agitation. We cannot define the precise form of the molecule but we can specify some of the statistical properties such as the root mean square distance between any two points of the molecule (which is usually taken as the distance between the ends of the chain) and we can define the probability of any gives distance r between the ends.

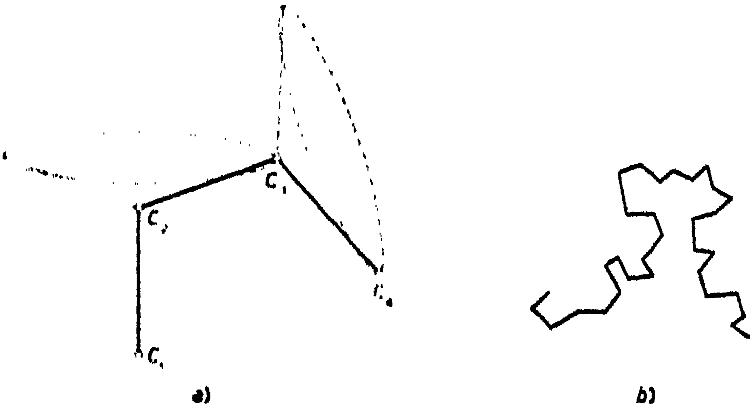

Fig. 20. – *a*) **Rotations about bonds in paraffin molecule;** *b*) **randomly kinked chain (after Treloar).**

For the polyethylene molecule, Eyring [25] has calculated the mean square length on the assumption that all configurations can occur with equal probability. For the polyethylene chain, the valence angle between adjacent bonds is 109.5°. Eyring's result is

$$r^2 = l^2[n + 2(n-1)\cos\alpha + 2(n-2)\cos^2\alpha + \ldots + 2\cos^{n-1}\alpha]\,, \tag{20}$$

where l is the length of a segment C_1–C_2, α is the semi-angle of the cone of rotation and n is the number of lengths. If n is large, this expression reduces to the simpler form

$$\sigma^2 = nl^2\left(\frac{1+\cos\alpha}{1-\cos\alpha}\right), \tag{21}$$

where σ is the root mean square value of r. Hence, the distance between ends is proportional to the square root of the number of segments. For polyethylene, $\alpha = 70.5°$ and hence

$$\sigma^2 = 2l^2n\,. \tag{22}$$

These considerations assume free rotation about the C—C bonds. Very often, however, there are attractions between adjacent molecules and steric hindrance to free rotation. These considerations result in energy barriers which have to be surmounted by thermal agitation. These effects result in values which are still proportional to the square root of n but with factors multiplying l which are somewhat temperature-sensitive.

Polyisobutylene, for which measurements are given in Section 3, follows an equation

$$\sigma^2 \doteq 1.1 \cdot 10^{-16} M, \tag{23}$$

where M is the molecular weight. Since the molecular weight of the repeating element shown by Table I is 56, the effective length of a chain segment is 7.8 Å compared to the measured values of 3.4 Å, a factor of 2.3.

5'2. *The probability function of long chain molecules.* – For a more complete discussion of the elastic properties of long chain molecules, it is necessary to specify more completely the distribution of r values about the mean. This requires the determination of a distribution function which expresses the probability of a chain having an end-to-end separation having a value r. Thus, if one end of the chain is fixed at the origin of co-ordinates as shown by Fig. 21, the other end B will move in a random manner through space. Choosing a small element of volume dV in the neighborhood of the point P, the probability that the end B will be found at any instant within this volume will be some function $\Psi(x, y, z)$ times the volume element dV. The problem of finding this function Ψ has only been solved in the case of the idealized chain of equal lengths joined entirely at random. The conception of the completely random jointing is in the sense that the direction in space of any given length is entirely independent of the direction of neighboring lengths. When valence-angle corrections or partially hindered rotations are taken account of, this is done by increasing the fundamental length l by the appropriate factor.

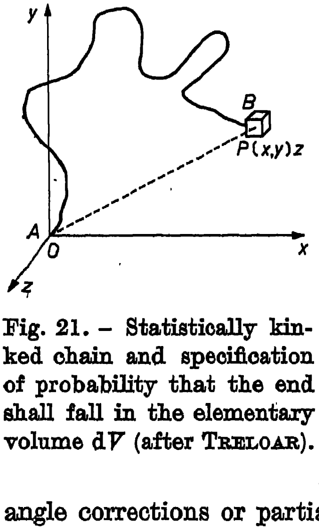

Fig. 21. – Statistically kinked chain and specification of probability that the end shall fall in the elementary volume dV (after Treloar).

The problem of evaluating the function Ψ consists essentially in evaluating the relative number of configurations of the chains for given values of x, y and z. The solution was first given in approximate form by Kuhn [26] and by Guth and Mark [26]. The required probability is proportional to the number of configurations, and for a chain of n lengths, each having a length l, the solution was obtained in the form

$$\Psi(x, y, z)\, \mathrm{d}x\, \mathrm{d}y\, \mathrm{d}z = C \exp[-\beta(x^2 + y^2 + z^2)]\, \mathrm{d}x\, \mathrm{d}y\, \mathrm{d}z, \tag{24}$$

where C and β are constants. Since $x^2+y^2+z^2=r^2$ and $\mathrm{d}x\,\mathrm{d}y\,\mathrm{d}z=4\pi r^2\,\mathrm{d}r$, the integral of the probability function is

$$4\pi C\int \exp\,[-\beta r^2]r^2\,\mathrm{d}r = 4\pi C\left[\frac{1}{4\beta}\sqrt{\frac{\pi}{\beta}}\right]. \tag{25}$$

Since the probability of finding the chain somewhere in the volume is unity,

$$C=(\beta/\pi)^{\frac{3}{2}}. \tag{26}$$

The constant β can be evaluated in terms of the root mean square value of $r=\sigma$. This value can be obtained by evaluating the integral

$$\sigma^2=\bar{r}^2=\int_0^\infty r^2(\Psi(r)\,\mathrm{d}V= \tag{27}$$

$$=4\pi\left(\frac{\beta}{\pi}\right)^{\frac{3}{2}}\int_0^\infty r^4\exp\,[-\beta r^2]\,\mathrm{d}r=4\pi\left(\frac{\beta}{\pi}\right)^{\frac{3}{2}}\left(\frac{1\times 3}{2\times 4\beta^2}\sqrt{\frac{\pi}{\beta}}\right)=\frac{3}{2\beta}.$$

Hence,

$$\beta=\frac{3}{2\sigma^2}.$$

The formula (24) is of fundamental importance in the theory of rubber elasticity and in the properties of polymer solutions, liquids and solids. Its form is that of a Gaussian error function, which appears often in statistical problems involving the superposition of random effects. It has interesting properties which will now be discussed.

The form of eq. (24) with $x^2+y^2+z^2$ being replaced by r^2 shows that the function is spherically symmetrical. Furthermore, the function Ψ will be a maximum when $r=0$, which shows that if a chain is fixed at one point, the most probable position for the other end is at the same point. Secondly, the distribution $\Psi(x, y, z)$ can be regarded as the product of three separate probabilities

$$\Psi(x,y,z)=(\beta/\pi)^{\frac{3}{2}}\exp\,[-\beta x^2]\,\mathrm{d}x\exp\,[-\beta y^2]\,\mathrm{d}y\exp\,[-\beta z^2]\,\mathrm{d}z \tag{28}$$

so that integrating over all the values of y and z, we are left with the distribution function for the components of length in the direction of x in the form

$$\Psi(x)\,\mathrm{d}x=(\beta/\pi)^{\frac{1}{2}}\exp\,[-\beta x^2]\,\mathrm{d}x. \tag{29}$$

A plot is equation is shown by Fig. 22(*a*). The most probable value of x is zero, while the probability of any other value of x is independent of the values of y and z. Although the most probable value of x is zero, this does not imply that the most probable length of the chain is zero. This follows because we have to multiply the probability density by the magnitude of the appropriate volume element $\mathrm{d}V$. For the case of spherical symmetry, this volume element will be $4\pi r^2\,\mathrm{d}r$. Hence, the required probability is

$$\Psi(r)\,\mathrm{d}V = \tag{30}$$
$$= (\beta/\pi)^{\frac{3}{2}} \exp[-\beta r^2](4\pi r^2)\,\mathrm{d}r\,.$$

This function is a maximum, as shown by Fig. 22(*b*), when

$$r^2 = \frac{1}{\beta} = \frac{2}{3}\sigma^2 = \frac{2l_E^2}{3}n\,, \tag{31}$$

where l_E is the effective length of the chain segment and n the number of segments. Hence, the most probable length is proportional to the square root of the number of segments times their effective length.

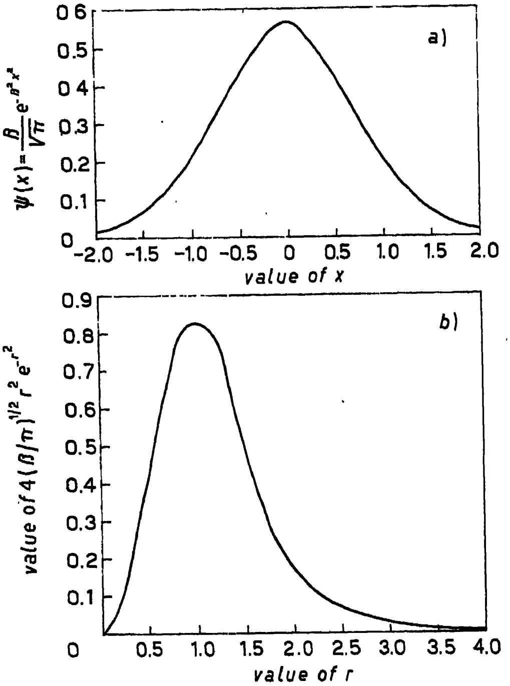

Fig. 22. – Distribution functions
(*a*) $\Psi(x) =$ constant $\exp[-\beta x^2]$,
(*b*) $\Psi(r) =$ constant $r^2 \exp[-\beta r^2]$ (after TRELOAR).

5·3. *The elasticity of long chain molecules.* – When the motion of the molecule is unrestricted by internal energy barriers, the internal energy will be the same for all configurations. With this assumption the Helmholtz free energy A, which is defined as

$$A = U - TS \tag{32}$$

will be determined solely by the last term which is the product of the absolute temperature T by the entropy S. If the chain is considered to be isolated and free, as can be realized by dissolving molecules in a large excess of a neutral liquid, *i.e.*, a solvent such that there is no heat of mixing, all configurations are possible. The reaction of such dissolved molecules is discussed in the next section.

If we fix one end of the molecules at the point of Fig. 21, and restrict the other end to the small volume $\mathrm{d}V$, the number of configurations available to the chain is proportional to the probability function Ψ times the elementary volume $\mathrm{d}V$. If we let the point P take different positions keeping $\mathrm{d}V$ constant, the relative number of positions will depend only on r and will be given by $\exp[-\beta r^2]$. The entropy being proportional to the logarithm of the number of available configurations will be

$$S = C - k\beta r^2 , \tag{33}$$

where C is an arbitrary constant and k is Boltzmann's constant. The constant C includes the size of the volume element $\mathrm{d}V$ and shows that we are concerned only with differences in entropy and not in absolute values.

Equation (33) shows that the entropy is a maximum when $r=0$ and decreases as r increases. If now we move one end from r to $r+\mathrm{d}r$, work is done. This requires a force

$$F = \frac{\mathrm{d}w}{\mathrm{d}r} = \frac{\mathrm{d}A}{\mathrm{d}r} = -T\frac{\mathrm{d}S}{\mathrm{d}r} = 2kT\beta r = \frac{3kTr}{\sigma^2} . \tag{34}$$

Thus, a molecule with its ends fixed at specified points is acted on by a tensile force in the direction of the line joining its ends and proportional to the length of the line. Since the tension is proportional to the length, the molecule can be considered to have an elasticity governed by Hooke's law, with a constant which is proportional to the absolute temperature. This stress is of course a fluctuating quantity and eq. (34) represents the average value.

5·4. *Theory of coiled molecules in solutions.* – Although the phenomenological description given in Section 4 is of great value in interrelating various types of measurements, it provides no insight into the molecular origin of viscoelastic behavior. Qualitatively, it has been emphasized that the effects are associated with the possibility of motion for various parts of the thread-like molecules.

The most complete theories of polymer motions deal only with deformation by shear stresses or the related extension with negligible change in volume. The subject of bulk behavior has not yet been theoretically treated. The most comprehensive treatments have dealt with the behavior of polymer molecules in dilute solutions of solvents. When a dilute solution of polymer molecules is subject to a shearing stress, the flowing solvent distorts the molecule from its Gaussian distribution. Thermal agitation tends to restore the equilibrium and the viscoelastic behavior is determined by the interaction of the two effects.

The first complete theory of this effect was due to ROUSE [27], who assumes that the polymer molecule can be divided into N segments of such a length that at equilibrium the separation of its ends obeys the Gaussian probability function (24). The model considered by ROUSE lumps all the thermodynamic spring action in one element and all the viscous effect in a weightless bead which is dragged through the solution. Figure 23(a) shows a slight modification of the Rouse model for which the chain ends up in a spring corresponding to half a segment, since it is assumed that the location of the bead is at the center of the segment. This arrangement fits better with the derivation to be given below. It should be emphasized that each spring represents the action of a kinked chain of the form shown by Fig. 20(b) while the bead represents the viscous drag of the whole segment as it is pulled through the solvent. A similar model was later discussed by BUECHE [28] without specifically taking account of the Brownian motion effect, but with quite similar results. Rouse's model can be considered a free draining model since no account was taken of the hydrodynamic interaction between chain segments. This interaction was later taken account of by ZIMM [29]. The present discussion is limited to the free draining model.

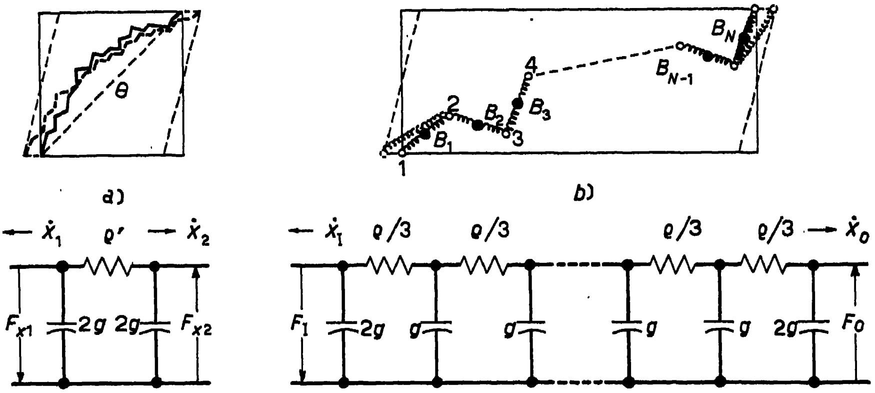

Fig. 23. – Representation of the action of a polymer segment by springs and beads. Dashed lines show distortion of chain by shearing strain in liquid.

The measurements of Fig. 7, 8 and 9, at high frequencies show that the viscosity of the polymer solution is only about 10 % higher than the viscosity of the solvent alone. This result strongly supports the hypothesis that the primary effect of the velocity gradient is to carry each segment along with the liquid. The motion, however, will disturb the equilibrium distribution of the molecular segments, and thermal agitation will cause a redistribution of positions with a subsequent motion of the polymer segments through the liquid. At low frequencies, this effect manifests itself as an increased viscosity of the solution over that of the solvent. As the frequency becomes higher, there is no time for all redistributions to become complete and the polymer motion lags behind the applied stress, giving a complex viscosity, *i.e.*, a shear stiffness effect. At the highest frequencies, no complete motions can occur, and the polymer reaction is a stiffness reaction for which a displacement of the polymer segments can take place in synchronism with the shearing motion of the liquid, but no motion of the segment through the liquid occurs. Under these conditions, the viscosity is the viscosity of the solvent, whereas the stiffness is the sum of the stiffness of all the segments.

Rouse's method of solution is to evaluate the normal modes of the network under the condition that the probability function ψ satisfies the equation of continuity. This method does not take full advantage of network theory and in the interest of simplicity and in order to apply the network theory for a higher frequency approximation, a somewhat different method is adopted here. The method of deriving the equations can be illustrated by means of the single segment of Fig. 23(*a*). Suppose that the ends of the segment 1, 2 lie in the x-z plane at an angle θ with the x axis. If the liquid is sheared by a plane wave propagating along the z axis with its displacement direction along x, the liquid will be disturbed as shown by the dashed line. As mentioned above experiment indicates that the effect of the shearing displacement is to carry the ends of the segment along with the liquid so that point 1 goes to 1′ and 2 to 2′. All the motion occurs in the x direction.

The form of the probability function ψ of eq. (24), when both ends can move is

$$\psi(x, y, z) = C \exp\left[-\beta((x_2 - x_1)^2 + (y_2 - y_1)^2 + (z_2 - z_1)^2)\right] . \tag{35}$$

Hence the force exerted by the medium on the segment is

$$\begin{cases} F_{x_2} = -kT \dfrac{\partial \log \psi}{\partial x_2} = 2\beta kT(x_2 - x_1) = \dfrac{3kT}{\sigma^2}(x_2 - x_1) , \\ F_{x_1} = -kT \dfrac{\partial \log \psi}{\partial x_1} = -2\beta kT(x_2 - x_1) = -\dfrac{3kT}{\sigma^2}(x^2 - x_1) , \end{cases} \tag{36}$$

when use is made of eq. (27) to evaluate β. If the shearing strain in the liquid is $S_{13} = \partial u/\partial z$, where u is the displacement in the x direction, then the distance $x_2 - x_1$ can be written in the form

$$x_2 - x_1 = x_{20} - x_{10} + S_{13}\sigma \cos\theta , \tag{37}$$

where σ is the chain end separation and θ is the angle between the direction of the chain ends and the z axis. Hence the force on the chain exerted by the fluid motion is

$$(38) \qquad F_{x_2} = \frac{3kT}{\sigma} S_{13} \cos\theta ; \qquad F_{x_1} = -\frac{3kT}{\sigma} S_{13} \cos\theta .$$

The displacement of each end of the segment is

$$(39) \qquad x_2 = \frac{S_{13}\sigma}{2} \cos\theta ; \qquad x_1 = -\frac{S_{13}\sigma}{2} \cos\theta .$$

Hence the rate of doing work is for sinusoidal vibrations

$$(40) \qquad F_{x_2}\dot{x}_2 + F_{x_1}\dot{x}_1 = j\omega(3kTS_{13}^2) = -\frac{j}{\omega}(3kT\dot{S}_{13}^2 \cos^2\theta) ,$$

where $\dot{S}_{13}$ is the time rate of change of the shearing stress. Since segments can occur in all directions, we have to average the values of $\cos^2\theta$. This is given by

$$(41) \qquad \overline{\cos^2\theta} = \frac{\int_0^\pi \cos^2\theta \sin\theta \, d\theta}{\int_0^\pi \sin\theta \, d\theta} = \frac{1}{3} .$$

Hence the effect of a single segment is to introduce a shear stiffness equal to kT. If there are N segments per unit volume, the stiffness introduced is NkT. The shearing strain will also introduce a dissipation in the solvent which becomes equal to

$$(42) \qquad \dot{S}_{13}^2 \eta_s .$$

Hence the effect of introducing a number of single segments into the liquid is the cause a stiffness proportional to NkT. It turns out that at very high frequency for which the long chain segments cannot move through the liquid, the same expression holds.

On examining Fig. 23(*a*), it is seen that the reason why the single segments do not contribute to the viscosity, is that with the symmetrical application of the shearing motion only the ends move out and there is no motion of the viscous bead with respect to the liquid. For structures having N elements, as shown by Fig. 23(*b*), and two adjacent segments at angles of θ_1 and θ_2 respectively with the z axis, the force on the point 2 is the sum of the force exerted by the medium and the reaction between the two chains. Hence F_2 does not necessarily equal F_1 and motions of beads 1 and 2 now occur through the liquid. These produce an extra drag due to the polymer molecules. At the common point 2 all the displacements of chain 1 equal those of chain 2 and the force exerted by chain 1 on chain 2 is the negative of that exerted by chain 2 on chain 1.

An equivalent electrical circuit which represents the action of a single segment is shown by Fig. 23(*a*). Here $2g$ is twice the stiffness constant, *i.e.*, $6kT/\sigma^2$. The resistance ϱ' shown represents the viscous drag introduced by the bead as it is pulled through the liquid in the x direction. It is evident from Fig. 23(*b*) that all the motion is not necessarily along the x direction and in general the total drag will be larger than ϱ'. The relation requires a solution of the diffusion equations for the probability functions ψ which is not attempted here. As might be expected the result indicates that $\varrho' = \varrho/3$, where ϱ is the total drag on the bead as it moves through the liquid. From the equivalent circuit of Fig. 23(*a*), with the forces and velocities directed as shown we have the mesh equations

$$(42)\qquad \left\{\begin{aligned} & F_1 - \frac{2jg}{\omega}\dot{x}_A = 0; \quad \dot{x}_1 + \dot{x}_m + \dot{x}_A = 0; \quad \dot{x}_m = \dot{x}_B + \dot{x}_1; \quad F_2 = -\frac{j2g\dot{x}_B}{\omega}, \\ & F_1 + F_2 = \frac{\varrho}{3}\dot{x}_m . \end{aligned}\right.$$

In terms of the output and input forces and velocities, these equations can be assembled in the form

$$(43)\qquad \left\{\begin{aligned} & \dot{x}_2 = -\dot{x}_1\left[1 + \frac{j\omega\varrho}{6g}\right] + \frac{j\omega}{g}F_1\left[1 + \frac{j\omega\varrho}{12g}\right], \\ & F_2 = -F_1\left[1 + \frac{j\omega\varrho}{6g}\right] + \frac{\varrho}{3}\dot{x}_1 . \end{aligned}\right.$$

At this point it becomes convenient to introduce the propagation constant Γ and the characteristic impedance Z_0 of a network, which in terms of the forces and velocities shown in Fig. 23(*a*) will be written [30] in the form

$$(44)\qquad \dot{x}_2 = -\dot{x}_1\cosh\Gamma + \frac{F_1}{Z_0}\sinh\Gamma; \qquad F_2 = -F_1\cosh\Gamma + \dot{x}_1 Z_0\sinh\Gamma .$$

Comparing this equation to (39), we have

$$(45)\qquad \left\{\begin{aligned} & \cosh\Gamma = 1 + \frac{j\omega\varrho}{6g} = 1 + \frac{j\omega}{2\omega_0}, \\ & Z_0 = \frac{\varrho}{3}\sqrt{-\frac{j3g/\varrho}{\omega(1 + j\omega\varrho/12g)}} = \frac{\varrho}{3}\sqrt{-\frac{j\omega_0}{\omega(1 + j\omega/4\omega_0)}}, \\ & \sinh\Gamma = \cosh^2\Gamma - 1 = \sqrt{\frac{j\omega}{\omega_0} - \frac{\omega^2}{4\omega_0^2}}; \end{aligned}\right.$$

where

$$\omega_0 = \frac{3g}{\varrho} = \frac{9kT}{\varrho\sigma^2} \,. \tag{46}$$

Since the two sections are joined together and the forces at their junctions are equal and opposite, we have the relation between two adjacent sections

$$\dot{x}_3 = -\dot{x}_2 \,; \qquad F_3 = -F_2 \,. \tag{47}$$

If we apply these conditions between two adjacent sections, having equations of the type shown by (44), we find that in terms of the input velocity $\dot{x}_I$ and input force F_I and the output velocity and force $\dot{x}_0$ and F_0, the relations

$$\left\{\begin{aligned} F_0 &= -F_I[\cosh^2\Gamma + \sinh^2\Gamma] + \dot{x}_I Z_0[2\sinh\Gamma\cosh\Gamma] \\ &= -F_I\cosh 2\Gamma + \dot{x}_I Z_0 \sinh 2\Gamma \,, \\ \dot{x}_0 &= -\dot{x}_I[\cosh^2\Gamma + \sinh^2\Gamma] + \frac{F_I}{Z_0}[2\sinh\Gamma\cosh\Gamma] \\ &= -\dot{x}_I\cosh 2\Gamma + \frac{F_I}{Z_0}\sinh 2\Gamma \,. \end{aligned}\right. \tag{48}$$

Hence with these parameters the propagation constants are additive and similar equations hold for N adjacent segments with N replacing the 2 of eqs. (48).

To calculate the effect of such a molecule introduced in the solvent we note that the effect of a shearing wave is to move the various segments without moving the center of gravity of the polymer. Since the forces on the two ends are equal and opposite, this requires that the force at the center be zero. Hence F_0 is zero if the number of sections in (44) is $N/2$ and the ratio of the input force to the input velocity is

$$F_I = \dot{x}_I Z_0 \operatorname{tgh} N\Gamma/2 \,. \tag{49}$$

The energy into the network can be calculated with reference to the arrangement of Fig. 23(*c*). The end-to-end chain length of the total molecule is by eq. (22)

$$l^2 = l_0^2 n_t \,, \tag{50}$$

where l_0 is the effective length of a single monomer and n_t is the total number of monomer lengths. If there are n_s of these lengths in the fundamental segment under consideration then

$$\sigma^2 = l_0^2 n_s \,. \tag{51}$$

The total number of segments N will be

$$N = n_l/n_s \tag{52}$$

and hence

$$l^2 = N\sigma^2 . \tag{53}$$

The velocities imparted to the ends of the chain will be

$$\dot{x}_l = -\left[\frac{\dot{S}_{13} l \cos\theta}{2}\right] = -\left[\frac{\dot{S}_{13}\sqrt{N}\sigma\cos\theta}{2}\right]; \qquad \dot{x}_N = \left[\frac{\dot{S}_{13}\sqrt{N}\sigma\cos\theta}{2}\right]. \tag{54}$$

The force exerted by this displacement velocity is $\dot{x}_1 Z_0 \operatorname{tgh} N\Gamma/2$ and hence the rate of doing work is

$$F_l\dot{x}_l + F_0\dot{x}_0 = 2\left[\frac{\dot{S}_{13}\sqrt{N}\sigma\cos\theta}{2}\right]^2 Z_0 \operatorname{tgh} N\Gamma/2 . \tag{55}$$

Averaging over the square of $\cos\theta$, adding the dissipation due to the solvent and assuming n molecules per cm^3, the effective complex stiffness of the solution is

$$\eta_A - \frac{j\mu_A}{\omega} = \eta_s + \frac{nN\sigma^2}{6} Z_0 \operatorname{tgh} N\Gamma/2 . \tag{56}$$

Several limiting values are evident from this equation. For very low frequencies

$$Z_0 \operatorname{tgh} N\Gamma/2 \doteq \frac{\varrho}{3}\sqrt{-\frac{j\omega_0}{\omega}} \times \frac{N}{2}\left(\sqrt{\frac{j\omega}{\omega_0}}\right) = \frac{N\varrho}{6}, \tag{57}$$

and the viscosity of the solution is

$$\eta_0 = \eta_s + \frac{nN^2\sigma^2\varrho}{36}, \tag{58}$$

in agreement with the results of Rouse. At very high frequencies, $\operatorname{tgh} N\Gamma/2 \to 1$ and

$$\mu_A = \frac{nN\sigma^2}{6} Z_0 = \frac{nN\sigma^2 g}{3} = nNkT . \tag{59}$$

Hence at very high frequencies, the liquid acts like a material with the viscosity of the solvent and a shear stiffness proportional to the total number of segments.

For the intermediate range determined by $\omega' < 4\omega_0 = N^2(nkT)/(\eta_0 - \eta_s)$ the viscosity and stiffness can be put in the form

$$\eta_A - \frac{j\mu_A}{\omega} = \eta_s + \sqrt{\frac{nkT(\eta_0 - \eta_s)}{\omega}}\left(\frac{1-j}{\sqrt{2}}\right) \operatorname{tgh}\left[\sqrt{\frac{(\eta_0 - \eta_s)\omega}{nkT}}\left(\frac{1+j}{\sqrt{2}}\right)\right]. \tag{60}$$

As long as $\sqrt{(\eta_0 - \eta_s)\omega/nkT}$ is equal to or greater than $2\sqrt{2}$ — for the solution of Fig. 9 this requires a frequency of 300 Hz —

$$\operatorname{tgh}(2 + 2j) = \frac{0.965 + j\,2.04}{1 + j\,1.96} = 1.025 - j\,0.03\,, \tag{61}$$

and hence within less than three per cent the value of the hyperbolic tangent is equal to unity and approaches it more closely as the argument gets larger. For frequencies above this point

$$\eta_A = \eta_s + \sqrt{\frac{nkT(\eta_0 - \eta_s)}{2\omega}}\,; \qquad \mu_A = \sqrt{\frac{nkT(\eta_0 - \eta_s)\omega}{2}}\,. \tag{62}$$

Below this point, the value of the hyperbolic tangent function enters according to the equation

$$\operatorname{tgh}\sqrt{\frac{(\eta_0 - \eta_s)\omega}{nkT}}\left(\frac{1+j}{\sqrt{2}}\right) = \frac{\operatorname{tgh}\sqrt{\dfrac{(\eta_0 - \eta_s)\omega}{2nkT}} + j\operatorname{tg}\sqrt{\dfrac{(\eta_0 - \eta_s)\omega}{2nkT}}}{1 + j\operatorname{tgh}\sqrt{\dfrac{(\eta_0 - \eta_0)\omega}{2nkT}}\operatorname{tg}\sqrt{\dfrac{(\eta_0 - \eta_s)\omega}{2nkT}}}\,. \tag{63}$$

Hence when one knows the number of molecules per cm³, n, and the difference between the static solution and solvent viscosities, the complete stiffness and viscosity of the solution is obtained.

Figures 7, 8 and 9 show how well the measurements agree with the theory up to frequencies as high as a megaherz. Divergences are indicated at the highest frequency measurement which will be discussed in the Section 6. The formulation of the Rouse theory is useful when the same polymer is dissolved in different solvents. Figure 8 shows measurements of low molecular weight polyisobutylene in various solvents and the difference in the shear stiffness is very marked. The cause of the reduction in stiffness is the lower relative viscosity due to the smaller separation σ^2 of the segments ends. The Rouse theory does not allow a separation of the separate quantities σ^2, ϱ and N but simply determines the product according to the equation

$$N^2\sigma^2\varrho = 36(\eta_0 - \eta_s)/n\,. \tag{64}$$

5·5. *Reduction formulas.* – There are only two types of elements in the generalized network of Fig. 23(*c*), a stiffness proportional to the absolute temperature and a viscous element which should have the same temperature variation for each element—*i.e.*, the same activation energy. Hence for a given liquid at a given frequency the effective stiffness μ_A should be proportional to the absolute temperature and also to the concentration due to the factor n of eq. (56). Hence with respect to the stiffness at some temperature T_0 and concentration C_0

$$\mu_i = \mu_{i_0} T_0 C_0 / TC \,, \tag{65}$$

where T and C are the actual temperatures and concentrations. It is also assumed that all relaxation times τ_i depend identically on the temperature and concentration and that there are proportionality constants a_T and a_C such that

$$\tau_i = a_T a_C \tau_{i_0} \,. \tag{66}$$

We can evaluate the factor $a_T a_C$ by noting that the static viscosity η_0 is by eq. (19)

$$\eta_0 = \sum_i \mu_i \tau_i = \frac{TC}{T_0 C_0} a_T a_C \sum_i \mu_{i_0} \tau_{i_0} = \frac{TC}{T_0 C_0} a_T a_C \eta_{R_0} \,, \tag{67}$$

where η_{R_0} is the static viscosity in the reference state. Hence

$$a_T a_C = \frac{\eta_0}{\eta_{R_0}} \frac{T_0 C_0}{TC} = \frac{\eta_0 T_0}{TC} \,, \tag{68}$$

if we choose C_0 and η_{R_0} equal to unity in the reference state. Hence we can define reduced stiffnesses, viscosities and angular frequencies

$$\mu_R = \frac{\mu T_0}{TC} ; \qquad \eta_R = \frac{\eta}{\eta_0} ; \qquad \omega_R = \frac{\omega \eta_0 T_0}{TC} \,, \tag{69}$$

such that data taken under a variety of temperature and concentration conditions should form a single curve which gives parameters of interest for the reference state. Figure 10 shows measurements of polyisobutylene in a decalin solution with concentrations ranging from 5 to 22 %, temperatures from 5 °C to 35 °C and frequencies from 0.005 Hz to 100 Hz which can be fitted on single reduced variable curves.

Recent work by BARLOW and LAMB [31] has shown that the effect of pressure can be incorporated into the reduction formulas. The viscosity η_0 is the viscosity measured at the hydrostatic pressure used. This finding has important consequences for lubrication theory since oils are used under high hydrostatic pressure and hence viscoelastic effects may be expected at the frequencies for which gear teeth mesh.

However, violations of the reduction formulas begin to appear if measurements are made for stiffnesses above 10^8 dyn/cm^2 or for very high frequencies. The measurements of Fig. 9 at 14 MHz appear to be definitely removed from the theoretical curve. The data of Fig. 13 for pure polymer liquids fit the reduction formulas well up to stiffnesses of 10^7 dyn/cm^2 but diverge for higher stiffnesses measured at higher frequencies. This matter is discussed further in Section 6.

5'6. *Interpretation in terms of a free volume model.* – An interesting relation between the temperature transformation factor a_T and the free volume state has been pointed out by WILLIAMS, LANDEL and FERRY [32]. If we plot the total volume per gram of material as a function of the temperature, a relation results of the form shown by Fig. 24. At temperatures high enough so that thermally produced segment motion is rapid an extra volume is occupied due to this motion. As the temperature is lowered, a collapse of this free volume occurs until a further collapse does not occur in the time of the measurement. A further lowering of temperature is accompanied by normal thermal compression coefficients existing in other type solids. The extra volume due to the segment nature of the polymer does not change. The temperature for which a change occurs in the temperature expansion coefficient is known as the glass temperature T_g. The dependence of the free volume on temperature is taken by several authors to be the difference between the thermal expansion coefficients above and below the glass transition temperature or

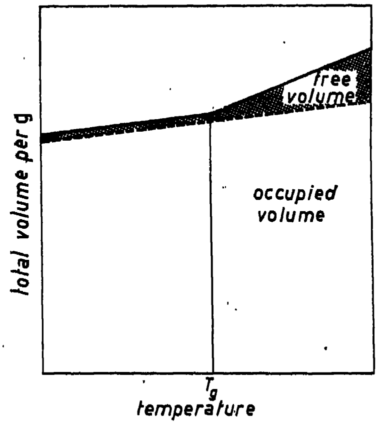

Fig. 24. – Free volume and glass temperature T_g:

$$f = f_g + (\alpha_2 - \alpha_1)(T - T_g)\,. \tag{70}$$

In the intermediate region, which extends from the glass temperature T_g to about 100 °C above the glass temperature, a universal equation of the form

$$\log_{10} a_t = A(T - T_g)/(B + T - T_g) \tag{71}$$

has been shown to hold experimentally. At first the constants A and B were thought to be universal constants with values of

$$A = 17.44\ ; \qquad B = 51.6\ . \tag{72}$$

More recent data taken [33] over a wide range of materials give values of

$$A = 15.6 \text{ to } 22.2\ ; \qquad B = 32 \text{ to } 114\ . \tag{73}$$

Above $T_g+100°$ the viscosity depends on details of the molecular structure while as the glass temperature is approached, the reduction formula becomes invalid.

An interpretation in terms of the free volume of the polymer has been given. In terms of the ratio of the free volume to the total volume, the viscosity of a liquid can be expressed by the equation

$$\ln \eta = \ln A + \frac{1}{f}\,, \tag{74}$$

where A is a different constant for each liquid.

For a pure liquid the factor a_T of eqs. (68) can be expressed in the form

$$a_T = \frac{\eta T_g \varrho_g}{\eta_g T \varrho}\,, \tag{75}$$

where ϱ_g and ϱ are the densities at the glass temperature T_g and at any temperature T. Neglecting the variations of T and ϱ compared to η

$$\log_{10} a_T = \frac{1}{2.303}\left(\frac{1}{f} - \frac{1}{f_g}\right). \tag{76}$$

Substituting (70) in (76) we find

$$\log_{10} a_T = -\frac{(T-T_g)}{2.303 f_g}\bigg/\left(\frac{f_g}{\alpha_2-\alpha_1} + T - T_g\right). \tag{77}$$

This is identical in form with (71) and if $\alpha_2-\alpha_1 = 4.8\cdot10^{-4}\,°\mathrm{C}$ and $f_g = 0.025$ the original constants are obtained. The differences in the temperature expansion coefficients for most polymers are in this range.

A consequence of this type of relationship is that the activation energy for viscous flow, given by

$$\eta = \eta_0 \exp\left[-\Delta H/RT\right] \tag{78}$$

will depend markedly on how close the temperature is to the glass temperature. From the relation

$$\Delta H = R\,\frac{\mathrm{d}\ln a_T}{\mathrm{d}(1/T)}\,, \tag{79}$$

we find

$$\Delta H \doteq R[T^2/(\alpha_2-\alpha_1)]\Big/\left(\frac{f_g}{\alpha_2-\alpha_1}+T-T_g\right) \approx \frac{2.08\cdot 10^3\,RT^2}{(B+T-T_g)^2}\,. \tag{80}$$

Close agreement is found with this equation for a number of polymer liquids.

6. – High frequency behavior of polymer solutions, liquids and solids.

The data of Figs. 9 and 13 on polymers in solution and short chain polymer liquids show deviations from the type of curve expected from the above treatment. This might be anticipated since there is a limit to the rapidity with which the polymer chain can adjust its position under the effect of thermal agitation alone. Suppose now that the stress is applied in a time much shorter than the time required to establish thermal equilibrium of the chain. The chain will still displace but with a stiffness determined by the intrinsic stiffness of the chain, *i.e.*, that due to mechanical bending of the joints. Furthermore when the joints are moved by thermal agitation there is an internal friction caused by the motion of the joints which has so far not been taken account of. Since these two deviations from the action of a simple spring are occasioned by the separation of the ends of the segment, we should expect that their effect will be represented by extra elements in the shunt coupling elements and Fig. 25(*a*) shows the type of network proposed. In this network g_3 represents the thermodynamic stiffness $3\,kT/\sigma^2$ and ϱ_2 represents the internal

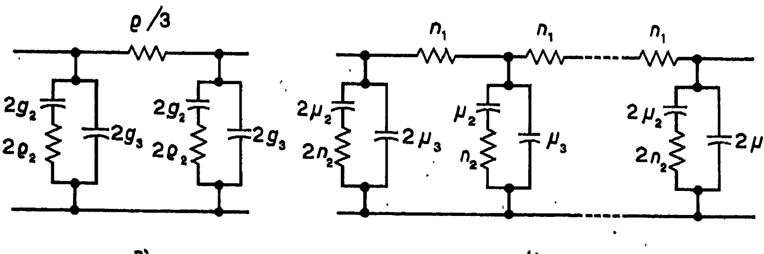

Fig. 25. – Modification of thermodynamic network to take account of internal friction and inherent segment stiffness.

friction caused by the motion of the polymer joints. The ratio

$$\varrho_2/g_2 = \tau_2 \tag{81}$$

is the relaxation time required to establish thermodynamic equilibrium.

As long as the time of the application of the alternating shearing strain is large compared to τ, we can neglect ϱ_2 and join g_2 and g_3 by the equation

$$g_0 = \frac{g_2 g_3}{g_2 + g_3} \doteq g_2 \,, \tag{82}$$

since g_3 will ordinarily be much larger than the thermodynamic stiffness g_2. Under these circumstances the network reduces to the network of Fig. 23(a), and the development given there will hold. However for $t < \tau$, it is necessary to take account of the other elements.

From the discussion of Section 6, it will be seen that the value of tgh $N(A+jB)/2$ is going to be equal to unity and the shear stiffness and viscosity of such a network will be represented by the equation

$$\eta_A - \frac{j\mu_A}{\omega} = \eta_s + \frac{\eta N \sigma^2}{6} Z_0 \,, \tag{83}$$

where Z_0 for this network is given by the equation

$$Z_0 = \sqrt{\frac{4Z_1 Z_2^2}{Z_1 + 4Z_2}}; \qquad Z_1 = \frac{\varrho_1}{3}; \qquad Z_2 = -\frac{j g_2 g_3}{\omega(g_2 + g_3)} \left[\frac{1 + j\omega\tau_2}{1 + j\omega\tau_3}\right], \tag{84}$$

where

$$\tau_3 = \left(\frac{\varrho_2}{g^2 + g_3}\right).$$

Inserting these values, the viscosity and stiffness of the solution become

$$\eta_A - \frac{j\mu_A}{\omega} = \eta_s + \frac{nN\sigma^2\varrho}{18} \left[\sqrt{\frac{((j\omega_0/\omega)((1 + j\omega\tau_2)/(1 + j\omega\tau_3))}{1 + (j\omega/4\omega_0)((1 + j\omega\tau_3)/(1 + j\omega\tau_2))}}\right], \tag{85}$$

where

$$\omega_0 = \frac{3 g_2 g_3}{(g_2 + g_3)\varrho_1} .$$

At frequencies below ω_0, but large enough so that tgh $N\Gamma/2 \to 1$, the values reduce to the values of eq. (60). However for values of ω greater than ω_0, divergence from the Rouse curve occurs. For the measurements of Fig. 9, two of the parameters are determined by the difference in the solution and solvent viscosity, *i.e.*, 0.265 poise, and by the number of molecules per cm^3, 1 g per 100 cm^3 of $3.9\cdot10^6$ molecular weight molecules. Since 1 molecule will weigh

$$3.9\cdot10^6\cdot1.66\cdot10^{-24}=6.48\cdot10^{-18}\,\mathrm{g}\,, \tag{86}$$

there are $1.54\cdot10^{15}$ molecules per cm^3 giving a value for the other parameter of

$$nkT=63.5\,. \tag{87}$$

If we express the measured values in terms of the equivalent network shown in Fig. 25(*b*), the complex stiffness measured above 300 Hz will be in the form

$$\eta_A-\frac{j\mu_A}{\omega}=\sqrt{-\frac{(j(nkT)(\eta_0-\eta_s)/\omega)\big((1+j\omega\tau_2)/(1+j\omega\tau_3)\big)}{1+(j\omega(\eta_0-\eta_s)/4N^2(nkT))\big((1+j\omega\tau_2)/(1+j\omega\tau_3)\big)}}\,. \tag{88}$$

At low frequencies one can determine two values according to the relations

$$\left\{\begin{aligned}\eta_1&=\frac{(\eta_0-\eta_s)}{N}=\frac{0.265}{N}\,,\\ \frac{2\mu_2\mu_3}{\mu_2+\mu_3}&=N(nkT)=N(63.5)\,.\end{aligned}\right. \tag{89}$$

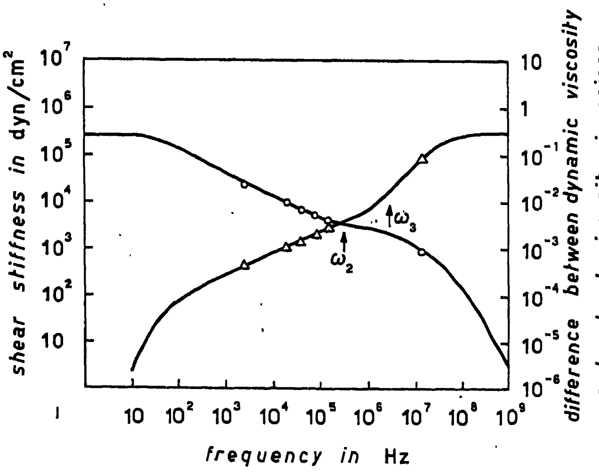

Fig. 26. – Calculation of shear stiffness and viscosity for 120X solution taking account of the thermodynamic relaxation and the structural stiffness: ○ measured viscosity values; △ measured shear stiffness; —— calculated curves.

To determine the other values, choices are made for τ_2, τ_3 and μ_3 to give the best fit for the measured points. Figure 26 shows the curve obtained by taking

$$(90)\qquad \begin{cases} \mu_2 = 2.5\cdot 10^4\ \text{dyn/cm}^2\ ; & \mu_3 = 1.9\cdot 10^5\ \text{dyn/cm}^2\ , \\ \eta_1 = 3.8\cdot 10^{-4}\ \text{poises}\ ; & \eta_2 = 1.1\cdot 10^{-2}\ \text{poises}\ . \end{cases}$$

These values allow a determination of the number of independent segments in the chain of $3.9\cdot 10^6$ molecular weight. N is determined by taking the ratio of the measured static viscosity $\eta_0 - \eta_s = 0.265$ poise to η_1 or

$$(91)\qquad N = \frac{0.265}{3.8\cdot 10^{-4}} = 700\ ,$$

corresponding to a segment length of

$$(92)\qquad \frac{3.9\cdot 10^6}{56\cdot 700} = 100\ ,$$

where 56 is the molecular weight of a single segment. The element

$$(93)\qquad \frac{2\mu_2\mu_3}{\mu_2+\mu_3} = 4.45\cdot 10^4\ \text{dyn/cm}^2 = N(nkT) = 700\times 63.5\ .$$

Hence we conclude that shear impedances of polymer solutions measured over wide frequency ranges allow one to estimate the number N of independent segments, the thermal relaxation time

$$(94)\qquad \tau_2 = \frac{\eta_2}{\mu_2} = \frac{1.1\cdot 10^{-2}}{2.5\cdot 10^4} = 4.4\cdot 10^{-7}\ \text{s}\ ,$$

occurring when the shape of the chain is altered and the stiffness to bending of the chain for this case appears to be about 8 times the thermal stiffness. Since this stiffness is determined by constraints rather than by thermal agitation, one would expect that the reduction formulas would not be valid in this region.

Several checks can be made on the value of 100 monomer units for the smallest chain segments. Since

$$(95)\qquad \eta_0 - \eta_s = \frac{n\sigma^2 N^2 \varrho}{36} = 0.265\ ,$$

we find

$$(96)\qquad \sigma^2\varrho = 1.27\cdot 10^{-20}$$

when we substitute $n = 1.54 \cdot 10^{15}$ and $N = 700$. The distance between chain ends for this segment can be calculated from eqs. (23) to be

$$\sigma^2 = 6.25 \cdot 10^{-13}\ \text{cm}^2 \tag{97}$$

giving a value of $\varrho = 2.04 \cdot 10^{-8}$. ϱ is defined as the viscous drag as the polymer segment is moved through the solvent. From Stokes law,

$$\varrho = 6\pi a \eta_s \tag{98}$$

for a sphere of radius a dragged through the solvent of viscosity $\eta_s = 0.0086$ poise. We find that the effective radius of the equivalent bead is equal to $12.5 \cdot 10^{-8}$ cm. This appears to be a reasonable value to represent a polymer chain of total length equal to $340 \cdot 10^{-8}$ cm with a chain end separation of $79 \cdot 10^{-8}$ cm.

6'2. *Complex stiffness of short network polymer liquids*. – A pure polymer liquid differs from a solution of polymer molecules in that there are intrachain connections as well as interchain connections. Hence the molecule cannot be considered as a linear network but must in general be considered as part of a three-dimensional network.

Very short networks, however, can be considered as linear networks since the interchain connections are more important than the intra-chain connections. Figure 11, circles and triangles, shows measurements of a polyisobutylene liquid of viscosity average molecular weight of 1600 which corresponds to a chain having 30 repeating elements. Attempts have been made to fit a Rouse function on the assumption that the solvent has the same viscosity as the liquid. The result as seen from the dash-double dot lines is not very good.

A considerably better result is obtained by considering that the polymer has two sections of the type shown by Fig. 25(*a*). Although neither section is long enough to develop its true thermodynamic stiffness or viscous drag, it appears that the center part can be considered as having no stress on it while the two halves move in and out with respect to the center. The equivalent circuit for this case is that shown by Fig. 27(*a*). By assuming $\eta_1 = 39$ poise; $\mu_2 = 1.2 \cdot 10^6$ dyn/cm²

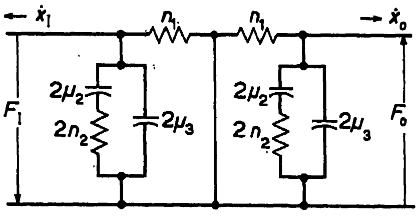

Fig. 27. – Representation of equivalent circuit for a short chain-length polymer liquid.

$$\eta_2 = \frac{\eta_1}{2} = 19.5\ \text{poise}; \qquad \mu_3 = 5.0 \cdot 10^8\ \text{dyn/cm}^2\,, \tag{99}$$

and using the equations for the shear stiffness and viscosity

$$(100)\qquad \left\{\begin{aligned} &\eta_s-\frac{j\mu_A}{\omega}=\frac{\eta_1(1+j\omega/\omega_2)}{1+(j\omega/\mu_2)\bigl(\eta_1(1+(\mu_2/\mu_3))+\eta_2\bigr)-\omega^2/\omega_2\omega_3};\\ &\omega_2=\frac{\mu_2}{\eta_2};\qquad \omega_3=\frac{2\mu_3}{\eta_1},\end{aligned}\right.$$

one obtains the match shown by the dot-dash line of Fig. 11. This value of μ_2 is less than that expected from the formula

$$(101)\qquad 2\mu_2=NnkT=2\left(\frac{0.866}{1660\cdot 1.66\cdot 10^{-24}}\right)(1.38\cdot 10^{-16}\cdot 298)=2.6\cdot 10^7\ \text{dyn/cm}^2\,.$$

The viscosity η_1 of the half segment, *i.e.*, 19.5 poise, is smaller than that for a fully developed segment which will be shown to be about 58 poise. Hence it appears that the two halves of the network with 15 repeating elements are not sufficiently long to develop the full thermodynamic stiffness and viscous drag.

At the high frequencies, the measured increase in stiffness and the measured decrease in viscosity change too slowly to be represented by a single relaxation. The same thing is true for the longer chain polymers shown by Fig. 12 and 13 and for the longitudinal wave measurements of Fig. 14. In these measurements the attenuation per wavelength approaches a constant which is indicative of a « hysteresis » type response for which the energy loss per cycle is a constant independent of the frequency. As discussed previously [34], this type of behavior is quite general in solid polymers, glasses and metals.

This behavior originates in the bending stiffness constant μ_3. It is believed to be due to the motion of smaller segments than the whole thermodynamic segment. For example any combination of segments up to 100—the length of the thermodynamic segment—can move at a higher frequency than the thermodynamic relaxation angular frequency μ_2/η_2. This action can be represented by a series of relaxation networks of the type discussed by eq. (19). Since the energy required to move segments smaller than the thermodynamic segment is smaller than that required to move the complete segment, the activation energy for this « hysteresis » component should be lower than the viscosity-determined activation energy in agreement with measurements by LITOVITZ [35] and LYON.

While the action of a « hysteresis » component can be obtained by adjusting the relaxation times of eq. (19) to cover a smooth range, a simpler approximation, holding for sinusoidal vibrations is to let the stiffness μ_3 have an imaginary component of the form

$$(102)\qquad Z=\frac{[\mu'_3-j\mu_3]}{\omega}=-\frac{j\mu_3^*}{\omega}\,.$$

The dashed line of Fig. 11 shows the effect of replacing μ_3 by the expression in (96) with $\mu_3' = 0.4\,\mu_3$. The agreement over the complete frequency range is much better.

6'3. *High frequency range for polymer liquids.* – As shown particularly in Fig. 12, the complex stiffness of a long polymer chain liquid has two ranges, a rubbery range for which the stiffness is in the order of 10^6 to 10^7 dyn/cm², and a glassy range for which the stiffness climbs to the order of 10^{10} dyn/cm². Below the rubber range, there is a viscous range and between the two stiffness regimes, there is a region for which the real and imaginary parts of the stiffness increase at a rate greater than the square root of the frequency. The frequency breadth of the rubber region depends markedly on the length of the polymer chains and is determined by intra-chain reactions as well as inter-chain reaction as discussed in Section 6.

On the other hand, as can be seen by comparing the data of Fig. 11, 12 and 13, the glassy region and the approach to it depend little on the length of the polymer chain. Furthermore, there are indications from Fig. 13, that this region does not obey a reduction formula at least as far as the shear modulus is concerned. Hence it appears that this phase can be interpreted in terms of the mechanical bending of the polymer segments at frequencies above the thermal relaxation time τ_2.

Assuming that the network of Fig. 25(*b*) represents the action of the chains in the high frequency region, the complex stiffness will be represented by the equation

$$(103)\qquad \left\{\begin{aligned} &\eta_A - \frac{j\mu_A}{\omega} = Z_0 = \sqrt{\frac{Z_1 Z_2}{1 + Z_1/4Z_2}}\,; \qquad Z_1 = \eta_1\,; \\ &Z_2 = -\frac{j\mu_2\mu_3^*}{\omega(\mu_2 + \mu_3^*)}\left[\frac{1 + j\omega\eta_2/\mu_2}{1 + j\omega\eta_2/(\mu_2 + \mu_3^*)}\right]. \end{aligned}\right.$$

The circles and triangles show the degree of agreement obtained with this model — above $\log\omega = 4$ — when we assume the values

$$(104)\qquad \left\{\begin{aligned} &\eta_1 = 58 \text{ poise}\,; && \mu_2 = 2\cdot 10^6 \text{ dyn/cm}^2\,; \\ &\mu_3^* = 5\cdot 10^9[1 + j0.4] \text{ dyn/cm}^2\,; && \eta_2 = 9\cdot 10^3 \text{ poise}\,. \end{aligned}\right.$$

The final value η_2 is not well determined from these measurements but determinations from considerations of the next section indicate the value shown.

The value of μ_2 agrees with the formula

$$(105)\qquad 2\mu_2 = nNkT = \left(\frac{0.914}{1.5\cdot 10^6\cdot 1.66\cdot 10^{-24}}\right)\left(\frac{1.5\cdot 10^6}{100\cdot 56}\right)(1.38\cdot 10^{-16}\cdot 298) =$$

$$= (3.68\cdot 10^{17})(268)(4.1\cdot 10^{-14}) = 4\cdot 10^6 \text{ dyn/cm}^2\,,$$

since the density $\varrho = 0.914\ \text{g/cm}^3$. This calculation assumes that the segment length is about 100 repeating units as found in Section 6'1. If we interpret the viscosity η_1 as being due to the drag of a segment through a surrounding medium and use the values established in Section 6'1, we have

$$(106)\qquad \eta_1 = 58\ \text{poise} = \frac{\eta\sigma^2 N\varrho}{36} \quad \text{or} \quad \varrho = 3.38\cdot 10^{-5}\,.$$

This corresponds to a sphere of $25\cdot 10^{-8}$ cm in diameter dragged through a liquid having a viscosity of 14.3 poises, which is close to that for a light polymer polyisobutylene liquid.

The data of Fig. 13 for molecular weights under 10 000 are fitted for

$$(107)\qquad \eta_1 = 50\ \text{poise}\,; \quad \mu_3 = 3\cdot 10^{9}\ \text{dyn/cm}^2$$

showing that both elements increase slightly as a function of the molecular weight. This is probably due to the slight increase in density with increase in molecular weight which causes a crowding of the chains making it more difficult for them to move.

6'4. *Rubbery region for polymer liquids.* – The measured values in the rubberlike region depend markedly on the molecular weight of the liquid as can be seen from Fig. 12 and 13. For the highest molecular weight of Fig. 12 there is a region of nearly constant elasticity from $\omega = 10^{-4}$ to 10^3, a range of nearly 10^7 Hz. This is presumably connected with the intra-chain connections which cause motions in surrounding chains when one chain is actuated. Several suggestions [32, 36] have been made on how to incorporate this coupling into the network but it appears to the writer that the most logical way is to incorporate the chain as part of a three-dimensional network. Since the calculations have been given previously [34] only a discussion of the principle is given here and the reader is referred to the previous publication for the details.

The data given previously indicate that we are dealing with polymer chains which have movable segments in the order of 100 repeating monomer units. It has been suggested [32] that this segment length is a measure of the ave-

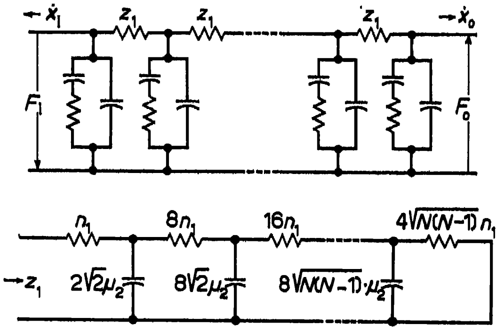

Fig. 28. – Representation of equivalent circuit for a long chain-length polymer liquid showing coupling to the side chains.

rage separation of the entanglement points between the chain under consideration and adjacent chains of the liquid. A simple network based on these considerations is shown by Fig. 28. The coupling of the segment under consideration to the adjacent chains is assumed to occur through the thermal motions of the segments. The adjacent chains in turn couple to other chains by means of thermal motions, so that the total number of chains driven increases as the square of the distance from the original chain. These adjacent chains dissipate energy in proportion to the number of segments driven. A flat cylindrical section is assumed to be connected with each segment since the energy lost to the sides is made up by energy received from the sides of the flat section. The inner segment should have a volume equal to $\pi\sigma^3/4$, while the next layer should have a volume $\pi[(3\sigma)^2-\sigma^2]\sigma/4$ or 8 times that of the first layer. The N-th layer will have a viscosity

$$[(2N+1)^2-(2N-1)^2]\eta_1=8N\eta_1 . \tag{108}$$

Eeach layer then will have a viscosity associated with it equal to the number of elements times the viscosity of a single segment η_1. The value of η_1 was determined by the higher frequency measurements of Section 6·3 and was found to be

$$\eta_1=50\left(\frac{MW}{10\,000}\right)^{0.05}\text{poise} . \tag{109}$$

The length of the sidewise chain actuated by each segment is in the order of the main chain, but may be somewhat longer on account of Van der Waals coupling to adjacent chains. The present model assumes that the number of layers activated is A times N where N is the number of chain elements. At the end of this chain it is assumed that there is a complete reflection of energy, *i.e.*, the chain is short-circuited as shown by Fig. 28.

There does not appear to be any way to calculate the length of the region of activation but by comparing the viscosity of various length polymer chains, a factor of $2.35N$ is derived. The total number of segments in each side chain is

$$1+8(1+2+\ldots+2.35N)=8\left(\frac{(2.35N-1)(2.35N+1)}{2}\right)\approx 22N^2 . \tag{110}$$

Since there are $2.35N$ of the side chains along the main chain, the total number of segments will be $52N^3$. Multiplying this value by the viscosity of a single segment, given by (109), the viscosity molecular weight relation

$$\eta_0=50\left(\frac{MW}{10\,000}\right)^{0.05}52N^3=50\cdot52\left(\frac{MW}{56\cdot100}\right)^3\left(\frac{MW}{10\,000}\right)^{0.05}=9.3\cdot10^{-9}(MW)^{3.05}, \tag{111}$$

valid for molecular weigths above 10 000.

Table II shows a comparison of this formula with the measurements of Fox and Flory [38] on the viscosity of polyisobutylene at 25 °C.

TABLE II.

Molecular weight	Measured η_0 in poise	n number of repeating elements	N number of segments	Calculated viscosity from (104)
11 200	22 000	200	2.0	20 800
80 000	$5.0 \cdot 10^6$	1 430	14.3	$8.2 \cdot 10^6$
600 000	$2.0 \cdot 10^9$	11 500	115	$5.2 \cdot 10^9$
1 500 000	$6.16 \cdot 10^{10}$	26 800	268	$5.85 \cdot 10^{10}$

This calculation assumes that the frequency is so low that all the chain elements can be activated. These elements will be driven by the thermal agitation of the chains which is represented by the thermodynamic stiffness of the segment μ_s. Between adjacent layers this stiffness increases since there are more segments to interact and the thermodynamic stiffness between layers is taken as

$$\mu = \mu_s \sqrt{64N(N+1)} \approx 8N\mu_s , \tag{112}$$

where μ_s is the thermodynamic stiffness which has been evaluated as $2 \cdot 10^6$ dyn/cm^2 for the B.S. polyisobutylene.

As the frequency increases, the sidewise distance that a vibration can penetrate is reduced and at a frequency greater than

$$\omega = \frac{\sqrt{2}\mu_s}{\eta_1} = \frac{2.83 \cdot 10^6}{58} = 4.9 \cdot 10^4 , \tag{113}$$

the molecule acts again as a single chain molecule, with a viscosity $\eta_1 = 58$ poise for the Bureau of Standards polyisobutylene and hence the calculations given in Section 6·3 are valid. For lower frequencies a good approximation can be obtained by taking the first few elements of the chain and the values at $\omega = 10^4$ and $\omega = 10^3$ were obtained in this way.

The complete solution of this tapered network has not been obtained but when $\omega \ll \mu_s/\eta_1$ a differential equation was derived which can be solved in terms of Bessel's functions. For low frequencies for which series expansions can be used, the side branch impedance Z_1 of Fig. 28 becomes

$$Z_2 = 4\eta_1 \left(\frac{r_2}{r_1}\right)^2 \approx 4\eta_1 (2.35N)^2 \approx 22\eta_1 N^2 , \tag{114}$$

in agreement with the static value. For higher frequencies the impedance Z_s can be derived from the equation

$$Z_s = 8\sqrt{\frac{j\eta\mu_2}{\omega}}\left[\frac{-J_1(\beta r_0) + [J_1(\beta r_1)/Y_1(\beta r_1)]\,Y_1(\beta r_0)}{J_0(\beta r_0) - [J_1(\beta r_1)/Y_1(\beta r_1)]\,Y_0(\beta r_0)}\right], \tag{115}$$

where

$$\beta = \frac{1}{r_0}\sqrt{-\frac{j\omega\eta_1}{\mu_2}}\,.$$

One can evaluate the side branch impedance from tables of Bessel's functions of complex arguments and the circles and triangles of Fig. 12 show the degree of agreement. At the low frequency end, the rise in impedance seems to come about a factor 10 higher in frequency than the measurements.

6'5. *Mechanical impedance of rubbers and polymer solids.* – Rubbers are also made from long chain polymer molecules but differ from liquids on account of cross linking between chains. Effectively this forms a three-dimensional network. As can be seen from Fig. 15(*a*) and 15(*b*), the « rubber » region and the high frequency « glassy » region are very similar to these regions in long chain polymer liquids. However there is no viscous region occurring at very low frequencies, since even for static stresses there is no flow but a finite « rubbery » stiffness. On the model presented in the last section the effective chain length coupled to the main chain becomes very large and the flow viscosity approaches infinity. A fairly good agreement with the complex stiffness of a rubber is obtained by using eq. (115) for the side branch impedance and letting r_1 become very large. The real part of the stiffness varies only by a factor of 2 over a frequency range $f_2/f_1 = 10^8$, while the imaginary part of the stiffness is about 1/30-th of the real part in relatively good agreement with Fig. 15.

A further inhibition of segment motion is obtained when linear polymers such as polyethylene form in partly crystalline form as shown by Fig. 2. The crystalline regions for which the molecules form close bonds as in an ordinary crystal are connected with other crystalline regions by amorphous regions where the polymer chains have the capability of some relative motion. The measurements of Fig. 16 and 17 for polyethylene show velocity dispersion and attenuation maximums which are thought to be related to the motion of a shortest chain segment in the amorphous region. For frequencies above this region a constant loss per wavelength is measured. According to the interpretation given previously this is due to the motion of one or more monomer units of the chain, which can still move at frequencies above which any chain segment motion is relaxed out.

If we compare the attenuations associated with the longitudinal and shear motions, it appears that most of the loss is accounted for by shear dissipative mechanisms, but a compressional viscosity about $\frac{1}{4}$-th of the shear viscosity is indicated.

7. – Some applications of the mechanical properties of polymers.

Although the main interest of this course is on the fundamental principles of sound absorption and dispersion, it appears worth-while to mention briefly a few of the applications. Polymer materials are the materials having the largest damping factors, *i.e.*, ratios of imaginary stiffness to real stiffness or alternatively, values of Q^{-1}, of any of the solid materials. Hence they are rather widely used in noise reduction and vibration reduction material. The materials are usually coated onto metal panels by a spraying or cementing technique to a thickness of about 20 % of the total panel thickness. They are sometimes used on both sides but more commonly on one side. In particular automobile bodies, blowers, air compressors and many building panels are treated this way.

As can be seen from Fig. 15, the highest value of the imaginary part of the stiffness modulus will occur in the region intermediate between rubbery and glassy regions. It is also obvious that such properties are very temperature-sensitive and somewhat frequency-sensitive. For a given frequency and temperature, a very high damping may be obtained but the results may vary considerably if the temperature is varied by ±10 °C.

A much wider temperature range of applicability has been obtained by OBERST [39], BOHN and LINHARDT by using a series of copolymers of vinyl acetate, vinyl chloride mixtures and other polymer chains. Each component has a different transition temperature and although the value of the imaginary stiffness component E_2 does not become as high as that for a single component, the temperature-frequency properties are much improved. Fillers are sometimes used to raise the stiffness E_1 and the imaginary stiffness E_2. They act by reducing the amount of material that is strained. Since such dampers reduce the amplitude of vibration of metal plates subject to air or solid vibrations, they are often used to prevent sonic fatigue in metals.

The heat generated in automobile tires is a cause for wear and degradation. For this reason natural rubbers, coupled with the use of carbon black to prevent radiation degradation, have been most often used in tires. However it has been shown [40] that higher static losses are beneficial in obtaining braking power. Both objectives may be obtained if a rubber is used which has high loss for low frequencies but low loss at frequencies corresponding to wheel rotations and vibrations, at a temperature corresponding to the steady state temperature of the tire. It has been suggested [40] that butyl-rubber has merit.

When a rigid sphere under pressure is rolled across a viscoeleastic surface, the viscoelastic material undergoes a shearing stress and compression followed by a recovery. The fractional force required to maintain a constant velocity is determined [41] by the viscoelastic loss in the material. In fact such a method has been used to measure losses in solid and rubbery polymers.

REFERENCES

[1] T. Alfrey jr.: *Mechanical Behavior of High Polymers* (New York, 1948).

[2] J. D. Ferry: *Viscoelastic Properties of Polymers* (New York, 1961), Chapter I.

[3] See W. P. Mason: *Physical Acoustics and the Properties of Solids*, Chapter IV (New York, 1958); Chapter XI by J. G. Ferry: *Rheology; Theory and Applications*, vol. II (New York, 1958).

[4] W. P. Mason, W. O. Baker, H. J. McSkimin and J. H. Heiss: *Phys. Rev.*, **75**, 936 (1949). This device is the work of H. J. McSkimin.

[5] W. P. Mason: *Trans. Am. Soc. Mech. Engs.*, **69**, 359 (1947).

[6] J. K. Appeldoorn, E. H. Okrent and W. Philippoff: 27-*th Midyear Meeting of Am. Petrol. Inst.* (1962).

[7] K. Sittel, P. E. Rouse jr. and E. D. Bailey: *Journ. Appl. Phys.*, **25**, 1312 (1954).

[8] E. R. Fitzgerald and J. D. Ferry: *Journ. Coll. Sci.*, **8**, 1 (1953).

[9] W. P. Mason: *Electromechanical Transducers and Wave Filters* (New York, 1942), p. 187; 2nd Edition (New York, 1948).

[10] W. O. Baker, W. P. Mason and J. H. Heiss: *Journ. Pol. Sci.*, **8**, 129 (1952).

[11] *a*) F. J. Padden and T. W. DeWitt: *Journ. Appl. Phys.*, **25**, 1086 (1954); *b*) F. J. Padden and T. W. DeWitt: *Journ. Appl. Phys.*, **22**, 718 (1951).

[12] W. P. Mason: *Dispersion and Absorption of Sound in High Polymers*, Vol. XI-1 (Berlin, 1961), p. 396.

[13] R. S. Marvin: *Proc. 2-nd Int. Congress on Rheology* (London, 1954), p. 156.

[14] W. P. Mason, W. O. Baker, H. J. McSkimin and J. H. Heiss: *Phys. Rev.*, **75**, 936 (1949).

[15] H. C. Rorden and A. Grieco: *Journ. Appl. Phys.*, **22**, 842 (1951).

[16] I. L. Hopkins: *Trans. Am. Soc. Mech. Engrs.*, **73**, 195 (1951).

[17] A. W. Nolle: *Journ. Pol. Sci.*, **15**, 1 (1950); *Journ. Appl. Phys.*, **19**, 753 (1948).

[18] W. P. Mason and H. J. McSkimin: *Bell Sys. Tech. Journ.*, **31**, 122 (1952)

[19] J. C. Maxwell: *Phil. Trans. Roy. Soc. London*, **157**, 49 (1837); *Phil. Mag.*, **35**, 129 (1868).

[20] See W. P. Mason: *Physical Acoustics and the Properties of Solids* (New York, 1958), p. 300.

[21] R. de L. Kronig: *Journ. Opt. Soc. Am.*, **12**, 547 (1926); H. A. Kramers: *Atti Congr. di Fisica* (Como, 1927), p. 545.

[22] B. H. Zimm: *Journ. Pol. Sci.*, **26**, 101 (1957).

[23] See J. Ferry: *Viscoelastic Properties of Polymers*, Chapter III (New York, 1961).

[24] See L. R. G. Treloar: *The Physics of Rubber Elasticity*, Chapter VI (Oxford, 1949).

[25] H. Eyring: *Phys. Rev.*, **39**, 746 (1932).

[26] W. Kuhn: *Kolloidschrift*, **68**, 2 (1934); E. Guth and H. Mark: *Mh. Chem.*, **65**, 93 (1934).

[27] P. E. Rouse jr.: *Journ. Chem. Phys.*, **21**, 1272 (1953).

[28] F. Bueche: *Journ. Chem. Phys.*, **22**, 603 (1954).

[29] B. H. Zimm: *Journ. Chem. Phys.*, **24**, 269 (1956). See also *Rheology*, III, Chapter I (New York, 1960).

[30] See for example, W. P. Mason: *Electromechanical Transducers and Wave Filters* (New York, 1942), p. 22, for a derivation of these relations.

[31] A. J. Barlow and J. Lamb: *Proc. Roy. Soc. London*, A **253**, 52 (1959).

[32] J. D. Ferry, R. F. Landel and M. L. Williams: *Journ. Appl. Phys.*, **26**, 359 (1955).

[33] J. D. Ferry: ***Viscoelastic Properties of Polymers*** (New York, 1961), Chapter 11.

[34] W. P. Mason: *Dispersion and absorption of sound waves in high polymers* in *Encyclopedia of Physics*, Vol. **11**-1 (Berlin, 1961), p. 402.

[35] T. A. Litovitz and T. Lyon: *Journ. Ac. Soc. Am.*, **26**, 577 (1954).

[36] F. Bueche: *Journ. Chem. Phys.*, **20**, 1959 (1952).

[37] W. P. Mason: *Dispersion and absorption of sound in high polymers*, in *Encyclopedia of Physics*, Vol. **11**-1 (Berlin, 1961), p. 407.

[38] T. G. Fox and P. J. Flory: *Journ. Am. Chem. Soc.*, **70**, 2384 (1948).

[39] H. Oberst, L. Bohn and F. Linhardt: *Kunstoffe*, **9**, 495 (1961).

[40] D. Tabor: *Phil. Mag.*, **45**, 1081 (1954); *Paper Trans. A.S.L.E.* (1956); D. Atack and D. Tabor: *Proc. Roy. Soc.*, A **246**, 539 (1958).

[41] D. G. Flom and A. M. Bueche: *Journ. Appl. Phys.*, **30**, 1725 (1959).

Theories of Relaxation Times.

K. F. HERZFELD

Catholic University of America - Washington D.C.

1. – Introduction [1, 2].

1·1. *General statement about collisions.* – If we have two particles of mass m_A and m_B and velocities $\boldsymbol{w}_A$ and $\boldsymbol{w}_B$, it is useful to define the motion of the center of mass

$$\boldsymbol{w}' = \frac{1}{m_A + m_B}(m_A \boldsymbol{w}_A + m_B \boldsymbol{w}_B)\,, \tag{1.1}$$

and the relative velocity

$$\boldsymbol{w}_r = \boldsymbol{w}_B - \boldsymbol{w}_A\,. \tag{1.2}$$

If no external force acts on the particle, $\boldsymbol{w}'$ remains constant during the whole motion, including collisions.

Furthermore, one has, for the total kinetic energy

$$\frac{1}{2} m_A w_A^2 + \frac{1}{2} m_B w_B^2 = \frac{1}{2}(m_A + m_B)(w')^2 + \frac{1}{2}\tilde{m}\, w_r^2\,, \tag{1.3}$$

where the effective mass, $\tilde{m}$, is

$$\tilde{m} = \frac{m_A m_B}{m_A + m_B}\,, \tag{1.4}$$

(1.3) says that the total kinetic energy is the sum of two parts: the kinetic energy of mass $m_A + m_B$, moving with the speed of the center of mass, and of a particle of mass $\tilde{m}$, moving with the relative velocity. In the absence of external forces, the first of these sums remains constant during the whole motion, and therefore only the second part can be affected by the collision.

Consider now the motion for regions where the particles are so far apart that the mutual potential energy is negligible. One such region will exist long before the collision, the other long after the collision.

In an elastic collision, the total kinetic energy long before and long after collision will be equal. That means that such a collision only changes the angle between w' and w_r, without changing their magnitudes.

In an inelastic collision, energy is lost to internal degree of freedom; and therefore, long after the collision, the relative velocity w_r is smaller than long before the collision.

In a « super elastic » collision (occasionally also called inelastic), kinetic energy of translation is gained from internal degree of freedom and therefore w_r long after collision is larger than long before the collision.

From the preceding it follows that, for the discussion of collision processes the motion of the center of gravity may be ignored, and one of the particles may be considered at rest, while the other, with the fictious mass $\mathfrak{M}$, moves against it with the relative velocity w_r.

1'2. *Exchange between translational and internal degrees of freedom as chemical reaction.* – We can describe the energy distribution over the internal states by stating that N_s particles are in the quantum states s.

The changes can than be described by chemical reaction equations of the second order (collisions) of the form

$$\frac{\mathrm{d}N_s}{\mathrm{d}t} = \sum_q \sum_j k^{(q)}_{j\to s} N^{(q)} N_j - \sum_q \sum_j k^{(q)}_{s\to j} N^{(q)} N_s \,, \tag{1.5}$$

$k^{(q)}_{j\to s} N^{(q)}$ is the number of processes per second in which a molecule which was in the state j is brought into state s by a collision with a molecule in state q.

It is of interest to remember that according to quantum theory equations like (1.5) require interference between a dense number of states, *i.e.* (1.5) is only possible because the molecules have, besides their discrete internal quantum states, a continuous spectrum of translation states.

In thermodynamic equilibrium, the numbers N_s are fixed. The principle of detailed balancing requires, that this constancy is achieved by exact balancing of each separate reaction pathway, *i.e.*

$$k^{(q)}_{j\to s}(N^q N_j)_{\text{equ}} = k^{(q)}_{s\to j}(N^q N_s)_{\text{equ}}$$

or

$$\frac{k_{j\to s}}{k_{s\to j}} = \left(\frac{N_s}{N_j}\right)_{\text{equ}} ,$$

for each q separately. The right side is, however, from statistical mechanics

$$\frac{g_s}{g_j} = \exp\left[-\frac{\varepsilon_s - \varepsilon_j}{RT}\right],$$

where the g's are the quantum weights (degeneracies) of the respective states. One has therefore the following fundamental relationships between the reaction constants of the forward and backward reaction

$$k^{(q)}_{j\to s} : k_{s-j} = \frac{g_s}{g_j} \exp\left[-\frac{\varepsilon_s - s_j}{RT}\right]. \tag{1.6}$$

The task, in the following is the calculation of the k's, which are directly related to the relaxation times. According to (1.6), one has only to calculate the rate for either excitation *or* deactivation (*).

In chemical kinetics, one is accustomed to write

$$k = f(T) \exp\left[-\frac{E'}{RT}\right], \tag{1.7}$$

where E' is called the heat of activation, $f(T)$ is usually a function which depends only mildly on the temperature, so that the temperature-dependence is dominated by the exponential. This form arises from the assumption that one has a Maxwell distribution, that a minimum energy E' is necessary for the reaction (per mole) and that the rate at which molecules with energy E larger than E' react is not too strongly dependent on $(E - E')$.

For activation of a vibration of an energy with quantum jumps $h\nu$, $E = h\nu$ is the minimum energy necessary for the reacting molecules, but the rate depends so enormously on the excess of energy that the rate formula has (in general) a form quite different from (1.7).

One more remark should be made about (1.5).

Since collisions are involved, the reaction is a second-order reaction, the right side is quadratic in the N's.

In the «acoustical» case—in contradistinction to the shock-wave case—the deviation of the N's from their equilibrium value is small, because of the small amplitude of the sound wave, and one can linearize the equation by writing

$$N^{(q)} = (N^{(q)})_{\text{equ}} + \delta N^{(q)},$$

$$N_j = (N_j)_{\text{equ}} + \delta N_j.$$

(*) The deeper reason for the existence of (1.6) is the symmetry of the quantum theoretical transition rates in respect to initial and final state, together with the Maxwell distribution law in equilibrium, which, for translational energy, is assumed preserved.

Taking the equilibrium conditions into account, (1.5) takes the form

$$\frac{\mathrm{d}}{\mathrm{d}t}(\delta N_s) = \sum_j \Big(\sum_q k^{(q)}_{j\to s} N^{(q)}_{\text{equ}}\Big)\,\delta N_j - \Big(\sum_j \sum k^{(q)}_{s\to j} N^{(q)}_{\text{equ}}\Big)\,\delta N_s = \\ = \sum_j k_{j\to s}\,\delta N_j - \Big(\sum_j k_{s\to j}\Big)\,\delta N_s\,,$$

with the abbreviation

$$k_{j\to s} = \sum_q k^{(q)}_{j\to s} N^{(q)}_{\text{equ}}\,.$$

1·3. *Formal description of elastic and inelastic cross-section.* – In the simplest case where there is direct exchange between internal and translational energy, the exchange rate does not depend on an internal quantum state of the colliding molecule q, but usually depends very strongly on its translational kinetic energy. We can then consider q as signifying the relative velocity w_r, and

$$\sum k^{(q)}_{j\to q} N^{(q)} = N_A \sum k^{(q)}_{j\to s} \frac{N^{(q)}}{N_A} = N_A k_{s\to j} \tag{1.8}$$

represents then the integration over relative velocities, which we assume to be distributed according to the Maxwell distribution law. Because of the factor N_A the rate is therefore proportional to the density of A, the relaxation time inversely proportional to this quantity.

We can make successive approximations in two steps:

First, we treat the problem as one-dimensional. Then the model of the molecule being bombarded is that of two parallel plates representing the two atoms B and C of the molecule, separated by springs of such strength that they have free vibrations of frequency ν or wave number $\tilde{\nu} = \nu/c$ (c light velocity). These are bombarded colinearly by a stream of molecules A, $w_r N_A$ molecules hitting unit area per second, where w_r is the mean one-dimensional relative thermal speed,

$$w_r = \sqrt{\frac{kT}{2\pi\bar{m}}}\,. \tag{1.9}$$

All incoming molecules are reflected, some elastically, some inelastically. The fraction of molecules A reflected inelastically, after producing the transitions $j\to s$, is

$$= k_{j\to s}(w_r)^{-1}\,. \tag{1.10}$$

In the calculation it will be assumed that this is a small fraction of the total.

In the three-dimensional case, the model of molecule BC will be at first that of a spherical, « breathing » sphere with proper frequency ν. Such a sphere will be arranged as « scatterer » at the origin and bombarded by a stream of particles A. As before, the number of particles hitting a unit area normal to the stream in unit time is given by $N_A w_r$ (1.9) being valid (*) for w_r.

The number of particles A scattered elastically per unit time is

$$Q_{\text{elast}} w_r N_A , \tag{1.11}$$

Q_{elast} is called the elastic cross-section. This would be $\pi(2r_0)^2$ for hard molecules and is in general well defined, except for such force laws for which most of the scattering goes into very small angles.

If the inelastic collisions form only a small fraction of all collisions, one can write

$$Q_{\text{elast}} w_r N_A = \frac{1}{\tau_c} , \tag{1.12}$$

where τ_c is the « average » time interval between collisions a molecule BC makes with molecules A (actually, the average is taken over $1/\tau_c$). As to the connection of τ_c and directly measurable quantities, see (6.23) p. 299, with

$$\tau_e = 0.499 \frac{8}{\pi} \tau_c = 1.271 \tau_e .$$

One can similarly define an inelastic cross-section for the process $j \to s$

$$N_A k_{j\to s} = N_A Q_{j\to s} w_r , \tag{1.13}$$

so that

$$k_{j\to s} = Q_{j\to s} w_r , \tag{1.13}$$

ndependent of the density N_A.

One may now write the rate for the process

$$N_A k_{j\to s} = \left(\frac{Q_{j\to s}}{Q_{\text{elast}}}\right) \frac{1}{\tau_c} . \tag{1.14}$$

In the particular case where one deals with activation or deactivation of simple harmonic oscillators representing the internal (vibrational) degrees of freedom, one is subject in first approximation to the selection rules for these

---

(*) In this notation, w_r is the average value of the speed of *one* component say the x-component. This is one-quarter of the average three-dimensional speed.

oscillators:

$$s \to s+1 \qquad \text{or} \qquad s \to s-1 .$$

LANDAU and TELLER [3] have pointed out that in this case

$$k_{s\to s-1} = s k_{10} \tag{1.15}$$

and

$$k_{s\to s+1} = (s+1)k_{01} = (s+1)k_{10} \exp\left[-\frac{h\nu}{kT}\right], \tag{1.15'}$$

see eq. (1.6).

If one deals with a system of simple harmonic oscillators nearly in equilibrium, LANDAU and TELLER find for the relaxation time

$$\frac{1}{\tau} = k_{10} - k_{01} = k_{10}\left[1 - \exp\left[-\frac{h\nu}{kT}\right]\right] = \frac{1}{\tau_0}\left(\frac{Q_{10}}{Q_{\text{elast}}}\right)\left[1 - \exp\left[-\frac{h\nu}{kT}\right]\right]. \tag{1.16}$$

For convenient writing, we will introduce, for the future, the characteristic temperature of the vibration, defined by

$$\theta = \frac{h\nu}{k} = \frac{kc}{k}\tilde{\nu} . \tag{1.17}$$

2. – Short characterization of methods of calculating k_{10} or k_{01}.

There are essentially four method available to calculate the k's. Two are partly classical, two are quantum theoretical.

The classical methods are called completely classical and semi-classical.

The quantum-theoretical methods use either time-dependent or time-independent (*i.e.* stationary state) perturbation theory.

All the methods can be applied to the one-dimensional or to the three-dimensional case.

We will first describe the general procedure for the one-dimensional case and draw general conclusions.

The interaction potential between the molecule BC and the hitting particle A is assumed to be of the form

$$V = H'(x, X) . \tag{2.1}$$

Here, x is the momentary distance between the centre of gravity of BC and A, and X is the vibrational amplitude. If H' would not contain X, the motion would not act on the vibration at all. On the other hand, it is assumed that the effect of the vibration is small—in other words, that the inelastic collisions are a small fraction of the elastic ones. One then writes

$$V = H'(x, 0) + \{H'(x, X) - H'(x, 0)\} .$$

The first term describes interaction with a nonvibrating molecule, the second term the perturbation due to the interaction between motion and vibration. This second term can usually be written

$$H'(x, X) - H'(x, 0) = \frac{\partial H'}{\partial X} X + \frac{1}{2} \frac{\partial^2 H'}{\partial X^2} X^2 + \dots , \tag{2.2}$$

and often only the first term is kept.

In the free vibration of BC, its center of mass is at rest, so that the vibrational motion of atom B is described by

$$X_B = \frac{m_C}{m_B + m_C} X = \beta X . \tag{2.3}$$

Often it is assumed that the interaction depends only on the momentary distance of B and A, so that

$$H'(x, X) = H'(x - X_B) = H'(x - \beta X) . \tag{2.4}$$

In that case

$$\frac{\partial H'}{\partial X} = -\frac{\partial H'}{\partial x} \beta ; \qquad \frac{\partial^2 H'}{\partial X^2} = \frac{\partial^2 H'}{\partial x^2} \beta^2 .$$

The procedure, both classically and quantum theoretically is as follows: one describes the relative motion of A and BC by $H'(x, 0)$, *i.e.* by the elastic motion, and then uses this unperturbed motion to calculate the effect on the vibration.

There is one even simpler approximation possible, the Born approximation [4, 5].

In this, $H'(x, 0)$ is neglected, *i.e.* the particle A is assumed classically to continue moving in a straight line with constant speed, and the force acting on the vibration is calculated under this assumption. Quantum theoretically, the stream of particles A is described by a plane wave even at BC.

WIDOM [6] has pointed out that this leads to transfer efficiencies which are far too high in the range of small kinetic energies, which interest us here.

In the following, we are going to talk first about the excitation and deexcitation of vibrational degrees of freedom. The vibrational motion is considered as simple harmonic, characterized by a frequency ν.

3. – Fundamental viewpoints on efficiency of inelastic collisions.

3·1. *Classical.* – The following argument is common to the completely classical and the semi-classical development. A simple harmonic oscillator of frequency ν is affected only by a force of the same frequency. If a force of arbitrary time-dependence, $F(t)$, acts on it, one has to calculate the Fourier component of frequency ν, *i.e.*:

$$\mathscr{F}(\nu)=\int_{-\infty}^{\infty}F(t)\exp\left[-2\pi i\nu t\right]\mathrm{d}t\,. \tag{3.1}$$

If the force varies relatively slowly compared to the period of vibration, the Fourier component of frequency ν increases with the rate of change of the force, *i.e.* the steepness of the force, *e.g.*, if the plot of the force against time consisted of two straight lines, starting at $-t'$ (*) with zero, rising to F_0 at $t=0$ and falling to zero at $+t'$, one has

$$\mathscr{F}(\nu)=\frac{F_0}{2\pi\nu^2}\,\frac{1}{t'}\,(1-\cos 2\pi\nu t')\,.$$

Apart from the last factor which gives interferences, F is inversely proportional to the rise time t'.

That means that forces which, during the relative motion of the particles, do not vary rapidly in time, do not have an appreciable Fourier coefficient of high frequency ν and are therefore inefficient for exchange between variational and translational energy. But the time variation of the force depends on two factors: the rate of variation of the potential in space and the relative speed of collision.

One therefore expects that those parts of the potential which do not vary rapidly in space are not very effective and that slowly moving molecules are not very effective [3].

The force is calculated from the elastic motion (without energy exchange).

3·2. – A similar conclusion can be reached by using quantum theoretically the time-dependent perturbation theory. If a system (the molecule BC) is in a certain quantum state j, of energy E_j, and if now a perturbating potential is applied (here, due to the approach of molecule A) one has to distinguish two cases:

(*) Assume $\tilde{\nu}=500$, $\nu=1.5\cdot10^{13}$ and the «range» of the force $l=0.2$ Å. The «rise time» of the force is $l/W=2\cdot10^{-9}/W$ compared to $7\cdot10^{-14}$, *i.e.*, slow for $W<3\cdot10^{4}$ cm s^{-1}.

If the potential changes slowly with time, this will affect the energy E_j, but the system stays in state j, the energy E_j has at every moment the value it would have if the external perturbation were frozen at its momentary value. If the perturbation finally disappears again (here, because A has moved away), the energy returns to its original value E_j and the state is still j. Such a process is called, with **Ehrenfest** [7, 8], « adiabatic ».

« Slow » means here that the relative change of the perturbing potential is small during the time $h|E_j - E_s|^{-1}$ where E_s is the energy of the nearest state to j which could be reached due to the perturbation. That is

$$\left|\frac{1}{H'}\frac{\mathrm{d}H'}{\mathrm{d}t}\right| < \frac{|E_j - E_s|}{h}. \tag{3.2}$$

If on the other hand the change is rapid, *i.e.* condition (3.2) is violated —nonadiabatic perturbation—the perturbation produces transitions to states different from j, and at the end the system may be in any of a number of states besides j, the theory giving the probability for these different states.

Slawsky and **de Wette** [8] have made a careful investigation of the effect of adiabatic and nonadiabatic forces.

3'3. *Maxwell distribution of molecules* A. – In view of what had been said earlier the efficiency of the collision increases rapidly with the speed of relative motion. On the other hand—except at extremely high temperature—the number of molecules with significantly high speeds decreases rapidly according to the Maxwell distribution law. This will have the effect of selecting a molecular energy which produces the majority of transitions; for lower energy, there are more but less efficient molecules; for higher energy, the molecules are more efficient, but fewer in number.

Considering the exchange of translational and vibrational energy, $N^{(\alpha)}$ in eq. ((3.3) should be written $N(E)$ where E is the translational energy, and $k^{(\alpha)}_{j\to s}$ would be $k_{j\to s}(E)$. Omitting the indices j, s for the time being, we have

$$N_A k = N_A \int k(E)\left(\frac{\tilde{m}}{2\pi kT}\right)^{\frac{1}{2}} \exp\left[-\frac{E}{kT}\right] \mathrm{d}w\,, \tag{3.3}$$

for the one dimensional case. Or

$$k = \frac{1}{(\pi kT)^{\frac{1}{2}}}\int_0^\infty k(E)\exp\left[-\frac{E}{kT}\right] \mathrm{d}\sqrt{E}\,. \tag{3.4}$$

One now looks for the maximum of the exponent $\ln k(E) - (E/kT)$.

Let E_m be the solution of the equation

$$\frac{\mathrm{d}\ln k(E)}{\mathrm{d}E}-\frac{1}{kT}=0\,. \tag{3.5}$$

For $\mathrm{d}\sqrt{E}$ we write $\frac{1}{2}(\mathrm{d}E/\sqrt{E})\sim(1/2\sqrt{E_m})\,\mathrm{d}E$, for the exponent

$$\ln k(E)-\frac{E}{kT}=\ln k(E_m)-\frac{E_m}{kT}+\frac{1}{2}\left[\frac{\mathrm{d}^2}{\mathrm{d}E^2}\ln E\right]_{E_m}(E-E_m)^2\,. \tag{6.3}$$

Then

$$k=\frac{1}{2}\left[\pi kTE_m\right]^{-\frac{1}{2}}k(E_m)\exp\left[-\frac{E_m}{kT}\right]\cdot\int\limits_{-\infty}^{\infty}\exp\left[\left(-\frac{1}{2}\frac{\mathrm{d}^2}{\mathrm{d}E^2}\ln k\right)(E-E_m)^2\right]\mathrm{d}E= \tag{3.7}$$

$$=\left\{\frac{1}{2}\,kTE_m\frac{\mathrm{d}^2}{\mathrm{d}E^2}\ln k(E)\right\}^{-\frac{1}{2}}\cdot\frac{1}{2}\,k(E_m)\exp\left[-\frac{E_m}{kT}\right].$$

The use of the infinite limits in (3.7) is justified because E_m is large compared with both kT and $h\nu$.

For three dimensions, the integrand in (3.3) is multiplied by the factor $4E/kT$, which change the $\{\}$ in (3.7) to

$$4(2E_m)^{\frac{1}{2}}\left\{(kT)^3\frac{\mathrm{d}^2}{\mathrm{d}E^2}\ln k(E)\right\}^{-\frac{1}{2}}.$$

The quantity $\{\frac{1}{2}(\mathrm{d}^2/\mathrm{d}E^2)\ln k(E_m)\}^{-\frac{1}{2}}$ measures the width of the energy interval around E_m which contributes appreciably to k.

4. – The formal procedure according to the different methods.

As had been mentioned in Section 3, the completely classical and the semi-classical method have in common the calculation of the force exerted by an elastically deflected particles as function of time. They differ in the way they use this force to calculate the excitation probability.

4·1. *Completely classical method* [9, 10]. – A simple harmonic oscillator of characteristic frequency ν receives, from an impulsive force $F(t)\,\mathrm{d}t$ impressed on it at time t, a change of velocity

$$\frac{1}{\tilde{\tilde{m}}}F(t)\,\mathrm{d}t\,.$$

At a later time t', this velocity will be

$$\frac{1}{\overset{\approx}{m}} F(t)\,\mathrm{d}t \cos 2\pi\nu(t'-t)\,.$$

If there is a sequence of such impulses, the velocity at time t' will be

$$\frac{1}{\overset{\approx}{m}} \int_{-\infty}^{t'} F(t) \cos 2\pi\nu(t'-t)\,\mathrm{d}t\,, \tag{4.1}$$

and if $F(t)$ has the character that it is zero up to a certain (negative) time and again zero beyond a certain positive time, the velocity, at a time t' beyond the cessation of the force, will be

$$\dot{X} = \frac{1}{\overset{\approx}{m}} \left\{ \cos 2\pi\nu t' \int_{-\infty}^{\infty} F(t) \cos 2\pi\nu t\,\mathrm{d}t + \sin 2\pi\nu t' \int_{-\infty}^{\infty} F(t) \sin 2\pi\nu t\,\mathrm{d}t \right\}.$$

The corresponding kinetic energy is, on the average

$$\frac{\overset{\approx}{m}}{2}\overline{\dot{X}^2} = \frac{1}{2\overset{\approx}{m}}\,\frac{1}{2} \left\{ \left(\int_{-\infty}^{\infty} F(t) \cos 2\pi\nu t\,\mathrm{d}t \right)^2 + \left(\int_{-\infty}^{\infty} F(t) \sin 2\pi\nu t\,\mathrm{d}t \right)^2 \right\}.$$

The bracket $\{\,\}$ can be rewritten as

$$\left| \int F(t) \exp[2\pi i\nu t]\,\mathrm{d}t \right|^2 = |\mathcal{F}(\nu)|^2\,.$$

The total energy is twice the average kinetic energy. Accordingly, in classical theory, the vibrational energy increase in each collision is

$$\Delta E = \frac{1}{2\overset{\approx}{m}} |\mathcal{F}(\nu)|^2\,,$$

equal for all oscillators originally at rest. In quantum theory, where only energy jumps of $h\nu$ are possible, this is interpreted as an excitation probability

$$\frac{\Delta E}{h\nu} = \frac{1}{2\overset{\approx}{m} h\nu} |\mathcal{F}(\nu)|^2\,. \tag{4.2}$$

4·2. *Semiclassical* [11, 12]. – Here, the time-dependent force is assumed the same as under 4·1, but one calculates according to quantum theory the probability that it will produce a transition from vibrational state j to state $j+1$.

One makes a time-dependent perturbation calculation for transition between vibrational states j and $j+1$, writing for the total wave function

$$\psi = \psi_j \exp\left[\frac{2\pi i E_j t}{h}\right] + b(t)\,\psi_{j+1} \exp\left[\frac{2\pi i E_{j+1} t}{h}\right]. \tag{4.3}$$

If, in eq. (2.3) only the term linear in X is kept, the perturbation energy is

$$-\beta\frac{\partial H'}{\partial x}\,X = \beta F(t)X\,, \tag{4.4}$$

(this is analogous to the interaction of an oscillating dipole with an electromagnetic field $F(t)$). Let $\tilde{\tilde{m}}$ be the effective mass of the vibration. Writing the Schrödinger equation for the oscillator

$$\frac{h}{2\pi i}\,\frac{\partial\psi}{\partial t} = -\frac{h^2}{8\pi^2\tilde{\tilde{m}}}\,\frac{\partial^2\psi}{\partial X^2} + [2\pi^2\tilde{\tilde{m}}\nu_0^2X^2 - \beta XF(t)]\,\psi\,, \tag{4.5}$$

one gets, in first approximation

$$\frac{h}{2\pi i}\,\psi_{j+1}\,\frac{\partial b}{\partial t} = \beta XF(t)\psi_j \exp\left[\frac{2\pi i(E_{j+1}-E_j)}{h}\,t\right] = \tag{4.6}$$

$$= \beta XF(t)\exp[2\pi i\nu t]\,\psi_j = \beta X\psi_j\int\mathscr{F}(\nu')\exp[2\pi i(\nu-\nu')t]\,\mathrm{d}\nu'\,.$$

Multiplying by ψ_{j+1} and integrating over X one has

$$\frac{\mathrm{d}b}{\mathrm{d}t} = \frac{2\pi i}{h}\,\beta\int\psi_{j+1}X\psi_j\,\mathrm{d}X\int\mathscr{F}(\nu')\exp[2\pi i(\nu-\nu')t]\,\mathrm{d}\nu'\,. \tag{4.7}$$

The first integral is the matrix element of the « dipole » moment between the state $j+1$ and j. It has the dimensions of a length. To make it dimensionless, we will divide it by an appropriately chosen length l; it is also multiplied with the dimensionless mass ratio β. We define a quantity

$$Z_{\text{osc}}^{-1} = \left(\beta\,\frac{1}{l}\int\psi_{j+1}X\psi_j\,\mathrm{d}X\right)^2. \tag{4.8}$$

If the ψ are wave functions of the simple harmonic oscillator, the matrix element is

$$\int\psi_{j+1}X\psi_j\,\mathrm{d}X = X_{j,j+1} = \left(\frac{j+1}{8\pi^2\tilde{\tilde{m}}\nu}\,h\right)^{\frac{1}{2}}. \tag{4.9}$$

One now integrates (4.7) over t from zero and remembers that b is zero for $t=0$

$$b(t)=\frac{1}{h}\beta X_{j,j+1}\int\mathcal{F}(\nu')\frac{\exp[2\pi i(\nu-\nu')t]-1}{\nu-\nu'}\,\mathrm{d}\nu',$$

$(b(t))^2$, which represents the small fraction of particles in state $j+1$ at time t, is then

$$(4.10)\qquad |b(t)|^2=\frac{\beta^2}{h^2}(X_{j,j+1})^2\int|\mathcal{F}(\nu)|^2\,2\,\frac{1-\cos 2\pi(\nu-\nu')t}{(\nu-\nu')^2}\,\mathrm{d}\nu'=$$
$$=\frac{4\beta^2}{h^2}(X_{j,j+1})^2\int|\mathcal{F}(\nu')|^2\frac{\sin^2\pi(\nu-\nu')t}{(\nu-\nu')^2}\,\mathrm{d}\nu'.$$

The argument of the integral is sharply peaked at $\nu'=\nu$ and one gets (*)

$$(4.11)\qquad |b(t)|^2=\frac{4\pi^2\beta^2 l^2}{h^2}(X_{j,j+1})^2|\mathcal{F}(\nu)|^2 t.$$

If the collisions are sufficiently far apart and random, $|\mathcal{F}(\nu)|^2$ is proportional to the number of collisions per second and $|\mathcal{F}(\nu)|^2 t$ is the product of $|\mathcal{F}(\nu)|^2$ for one collision times the total number of collisions during t. If one takes this modified meaning of $|\mathcal{F}(\nu)|^2$ and (4.9) into account, the eq. (4.11) agrees exactly with eq. (4.2) apart from the factor $\beta^2(j+1)$.

4·3 *Quantum-theoretical treatment* [13, 14]. – One considers the molecule BC as a scatterer, fixed in space, on which a beam of molecules A, of fixed velocity w_0 impinges. The incident beam is described as a plane wave, $\exp[ik_0x]$ where the propagation constant k_0 is (p_0 linear momentum)

$$(4.12)\qquad k_0=\frac{2\pi p_0}{h}=\frac{2\pi\tilde{m}w_0}{h}.$$

(*) The integral is evaluated by changing the variable to $y=\pi(\nu-\nu')t$. Then it takes the form

$$|\mathcal{F}(\nu)|^2\pi t\int_{-\infty}^{\infty}\frac{\sin^2 y}{y^2}\,\mathrm{d}y.$$

The latter integral is π.

In the expressions (4.7-4.10), the energy is *not* conserved for each value of the integrand, since $h\nu\neq h\nu'$. Only at the end, by the interference process, is conservation of energy reached, since absorption of a phonon $h\nu$ leads to a vibrational energy jump $h\nu$. Without the integration, $|b(t)|^2$ would not be proportional to t, and one could not write equations of the type familiar in reaction kinetics. See the remark to eq. (4.1-4.5).

Since a plane wave of unit amplitude is associated with unit spatial density, the number of particles passing through unit area per second is w_0. Here, $\tilde{m}$ is the effective mass of the relative motion.

The scatterer produces both elastically and inelastically scattered waves. Both of these obey the same differential equation as the primary waves, namely far from the scatterer the usual wave equation, near the scatterer a wave equation corresponding optically to a region of variable refractive index, the latter due to the interaction potential. This is called the method of distorted waves; the Born approximation neglects this effects. Far from the scatterer, both the elastic and the inelastically scattered wave behave as spherical waves (*i.e.* are proportional to $1/r \exp[-ikr]$) although the amplitude may depend on the angle. The elastically scattered wave has the propagation constant k_0, equal to that of the incident wave, the inelastically scattered wave a different one, due to the change of energy,

$$\frac{\tilde{m}}{2} w^2 = \frac{\tilde{m}}{2} w_0^2 \pm h\nu ,$$

or

$$k = k_0 \left(1 \pm \frac{h\nu}{\tilde{m} w_0^2/2}\right)^{\frac{1}{2}} \sim k_0 \pm \frac{2\pi\nu}{w_0} , \tag{4.13}$$

if

$$h\nu \ll \frac{\tilde{m}}{2} w_0^2 .$$

The amplitude of the elastic wave is determined by the boundary condition at the scatterer, that of the inelastically scattered wave by the perturbation potential, acting on the combination of incoming and elastically scattered wave. In the one-dimensional case we are dealing with plane reflected waves, the elastic wave having in first approximation the same amplitude as the incoming wave.

If the amplitude of the inelastically scattered wave is $a(\varphi)$ (where φ in the three-dimensional case stands for any angle), the total fraction of inelastically scattered particles is ($\mathrm{d}\Omega$ element of steric angle)

$$\frac{k}{k_0} \int |a^2| \,\mathrm{d}\Omega ,$$

for three dimensions,

$$\frac{k}{k_0} |a^2| ,$$

for one dimension.

The fraction of inelastically scattered particles is equal to the fraction of collisions which produce excitation (de-excitation).

We now discuss the two methods of time-dependent and stationary perturbation theory.

4'4. *Time-dependent perturbation.* – The procedure is analogous to that under 4'2, except that the Schrödinger equation is written not for the vibration alone (eq. (4.5)), but for the complete process, relative translational motion and vibration. Accordingly, the (partial) wave function is the product of a translational wave function $\psi_A(kx)$ and a vibrational wave function $\psi_{BC}(X)$. The Schrödinger equation for the complete process, including primary wave, elastically and inelastically scattered waves, is then

$$(4.15)\qquad \frac{h}{2\pi i}\frac{\mathrm{d}\psi}{\mathrm{d}t} = -\frac{h^2}{8\pi^2\tilde{m}}\frac{\partial^2\psi}{\partial x^3} - \frac{h^2}{8\pi^2\tilde{\tilde{m}}}\frac{\partial^2\psi}{\partial X^2} + \left[H(x) + 2\pi^2\tilde{\tilde{m}}\nu^2X^2 - \beta\frac{\partial H}{\partial x}X\right]\psi = 0,$$

instead of (4.5).

The terms with x control the relative motion of A and BC, those with X alone govern the unperturbed vibration of BC, and the last term in [ ] is responsible for the coupling of the two inelastic transitions.

The total energy when the particles are still far apart, is equal to

$$E_0 = \frac{\tilde{m}}{2}w_0^2 + \left(v + \frac{1}{2}\right)h\nu = \frac{h^2}{8\pi^2\tilde{m}}k_0^2 + \left(v + \frac{1}{2}\right)h\nu\,.$$

For the solution one proceeds as in (4.3). In addition, because of eq. (1.15), we can simplify our expression by putting $v = 0$. Therefore

$$(4.16)\qquad \psi = \psi_A(k_0x)\,\psi^0_{BC}(X)\exp\left[\frac{2\pi iE_0t}{h}\right] + b(t)\,\psi_A(kx)\,\psi^{(1)}_{BC}(X)\exp\left[\frac{2\pi iE't}{h}\right],$$

where $\psi_A(kx)$ satisfies the equation for the relative « elastic » motion

$$(4.17)\qquad \frac{\mathrm{d}^2}{\mathrm{d}x^2}\psi_A - \left[\frac{8\pi^2\tilde{m}}{h}H(x) - k^2\right]\psi_A = 0\,.$$

In (16) conservation of energy is *not* presupposed. After introducing (4.16) into (4.15), making use of (4.17) and of the oscillator equation, neglecting terms of the second order, namely $b(\mathrm{d}b/\mathrm{d}t)$ and bX, one is left with

$$(4.18)\qquad \frac{h}{2\pi i}\psi_A(kx)\,\psi^{(1)}_{BC}(X)\frac{\mathrm{d}b}{\mathrm{d}t} = -\beta\frac{\mathrm{d}H}{\mathrm{d}x}X\,\psi_A(k_0x)\,\psi^0_{BC}(X)\exp\left[\frac{2\pi i}{\hbar}(E' - E_0)t\right].$$

One now multiplies by $\psi_{\mathrm{A}}(kx)\,\psi^{(1)}_{\mathrm{BO}}(X)$ and integrates over x and X:

$$\int \psi^{*}_{\mathrm{A}}(kx)\,\frac{\mathrm{d}H}{\mathrm{d}x}\,\psi_{\mathrm{A}}(k_0 x)\,\mathrm{d}x = H'_{k_0 k}\,. \tag{4.19}$$

Normalize ψ_{A} so that the density is one particle per unit volume. Call L the (large) region of integration for x (in three dimensions, this would be a volume). One then has

$$\frac{h}{2\pi i}\,L\,\frac{\mathrm{d}b}{\mathrm{d}t} = -\,\beta H'_{k_0 k} X_{10} \exp\left[\frac{2\pi i}{h}\,(E'-E)\,t\right]. \tag{4.20}$$

From now on proceed as before (eq. (4.10)), integrating first over time, then over a narrow range of E' near the value E which alone satisfies the conservation of energy. The integration over E' takes the place of the integration over ν' in (4.10) but requires the introduction of a « density of states » $G(E)$, defined so that $G(E)\,\mathrm{d}E$ is the number of states lying within $\mathrm{d}E$. $L^{-1}G(E)$ is independent of L; Lb^2 is the total number of transitions. One finds therefore (see (4.11))

$$L\,\frac{b^2}{t} = \frac{4\pi^2}{h}\,L^{-1}\mathcal{G}(E)\,X^2_{10}\,|H'_{k_0 k}|^2\,. \tag{4.21}$$

4.5. *Method of perturbed stationary states.* – The scatterer is supposed to have only states 0 and 1. A beam of particles A, represented by a plane wave with propagation constant k_0, falls on it. If not one sample of the system but an ensemble if considered, the number N_1 of the scatterers will be in state one, the number $N_0 = N - N_1$ in state zero. In the stationary state, the number of scatterers

$$k_{0\to 1}(E)\,N_0$$

will be excited per second, the number $k_{10}(E_0)N_1$ will be de-excited, if there is one particle A of energy E per unit volume. Therefore, N_1 will be determined by

$$N_1 = \frac{k_{01}(E)}{k_{10}(E)}\,N_0 \sim \frac{k_{01}(E)}{k_{10}(E)}\,N,$$

neglecting N_1 besides N_0.

For each excitation, one incoming particle has its energy diminished to $E_0 - h\nu$, for each de-excitation, one particle has its energy increased to $E_0 + h\nu$. If therefore all the particles scattered per second with $k = k_0[1-(h\nu/E_0)]^{\frac{1}{2}}$ are counted, this is equal to the number of excitations per scatterer per second.

Therefore the inelastic cross-sections

$$Q_{1\to 0}=\frac{k}{k_0}\int |a|^2\,\mathrm{d}\Omega\,. \tag{4.22}$$

One now again writes eq. (4.16), but assumes directly conservation of energy, so that everything is proportional to $\exp[(2\pi i/h)E_0t]$ and one has the time-independent Schrödinger equation

$$-\frac{h^2}{8\pi^2\tilde{m}}\frac{\partial^2\psi}{\partial x^2}-\frac{h^2}{8\pi^2\tilde{\tilde{m}}}\frac{\partial^2\psi}{\partial X^2}+\left[H(x)+2\pi^2\tilde{\tilde{m}}\nu^2X^2-\beta\frac{\mathrm{d}H}{\mathrm{d}x}X-E_0\right]\psi=0\,. \tag{4.23}$$

One tries the solution (compare with (4.16))

$$\psi=\psi_{\mathrm{A}}(k_0x)\,\psi^0_{\mathrm{BC}}(X)+a\tilde{\psi}_{\mathrm{A}}(kx)\,\psi^{(1)}_{\mathrm{BC}}(X)\,, \tag{4.24}$$

where a is time-independent and is considered, like X, as small quantity, the squares of which are neglected. After considering the Schrödinger equation to which $\psi_{\mathrm{BC}}(X)$ obeys, one finds for $\tilde{\psi}_{\mathrm{A}}$ ·

$$\left(\frac{\mathrm{d}^2}{\mathrm{d}x^2}-\frac{8\pi^2\tilde{m}}{h^2}H+k^2\right)\tilde{\psi}_{\mathrm{A}}(kx)=-\frac{8\pi^2\tilde{m}}{h^2}\beta X_{10}\frac{\mathrm{d}H}{\mathrm{d}x}\psi_{\mathrm{A}}(k_0x)\,. \tag{4.25}$$

The square of the amplitude of the inelastically scattered wave follows then as

$$|a|^2=\frac{\beta^2}{p_0p}X^2_{10}\left|\frac{4\pi\tilde{m}}{h}H'_{k_0k}\right|^2. \tag{4.26}$$

For a comparison, see addendum at end of Section 11.

We have made the following approximations.

We have stopped, in (4.24), with the first-order perturbation. This means that we have neglected processes like 0 → 2 → 1; but this is forbidden by the selection rules of the simple harmonic oscillator. But we have also neglected processes like 1 → 2, which also require $h\nu$ and therefore also result in inelastic waves with the same k. This requires that the number of excited states N_1 is so small compared to N_0 that this process is negligible.

5. – Transition from the one-dimensional to the three-dimensional spherical case for the calculation of the umperturbed motion.

5·1. *Classical.* – In one dimension, the energy equation for the relative motion is

$$\frac{\tilde{m}}{2}\left(\frac{\mathrm{d}x}{\mathrm{d}t}\right)^2+H(x)=E_0=\frac{1}{2}\tilde{m}w_0^2\,. \tag{5.1}$$

Solving for $\mathrm{d}x/\mathrm{d}t$ and separating variables, one has

$$(5.2)\qquad \int \mathrm{d}t = \left(\frac{\tilde{m}}{2}\right)^{\frac{1}{2}} \int \frac{\mathrm{d}x}{\sqrt{E_0 - H(x)}} = \frac{1}{w_0} \int \frac{\mathrm{d}x}{\sqrt{1-(1/E_0)H(x)}}\,.$$

In three dimensions, the orbit is plane, if $H(r)$ has spherical symmetry. In polar co-ordinates r and φ, the energy equation has the following form:

$$(5.3)\qquad \frac{\tilde{m}}{2}\left(\frac{\mathrm{d}r}{\mathrm{d}t}\right)^2 + \frac{\tilde{m}}{2} r^2 \left(\frac{\mathrm{d}\varphi}{\mathrm{d}t}\right)^2 + H(r) = E\,.$$

In addition, we have the equation for the conservation of angular momentum

$$(5.4)\qquad P_\varphi = \tilde{m} r^2 \frac{\mathrm{d}\varphi}{\mathrm{d}t}\,.$$

Eliminating $\mathrm{d}\varphi/\mathrm{d}t$, one gets

$$\frac{\tilde{m}}{2}\left(\frac{\mathrm{d}r}{\mathrm{d}t}\right)^2 + \frac{1}{2\tilde{m}} \frac{1}{r^2} P_\varphi^2 + H(r) = E_0\,.$$

In general, this is too difficult to integrate in closed form. However, one can also here use an approximation, which was first introduced in the quantum-theoretical method by TAGAYANAKI [14, 15] and SCHWARTZ and HERZFELD [16], the method of « modified wave length ».

One substitutes in the centrifugal quasi-energy the distance of closest approach, the collision radius r_c, for the variable r, *i.e.* writes the second term

$$\frac{1}{2\tilde{m}} \frac{1}{r_c^2} P_\varphi^2\,,$$

and brings this to the right side, so that it acts as a subtrahend from the energy.

The equation is then

$$(5.5)\qquad \frac{\tilde{m}}{2}\left(\frac{\mathrm{d}r}{\mathrm{d}t}\right)^2 + H(r) = E_0 - \frac{1}{2\tilde{m}} \frac{1}{r_c^2} P_\varphi^2\,.$$

The rest of the calculation follows as in the one-dimensional case, except that one uses a modified velocity w' instead of w_0, namely

$$w' = w_0 \left\{1 - \frac{1}{\tilde{m}^2 w_0^2 r_c^2} P_\varphi^2\right\}^{\frac{1}{2}}.$$

Finally, one has to sum over P_φ. At large distance from the scatterer one has

$$P_\varphi = \tilde{m} w_0 \sigma \,, \tag{5.6}$$

where σ is the minimum distance of A from the mass center of BC, if A were proceeding on a straight line, or

$$w' = w_0 \left\{1 - \left(\frac{\sigma}{r_c}\right)^2\right\}^{\frac{1}{2}} .$$

In a beam of particles in which N' particles fall per second on the unit area, the number having an (original) distance between σ and $\sigma + \mathrm{d}\sigma$ is

$$N' 2\pi\sigma \, \mathrm{d}\sigma = N' 2\pi \frac{1}{(\tilde{m} w_0)^2} P_\varphi \, \mathrm{d}P_\varphi \,. \tag{5.7}$$

Therefore, after one has found the quantity $\mathscr{F}(\nu, w_0, P_\varphi)$ (see eq. (4.1)) one calculates

$$\frac{2\pi}{(\tilde{m} w_0)^2} \int |\mathscr{F}(P_\varphi)|^2 P_\varphi \, \mathrm{d}P_\varphi \,,$$

and multiplies by $|(2\pi\beta l/h) X_{01}|^2$ to get the inelastic cross-section for particles of original velocity w_0. Finally, one integrates over w_0 using the Maxwell distribution law to get the average cross-section. From the computational standpoint, it is easier to invert the order of integration.

5·2. *Quantum-theoretical.* – The Schrödinger equation in the one-dimensional case is given by (4.17). In the 3-dimensional case some modifications have to be introduced. The kinetic energy of particles is now given by

$$-\frac{h^2}{8\pi^2 \tilde{m}} \left[\frac{1}{r^2} \frac{\partial}{\partial r} r^2 \frac{\partial}{\partial r} + \frac{1}{r^2 \sin\theta} \frac{\partial}{\partial\theta} \sin\theta \frac{\partial}{\partial\theta} + \frac{1}{r^2} \frac{1}{\sin^2\theta} \frac{\partial^2}{\partial\varphi^2}\right] . \tag{5.8}$$

The latter part requires that the wave function, $\psi_A(kr)$ has to be multiplied by a generalized (normalized) spherical harmonic $S_j(\theta, \varphi)$. However, this is not changed in the collision, since the total angular momentum must be preserved and in the present spherical model there is no way to take up any change in orbital angular momentum. Therefore the same angular-momentum quantum number j belongs to the partial wave of the primary, of the elastic and the inelastically scattered waves. The result is the operator

$$-\frac{h^2}{8\pi^2 \tilde{m}} \left\{\frac{1}{r^2} \frac{\mathrm{d}}{\mathrm{d}r} r^2 \frac{\mathrm{d}}{\mathrm{d}r} - \frac{j(j+1)}{r^2}\right\} . \tag{5.9}$$

As in a classical case, we approximate by choosing a constant r, namely r_c and therefore the centrifugal term contributes an additional term to the energy:

$$E_{\text{eff}} = E_0 - \frac{h^2}{8\pi^2 \tilde{m}} \frac{1}{r_c^2} j(j+1)\,.$$

After the calculation is completed, one has to sum properly over j. Furthermore one can show the following by direct substitution: if $f(kr)$ is a solution of the one-dimensional Schrödinger equation (4.17) then $f(k'r)/r$ is a solution of

$$\frac{1}{r^2}\frac{\mathrm{d}}{\mathrm{d}r} r^2 \frac{\mathrm{d}}{\mathrm{d}r}\left(\frac{f}{r}\right) - \left[\frac{8\pi^2 \tilde{m}}{h^2} H(r) - (k')^2\right]\frac{f}{r} = 0\,. \tag{5.10}$$

Therefore, the transition to three dimensions can be made by writing ψ_A/r instead ψ_A and by modifying the energy. The former change, however, does not change the quantity $H_{k_0 k}$; integration over x is replaced by integration over $r^2\mathrm{d}r$:

$$\int \frac{\psi_A(k'r)}{r} \frac{\mathrm{d}H}{\mathrm{d}r} \frac{\psi_A(k_0 r)}{r} r^2\,\mathrm{d}r\,, \tag{5.11}$$

except for a possible effect of a change in the range of integration.

6. - The model used.

It follows from the preceding that the transition probability depends very sensitively on the steepness of the potential in the region of the classical turning point of the collisions which contribute most to the effect.

If one wants therefore to calculate this probability *a priori* one must have sources other than experimental determinations of the relaxation times from which to get the shape of the interaction potential.

On principle, one should be able to calculate this interaction potential theoretically, but except for He—He and H_2—H_2, this is not possible at present. The largest source exists at present in the calculations in which HIRSCHFELDER and his co-workers have evaluated the viscosity of an ideal gas and its temperature-dependence, for spherical molecules which interact by a Lennard-Jones potential

$$H(r) = 4\varepsilon\left[\left(\frac{r_0}{r}\right)^{12} - \left(\frac{r_0}{r}\right)^{6}\right]. \tag{6.1}$$

The inelastic scattering by such a potential cannot be calculated in closed form, and so SLAWSKY, SCHWARTZ and HERZFELD [17] have replaced it by an exponential expression

$$H(r) = H_0 \exp\left[-r/l\right] - \varepsilon \,. \tag{6.2}$$

The asymptote of H for $r = \infty$ lies at the depth of the well of the Lennard Jones formula, namely at $-\varepsilon$, the other two constants, H_0 and l, may be determined in several ways. It has been found most useful, according to DE WETTE and SLAWSKY [8], to make H and $(H)_{LJ}$ equal at two points: at $r = r_0$, where the Lennard-Jones potential is zero and therefore

$$H_0 \exp\left[-r_0/l\right] = \varepsilon \tag{6.3}$$

and at the classical turning point of the most important molecules, those with kinetic energy E_m.

Call that distance the collision radius r_c. Then

$$E_m = 4\varepsilon \left[\left(\frac{r_0}{r_c}\right)^{12} - \left(\frac{r_0}{r_c}\right)^{6}\right] = H_0 \exp\left[-\frac{r_c}{l}\right] - \varepsilon \,. \tag{6.4}$$

The result is

$$\frac{r_0}{l} = \left\{\ln\left(\frac{E_m}{\varepsilon} + 1\right)\right\}\left\{1 - \left[\frac{1}{2}\left(1 + \sqrt{\frac{E_m}{\varepsilon} + 1}\right)\right]^{-\frac{1}{2}}\right\}, \tag{6.5}$$

r_0/l is 24 for $E_m = 0$ and has a broad minimum of 18.48 between $E_m/\varepsilon = 99$ and 730, the value of r_0/l being 1 % above the minimum at the lower end of the above range of E_m/ε.

H_0 which will not directly appear in our calculations is given by

$$H_0 = (E_m + \varepsilon)\left(\frac{E_m}{\varepsilon} + 1\right)^{-[\,]} ,$$

where [ ] signifies this brackets in eq. (6.5).

This procedure makes use of the fact that the attractive part of the Lennard-Jones curve is much less steep than the repulsive part, and for this reason it will only cause a negligible number of transitions.

At the classical turning point, the first and second differential quotients of the exponential expression are

$$-\,lH_0 \exp\left[-r_c/l\right] , \qquad l^2 H_0 \exp\left[-r_c/l\right] .$$

We now use, in succession, the following models, mentioned earlier:

a) One-dimensional. The molecule BC is approached by the particle A of effective mass $\mathfrak{M}$ with the relative velocity w_0. The interaction is supposed to be of such short range that only that between nearest particles, B and A, need to be taken into account. If B-C vibrates, the distance between B and A is $x-L_B-\beta X$, and therefore the interaction potential

$$(6.6)\qquad H=-\varepsilon+H_0\exp\left[-\frac{1}{l}(x-L_B-\beta X)\right]=$$

$$=-\varepsilon+\left(H_0\exp\left[\frac{L_B}{l}\right]\right)\exp\left[-\frac{1}{l}(x-\beta X)\right]=-\varepsilon+H_0'\exp\left[\frac{-x}{l}\right]\cdot\left(1-\frac{\beta X}{l}\right),$$

provided $\beta X<l$ (6.7).

Here x is the distance from A to the center of mass of BC, L_B the equilibrium distance of B from the center of mass of BC, and

$$H_0'=H_0\exp\left[\frac{L_B}{l}\right].$$

b) *Three-dimensional, spherical symmetry.* Here the linear model of the molecule BC is replaced by two concentric spheres, C and B, which can vibrate against each other. The only change is the replacement of x by r, the distance between A and the center of the spherical molecule BC.

c) *Three-dimensional, linear.* Here we consider the linear molecule BC; each atom, B and C, interacts separately by an exponential repulsion with the approaching molecule A, while the effect of the attractive force, $-\varepsilon$, remains as coming from the center of BC. The details of the calculation will be given in Section 8·3 for the special case where B and C are atoms of the same kind.

Translational motion for an exponential force law:

α) *Classical* [10]. One has from the energy principle (5.1)

$$(6.8)\qquad dt=\pm(E_0+\varepsilon)^{-\frac{1}{2}}\left\{1+\frac{H_0'}{E_0+\varepsilon}\exp\left[-\frac{x}{l}\right]\right\}^{-\frac{1}{2}}dx\,.$$

The substitution

$$u^2=\frac{E_0+\varepsilon}{H_0'}\exp\left[\frac{x}{l}\right],$$

results finally in

$$(6.9)\qquad F(t)=\frac{E_0+\varepsilon}{l}\left[\cosh\frac{w_0'}{2l}(t-t_0)\right]^{-2},$$

which has, as square of the Fourier amplitude

(6.10) $$|\mathscr{F}(\nu)|^2 = 16\pi^4\tilde{m}^2\nu^2 l^3 \left[\sinh\frac{2\pi^2\nu l}{w_0'}\right]^{-2} .$$

For large value of $2\pi^2\nu l/w_0'$ this takes the form

(6.11) $$|\mathscr{F}(\nu)|^2 = 4\tilde{m}\, 16\pi^4\tilde{m}\nu^2 l^2 \exp\left[-\frac{4\pi^2\nu l}{w_0'}\right] ,$$

where

$$w_0' = w\left(1+\frac{\varepsilon}{E_0}\right)^{\frac{1}{2}} .$$

It will be useful to introduce here two « temperatures », θ and θ'. θ is the characteristic temperature of the molecular vibration,

$$\theta = \frac{h\nu}{k} = \frac{hc}{k}\tilde{\nu} = 1.44\tilde{\nu} ,$$

θ' is defined by

$$\theta' = \frac{1}{k}\,16\pi^4\tilde{m}\nu^2 l^2 = 0.8153\tilde{M}\theta^2 l^2 .$$

Then

(6.11a) $$l^2|\mathscr{F}(\nu)|^2 = \frac{h^2}{4\pi^4}\left(\frac{\Theta'}{\Theta}\right)^2 \exp\left[-\frac{4\pi^2\nu l}{w_0'}\right] ,$$

where l is measured in ångstroms in the last expression.

$2\pi^2\tilde{m}\nu l^2$ would be the energy necessary to stretch the molecular oscillator by l. Furthermore

(6.11b) $$E_m = k\frac{1}{2}(\theta')^{\frac{1}{3}}T^{\frac{2}{3}} .$$

(see eq. (3.5)).

One of the difficulties of the classical calculations is the fact that, because of its very nature, only the initial velocity w_0' enters. As a method of improving this, it has been suggested that

$$\frac{1}{w_0'} \text{ be replaced by } \frac{1}{2}\left(\frac{1}{w_0'}+\frac{1}{w_1'}\right) \quad \text{or} \quad E \text{ by } \tfrac{1}{2}(E_0+E_1) ,$$

$$(w_1')^2 = (w_0')^2\left[1 \mp \frac{h\nu}{E_0'}\right] ,$$

β) Quantum-dynamical.

A) One-dimensional. The Schrödinger equation (4.17) with $H = H_0 \cdot \cdot \exp[-x/l]$ has been integrated by JACKSON and MOTT [18]. The solution is a Bessel function of argument

$$\zeta = \pm \frac{i}{\pi 0}\left(20' \frac{H'_0}{k}\right) \exp\left[-\frac{x}{2l}\right],$$

and index

$$\pm i \frac{4\pi p l}{h}.$$

The model is a plane in the yz plane, exerting a repulsive potential $H_0 \exp[-x/l]$. This becomes infinity at $x = -\infty$ so that the particles A cannot penetrate to $x = -\infty$. The resultant elastically scattered wave is determined by the fact that the total wave function is zero at $x = -\infty$ (*i.e.*, for a value of the argument $\pm i\infty$). This determines the choice of the amplitude of the elastically scattered wave; from the geometry of the case, it is clear that this reflected wave is of equal amplitude as the incident wave, *i.e.*, the reflection is total—of course only in zero approximation, as has been mentioned before. Both the incident and the elastically reflected wave contribute equally to the amplitude of the inelastically scattered wave so that the total energy of the latter (*i.e.*, the fraction of inelastically scattered particles) is four times that produced by the primary wave alone.

The result is

$$(6.12) \qquad \frac{4\pi \tilde{m}}{h\sqrt{p_0 p_1}} H_{kk_0} = 8 \frac{\pi^3 l^2}{h^2} (p_1^2 - p_0^2)(\sinh g_0 \sinh g_1)^{\frac{1}{2}}(\cosh g_1 - \cosh g_0)^{-1},$$

where

$$(6.13) \qquad g = \frac{4\pi^2 p l}{h} = 4\pi^2 \frac{l}{\lambda},$$

λ being the de Broglie wave length of the relative motion of particle A. In general g_0, $g_1 \gg 1$ (which is the condition for the approximate agreement of classical and quantum theoretical calculation).

Under this condition

$$\sinh g = \cosh g = \tfrac{1}{2} e^g$$

and the last two factors give

$$\exp\left[\frac{g_0 + g_1}{2}\right] [\exp[g_1] - \exp[g_0]]^{-1} = \left[\exp\left[\frac{g_1 - g_0}{2}\right] - \exp\left[\frac{g_0 - g_1}{2}\right]\right]^{-1}.$$

One has now to distinguish two cases

$$|g_1 - g_0| > 1$$

and

$$|g_1 - g_0| < 1 .$$

The former case requires

$$g_0 \left| \frac{g_1}{g_0} - 1 \right| > 1 ,$$

or

$$g_0 \left| \sqrt{1 \mp \frac{h\nu}{E}} - 1 \right| > 0 ,$$

or

$$g_0 \frac{1}{2} \frac{h\nu}{E_0} > 0 ,$$

or

$$\frac{4\pi^2 l\nu}{w_0} > 1 , \tag{6.14}$$

which is the same condition as in the classical case (6.11).

This can also be written (by squaring)

$$k\theta' \gg 2E .$$

If for E there is substituted E_m, it can be seen that this may be rewritten

$$\theta' \gg (\theta')^{\frac{1}{3}} T^{\frac{2}{3}} \qquad \text{or} \qquad \theta' \gg T \tag{6.15}$$

which is always the case for « nonresonance transfer ».

Under the assumption of transfer of one vibrational quantum we find therefore

$$\frac{4\pi\tilde{m}}{h\sqrt{p_0 p_1}} H_{kk_0} = \frac{8\pi^3 l^2}{h^2} 2\tilde{m}h\nu \exp\left[- \frac{|g_1 - g_0|}{2} \right] ,$$

and for the square

$$\left(\frac{4\pi\tilde{m}}{h\sqrt{p_0 p_1}} H_{kk_0} \right)^2 = \frac{1}{\pi^2} \left(\frac{\theta'}{\theta} \right)^2 \exp\left[- |g_1 - g_0| \right] , \tag{6.16}$$

$$|g_1 - g_0| = - \frac{4\pi^2 l\nu}{w_0} \left(1 \mp \frac{h\nu}{2mw_0^2} \right) . \tag{6.17}$$

The negative sign applies to de-activation, the positive sign to activation.

If one compares the quantum theoretical expression for $|(4\pi\tilde{m}/\sqrt{p_0 p_1})H_{kk_0}|^2$ (6.16), (6.17) with the classical expression for $4\pi^2 l^2/h^2|\mathscr{F}(\nu)|^2$ ((4.11) and (6.11*a*)) one finds that, for high kinetic energies ($>10kT$) they are identical. However, Cottrell and McCoubrey [19] have shown that the agreement is excellent throughout the whole energy range, provided that the velocity w in the classical formula is symmetrized according to

$$w = \tfrac{1}{2}(w_0 + w_1)\,.$$

If one now integrates over the Maxwell distribution function according to the expressions of Section 3'3, in particular (3.7), one finds, with the definition of a new quantity Z_{tr}

$$\frac{1}{Z_{\mathrm{tr}}} = \left[\frac{(4\pi\tilde{m})^2}{h^2 P_0 P_1}\,|H_{kk'}|^2\right]_{\mathrm{ave}} = \frac{1}{\pi^2}\sqrt{\frac{2\pi}{3}}\left(\frac{\theta'}{\theta}\right)^2\left(\frac{\theta'}{T}\right)^{\frac{1}{6}}\exp\left[-\frac{3}{2}\left(\frac{\theta'}{T}\right)^{\frac{1}{3}} + \frac{\theta}{2T} + \frac{\varepsilon}{T}\right]. \tag{6.18}$$

In eq. (6.18) the last two terms of the exponent need discussion: $+\theta/2T$ is the result of the second term on the right in (6.17) and is valid for deactivation; for activation the sign would be negative. This conforms with the general rule (1.6). ε/kT results from substituting for w_0 in (6.17) the velocity w_0' as modified by the attractive potential

$$\frac{4\pi^2 l\nu}{w_0'} = \frac{4\pi^2 l\nu}{w_0}\left(1 + \frac{\varepsilon}{E_0}\right)^{-\frac{1}{2}} = \frac{4\pi^2 l\nu}{w_0} - \frac{4\pi^2 l\nu\varepsilon}{2w_0 E_0}\,,$$

and using, for E_0 in the second term, the values for E_m.

We have to discuss the second case in passing, $|g_1 - g_0| < 1$ where very little energy is exchanged. Then

$$\frac{4\pi\tilde{m}}{h\sqrt{p_0 p_1}}\cdot H_{kk_0} = \frac{8\pi^3 l^2}{h^2}\,\frac{p_1^2 - p_2^2}{g_1 - g_0} = \frac{2\pi l}{h}\,(p^0 + p_1) \sim \frac{4\pi l}{h}\,p_0\,,$$

and

$$\frac{1}{Z_{\mathrm{tr}}} = \left[\left(\frac{4\pi\tilde{m}}{h}\right)^2 \frac{1}{p_0 p_1}\,|H_{kk_0}|^2\right]_{\mathrm{ave}} = \frac{16\pi^2 l^2}{h^2}\,[p_0^2]_{\mathrm{ave}} = \frac{16\pi^2 l^2}{h^2}\,2\tilde{m}2kT = \frac{4}{\pi^2}\,\frac{\theta' T}{\theta^2}\,. \tag{6.19}$$

B) 3-*dimensional case.* As mentioned earlier, the transfer of the one-dimensional results to three dimensions can be done relatively easily. There are, however two points to be mentioned. While the general form of the solutions for the combination of primary and elastically scattered waves are the same, the boundary conditions are somewhat different. In the plane case, the solutions must be zero deep in the reflecting body, at $x = -\infty$; in the spherical case, it must be zero at the center of the scatterer, at $r = 0$, where the argument of the Bessel function is not infinite. However, because of the actual values of H_0, this argument is quite large at the center. This means that, while the elastically scattered wave will not have in the spherical case exactly the same amplitude as the primary wave, the difference should not be great; it has been neglected here and the one-dimensional result been taken over.

The primary wave

$$\exp\,[ik_0 z]$$

can be analysed into partial waves, to each of which corresponds a partial elastic and inelastically scattered wave. If there is a stream of one particle A per second and unit area coming in, the angle distribution (square of the amplitude times p_1/m) of the scattered wave is given by

$$\left(\frac{h}{2\pi r}\,\frac{2j+1}{2p_0}\right)^2 Q_{j,v\to v'} P_j^2\,,$$

where $Q_{j\,v\to v'}$ is a partial inelastic cross-section and P_j a Legendre function of order j. Integrating over the sphere

$$2\pi r^2\int P_j^2 \sin\theta\,\mathrm{d}\theta = 2\pi r^2\,\frac{2}{2j+1}\,,$$

gives

$$\frac{h^2}{4\pi p_0^2}\,(2j+1)Q\,,$$

where Q is the corresponding solution of the one-dimensional problem. Integrating this over the three-dimensional Maxwell distribution for a stream of molecules this contributes, compared with the one-dimensional expression, a factor

$$\frac{1}{4}\,4\pi\,\frac{\tilde{m}}{2\pi kT}\,w^2 = \frac{1}{2\tilde{m}kT}\,p_0^2\,.$$

Therefore

$$(Q_j)_{\text{ave}} = \frac{h^2}{8\pi\tilde{m}kT}\,(2j+1)\,\frac{1}{Z_{\text{osc}}}\,\frac{1}{Z_{\text{tr}}}\,, \tag{6.20}$$

where the latter quantities are those for the one-dimensional case, eqs. (4.8) and (6.18).

Finally, taking the effect of the quasi-centrifugal (slowly varying and considered constant) quasi-potential

$$(6.21)\qquad \frac{h^2}{8\pi^2\widetilde{m}}\,\frac{j(j+1)}{r^2} \sim \frac{h^2}{8\pi^2\widetilde{m}}\,\frac{j(j+1)}{r_c^2}$$

into account in the same manner as that of the attractive potential (by an exponential) and summing over j, one finds

$$(6.22)\qquad (Q_{v\to v'})_{\text{ave}} = \pi r_c^2\,\frac{1}{Z_{\text{osc}}}\cdot\frac{1}{Z_{\text{tr}}}\,,$$

πr_c^2 is a cross-section, the next two factors are pure numbers. We will add a third number to these, $1/Z_0$ which we call the steric factor and will discuss later.

Before we proceed, the influence of the value of H_0 on the result should be discussed. In the one-dimensional case there is exactly *no* effect on the intensities of the elastic and the inelastically scattered wave far enough from the reflector. This is due to the fact that

$$H_0 \exp\left[-\frac{x}{l}\right] = \exp\left[-\frac{1}{l}\,(x - l\ln H_0)\right],$$

so that a change in H_0 can be compensated by a shift in the origin. The same is true for the variable ξ of the wave function, and as the integral in H_{kk_0} goes from $-\infty$ to $+\infty$, its value remains unchanged.

In the three-dimensional case this is not quite true, since at the origin, $r = 0$ (which also appears as limit of the integral) the argument of the wave function is

$$\pm i\left(\frac{2}{\pi^2}\,\frac{\Theta'}{\Theta^2}\,\frac{H_0}{k}\right)^{\frac{1}{2}}.$$

But since this value is large, we have neglected the dependence of the result on the particular value H_0.

Returning to eq. (6.22) we express πr_c^2 in a slightly different way:

$$(6.23)\qquad \pi r_c^2 = \pi\left(\frac{r_c}{r_0}\right)^2 r_0^2 = \left(\frac{r_c}{r_0}\right)^2 \frac{1}{N_A\overline{w}_r}\,[1.017\,Y(2,2)]^{-1}\,\frac{1}{\tau_c}\,.$$

The function $Y(2,2)$ has as its argument kT/ε and is tabulated by HIRSCHFELDER *et al.* It corrects the actual viscosity cross-section for the effect of the attractive forces, as compared to the hard sphere cross-section (see Sect. 4, p. 281 and Sect. 6, p. 291).

Finally we have to get the connection between the relaxation time τ and the inelastic cross-section (Q_{10}). This relation is given by (1.16). If we define Z by

$$\frac{1}{Z}=\frac{\tau_0}{\tau}, \tag{6.24}$$

we find

$$Z=1.017\left(\frac{r_0}{r_c}\right)^2 Y(2,2)\left(1-\exp\left[-\frac{\theta}{T}\right]\right)^{-1}\exp\left[-\frac{\varepsilon}{kT}\right]Z_0 Z_{\text{osc}} Z_{\text{tr}}\,. \tag{6.25}$$

Except for the factor $(1-\exp[\theta/T])^{-1}$, Z can be interpreted as the number of collisions needed to reduce an excess of molecules excited to $v=1$ to the equilibrium number. The number of collisions needed for excitation is found by changing the sign of the exponent $\theta/2T$ appearing in Z_{tr}.

7. - Discussion of the equation for Z.

Before starting on the calculation of the steric factor Z_0, it will be useful to discuss the general behaviour of Z. For this purpose we will re-order the terms regardless of their origin,

$$Z=0.703\,\frac{M_B M_C}{M_B^2+M_C^2}\,\frac{M_A+M_B+M_C}{M_A}\left(\frac{r_0}{r_c}\right)^2 Y(2,2)\exp\left[-\frac{\varepsilon}{kT}\right]\cdot$$
$$\cdot\exp\left[\frac{\theta}{2T}\right]\cdot\frac{\theta}{T}\left(\exp\left[\frac{\theta}{T}\right]-1\right)^{-1}\left(\frac{T}{\theta'}\right)^{7/6}\exp\left[\frac{3}{2}\left(\frac{\theta'}{T}\right)^{\frac{1}{3}}\right]. \tag{7.1}$$

In this expression, $Y(2,2)\exp[-\varepsilon/kT]$ corrects for the effect of the attractive forces. The first seven factors multiplied out are in general of the order of magnitude unity.

$\theta/T(\exp[\theta/T]-1)^{-1}$ is the energy of oscillation, divided by kT, of a Planck oscillator and approaches the value unity for increasing temperature.

The last two factors together dominate the value of Z. Only if their product is large, are the approximations made justified; it will be useful to introduce provisionally the abbreviation

$$u^3=\frac{\theta'}{T},$$

so that the last two factors give

$$u^{-\frac{7}{2}}e^{\frac{3}{2}u}, \tag{7.2}$$

u ought to be at least 3 or $\theta' > 27T$ to justify our calculations; for the examples given later, this is always fulfilled. From $u = 3$ on, Z increases strongly with increasing θ' and decreasing T.

To get a better idea of the physical meaning of θ', one sees that (see after eq. (6.11))

$$k\theta' = 8\pi^2 \cdot 2\pi^2 \mathfrak{m} \nu^2 l^2 \tag{7.3}$$

is $8\pi^2$ times the work necessary to stretch the oscillator by the amount 1.

One sees that θ' increases with increasing $\mathfrak{m}$, ν and l, so that more tightly-bound molecules (larger quanta $h\nu$ to be transferred), larger molecules (those with greater l, *i.e.*, with less steep force fields) and those with large mass $\mathfrak{m}$ are more difficult to excite (have a larger Z). The latter point explains the high efficiency of H_2 as impurity.

However, it is of interest that the effect of the mass is indirect. Equations (6.16), (6.17) contain the *velocity*. If molecular beams of H_2 and N_2 of the same velocity were used to excite a molecule BC, their efficiency would be nearly equal. Only when, through Maxwell's distribution, a transition is made to equal kinetic *energy* or temperature, is H_2 strongly favored over N_2, because at given T it contains many more molecules of a given high velocity.

To illustrate numerically, Table I shows the function $\log[u^{-\frac{7}{2}} e^{\frac{3}{2}u}]$ (see eq. (7.2)):

TABLE I.

$u \rightarrow$ θ'/T $\log(u^{-\frac{7}{2}}\exp[\frac{3}{2}u])$	3 27 0.2398		55 125 0.6243		7.5 422 1.7126	10 1000 2.8658
u θ'/T $\log(u^{-\frac{7}{2}}\exp[\frac{3}{2}u])$	12 1328 3.8618	13.5 2460 4.6376	15 3375 5.4639	18 5832 7.0151	20 8000 8.1781	24 10624 10.4472

8. - Calculation of the steric factor Z.

There are two methods available to calculate the steric factor Z.

a) In the simplest procedure, it is assumed that only the component of velocity in the direction of the molecular axis matters. One then generalizes the one-dimensional model by allowing the molecular axis a fixed position, inclined toward the direction of the relative velocity by the angle. Equation (2.4) is therefore written

$$H'(x - \beta X \cos\theta)\,. \tag{8.1}$$

In the power development, $\beta \cos\theta$ appears in the vibrational transition matrix element instead of β, and $\cos^2\theta$ appears therefore as additional factor in the transition probability. Accordingly

$$\frac{1}{Z_0} = (\cos^2\theta)_{\text{ave}} = \frac{1}{3}. \tag{8.2}$$

For the bending vibration of a linear triatomic molecule, it is assumed that the velocity component *normal* to the axis matters. Therefore $\sin\theta$ is substituted for $\cos\theta$, and

$$\frac{1}{Z_0} = (\sin^2\theta)_{\text{ave}} = 1 - (\cos^2\theta)_{\text{ave}} = \frac{2}{3}. \tag{8.3}$$

It seems clear from a close consideration of the model, that simultaneous excitation or de-excitation processes of the rotational motion are included. More on this in the next section.

b) The steric factor: vibrational, rotational, translational energy exchange. We finally take our assumption, that the interaction occurs between individual atoms, seriously. This introduces an angle-dependence into the interaction between BC and A and couples rotational transition to the other processes.

We assume for the sake of simplicity that the atoms B and C are alike, and that each interacts independently with A by an exponential function

$$H_0 = H_0 \exp\left[-\frac{r_{AB}}{l}\right] + \tilde{H}_0 \exp\left[-\frac{r_{AC}}{l}\right]. \tag{8.4}$$

We call L the equilibrium distance between B and C, and assume $L \gg l$. Next, call r the distance between the center of BC and A, and Γ the angle between r and the molecular axis.

Then, in first approximation (*),

$$r_{AB} = r - \tfrac{1}{2}(L + X)\cos\Gamma; \tag{8.5}$$

$$r_{AC} = r + \tfrac{1}{2}(L + X)\cos\Gamma. \tag{8.6}$$

Developing the exponential according to powers of the small quantity X/l

---

(*) The factor β is here equal to $\frac{1}{2}$.

and keeping only the linear term, one finds

$$(8.7)\qquad H=\widetilde{H}_0\left\{\exp\left[-\left(\frac{r}{l}+\frac{1}{2}\frac{L}{l}\cos\Gamma\right)\right]+\exp\left[-\left(\frac{r}{l}-\frac{1}{2}\frac{L}{l}\cos\Gamma\right)\right]\right\}-$$
$$-\widetilde{H}_0\frac{X}{2l}\cos\Gamma\left\{\exp\left[-\left(\frac{r}{l}+\frac{1}{2}\frac{L}{l}\cos\Gamma\right)\right]-\exp\left[-\left(\frac{r}{l}-\frac{1}{2}\frac{L}{l}\cos\Gamma\right)\right]\right\}.$$

The first term produces truly elastic scattering plus scattering involving changes in rotational states, the second term inelastic scattering, involving exchanges in both vibrational and rotational states (*).

An attempt to calculate the probability of each rotational transition is extremely difficult at the present state, since the probability is so high that the validity of first-order perturbation theory is very doubtful.

On the other hand, the task is much simpler if we ask only for the overall result of all rotational transitions, and make the following simplification: In general (apart from H_2, D_2, etc.) the energy difference between significant, rotational states is small compared to kT and to $h\nu$. We therefore neglect the change in w (or k) if only rotational jumps occur; if a vibrational jump occurs, we neglect the effect of a simultaneous rotational transition on the k. In other words, we assume that the « elastic » collisions, of which we see the effect in viscosity, include collisions in which rotational jumps occur.

To make the proper calculation, one has to multiply the wave function (4.24) with a rotational factor, S_J. S is a generalized spherical harmonic and the index J stands for both the angular momentum quantum number J and the magnetic quantum number (orientation). In addition the scattering has not anymore cylindrical symmetry around the direction of the incoming beam, which is chosen as the polar axis, so that (P_j) must be replaced by another generalized spherical harmonic S_j, with j the angular momentum quantum number of the relative motion.

Since the factor $\exp[-r/l]$ can be taken out of all terms of the perturbation potential, we have, for the elastic scattering a term

$$(8.8)\qquad \widetilde{H}_0\int\frac{f_1}{r}\exp\left[-\frac{r}{l}\right]\frac{f_2}{r}r^2\,\mathrm{d}r\,|\psi^0_{\mathrm{BC}}|^2\,\mathrm{d}X\cdot$$
$$\cdot\int S_{J'}S_{j'}\left\{\exp\left[-\frac{L}{2l}\cos\Gamma\right]+\exp\left[+\frac{L}{2l}\cos\Gamma\right]\right\}S_J S_j\,\mathrm{d}\Omega\,\mathrm{d}\omega\,,$$

(*) The treatment in our book Section 64 here is wrong, since a term $2H_0\exp[-r_0/l]$ was unjustifiedly isolated as determining the viscous scattering, in which no rotational transitions were assumed present.

which describes a transition $j \to j'$ in the orbit and $J \to J'$ in the rotational state. $d\Omega$ and $d\omega$ are the elements of steric angle for the orbit and the molecular orientation. The f's are explained below.

In the method of distorted waves which we have been using in Section 4, one uses a wave function which is an exact solution for the unperturbed potential $H(x)$. This wave function which contains the primary wave and also the elastically or quasi-elastically (*i.e.* one including the result of rotational transitions) scattered wave, can on principle also be used to calculate viscosity. However, there is no theory of the viscosity of a rotating diatomic molecule with our assumed forces, and correspondingly no exact solution of the wave equation if $H(r, \Gamma)$ is identified with the first line of (8.7). On the other hand, one can also not select as unperturbed interaction energy a term $\tilde{H}_0 \exp[-r/l]$ and treat the difference between it and the first line of eq. (8.7) as perturbation since this difference may be very large depending on the value of Γ.

The only way available seems the following:

Take $(1/r)f_1(kr)$ as the incident and $(1/r)f_2(kr)$ as the quasi-elastically scattered wave satisfying the Schrödinger eq. (5.10) so that

$$f_1 + f_2 = f\,, \tag{8.9}$$

where f is the function used in Section 5·2).

The f are wave functions belonging to the spherically symmetrical potential $H_0 \exp[-r/l]$.

Then a partial wave function, belonging to the initial state, will be

$$\psi^0_{\mathrm{BO}} \frac{f_1(k_0 r)}{r}\, S_j S_J\,, \tag{8.10}$$

a corresponding partial wave function for the elastically scattered wave will be

$$\psi^0_{\mathrm{BO}} \frac{f_2(k_0 r)}{r}\, S_{j'} S_{J'}\,. \tag{8.11}$$

and a partial wave function for the inelastically scattered wave

$$\psi^{(1)}_{\mathrm{BO}} \frac{f_3(kr)}{r}\, S_{j''} S_{J''}\,. \tag{8.12}$$

If, for the moment we call the first line in eq. (8.9) H^{I} and the second line H^{II}, the elastic cross-section will be proportional to

$$\sum_j \sum_J \left| \int \psi_1 H^{\mathrm{I}} \psi_2 r^2\, dr\, dX\, d\Omega\, d\omega \right|^2, \tag{8.13}$$

the inelastic cross-section to

$$\sum_j \sum_J \left| \int (\psi_1 + \psi_2) H^{\text{II}} \psi_3 r^2 \,\mathrm{d}r \,\mathrm{d}X \,\mathrm{d}\Omega \,\mathrm{d}\omega \right|^2 , \tag{8.14}$$

where ψ_1, ψ_2, ψ_3 are momentary abbreviations for (8.10)–(8.12).

In the spherical harmonics, ϑ, φ are angles defining the relative motions of A; they are the arguments in S_j. ψ and φ' characterize the direction of the molecular axis, they are the arguments in S_J. Further

$$\begin{aligned} \mathrm{d}\Omega &= \sin\vartheta \,\mathrm{d}\vartheta \,\mathrm{d}\varphi , \qquad \mathrm{d}\omega = \sin\chi \,\mathrm{d}\chi \,\mathrm{d}\varphi' , \\ \cos\Gamma &= \cos\vartheta \cos\chi + \sin\vartheta \sin\chi \cos(\varphi' - \varphi) . \end{aligned} \tag{8.15}$$

In detail, a term in (8.14) looks so: for the vibrational jump from 0 to 1, rotational jump $J \to J'$

$$\begin{aligned} -\beta\widetilde{H}_0 \int \frac{f(k_0 r)}{r} \exp\left[-\frac{r}{l}\right] \frac{f_3(kr)}{r} r^2 \,\mathrm{d}r \int \psi^0_{\text{BC}} \frac{X}{l} \psi^1_{\text{BC}} \,\mathrm{d}X \cdot \\ \cdot \left\{ S_{J'} S_{j'} \left\{ \exp\left[-\frac{L}{2l}\cos\Gamma\right] - \exp\left[\frac{L}{2l}\cos\Gamma\right] \right\} S_J S_j \cos\Gamma \,\mathrm{d}\Omega \,\mathrm{d}\omega \right\} . \end{aligned} \tag{8.16}$$

The first factor in (8.8) and the first two factors in (8.16) are the same quantities which we have considered in the case of the « breathing » sphere. Only the last factor is new.

To get the total elastic and inelastic scattering, we have to take the sum of the squares of the matrix elements, weighted with the proper number of molecules.

Call A_j the fraction of incoming molecules A which have originally the orbital angular momentum j, and B the fraction of scatterers which have originally the rotational quantum number J. The number of particles elastically scattered is then proportional to

$$|H_{k_0 k_0}|^2 \sum_J B_J \sum A_j \sum_{J'} \sum_{j'} V^2_{J'j',Jj} , \tag{8.17}$$

the number of particles scattered inelastically is proportional to

$$|H_{k_0 k}|^2 \beta^2 |X_{10}|^2 \sum_{J,j} B_J A_j \sum (V'_{J'j',Jj})^2 . \tag{8.18}$$

Here, V and V' are the last integrals in (8.8) and (8.16). One can now directly sum up over the final states in these integrals, by using the expression for the square of a matrix.

Therefore, one gets, in (8.17), for

$$V^2_{Jj',Jj}=\int S_J^* S_j^* \left[\exp\left[-\frac{L}{2l}\cos\Gamma\right]+\exp\left[+\frac{L}{2l}\cos\Gamma\right]\right]^2 S_J S_j \,\mathrm{d}\Omega\,\mathrm{d}\omega\,, =$$

$$=\int S_J^* S_j^* \left[\exp\left[-\frac{L}{l}\cos\Gamma\right]+\exp\left[-\frac{L}{l}\cos\Gamma\right]+2\right] S_J S_j \,\mathrm{d}\Omega\,\mathrm{d}\omega\,.$$

In the case of inelastic scattering one has in addition a factor $\cos^2\Gamma$ under the integral, and replaces $+2$ by -2.

We next sum over the different rotational states of the molecule BC which involves the summation

$$\sum_J B_J \int [\;]\, S_J^* S_J S_j S_j^* \,\mathrm{d}\Omega\,\mathrm{d}\omega\,.$$

The summation is first made over the different magnetic quantum number for a fixed total angular momentum J. There are $2J+1$ such states, and they are equally populated in equilibrium, since they are nondegenerate and have equal energy. The sum over $S_J^* S_J$ gives a result which is independent of the the angle χ (*) and equal to $\frac{1}{2}(2J+1)$, so that the contribution per state is $\frac{1}{2}$. Accordingly

$$\sum B_J S_J^* S_J = \tfrac{1}{2}$$

and we end up with an averaged square of the interaction energy for elastic scattering which is proportional to

$$(\widetilde{H}_0)^2\,|H_{k_0k_0}|^2\,|X_{10}|^2\,\frac{1}{2}\sum_j A_j \iint \left[\exp\left[-\frac{L}{l}\cos\Gamma\right]+\exp\left[\frac{L}{l}\cos\Gamma\right]+2\right] S_j^* S_j \,\mathrm{d}\Omega\,\mathrm{d}\omega\,.$$

In other words, the ratio of the elastic scattering cross-section for the present model to that in the spherical model is (**)

$$\text{(8.18)}\qquad \frac{1}{2}\left(\frac{\widetilde{H}_0}{H_0}\right)^2 \sum_j A_j \iint \left[\exp\left[-\frac{L}{l}\cos\Gamma\right]+\exp\left[\frac{L}{l}\cos\Gamma\right]+2\right] S_j^* S_j \,\mathrm{d}\Omega\,\mathrm{d}\omega : 4I\,.$$

where I is the integral (8.19*a*).

(*) In atomic theory, the spherical symmetry of filled subshells is a consequence of this.

(**) In a sense, this can be considered as the beginning of the theory of viscosity for a dumbbell molecule, each atom of which exerts an exponential repulsive force. However, there is the inconsistency that the radial wave functions (primary plus elastically scattered) are nearly zero at the center of the spherical molecule, not at the nuclei of the individual atoms. Whether this accounts for the difficulties in the steric factor later reported in this section, I do not know.

Similarly, the same ratio for the inelastic cross-section is

$$(8.19)\qquad \frac{1}{2}\left(\frac{\tilde{H}_0}{H_0}\right)^2 \sum_j A_j \iint \left[\exp\left[-\frac{L}{l}\cos\Gamma\right] + {} \right.$$
$$\left. {}+\exp\left[\frac{L}{l}\cos\Gamma\right] - 2\right]\cos^2\Gamma\, S_j^* S_j\, \mathrm{d}\Omega\, \mathrm{d}\omega : 4I,$$

where for the spherical model no Z_0 is taken into account.

Under the assumption $L > l$, the expression in the bracket is large if $\cos\Gamma$ is either near (-1) (first term) or near $(+1)$ (second term), under which conditions the molecular axis of BC nearly points at A. This is intuitively understandable.

Since in the integrals now only the wave functions S_j^*, S_j (no those $S_{j'}$ of the scattered wave) appear, one can limit oneself to the cylindrically symmetrical Legendre polynomials ($\tilde{P}_j$) (the tilde implies the inclusion of the normalization factor).

We have therefore to evaluate, for (8.18), the sum

$$\sum A_j \int \tilde{P}_j^2[\ ]\sin\theta\, \mathrm{d}\theta\, \frac{\mathrm{d}\varphi}{2\pi}\sin\chi\, \mathrm{d}\chi\, \frac{\mathrm{d}\varphi'}{2\pi}\,.$$

Because of the expression for $\cos\Gamma$, $\Gamma = 0$ or π means $\varphi' - \varphi = 0$, $\theta - \chi = 0$ or π.

One can therefore make in the integral a change in variables from φ, φ' to $\varphi'' = \varphi' - \varphi$ and φ' and immediately integrate over φ'. In the neighborhood of $\cos\Gamma = \pm 1$ we write $\chi = \theta + \delta$

$$\cos\Gamma = \cos\delta + \sin\theta(\sin\theta\cos\delta + \cos\theta\sin\delta)(\cos\varphi'' - 1)\,.$$

Treating δ and φ'' as small quantities of zero order, one has

$$\cos\Gamma = \pm 1 - \tfrac{1}{2}(\delta^2 + (\varphi'')^2\sin^2\theta)$$

and therefore the bracket in (8.18) can be written

$$2\exp\left[+\frac{L}{l} - \frac{L}{2l}(\delta^2 + (\varphi'')^2\sin^2\theta)\right],$$

and the ratio (8.18)

$$\left[\frac{\tilde{H}_0\exp(L/2l)}{H_0}\right]^2 \sum_j A_j \iint \exp\left[-\frac{L}{2l}(\delta^2 + (\varphi'')^2\sin^2\theta)\right]\tilde{P}_j^2\sin\theta\, \mathrm{d}\theta\, \frac{\mathrm{d}\varphi''}{2\pi}\sin\chi\, \mathrm{d}\chi\,.$$

The integration over φ'' gives immediately the factor

$$\sqrt{\frac{2l}{4\pi L}}\,\frac{1}{\sin\theta}\,.$$

The change of variables from θ, χ to θ, $\delta_s=\chi-\theta$ gives, instead of

$$\sin\theta\,\mathrm{d}\theta\,\sin\chi\,\mathrm{d}\chi\to\sin^2\theta\,\mathrm{d}\theta\,\mathrm{d}\delta\,.$$

Integration over δ provides a factors $\sqrt{2l\pi/L}$, so that we end up with

$$\left[\frac{\tilde{H}^0\exp\left[L/2l\right]}{H_0}\right]^2\frac{l}{L}\sum A_s\int\tilde{P}_s^2\sin\theta\,\mathrm{d}\theta\,.$$

In the « spherical » model, the expression was

$$I=\sum A_s\int P_s^2\sin\theta\,\mathrm{d}\theta\,. \tag{8.19a}$$

Therefore, the ratio (8.18) is

$$\left[\frac{\tilde{H}_0\exp\left[L/2l\right]}{2H_0}\right]^2\frac{l}{L}\,. \tag{8.20}$$

Therefore, the effect of the substitution of the spherical model for one in which the interaction energy is exerted by the individual atoms is only on the numerical constant H_0, which does not enter into the strength of the « elastically » scattered wave. The apparent constant H_0, which appears in the spherical model, differs from the « true » constant H_0 by two factors, $\exp\left[+L/2l\right]$, which results from carrying the exponential back to the centre of the molecule, and a factor $(l/4L)^{\frac{1}{2}}$. For $L/l=5$, the factor is 1.35.

In any case, it follows that the same l, which is found from viscosity measurements under the assumption of a potential originating from the center of the molecule, is also valid if the forces are centered in the separate atoms B and C.

A similar argument can now be applied to the matrix element of the perturbation energy responsible for inelastic scattering (vibrational activation or deactivation). The only difference is a factor $\cos^2\Gamma$ appearing under the integral.

However, under the assumption previously made, this will not be far from unity. Putting

$$\cos^2\Gamma=1-\delta^2-\sin^2\theta(\varphi'')^2$$

one finds that the correction factor to be applied, because of angle-dependence of the forces, to the square of the inelastic matrix element differs from the factor to be applied to the square of the elastic matrix element, only by the numerical factor $1-(2l/L)$. Therefore the steric factor is

$$\frac{1}{Z_0}=\frac{L-2l}{L}, \tag{8.21}$$

contrary to the result found in Subsection 8-*a*). The result is plausible from the conclusion that strong interaction occurs only when the molecular axis is nearly pointed at A.

If one next considers the transversal vibration in a molecule BCB, there appears approximately $\sin^2\Gamma$ instead of $\cos^2\Gamma$, and therefore the steric factor should be

$$\left\{\begin{aligned}&\frac{1}{Z_0}=1-\left(1-\frac{2l}{L}\right),\\&\text{or}\\&Z_0=\frac{L}{2l}.\end{aligned}\right. \tag{8.22}$$

If one replaces [20] the colliding particle A by another molecule BB and uses a similar procedure, one finds (*) again that only approximately head-on collisions where the molecular axes are nearly aligned, contribute to both « elastic » and inelastic scattering, and (8.21) and (8.22) remain unaltered. To sum up the preceding, it has been shown that

$$\frac{1}{Z_0}=\overline{\cos^2\Gamma}\quad\text{or}\quad\overline{\sin^2\Gamma}=1-\overline{\cos^2\Gamma},$$

for longitudinal and transversal vibrations, respectively.

For nearly spherical molecules, all kinds of collisions are effective in both « elastic » and inelastic scattering, the averages are taken over the whole sphere and are $\frac{1}{3}$ and $\frac{2}{3}$. For elongated molecules, only approximately head-on collisions are important for both elastic and inelastic scattering, and the averages are to be taken only in the neighborhood of alignment, giving a value much closer to unity for $\cos^2\Gamma$ and much smaller than $\frac{2}{3}$ for $\sin^2\Gamma$.

9. – Comparison between theory and experiment.

In the following tables the results of eq. (7.1) and of experiment are compared. This had been attempted in Section 66 of our book, but unfortunately,

---

(*) The same misinterpretation occurs in ref. [20] as in Section 66 of our book.

Table 66-5 of our book is marred by errors, as Professor F. C. SHIELDS has kindly pointed out to me. Therefore, all the theoretical Z values have been recalculated, about half of them twice.

The table also shows tha values of l and ϑ'. It is found (*) that these are correctly given in Table 66.5. Two sets of theoretical Z values are shown: Z_{theor} (a) uses $Z_0 = 3$ for longitudinal and $\frac{3}{2}$ for transversal vibrations, Z_{theor} (b) uses the expressions (8.21) and (8.22).

The experimental Z_{exp} are listed in the column before last. The last column, Ref., gives the source of these data. So as not to overburden this article with references, the following procedure was followed. Most of the data are either taken from our book (indicated by ref. [1]) or from the COTTRELL-McCOUBREY book (indicated as ref. [2]) but then the particular reference is added: *e.g.* [2; 7] means ref. [7] (F. ANGONA) of the COTTRELL-McCOUBREY book. However, it has to be noted that the latter lists Z_{10} instead of our Z; the two are connected by

$$Z = Z_{10}\left(1 - \exp\left[-\frac{\vartheta}{T}\right]\right)^{-1}.$$

This correction has been made.

The experimental data below 600 °K have usually been determined with the acoustic interferometer and should in general be reliable, although the presence of an undetected impurity would make them too low.

On the other hand, the values at higher temperatures usually come from shock tube data, and here the τ's found by different experimenters may differ by a factor as large as 3. This is not so much a question of the direct measurement as of its evaluation, since the temperature behind the shock varies over a considerable range, and C and Z are temperature-dependent. *E.g.*, newer measurements by WITTEMAN [22] on CO_2 at about 800 °K differ appreciably from the older ones of EUCKEN and WINKLER and SMILEY.

If one now makes the actual comparison for the smaller diatomic molecules without impurities (7 measurements of O_2, 7 of N_2, 4 of CO, 1 of F_2 and 4 at Cl_2), one finds that the agreement is appreciably better for $Z_0 = 3$;

(*) A simplified method has been developed to calculate l. Originally (6.5) connects E_m/ε and r_0/l but E_m itself contains l, and therefore iteration had to be used. Instead there has now been calculated an extensive table for r_0/l as a function of E_m/ε.

From this original table, a new one has been found, showing r_0/l as function of a new quantity

$$\frac{1}{2}\left(\frac{0.8153\, M\vartheta^2 r_0^2}{T}\right)^{\frac{1}{3}} \frac{kT}{\varepsilon}.$$

This latter expression does not contain l, but only known molecular quantities. This speeds up the procedure considerably.

TABLE II. – *Comparison of theory and experiment.*

θ, T	l in Å	$\theta' \cdot 10^{-6}$	Z_{theor} (a)	Z_{theor} (b)	Z_{exp}	Ref.
O_2-O_2						
$\theta = 2\,230$						
$T =$ 288	0.1786	2.0692	$4.2 \cdot 10^7$	$2.0 \cdot 10^7$	$1.6 \cdot 10^7$	[1]
300	—	—	—	—	$9.9 \cdot 10^7$	[46]
323	0.1789	2.0762	$2.4 \cdot 10^7$	$1.2 \cdot 10^7$	$1.0 \cdot 10^7$	[22]
482	—	—	—	—	$7.4 \cdot 10^6$	[47]
1 372	0.1833	2.1796	15 000	7 200	36 000	[1]
1 953	0.1840	2.1963	4 100	2 000	12 000	[1]
2 912	0.1847	2.2130	1 000	480	1 800	[1]
3 000	—	—	—	—	2 700	[23]
4 000	0.1851	2.2226	370	180	780	[23]
6 000	0.1855	2.2322	140	65	190	[23]
O_2-N_2						
323	0.1862	2.100	$2.82 \cdot 10^7$	$1.4 \cdot 10^7$	$4 \cdot 10^6$	[22]
1 953	0.1910	2.208	3 800	1 900	5 000	[1]
O_2-A						[23]
1 200	0.1826	2.408	46 600	22 000	$7.1 \cdot 10^5$	[23]
2 400	0.1840	2.438	2 500	1 200	33 000	[23]
6 000	0.1851	2.467	150	70	970	[23]
O_2-H_2						
288	0.1657	0.2095	1 000	460	31 900	[24]
O_2-He						
288	0.1895	0.3860	6 600	3 200	290 000	[24]
N_2-N_2						
$\theta = 3\,380$						
$T =$ 475	0.1960	5.008	$2.1 \cdot 10^9$	$1.1 \cdot 10^9$	$> 8.10^8$	[22]
558	0.1963	5.026	$8.2 \cdot 10^8$	$4.3 \cdot 10^8$	$1.1 \cdot 10^8$	[1]
778	0.1971	5.064	$7.0 \cdot 10^7$	$3.6 \cdot 10^7$	$6.5 \cdot 10^6$	[1]
1 168	0.1978	5.102	$4.7 \cdot 10^6$	$2.4 \cdot 10^6$	$2.3 \cdot 10^6$	[1]
2 450	0.1988	5.152	75 000	39 000	150 000	[2; 41]
3 640	0.1990	5.166	11 600	6 000	24 000	[1]
4 630	0.1991	5.171	4 300	2 200	8 000	[1]
CO-CO						
$\theta = 3\,450$						
$T =$ 300	0.1886	4.837	$3.3 \cdot 10^{10}$	$1.6 \cdot 10^{10}$	$> 10^9$	[25]
1 447	0.1928	5.052	$1.2 \cdot 10^6$	$6 \cdot 10^5$	$1.4 \cdot 10^6$	[2; 267]
1 919	0.1933	5.074	$2 \cdot 10^5$	$1. \cdot 10^5$	$3.4 \cdot 10^5$	[2; 267]
2 985	0.1956	5.102	20 000	10 000	68 000	[2; 267]
F_2-F_2						
$\theta = 1\,284$						
$T =$ 301	0.1874	0.8970	$2.3 \cdot 10^5$	$1.0 \cdot 10^5$	$2.6 \cdot 10^5$	[26]

TABLE II (*continued*)

θ, T	l in Å	$\theta' \cdot 10^{-6}$	Z_{theor} (a)	Z_{theor} (b)	Z_{exp}	Ref.
Cl_2-Cl_2						
$\theta =$ 802						
$T =$ 298	0.2009	0.7505	79 000	33 000	46 000	[2; 220]
528	0.2048	0.7802	8 700	3 700	8 500	[2; 220]
1 000	0.2090	0.8122	860	360	550	[1]
1 372	0.2109	0.8268	390	160	200	[1]
Cl_2-He						
$T =$ 288	0.1681	0·08018	200	80	1 200	[2; 73]
Br_2-Br_2						
$\theta =$ 462						
$T =$ 301	0.2032	0.5744	15 000	7 100	7 200	[2; 220]
529	0.2069	0.5952	2 500	1 200	2 100	[2; 220]
I_2-I_2						
$\theta =$ 309						
$T =$ 385	0.2385	0.5619	6 800	2 750	760	[2; 220]
N_2O-N_2O						
$\theta =$ 847						
$T =$ 293	0.1924	0.4753	4 300	17 300	7 500	[2; 76]
473	0.1952	0.4903	680	2 700	2 900	[2; 76]
673	0.1975	0.5008	300	1 200	1 600	[2; 76]
CO_2-CO_2						
$\theta =$ 960						
$T =$ 296°	0.2008	0.6693	18 400	69 000	49 000	[2; 7]
579	0.2048	0.6932	1 350	5 100	11 400	[2; 219]
1 000	0.2076	0.7123	230	850	300	[1]
CO_2-A						
$T =$ 296	0.1875	0.5527	7 300	30 000	$4 \cdot 10^5$	[2; 126]
COS-COS						
$\theta =$ 755						
$T =$ 293	0.2004	0.5641	2 900	13 000	17 700	[2; 72]
475	0.2047	0.5886	930	4 100	6 600	[2; 72]
CS_2-CS_2						
$\theta =$ 570						
$T =$ 296	0.2108	0.4478	900	4 500	6 700 7 000	[2; 84] [2; 7]
433	0.2140	0.4609	312	1 500	3 600	[2; 91]

in general, it lies within a factor 2. There are exceptions: *e.g.*, for N_2 at 558 °K and 778 °K, the theoretical values are 8 to 10 times too great. But one may expect that these experimental Z are too small because of the presence of water vapor; the Z found at 778 is only 3 times larger than the value found at 1167 with the shock tube. Camac's Z for O_2 is appreciably higher than Blackman's.

That these small molecules act nearly as if they were spherical (*i.e.*, that the mathematical approximations used to deduce (8.21) and (8.22) are not justified) is not too astonishing.

On the other hand, for elongated diatomic molecules and for all triatomic molecules (2 Br_2, 1 I_2, 3 N_2O, 3 CO_2, 2 COS and 2 CS_2), eqs. (8.21) and (8.22) fit much better (the agreement is whithin a factor 2.4 except for I_2 where the theoretical value is four times too great).

However, there is great disagreement for the 9 cases of impurity effects. For impurities of small mass (H_2, He) an even higher efficiency is calculated than is found: the error in the calculation may be as high as a factor $30 \div 40$. The impurity N_2 in O_2 at 323 °K is found to be about 2.5 times as efficient as O_2, while the calculation gives a factor 1.2 in the other direction. Argon as an impurity in CO_2 should be more efficient than CO_2 having a smaller mass and smaller radius, while experimentally it is found to have only one eighth the efficiency of a CO_2. The only explanation I can think of is the failure of the rule which says that the r_0 in the interaction of two different molecules is the arithmetical mean of that of the two partners. To explain the results, it would have to be larger than the mean.

E.g.: to get 27000 for O_2–H_2, one needs an l of 0.2500 instead of 0.1657; to get a Z of $4 \cdot 10^5$ for CO_2–A, one needs an l for 0.2380 instead of 0.1875.

The question is now: does the reason for the deviations lie in the mathematical approximations made?

Or does it lie in the problem of the steric factor Z_0?

Or does it lie in the use of the wrong interaction potential?

The first question can—and will probably soon—be tested by the use of a computer and numerical methods. The second question requires first a theory of the viscosity of nonspherical, nonhard molecules. The third question will be discussed in the next section.

McCoubrey, Milward and Ubbelohde [27] have made a comparison

Table III. – *Range l of forces which gives best agreement with experiment.*

Gas	O_2	N_2	Cl_2	Br_2	N_2O	COS	CS
l_{exp} in Å	0.154	0.141	$0.205 \div 0.149$	0.159	0.134	0.151	0.169
l_η in Å	$0.179 \div 0.185$	$0.196 \div 0.199$	$0.200 \div 0.211$	0.207	0.192	0.201	0.211

between theory (eq. (6.25) with $Z_0=3$) and experiment by calculating the l (or, as they call it, the quantity $1/\alpha$) which fits the data best. Their curves show that this l (which shall be called here l_{exp}) permits a good representation of the temperature-dependence of Z. In Table III, this l_{exp} is compared with the quantity determined from viscosity data, l_η, which we have used before.

The most effective energy E_m is given by eq. (6.11*b*). One has, therefore, the following examples.

TABLE IV.

Gas, T °K	O_2, 288 °K	O_2, 2 912 °K	CO_2, 300 °K	CO_2, 1 000 °K
E_m/k	5 600 °K	36 500 °K	3 900 °K	9 000 °K

Therefore we are making use of a high part of the $H-r$ curve, which is not easily accessible otherwise.

10. – Dependence of the calculated Z on the force law.

a) An important paper by WIDOM [6] discusses this problem in general. He restricts himself to the one-dimensional case and introduces, as a separate quantity the energy transferred, $\Delta=h\nu$, so that for the simple harmonic oscillator $\nu=\Delta/h$ and, for the exponential potential:

$$\ln Z=\frac{3}{2}\left(\frac{16\pi^4}{kT}\,\widetilde{m}l^2\,\frac{\Delta^2}{h^2}\right)^{\frac{1}{3}}-\frac{\Delta}{2kT}-\frac{\varepsilon}{kT}-\frac{4}{3}\ln\frac{\Delta}{h}-\ln c\,, \tag{10.1}$$

where c does not contain h. He now considers this as a function of h considered variable to smaller and smaller values; then the first term is the most important term.

This arose from integration, over the Maxwell distribution law, of a cross-section

$$Q'\sim\exp\left[-\frac{4\pi\,l\nu}{w}\right]=\exp\left[-\frac{4\pi l}{w}\,\frac{\Delta}{h}\right]. \tag{10.2}$$

He now applies an expression of Landau, according to which, if the elastic motion is practically classical,

$$Q'\sim\frac{32\pi^2\widetilde{m}}{h^2\sqrt{E(E+\Delta)}}\,|X_{01}|^2\exp\left[-\frac{4\pi}{h}\sqrt{2\widetilde{m}}\lim_{u=\infty}\left[\int\limits_{E+.1}^{u}\sqrt{H-(E+\Delta)}\,\frac{\mathrm{d}x}{\mathrm{d}H}\,\mathrm{d}H-\right.\right.$$
$$\left.\left.-\int\limits_{E}^{u}\sqrt{H-E}\,\frac{\mathrm{d}x}{\mathrm{d}H}\,\mathrm{d}H\right]\right]. \tag{10.3}$$

In this equation $|E+\Delta|>E$ and $\mathrm{d}x/\mathrm{d}H$ means $(\mathrm{d}H/\mathrm{d}x)^{-1}$ with x expressed by H. H is the quantity previously called $H(x, 0)$.

Widom shows for some examples, that Landau's approximate equation gives the correct result wherever it can be compared with a known exact solution.

Widom then integrates Q' (10.3) over the Maxwell distribution keeping only those terms which are pre-eminent in the limit $h \to 0$.

Introducing the function

$$F(E)=\int_E^\infty \frac{1}{\sqrt{H-E}}\,\frac{\mathrm{d}x}{\mathrm{d}H}\,\mathrm{d}H\,, \tag{10.4}$$

(this is related to our classical integral (5.2))

$$\sqrt{\frac{2}{\tilde{m}}}\int \mathrm{d}t=\int_\lambda^\infty \frac{\mathrm{d}x}{\sqrt{E-H}}\,,$$

he defines a number E^* as the solution of the transcendent equation

$$\sum_{n=1}^\infty \frac{1}{n!}\,\Delta^n\,\frac{\partial^n F}{\partial E^n}=\frac{h}{2\pi}\sqrt{2\tilde{m}}\,kT\,, \tag{10.5}$$

and finds for Q

$$Q\sim\exp\left[-\frac{E^*}{kT}+\frac{2\pi}{h}\sqrt{2\tilde{m}}\,\Delta\sum_{n=1}^\infty\frac{1}{n!}\,\Delta^{n-1}\,\frac{\partial^{n-1}F}{\partial E^{n-1}}\right]. \tag{10.6}$$

It seems to me that the equation defining E^* can also be written

$$F(E^*+\Delta)-F(E^*)=\frac{h}{2\pi}\sqrt{2\tilde{m}}\,kT\,, \tag{10.7}$$

while the expression for Q can be given the form

$$Q\sim\exp\left[-\left\{-\frac{E^*}{kT}+\frac{2\pi}{h}\sqrt{2\tilde{m}}\left[\int_0^1 F(E^*+\Delta')\,\mathrm{d}\Delta'\right]\right\}\right]. \tag{10.8}$$

One may now write, as a very general form,

$$\frac{\mathrm{d}x}{\mathrm{d}H}=-aH^{-N}[1+g(H)]\,;\quad N\geqslant 1,\qquad g(\infty)=0\,. \tag{10.9}$$

As examples, the exponential potential is represented by $a=1$, $N=1$, $g\equiv 0$; the inverse power potential A x^{-m} follows from $N=1+(1/m)$, $a=(1/m)A^{1/m}$. $g\equiv 0$. A long as H becomes very large for very small x, N is close to unity.

If one now evaluate those terms of the exponent in Q which do not vanish with $h\to 0$, one gets

$$Q \sim \exp\left[-\frac{E^*}{kT}+\frac{2\pi}{k}\sqrt{2\tilde{m}}\,\Delta F(E^*)+\frac{\Delta}{2kT}\right]= \tag{10.10}$$

$$=\exp\left[-\frac{N+\frac{1}{2}}{N-\frac{1}{2}}\frac{1}{kT}\left[\left(\frac{\Gamma(N+\frac{1}{2})}{\Gamma(N)}\right)^2\frac{8\pi^3\tilde{m}l^2\Delta^2}{h^2}\,kT\right]^{1/2N+1}+\frac{\Delta}{2kT}\right].$$

For $N=1$ this goes into the expression for the exponential potential. However there is no guarantee that no other terms independent of h will appear in the exponent besides $\Delta/2kT$. For example, if $g(H)=b/H$ for large H, an additional term b/NkT will appear in the exponent. For the Morse or Lennard-Jones potential, $g\sim H^{-\frac{1}{2}}$ for large H. If there is an attractive branch of H, then for high H one can write

$$\frac{\mathrm{d}x}{\mathrm{d}H}=-a(H+\varepsilon)^{-N}\sim aH^{-N}\left(1-\frac{N\varepsilon}{H}\right),$$

in which case the correction ε/kT we have previously introduced is correct.

The conclusion of the paper is as follows: for reasonable potentials, the first two terms in the exponent of Z, eq. (10.1), are nearly correct, however, if the ν of the oscillator is replaced by Δ/k, there may be other terms not containing h and replacing ε/kT, which one can only calculate if the *exact* shape of the potential, including the attractive part, is known.

We next discuss specific potentials, for which calculations have been made.

b) The most important is the Morse potential. The following investigation *s* are available here:

DEVONSHIRE [28] has exactly calculated the matrix element H_{k_0k} for this potential. However, for this interaction between two molecules, in contradiction to the vibration within a molecule, ε is not large compared to kT, so that certain approximations applicable in the latter case cannot be used. COTTRELL and his co-workers [29] have made use of Devonshire's results.

TURNER and RAPP [30] have given an expression of the same form as for the exponential potential, but with modified constants. BAUER and his co-workers [31] have made numerical calculations for the efficiency of energy transfer, both as function of E and the angular momentum quantum number j, for a vibrating H_2 molecule, but no comparison with the corresponding Lennard-Jones data have been made. TAKAYANAGI and KANEKO [32] have calculated extensive tables, presented in graph form, of a function they call Ω. Since the Morse function contains three parameters, these tables have as independent variable kT/ε, and also two parameters. One is a quantity d, introduced by DEVONSHIRE. The other is called Δq^2 and is

$$\Delta q^2 = \frac{8\pi^2 \tilde{m} l^2}{h^2} \Delta , \tag{10.11}$$

where Δ is the energy transferred in the collision. One gets then the inelastic cross-section,

$$Q_{v\to v'} = \pi r_c^2 \frac{\pi^2}{4} (\Delta q^2)^2 \left| \frac{1}{l} X_{v-v'} \right|^2 \Omega . \tag{10.12}$$

If just one quantum is transferred

$$\frac{\pi^2}{4} (\Delta q^2)^2 = \frac{1}{16\pi^2} \left(\frac{\theta'}{\theta}\right)^2 .$$

To compare all these results with the calculation according to Lennard-Jones, what need now to be done, but has not yet been done, is the following: A gas should be selected, for which the temperature variation of viscosity can be well represented through the Lennard-Jones expression. A combination or a set of combinations of parameters must then be found, which allows the representation of the viscosity data with equal accuracy by the Morse function. Will these parameters and the help of the Takayanagi curves, the Z should then be calculated over an appreciable temperature range, and this compared with experiment and the calculation according to Lennard-Jones. None of this has yet been done.

COTTRELL and MCCOUBREY [33] have developed the most general expression available, using the semiclassical method. They write the potential

$$H = \lambda \exp\left[-\frac{r}{l}\right] - \mu \exp\left[-\frac{r}{2l}\right] = \lambda\left\{\exp\left[-\frac{r}{l}\right] - \frac{\mu}{\lambda}\exp\left[-\frac{r}{2l}\right]\right\} . \tag{10.13}$$

One gets the purely exponential repulsion by setting $\mu = 0$; one gets the Morse potential by setting

$$\lambda = D \exp\left[\frac{r_e}{l}\right] \qquad \mu = 2D \exp\left[\frac{r_e}{2l}\right] , \tag{10.14}$$

(r_e is the equilibrium distance).

Then they find eq. (6.11), except that the exponent is multiplied by a factor

$$1-\frac{2}{\pi}\,\mathrm{arctg}\sqrt{\frac{\mu^2}{4E\lambda}}\,. \tag{10.15}$$

COTTRELL and REAM [34] have attempted to apply the Lennard-Jones potential directly, using numerical methods.

Two other force laws have been investigated, mainly to test quantitatively the statement that a « *steep* » force is favorable for transitions.

c) Chemical forces. To test the idea that the efficiency of transfer is higher when « chemical forces » act, KOROBKIN [35] has investigated the collision between an H_2 molecule and a proton. For the sake of simplicity, the proton is restricted to the plane normal to the molecular axis of H_2 and bisecting it. Two calculations are made: in the first, the interaction is purely electrostatic, and therefore the efficiency of transfer is low. In the second, sharing of the two H_2 electrons by the proton is allowed by building molecular orbitals connecting all three nuclei; this introduces a typical « chemical » force. As a result, the transfer efficiency is so high that the first-order perturbation calculation is not justified.

d) Hard spheres. For hard spheres the time of interaction is infinitely short and therefore the energy transfer should be very efficient (the process is extremely nonadiabatic). A direct classical calculation is easy to make. Assuming the spheres to be smooth and the molecule BC originally at rest; we may consider B for the collision process to be free since during the infinitely small collision time the spring has transferred only infinitely little momentum to C. One then introduces the line of centres, which joins the centers of A and B at the moment of collision and makes an angle χ with the direction of the velocity w_A. The law of collision says then that B does not receive any momentum normal to the line of centres, but receives a velocity

$$w_B = 2\,\frac{m_A}{m_A+m_B}\,w_A\cos\chi\,, \tag{10.16}$$

in the direction of the line of centres.

Immediately after the collision we can forget the fate of A, but consider now the combination B-C.

After the collision, this has a velocity of its center of mass

$$w'_{BC}=\frac{1}{m_C+m_B}\,(m_B w_B + m_C 0)\,.$$

One can now write for the energy E_i of the internal motion (rotation plus vibration) of the molecule BC:

$$E_i = E_{\text{total}} - E' ,$$

E' being the energy of center-of-mass motion; *i.e.*,

$$E_i = \frac{1}{2} m_B w_B^2 - \frac{1}{2}(m_B + m_C)\left(\frac{m_B}{m_B + m_C}\right)^2 w_B^2 = \frac{1}{2}\overset{\approx}{m} w_B^2 = \tag{10.17}$$

$$= \frac{1}{2}\overset{\approx}{m}\cdot 4\frac{m_A^2}{(m_A + m_B)^2} w_A^2 \cos^2\chi = 4\frac{m_A m_B m_C \cdot E_A \cos^2\chi}{(m_A + m_B)^2(m_B + m_C)} ,$$

where E_A is the original energy of A.

If one takes the average of $\cos^2\chi$ over the half sphere (the number of particles A hitting a ring $d\chi$ is proportional to $\cos\chi \sin\chi\, d\chi$) one finds

$$\bar{E}_{\text{int}} = 2\frac{m_A m_B m_C}{(m_A + m_B)^2(m_B + m_C)} E_A , \tag{10.18}$$

and if one considers that the chance is $\frac{1}{2}$ that either B or C is hit (this is an approximation) one finds the average fraction of the energy E transferred to internal energy (*)

$$\frac{m_A m_B m_C}{m_B + m_C}\left[\frac{1}{(m_A + m_B)^2} + \frac{1}{(m_A + m_C)^2}\right] . \tag{10.19}$$

If the masses are about equal this is of order of magnitude unity; the result of SHULER and ZWENZIG [36, 37] is thereby explained. Separation of rotation and vibration is somewhat more complicated.

The above calculations assume $m_A \ll m_B$, so that no multiple collisions occur, and that BC is originally vibrationless. BENSON [38] has recently dropped both assumptions. He finds that if BC is originally highly excited, the energy transfer is small. This can be understood, since his result corresponds to the difference between excitation and de-excitation.

11. - Complex collisions.

In the previous deductions, only the term $-\beta(\partial H/\partial x)X$ was kept as perturbation term. For an exponential H, this is equal to

$$H\beta\frac{X}{l} ,$$

(*) If one wishes to use the energy of the relative initial motion instead of E_A for comparison, one must multiply the result (10.19) by $(m_B + m_C + m_A)/(m_B + m_C)$.

and led to a selection rule $v \rightarrow v \pm 1$, and an oscillation factor

$$\left|\beta^2 \frac{X_{10}}{l}\right|^2 . \tag{11.1}$$

The next term

$$\frac{1}{2} \beta^2 \frac{\partial^2 H}{\partial x^2} X^2 = \frac{1}{2} H \left(\frac{\beta X}{l}\right)^2 ,$$

for an exponential force law, permits jumps $v \rightarrow v \pm 2$.

It has been neglected in the previous development, for two reasons:

a) It is assumed that $\beta^2 |X_{10}/l|^2 < 1$. The quadratic term would led to an oscillatory factor for the jump $v \rightarrow v + 2$,

$$(v+1)(v+2)\left(\frac{\beta X_{10}}{l}\right)^4 < (v+1)\left|\frac{\beta X_{10}}{l}\right|^2 . \tag{11.2}$$

But much more important, the translational factor in Q is very much smaller for an energy transfer of $2h\nu$ than for an energy transfer $h\nu$.

There are however circumstances where these arguments do not hold.

Firstly [39], if one deals not with states at the bottom of the inner molecular binding curve but with states near the top, near to dissociation (11.2) is not fulfilled because the binding curve is far from that of a harmonic oscillators. Secondly, the energy steps Δ are much smaller, and therefore the effect of the translantional factor much smaller.

Secondly, however, there are cases where more than one characteristic vibration is present, either in the same molecule BC, or some in BC, others in A, if the latter is also a molecule containing more than one atom. Then one can write for βX

$$\sum \beta_s X^{(s)} ,$$

where the index s refers to the particular characteristic vibration and the β_s are numerical coefficients of order unity, not any more the special value (2.3). Since X^2 appears in

$$\frac{1}{2} \frac{\partial^2 H}{\partial x^2} X^2 = \frac{1}{2} H \frac{X^2}{l^2} ,$$

there will therefore be a term

$$H \beta_s \beta_j \frac{X^{(s)}}{l} \frac{X^{(j)}}{l} .$$

This will produce transitions $v_s \to v_{s\pm1}$, $v_j = v_{j\pm1}$ and provide an oscillatory factor in Q

$$\frac{1}{Z_{\text{osc}}} = (\beta_0 \beta_j)^2 \left| \frac{X_{10}^{(s)}}{l} \right|^2 \left| \frac{X_{10}^{(j)}}{l} \right|^2 , \tag{11.3}$$

multiplied by factors v_s or (v_{s+1}), v_j or (v_{j+1}), depending on the question whether we are dealing with deactivation or excitation. (11.3) will in general be smaller than (11.1). On the other hand if one oscillation (say s) suffers deactivation, the other (j) activation, only the difference of the quanta, $h\nu_s - h\nu_j$, has to be exchanged against translational energy, and this decrease in energy involved in the exchange into translational energy might increase $1/Z$ sufficiently that the product is larger (Z smaller) than for the single quantum process.

This is important for several reasons.

Complicared organic molecules have usually a rather small Z, although they contain no very low frequencies and should therefore, from the elementary theory, have large Z's. However they contain usually so many characteristic vibrations, that one can form combinations of $h\nu$'s so that the transfer to translational energy is small while a vibration with large ν looses one quantum and at the same time one with lower ν gains one.

Another interesting case is one where practically no transfer to kinetic energy takes place (« exact resonance »). In exact resonance, Z is little dependent on temperature, $\sim 1/T$ (see (6.19)). Exact resonance may happen because two molecules of different kind happen to have two characteristic vibrations of the same frequency. An example is N_2 and CO_2 recently investigated by HENDERSON [40]. The θ values for the single vibration of N_2 ($\theta = 3380$) and of the symmetrical vibration of CO_2 ($\theta = 3380°$) are the same. If N_2 is excited, it can loose its large quantum only in one step, which is a slow process. But if some CO_2 is mixed in, the transfer of this quantum to the assymetric valence bond vibration is easy, and from there it can leak out into translational energy, using in a stepwise process the other vibrational modes of CO_2, which have all lower frequencies. As a consequence, CO_2 is a rather effective impurity in shortening the relaxation time of N_2, which one would not have expected otherwise.

Another case of nearly exact resonance occurs [41] in CO_2, where the frequency of the symmetric valence bond vibration ($\theta = 1920$) is about twice that of the bending vibration. In this case, the former is deactivated by giving the bending vibration two quanta, with negligible transfer to translational energy. In spite of this fact, all the complex processes including those at exact resonance, can only occur during collision, so that the relaxation time is still inversely proportional to the pressure.

Consider a system with two vibrational degrees of freedom, such that only

I exchanges directly with kinetic energy while II exchanges its energy in practice in a complex collision which involves I and kinetic energy. This is a coupled system and the two effective relaxation times have to be calculated by the method of normal co-ordinates or network theory, as Dr. MASON has discussed. Assume $\tau_{\mathrm{I}} > \tau_{\mathrm{I\,II'}}$. Then at low frequency, there will be near equilibrium energy in both I and II. But for a frequency $\omega\tau'_{\mathrm{I}} > 1$, $\omega\tau'_{\mathrm{I\,II'}} < 1$, there will still be an influence of the sound wave on the process $h\nu_{\mathrm{II}} \rightleftharpoons h\nu_{\mathrm{I}} +$ kinetic energy, while the process $h\nu_{\mathrm{I}} \rightleftharpoons$ kinetic energy will be undisturbed, *i.e.*, the system will show two relaxation times. A general system with n vibrational degrees of freedom has on principle n relaxation times, although there may be many more individual reaction paths and although some of the relaxation times may be so close together as to be indistinguishable. We do not have yet a theory which allows us to predict without elaborate calculation, when a system will have more than one experimentally distinguishable relaxation time. As an example, consider CX_3Y and CX_4 againt CX_2Y_2; theoretical elaborate calculations, have been made by TANCZOS [42] and by DICKENS and LINNETT [43].

Another problem which may need theoretical treatment is the following: There are experimental indications that in a molecule with several vibrations, in which the relaxation times are sufficiently close together so as not to be experimentally separable, these relaxation times may be pulled apart by an impurity (possible examples CO_2 with H_2O [44], CO_2 and A [45]). This would mean that the impurity would act with different efficiency on different processes in the same molecule.

Addendum to Section 4. - Comparing the different expressions for the probability of excitation for one collision in the one dimensional case, one has

$$\frac{4\pi^2\beta^2}{h^2} X_{10}^2 |\mathscr{F}(\nu)|^2 , \tag{4.2, 4.11}$$

$$L\beta^2 = \frac{4\pi^2\beta^2}{h} X_{10}^2 L^{-1} \mathscr{G}(E) |H'_{k_0,k}|^2 \tau_0 , \tag{4.21}$$

$$|a|^2 \frac{p}{p_0} = \frac{16\pi^2\beta^2}{h^2} \frac{\tilde{m}^2}{p_0^2} X_{10}^2 |H'_{k_0,k}|^2 . \tag{4.26}$$

Probably, (4.21) should be multiplied by 4, since the elastically reflected wave also excites inelastic waves. One has then agreement between (4.21) and (4.26) since

$$\mathscr{G}(E)\,\mathrm{d}E = \frac{L\,\mathrm{d}p}{h} = \frac{L\tilde{m}}{hp_0}\,\mathrm{d}E \qquad \text{and} \qquad \tau_0 = \frac{\tilde{m}}{p_0} .$$

REFERENCES

[1] K. F. Herzfeld and T. A. Litovitz: *Absorption and Dispersion of Ultrasonic Waves* (New York, 1959).

[2] T. L. Cottrell and J. C. McCoubrey: *Molecular Energy Transfer in Gases* (London, 1961).

[3] L. Landau and E. Teller: *Phys. Zeits. der Sovjet Union*, **10**, 34 (1936).

[3] M. Born: *Zeits. Phys.*, **38**, 803 (1926).

[5] See N. F. Mott and H. S. W. Massey: *The Theory of Atomic Collisions* 2nd. ed. (Oxford, 1949).

[6] B. Widom: Discussions of the Faraday Soc. **33**, 37 (1962).

[7] P. Ehrenfest: *Kon. Ned. Akad. Wetenschap Proc.*, **16**, 591 (1914); *Ann. d. Phys.*, **51**, 327 (1916).

[8] F. W. de Wette and Z. I. Slawsky: *Physica*, **20**, 1169 (1954) See also Z. I. Slawsky, F. W. de Wette and S. R. de Groot: *Colloque Intern. sur les Ultrasons* (Brussel, 7-8-9 June 1951), p. 82.

[9] J. G. Parker: *Phys. of Fluids*, **2**, 449 (1959).

[10] D. Rapp: *Journ. Chem. Phys.*, **32**, 735 (1961).

[11] Cl. Zener: *Phys. Rev.*, **38**, 277 (1931).

[12] B. Widom and S. H. Bauer: *Journ. Chem. Phys.*, **21**, 1670 (1953).

[13] Cl. Zener: *Phys. Rev.*, **37**, 556 (1931).

[14] O. K. Rice: *Phys. Rev.*, **38**, 1943 (1931).

[15] K. Takayanaki: *Progr. Theor. Phys. Japan*, **8**, 111, 497 (1952).

[16] R. N. Schwartz and K. F. Herzfeld: *Journ. Chem. Phys.*, **22**, 767 (1954).

[17] R. N. Schwartz, Z. I. Slawsky and K. F. Herzfeld: *Journ. Chem. Phys.*, **20**, 1591 (1952).

[18] N. F. Mott and J. M. Jackson: *Proc. Roy. Soc.* (*London*), A **137**, 703 (1932).

[19] Ref. [2], p. 135.

[20] K. F. Herzfeld: *Zeits. f. Phys.*, **156**, 265 (1959).

[21] W. J. Witteman: *Journ. Chem. Phys.*, **37**, 655 (1962).

[22] M. C. Henderson: *Journ. Acoust. Soc. Am.*, **34**, 349 (1962).

[23] M. Camac: *Journ. Chem. Phys.*, **34**, 448 (1961).

[24] J. G. Parker: *Journ. Chem. Phys.*, **34**, 1763 (1961).

[25] R. C. Millikan: *Phys. Rev. Lett.*, **8**, 253 (1962).

[26] F. D. Shields: *Thermal relaxation in fluorine*, Technical Rep. NONR 3078 (01) (University of Mississippi, 1961).

[27] J. C. McCoubrey, R. Milward and A. R. Ubbelohde: *Trans. Far. Soc.*, **57**, 1472 (1961).

[28] A. F. Devonshire: *Proc. Roy. Soc.* (*London*), A **158**, 269 (1937).

[29] A. R. Blythe, T. L. Cottrell and A. W. Read: *Trans. Far. Soc.*, **57**, 935 (1961).

[30] R. E. Turner and D. Rapp: *Journ. Chem. Phys.*, **35**, 1076 (1961).

[31] M. Salkoff and E. Bauer: *Journ. Chem. Phys.*, **29**, 26 (1958).

[32] K. Takayanagi and S. Kaneko: *Science Reports of the Saitama University*, A **3**, 167 (1960); **4**, 15 (1961).

[33] Ref. [2], p. 127.

[34] T. L. Cottrell and N. Ream: *Trans. Far. Soc.*, **51**, 159 (1955).

[35] A. Korobkin and Z. I. Slawsky: *Journ. Chem. Phys.*, **37**, 226 (1962).

[36] K. E. SHULER and R. ZWANZIG: *Journ. Chem. Phys.*, **33**, 1778 (1960).
[37] F. H. MIES and K. E. SHULER: *Journ. Chem. Phys.*, **37**, 177 (1962).
[38] S. W. BENSON, G. D. BEREND and J. C. WU: *Journ. Chem. Phys.*, **38**, 25 (1963).
[39] *E.g.*, E. BAUER and F. W. CUMMINGS: *Journ. Chem. Phys.*, **36**, 618 (1962).
[40] M. C. HENDERSON: unpublished.
[41] K. F. HERZFELD: *Discussions Far. Soc.*, **33**, 22 (1962).
[42] F. TANCZOS: *Journ. Chem. Phys.*, **25**, 439 (1956).
[43] P. G. DICKENS and J. W. LINNETT: *Proc. Roy. Soc.* (*London*), A **243**, 84 (1957).
[44] W. H. PIELEMEIER, H. L. SAXTON and D. TELFAIR: *Journ. Chem. Phys.*, **8**, 106 (1940).
[45] H. O. KNESER and H. ROESLER: *Acoustica*, **9**, 224 (1959).
[46] R. HOLMES, F. A. SMITH and W. TEMPEST: *Proc. Phys. Soc. London*, **81**, 311 (1963).
[47] F. D. SHIELDS and KUN PAI LEE: *Journ. Acoust. Soc. Am.*, **35**, 251 (1963).

Phenomenological Theory of Multiple Relaxation Processes.

H.-J. BAUER

I. Physikalisches Institut der Technischen Hochschule - Stuttgart

Before entering into the theory of multiple relaxation processes I would like to make some general remarks on this subject:

1) The physical concept of multiple relaxation is the same as that of a single relaxation process. The fundamental equations, however, have a more complicated mathematical form. This forces us to obtain these fundamental equations in a quasi-automatic manner, otherwise errors could easily result.

2) The theoretical path from the fundamental equations to the results requires scarcely more then some algebraic operations and some termodynamic considerations. The algebraic operations, however, lead to many complicated equations. The use of matrix algebra could solve some problems here.

3) The results, which are equations of sound absorption and dispersion, are not very convenient for practical purposes, if they are given as a fraction of two polynomials in ω, involving several parameters. One should prefer a sum of functions for single relaxation.

The following theory of multiple relaxation processes is based on the thermodynamics of irreversible processes. For the sake of completeness the general concept of this foundation is reviewed. We start from the second law of thermodynamics:

$$\mathrm{d}S \geqslant \mathrm{d}Q/T\,. \tag{1}$$

We extend this inequality to an equation by adding another term to the right side:

$$\mathrm{d}S = \mathrm{d}Q/T + \mathrm{d}_i S = \mathrm{d}_a S + \mathrm{d}_i S\,. \tag{2}$$

There $\mathrm{d}Q/T$ is identified as fed-in entropy $\mathrm{d}_a S$, where as $\mathrm{d}_i S$ means the amount of entropy produced in the system by irreversible processes. The entropy production per second, also called the entropy source $\sigma = \mathrm{d}_i S/\mathrm{d}t$, gives a measure for the irreversibility of the processes. Instead of the entropy source we could also use the dissipation of energy $\mathrm{d}W - \mathrm{d}W_{\mathrm{rev}}$. Here $\mathrm{d}W$ is the work brought into the system for an irreversible change of state. $\mathrm{d}W_{\mathrm{rev}}$ is the necessary work for the same change of state along a reversible path. Since $\mathrm{d}U$ is the same for both paths, one gets by the use of the first law

$$\mathrm{d}W - \mathrm{d}W_{\mathrm{rev}} = \mathrm{d}Q_{\mathrm{rev}} - \mathrm{d}Q = T\,\mathrm{d}_i S\,. \tag{3}$$

The dissipation of energy per second or dissipation function is

$$\theta = \frac{\mathrm{d}W - \mathrm{d}W_{\mathrm{rev}}}{\mathrm{d}t} = T\sigma\,. \tag{2}$$

Investigations of the entropy source in many systems have shown that it is a bilinear form:

$$\sigma = X_1 J_1 + X_2 J_2 + \dots\,. \tag{5}$$

The X are the so-called forces. They are connected with the departure of the system from equilibrium. The fluxes J represent the velocity of the irreversible processes. One expects the fluxes to be functions of the forces alone, at least in a first approximation. In this approximation the fluxes are assumed to be linear functions of the forces:

$$J_i = \sum_k L_{ik} X_k\,. \tag{6}$$

These are the so-called phenomenological equations. For the phenomenological coefficients L_{ik} we make the following statements:

1) The matrix of the L_{ik} is positive definite. This is a result of the second law, since the entropy production always has to be positive.

2) Under certain conditions the L_{ik} matrix is symmetric. These are the Onsager relations. They are closely related to the principle of detailed balancing. These conditions are always fulfilled in our case.

Now we apply the thermodynamics of irreversible processes to the relaxation processes. First we have to investigate the meaning of the forces and fluxes. For this purpose we must calculate the entropy source. We neglect as usual heat conduction, internal friction, and diffusion and call their influence «classical absorption». Then it is possible to study our medium in a homogeneous, closed system; in which the only irreversible processes are reactions. The stoichiometric equations are

$$\sum_i \nu_{i\alpha}[M_i] \rightleftharpoons \sum \nu'_{i\alpha}[M_i] \qquad (\nu = 1, 2, ..). \tag{7}$$

The only work done on our system is expansion work

$$\mathrm{d}W = -p\,\mathrm{d}V. \tag{8}$$

$\mathrm{d}W_{\mathrm{rev}}$ is different from this value, if there are irreversible processes. For each reaction we have to introduce one more independent variable. We choose the reaction parameters ξ_α. They are defined so, that they are increased by unity, if the corresponding reaction has executed a fundamental step. $\mathrm{d}W_{\mathrm{rev}}$ is expected to be a function of all independent variables except the temperature:

$$\mathrm{d}W_{\mathrm{rev}} = -p\,\mathrm{d}V - \sum_\alpha A_\alpha \mathrm{d}\xi_\alpha . \tag{9}$$

The temperature is excepted, since there is no work necessary for a reversible temperature rise at constant volume and constant reactions. The affinities A_α are introduced here quite formally as the negative coefficients of work, corresponding to the ξ_α. From (8) and (9) we get

$$\mathrm{d}W - \mathrm{d}W_{\mathrm{rev}} = \sum_\alpha A_\alpha \mathrm{d}\xi_\alpha . \tag{10}$$

One obtains an expression for the dissipation function and for the entropy source:

$$\Theta = \sum_\alpha A_\alpha \dot{\xi}_\alpha , \tag{11}$$

$$\sigma = \frac{1}{T} \sum_\alpha A_\alpha \dot{\xi}_\alpha . \tag{12}$$

In this expression the reaction velocities $\dot{\xi}_\alpha$ represent the fluxes and the quantities A_α/T the forces. The phenomenological equations are

$$\dot{\xi}_\alpha = \sum_\beta L_{\alpha\beta} \frac{A_\beta}{T} . \tag{13}$$

We now investigate the affinities A_α. For this purpose we establish the differential internal energy change:

$$\mathrm{d}U = \mathrm{d}Q_{\mathrm{rev}} + \mathrm{d}W_{\mathrm{rev}} = T\,\mathrm{d}S - p\,\mathrm{d}V - \sum_\alpha A_\alpha \mathrm{d}\xi_\alpha . \tag{14}$$

One obtains from this equation

$$A_\alpha = -\left(\frac{\partial U}{\partial \xi_\alpha}\right)_{VS}. \tag{15}$$

In the Gibbs fundamental equation (14) one can replace the « physical » variables V and S by their conjugated ones. Then one has to carry out a Legendre transformation from the internal energy to the other thermodynamic potentials H, F, and G. It then follows that

$$A_\alpha = -\left(\frac{\partial U}{\partial \xi_\alpha}\right)_{VS} = -\left(\frac{\partial H}{\partial \xi_\alpha}\right)_{pS} = -\left(\frac{\partial F}{\partial \xi_\alpha}\right)_{VT} = -\left(\frac{\partial G}{\partial \xi_\alpha}\right)_{pT}. \tag{16}$$

The affinities represent the variables thermodynamically conjugated to the reaction parameters ξ_α. Therefore an equation of state exists for the affinities. We expand these « chemical » equations of state in a first order approximation. The zero point is chosen as an equilibrium point of the system, in which all affinities equal 0. For the independent variables p and T we get

$$A_\alpha = \left(\frac{\partial A_\alpha}{\partial p}\right)_{\xi T}(p-p_0) + \left(\frac{\partial A_\alpha}{\partial T}\right)_{\xi p}(T-T_0) + \sum_\beta \left(\frac{\partial A_\alpha}{\partial \xi_\beta}\right)_{pT}\xi_\beta. \tag{17}$$

One can see that we have set the $\xi^0 = 0$ in the last terms of this equation. This is allowed from our definition of the reaction parameters which was only a differential one.

Now it is useful to introduce matrices and vectors, which rather reduces the number of equations and terms. We introduce: the vector $\boldsymbol{\xi}$ with the components ξ_α and the vector $\boldsymbol{A}$ with the components A_α: The vector with the components $(\partial A_\alpha/\partial p)_{\xi T}$ and $(\partial A_\alpha/\partial T)_{\xi p}$ is called in what follows $\boldsymbol{G}_p$ and $\boldsymbol{G}_T$. The square matrix with the components $(\partial A_\alpha/\partial \xi_\beta)_{pT}$ is called $\boldsymbol{G}$. Then our chemical equations of state are

$$\boldsymbol{A} = \boldsymbol{G}_p(p-p_0) + \boldsymbol{G}_T(T-T_0) + \boldsymbol{G}\boldsymbol{\xi}. \tag{18}$$

One can immediately see one property of the matrix $\boldsymbol{G}$ from (16) and (17). An exchange of the order of differentiation in

$$\left(\frac{\partial A_\alpha}{\partial \xi_\beta}\right)_{pT} = -\left(\frac{\partial^2 G}{\partial \xi_\alpha \partial \xi_\beta}\right)_{pT} = \left(\frac{\partial A_\beta}{\partial \xi_\alpha}\right)_{pT}, \tag{19}$$

yields the symmetry of the matrix $\boldsymbol{G}$. Another property of this matrix can be shown by the expansion of the Gibbs function G about the equilibrium point under constant pressure, constant temperature circumstances. One gets

$$G - G_0 = -\tfrac{1}{2}\xi' A = -\tfrac{1}{2}\xi' G \xi \,. \tag{20}$$

Herein ξ' is the transposed vector ξ. Since the Gibbs function G has an absolute minimum in equilibrium at constant p and T, the quadratic form (20) is always positive. So G is negative definite.

We now insert the chemical equations of state (18) into the phenomenological eqs. (13). The matrix form of (13) is

$$\dot{\xi} = \frac{1}{T} L A \,, \tag{21}$$

or, after multiplication with L^{-1} from the left side,

$$L^{-1}\dot{\xi} = \frac{1}{T} A \,. \tag{22}$$

Insertion of (18) gives us

$$L^{-1}\dot{\xi} = \frac{1}{T} G\xi + \frac{1}{T} G_p(p - p_0) + \frac{1}{T} G_T(T - T_0) \,. \tag{23}$$

Now we consider the relaxation experiment at constant pressure and temperature $p = p_0$, $T = T_0$. The last two terms of (23) then vanish and we get a system of linear, homogeneous differential equations of first order in ξ. These equations are normally coupled. Only in the case, where L^{-1} and G have diagonal form, are the differential eqs. (23) decoupled and solutions can easily be obtained.

In the general case one has to carry out a transformation of the reaction co-ordinates to main axes. We perform the linear substitution

$$\xi = C\zeta \,. \tag{24}$$

Then we get

$$C' L^{-1} C \dot{\zeta} = \frac{1}{T} C' G C \zeta \,. \tag{25}$$

It is possible to select a transformation matrix C which leads to $C'L^{-1}C$ being equal to the unit matrix L and $C'GC$ achieving a diagonal form. The reason is the symmetry of both matrices L^{-1} and G and the positive definiteness of L and therefore of L^{-1}. To find this transformation matrix C forms the algebraic part of our task. It consists in the solution of the general eigenvalue problem for the pair of matrices L^{-1} and G. It is treated in the textbooks on matrix algebra. After the transformation, the diagonal form of the matrix $C'GC$ is composed of the eigenvalues λ_i^{pT}. They are all negative and connected with the isothermal-isobaric relaxation times by

$$\tau_i^{pT} = -T/\lambda_i^{pT}. \tag{26}$$

With these relaxation times, the transformed reaction parameters relax to the equilibrium value zero.

We have considered relaxation under isothermal-isobaric conditions and we now treat the isentropic-isobaric relaxation. For this problem the most convenient physical variables are p and S and the corresponding thermodynamic potential is the enthalpy H. The chemical equations of state are now

$$\boldsymbol{A} = \boldsymbol{H}_p(p - p_0) + \boldsymbol{H}_s(S - S_0) + \boldsymbol{H}\boldsymbol{\xi}. \tag{27}$$

From the phenomenological equations, which remain unchanged, we get the relaxation equations

$$\boldsymbol{L}^{-1}\dot{\boldsymbol{\xi}} = \frac{1}{T}\boldsymbol{H}\boldsymbol{\xi} + \frac{1}{T}\boldsymbol{H}_p(p - p_0) + \frac{1}{T}\boldsymbol{H}_s(S - S_0). \tag{28}$$

In the description of relaxation experiments the last two terms again vanish. For the solution of (28) we have to transform to main axes. After the transformation the matrix at the left side is the unit matrix, the matrix at the right side is diagonal and composed of the eigenvalues λ_i^{pS}, which are different from the λ_i^{pT}. The isentropic-isobaric relaxation times are

$$\tau_i^{pS} = -T/\lambda_i^{pS}. \tag{29}$$

We now treat the dynamic experiment. In the dynamic case $(p - p_0)$ and $(T - T_0)$ are not always zero. In the acoustical dynamic experiment, however, $(S - S_0)$ equals zero in a first order approximation, since acoustical processes are adiabatic under neglect of heat conduction and the entropy produced is small—of second order. Therefore the independent variables p and S are more convenient than p and T.

The best way of describing the dynamic experiment is the dynamic equation of state. We derive this equation from the normal equation of state by elimination of all reaction parameters. In the acoustic case we regard the density ϱ as the dependent variable and we get the normal equation of state

$$\varrho - \varrho_0 = \left(\frac{\partial \varrho}{\partial p}\right)_{\xi S} (p - p_0) + \sum_{\alpha} \left(\frac{\partial \varrho}{\partial \xi_\alpha}\right)_{pS} \xi_\alpha \,. \tag{30}$$

The term with $(S - S_0)$ has already been omitted. If the vector with the components $(\partial\varrho/\partial\xi_\alpha)_{pS}$ is called $\boldsymbol{Z}$, the eq. (30) takes the form

$$\varrho - \varrho_0 = \left(\frac{\partial \varrho}{\partial p}\right)_{\xi S} (p - p_0) + \boldsymbol{Z}'\boldsymbol{\xi} \,. \tag{31}$$

The elimination of the vector $\boldsymbol{\xi}$ is done by use of the relaxation eqs. (28). We consider only harmonic changes of state so that the differentiation means a multiplication by $j\omega$. (28) then changes to

$$\left(j\omega \boldsymbol{L}^{-1} - \frac{1}{T}\boldsymbol{H}\right)\boldsymbol{\xi} = \frac{1}{T}\boldsymbol{H}_p (p - p_0) \,, \tag{32}$$

or

$$\boldsymbol{\xi} = \left(j\omega \boldsymbol{L}^{-1} - \frac{1}{T}\boldsymbol{H}\right)^{-1} \frac{1}{T}\boldsymbol{H}_p (p - p_0) \,. \tag{33}$$

Insertion of (33) in the equation of state (31) gives us the acoustic equation of state

$$\varrho - \varrho_0 = \left[\left(\frac{\partial \varrho}{\partial p}\right)_{\xi S} + \boldsymbol{Z}'\left(j\omega\, \boldsymbol{L}^{-1} - \frac{1}{T}\boldsymbol{H}\right)^{-1} \frac{1}{T}\boldsymbol{H}_p\right] (p - p_0) \,. \tag{34}$$

For the compressibility we get

$$\varkappa_S^{\mathrm{eff}} = \frac{1}{\varrho_0}\frac{\varrho - \varrho_0}{p - p_0} = \frac{1}{\varrho}\left(\frac{\partial \varrho}{\partial p}\right)_{\xi S} + \frac{1}{\varrho T}\boldsymbol{Z}'\left(j\omega \boldsymbol{L}^{-1} - \frac{1}{T}\boldsymbol{H}\right)^{-1} \boldsymbol{H}_p \,. \tag{35}$$

This compressibility $\varkappa_S^{\mathrm{eff}}$ is complex and frequency-dependent. Therefore we call it the effective or dynamic compressibility. Its representation in the form (35) is due to MEIXNER.

If we now insert the matrices $\boldsymbol{L}^{-1}$ and $\boldsymbol{H}$ we get a fraction of two complex polynomials in ω. After transformation to main axes however, we get a more convenient form, since the $\boldsymbol{L}^{-1}$ is then the unit matrix and $\boldsymbol{H}$ is diagonal. But then we have also to transform the vectors $\boldsymbol{Z}$ and $\boldsymbol{H}_p$: These vectors contain differential coefficients whith respect to the reaction parameters. The differentiation now has to be carried out with respect to the transformed reaction parameters ζ. We call these new vectors $\boldsymbol{z}$ and $\boldsymbol{h}_p$. If one remembers

$$\lambda_i^{pS}/T = -1/\tau_i^{pS}$$

one gets the form

$$\varkappa_S^{\text{eff}} = \varkappa_S^{\infty} + \frac{1}{\varrho T}\boldsymbol{Z}'\,[\text{Diag}\,(1 + j\omega\tau_i^{pS})/\tau_i^{pS}]^{-1}\,\boldsymbol{h}_p\,.$$

This is a bilinear form of the vectors $\boldsymbol{z}$ and $\boldsymbol{h}_p$ with the matrix

$$\text{Diag}\left[\frac{\tau_i^{pS}}{(1+j\omega\tau_i^{pS})}\right].$$

In components, we have

$$\varkappa_S^{\text{eff}} = \varkappa_S^{\infty} + \sum_i \frac{(\tau_i^{pS}/\varrho T)(\partial\varrho/\partial\zeta_i)_{pS}(\partial V/\partial\zeta_i)_{pS}}{1 + j\omega\tau_i^{pS}}\,. \tag{37}$$

For the normalized compressibility $\varkappa_S^{\text{eff}}/\varkappa_S^{\infty}$ we get the final form

$$\varkappa_S^{\text{eff}}/\varkappa_S^{\infty} = 1 + \sum_i \frac{(\tau_i^{pS}/VT\varkappa_S^{\infty})(\partial V/\partial\zeta_i)_{pS}^2}{1 + j\omega\tau_i^{pS}}\,. \tag{38}$$

The numerator can be interpreted as $\varepsilon_i^{\infty} = \delta_i\varkappa_S/\varkappa_S^{\infty}$. Here $\delta_i\varkappa_S$ is the part of the compressibility due to the i-th transformed reaction. So $\delta_i\varkappa_S$ is the compressibility which one would get, if only the i-th reaction is in equilibrium minus the instantaneous compressibility $\varkappa_S^{\infty}$.

The quantities ε_i^{∞} correspond to the relaxation strength of single relaxation processes, but normalized with $\varkappa_S^{\infty}$ instead of $\varkappa_S^{0}$. For the calculation of the ε_i^{∞} we properly introduce the $(\partial V/\partial\xi)_{pS}$ instead of the $(\partial V/\partial\zeta)_{pS}$ by use of the linear substitution (24). In this operation we must notice that co-ordinates and differential coefficients transform in contragredient fashion:

$$\left(\frac{\partial V}{\partial\zeta}\right)_{pS} = C'\left(\frac{\partial V}{\partial\xi}\right)_{pS}. \tag{39}$$

The quantities $(\partial V/\partial\xi_\alpha)_{pT}$ are connected with the volume changes $\Delta_\alpha V = (\partial V/\partial\xi_\alpha)_{pT}$ and the reaction entropies $\Delta_\alpha S = (\partial S/\partial\xi_\alpha)_{pT}$ in the same way as in the single relaxation process.

Our final form of the normalized compressibility was

$$\varkappa_S^{\text{eff}}/\varkappa_S^{\infty} = 1 + \sum_i \frac{\varepsilon_i^{\infty}}{1 + j\omega\tau_i^{pS}}\,. \tag{40}$$

The real part of this expression equals c_∞^2/c^2, the imaginary part equals $(\mu/\pi)\cdot(c_\infty^2/c^2)$ and is mainly connected with the absorption. Since (40) involves a sum of several complex relaxation terms, they can be split into their real and imaginary parts separately. Therefore we get a simple superposition of single relaxation functions for some properly chosen absorption and dispersion quantities:

$$\frac{c_\infty^2}{c^2} = 1 + \sum_i \frac{\varepsilon_i^\infty}{1+\omega^2\tau_{i\nu s}^2}\,, \tag{41}$$

$$\mu\frac{c_\infty^2}{c^2} = \sum_i \frac{\pi\varepsilon_i^\infty\,\omega\tau_{i\nu s}}{1+\omega^2\tau_{i\nu s}^2}\,. \tag{42}$$

We now consider the matrices ***P***, ***G***, ***H***, and ***L*** and discuss the way in which they can be established. First we connect the affinities A_α with the chemical potentials μ_i:

$$A_\alpha = -\left(\frac{\partial F}{\partial\xi_\alpha}\right)_{VT} = -\sum_i\left(\frac{\partial F}{\partial n_i}\right)_{VT}\frac{\partial n_i}{\partial\xi_\alpha} = -\sum_i \mu_i\Delta\nu_{i\alpha}\,. \tag{43}$$

Here the $\Delta\nu_{i\alpha}$ are the differences between the stoichiometric coefficients at the right and left side of the α-th reaction.

For the differentiation with respect to ξ_β we now have to assume our medium to be an ideal mixture. Then $\mu_i=\mu_i^0+RT\ln x_i$, where μ_i^0 is the chemical potential of the pure substance i, x_i is its mole fraction. In ideal gases the differentiation process works only on the second term and we get

$$\left(\frac{\partial A_\alpha}{\partial\xi_\beta}\right)_{VT} = -\frac{RT}{V}\sum_i\frac{\Delta\nu_{i\alpha}\Delta\nu_{i\beta}}{c_i}\,. \tag{44}$$

One can establish this expression quite easily by the use of two further matrices. A matrix $\boldsymbol{\nu}$ contains these $\Delta\nu_{i\alpha}$ where each reaction furnishes one column. The other matrix is diagonal and contains the reciprocal concentrations of all substances in the same order as in the matrix $\boldsymbol{\nu}$. We call this matrix $\mathrm{Diag}\,(1/c)$. Then one gets the matrix ***F*** with the components $(\partial A_\alpha/\partial\xi_\beta)_{VT}$ by the use of these two matrices:

$$\boldsymbol{F} = -\frac{RT}{V}\boldsymbol{\nu}'\,\mathrm{Diag}\,(1/c)\boldsymbol{\nu}\,. \tag{45}$$

From the matrix ***F*** we get the matrix ***G*** by the use of the thermodynamic relation

$$\left(\frac{\partial A_\alpha}{\partial\xi_\beta}\right)_{pT} = \left(\frac{\partial A_\alpha}{\partial\xi_\beta}\right)_{VT} + \frac{1}{V\varkappa_T^\infty}\Delta_\alpha V\Delta_\beta V\,. \tag{46}$$

One sees from this equation that we have to add a matrix with the components $\Delta_\alpha V \Delta_\beta V / V \varkappa_T^\infty$ to our matrix $\boldsymbol{F}$. This can be done by an extension of the matrix $\boldsymbol{\nu}$ by one row, containing all ΔV and by continuation of the matrix Diag$(1/c)$ by the component $-1/RT\varkappa_T^\infty$.

In the same way we can establish the matrix $\boldsymbol{H}$. The proper thermodynamic relation is

$$\left(\frac{\partial A_\alpha}{\partial \xi_\beta}\right)_{vS} = \left(\frac{\partial A_\alpha}{\partial \xi_\beta}\right)_{vT} - \frac{T}{nC_v^\infty} \Delta_\alpha S \Delta_\beta S . \tag{47}$$

We extend the matrix $\boldsymbol{\nu}$ again by one row, containing all ΔS. The diagonal matrix is continued another time by the component $+v/RC_v^\infty$.

Finally, we need a relation between the matrix $\boldsymbol{L}$ and a kinetic model. In the following we assume our reactions to be elementary reactions. This means that the exponents in the rate equations are the stoichiometric coefficients of each substance. The rate of the reaction in the forward direction is $k_\alpha \Pi c_i^{\nu_{i\alpha}}$ and the rate in the backward direction is $k'_\alpha \Pi c_i^{\nu'_{i\alpha}}$. In equilibrium both reaction ratese are equal. For equilibrium concentrations, a macroscopic reaction rate can be observed:

$$\dot{\xi}_\alpha = V[k_\alpha \Pi c_i^{\nu_{i\alpha}} - k'_\alpha \Pi c_i^{\nu'_{i\alpha}}] . \tag{48}$$

We consider only small departures from equilibrium. Then this expression can be expanded:

$$\dot{\xi}_\alpha = - V\, k_\alpha \Pi c_i^{\nu_{i\alpha}} \sum_i \Delta \nu_{i\alpha} \frac{c_i - c_{i0}}{c_{i0}} . \tag{49}$$

We now express the concentration departures in the reaction parameters and get the final form

$$\dot{\boldsymbol{\xi}} = - \mathrm{Diag}\, (k_\alpha \Pi c_i^{\nu_{i\alpha}}) \boldsymbol{\nu}' \, \mathrm{Diag}\, (1/C) \boldsymbol{\nu} \boldsymbol{\xi} . \tag{50}$$

Taken together, the last three matrices are $-(V/RT)\boldsymbol{F}$. (50) represents the relaxation equation for isothermal-isochoric relaxation. For this case the thermodynamics of irreversible processes furnishes the form

$$\dot{\boldsymbol{\xi}} = \frac{1}{T} \boldsymbol{L}\boldsymbol{F}\boldsymbol{\xi} . \tag{51}$$

By comparison with (50) we get

$$\boldsymbol{L} = \frac{V}{R} \mathrm{Diag}\, (k_\alpha \Pi c_i^{\nu_{i\alpha}}) . \tag{52}$$

An example is now given to illustrate the method. We consider two independent reactions in parallel according to the stoichiometric equations

$$\left\{\begin{array}{ll} A_0 + C \rightleftharpoons A_1 + C & (A) \\ B_0 + C \rightleftharpoons B_1 + C & (B) \end{array}\right. . \tag{53}$$

They can be interpreted as activation and de-activation of two different molecules A and B in the collisions with a molecule C, which remains unchanged. C is not further specified in this simple model. From the stoichiometric equations we derive

$$\nu = \begin{pmatrix} -1 & 0 \\ 1 & 0 \\ 0 & -1 \\ 0 & 1 \end{pmatrix} \quad \text{and} \quad \mathrm{Diag}\,(1/c) = \begin{pmatrix} \frac{1}{c_{A_0}} & 0 & 0 & 0 \\ 0 & \frac{1}{c_{A_1}} & 0 & 0 \\ 0 & 0 & \frac{1}{c_{B_0}} & 0 \\ 0 & 0 & 0 & \frac{1}{c_{B_1}} \end{pmatrix}, \tag{54}$$

and get

$$\boldsymbol{F} = -\frac{RT}{V}\begin{pmatrix} \frac{1}{c_{A_0}} + \frac{1}{c_{A_1}}, & 0 \\ 0 & , \frac{1}{c_{B_0}} + \frac{1}{c_{B_1}} \end{pmatrix}, \tag{55}$$

Since neither reaction changes the number of moles, the ΔV are zero and $\boldsymbol{G} = \boldsymbol{F}$. $\boldsymbol{L}$ is

$$\boldsymbol{L} = \frac{V}{R}\begin{pmatrix} k_A c_C c_{A_0} & , & 0 \\ 0 & , & k_B c_C c_{B_0} \end{pmatrix}. \tag{56}$$

From the three matrices $\boldsymbol{F}$, $\boldsymbol{G}$, and $\boldsymbol{L}$ one sees that the isothermal-isochoric and isothermal-isobaric relaxation equations are already decoupled. The isothermal relaxation times are

$$\left\{\begin{array}{l} \tau_A^{VT} = \tau_A^{pT} = 1/k_A c_C\left(1 + \dfrac{c_{A_0}}{c_{A_1}}\right) = 1/c_C(k_A + k'_A)\,, \\ \tau_B^{VT} = \tau_B^{pT} = 1/c_C\,(k_B + k'_B)\,. \end{array}\right. \tag{57}$$

This is the result which one would obtain also, if each reaction were occuring alone.

Before considering the acoustic relaxation we have to form the matrix $\boldsymbol{H}$. $\boldsymbol{H}$ contains nondiagonal components, since the reaction entropies ΔS do not vanish. One gets

$$H = -\frac{RT}{V}\begin{pmatrix} \dfrac{1}{c_{A_0}} + \dfrac{1}{c_{A_1}} + \dfrac{v}{RC_p^\infty}\Delta_A S^2, & \dfrac{v}{RC_p^\infty}\Delta_A S\,\Delta_B S \\ \dfrac{v}{RC_p^\infty}\Delta_A S\,\Delta_B S & , \dfrac{1}{c_{B_0}} + \dfrac{1}{c_{B_1}} + \dfrac{v}{RC_p^\infty}\Delta_B S^2 \end{pmatrix}. \tag{58}$$

Now the eigenvalue problem has to be solved. The way of solution is not shown here in particular, neither shall I write down the complicated general expressions for the isentropic-isobaric relaxation times and for the relaxation strengths. Results are only given here for two special cases. We assume the two isothermal relaxation times to be very different and τ_A to be much shorter than τ_B, since the reaction A takes place rapidly compared with the reaction B. Than the results are, in a first order approximation:

$$\left\{\begin{aligned} \frac{1}{\tau_1^{pS}} &= \frac{C_p^\infty + \delta_A C}{\tau_A C_p^\infty}\left[1 + \frac{\tau_A}{\tau_B}\cdot\frac{\delta_A C\,\delta_B C}{(C_p^\infty + \delta_A C)^2} + \dots\right], \\ \frac{1}{\tau_2^{pS}} &= \frac{C_p^\infty + \delta_B C}{\tau_B C_p^\infty}\left[1 - \frac{\tau_A}{\tau_B}\cdot\frac{\delta_A C\,\delta_B C}{(C_p^\infty + \delta_A C)^2} + \dots\right], \\ \delta_1 \varkappa_S &= \frac{v\,\delta_A C}{T C_p^\infty (C_p^\infty + \delta_A C)}\left[1 + \frac{\tau_A}{\tau_B}\cdot\frac{2C_p^\infty\,\delta_B C}{(C_p^\infty + \delta_A C)^2} + \dots\right], \\ \delta_2 \varkappa_S &= \frac{v\,\delta_B C}{T(C_p^\infty + \delta_A C)(C_p^\infty + \delta_A + \delta_B C)}\left[1 - \frac{\tau_A}{\tau_B}\cdot\frac{2\,\delta_A C(C_p^\infty + \delta_A C + \delta_B C)}{(C_p^\infty + \delta_A C)^2} + \dots\right]. \end{aligned}\right. \tag{59}$$

The quantities in front of the brackets are the values which one would expect from the theory of single relaxation for the reaction A with B neglected or B with A treated as instantaneous. One can see from the first two equations that the smaller relaxation time τ_1^{pS} gets smaller, the longer relaxation time τ_2^{pS} longer than expected from simple theory. The interaction of the two relaxation processes makes them «repel» each other. The $\delta_1\varkappa_S$ and therefore the relaxation strength ε_1^∞ of the faster process is always larger than expected for simple theory. The reverse is true for the slower process.

Another special case exists where $(C_p^\infty + \delta_A C)/\tau_A = (C_p^\infty + \delta_B C)/\tau_B$: Then the two processes are very close. We get

$$(60)\qquad \left\{\begin{aligned} &\frac{1}{\tau_{1,2}^{pS}} = \frac{C_p^\infty + \delta_A C}{\tau_A C_p^\infty} \pm \frac{1}{C_p^\infty}\sqrt{\frac{\delta_A C\,\delta_B C}{\tau_A\tau_B}}\,,\\ &\varepsilon_{1,2} = \frac{R}{C_V^\infty(C_p + \delta_A C + \delta_B C)}\,.\\ &\cdot\left[\frac{1}{2}\left(\frac{\partial_A C}{\tau_A} + \frac{\delta_B C}{\tau_B}\right) \pm \sqrt{\frac{\delta_A C\delta_B C}{\tau_A\tau_B}}\right]\Bigg/\left[\frac{C_p^\infty + \delta_A C}{\tau_A C_p^\infty} \pm \frac{1}{C_p^\infty}\sqrt{\frac{\delta_A C\,\delta_B C}{\tau_A\tau_B}}\right]. \end{aligned}\right.$$

In this case the theory of single relaxation would make both isentropic-isobaric relaxation times equal. However a difference still can be seen from the first equation, and this difference is the minimum distance of the two relaxation processes. The relaxation strength ε_1^∞ of the faster process contains approximately the effects of both reactions. One can see this easily, since in the numerator we have the sum of the arithmetic and geometric means of the quantities $\delta_A C/\tau_A$ and $\delta_B C/\tau_B$. The low-frequency relaxation strength ε_2^∞, however, has a small value. The numerator then contains the difference between the arithmetic and the geometric mean of the same quantities.

There are some final remarks to be made on the example « two independent elementary reactions in parallel ».

In this case the two matrices L and G already had diagonal form. The nondiagonal components of H were the result of coupling by the reaction entropies. We have cancelled this coupling by a transformation to main axes. For all reactions that lead to double relaxation, then one part of the work is already done. We can use the results of our example for all systems of reactions with diagonal 2×2 matrices L and G. The only values we must know are the isothermal relaxation times and the contributions to the specific heat. For reactions that are already coupled in the stoichiometric equations, it is sufficient to diagonalize the matrix G. This means a transformation from the original reactions to those which behave like « two independent elementary reactions in parallel ». When the diagonalization of the matrix G is done, we know the isothermal relaxation times. The contributions to the specific heat can be calculated from the reaction heats by means of some thermodynamic relations and the transformation matrix C.

Thus it is possible, to proceed from simple to more complicated multiple relaxation processes by putting several transformations in series. This is another advantage, if not the main one, of the method given here.

Rotational Relaxation in the Sound Absorption of Hydrogen Isotopes.

C. G. Sluijter

Kamerlingh Onnes Laboratorium - Leiden.

Measurements of sound absorption have been made in normal H_2, para-H_2, normal D_2, ortho-D_2 and HD using a method developed by Meyer and Sessler [1]. This method has been modified in order to use it at low temperatures. Some of our results are shown in Fig. 1, 2 and 3. Figure 1 shows the experimental points of α'/f as function of f/p at 293 °K of para-H_2 (△), normal D_2 (□) and HD (○). Figure 2 and 3 show the experimental points of $\alpha'\lambda(V_0/V)^2$ as function of f/p of ortho-D_2 at 90 °K and of para-H_2 at 77 °K.

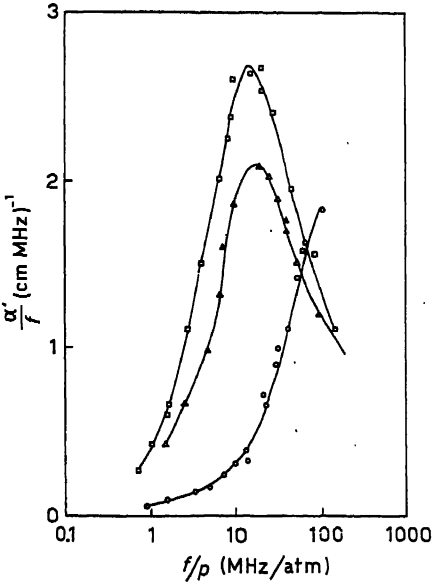

Fig. 1.

The notation is taken from HERZFELD and LITOVITZ [2]. They derive in the case of a single relaxation time the absorption formula

$$\alpha'\lambda\left(\frac{V_0}{V}\right)^2=\frac{\Delta C'}{C_V(C_p-C')}\,\frac{\omega\tau'}{1+\omega^2\tau'^2}\,.$$

This formula is represented by the solid curve in the Fig. 2 (ortho-D_2 at 90 °K) and 3 (para-H_2 at 77 °K). The specific heat data were taken from FARKAS [3].

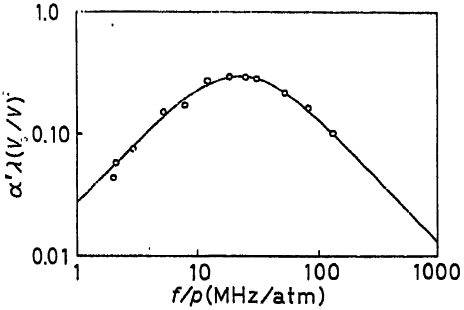

Fig. 2.

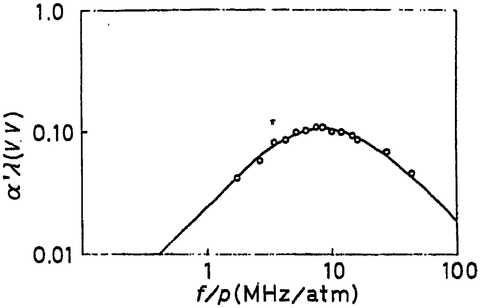

Fig. 3.

In this way it is proved that ortho-D_2 and para-H_2 at temperatures below 100 °K behave as a two-level gas with one single relaxation time. Full details will be published in *Physica* (1963).

This research has been done in the Kamerlingh Onnes Laboratory, Leiden in cooperation with Dr. J. J. M. BEENAKKER, as part of the research program of the Molecular Physics group of the Stichting voor Fundamenteel Onderzoek der Materie (F.O.M.) financially supported by the « Stichting voor Zuiver Wetenschappelijk Onderzoek » (Z.W.O.) in the Netherlands.

REFERENCES

[1] E. MEYER and G. SESSLER: *Zeits. Phys.*, **149**, 15 (1957).
[2] K. F. HERZFELD and T. A. LITOVITZ: *Absorption and Dispersion of Ultrasonic Waves* (New York and London, 1959).
[3] A. FARKAS: *Orthohydrogen, Parahydrogen and Heavy Hydrogen* (Cambridge, 1935).

Measurements of Ultrasonic Velocity and Absorption in Liquids at High Frequencies, at High Temperatures and under High Hydrostatic Pressure.

R. T. BEYER

Brown University - Providence R. I.

Under this title, I wish to discuss absorption and velocity measurements in liquids under a number of extreme conditions—high frequency, high pressure, high temperature. Some of these measurements are today in their early stages, and what I shall say is undoubtedly behind the most recent work, which, in a number of cases, is being done by members of the group lecturing here. Nevertheless, I hope to give you some picture of the more recent advances.

1. – Absorption measurements at high frequency.

1·1. *Pulse techniques.* – For many years now, the standard range of measurement of ultrasonic absorption by the pulse technique has been from about 10 MHz up to perhaps 200 MHz. Commercial instruments are now available which are capable of performing absorption and relatively rough velocity measurements in this range. A detailed analysis of one such system is given by CHICK, ANDERSON and TRUELL [1]. Because it is useful for comparison of methods, a few words about such circuits are appropriate. A rectangular pulse is used to modulate the radiofrequency carrier signal, and the result is applied to a transducing crystal at one of its resonant frequencies. In a typical case, the pulse is about 5 μs in length, with a repetition rate of 1000 per second. The pulse must be of sufficient length so that the frequency spread of the Fourier analysis of the pulse is negligible.

Such an electric pulse is converted by the transducer to an acoustic pulse which passes through the medium. It is then reflected by a polished surface (metal or quartz) and is then received by the crystal during the quiescent part of its cycle. This reflected signal is now re-converted to an electric one, amplified and detected, so that the returned pulse envelope is presented on an oscilloscope screen. A typical successful trace is shown in Fig. 1. The peaks of the curve or « pips » give the relative amplitudes of the original signal and the successive reflections.

To measure the attenuation, one can superpose a calibrated exponential decay curve on the oscilloscope screen. This curve can be adjusted to fit as a tangent curve to the individual pips. An absorption coefficient can then be read from the information on the decay curve.

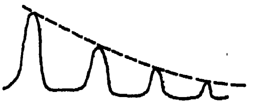

Fig. 1. – Typical oscilloscope pattern for reflected acoustic pulses.

Alternatively, the reflected pulse is passed through a calibrated attenuator. The reading of this attenuator is adjusted until the reflected pulse reaches a certain height. The reflector is then moved closer to the source until the reflected pulse regains its original height. This process is repeated at a number of different points along the beam. The attenuation can then be read from the number of db attenuation introduced in the system.

As the reflector is moved, the reflected pulse moves across the screen of the oscilloscope. A velocity measurement can then be made by reading the reflector positions for which the pulse front coincides with time markers superposed on the trace. The distance that the reflector has moved is equal to one half the distance the sound beam travels in the time interval between the time markers.

In giving this brief account, we have passed over a variety of difficulties. For example, it is necessary that the pulse have a very steep leading edge for velocity measurements; in general, such a lack prevents very accurate measurements. Great care must also be taken to assure that the faces of the crystal and reflector are accurately flat and parallel, and that the reflector moves perpendicular to these faces. Finally, one is never dealing with a plane wave, so that there is a certain amount of beam spreading, especially at the lower frequencies, which must be taken into account. A recent analysis of these diffraction effects has been given by Bass [2].

In the effort to work at higher and higher frequencies, one used more and more compact apparatus. This is necessary both for electrical reasons and for the reason that the absorption becomes very great so that only a very short path length can be employed. It is also necessary to use very high harmonics of the quartz crystal. Recently, measurements have been reported by Dunn and Breyer [3] in which a 4 MHz crystal was driven up to its 487th harmonic. The authors used a single acoustic pulse of rectangular shape and with a duration of 0.1 s. A specially prepared copper-constantan thermocouple probe was used as the detector. This probe had a working surface of 5 μm maximum width, and its motion was measured by a micrometer having a least count of 0.000 01 in. In this first report, they measured the attenuation in castor oil up to 400 MHz, and in DC-710 silicone oil to 2 GHz. The highest absorption coefficient measured was more than 1000 neper/cm.

In working with a more conventional system at higher frequencies, it has become customary to alter the transducer arrangement so that the driving crystal is mounted on one end of a fused quartz rod, and a second, receiving crystal is mounted on another such rod. The attenuation in the quartz is quite low and can be neglected up to very high frequencies. With this arrangement, overlap between the initial pulse and its subsequent reflections is avoided.

1·2. *Shear waves.* – It is also possible to measure the properties of shear waves in liquids. Such waves, which require the presence of viscosity for their existence, are very rapidly absorbed. Now the shear wave impedance of such a wave can be written as

$$Z_L=\frac{i\omega\varrho_0}{ik+\alpha}=R_L+iX_L\,. \tag{2}$$

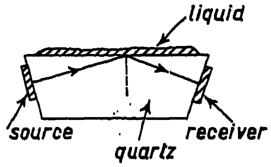

Fig. 2. – Arrangement for production of shear waves in a liquid (after Mason *et al.* [4]).

A method was developed by Mason *et al.* [4] to make use of these facts to measure the shear wave impedance in liquids by reflecting a shear wave from a quartz-liquid interface and comparing this with reflection from a quartz-air interface. The arrangement is sketched in Fig. 2. The governing relation is [5]

$$Z_L=Z_s\cos\varphi\left[\frac{1-R^2+2iR\sin\theta}{1+R^2+2R\cos\theta}\right], \tag{3}$$

where R is the modulus of the complex reflection coefficient and θ is the phase shift. The impedance of the quartz is Z_s and φ is the angle of inclination of the beam. In the modification employed by Lamb and his co-workers [6], a comparison pulse of the same frequency is displayed on the oscilloscope screen next to the received pulse from the quartz. In the absence of the test liquid, the two pulses are adjusted to the same height by an attenuator. When the liquid is inserted, a second adjustment is made, and the modulus of the reflection coefficient is thereby determined.

To measure the phase shift, a second, identical quartz bar is used as a reference unit. Signals from the two bars (in the absence of liquid) are added electrically, and the amplitudes and phases appropriately adjusted to give zero signal. The insertion of the liquid upsets this balance, which can then be restored by varying the acoustic delay.

Such measurements have been carried out successfully by these authors up to frequencies of 250 MHz. For its accurate use, the method requires the magnitudes of R_L and X_L to be approoximately the same. Since this is never the case for longitudinal waves, where the real part is extremely large in comparison with the imaginary, the method is not applicable for measuring the attenuation of longitudinal waves.

1·3. *Microwave techniques.* – To go to even higher frequencies, it is necessary to make use of microwave techniques. This was first done in quartz by **Baranskii** [7] and generation and detection of ultrasonic waves in a quartz specimen were carried out by **Bömmel** and **Dransfeld** [8].

It has been pointed out by these latter authors that ultrasonic waves will be excited at every surface of discontinuity in a piezoelectric specimen, so that the free surface of a piece of quartz will be the transducer of the hypersonic waves, while the rest of the specimen will serve as the transmission medium. The reverse operation is also true. Therefore, they employed a quartz rod 2.5 cm in length, with optically flat, parallel faces. Each end of the rod (Fig. 3) was placed in a re-entrant microwave cavity, one cavity serving as the transmitter and the other as the receiver. The transmitter cavity was then coupled to a generator giving 2 μs pulses with the frequency available up to 4 kHz. The average power was below 1 mW. Absorption could be measured by the decay of successive echoes.

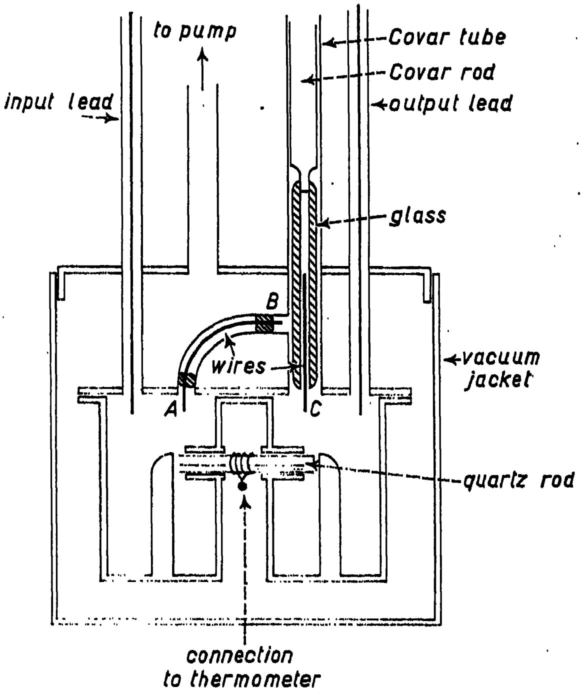

Fig. 3. – Re-entrant microwave cavity for ultra high frequency sound wave production in quartz (**Bömmel** and **Dranfeld** [7]).

Of course, these measurements are in solids, and we are here concerned with liquids. A method somewhat different above has been applied by the **Stewarts** to the liquid case, but few details are yet available [9]. To quote from their letter,

> « We have recently observed the resonance of X-cut quartz crystals 0.1 mm thick at several odd harmonics between 2 950 and 3 600 MHz at room temperature. The crystal, 1.0 cm in diameter, is located in the gap of a re-entrant cylindrical cavity as suggested by SLATER. The reaction of the mechanical resonance of the piezoelectric quartz on the electrical resonance of the cavity has been observed by sweeping the frequency of the microwave oscillator. The photograph [Fig. 4*a*] of an oscilloscope trace ... shows the sharper inverted resonance or „crevasse" of the quartz crystal superimposed on the broader resonance of the cavity tuned to the same frequency. »

In the same experiment, the STEWARTS placed a thin layer of water on the crystal and caused the crevasse to disappear [Fig. 4*b*].

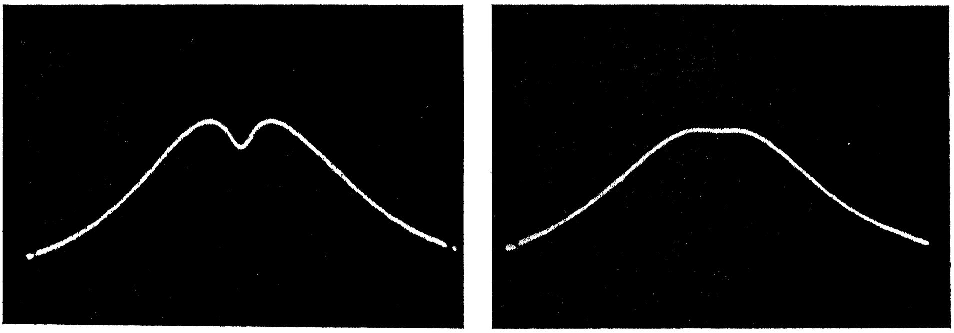

a) *b*)

Fig. 4. – *a*) Resonance curve of quartz crystal in microwave cavity. *b*) Same crystal with thin layer of water on its surface (J. L. STEWART and E. S. STEWART [9]).

LAMB and his associates have followed a somewhat similar path in the case of shear waves in liquids [6]. In this case, the apparatus was similar to that used by them for lower frequency measurements, except that normal incidence at the quartz-liquid interface is used, and one end of the crystal is placed inside an electrical cavity resonator. This method has the advantage that the liquid is applied to the surface of the quartz *outside* the resonator. Lamb's apparatus has operated up to 3 GHz.

2. – Velocity measurements.

2·1. *High accuracy measurements.* – As was mentioned above, the measurement of the velocity of sound by direct observation of pulses on the oscilloscope is rather inaccurate. The error amounts to about one part in 1 000, which means approximately (1.5 ÷ 2) m per s. This value range is of the same order of magnitude as observed dispersions in liquids, so that the technique is of little use in dispersion measurements.

A much more accurate method is that advanced by GREENSPAN and TSCHIEGG [10]. Two quartz crystals are installed with a fixed separation distance. An electrical rectangular pulse is applied to one of the crystals. The repetition rate of these pulses is variable, the period of repetition being chosen to be approximately equal to the time required for the ultrasonic pulse to complete a round trip in the test liquid.

The second crystal records the arrival of the first pulse and reflects it back to the first crystal. At about the time the first pulse has completed the round trip, the second pulse is emitted. The time relations are indicated in Fig. 5. The combined signal of the various reflected pulses is viewed on an oscilloscope, and the repetition frequency is adjusted so that the first or second peak of the combination signal is a clear maximum. This frequency, which is of the order of (5 ÷ 10) kHz, is measured by a counter.

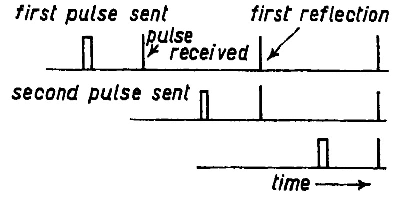

Fig. 5. – Succession of received pulses in velocimeter (after GREENSPAN and TSCHIEGG [10]).

This technique is capable of measurements to within one part in 10 000 and possibly a little better.

The older, interferometric method of measuring sound velocity is also capable of this level of accuracy when care is taken to make all necessary corrections. Since this method is also widely used in gases, it will not be discussed further here.

2·2. *Hypersonic velocity measurements.* – The thermal energy of a liquid can be expressed in terms of standing sound vibrations of frequencies of the order of 10^{10} per second. Light waves passing through such a medium undergo Rayleigh scattering. This is a sort of Bragg diffraction, with the hypersonic wavelength λ, playing the same role as the lattice constant of the crystal in the solid case. The scattering angle is then given by

$$\Lambda = 2\lambda_s \cos\theta\,, \tag{4}$$

where Λ is the optical wavelength, and θ is the angle between the light beam and the sound wave. However, because of the Doppler effect, there will be a frequency splitting in the scattered light, given by

$$\frac{\delta\nu}{\nu} = 2\frac{c_s}{c_l}\cos\theta\,. \tag{5}$$

This effect is sometimes called Brillouin scattering. The method was early used by VENKATESWAREN and the Indian school to obtain hypersonic velocities. More recently, FABELINSKII and his co-workers [11] in Moscow have determined a number of hypersonic velocities that agree well with those predicted from measured relaxation strengths. Unfortunately, the uncertainty in these hypersonic velocity measurements is of the order of one percent. Thus the value obtained by them for water was (1509 ± 25) m/s, as compared with the low frequency value of 1492 m/s. More accurate measurement of the frequency shift is necessary here if the method is to become a satisfactory working instrument.

3. – Measurements at elevated pressures.

In recent years, interest has developed in the measurement of both velocity and absorption in liquids under elevated pressures. A typical set-up for such measurements is shown in Fig. 6 [12]. The system used inside the pressure vessel was either a fixed-path or a variable-path interferometer. In the case of variable path, a pulse is transmitted through the medium and reflected to the receiver. Here, the electrical signal is amplified and mixed with some continuous r.f., and the result is portrayed on an oscilloscope. The resultant amplitude of signal is dependent on the relative phase of the returned signal

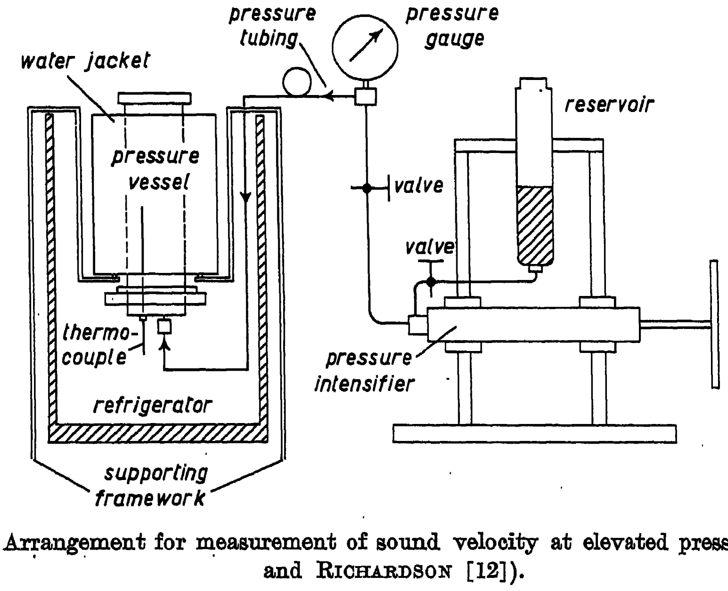

Fig. 6. – Arrangement for measurement of sound velocity at elevated pressures (EDEN and RICHARDSON [12]).

and the continuous r.f. As the reflector is moved outward, the oscilloscope trace passes through a series of maxima and minima. By recording a large number of these, the sound velocity can be measured to one part in 1000 or better. For fixed-path interferometry, the pressure is varied. Under these circumstances, the pulse on the oscilloscope again passes through maxima and minima, since the variation in pressure changes the sound velocity, and hence the effective path length. The relation between the sound velocity at atmospheric pressure v_0 and that at a particular pressure p is given by

$$v_0/v_p = 1 \pm nv_0/2fd\,, \tag{6}$$

where n is the number of maxima counted in the pressure change, d is the separation of crystal and reflector, and f is the frequency. The accuracy is comparable with that of the variable path system and is of course more convenient. For absorption measurements, the variable-path method was the same as that outlined for pulse systems previously. For a fixed path length, the system was equipped with an auxiliary reflector. Two sets of echoes were thereby received, with a known path length difference. As a result, the absorption over this path length difference could be deduced. These measurements were carried out at pressure up to 1000 atmospheres.

Of course, such measurements can also be made with standard pulse systems. In addition, the Greenspan method has been employed by WILSON [13] in measurements in water and ethyl alcohol.

Knowledge of the variation of α and v with sound pressure has been useful in a number of ways. Thus, LITOVITZ has been able to relate the pressure variation of the relaxation frequency with the type of relaxation process [14]. In the case of vibrational relaxation, the relaxation frequency increases with the pressure, while for a structural relaxation such as in glycerol, the relaxation frequency decreases. Finally, in the case of rotational isomerism, there is no pressure-dependence.

In another direction, data on the dependence of the sound velocity on pressure can be used in deducing the adiabatic equation of state of a liquid. Such an equation can be written in the form of a Taylor series

$$p - p_0 = A\left(\frac{\varrho - \varrho_0}{\varrho_0}\right) + \frac{B}{2}\left(\frac{\varrho - \varrho_0}{\varrho_0}\right)^2, \tag{7}$$

where $A = \varrho_0(\partial p/\partial \varrho)_s$ and $B = \varrho_0^2(\partial^2 p/\partial \varrho^2)_s$. By appropriate transformations, B can be recast in the form

$$\frac{B}{A} = 2\varrho_0 c_0 \left(\frac{\partial c}{\partial p}\right)_T + \frac{2c_0 T\beta}{c_p}\left(\frac{\partial c}{\partial T}\right)_p. \tag{8}$$

β = thermal expansion coefficient
c = specific heat (const. p).

Thus a knowledge of c, $\partial c/\partial p$ and $\partial c/\partial t$ can serve to deduce A and B, the ratio of which is of great importance in work in nonlinear acoustics.

4. – Ultrasonic absorption and velocity at high temperatures.

The principal problems associated with the measurement of ultrasonic absorption and velocity at high temperatures are the maintenance of the transducer at a sufficiently low temperature to prevent loss of its piezoelectric properties, and the securing of an adequate contact between the crystal and the melt.

The first of these problems is solved by the use of long fused-quartz rods, which enable the driving and pickup crystals to be kept out of the operating furnace. A typical apparatus is shown in Fig. 7 [15]. The rods used were of 30 and 45 cm length, with the crystals mounted at the outer ends. A small quartz cup was fitted to the lower rod and cemented in place with Saureisen cement. In this particular case, molten nitrate salts were to be measured. The salts were placed in the lower part of the cup. The entire system could be closed and nitrogen introduced in place of air above the salt. The furnace was used to melt the salt, after which the system was opened sufficiently to permit insertion of the upper rod, after which the nitrogen was restored. This enables the system to operate without oxidation problems.

This system was used at temperatures between 200 and 650 °C and yields ab-

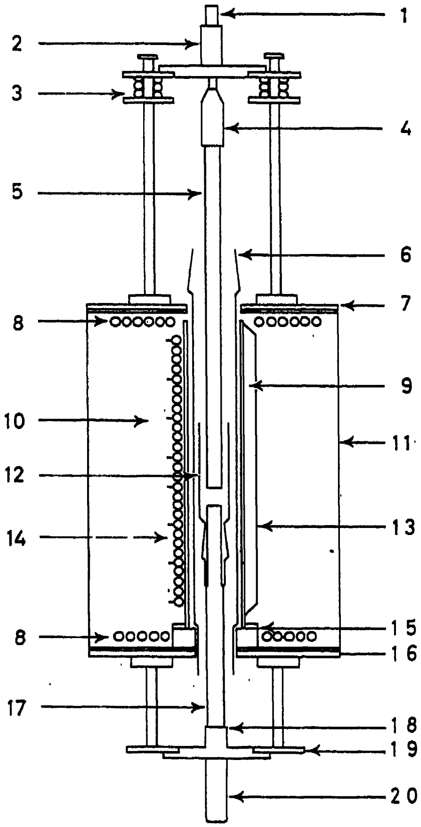

Fig. 7. – Arrangement for measuring ultrasonic absorption in a liquid metal (Higgs and Litovitz [15]): 1) micrometer, 2) drive mechanism, 3) leveling mechanism and upper rod support, 4) upper rod holder, 5) 18 in. upper rod, 6) Vycor furnace tube, 7) brass and asbestos top plates, 8) cooling coils, 9) stainless steel furnace tube, 10) tops, 11) transite furnace case, 12) quartz cup, 13) alumina cement, 14) furnace winding, 15) insulating base, 16) brass and asbestos base plates, 17) 12 in. lower rod, 18) lower rod holder, 19) lower rod support, 20) bakelite handles.

sorption values estimated to be accurate within five per cent and sound velocity to within 0.3 %.

The second problem—that of getting the sound into the liquid—is unfortunately not always discussed in research papers. Perhaps the best account of such troubles is given by KLEPPA [16] whom I quote:

> « The main experimental difficulty was associated with obtaining a reflected signal of sufficient strength and persistence to allow measurements to take place. In preliminary work on mercury it was, for example, found that when the metal was carefully dried and filtered in the usual way, some difficulty was experienced in getting a signal through. This is believed to be due to the fact that mercury does not wet glass and that, therefore, the thin gas film between the rod and the metal prevents the transmission of the pulses. However, a few drops of mineral oil effectively reduced this „surface barrier" and gave the required signal in good strength. It was found that a layer of molten paraffin wax apparently served the same purpose at higher temperatures. All later experiments, except those performed in zinc, were accordingly carried out with the liquid metal contained under a layer of liquid wax or mineral oil.... All measurements involving use of liquid wax were carried out below 400 °C.
>
> After unsuccessful attempts at measurement under a cover of liquid wax of the velocity of sound in liquid zinc (m.P. 420 °C), the measurements were finally carried out with the liquid metal covered by a layer of the eutectic mixture of LiCl and KCl. The salt melt unfortunately attacked the glass to some extent, which in turn led to a gradual deterioration of the signals. »

Recently, the author learned of another technique, used by PLASS at Göttingen for measuring sound absorption in liquid indium. The quartz rod was first covered by a thin evaporated layer of chromium. This was followed by a layer of iron, and finally, by one of indium. This made a very good contact until the indium began to melt away (two or three hours duration). Clearly, such a technique is useful only at temperatures close to the melting point, and in that case even, only for short time intervals.

5. – Conclusions.

All of the methods and techniques that have been discussed in this lecture have served to open up the available range of measurement of the velocity and absorption of ultrasonic waves in liquids. In so doing, they should make new information and new insights available as to the properties of the liquid state.

REFERENCES

[1] H. B. Chick, G. Anderson and R. Truell: *Journ. Acoust. Soc. Am.*, **32**, 186 (1960).

[2] R. Bass: *JASA*, **30**, 602 (1958).

[3] F. Dunn and J. E. Breyer: *JASA*, **34**, 775 (1962).

[4] W. P. Mason, W. O. Baker, H. J. McSkimin and J. H. Heiss: *Phys. Rev.*, **75**, 936 (1949).

[5] W. P. Mason, W. O. Baker, H. J. McSkimin and J. H. Heiss: *Phys. Rev.*, **75**, 936 (1949); H. T. O'Neil: *Phys. Rev.*, **75**, 928 (1949).

[6] A. J. Barlow: *Laboratory Practice*, **10**, 786 (1961).

[7] K. N. Baranskii: *Soviet Phys. Doklady*, **2**, 237 (1958).

[8] H. Bömmel and K. Dransfeld: *Phys. Rev. Lett.*, **1**, 234 (1958); *Phys. Rev.*, **117**, 1245 (1960).

[9] J. L. Stewart and E. S. Stewart: *Journ. Acoust. Soc. Am.*, **33**, 538 (1961); see also E. Stewart: 4-*th ICA* (Copenhagen, August 21-28 (1962).

[10] M. Greenspan and C. E. Tschiegg: *Journ. Res. Nat. Bur. Standards* (*U.S.*), **59**, 249 (1957).

[11] I. L. Fabelinskii: *Usp. Fiz. Nauk.*, **63**, 355 (1957).

[12] H. F. Eden and E. G. Richardson: *Acustica*, **10**, 309 (1960).

[13] W. Wilson: *Journ. Acoust. Soc. Am.*, **31**, 1067 (1959).

[14] T. Litovitz and E. Carnevale: *Journ. Acoust. Soc. Am.*, **30**, 134 (1958).

[15] R. W. Higgs and T. A. Litovitz: *Journ. Acoust. Soc. Am.*, **32**, 1108 (1960).

[16] O. J. Kleppa: *Journ. Chem. Phys.*, **18**, 1331 (1950).

Measurements of Ultrasonic Velocity and Absorption in Liquids under High Sound Intensities.

R. T. Beyer

Brown University - Providence, R. I.

1. – Theoretical analysis.

1·1. *Introduction*. – From its beginning, the science of acoustics has been based on the approximation that the amplitude of the sound waves was extremely small. The theory of acoustic wave propagation is therefore an infinitesimal theory.

The question as to what constitutes a wave of infinitesimal amplitude can best be answered from a consideration of the one-dimensional equation for the particle displacement in a viscous, ideal gas:

$$\left(1+\frac{\partial\xi}{\partial x}\right)^{1+\gamma}\left[\ddot{\xi}-\left(\frac{4}{3}\eta+\eta_B\right)\frac{1}{\varrho}\frac{\partial^3\xi}{\partial x^2\partial t}\right]=c_0^2\frac{\partial^2\xi}{\partial x^2}\,, \tag{1}$$

where η is the shear, and η_B the bulk viscosity, γ is the ratio of specific heats and c_0 is the sound velocity as measured in waves of infinitesimal amplitude. To make this equation linear (so that the periodic solutions are those of a damped plane wave), it is necessary that $(\partial\xi/\partial x)_{\max}\ll 1$. Now $(\partial\xi/\partial x)_{\max}$ can, for a sinusoidal wave, be written also as $p_{ac}/\varrho_0c_0^2$, where p_{ac} is the pressure amplitude in the wave, or also as u_0/c_0, where u_0 is the maximum particle velocity. This latter ratio is known as the acoustic *Mach number*, *M*. Therefore, in order that $(\partial\xi/\partial x)_{\max}\leq 0.01$, it is necessary that $p_{ac}\leq 14200$ dyn/cm², which corresponds to 154 db above the usual acoustic reference level of an rms pressure of 0.0002 dyn/cm². Sounds of this intensity are actually produced by jet engines, but the intensity is far above the level commonly encountered in acoustical research.

To obtain the corresponding reference level for liquids, we must replace the adiabatic relation $p\varrho^{-\gamma}=\text{const}$, used in the derivation of (1), by the adiabatic Taylor's series for the pressure in terms of the density:

$$p = p_0 + A\left(\frac{\varrho - \varrho_0}{\varrho_0}\right) + \frac{B}{2}\left(\frac{\varrho - \varrho_0}{\varrho_0}\right)^2, \tag{2}$$

where p_0 is the hydrostatic pressure and A, B are temperature-dependent coefficients. Under these circumstances, we can replace γ in eq. (1) by the factor $1+B/A$. The ratio B/A is approximately 5 for water. Then, in order that $M \leqslant 0.01$ for water, we get $p_{a0} \leqslant 225$ atm, which corresponds to an intensity of 18 000 W/cm², a level not easily obtainable, even with the best of focussing devices.

At first glance, it would seem therefore that the infinitesimal requirement is not a very stringent one. However, one fact has been neglected, namely, that the products of $\partial\xi/\partial x$ with the terms in the second factor on the left side of eq. (1) accumulate in space, and can ultimately have a considerable effect. This will be made clear in what follows.

1'2. *Nonviscous case.* – The case of the propagation of a finite amplitude wave in a nonviscous medium was partially solved by EARNSHAW [1] and RIEMANN [2] one hundred years ago, but the complete form of the solution is due to Fubini-Ghiron [3]. In implicit form, the solution given by

$$u(x, t) = u_0 \sin\left[ut - \left(1 + \frac{\gamma - 1}{2}\,\frac{u}{c_0}\right)^{(-\gamma+1)/(\gamma-1)}\right], \tag{3}$$

for the case in which $u(0, t) = u_0 \sin \omega t$.

It is evident from eq. (3) that at a certain distance $x = l$ the slope $\partial u/\partial x$ becomes negatively infinite, so thet a discontinuity appears in the wave, and the solution (3) becomes invalid beyond this point. The quantity is known as the discontinuity distance, and is given by the relation

$$l = \frac{2}{(\gamma + 1)Mk}\,. \tag{4}$$

The explicit solution for u (for $M \ll 1$) can be found by expanding $u(x, t)$ in a Fourier series in the variable $\omega t - kx$:

$$u = u_0 \sum_{n=1}^{\infty} B_n \sin n(\omega t - kx)\,, \tag{5}$$

where

$$B_n = \frac{1}{\pi}\int_0^{2\pi} \frac{u}{u_0} \sin n(\omega t - kx)\, \mathrm{d}(\omega t - kx)\,. \tag{6}$$

By substitution of (3) in (6) under the condition $M \ll 1$, we get integrable relations for the B_n. As a final result, we have

$$u = 2u_0 \sum_{n=1}^{\infty} \frac{J_n(nx/l)}{nx/l} \sin n(\omega t - kx) \,, \tag{7}$$

where $J_n(nx/l)$ is the Bessel function of order n.

The gradual distortion of the wave and the growth of the various harmonics can be seen from eq. (7). We are now in a position to judge the cumulative effect mentioned earlier. For a 2.5 kHz sound in air, with $M = 0.01$, $l = 180$ cm. For a sound of the same frequency in water, but with M equal only to 10^{-4} (a more reasonable figure), $l = 3\,300$ m. At the ultrasonic frequency of 2.5 MHz, however, this length would be reduced to 3.3 m.

It is thus evident that a sound wave of low Mach number can nevertheless undergo appreciable distortion during its propagation.

1'3. *Viscous case. Perturbation analysis.*

– When viscosity is present, it must be expected that the higher harmonics in the distorted wave will be attenuated more rapidly, because of the higher absorption coefficient for the higher frequencies. One should therefore expect the discontinuity or shock front to be delayed in its appearance beyond the point $x = l$.

Quantitative consideration is carried out by use of a perturbation technique due to AIRY and first applied to this problem by ECKART in 1948 [4]. In the nonviscous case, ECKART used the Mach number M as the factor separating the terms of different order, and assumed that the hydrodynamic variables could be written in the series

$$\xi = \xi_1 + \xi_2 + \dots \,, \tag{8}$$

where each succeeding term is smaller than its predecessor by the factor M. In the viscous case, one must estimate the relative size of the viscous terms. Usually this is done by regarding the first term involving the viscosity to be of first order in the expansion. This is equivalent to regarding the acoustic *Reynolds' number*, $p_{ac}/\omega\eta b = \mathrm{Re}$, as small compared with unity. Here $b = \frac{4}{3} + \eta_B/\eta$ is introduced for convenience. The assumption of low Reynolds' number is equivalent to the assumption of high viscosity. In actual practice, however, the Reynolds' number in liquids may very well be of the order of unity, which presents certain convergence difficulties.

If we substitute eq. (8) in eq. (1) (under the assumption that $\mathrm{Re} \ll 1$) and equate terms of like order, and make the further approximation that $\alpha/k \ll 1$ so that all terms of a given type that are smaller than their counterparts by this factor can be neglected, the linearized equation can be put into the following operator form:

$$
(9)\qquad \left\{
\begin{aligned}
&\Omega \equiv \frac{1}{c_0^2}\frac{\partial^2}{\partial t^2} - \frac{\eta b}{\varrho_0 c_0^2}\frac{\partial^3}{\partial x^2 \partial t} - \frac{\partial^2}{\partial x^2}\,;\\
&\Omega(\xi_1) = 0\,,\\
&\Omega(\xi_2) = \frac{(\gamma+1)}{2}\frac{\partial}{\partial x}\left(\frac{\partial \xi}{\partial x}\right)^2,\\
&\dots\dots\dots\dots\dots\dots\dots\\
&\Omega(\xi_n) = \left(\frac{\gamma+1}{2}\right)\frac{\partial}{\partial x}\sum_{i=1}^{n-1}\frac{\partial \xi_i}{\partial x}\frac{\partial \xi_{n-i}}{\partial x}\,.
\end{aligned}
\right.
$$

These equations can then be solved successively for both the homogeneous and the inhomogeneous parts, subject to the boundary condition $u(0, t) = u_0 \sin \omega t$. These solutions have been carried out through several orders of approximation for the fundamental frequency and the first few harmonics. All of the expressions are power series in a variable $K(x)$, where

$$
(10)\qquad K = \frac{1-\exp[-2\alpha x]}{4\alpha l}\,.
$$

The cumulative effect can be seen from a consideration of $K(x)$, which must be small compared with unity. If the viscosity is small, so that $\alpha x \ll 1$, then K becomes

$$
K = \left(1 + \frac{B}{2A}\right)\frac{kx}{2}\,M\,,
$$

so that the effective parameter is the product of the Mach number and kx, which ultimately becomes comparable with unity, no matter how small M may be. On the other hand, if αx becomes large, the expansion parameter gradually transforms so that, in the extreme limit as $\alpha x \to \infty$, $K \to (1+B/A)\,\mathrm{Re}/2$, which can well be larger than unity.

The first terms in the various expansions are given below:

$$
(11)\qquad \left\{
\begin{aligned}
&u_1 = u_0 \exp[-\alpha x]\sin(\omega t - kx)\left[1 - \tfrac{1}{2}K^2 + \dots\right],\\
&u_2 = u_0 \exp[-2\alpha x]\sin 2(\omega t - kx)\left[K - \left(\frac{3+\exp[-2\alpha x]}{3}\right)K^3 + \dots\right],\\
&u_3 = u_0 \exp[-3\alpha x]\sin 3(\omega t - kx)\left[\frac{2+\exp[-2\alpha x]}{2}K^2 - \dots\right].
\end{aligned}
\right.
$$

The effective absorption coefficient for a finite-amplitude wave can be computed from (11). It has the form

$$\frac{\alpha_{\text{fin}}}{\alpha} = 1 + 3\exp[-2\alpha x]K^2 - (3 + 3\exp[-2\alpha x] - 8\exp[-4\alpha x] + \\ + 2\exp[-6\alpha x])\exp[-2\alpha x]K^4 + \dots \tag{12}$$

If $\alpha x \ll 1$, eq. (12) becomes

$$\frac{\alpha_{\text{fin}}}{\alpha} = 1 + 3\left(\frac{x}{l}\right)^2 - \dots \tag{13}$$

Since l is inversely proportional to the acoustic pressure, this means that the experimentally measured coefficient increases as a linear function of p_{a0}^2, provided that the acoustic intensity is sufficiently small.

1·4. *Viscous case. Comparatively stable wave.* – For still higher intensities, where the perturbation method clearly fails, another method can be used. This is the one developed by FAY in 1931 [5]. It first is assumed that $1 + (\partial\xi/\partial x)$ can be written in terms of a Fourier series, the coefficients of which are function of x:

$$1 + \frac{\partial\xi}{\partial x} = \text{const} - \sum_{n=0} X_n \sin n\left(\omega t - \frac{\omega x}{c_n} - \varphi_n\right)_n . \tag{14}$$

FAY then introduced the concept of the comparatively stable wave form—the X_n are fed energy from the lower harmonics and dissipate it in viscous absorption. After the wave has traveled a certain distance, then these two effects come to a quasi-balance, and the waveform remains roughly constant for some distance. This justified FAY in writing the X_n as a series of exponentials of $2\alpha x$:

$$X_n = \exp[-(n-2)\alpha x]\sum_{n=1}^{\infty} K_{nm}\exp[-m\alpha x] . \tag{15}$$

If this solution is introduced into eq. (14) and the terms of the corresponding exponential orders are equated, the K_{nm} can be evaluated. The final result is

$$p = \frac{4\varrho_0 c^3 \alpha}{(\gamma + 1)\omega}\sum_{n=1}^{\infty}\frac{\sin n(\omega t - kx)}{\sinh n\alpha(x + x_0)} , \tag{16}$$

where

$$x_0 = \sinh^{-1}\frac{\pi}{(\gamma + 1)\,\text{Re}} .$$

Equation (16) is very nearly that of a damped sawtooth wave. With little error, one can therefore approximate the summation by the expression

$$\sum\frac{\sin n(\omega t - kx)}{\sinh n\alpha(x + x_0)} \approx \frac{1}{\alpha(x - x_0)}\left(\frac{\pi - \omega t + kx}{2}\right); \qquad 0 < \omega t - kx < 2\pi , \tag{17}$$

so that

$$p = \frac{2\varrho_0 c^3}{\omega(\gamma+1)(x+x_0)}\,[\pi - \omega t + kx]\,. \tag{18}$$

This equation has the interesting result that the absorption coefficient has disappeared, and that the attenuation is no longer exponential. If we try to fit an exponential decay to eq. (18), however, we obtain the result that the effective absorption coefficient for the finite-amplitude wave in this case will be given by

$$\alpha = \frac{1}{x+x_0}\,. \tag{19}$$

1'5. *Case of a relaxing medium.* – All of the foregoing analysis has pertained to the case of a nonrelaxing medium, in which the (infinitesimal) absorption coefficient is proportional to the square of the frequency. In the case of propagation through a relaxing medium, the equations must be altered somewhat. In the perturbation treatment, the factor b in eq. (9) will be frequency-dependent. Therefore, wherever a higher harmonic term enters the solution (either via the complementary solution or the particular solution), the value of the absorption coefficient (and therefore of b) appropriate to that frequency must be used. As can be expected, this leads to much more involved solutions than those of eq. (11). Some results are indicated below:

$$\left\{\begin{aligned} u_1 &= u_2 \exp[\alpha_1 x]\sin(\omega t - kx)\,\cdot \\ &\qquad \cdot\left[1 - \frac{4N^2}{\alpha_2 - 2\alpha_1}\left\{\frac{1}{2\alpha_1} - \frac{1}{\alpha_2} - \frac{1}{2\alpha_1}\exp[-2\alpha_1 x] + \frac{1}{\alpha_2}\exp[-\alpha_2 x]\right\}\right] - \dots\,, \\ u_2 &= \frac{2N}{\alpha_2 - 2\alpha_1}\,u_0\bigl(\exp[-2\alpha_1 x] - \exp[-\alpha_2 x]\bigr)\sin 2(\omega t - kx) - \dots\,, \\ &\qquad\qquad N = \left(1 + \frac{B}{2A}\right)\frac{Mk}{4}\,. \end{aligned}\right. \tag{20}$$

The behavior of the relaxation frequency for very high intensities (equivalent to those for which the Fay theory is valid) has been studied by Polyakova [6]. She has been able to show that the absorption coefficient increases with increasing Reynolds' number, while the maximum shifts to lower frequencies, as shown in Fig. 1.

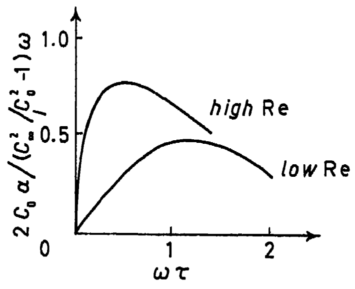

Fig. 1. – Dependence of ultrasonic absorption on frequency in a relaxing medium for different Reynolds number. (After Polyakova [6]).

2. – Experimental results.

The first distortion measurements known to the author were made in gases by Thuras, Jenkins and O'Neil in 1935 [7]. In these experiments, the second harmonic was measured that had been developed in a bent tube 3.8 cm in diameter and 15 m long. The measurements were made in air at frequencies between 300 and 2 000 Hz. The theory used was largely that due to Riemann, and the results indicated that the acoustic pressure of the second harmonic was approximately proportional to the distance traveled by the sound, to the frequency, and to the pressure of the original signal. In all cases, however, the experimental values were considerably different from the theoretical—not a surprising result in view of the corrections and calibrations necessary for audio-frequency measurements in a bent tube.

In the next stage of development, Fox and Wallace [8] measured the total intensity of a 5 MHz sound beam by means of radiation pressure detectors. The measurements were made both in water and in carbon tetrachloride, with the intensity in water reaching 4.00 $\mathrm{W/cm^2}$ ($p_{ac} = 3.5$ atm). At points of the order of several centimeters from the source, the rate at which the intensity fell off was equivalent to an absorption coefficient about five times that due to an infinitesimal wave. It was not possible, however, to observe the initial rise in the total absorption coefficient predicted by eq. (13). The

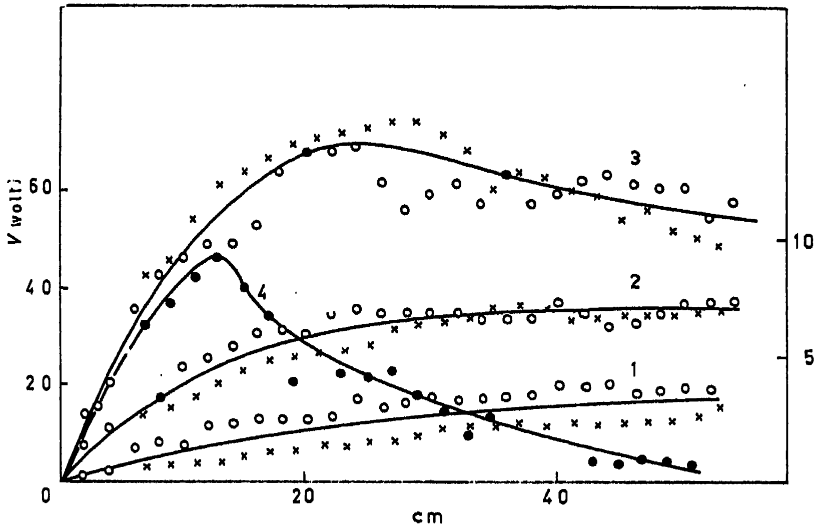

Fig. 2. – Relative amounts of second harmonic in water from a 1.5 MHz source as a function of distance from the source. Initial pressure amplitudes: Curve 1, 1.25 atm; Curve 2, 2.4 atm; Curve 3, 4.9 atm; Curve 4, gives the second harmonic in transformer oil for an initial pressure amplitude of 4.9 atm. (Krasilnikov *et al.* [9]).

results were consistent, however, with a numerical analysis that was equivalent to the perturbation solution.

In 1956, KRASILNIKOV, ZAREMBO and SHKLOVSKAYA-KORDI [9] made a striking improvement by measuring the harmonic content of a beam from a 1.5 MHz source in water. To filter out the unwanted harmonics, they employed glass or metal plates set at some oblique angle with respect to the beam. By suitable choice of plate composition and thickness as well as the setting angle, the authors were able to reduce the undesirable harmonics to very small amounts, and thus achieve a harmonic analysis. Some of the results of these measurements are shown in Fig. 2. The characteristic increase of the second harmonic to a maximum and its subsequent decrease is clearly evident.

The next improvement was that of RYAN, LUTSCH and BEYER [10]. In this case, a short radiofrequency pulse is applied to the source crystal. After its passage through the test liquid, the distorted wave is detected by a quartz transducer whose resonant frequency is well above that of the harmonic being tested, so that a nearly flat response is obtained. Experiments were made with a large receiving crystal in order to intercept as much of the beam as possible. Figure 3 shows the results obtained with a 2.5 MHz source and a 25 MHz receiver. The measurements were made in water with a source with an acoustic

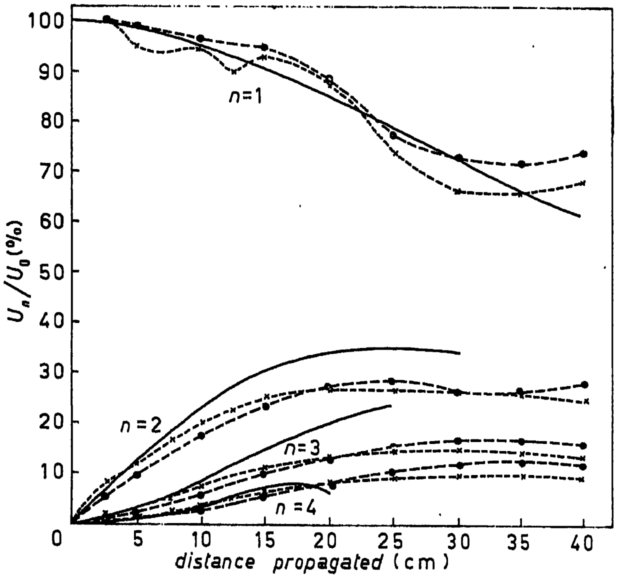

wig. 3. – Relative harmonic content in water from a 2.5 MHz source. The digital analysis Fas a computed Fourier analysis of distorted wave photographs; the analytic measurement was made on the received signal after passage through an electrical filter resonant ment was made on the received signal after passage through an electrical filter resonant at the respective harmonic. (RYAN, BEYER, LUTSCH [10].) ——— theory; ×--×--× digital analysis; ●—●—● analyser measurement.

pressure of 3.0 atm. Experimental and theoretical values are plotted for the fundamental frequency and the second, third and fourth harmonics.

In these measurements, the source and receiver were both calibrated so that the comparison is supposed to be an absolute one. The divergence of the various theoretical solutions is easily noted. It is also worth noting the onset of the comparatively stable waveform at a distance of (15 ÷ 20) cm from the source; from that point on, the relative content of the various harmonics remains roughly constant.

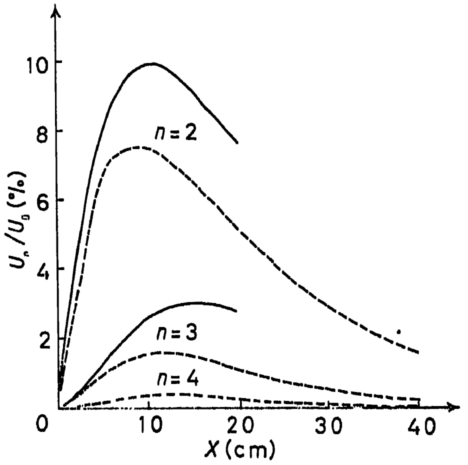

Fig. 4. – Relative harmonic content in 0.2 molal aqueous solution of $MnSO_4$ from a 2.5 MHz source. (RYAN, ATTANASIO and BEYER, unpublished). —— theory; – – – analyser measurement.

Measurements have also been made in an 0.2 molal aqueous solution of $MnSO_4$, which has a relaxation frequency of about 4.0 MHz. The results are shown in Fig. 4. Here again, the agreement between experiment and theory is quite satisfactory.

Quite a different method of studying nonlinear distortions in liquids has been developed by HIEDEMANN and his students, and also by MIKHAILOV and SHUTILOV [11]. It is well known that a plane sound-wave traveling through a medium can act as a diffraction grating to a beam of monochromatic light passing transverse to it. After passage through a sound beam of low intensity, the phase of the resultant optical wavefront becomes sinusoidally modulated (corrugated), as shown in the diagram in Fig. 5*a*. The resulting diffraction pattern will then be symmetric in its positive (forward) and negative (backward) orders.

If the sound intensity were to be increased so that the wave becomes a sawtooth, then the corrugation of the wavefront will also be a sawtooth, and the positive and negative

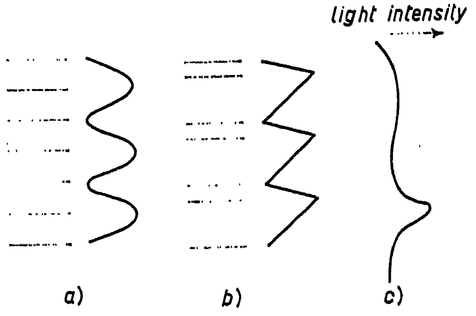

Fig. 5. – (*a*) Crests (– – –) and troughs (——) of a sinusoidal wave propagating upward; (*b*) Same situation for a sawtooth wave; (*c*) Relative diffracted light intensity along the propagation direction. (After SHUTILOV [11].)

orders will be asymmetric [Fig. 5b]. A diffraction maximum exists in both the positive and negative orders, but the negative maximum is the higher [Fig. 5c]. SHUTILOV has been able to relate the diffraction order at which this maximum occurs with the condensation gradient φ of the corresponding part of the sawtooth [Fig. 5c]:

$$\varphi_1 = \frac{\lambda}{\Lambda} m_1; \qquad \varphi_2 = \frac{-\lambda}{\Lambda} m_2, \tag{20}$$

where m_1, m_2 are the orders of the positive and negative intensity maxima.

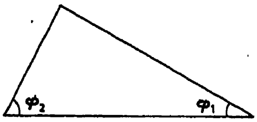

Fig. 6. – Indentification of sawtooth angles in eq. (20).

HIEDEMANN and his students have worked with much lower intensities, and have enlarged upon the infinitesimal amplitude theory of Raman and Nath. In essence, the distorted wave is analysed into Fourier components. The diffraction effect of each of these components is then combined to obtain the total result.

The mathematical analysis is extremely complicated in the general case, but can be reduced to relatively simple calculations when the intensity of the sound wave is sufficiently low that only second and third harmonic distortions need be considered. By making use of the perturbation analysis for the harmonics, the relative intensities for the different diffraction orders can be computed and compared with the values obtained experimentally. The agreement is excellent as is shown in Fig. 7.

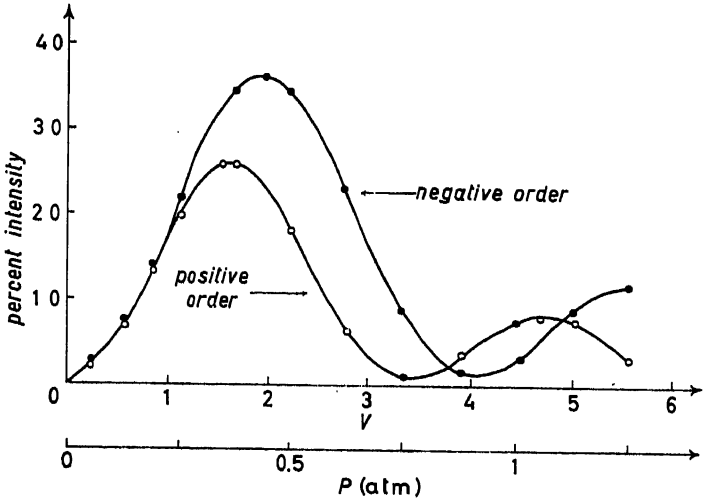

Fig. 7. – Experimental values of the intensity of the first diffraction orders as a function of the original pressure p in atmosphere for water at 2 MHz. (HIEDEMANN ZANKEL [11].)

Recently, a detailed study has been made by BARNES of the absorption coefficient for finite amplitudes [12]. In these measurements, the radiofrequency carrier applied to the source crystal is 100 per cent modulated by an audiofrequency square wave. As a result, the radiation pressure oscillates at this audio frequency. This pressure, which is proportional to the ultrasonic intensity (from all the harmonic components) is detected by means of a con-

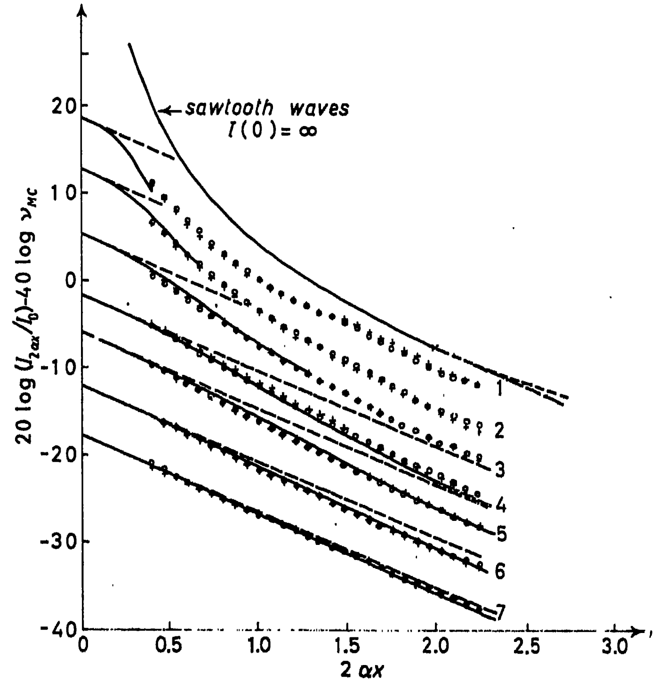

Fig. 8. – Relative intensity of 11.6 MHz beam in water as a function of $2\alpha x$, x = distance from source. In the legend, P_0 is the initial intensity in atmospheres, while $N = (1/4\alpha)l$. l being the discontinuity distance. The curve labeled « sawtooth waves » is the intensity predicted by the Fay analysis in the limiting case of infinite initial intensity. (BARNES [12].) Water at 20 °C, O_{DB} = 1.91 W cm³; – – – slope at infinitesimal amplitudes.

Frequency: 11.6 MC.

Case	N	P_0 (atmospheres)
1	2.91	4.84 estimated
2	2.08	3.45 measured
3	1.36	2.26 measured
4	0.912	1.52 measured
5	0.704	0.17 estimated
6	0.498	0.828 estimated
7	0.357	0.594 estimated

denser microphone. In this way, the ultrasonic intensity could be measured as a function of the distance.

A more accurate comparison of experiment and theory was obtained by using the eqs. (11) to compute the effective sound intensity, and to plot this against the measured intensity. The results of this comparison are shown in Fig. 8. Here the theoretical calculations have been carried in each case to the point were $K=1$. The dashed lines on the drawing indicate the slope to be expected for the case of infinitesimal amplitude. It can be seen that the absorption coefficient (which is the negative of the slope) starts from the value for infinitesimal amplitude increases to a maximum, and thereafter declines, again approaching the infinitesimal-amplitude value. These measurements indicate the close agreement between measured and computed values.

3. – Conclusion.

From the viewpoint of molecular acoustics, the most important contribution of nonlinear work is the statement of the conditions under which the wave can safely be regarded as infinitesimal, so that the measured values of α can be used in the standard theoretical treatments.

REFERENCES

[1] S. Earnshaw: *Proc. Roy. Soc. (London)*, **9**, 590 (1859).
[2] B. Riemann: *Göttingen Abhandlungen* (1860), reprinted in *Collected Works* (New York, 1953), p. 156).
[3] S. Fubini-Ghiron: *Alta Frequenza*, **4**, 530 (1935).
[4] C. Eckart: *Phys. Rev.*, **73**, 68 (1948).
[5] R. D. Fay: *JASA*, **3**, 222 (1931).
[6] L. A. Polyakova: *Soviet Phys. Acoustics*, **5**, 85 (1959).
[7] A. L. Thuras, R. T. Jenkins and H. T. O'Neill: *Journ. Acoust. Soc. Am.*, **6**, 173 (1935).
[8] F. E. Fox and W. A. Wallace: *Journ. Acoust. Soc. Am.*, **26**, 994 (1954).
[9] V. A. Krasilnikov, L. K. Zarembo and V. V. Shklovskaya-Kordi: *Journ. Acoust. Soc. Am.*, **29**, 642 (1957).
[10] R. P. Ryan, A. G. Lutsch and R. T. Beyer: *Journ. Acoust. Soc. Am.*, **34**, 31 (1962).
[11] For a review, see E. A. Hiedemann and K. L. Zankel: *Acustica*, **11**, 213 (1961). See also V. A. Shutilov: *Soviet Phys. Acoustics*, **5**, 230 (1959).
[12] R. P. Barnes, jr.: *Ph. D. Thesis* (Brown University, 1962).

Determination of the Kinetics of Chemical Reactions by Sound Absorption or Dispersion.

L. LIEBERMANN

University of California - San Diego, La Jolla, Cal.

1. – Introduction.

A fluid containing chemically reactive ingredients in equilibrium may exhibit acoustic relaxation analogous to the familiar phenomenon observed in pure liquids and gases. In pure gases relaxation is usually explained by the slowness of energy exchange between the internal rotational or vibrational energies and translational energy of the molecules as a whole; stated more generally, the energy exchange takes place between 2 degrees of freedom. Similarly, the left and right sides of a chemical equation *in equilibrium*, can be considered to represent 2 degrees of freedom with energy divided between each side. The relative slowness of the chemical reaction leads to acoustic relaxation exactly in the manner found in gases (^{1}).

The acoustic relaxation time of a chemical reaction is explicitly related to its fundamental kinetic and thermodynamic constants. Hence, determination of the acoustic relaxation time is the primary experimental objective, although the magnitude of the absorption coefficient can be of some value. There does not appear to exist any practical experimental technique for the determination of the relaxation time other than the usual method of absorption measurements at different frequencies. It might appear that the relaxation time could be determined more simply by observing the frequency-dependence of acoustic level in a closed box containing the chemically active constituents; however, this would require relative calibration of the sound source over a wide range of frequencies, a procedure equivalent to determining the acoustic absorption.

2. – Acoustic relaxation and reaction rates.

The relationship between the chemical reaction rate and the acoustically observed relaxation time can best be described by reference to a specific example: consider the reaction $\mathrm{AB} \rightleftarrows \mathrm{A}+\mathrm{B}$. Let N be the mole fraction of the dissociated molecules (A or B) and $1-N$ the fraction of undissociated molecules (AB). The rate of reaction in the forward direction (dissociation) is given by $k_f(1-N)$ where k_f is the chemical reaction rate constant in the forward direction (*). Similarly, the recombination rate is given by k_b, the backward rate constant. Thus the rate of return for a slight perturbation, ΔN, from equilibrium is given by

$$-d(\Delta N)/dt = k_b(N+\Delta N)^2 - k_f[1-(N+\Delta N)]\,. \tag{1}$$

However, $k_b N^2 - k_f(1-N) = 0$ at equilibrium. Hence, eq. (1) becomes

$$-\mathrm{d}(\Delta N)/\mathrm{d}t = (2k_b N + k_f)\,\Delta N\,. \tag{2}$$

The solution to this first order differential equation will be recognized as simply an exponential decay with relaxation time,

$$\tau = (2k_b N + k_f)^{-1}\,. \tag{3}$$

The quantity τ is clearly identical with the familiar relaxation time obtained in acoustical experiments.

Each type of reaction will yield a different relationship for τ. For example, the first order reaction $A \rightleftarrows B$ gives

$$\tau = (k_f + k_b)^{-1}\,. \tag{4}$$

In general, it can be shown that for any reaction (2),

$$1/\tau = k_f(A^a B^b \ldots)\,\mathrm{d}\ln K/\mathrm{d}N\,. \tag{5}$$

The equilibrium constant K of a chemical reaction is probably the most useful single thermodynamic parameter from which are derived other parameters. It is related to the reaction rate constants by $K = k_f/k_b$ so that both the kinetic and the thermodynamic properties of the chemical reaction become accessible if the reaction rates are known. However, it is noted that neither eq. (3) nor eq. (4) relates the acoustic observable, τ, to the individual reaction rate constants explicitly. In the next section methods for extracting these parameters are discussed.

(*) Activity coefficients are assumed to be unity in the illustrations used here.

3. - Experimental determination of reaction rates.

Method 1: *Temperature variation.* - At stated above, it is not possible to determine k_f and k_b explicitly from a single determination of τ. However, τ varies with temperature and the determination of its temperature-dependence can lead to the evaluation of the two constants. The effect of temperature on τ can be considered as two-fold: the effect on the rate constants k (which follows the Arrhenius law) and the effect on the equilibrium constant, K.

Consider what happens if the logarithm of τ is plotted *vs.* $1/T$ (as in an Arrhenius plot). For example, assume that $\tau = (k_f + k_b)^{-1}$. In this case

$$-\mathrm{d}\ln\tau/\mathrm{d}(1/T) = \mathrm{d}\ln(k_f + k_b)/\mathrm{d}(1/T)\,.$$

If $K \gg 1$ or $k_f \gg k_b$ then

$$\mathrm{d}\ln\tau/\mathrm{d}(1/T) = E_f/R = (E_b + \Delta H)R\,, \tag{6}$$

where E_f is the activation energy in the forward direction. Hence, the logarithm of the relaxation time will be a linear function of $1/T$, as is shown in Fig. 1. Similarly, for the case of $K \ll 1 (k_f \ll k_b)$

$$\mathrm{d}(\ln\tau)/\mathrm{d}(1/T) = E_b/R\,. \tag{7}$$

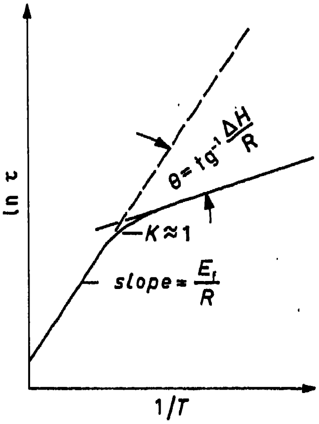

Fig. 1.

Thus, Fig. 1 shows two linear regions differing in slope by $\Delta H/R$. The transition region occurs when $K \approx 1$; stated in another manner, $k_f \approx k_b$. The value of ΔH, determined from the slopes as shown in Fig. 1, is utilized to calculate K from the van't Hoff equation,

$$(\partial(\ln K)/\partial T)_p = \Delta H/RT^2 \tag{8}$$

which when integrated leads to

$$\ln[K(T_1)/K(T_2)] = (\Delta H/R)(1/T_1 - 1/T_2)\,. \tag{9}$$

Having obtained in this manner the magnitude of the equilibrium constant and its variation with temperature, the evaluation of k_f and k_b follows with the aid of eqs. (3) or (4).

Method 2: *Variation of composition.* – This method is useful provided the reaction rate is composition-dependent, *i.e.*, if it is bimolecular or of higher order in at least one direction. For example, the relaxation time for $AB \rightleftarrows A+B$ according to eq. (3) depends on N, which implies composition-dependence. On the other hand the relaxation time for the unimolecular reaction $A \rightleftarrows B$ given by eq. (4) is independent of N (independent of the composition or the concentration).

As a specific illustration, consider the dissociation, $AB \rightleftarrows A+B$ of substances in solution (A and B might represent the ionic products of electrolytic dissociation). Let c be the concentration of the solution and α the degree of (ionic) dissociation. Then the previously defined quantity N (the mole fraction in the dissociated state) is related to c by

$$N = c\alpha \quad \text{with} \quad k_f/k_b = K = c\alpha^2/(1-\alpha)\,.$$

Hence, it follows that

$$(10) \qquad \tau = (2Nk_b + k_f)^{-1} = (k_f^2 + 4k_f k_b c)^{-\frac{1}{2}}\,.$$

Thus, a plot of $(\tau)^{-2}$ *vs.* concentration, c, yields a straight line as is shown inFig. 2 whose intercept is k_f^2 with slope, $4k_f k_b c$. Hence, the rate constants, k_f and k_b are given directly.

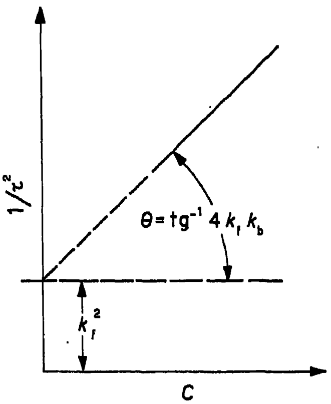

Fig. 2.

Method 3: *Utilization of the acoustic absorption coefficient.* – In case the temperature variation is not sufficiently large to satisfy the requirements of Method 1, the acoustic absorption coefficient can be utilized to determine the rate constants. The magnitude of the absorption is given by the familiar expression [1]

$$(11) \qquad 2\alpha = (C_0'\Delta/C_0^2 + \beta_0'/\beta_0)\,\omega^2\tau\big/(\omega^2\tau^2+1)\,,$$

where C_0' is the partial molal specific heat of the chemical reaction; Δ is $C_p - C_v$, and C_0 is the total specific heat. The compressibilities, β_0' and β_0, are similarly defined for the chemical reaction. Consider again the reaction $AB \rightleftarrows A+B$ whose equilibrium is assumed to be *temperature-dependent*, but not pressure-dependent. Absorption measurements at different frequencies and temperatures will yield τ and $C_0'(T)$ (C_0 and Δ are usually available in tables; the compressibility β_0' may be neglected for a temperature-dependent reaction). The temperature-dependence of the molal specific heat C_0' is given by

$$(12) \qquad C_0'(T) \equiv \Delta H\, \partial N/\partial T\,,$$

where ΔH is a constant. The equilibrium constant K is related to N for this reaction according to

$$K = N^2/(1-N)\,.$$

The van't Hoff equation provides another independent relationship between K and ΔH:

$$\partial \ln K/\partial T = \Delta H/RT^2\,.$$

Hence, if C_0' is determined at two different temperatures (by measuring the absorption at two different temperatures), these three equations can be solved simultaneously to yield K (and also ΔH); when combined with τ the rate constants can be evaluated.

This method has been employed to evaluate the thermodynamic properties of the monomer-dimer equilibrium reaction in acetic acid (^{3}). Absorption measurements at the two temperatures, 20 °C and 50 °C, provided sufficient data to yield the equilibrium constant K in the manner described above.

In the case of a *pressure*-dependent rather than temperature-dependent chemical reaction, an analogous procedure would be followed: The acoustic absorption coefficient will yield β_0' rather than C_0'. The partial molal compressibility, β_0', is defined as

$$\beta_0' = -\,\partial V/V\,\partial P\,. \tag{13}$$

In addition, one has the van't Hoff isothermal analogue

$$(\partial \ln K/\partial P)_T = -\,\Delta V/RT \tag{14}$$

with $\mathrm{d}V/\mathrm{d}N = \Delta V$ and $K = f(N)$. Consequently, these equations can be solved simultaneously to obtain the equilibrium constant, K. The required acoustic absorption data will be measurements at two different pressures, as well as the determination of the relaxation time, τ.

REFERENCES

[1] L. N. Liebermann: *Phys. Rev.*, **76**, 1520 (1949).
[2] M. Manes: *Journ. Chem. Phys.*, **21**, 1791 (1953).
[3] E. Freedman: *Journ. Chem. Phys.*, **21**, 1784 (1953).

The Dielectric Properties of Quartz Crystals and Fused Silica in Relation to their Imperfections (*).

J. M. STEVELS

Philips Research Laboratories - Eindhoven

1. – Introduction.

This lecture differs in three respects from the other ones in this Course:

1) It deals with *dielectric* relaxation instead of *acoustic* relaxation. In has been a very good idea to include a few lectures on the first subject in a course which is mainly dedicated to acoustic relaxations. On the one hand the problems are very much related and as was pointed out already, formulae of the same kind can be used. On the other hand there are differences: Dielectric relaxation can be studied over a much larger frequency range than can be done with acoustical (mechanical) relaxation. With present-day apparatus one can study a frequency range of 10^{-2} to 10^{11} Hz. A disavantage is of course, that the moving particles (molecules) must have an electric charge or an electric dipole moment, which respond to the A.C. electric field applied. An advantage of the measurement of the dielectric relaxation is that it can be carried out with very high precision as the figures will show.

2) This paper deals with solid systems, contrary to the lectures given so far which deal with fluids (*i.e.* gases or liquids).

3) The third difference is that this paper will treat a very practical problem, *i.e.* how we can interprete dielectric relaxation measurements of a crystal in terms of certain well-defined imperfections.

As a crystal I have chosen the quartz crystal for a number of reasons: In the first place because we have studied it in an extensive way in our laboratory.

In the second place because quartz crystal and also SiO_2 in its vitreous

---

(*) The contents of this lecture are treated in a more extensive way in a paper by J. M. STEVELS and J. VOLGER: *Philips Research Reports*, **17**, 283 (1962).

form, fused silica, is applied in so many devices to measure the acoustic relaxation. People working with these devices do not always realize that a given quartz crystal is practically always different from another quartz crystal; for fused silica, a frequently used material in acoustic research, this situation is even worse.

In the third place the knowledge of the behaviour of SiO_2 is very important to understand the behaviour of silicate glasses.

It is known that both quartz crystals and fused silica contain imperfections. The usual imperfections are aluminium ions which replace silicon ions (of the order of $(10 \div 1000)$ ppm). The balance of the charge is given by the presence of H^+, Li^+, Na^+ or K^+ ions in the neighbourhood of these Al^{3+} ions. They may be studied by measuring the dielectric relaxation phenomena (dielectric losses). There are practically no other physical means which may detect them unless perhaps the acoustic relaxation.

After treatment with ionizing radiation, these imperfections, (called the progenitors) give rise to new centres, which will be called the colour centres.

The latter may be studied with the help of different tools, for instance the optical absorption, the electron spin paramagnetic resonance, the nuclear magnetic resonance, and also with the aid of dielectric loss measurements, as will be shown in this paper.

Generally speaking there are different types of dielectric losses, viz.

1) *Migration losses*. – These have a relaxational character, and are due to the migration of the ions over a certain distance under influence of the A.C. field. They can be easily measured at room temperature and have a relaxation time, which is determined by a fairly large activation energy (of the order of $(0.5 \div 1)$ eV). They occur in all types of crystals and glasses, but will not be discussed in this paper.

2) *Deformation losses*. – Built-in chemical impurities may carry an electric dipole moment giving rise to dielectric losses in an A.C. field. These are governed by a relaxation time which in turn is determined by a small activation energy (of the order of 0.1 eV); they have been named deformation losses. They were found first in silicate glasses [1] and afterwards in crystalline quartz and fused silica.

The dipole orientation is probably a local process in which there are only relatively small displacements of the ions.

They can be measured at rather low temperatures with the aid of a medium frequency A.C. field.

3) *Colour-centre dipole losses*. – Their character has been discussed tentatively [2] as being due to electrons or holes trapped at various positions, be-

tween which electrically active transitions can occur. They are only present in quartz crystals and not in fused silica or glasses. They have a relaxational character, their relaxation time being determined by a very small activation energy (of the order of 0.01 eV).

Besides the reason mentioned already quartz crystals seem to be a particularly suitable substance for the study of dielectric relaxation for the following reasons:

1) Both natural and synthetic crystals are available containing a great variety of contaminations in various concentrations, giving rise to a wealth of phenomena.

2) Although the crystal is rigid, the interstices and channels in the structure permit the entrance (for instance by electrolysis) and exchange of interstitial foreign ions.

3) Colour centres are readily obtainable and fairly stable at room temperature.

2. – The measurements and the scheme of their interpretation.

The losses are measured with the help of the bridge described elsewhere [3]. Specimens have a thickness of about 1 mm and a surface area of about 1 cm^2.

Electrodes are obtained by applying colloidal silver paint. The temperature range explored is mostly 14 °K up to 150 °K.

The results are mostly presented in the form of $\operatorname{tg}\delta$ *vs.* T curves, measured at a frequency of 32 kHz. They proved to be of such a nature that the discussion could be based on the well-known relaxation formula

$$\operatorname{tg}\delta = \frac{\Delta\varepsilon}{\varepsilon}\,\frac{\omega\tau}{1+\omega^2\tau^2} = \frac{\varepsilon''}{\varepsilon'}\,, \tag{1}$$

in which

$$\tau = \tau_0 \exp\left[\frac{Q}{kT}\right]. \tag{2}$$

Moreover,

$$\Delta\varepsilon = \frac{4\pi f N p^2}{3kT}\,, \tag{3}$$

if N, the concentration of permanent dipoles with momentum p, is small. f depends on the *internal field correction*, and is $((\varepsilon+2)/3)^2$ assuming that the Lorentz field approximation holds. Since $\Delta\varepsilon/\varepsilon \ll 1$ f is independent of temperature.

In a number of cases measurements at frequencies other than 32 kHz were carried out (for instance to provide the data for Fig. 11).

From the formulae (1), (2), (3) it is seen that N, p, τ_0 and Q are the important quantities to be deduced from the experiments.

τ_0 and Q can be obtained from loss measurements as a function of both frequency and temperature. Strictly speaking, a number of tg δ *vs.* ω curves should be measured at various temperatures, but for practical reasons we usually confine ourselves to the less elegant method of taking the tg δ *vs.* T curves mentioned.

We now define T_m as the temperature where the tg δ *vs.* T curve shows its maximum.

Since tg δ is proportional to $f(T)$, and

$$(4)\qquad f(T)=\frac{1}{T}\,\frac{\omega_0\tau\exp\left[Q/kT\right]}{1+\omega^2\tau_0^2\exp\left[2Q/kT\right]}\,,$$

and since under the experimental conditions chosen $\omega\tau_0<1$, τ_0 and Q can easily be obtained from T_m and its shift when the frequency is set at a different value [1].

From eq. (4) it follows that

$$(5)\qquad kT_m=-\frac{Q}{\ln\omega\tau_0}\left(1-\frac{1}{(\ln\omega\tau_0)^2}+\dots\right).$$

We can also make use of T_{mc}, the temperature where the T. tg δ *vs.* T curve shows its maximum. At T_{mc} the slope of the tg δ *vs.* T curve is $-\mathrm{tg}\delta/T$ (Fig. 1) and

$$(6)\qquad kT_{mc}=-\frac{Q}{\ln\omega\tau_0}\,.$$

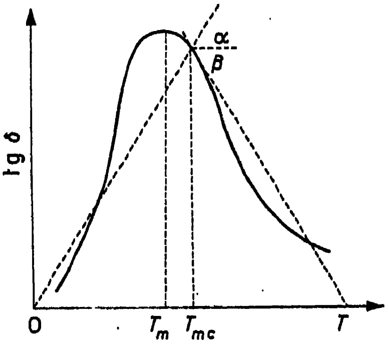

Fig. 1. – Overall picture of the positions of T_m and T_{mc} in a tg δ *vs.* T curve taken at fixed frequency ($\sphericalangle\alpha=\sphericalangle\beta$).

When $\omega\tau_0\ll 1$, $T_{mc}\simeq T_m$. This case is experimentally found when studying the deformation losses (Sections **5-10** incl.).

When $\omega\tau_0$ approaches 1 (for instance if $\omega\tau_0$ is of the order of 0.01) a noticeable difference exists between T_{mc} and T_m. This will be found when the colour centres are discussed (Sections **11-12** incl.).

From the heights of the peaks of tg δ *vs.* T curves we can obtain Np^2. This means that p can be derived, provided that the concentration N of the centres is known, *e.g.* from chemical or spectrographical analysis, and on the other hand N may be deduced, once the value of p has been verified.

3. – Relation between deformation losses and colour-centre dipole losses.

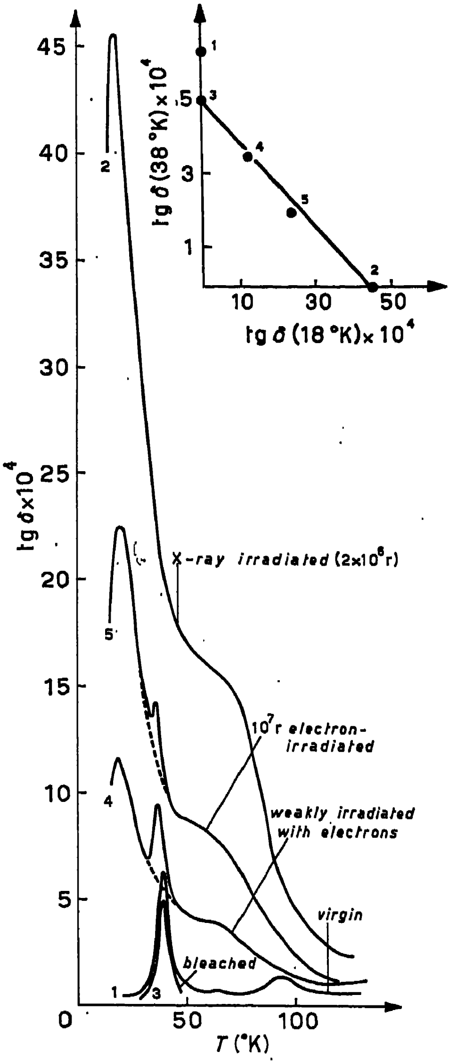

Fig 2. – Tg δ *vs.* *T* curves for a synthetic quartz crystal, C4, measured at 32 kHz. The insert shows the relation between the peak heights, at 18° and 38 °K respectively, which are supposed to be proportional to the concentratoins of colour centres and progenitors.

In Fig. 2 we present tg δ *vs.* *T* curves for a synthetic quartz crystal, in fact the same as specimen, C4, studied earlier [1] (*). Curve 1 holds for the virgin crystal, curves 4, 5 and 2 hold for the same crystal, but with increasing colouration, curve 4 viz. by weak irradiation with electrons, curve 5 by electron irradiation in a dose of 10^7 r, curve 2 by X-ray irradiation ($2\cdot10^6$ r), curve 3 after bleaching. The numbers give the chronological order of the experiments. The virgin crystal (Curve 1) shows three peaks, viz. at 38°, 60° and 95 °K.

Apparently the 38° peak of the bleached crystal is somewhat smaller than that of the virgin crystal. The peaks all disappear gradually upon irradiation, but at the same time a new peak, due to colour centres, appears at 18 °K.

As is known from earlier work [1] a broad hump also appears at about 70 °K; these will be analysed in sections **11** et seq.

The insert in Fig. 2 shows the relation between the height of the peak at 38 °K (deformation loss) and the height of the peak at 18 °K (colour-centre dipole loss). It is seen that the relation is practically linear, as long as we compare curves 2, 3, 4 and 5, thus showing that the colour centres are formed at the cost of those original defects (progenitors) which cause the deformation losses.

(*) This crystal was provided by Bell Telephone Laboratories, Murray Hill, N. J.

It seems, however, that a (small) part of the progenitors (difference between the curves 1 and 3) does not act in such a way that the original defect is found again after a subsequent irradiation and bleaching.

A similar case is given in Fig. 3, representing the behaviour of a synthetic quartz crystal, C9 (*), the difference compared with C4 being that here relatively large amounts of Al^{3+} and Na^{+} ions were deliberately built in (a quantitative analysis of the effect of the amount of chemical defects will be postponed to Section 7).

Curve 1 is the curve for the virgin crystal, curve 2 is the one after X-ray irradiation ($6\cdot10^{6}$ r), curve 3 after bleaching, curve 4 after a second X-ray irradiation ($4.5\cdot10^{6}$ r). The numbers are given in the chronological order of the experiments.

The curves for C9 differ from those for C4 with respect to the following features:

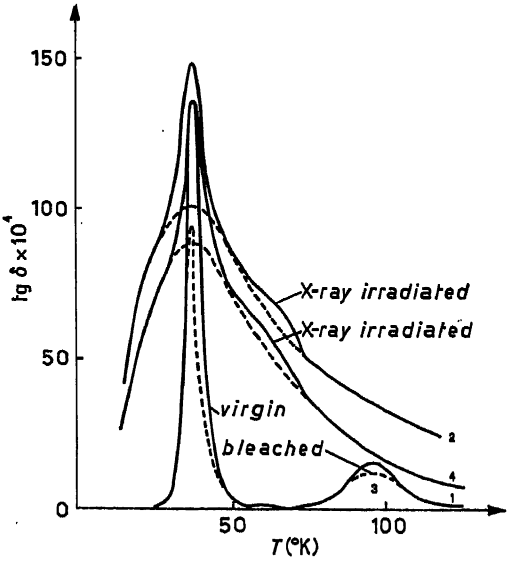

Fig. 3. – Tg δ *vs.* T curves for a synthetic quartz crystal, C9, measured at 32 kHz.

1) The peak for the colour-centre dipole losses of C9 has a different character (relatively broader).

2) Its maximum is found at a different temperature (between 35 and 40 °K).

This accounts for the peculiar form of the curves 2 and 4, since here the peak of the colour-centre dipole losses coincides — quite incidentally, as will be shown later — with the peak caused by the non-affected progenitors. Again it can be concluded that colour centres are formed at the cost of progenitors, although it seems that in this case the conversion factor is smaller.

4. – The effect of irradiation by neutrons.

Though the majority of our experiments relating to the effect of irradiation on crystals were performed with the aid of electrons or X-rays, a few were carried out with neutron fluxes.

(*) This crystal was provided by G.E.C. Research Laboratories, now Hirst Research Centre, Wembley.

The crystals were exposed to a neutron flux in a reactor with the normal energy distribution (that is to say, part of the neutrons having energies lower than 1 eV (slow neutrons), the other part having higher energies up to about 1 MeV (fast neutrons).

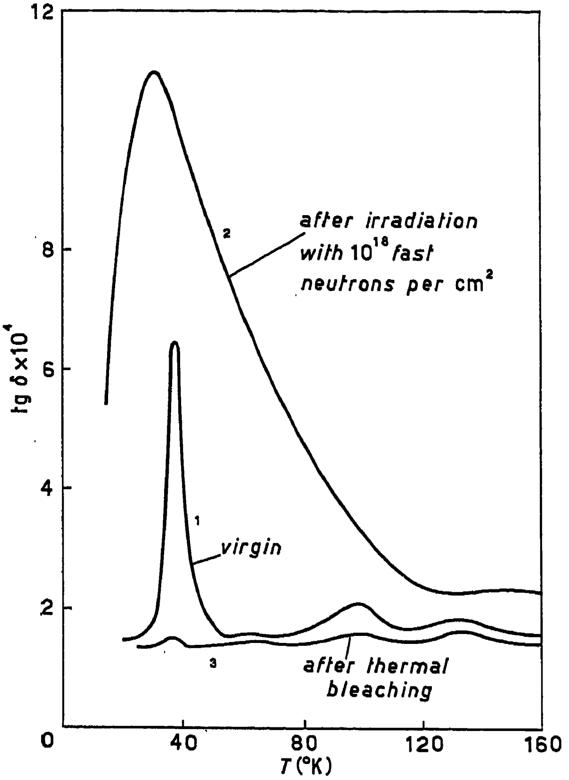

Fig. 4. – Effect of neutron irradiation on the tg δ *vs.* T curves of a synthetic quartz crystal, C6. Measuring frequency 32 kHz.

Whereas the primary effect of X-ray or electron beams is ionization, (the colour-centre formation being a secondary process involving electric-field induced ion transport), fast neutrons primarily cause direct knock-off processes by impact, in which case the above mentioned ionization process also occurs.

In the latter case radiation damage (thermal spikes, local vitrification) of a rather serious character is found. A typical result is shown in Fig. 4 [4].

Curve 1 shows the deformation losses of a clear synthetic crystal, C6. Curve 2 gives the loss after irradiation by a flux of 10^{18} fast neutrons per cm^2 (*). The typical form of a colour-centre dipole loss curve is obtained ($T_m = 32$ °K, $T_{mo} = 45$ °K). Curve 3 is obtained after subsequent thermal bleaching at 300 °K for 5 hours. Now, the original curve is not restored, so the conclusion is that those progenitors that give rise to deformation losses are not regenerated. It seems plausible that the locally vitrified regions act as a sink for certain mobilized ions, although a very small amount of the progenitors are seen to come back since low maxima of a few times 10^{-5} are visible in curve 3.

(*) The irradiation by neutrons has been performed by the courtesy of the Reactor Centre Mol, Belgium.

5. – Anisotropy of deformation losses.

Table I gives some results on synthetic crystals (*) from which samples had been sawn in different directions.

TABLE I.

Crystal	θ (between z-axis and electric field)	$\cos^2\theta$	Peak height at 38 °K	Peak height at 95 °K	Field
C11	0	1	$28 \cdot 10^{-4}$	$2.0 \cdot 10^{-4}$	$\parallel$ z-axis
	52° (rhomb. face)	0.38	$9.5 \cdot 10^{-4}$	$0.6 \cdot 10^{-4}$	
	90°	0	$1 \cdot 10^{-4}$	0	$\perp$ z-axis
C12	0	1	$20 \cdot 10^{-4}$	$1.5 \cdot 10^{-4}$	$\parallel$ z-axis
	52° (rhomb. face)	0.38	$13.7 \cdot 10^{-4}$	$1.2 \cdot 10^{-4}$	
C17	0	1	$6 \cdot 10^{-4}$	—	$\parallel$ z-axis
	90°	0	$0.2 \cdot 10^{-4}$	—	$\perp$ z-axis

The angle θ between the z-axis and the measuring electric field has been listed. The height of the peak at 38 °K and 95 °K in the $\operatorname{tg}\delta$ *vs.* T curves, measured at 32 kHz, is seen to be highly dependent on the orientation, in fact the heights of the peaks are approximately proportional to $\cos^2\theta$. The structure of the quartz crystal has channels in the z-direction and in the directions of the a-axis, the first of which may, obviously also in the case of the deformation losses under consideration, act as a guide to ionic movements.

6. – The relation between the peak at 38 °K and 95 °K in the tg δ *vs.* T curves.

From Table I in the preceding Section it is seen that the peak heights at 38 °K and 95 °K, measured for C11 and C12, have an almost constant ratio. In so far as they showed these peaks, and within the limit of the measuring accuracy, this feature was observed with *all* crystals investigated.

In Fig. 5 plot is made of all relevant data.

The straight line represents a ratio of 10 between the peak heights. It is seen that the proportionality mentioned holds fairly well over a wide range of loss angles, in fact almost three decades.

(*) Provided by Bell Telephone Laboratories, Murray Hill, N. J.

The provisional conclusion of this finding can be that both relaxation effects seem to be very closely related: either there are two imperfections involved, occuring in a fixed concentration ratio, or there is one imperfection that manifests itself in two relaxation effects. We shall return to this question in Section 10.

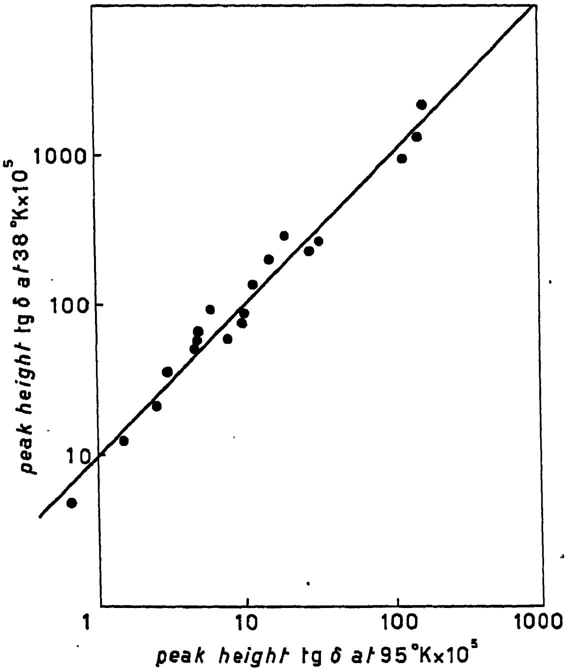

Fig. 5. – Peak height at 38 °K *vs.* peak height at 95 °K, taken from tg δ *vs.* T curves for a number of clear quartz crystals, measured at 32 kHz and plotted on logarithmic scales.

7. – Discussion of measurements on a series of crystals grown from source material with increasing amount of aluminium added.

In Fig. 6 a series of tg δ *vs.* T curves is displayed, measured on synthetic crystals (C7-C10) which were synthesized in a comparable manner by using the hydrothermal method with NaOH as a solvent (*).

(*) These crystals were provided by G.E.C. Research Laboratories, now Hirst Research Centre, Wembley.

The most striking feature is the occurence again of the pairs of peaks at 38 °K and 95 °K. It is the aim of this Section to compare our results with what is known about the preparation of the sample. Upon request of the present author, the crystals were grown after adding known amounts of aluminium to the melting quality quartz source material, which is normally used in the hydrothermal process.

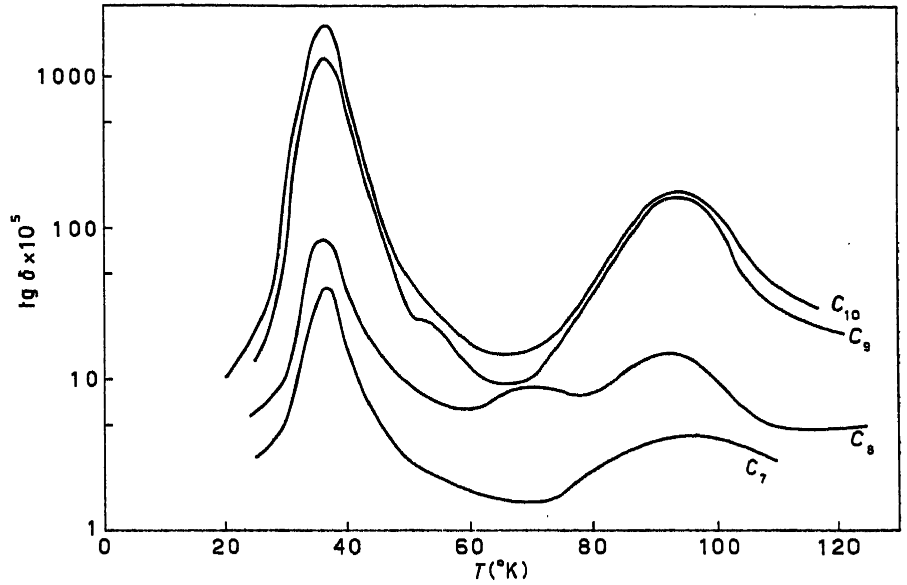

Fig. 6. – Tg δ *vs.* T curves for a number of synthetic quartz crystals, C7 to C10, measured at 32 kHz.

With amounts of aluminium added larger than 50 parts in 10^4 by weight (relative to source material) the crystalline quality of the synthetic deposit rapidly deteriorates so that specimens cannot be cut, and with 250 parts in 10^4 no growth is obtained (*).

In Table II the peak heights of the various crystals as given in Fig. 6 are listed together with the known amount of aluminium added to the source material.

The table also includes the ratios of the peak heights at 38 and 95 °K (which are also included in Fig. 5).

The tg δ peaks are found to increase monotonously with the amount of Al added to the source material.

In discussing these data a quantitive chemical analysis of the impurities

---

(*) Private communication of Dr. L. A. THOMAS.

actually built into the specimens would be very useful. Such an analysis, however, is very difficult, since very small quantities are involved and the detection of small quantities of sodium is complicated by a possible involuntary contamination during the process of analysis.

TABLE II.

	Known amount of Al added to source material (parts in 10^4 by weight	Peak height at 38 °K (32 kHz) $(\cdot 10^4)$	Peak heights at 95 °K (32 kHz) $(\cdot 10^4)$	Ratio of peaks	Concentration of Al in the mother crystal (*) (ppm)	Concentration of Na in the mother crystal (**) (ppm)	Concentration of Na in actual specimen (***) (ppm)
C7	5	3.8	0.3	13	67	45	—
C8	12.5	8.0	1.0	8	445	172	18
C9	25	135	15	9	670	365	272
C10	50	220	17	13	1100	390	—

(*) The values were obtained by spectrochemical analysis in the G.E.C. Research Laboratories, Wembley. Not the actual specimen investigated by us, but another piece of the mother crystal was analysed.

(**) Determined by flame photometrical methods in the G.E.C. Research Laboratories, Wembley. Same remark as under (*).

(***) Determined by flame photometrical methods by H. OORTWIJN and J. VISSER in this laboratory. The analysis was carried out on the some specimen as investigated by us.

In the table two sets of concentration values are given, one originating from the makers of the crystals (the analysis not being made of the measured specimens, but of the mother crystals) and one originating from this laboratory (made of the measured specimens themselves).

In view of possible inhomogeneities and contaminations during the analysis (these being so important according to Mr. H. OORTWIJN and Mr. J. VISSER that they had to take elaborate precautions) we are inclined to believe that the values of the last column are particularly useful for quantitatives comparison; it is striking that the increase by about a factor 15 for the peak heights both at 38° and 95° when passing from C8 to C9 is found again by the same increase in the sodium concentration found in this laboratory. On the other hand, it should be borne in mind, that sodium might be taken up in the crystal in such a form as to cause no contribution to the dielectric loss peak under discussion.

8. – Discussion of experiments with crystal subjected to ion exchange.

It is generally accepted that the aluminium ions in quartz crystals take silicon sites. The lack of positive charge can be compensated for by the presence of interstitial alkali or hydrogen ions, which are available in the solution. In earlier publications it was suggested that the peak at 38 °K is connected with the presence of hydrogen, since in a series of crystals it had appeared, fortuitously as we now know, that the infrared absorption band at 2.7 μ which doubtless is due to OH vibrations, and the height of the 38 °K peak varied monotonously under various conditions. However, apart from the evidence given in Section 7, that both the 38 and 95 °K peaks are related to the presence of sodium, we present here a few experiments likewise giving some evidence in favour of the sodium hypothesis. In the first type of experiment the role of hydrogen is taken over by deuterium. Measurements were first done on C24, a crystal grown in the usual way (*), except that the water of the

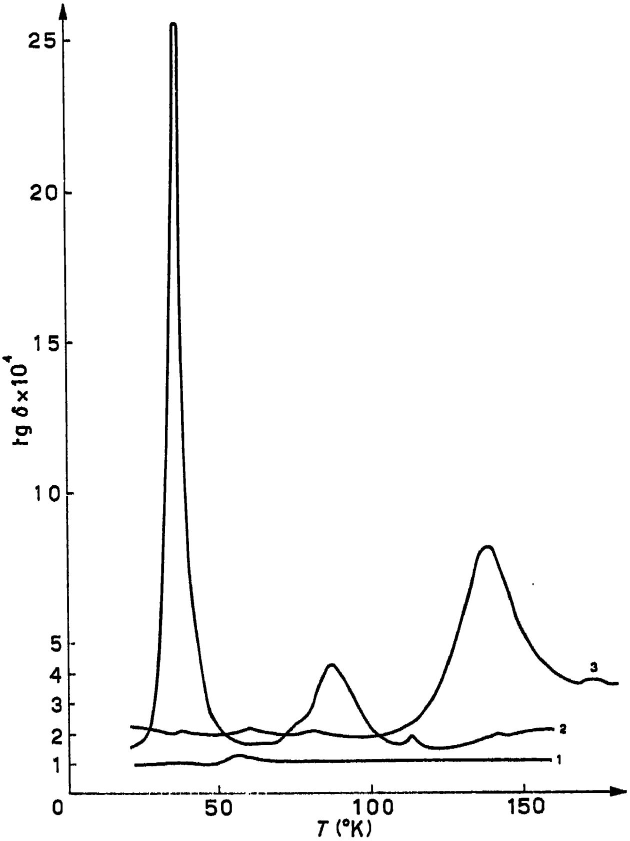

Fig. 7. – Sweep experiments with a natural quartz crystal, C29; tg δ *vs.* T curves at 32 kHz: 1) virgin crystal; 2) after introducing Na^+ ions; 3) after introducing K^+ ions.

(*) In Bell Telephone Laboratories, Murray Hill, N. J.

solvent was replaced by D_2O (the rates of H to D in the solvent being 1/200). The tg *vs.* *T* curve showed no deviation from its normal shape.

In particular, the normal 38 °K peak was found again.

In an other experiment, a crystal, C10, was heated for 2 days at 1000 °C under a pressure of 25 atm of D_2O vapour. It is known that under these circumstances [5], hydrogen will be exchanged for deuterium although such treatment may also affect mobile alkali ions. The tg δ *vs.* *T* curves of the treated specimen shows lower peaks but their positions are unaltered, and it seems also that no new peaks have been formed.

A second type of experiment was performed by means of electrolysis. In a crystal at least part of the alkali ions and protons were interchanged by a sweep experiment, *i.e.* the crystal cut perpendicular to the z-axis, was placed between electrodes, the anode being an alkali halide, so as to produce a stream of specific alkali ions into the crystal, and causing in particular the most mobile cations to disappear out of the crystal at the cathode. Fields of 10 to 1000 V/cm and a temperature of about 500 °C were applied (*).

In Fig. 7 curve 1 shows the tg δ *vs.* *T* curve for a natural Brazilian quartz crystal, C29. This crystal had been irradiated, after which it showed the normal colour-centre dipole losses, and bleached again.

A sweep experiment as described above was now carried out, exchanging Li^+ for Na^+ ions, and the tg δ *vs.* *T* curve taken. Curve 2 shows the results, suggesting that the two well-known peaks appearing at 38 and 95 °K are due to Na^+ ions.

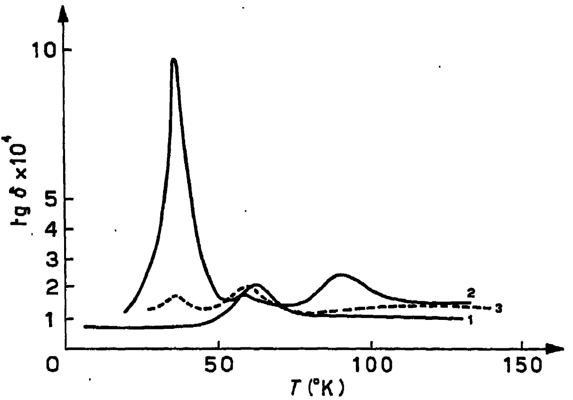

Fig. 8. – Sweep experiments with a natural quartz crystal, C25; tg δ *vs.* *T* curves at 32 kHz: 1) virgin crystal; 2) after introducing Na^+ ions; 3) after introducing Li^+ ions.

As a check Na^+ ions were replaced by Li^+ ions and a curve (not shown in Fig. 7) was found in which very small remnants of the peaks at 38 and 95 °K are seen and an indication is found for a small peak at 60 °K.

In a subsequent sweep experiment, K^+ ions were introduced and the tg δ *vs.* *T* curve taken, Curve 3 shows the result: remnants of the peaks at 38, 60 and 95 °C can still be seen, and

---

(*) Drs. Haven and Kats carried out these sweep experiments.

a new large peak has come into existence at about 140 °K. It is reasonable to ascribe this latter peak to K^+ ions.

In Fig. 8 the results of another sweep experiment are shown, starting from a crystal, C25, containing about $3 \cdot 10^8$ Li^+ ions per cm^3, which is a relatively high concentration.

Curve 1 shows the original tg δ *vs.* T curve with a marked peak at 60 °K only. After having introduced Na^+ ions by a sweep experiment, two peaks appear at 38 and 95 °K but the peak at 60 °K is considerably lowered (curve 2). After a new treatment in which Li^+ ions are introduced, obviously at the cost of Na^+ ions, the peak at 60 °K is markedly enlarged and only remnants of the peak at 38 °K, due to non-exchanged Na^+ ions are found (curve 3).

9. – Identification of the peaks in the loss curves at 32 kHz.

As discussed in foregoing sections, the quartz crystal may contain aluminium ions together with alkali ions or protons. As it is the aim of this section, to identify the various peaks in the loss curves, we shall restate some earlier conclusions and summarize the experimental facts.

We shall discuss the influence of the various alkali ions separately.

Lithium ions. – It is believed that the 60 °K peak is due to the presence of lithium ions. There are two reasons for this statement.

1) The sweep experiment mentioned in Section **8**, and illustrated by Fig. 8.

2) The fact that, although a small peak at 60 °K pratically always occurs in both natural and synthetic quartz crystals, a high peak is found in these cases (C25, for instance) where the chemically determined lithium concentrations are much larger than usual.

Sodium ions. – It is believed that both the 38 and 95 °K are due to the presence of sodium ions:

1) There is a striking proportionality between the peak heights at 38 and 95 °K (cf. Section **6**).

2) There is a proportionality between the peak heights and the sodium concentrations (cf. Table II in Section **7**).

3) Swept-in sodium gives rise to the two peaks mentioned in a correct peak-height ratio, whereas subsequent sweeping out makes these almost disappear.

Potassium ions. – It is believed that the peak at about 140 °K is due to potassium ions:

1) Apart from in amethyst, potassium has never been found by chemical analysis in natural quartz crystals, and normally the 140 °K peak is also absent. In synthetic crystals potassium has sometimes been traced, but in a crystal, C22, especially grown in 1 N KOH as solvent (*), the 140 °K peak, if any, has a height less than $2 \cdot 10^{-5}$.

2) However, with the help of a sweep experiment larger amounts of K^+ ions can be introduced (Section 8, Fig. 7) giving rise to the mentioned peak in the tg δ *vs.* T curve.

Rubidium ions. – A quartz crystal, C23, grown in 0.8 molar Rb_2CO_3 aqueous solution as a solvent, did not show any special new peaks. Apparently the Rb^+ ion is too big to enter the crystal. However, the few sodium and lithium ions originating from contaminations of either the Rb_2CO_3 or the source material may find their way with relative ease into the growing crystal, since even in this case rather high sodium peaks (for instance $25 \cdot 10^{-4}$ at 38 °K and $2.5 \cdot 10^{-4}$ at 95 °K) and a lithium peak ($2 \cdot 10^{-4}$ at 60 °K) are observed in the tg δ *vs.* T curve.

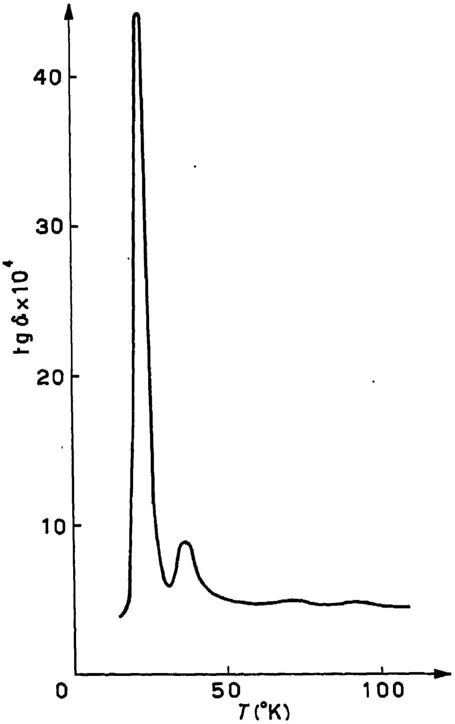

Fig. 9. – Tg δ *vs.* T curve at 32 kHz for a natural quartz crystal that has been subjected to a sweep experiment with AgCl as an electrode.

Protons. – These are present in many quartz crystals, since strong OH vibrations are detected spectroscopically. They cannot be conclusively detected by means of the dielectric loss experiments, at least, in the frequency and temperature ranges discussed in this paper.

Silver ions. – These can be swept in readily and show a typical peak at 22 °K (Fig. 9).

(*) This crystal was provided by Bell Telephoue Laboratories, Murray Hill, N. J.

10. – Determination of the dipole strength of the imperfections in clear crystals. Discussion of a model of these imperfections.

A determination of the dipole strength, p, for an imperfection that is electrically active, is complicated by the fact that concentration of the impurities causing such an imperfection cannot be accurately measured. It becomes even more doubtful when the possibility is envisaged that part of the foreign ions are hidden, as it were, in electrically inactive imperfections. A third point of doubt is the internal field correction as discussed in Section **2**.

Let us first discuss models of the imperfections in clear crystals. With the help of these models we shall try to systematize in the variety of data, and in particular we shall discuss the loss phenomena connected with ions of the following series: H^+, Li^+, Na^+, K^+.

We know from the discussion in Section **5** that ionic charges can move in the direction of the z-axis, that is in the main channels of the crystal.

The models proposed are given in Figs. 10*a-e*, showing in a schematic way the various possible positions for the mobile ions, and also qualitatively the potential energy of the ion involved as a function of a co-ordinate z in the direction of the z-axis. It should be emphasized that the models are over-simplified and are only meant as tentative proposals, but the following facts speak in their favour.

If H^+ ions are present, it is known from the infrared work of KATS [6] that these are very strongly bonded to the oxygen ions. This author arrived at two possible models: in the first one the hydrogen is found « ahead » of an oxygen ion adjacent to the Al^{3+} ion (Fig. 10*a*) the second model placed the hydrogen ion between two oxygen ions belonging to a tetrahedron of which the Al^{3+} ion is the centre (Fig. 10*b*). In both models the O—H bond can show both stretching and bending vibrations. Since the O—H bond is very strong we assume that there is no transition of H^+ ions to another oxygen ion in the wall of the channel—at least so at the low temperatures investigated. This is in accordance with the evidence, given in Section **8**, that at low temperature no dielectric relaxation is coupled with the presence of centres in which H^+ ions are involved.

Figures 10*c-e* show the models for the position of the alkali ions in the channel. The potentials are sketched so as to accord with the experimental facts.

There is an overall potential well around the Al^{3+} ion of the order of 1 eV depth. (This value determines roughly the diffusion and ionic conduction; cf. VERHOOGEN [7]).

Superposed on this overall potential are the series of relatively low barriers along the channel, due to binding forces, and the influence of ion size and steric hindrance.

Disregarding possible states of higher energy at the flanks of the potential well, which are supposed not to be occupied, the situation at the bottom, is

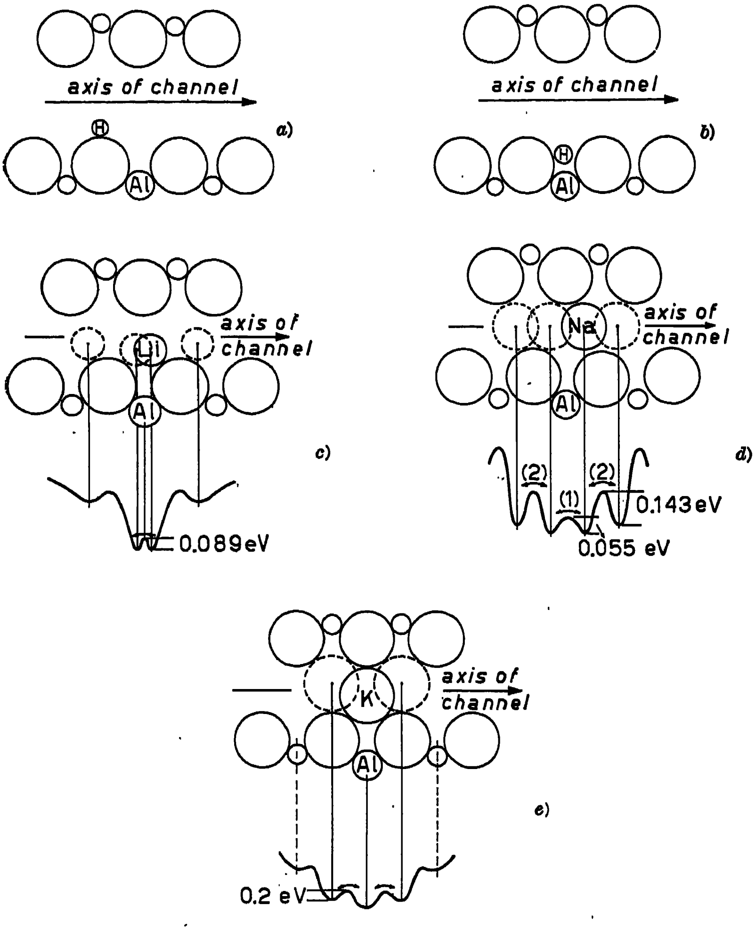

Fig. 10*a*-*e*. – Showing models of the positions of H^+ and alkali ions in the channel of the quartz crystal, and the corresponding trends of the potential-energy curves.

chosen in such a way that in the Li^+ case (Fig. 10*c*) only one kind of transition and therefore only the one relaxation process detected in our temperature interval shows up, whereas Fig. 10*d* (the Na^+ case) indicates two different kinds of transition and Fig. 10*c* (the K^+ case) one again. There is some continuity in this series of models. The known values of the activation energies involved (cf. also Table V) are used in Figs. 10*c*-*e*.

Let us now consider the Na^+ case in more detail in order to calculate the value of p related to the 38 °K peak in spite of the difficulties mentioned in the beginning of this Section. Our most reliable analyses are given in the following table.

TABLE III.

	Na/SiO_2 (ppm.)	N (cm^{-3})	$(\text{tg}\,\delta)_{\max}$	p (Debye units)
C8	18	$4.8\cdot10^{17}$	$8\cdot10^{-4}$	2.0
C12	60	$1.6\cdot10^{18}$	$14\cdot10^{-4}$	1.45
C9	272	$7.2\cdot10^{18}$	$135\cdot10^{-4}$	2.1

From eq. (1) and (3) and taking $f=((\varepsilon+2)/3)^2$ with $\varepsilon=4.8$ one finds

$$p^2 = 6.3\cdot10^{19}\,\frac{T}{N}\,\text{tg}\,\delta_{\max}\,, \tag{7}$$

where p is expressed in Debye-units ($=10^{-18}$ e.s.e.). With this equation the fifth column of Table III is calculated. If the internal field correction had been less drastic, the values of p would have been somewhat higher. The displacement of the ion is of the order of 1 Å.

As to the discussion of the 95 °K peak, p values are found which are about half the values for the 38 °K peak, since $\text{tg}\,\delta_{\max}$ is the factor of 10 lower, but T a factor of 2.5 higher.

The model in Fig. 10*d* is chosen in such a way that a Boltzmann distribution factor is not taken into account, although the necessity for such a procedure cannot be excluded.

A similar procedure for lithium using the peak height at 60 °K, yields p values as given in Table IV.

TABLE IV.

	Li/SiO_2 (ppm)	N (cm^{-3})	$(\text{tg}\,\delta)_{\max}$	p (Debye units)
C5	103	$2.7\cdot10^{18}$	$6\cdot10^{-5}$	0.29
C25	113	$3\cdot10^{18}$	$13\cdot10^{-5}$	0.40
C0	189	$5\cdot10^{18}$	$20\cdot10^{-5}$	0.39

In view of the possible and obvious errors the only conclusion can be that the p values in this case are remarkably smaller; *i.e.* of the order of $(0.3\div0.4)$ Debye units.

In conclusion Table V gives a survey of the activation energies belonging to relaxation effects due to a few discussed centres (progenitors). These activation energies are calculated from the shift of the peaks in the tg δ *vs.* T curves with frequency.

TABLE V.

Impurity symbol [8]	Peak temp. for 32 kHz (°K)	τ_0 (s)	Q (eV)
${}^{\mathrm{Al}}_{\mathrm{Na}}\mathrm{P}$	38	$2\cdot10^{-13}$	0.055
	95	$2\cdot10^{-13}$	0.143
${}^{\mathrm{Al}}_{\mathrm{Li}}\mathrm{P}$	60	$2\cdot10^{-13}$	0.089
${}^{\mathrm{Al}}_{\mathrm{K}}\mathrm{P}$	140	$2\cdot10^{-13}$	0.2

11. – The relaxation time connected with the low temperature effect in irradiated material.

In Fig. 11 the τ *vs.* $1000/T$ curve is given for a synthetic X-irradiated crystal, C11. A straight line appears, showing that the values obey eq. (2) quite well over a large temperature interval.

One finds in the case of C11

$$\tau_0 = 5\cdot10^{-7}\ \mathrm{s} \quad \text{and} \quad Q = 7.5\ \mathrm{meV}.$$

For a crystal containing a very large amount of colour centers (C9, cf. Fig. 3 or Table II in Section 7) we find a somewhat larger τ_0 value, *viz.* $10\cdot10^{-7}$ s, but the same activation energy, as can also be concluded from Fig. 11.

It should be added that the various coloured crystals generally

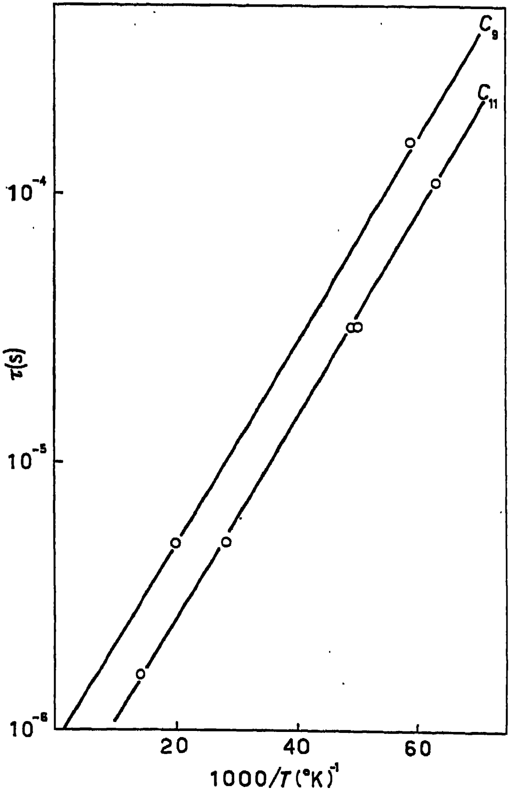

Fig. 11. – τ plotted on a logarithmic scale as a function of $1000/T$. The values refer to the low-temperature colour-centre peak.

differ not only in the value of their dielectric loss, but also in the position of their tg δ peaks along the T-axis. In connection with all data available this matter will be dwelt upon further in Section **12**, but here it may be remarked that, according to eq. (5) of Section **2** a slight change in τ_0 might have a marked influence upon T_m when $\omega\tau_0$ approaches 1.

With the measurements presented in this paper we generally have $\omega = 2 \cdot 10^5$, *so in this case a change of* τ_0 *from e.g.* 10^{-6} *to* $5 \cdot 10^{-7}$ s *alters the scale for the Q-values along the T-axis by a substantial factor, viz. roughly* 1.4.

It seems, therefore, that with the measuring frequency used the exact position of the peaks along the T-axis is a rather sensitive measure of τ_0, as long as one can be sure that cases with the same Q value are compared. If we compare the cases of C9 and C11 (Fig. 11) having T_{mc} values of 50 and 35 °K respectively (measured at 32 kHz), a difference which may seem quite alarming at first sight, we have indeed a good example of this phenomenon, since these crystals have the same activation energy of the colour-centre dipole relaxation and differ in τ_0 values by a factor of 2 only (*).

A possible reason for shifts in τ_0 will be discussed now. It seems likely that not only *the local lattice disturbance* at the point imperfection, but *also long range effects* (tension in the crystal) are involved.

12. – The spread in relaxation behaviour of various coloured crystals.

In this section we shall deal mainly with the low-temperature effect of coloured crystals, *i.e.* the peak in the tg δ *vs.* T curve at about 20 to 40 °K.

An important fact to be noticed is the spread of the T_m and T_{mc} values in the numerous measured curves at our disposal. T_m values are found ranging from 15 to 40 °K and corresponding T_{mc} values from say 16 to 50 °K. The reader is referred to the figures published earlier [1] and Figs. 2, 3 and 4 in this article, where a few examples are given. In view of the discussion in Section **11**, this should not worry us too much, since relatively small variations of τ_0 already involve such large variations of T_m and T_{mc}.

Let us first discuss briefly what happens when the crystal is irradiated. The progenitors, discussed in the foregoing sections, are the spots where the ionizing radiations give rise to the dissociation of the progenitor into 1) an aluminium ion with a hole trapped at the neighbouring oxygen ions (${}^{\text{Al}}\text{A}_+$ centre) and 2) an alkali ion associated with a trapped electron (${}_{\text{X}}\text{P}_-$ centre) [8]. *The latter centre must have found a relatively stable position at*

(*) These complications are not encountered in the discussion of deformation losses, since τ_0 is extremely small in that case.

some mooring, most likely at an already existing irregularity, imperfection or impurity (foreign ion) in the lattice (*).

The process can be visualised be the following reaction

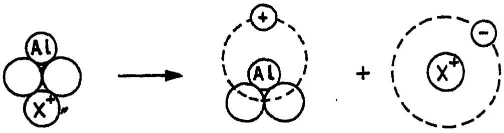

or written with the help of impurity symbols

(I) $${}^{Al}_{X}P \rightarrow {}^{Al}A_{+} + {}_{X}P_{-}$$

On the basis of this picture we venture the hypothesis that the ${}_{X}P_{-}$ centre gives rise to the main low-temperature loss peak, whereas the ${}^{Al}A_{+}$ centre should be connected with the hump at about 70 °K.

A similar hypothesis has been put forward earlier [1].

At the time the spread of the T_m values was interpreted in terms of the properties of the alkali ions (X^+ ions) involved, but taking into account the now available experimental evidence, we are inclined to believe that the influence of the said nature is small in relation to the influence of the nature of the moorings mentioned above. These moorings could be dislocations or in themselves rather inactive or harmless point defects, such as titanium or germanium on a silicon site, or an oxygen vacancy flanked by two substitutional aluminium ions.

The spread in the relaxational behaviour (*e.g.* T_m values), then, is related to the spread to the various moorings and to the stress fields due to the overall imperfection (dislocations, oxygen vacancies impurities) of the crystal.

We shall now give *evidence* for this point of view.

1) Those natural clear crystals which are characterized by low concentrations of alkali impurities (and consequently by low deformation losses) and which, moreover, are grown very slowly, show low T_m values upon irradiation. This applies particularly to most of the smoky quartz crystals, being natural crystals irradiated in nature, in which low concentrations of impurities are found and in which T_m values below 14 °K have been measured in all cases investigated by us [1].

2) Comparing natural clear crystals with increasing content of lithium as the characteristic impurity, that is with increasing peak height at 60 °K

(*) Since the word « trap » has generally been accepted for the place where electrons or holes are captured, we prefer to speak of « moorings » for places where ions are captured.

(at 32 kHz) it is found that after irradiation these crystals show increasing T_m and T_{mc} values, as appears from Table VI.

TABLE VI.

Crystal	Peak height (field $\parallel$ z-axis, at 60 °K and 32 kHz in the clear crystal)	T_m of colour-centre dipole losses	T_{mc} of colour-centre dipole losses
Smoky crystals mentioned sub 1)	Unknown	14	16
C3	Unknown	18	20
C2	$1.7 \cdot 10^{-5}$	22	30
C28	$5 \cdot 10^{-5}$	23	33
C25	$13 \cdot 10^{-5}$	23	40

3) A series similar to that discussed sub 2) is given in Table VII, where the data for a number of synthetic crystals are collected. Here, the impurity content is measured by the peak height at 38 °K (32 kHz) since ${}^{\mathrm{Al}}_{\mathrm{Na}}P$ centres are the main progenitors.

TABLE VII.

Crystal	(Peak height field $\parallel$ z-axis, at 38 °K and 32 kHz in the clear crystal)	T_m of colour-centre dipole losses	T_{mc} of colour-centre dipole losses
C4	$6 \cdot 10^{-4}$	18	24
C11	$28 \cdot 10^{-4}$	26	35
C23	$27 \cdot 10^{-4}$	40	50
C9	$135 \cdot 10^{-4}$	38	50

It should be remarked that in the case of C23 a considerable lithium peak of at least $10 \cdot 10^{-5}$ is present, besides the sodium content corresponding to the given height of the 38 °K peak.

4) An interesting case is formed by the crystals irradiated by a flux of neutrons. Without exception such crystals (C6, C14, C17) show high T_m values (> 30 °K) and T_{mc} values (> 45 °K). This will be due to irradiation damage, creating stress fields and an overall imperfection in the crystal as discussed above.

It is interesting to mention two specimens originating from the same mother crystal, one being irradiated by X-ray only showing a T_m value of 25 °K the other one by a flux of neutrons showing a T_m value of 32 °K.

13. – Some final remarks.

An interesting case is shown by the smoky quartz crystal shown in Fig. 12. A smoky quartz crystal is a crystal irradiated in nature. So the tg δ *vs.* T peak shows the typical form of the irradiated crystals, shown in Figs. 2 and 3. By gradual bleaching the progenitor (in this case the $^{\text{Al}}_{\text{Li}}P$ centre) shows up

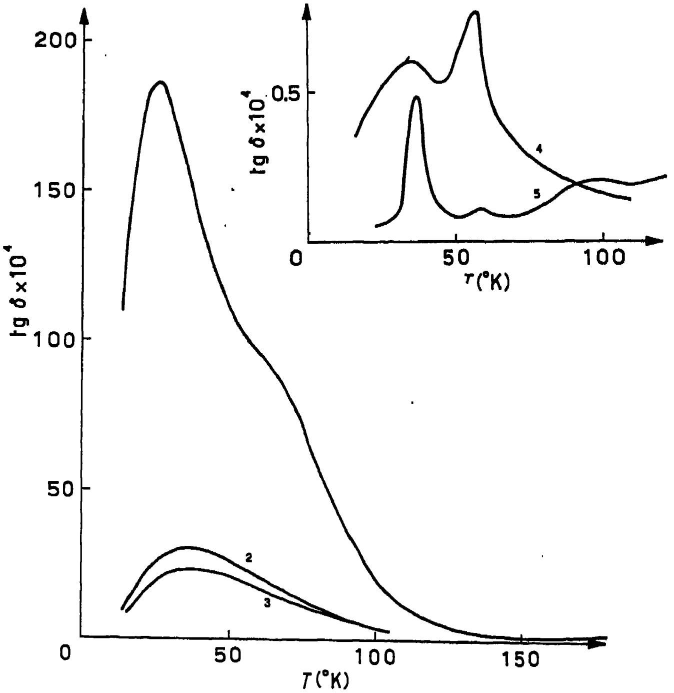

Fig. 12. – Tg δ *vs.* T curves for a natural smoky quartz crystal, C19, in different stages of bleaching. Measuring frequency 32 kHz.

finally (cf. the insert; curve 4). The insert also shows that by careless handling by the fingers the Li$^+$ ions were exchanged by Na$^+$ ions and a curve typical for a the presence of $^{\text{Al}}_{\text{Na}}P$ centres showed up (curve 5).

That the colour centres are really formed can also be detected by other physical tools, which are summarized Table VIII.

One can say therefore that the mechanism of the reaction of ionizing radiation with crystalline quartz is explained in a self-consistent way and the nature of both the progenitors and the colour centres is fairly well known.

If we now try to study fused silica with the same methods, the results are rather disappointing. Fused silica is contaminated with variable amounts of water, which are built in into the network as OH groups, bonded to silicon ions. Moreover, it turns out that fused silica is usually more contaminated than crystalline quartz and a contamination with 10 different elements in a arbitrarily chosen specimen is no exception. No wonder therefore, that practically every piece of fused silica shows an individual tg δ *vs.* T curve [1].

TABLE VIII.

$${}^{Al}_{X}P \rightarrow {}^{Al}A_{+} + {}_{X}P_{-}.$$

Dielectric losses at 32 kHz	X=Li : $T_{mc}=$ 60 °K X=Na: $T_{mc}=\begin{cases}38\ °K\\ 95\ °K\end{cases}$ X=K : $T_{mc}=$ 140 °K	$T_{mc}=70$ °K	Dependent on the kind of mooring
Optical absorption peak [9]	None	3 000 Å	X=Li : 4 200 Å X=Na: 4 600 Å X=K : 4 750 Å
g-values measured with electron spin resonance [10]	None	$g=2.011$	X=Li : $g=1.960$ X=Na: $g=1.964$ X=K : $g=1.97$

Colour centres *are* formed upon X-ray irradiation, but they cannot be detected by dielectric loss measurements, since they are not embedded in the same surroundings and the symmetry of a crystal field is absent.

Fortunately the colour centres can be studied by the optical absorption. Irradiated fused silica shows a typical rose colour due to an absorption band at 5 500 Å. There is much evidence, that the reaction I is followed by another reaction in which the oxygen atom is stripped of the ${}^{Al}A_{+}$ centre and a ${}^{Al}B_{-}$ centre is formed. The resulting reaction is then [9]

$$\text{(II)} \qquad {}^{Al}_{X}P \rightarrow {}^{Al}B_{-} + {}_{Na}P_{-} + O$$

The ${}^{Al}B_{-}$ centre is well-known from the research of the coloration of glasses and has an absorption at 5500 Å. The interstitial oxygen atom formed is very probably responsible for a new absorption band in the vacuum U.V. at about 1 600 Å. That reaction II takes place is also confirmed by the fact that with the help of the electron spin resonance technique two colour centres both with an unpaired electron, and none with an unpaired hole, are found.

Finally, an interesting remark can be made: Fused silica always shows the reaction II, no matter whether the ionizing radiation is U.V. light (wavelength shorter than 3000 Å) X- or γ-rays or neutrons. In crystalline quartz the three types of radiation first mentioned only result in a reaction of type I. If quartz crystal is irradiated with a flux of a least 10^{20} fast neutrons/cm^2

reaction II is found. One can express this also in this way that so much damage is done to the quartz lattice, that it is partially randomized (vitrified). This seems to be the reason that the original tg δ *vs.* T for such a crystal is not found back after thermal bleaching (cf. Fig. 4).

REFERENCES

[1] J. Volger and J. M. Stevels: *Philips Res. Rep.*, **11**, 452 (1956).
[2] J. Volger and J. M. Stevels: *Philips Res. Rep.*, **11**, 79 (1956).
[3] J. W. L. Köhler and C. G. Koops: *Philips Res. Rep.*, **1**, 416 (1946).
[4] J. M. Stevels: *Non-crystalline Solids* (New York, 1960), p. 431.
[5] A. Kats and Y. Haven: *Phys. and Chem. Glasses*, **1**, 99 (1960).
[6] A. Kats: *Philips Res. Rep.*, **17**, 249 (1962).
[7] J. Verhoogen: *Am. Mineral.*, **37**, 637 (1952).
[8] For the explanation of these symbols cf. J. M. Stevels and A. Kats: *Philips Res. Rep.*, **11**, 103 (1956).
[9] A. Kats and J. M. Stevels: *Philips Res. Rep.*, **11**, 115 (1956).
[10] J. S. van Wieringen and A. Kats: *Philips Res. Rep.*, **12**, 432 (1957).

Ultrasonic Attenuation in Liquid Metals.

R. W. B. STEPHENS

Department of Physics, Imperial College - London

In studying the structure of the liquid state, experimental investigation of the acoustical properties of liquid metals could be particularly useful because of their simple monatomic character. For example measurements on the temperature variation of sound velocity in liquid lead and tin have been applied by GORDON [1] to evaluate essential parameters in the « hole » theory of liquids. As pointed out by ABOWITZ and GORDON [2] ultrasonic attenuation measurements might give information on the nature of clusters giving rise to scattering in the fluid. These clusters are formed by heterophase fluctuations produced when the temperature of the liquid approaches that at which a phase change occurs and have been observed in organic fluids [3]. Further, the observation of structural or thermal relaxations would provide information about the structure of the liquid metal and the mobility of its atoms.

Mercury is a convenient liquid for initial experiments as there are fairly full physical data available, so that the expected classical attenuation as a function of frequency and temperature may be calculated and compared with the directly obtained experimental value. The only liquid metals for which ultrasonic absorption data have been published are mercury (BÄR [4]; RIECKMANN [5]; RINGO *et al.* [6]; ABOWITZ and GORDON [7]; JARZYNSKI [7]), bismuth (JARZYNSKI [9]) and gallium (PROFFIT and CAROME [10]; JARZYNSKI [11]).

The « classical » absorption of ultrasound in liquid metals is assumed to be given by the Stokes-Kirchhoff formula

$$\alpha = \frac{2\pi^2}{\varrho c^3} \cdot f^2 \left[\frac{4}{3}\eta_s + \frac{c\,\beta^2 K T}{J c_p^2}\right] = \alpha_s + \alpha_T\,, \tag{1}$$

where η_s is the shear viscosity coefficient, K the coefficient of thermal conductivity, c_p the specific heat at constant pressure, β the volume expansion coefficient, c the velocity of sound, f the frequency, ϱ the density and T the absolute temperature. In both mercury and bismuth the losses due to heat conductivity (α_T) are larger than those due to shear viscosity (α_s).

The results for mercury are as follows:

Author	Frequency range (MHz)	Temperature (°C)	Observed $\alpha/f^2 \cdot 10^{17}$ (s^2 cm^{-1})
BÄR	54	22	6.6
RIECKMANN	22÷ 54	24	6.4÷6.3
RINGO *et al.*	152÷996	24÷28	6.0÷4.7
ABOWITZ and GORDON	45÷115	−13 20 72	4.7 5.4 7.1
JARZYNSKI	68÷ 92	25 128 204	6.2 9.0 11.8

The reason for the difference in the absorption as measured at room temperature by ABOWITZ and GORDON and JARZYNSKI, is not clear. In both cases a pulse method was used, capable in principle of measuring the absorption to within 2% accuracy. The results of ABOWITZ and GORDON are in agreement with the classical absorption given by eq. (1). The results of JARZYNSKI, however, are consistently larger than the classical absorption. This excess absorption is interpreted by him as due to a bulk viscosity (η_B), which leads to an absorption coefficient

$$\alpha_B = \frac{2\pi^2}{\varrho c^3} \eta_B f^2 . \tag{2}$$

The classical absorption and the values of η_B calculated from the observed excess absorption are given below:

Temperature °C)	$\alpha_s/f^2 \cdot 10^{17}$ (s^2 cm^{-1})	$\alpha_T/f^2 \cdot 10^{17}$ (s^2cm^{-1})	η_B centipoise	η_B/η_s
25	0.98	4.26	1.9	1.2
128	0.84	7.33	1.6	1.4
204	0.83	10.15	1.3	1.3

A considerably larger excess absorption was found in liquid bismuth as shown below, the measurements being made at 68 and 92 MHz (see also Fig. 1).

Temperature (°C)	$\alpha_s/f^2\cdot 10^{17}$ (s^2 cm^{-1})	$\alpha_T/f^2\cdot 10^{17}$ (s^2 cm^{-1})	$\alpha_{ob}/f^2\cdot 10^{17}$ (*) (s^2 cm^{-1})	η_B centipoise	η_B/η_S
305	0.96	5.27	9.3	7.0	4.2
380	0.95	6.81	11.5	7.1	4.9
442	0.95	8.30	12.3	5.6	4.3

(*) α_{ob} is the experimentally observed attenuation coefficient

In both mercury and bismuth α/f^2 was found to be independent of frequency.

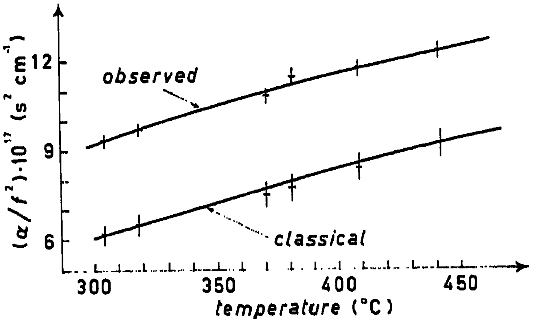

Fig. 1. Observed (exptl.) and classical (calcd.) ultrasonic absorption in liquid bismuth.

The classical absorption can be calculated with a fair degree of accuracy for liquid bismuth and mercury, as there are now sufficient reliable data. In the case of liquid bismuth the error in the classical absorption is mainly due to a ± 3 % uncertainty in the value of the specific heat and a ± 2% uncertainty in the value of the thermal conductivity. In the case of mercury the error in the classical absorption is mainly due to a ± 2 % uncertainty in the value of the thermal conductivity. JARZYNSKI estimates his measured absorption to be accurate to ± 2 % and gives the following estimates for the accuracy of η_B and η_B/η_S.

	T (°C)	η_B and η_B/η_S
Bismuth	305 442	± 13% ± 20%
Mercury	25 204	± 19% ± 42%

To determine the nature of the relaxation process, which could account for the observed excess absorption in the liquid metals the ratio η_B/η_S and the temperature dependence of η_B is compared with that of other liquids. The relatively low values of η_B/η_S and the observed decrease of η_B with temperature classifies liquid metals in the same group as associated polyatomic liquids and the fused salts, in which the volume viscosity has been attributed to structural, rather than thermal relaxation. Conclusions about the temperature dependence of η_B must, however, be taken as somewhat tentative in view of the large errors in the values of η_B. The structural simplicity of liquid metals provides the strongest argument against the possibility of thermal relaxation.

It is very unlikely that in monatomic liquids, such as the liquid metals, there is transfer of thermal energy from external to any internal degrees of freedom of the atom.

Gallium. – Although JARZYNSKI [12] places a large possible error in his results for gallium they are set out below together with some initial measurements made by PROFFIT and CAROME [13]. JARZYNSKI attributes the uncertainty to a lack of reliable physical data on gallium and to possible contamination by the air.

JARZYNSKI: 92 MHz

Temperature (°C)	56	292	348	413	438
α/f^2 (10^{17} cm^{-1} s^2)	2.9	3.1	3.6	4.2	4.3

PROFFIT and CAROME: 205 MHz

$$\text{Temperature } 30\ ^\circ\text{C} \quad \frac{\alpha}{f^2} = 2.5\cdot 10^{-17}\ \text{cm}^{-1}\ \text{s}^2\,.$$

The values of η_B/η_S for molten Bi and Ga as found by JARZYNSKI did not increase with increasing entropy of fusion as is the case for molten salts, which behave mechanically in a very similar way to monatomic liquids. ANDRADE [14] noted this different behaviour in his shear viscosity measurements on liquid metals and attributed it to the complex crystalline structure of bismuth and gallium.

ABOWITZ and GORDON [15] have also measured ultrasonic absorption in a series of mercury-thallium alloys. The absorption measurements were made as a function of frequency, from 15 to 115 MHz, temperature from 0 to 60 °C, and composition to 40 at. % thallium.

An excess absorption was found which increases with increasing thallium content. Also α/f^2 was found to decrease with increasing frequency, which is the case in the region of a relaxation effect. The extreme values of α/f^2 for the 40 at. % thallium-mercury alloy are shown below.

Although the data do not fit exactly the relaxation curves predicted by single relaxation time theory, by making a best fit **Abowitz** and **Gordon** estimate that at 1.4 °C the relaxation peak for the 40 at. % alloy would occur at approximately 270 MHz. Considering the process to be thermally activated and using the Arrhenius relation an activation energy of (3600 ± 300) cal/mole is obtained for the 40 at. % alloy and (2000 ± 400) cal/mole for the 14.5 at. % alloy. Extrapolation to zero per cent thallium yields a value of (1000 ± 500) cal/mole for pure mercury. Three recent measurements of self diffusion in liquid mercury give the activation energy for self diffusion as 1160, 1005 and 2400 cal/mole respectively. **Gordon** and **Abowitz** conclude that the relaxation observed in mercury-thallium alloys under the influence of the applied periodic stress, is of a structural nature involving a change in the average number of like and unlike nearest neighbours surrounding a given atom.

Temperature (°C)	f (MHz)	$\alpha/f^2 \cdot 10^{11}$ dβ s
1.4	15	13.8
	115	10.4
25.0	15	12.0
	115	9.7
65.0	15	11.1
	115	9.4

Magnetohydrodynamic Dispersion and Absorption at Ultrasonic Frequencies.

Alfvén [16], **Herlofson** [17] and **Lundquist** [18] show theoretically that both transverse and longitudinal magnetohydrodynamical waves may be propagated in conducting liquids, and **Anderson** [19] and **Robey** [20], a few years later, calculated the sound velocity and the absorption in liquids of finite conductivity when situated in transverse magnetic fields. More recently **Westphal** [21] has carried out a series of ultrasonic experiments in conducting liquids (and solids) in magnetic fields up to 20 kG. The general theoretical predictions were verified, namely that the magnetic field is « carried along » with the sound motion at acoustic frequencies below a characteristic value for a given substance and that the sound dispersion is greatest and the absorption per wavelength is a maximum in the region of this transition frequency (ν_t). Assuming that a plane sound wave is being propagated in a liquid of finite conductivity in say the x-direction, and a magnetic field is applied perpendicular to this direction, then the liquid movement created by the acoustic disturbance will give rise to induced electric currents. Energy will therefore be abstracted from the sound wave due to Joulean heating by these induced currents, and moreover these will react with the magnetic field and lead to the generation of compressions and rarefactions in direction opposed to that of the acoustic wave. The presence of the magnetic field thus produces attenuation of the amplitude of the sound-wave and velocity dispersion (see Fig. 2), the absorption and dispersion being determined by two magnetohydrodynamic quantities, the Alfvén velocity (a_m) and (R_m) the magnetohydrodynamic Reynolds number $a_m = B_0/(u_0\varrho^{\frac{1}{2}})$, where B_0 is the magnetic induction, μ_0 is the permeability and ϱ is the density of the medium. The Reynolds number is defined by $R_m = LV\mu_0\sigma$, where the velocity V is arbitrarily assumed to be given by a_0 (the sound velocity for $B=0$) and $L = \lambda/2\pi$, where λ is the wave length: *i.e.*

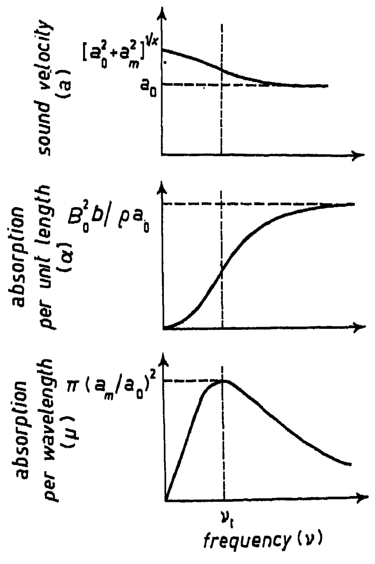

Fig. 2.

$$i.e. \qquad R_m = \frac{\lambda}{2\pi}\, a_0\mu_0\sigma = \frac{a_0^2\mu_0\sigma}{2\pi\nu}\,,$$

ν being the ultrasonic frequency.

If the Reynolds number R_m is $\gg 1$, then the diffusion will be dominated by the transport process and the magnetic field will be frozen in the conducting liquid. In Westphal's experiments this is the case at low frequencies and in consequence the magnetic pressure contributes to the fluid pressure, so that the sound velocity will be increased. On the other hand at high frequencies the diffusion process will be faster, and the magnetic pressure will be comparatively ineffective. The « unfreezing » of the magnetic field will mean that the magnetic pressure and fluid compression will become out of phase with each other leading to acoustic energy dissipation. It should be pointed out that the magneto-acoustic dispersion differs from the corresponding acoustic effect arising from relaxation phenomena in liquids, for the latter shows a smaller sound velocity at low frequencies.

The experimental liquids used by Westphal were mercury, hydrochloric acid and K-Na liquid alloy, which were contained within a cylindrical glass vessel (2.8 cm diam., 16.9 cm long) and ultrasonic pulses were generated by quartz crystals operating at frequencies of 0.885, 1.64, 2.54 and 4.21 MHz.

The electromagnet gave a field strength of 19.6 kG, and as a control in the experiment, WESTPHAL also measured the absorption in K-Na contained within a short vessel which was adjusted to be *parallel* to the magnetic field. The presence of the magnetic field was found to have no effect on the measured absorption in this control experiment.

Figure 3 illustrates the degree of agreement of Westphal's experimental results with the calculations from theory and in particular it is to be noted that the « freezing-in » of the magnetic field begins below the transition frequency (ν_t) of 2.5 MHz (cf. calculated value in Table below) *i.e.* in the region where $R_m \sim 1$.

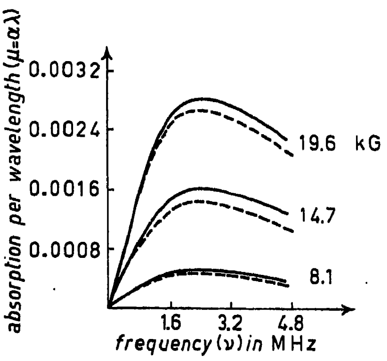

Fig. 3. – Theoretical (full lines) and experimental (dashed lines) curves for ultrasonic absorption in K-Na alloy for various frequencies and magnetic field strengths (after Westphal).

Liquid conductor	ϱ (kg m^{-3})	σ (Ω^{-1} m^{-1})	a_0 (m s^{-1})	ν_t (s^{-1})	a_m m s^{-1}	$\left(\frac{a-a_0}{a_0}\right)_{\nu\to 0}$	$(1/x)_{\nu\to\infty}$ (m)
HCl 20%	$1.03\cdot10^3$	$7.6\cdot10^1$	$1.58\cdot10^3$	$3.8\cdot10^1$	44.5	$7.2\cdot10^{-1}$	$4.6\cdot10^3$
Hg	$1.35\cdot10^4$	$1.04\cdot10^6$	$1.44\cdot10^3$	$4.13\cdot10^5$	15.0	$5.4\cdot10^{-5}$	0.49
K-Na (5:1)	$8.46\cdot10^2$	$3.08\cdot10^6$	$2.00\cdot10^3$	$2.46\cdot10^6$	59.9	$4.48\cdot10^{-1}$	0.145 .

Since the calculated transition frequency is very much smaller than the frequencies used in Westphal's experiments it was expected ($R_m \ll 1$), and confirmed, that no magnetoacoustic absorption would be observed in HCl.

ANDERSON [21] showed theoretically that the maximum absorption per wave length was independent of the conductivity.

The table below gives the calculated values for a number of liquids, the frequency (f_m) of maximum absorption correlating with ν_t.

Liquid conductor	σ (Ω^{-1} m^{-1})	f_m (s^{-1})
Sea water	$1.0\cdot10^1$	$0.5\cdot10^1$
HCl	$7.5\cdot10^1$	$4.0\cdot10^1$
Hg	$1.02\cdot10^6$	$4.7\cdot10^5$
Ga	$1.4\cdot10^6$	$6.7\cdot10^5$
Wood's metal	$2\cdot10^6$	$9.5\cdot10^5$
Sodium	$9\cdot10^7$	$4.7\cdot10^6$

In concluding it is interesting to note, having in mind the development of the acoustic n.m.r. technique, that ordinary n.m.r. techniques have been employed to examine the liquid state in metals. One of these techniques is concerned with the so-called Knight shift, which relates to the shift of the magnetic resonance frequency of the nucleus resulting from its interaction with the conduction electrons; the latter are polarized in the presence of a magnetic field and thus give rise to an extra effective field at the nucleus. The other technique which KNIGHT *et al.* [23] have applied is concerned with relaxation effects, such as quadrupolar broadening, and for the several metals he has examined, there appears to be an appreciable amount of zone structure retained above the melting point. Such investigations could be carried out by acoustic n.m.r., in which an ultrasonic excitation is used to perturb the nucleus instead of a R.F. field. The detection of the resonance may be as in ordinary n.m.r., or alternatively the changed impedance of the medium at resonance may be detected acoustically.

REFERENCES

[1] R. B. GORDON: *Acta Metallurgica*, **7**, 1 (1959).
[2] G ABOWITZ and R. B. GORDON: *Acta Metallurgica*, **10**, 671 (1962).
[3] W. A. HAYER and A. W. NOLLE: *Journ. Chem. Phys.*, **24**, 803 (1956).
[4] R. BÄR: *Helv. Phys. Acta*, **10**, 332 (1937).
[5] P. RIECKMANN: *Phys. Zeits.*, **40**, 582 (1939).
[6] G. R. RINGO, J. W. FITZGERALD and G. B. HURDLE: *Phys. Rev.*, **72**, 87 (1947).
[7] G. ABOWITZ and R. B. GORDON: loc. cit.
[8] J. JARZYNSKI: *Ph. D. Thesis* Univ. of London, (1961), also *Proc. Phys. Soc.* (April, 1963) .
[9] J. JARZYNSKI: loc. cit.
[10] R. L. PROFFIT and E. F. CAROME: ONR Technical Report No. 5 (John Carroll, Univ. Ohio) (March, 1962).
[11] J. JARZYNSKI: *Ph. D. Thesis* Univ. of London, (1961) and *Proc. Phys. Soc.*, **81** 745, 1963.
[12] J. JARZYNSKI: loc. cit.
[13] R. L. PROFFIT and E. F. CAROME: loc. cit.
[14] E. N. ANDRADE: *Proc. Phys Soc.*, **52**, 748 (1940).
[15] G. ABOWITZ and R. B. GORDON: loc. cit.
[16] H. ALFVÉN: *Cosmical Electrodynamics* (Oxford, 1950).
[17] N. HERLOFSON: *Nature, London*, **165**, 1020 (1950).
[18] S. LUNDQUIST: *Phys. Rev.*, **83**, 307 (1951).
[19] N. S. ANDERSON: *Journ. Acoust. Soc. Am.*, **25**, 529 (1953).
[20] D. H. ROBEY: *Journ. Acoust. Soc. Am.*, **25**, 603 (1953).
[21] W. WESTPHAL: *Zeits. f. Phys.*, **168**, 333 (1962).
[22] N. S. ANDERSON: loc. cit.
[23] W. KNIGHT, A. G. BERGER and V. HEINE: *Non-Crystalline Solids* (New York, 1960), p. 230.

Recouvrance de volume des verres; comparaison entre les expériences et une théorie phénoménologique.

A. J. Kovacs

Centre de Recherches sur les Macromolécules - Strasbourg

1. – Introduction.

Depuis les travaux de Simon [1] de nombreux auteurs ont reconnu qu'au dessous d'une zone critique de température les paramètres extensifs des *liquides surfondus* (volume, enthalpie, etc.) dépendent non seulement de la température, T, et de la pression, P, mais aussi du temps, et plus généralement de l'histoire thermique de l'échantillon. La zone critique sépare deux états dont la *stabilité* est fondamentalement différente, la structure liquide, (l'ordre à courte distance), n'étant pratiquement pas affectée par cette transition. Aux températures élevées le *liquide surfondu*, (ou le caoutchouc dans le cas des polymères amorphes), est en *équilibre métastable* (par rapport à l'état cristallin); par contre, aux basses températures, le *verre* se trouve dans un état *évolutif*, intermédiaire entre l'état métastable qu'il avait antérieurement à haute température, et celui correspondant à sa température réelle. La vitesse de réarrangement de la structure liquide diminue rapidement avec T, et la *transition vitreuse* se manifeste lorsque cette vitesse est du même ordre de grandeur que celle de la variation de la température, imposée par l'expérience. Cette définition de la transition peut être généralisée pour d'autres paramètres externes qui agissent éventuellement sur l'échantillon, par exemple des contraintes électro-magnétiques ou mécaniques. Aussi peut-on dire avec Kauzmann [2] que la transition vitreuse peut être localisée par une température, T_v, au dessous de laquelle le temps de relaxation (ou de retard) de certains degrés de liberté, qui caractérisent le mouvement des particules du liquide, est comparable à la durée de la variation, (ou la période), des paramètres externes. Parmi ces paramètres la température occupe une place privilégiée; dans ce cas l'échelle des temps accessibles est limitée par la conductivité thermique à des temps généralement plus longs que la minute, mais pouvant s'étendre à des durées considérables.

Cette lente évolution des verres peut être facilement mise en évidence en mesurant la variation isotherme de leur volume, à pression constante, après une impulsion thermique relativement courte (trempe), comparée au temps nécessaire pour atteindre l'équilibre (métastable) de structure. Dans le cas général la variation de volume dépend de l'histoire thermique de l'échantillon, et elle se complique singulièrement avec cette dernière, reflétant une sorte de « mémoire » des états antérieurs. Nous nous limiterons ici à quelques *classes* de traitements thermiques parmi les plus simples, qui ne dépendent que d'un paramètre unique, que l'on fait varier systématiquement; l'état de départ étant toujours un état d'équilibre métastable, qui ne dépend que de la température, T_0. Dans ce cas, on peut analyser les résultats à l'aide des théories phénoménologiques, dont nous développerons une ici.

Ces expériences ont été effectuées à l'aide d'une technique dilatométrique décrite auparavant [3] sur des échantillons de polymères amorphes (polystyrène, PS, polyacétate de vinyle, PVA), et du glucose. Mais les phénomènes observés peuvent être généralisés probablement à tous les systèmes vitreux. Ainsi, le comportement d'un verre de borosilicate est tout-à-fait comparable à celui de nos échantillons [4]. La constitution chimique des verres affecte surtout l'emplacement de T_g dans l'échelle des températures, mais les paramètres cinétiques de l'évolution isotherme sont du même ordre de grandeur dans leur zone respective de transition.

2. – Résultats expérimentaux.

La Fig. 1 représente typiquement la variation du volume spécifique, $v(t)$, d'un échantillon de polystyrolène (PS II), en fonction de la température. Dans la région de transition (A), qui sépare le domaine du *liquide surfondu* (B) de celui du *verre* (C), le coefficient de dilatation subit une variation importante. Dans le domaine (B) l'équilibre de volume est obtenu simultanément avec l'équilibre des températures (qui dans la plupart de nos exemples né-

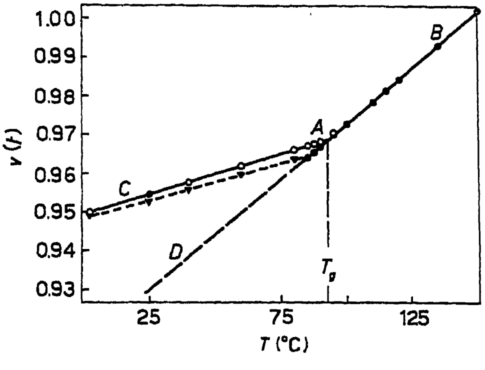

Fig. 1. – Variations du volume spécifique $v(t)$, en cm³/g, du polystyrolène (PS II), en fonction de la température, T, et du temps, t (en heures), après trempe de T_0=115°C; ○ $v(0,02)$; ● $v(\infty)$; ▲ $v(100)$.

cessite environ 1 minute), par contre dans le domaine (*C*) le volume n'est plus défini d'une manière univoque par la température, mais dépend de l'histoire thermique de l'échantillon. Les deux branches (*C*) de cette courbe ont été tracées à l'aide des volumes mesurés au bout des temps $t = 0.02$, et 100 heures, après avoir trempé l'échantillon de 115 °C (T_0), où il était en état d'équilibre.

Pendant la trempe on observe une contraction rapide, « instantanée », en phase avec la variation de T, puis une contraction additionnelle, isotherme. Lorsque la contraction cesse, le volume d'équilibre, $v(\infty)$, se situe sur le prolongement (*D*) de la courbe (*C*). Le temps nécessaire pour atteindre un tel équilibre croît rapidement avec la différence ($T_g - T$). La température de transition T_g, définie d'une manière *conventionnelle* par l'intersection des deux branches droites asymptotiques de $v(\infty)$ et de $v(0.02)$, est donc liée au temps de 0.02 h., et aussi au mode opératoire. La même convention localise T_g (100 h) environ 7 °C inférieure à T_g (0.02). Le rapport de corrélation: $\Delta T_g / \Delta \log t \approx$ ≈ -2 °C, est du même ordre de grandeur pour tous les systèmes étudiés, et sa valeur réduite explique la relative insensibilité de T_g vis-à-vis de l'échelle de temps.

Pour la même raison on voit que l'on ne peut atteindre la branche (*D*) de cette courbe prolongée vers les basses températures, à moins de recuire l'échantillon pendant des temps extrêmement longs. Il y a toute raison de croire que cette extrapolation quasi linéaire cesse d'être valable au dessous d'une zône critique de température [2]. La courbe d'équilibre présente probablement une singularité analogue à la transition vitreuse (*A*) qui, elle, serait une véritable transition du 2ème ordre [5], mais inacessible à l'expérience directe.

Il est surtout intéressant d'étudier la *variation isotherme du volume* en fonction du temps, qui reflète la cinétique du réarrangement de la structure liquide. La Fig. 2 représente cette variation pour l'échantillon PS I, à différentes températures (indiquées). L'origine des ordonnées est ici le volume mesuré au temps $t_i = 0.01$ h, après trempe de $T_0 (= 115$ °C). Toutes ces isothermes de volume ont une tangente d'inflexion (en pointillé) dont la pente $\bar{\beta} = (-\partial v / v \cdot \partial \log t)_{\max}$ ne varie que peu avec T. Exception faite de la courbe à 80 °C, on voit que le volume est loin de sa valeur d'équilibre $v(\infty)$, même au bout

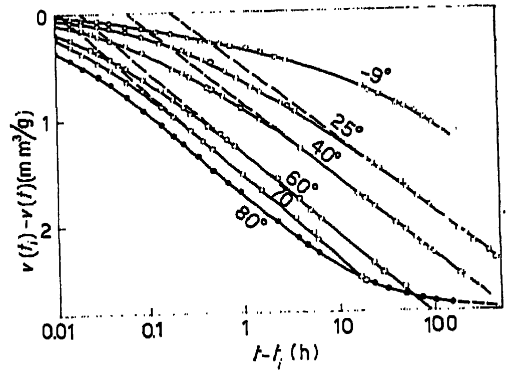

Fig. 2. – Isothermes de contraction de l'échantillon PS I, après trempe ($T_0 = 115$ °C) à différentes températures indiquées. L'isotherme à 80 °C coïncidant pratiquement avec celle à 70 °C, a été translatée vers le bas.

de 1000 heures. Nous n'insisterons pas ici sur les différents paramètres qui définissent ces isothermes [3, 6]. Notons seulement que si l'on admet l'extrapolation linéaire des volumes $v(\infty)$ (Fig. 1, branche *D*), la tangente d'inflexion de l'isotherme à 25 °C (Fig. 2) coupe l'ordonnée $v(\infty)$ pour un temps de l'ordre de 10^{32} heures.

Au voisinage de T_g ces temps sont évidemment plus courts. La Fig. 3 montre les isothermes de contraction dans cette région critique pour un échantillon PVA II, après trempe de 40 °C. L'origine des ordonnées est ici le volume d'équilibre, $v(\infty)$. Les tangentes d'inflexion (en pointillés) coupent les

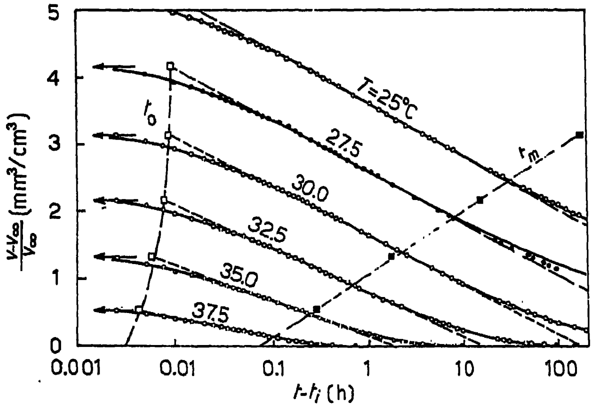

Fig. 3. – Isothermes de contraction du polycétate de vinyle (PVA II) dans le domaine de sa transition vitreuse. $T_0 = 40$ °C. Variations des paramètres t_0 et t_m avec la déformation initiale, indiquée par des flèches horizontales. La courbe de 27,5° a été calculée d'après la formule (13).

ordonnées: $(v_i - v_\infty)/v_\infty$ (correspondant à l'amplitude initiale, e_i, au temps t_i) pour des temps t_0, et l'ordonnée zéro ($v = v_\infty$) pour des temps t_m. En portant ces temps (à l'échelle logarithmique) en fonction de l'amplitude initiale e_i, marquée par des flèches horizontales, on obtient deux courbes (Fig. 3), dont l'écartement sur une parallèle à l'axe des abscisses représente l'intervalle de temps approximatif de la *recouvrance* (recovery) de volume.

Le paramètre t_0 ne varie que peu avec T (ou e_i), et il est du même ordre de grandeur que le temps $t_i = 0.01$ h. Par contre, t_m varie rapidement, le rapport de corrélation $\Delta T/\Delta \log t_m \approx -2.7$ °C, étant du même ordre de grandeur que $\Delta T_g/\Delta \log t \approx -2.3$ °C. La différence entre ces deux valeurs peut être attribuée à la variation relativement importante de ces rapports avec T. La variation de $\log t_m$, avec e_i est, par contre, sensiblement linéaire ($\Delta e_i/\Delta \log t_m = 9.3 \cdot 10^{-4}$). Enfin, lorsque e_i tend vers zéro, le rapport t_m/t_0 tend vers une valeur finie, et voisine de 15, pour tous les systèmes étudiés de la même manière. Or, ce rapport est sensiblement le même que celui obtenu (par une construction analogue) à partir d'une fonction exponentielle simple:

$$v - v_\infty = (v_i - v_\infty) \exp\left[-\frac{t - t_i}{\tau}\right], \tag{1}$$

où τ est le temps de retard caractéristique du processus de recouvrance. Il en résulte que la contraction isotherme consécutive à une trempe, d'une température T_0 à T, peut être caractérisée par un temps de retard unique, lorsque l'amplitude e_i tend vers zéro, c'est-à-dire lorsque T tend vers T_0 (40° dans le cas de la Fig. 3).

Bien entendu pour toute amplitude finie le rapport t_m/t_0 est supérieur à 15 (Fig. 3), ce qui signifie que la recouvrance du volume est plus lente que celle qui correspond à l'expression (1). On peut expliquer ce ralentissement en admettant une distribution des temps de retard [3]. Bien que l'existence d'une telle distribution soit très probable [7], nous allons montrer qu'elle ne constitue pas le paramètre essentiel de ces expériences. Elle ne permet pas d'expliquer notamment la cinétique de la recouvrance de volume, lorsque celle-ci procède par dilatation isotherme.

Ayant obtenu un état d'équilibre au bout d'un temps raisonnablement long, au dessous de T_g, on peut, en effet, imposer à l'échantillon un traitement thermique symétrique à la trempe, en le *réchauffant* rapidement à T. On observera dans ce cas, d'abord une dilatation « instantanée », caractérisée par le coefficient α_g du verre, puis, après l'établissement de l'équilibre thermique, une dilatation isotherme.

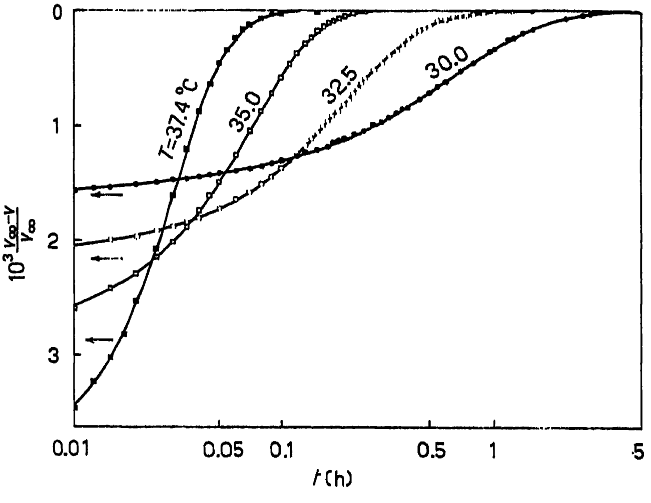

Fig. 4. – Isothermes de dilatation du glucose, après stabilisation à 25 °C (T_0) et réchauffement rapide à différentes températures T.

La Fig. 4 représente les résultats de telles expériences faites avec du glucose, après réchauffement à différentes températures T (indiquées), à partir de $T_0 = 25\,°C$. Pour obtenir l'équilibre de volume à 25 °C on a dû maintenir l'échantillon à cette température pendant au moins 150 heures (Fig. 8) avant *chaque* réchauffement à T. La différence entre ces isothermes et celles de la Fig. 3 est manifeste, car ces processus sont, en général, plus rapides qu'une recouvrance exponentielle, exceptée l'isotherme à 30 °C, qui représente pratiquement une telle fonction (1), avec $\tau = 0.85\,h$, et $e_i = -1.55 \cdot 10^{-3}$. En trempant cet échantillon de 40 à 30 °C, on obtient une isotherme de contraction de même amplitude initiale, mais de signe opposé. La Fig. 5 représente ces deux isothermes de recouvrance à 30 °C; leur dissymétrie est frappante. La vitesse initiale de contraction est environ 5 fois plus grande que celle de la dilatation isotherme. De même l'équilibre final $v(\infty)$ est beaucoup plus rapidement approché par contraction, que par dilatation.

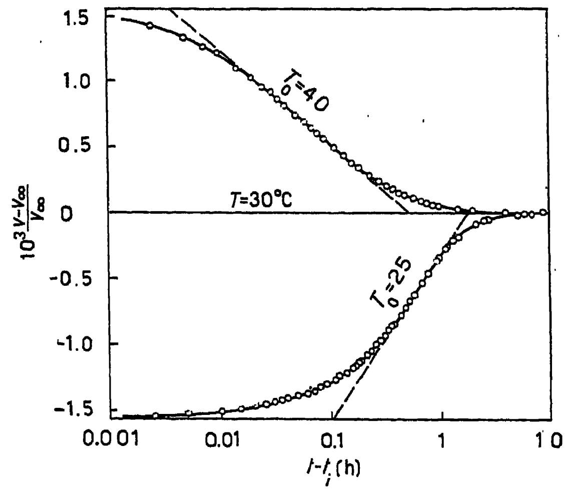

Fig. 5. – Isothermes de dilatation et de contraction du glucose à 30 °C, après réchauffement et trempe à partir des températures T_0.

D'après la Fig. 4 on peut voir que la dissymétrie est accentuée par l'accroissement de l'amplitude initiale, car la dilatation isotherme devient de plus en plus *autocatalytique*, alors que la vitesse de contraction diminue sensiblement proportionellement avec l'inverse du temps quelle que soit

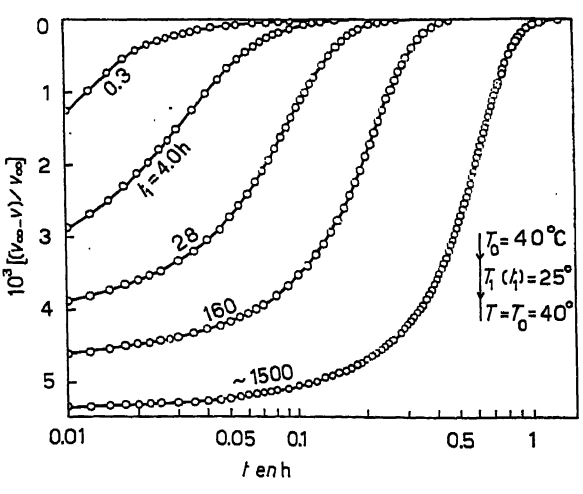

Fig. 6. – Isothermes de dilatation de l'échantillon PVA II, à 40 °C après trempe de T_0(40°C) à T_1(25 °C), et recuit à T_1, pendant des temps t_1 (indiqués), suivi de réchauffement à 40 °C.

l'amplitude initiale. Cette observation, déjà signalée par d'autres auteurs [3, 4, 8], constitue la caractéristique essentielle des phénomènes de la recouvrance des verres.

Le comportement autocatalytique, et son accentuation avec l'accroissement de l'amplitude de la dilatation isotherme est clairement illustré par la Fig. 6. Ces expériences, faites avec un échantillon de PVA II, ont été effectuées de la manière suivante: Trempé de $T_0 = 40\,°C$ à $T_1 = 25\,°C$, l'échantillon a été maintenu à T_1 pendant un temps t_1 variable (indiqué sur la figure), sans d'ailleurs atteindre l'équilibre de volume (Fig. 3), puis réchauffé de nouveau à 40 °C, où l'on a observé la dilatation isotherme résultant de ce traitement thermique (Fig. 6). Les courbes peuvent être convenablement représentées par une formule empirique de type:

$$v - v_\infty = (v_t - v_\infty) \exp\left[-\frac{t}{\tau}\right]^n \qquad ; \qquad t \geqslant t_t\,, \tag{2}$$

où l'exposant n est supérieur à l'unité, et il a la valeur de $n = 3$ lorsque $t_1 = \sim 1500$ heures. On sait qu'une telle fonction (2) n'a pas de transformée de Laplace, et ne peut donc être interprétée par aucune distribution réelle des temps de retard. S'il existe aussi, comme c'est vraisemblable, une distribution des temps de retard, son effet se manifeste par un ralentissement du processus. Il en résulte que l'effet des paramètres de structure qui confèrent le caractère autocatalytique au processus de dilatation *l'emportent* sur l'effet dû à la dispersion des temps de retard. Cette observation impose une hiérarchie des paramètres qui contrôlent les phénomènes de recouvrance.

D'autres exemples de traitements thermiques ont été décrits ailleurs [3, 6, 9] que nous ne pouvons pas discuter ici. La recouvrance de volume qui en résulte confirme les observations faites ici, tout en précisant la nature assez extraordinaire de ces phénomènes.

3. – Théorie phénoménologique.

On peut concevoir la recouvrance de volume comme un écoulement produit par une *pression interne effective* ΔP, engendrée par la variation de T [8], et écrire:

$$(1/v)(\mathrm{d}v/\mathrm{d}t) = \Delta P/\eta_v\,, \tag{3}$$

où η_v est une viscosité de volume. On doit admettre, d'autre part, que ΔP s'annule lorsque $v = v_\infty$, et poser:

$$\Delta P = -K(v - v_\infty)/v \tag{4}$$

où K est un module de compressibilité, qui ne dépend pas de v (les déformations sont suffisamment petites pour que la relation entre P et v puisse être considérée comme linéaire).

Les formules (3) et (4) expriment la recouvrance d'un élément Kelvin (ressort et amortisseur en parallèle) soumis à une pressione ΔP. On peut s'attendre d'ailleurs à ce qu'elles restent valables même pour une pression *externe* imposée au système [10].

En combinant (3) et (4) on obtient:

$$\mathrm{d}v/\mathrm{d}t = -(K/\eta_v)(v - v_\infty) = -(1/\tau_v)(v - v_\infty)\,, \tag{5}$$

où $\tau_v = \eta_v/K$, est le temps de retard associé au processus de recouvrance. Toutes les théories phénoménologiques ont comme point de départ une relation analogue, formulée d'une manière très générale par KRONIG [11] pour toutes sortes de phénomènes de relaxation.

Les différences entre ces théories proviennent de l'évaluation du paramètre τ_v [8-14].

Si τ_v était constant, le volume devrait varier exponentiellement avec t, en suivant la relation (1). Or, nous avons montré qu'en général τ_v dépend de l'amplitude, et que sa dérivée par rapport au volume doit changer de signe avec $(v - v_\infty)$, par suite de la dissymétrie des phénomènes de contraction et de dilatation. Le module K dépend probablement de la température, et aussi du temps, au cas où nous avons une distribution des temps de retard. Nous négligerons cependant, *en première approximation*, ces variations en supposant que K est une constante, son inverse étant de l'ordre de grandeur de la différence entre la compressibilité (isotherme) du liquide surfondu, et celle du verre [8]. La validité de ces hypothèses simplificatrices sera discutée en comparant les résultats des calculs aux expériences.

D'après les conceptions d'EYRING [13] le changement de la structure liquide en fonction de T, et de P consiste essentiellement dans la variation du nombre de « trous », distribués au hasard, ou plus généralement dans la variation du « volume libre ». Ce dernier résulte des *fluctuations* de densité, entretenues d'une part, par des *oscillations anharmoniques* des particules élémentaires autour de leur position d'équilibre momentanée (comme dans le milieu cristallin); et d'autre part, par des mouvements de *translation* et de *rotation* des unités structurales simples, ou associées.

A haute température $(T > T_g)$ tous ces mouvements sont plus rapides que la variation de la température extérieure. Le réajustement du volume libre suit donc sans retard les variations de T. Lorsque la température s'abaisse, et que $(\mathrm{d}T/\mathrm{d}t)$ devient du même ordre de grandeur que la vitesse de réarrangement, la contribution de ces mouvements au rétablissement de l'équilibre (du volume libre) sera en retard sur la variation de T, et elle se manifestera par une *variation isotherme* du volume (libre), et des autres paramètres (enthalpie, pression interne, etc.) liés à ce dernier. L'amplitude des variations isothermes de ces paramètres mesure ainsi la contribution des mouvements retardés au rétablissement de l'équilibre.

Lorsque le même corps peut être obtenu, dans un même domaine de $T < T_g$, sous forme cristalline et vitreuse (glucose, glycerol, etc.), on constate que le coefficient de dilatation «instantané» du verre, α_g, est sensiblement égal à celui du cristal. Il en est de même de la chaleur spécifique, C_p, et de la compressibilité, χ [2]. L'égalité de ces paramètres dans ces deux milieux, de structure essentiellement différente, doit être attribuée à la similitude des oscillations anharmoniques qui s'y opèrent. Corrélativement, *l'excès* de ces coefficients dans le milieu liquide (surfondu): $\Delta\alpha$, ΔC_p et $\Delta\chi$ peut être attribué à la contribution des mouvements de translation et de rotation caractérisant ce milieu.

Nous avons utilisé cette description phénoménologique de la transition vitreuse pour évaluer la variation de la viscosité η_v, à partir d'une formule proposé par DOOLITTLE [15], qui relie ce paramètre au volume libre par la relation:

$$(6)\qquad \left\{\begin{aligned} &\ln(\eta_v/A) = Bv_\infty/(v - v_0) = B/f\,, \\ &f = \frac{v - v_0}{v_\infty}\,, \end{aligned}\right.$$

où A est une viscosité de référence et B un paramètre de l'ordre de l'unité, v_0 le volume «occupé» par des particules (dans lequel nous incorporons le volume engendré par les oscillations anharmoniques), et f la fraction libre du volume. Pour un verre, le volume v dépend généralement de la température et du temps; nous admettrons, par contre, que v_0 n'est fonction que de la température. Dès lors, la viscosité sera aussi une fonction de T et de t, et l'on a, en omettant l'indice v:

$$(7)\qquad \eta_v = \frac{\eta(T, t)}{\eta(T, \infty)}\cdot\frac{\eta(T, \infty)}{\eta(T_g, \infty)}\cdot\eta(T_g, \infty) = \frac{\eta(T, t)}{\eta(T, \infty)}\, a_T\eta_g\,,$$

où le second membre comporte 3 facteurs: le rapport des viscosités isothermes au temps t, et à l'équilibre: $a_T = \eta(T)/\eta(T_g)$, qui ne dépend que de T; et η_g qui est la viscosité du liquide surfondu à une température de référence T_g, sans spécification aucune.

Explicitons ces facteurs à l'aide des relations (6), en précisant:

$$(8)\qquad f = \frac{v - v_0}{v_\infty} = \frac{v - v_\infty}{v_\infty} + \frac{v_\infty - v_0}{v_\infty} = f_T + \frac{v - v_\infty}{v_\infty}\,,$$

où f_T ne dépend que de T, on a

$$\ln\frac{\eta(T,t)}{\eta(T,\infty)} = B\left(\frac{1}{f}-\frac{1}{f_T}\right) = -\frac{Bv_\infty(v-v_\infty)}{(v-v_0)(v_\infty-v_0)} \equiv -s\,. \tag{9}$$

En posant, d'autre part:

$$\left\{\begin{array}{l} f_T = f_g + \alpha_f(T-T_g)\,,\\ \text{où}\\ \alpha_f = \mathrm{d}f_T/\mathrm{d}T \approx \alpha-\alpha_g = \Delta\alpha\,, \end{array}\right. \tag{10}$$

on obtient pour a_T l'expression WLF [16], qui s'écrit:

$$\ln a_T = -\frac{(B/f_g)(T-T_g)}{(f_g/\alpha_f)+T-T_g}\,. \tag{11}$$

En combinant les formules (7) et (9) avec (5), et en réarrangeant, on obtient l'équation différentielle de la recouvrance:

$$\frac{\exp[-s]}{1-(f_T/B)s}\,\frac{\mathrm{d}s}{s} = -\frac{\mathrm{d}t}{a_T\,\tau_g}\,, \tag{12}$$

où $\tau_g = \eta_g/K$, est le temps de retard caractéristique du processus à T_g.

L'intégrale de cette équation dépend du signe de s, donc du signe de $(v-v_\infty)$, car f est toujours positif, et l'on obtient deux expressions différentes. Nous ne les reproduirons ici que sous des formes simplifiées. L'approximation est basée sur le fait que $(f_T/B)s$ est généralement petit devant l'unité, car nous avons écarté le cas $v_0 = v_\infty$. L'erreur ainsi introduite est en général inférieure aux erreurs de mesure [9].

1) Si $v > v_\infty$, c'est-à-dire si la recouvrance procède par *contraction* isotherme, donc $s > 0$, on a:

$$Ei(-s_i) - Ei(-s) - (f_T/B)(\exp[-s_i] - \exp[-s]) = \frac{t-t_i}{a_T\tau_g}\,. \tag{13}$$

2) Si $v < v_\infty$, c'est le cas de la *dilatation* isotherme, on a, en posant $s' = -s > 0$:

$$\overline{Ei}(s'_i) - \overline{Ei}(s') + f_T/B\,(\exp[s'] - \exp[s'_i]) = \frac{t-t_i}{a_T\tau_g}\,. \tag{14}$$

Dans ces expressions s_i et s'_i correspondent au volume initial v_i, les fonctions $Ei(-s)$, et $\overline{Ei}(s')$ sont des exponentielles intégrales tabulées [17].

4. – Comparaison entre théorie et expériences.

Les deux expressions (13) et (14) contiennent implicitement la variable expérimentale: $(v - v_\infty)/v_\infty$, que l'on ne peut pas mettre sous forme explicite, sauf si s tend vers zéro ou vers l'infini. Nous ne pouvons pas insister ici sur l'emploi des fonctions (13) et (14) qui a été discuté ailleurs [9], et sur lequel nous reviendrons [18]. Notons seulement que la forme de chaque isotherme est définie par l'unique paramètre f_T, que l'on peut déterminer à partir de l'amplitude initiale e_i, et de la tangente d'inflexion $\tilde{\beta}$ des isothermes [18]. C'est ainsi qu'une des courbes ($T = 27.5$ °C) de la Fig. 3 a été calculée à partir de la formule (13), avec une valeur de $f_T = 0.0165$. On voit que l'accord est tout à fait satisfaisant. La superposition de cette courbe et de l'isotherme expérimentale déterminent, d'autre part, la valeur de $a_T \tau_g$. Le *facteur de translation*, a_T, dépend non seulement de f_T, mais aussi de f_g, c'est-à-dire de α_f (eq. (10)). Les isothermes de recouvrance dépendent donc (en admettant $B = 1$) de trois paramètres indépendants: f_g, α_f et τ_g. Toutefois, on ne doit pas considérer ces paramètres comme ajustables à volonté, car leur valeur est liée aux paramètres expérimentaux qui caractérisent le système vitreux. En effet, d'après ce que nous avons dit, f_g doit être de l'ordre de *l'excès* de volume du verre, par rapport au cristal; α_f est égal à $\Delta\alpha$; et τ_g, de l'ordre du temps t_i, qui caractérise l'échelle expérimentale des temps qui, elle, définit la température de transition T_g (τ_g).

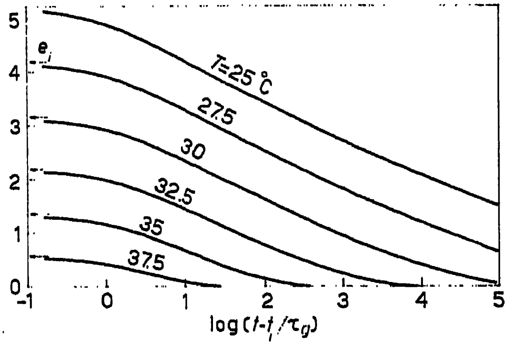

Fig. 7. – Isothermes de contraction du PVA II, calculées d'après la formule (13) avec $f_{27.5} = 0.0165$, et $\alpha_f = 4.2 \cdot 10^{-4}$/°C, pour $T_0 = 40$ °C (voir Fig. 3).

La Fig. 7 montre pour l'échantillon PVA II les isothermes de contraction calculées à partir de la valeur f_T, indiquée plus haut pour $T = 27.5$ °C, et $\alpha_f = 4.2 \cdot 10^{-4}$/°C, en laissant la valeur de τ_g indéterminée. Rappelons que pour cet échantillon $\Delta\alpha = 4.4 \cdot 10^{-4}$/°C. Ce réseau de courbes devrait pouvoir se superposer, *en bloc*, aux isothermes de la Fig. 3. Cette superposition est tout-à-fait satisfaisante, et la valeur de τ_g (c'est-à-dire τ_{40} dans ce cas précis) qui en résulte est égale à (0.015 ± 0.005) h, qui est bien du même ordre de grandeur que le temps $t_i = 0.01$ h. Il semble, cependant, que l'accroissement systématique de τ_g (de 0.01 à 0.02 h), lorsque l'on superpose les isothermes correspondant à des températures décroissantes, soit supérieur aux erreurs de mesure. Nous reviendrons sur ce point plus loin.

Les isothermes de contraction du glucose ont été calculées de la même manière à partir des paramètres suivants $f_g = 0.0252$, $\alpha_f = 3.6\cdot10^{-4}/°C$ et $\tau_g = (0.015 \pm 0.05)$ h; $T_g(\tau_g)$ étant égal à 35.5 °C. La Fig. 8 montre l'excellent accord entre ces isothermes et les points expérimentaux. On doit noter, cependant, que cet accord a été obtenu en admettant pour α_f une valeur nettement supérieure à $\Delta\alpha \approx 2.8\cdot10^{-4}/°C$. Un examen critique des résultats montre [18] qu'il convient mieux d'adopter: $\alpha_f = 3.0\cdot10^{-4}/°C$, et d'admettre que τ_g varie avec T, en associant à cette variation une énergie d'activation de l'ordre de 30 kcal/mole. Ce qui constitue l'introduction d'un paramètre supplémentaire. Nous avons supposé, en effet, avec **Doolittle**, que la viscosité ne dépend que du volume. Or, dans les calculs de la recouvrance la variation de viscosité intervient par deux facteurs (formule (7)): $-s$, et a_T; le premier mesurant la variation isotherme de η_v, le second sa variation à différentes températures, et à l'équilibre de volume. La variation importante de τ_g, dans le cas du glucose, montre qu'il existe une contribution propre de la température qui, tout en restant relativement petite (environ $\frac{1}{6}$ de l'effet total), ne peut être négligée. En réexaminant sous cet angle les résultats obtenus avec le PVA II, on trouve que la contribution propre de la température est de l'ordre de 8 kcal/mole seulement, ce qui correspond à la petite variation de τ_g signalée précédemment.

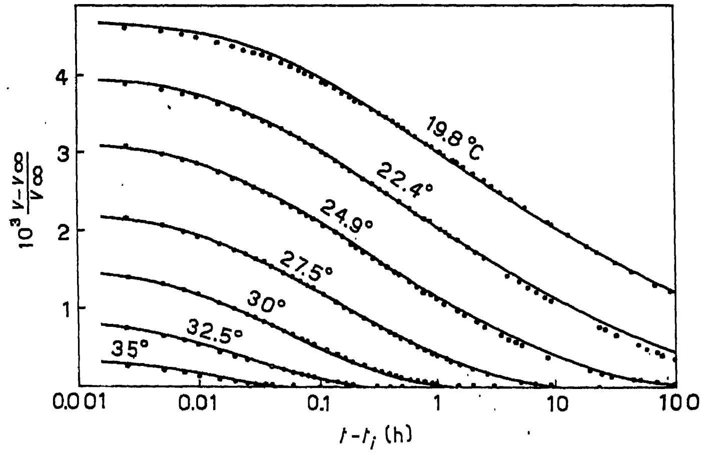

Fig. 8. – Isothermes de contraction calculées du glucose comparées aux résultats experimentaux. Paramètres: $f_{35.5}=0.0252$; $\alpha_f=3.6\cdot10^{-4}/°C$, et $0.01 \leqslant \tau_g \leqslant 0.02$ h.

On doit noter aussi, qu'en appliquant la relation de WLF (11) aux résultats obtenus par **Parks** [19] sur la variation de la viscosité de cisaillement du glucose, en fonction de T, on obtient pour $f_{35} \approx 0.0235$ et $\alpha_f \approx 3.2\cdot10^{-4}/°C$, en ayant déduit la contribution propre de la température. L'accord entre ces mesures et les nôtres est donc tout à fait satisfaisant. Enfin, l'excès de volume du glucose vitreux par rapport à sa forme cristalline est de l'ordre de 0.02 ± 0.003 (selon différentes estimations). Cette valeur est comparable à celles de f_g, évaluées plus haut à partir de deux séries de mesures.

L'accord entre théorie et expériences est loin d'être aussi satisfaisant pour les isothermes de dilatation. En effet, celles ci sont nettement *moins autocatalytiques* que les isothermes calculées avec les valeurs de f_g, obtenues précédemment. En ajustant le paramètre f_g on peut, certes, améliorer cet accord, mais pour ce faire on doit introduire des valeurs de l'odre de 0.04 qui sont beaucoup trop grandes, et incompatibles avec les isothermes de contraction. Nous avons interprété ce désaccord par une distribution des temps de retard, négligée dans ces calculs, dont l'effet est de *ralentir* le phénomène de recouvrance quel que soit le signe de $(v - v_\infty)$. L'existence d'une telle distribution se manifeste aussi lors des expériences de recouvrance après des traitements thermiques plus complexes [3, 6, 9], que ceux rapportés ici. L'introduction d'une telle distribution dans les calculs nécessite la spécification des mouvements coopératifs des unités structurales du liquide, et leur contribution à la compressibilité, peu connus à l'heure actuelle. On peut seulement affirmer que l'effet d'une distribution des temps de retard est, comparativement, plus important pour la dilatation isotherme que pour la contraction. De même, on peut conclure, que le fait dominant, dans les expériences de recouvrance des verres, est la variation de la viscosité avec le volume, variation dont l'effet excède aussi bien l'effet de la température, que celui qui résulte d'une distribution des temps de retard des mouvements moléculaires.

RÉFÉRENCES

[1] F. Simon: *Erg. Exakt. Naturwiss.*, **9**, 222 (1930).
[2] W. Kauzmann: *Chem. Rev.*, **43**, 219 (1948).
[3] A. J. Kovacs: *Contribution à l'étude de l'évolution isotherme du volume des hauts polymères, Thèse, Fac. Sci. Paris* (1954).
[4] H. R. Ritland: *Journ. Am. Ceram. Soc.*, **37**, 370 (1954).
[5] J. H. Gibbs et E. A. Di Marzio: *Journ. Chem. Phys.*, **38**, 373, 807 (1958).
[6] A. J. Kovacs: *Journ. Polym. Sci.*, **30**, 131 (1958).
[7] J. E. McKinney, H. V. Belcher et R. S. Marvin: *Trans. Soc. Rheol.*, **4**, 347 (1960).
[8] R. O. Davies et J. O. Jones: *Proc. Roy. Soc.*, **A 217**, 26 (1953).
[9] A. J. Kovacs: *Phénomènes de relaxation et de fluage en rhéologie non linéaire*, edité par le CNRS (Paris, 1961), p. 191.
10] A. J. Kovacs: *Trans. Soc. Rheol.*, **5**, 285 (1961).
11] R. de L. Kronig: *Phys. Zeits.*, **39**, 823 (1938).
12] M. W. Volkenstein et O. B. Ptitsyn: *Journ. Techn. Phys. URSS*, **26**, 2204 (1956).

[13] N. Hirai et H. Eyring: *Journ. Polym. Sci.*, **37**, 51 (1959).

[14] G. Adam: *Kolloid Zeits.*, **180**, 11 (1962).

[15] A. K. Doolittle: *Journ. Appl. Phys.*, **22**, 1471 (1951).

[16] M. L. Williams, R. F. Landel et J. D. Ferry: *Journ. Am. Chem. Soc.*, **77** 3701 (1955).

[17] E. Jahnke et F. Emde: *Tables of Functions* (New York, 1945).

[18] A. J. Kovacs: *Adv. in Polym. Sci.*, en préparation.

[19] G. S. Parks, L. E. Barton, M. E. Spaght et J. F. Richardson: *Physics*, **5**, 193 (1934).

Variations des paramètres viscoélastiques du polyacétate de vinyle dans le domaine de sa transition vitreuse.

A. J. KOVACS

Centre de Recherches sur les Macromolécules - Strasbourg

J. D. FERRY

Department of Chemistry, University of Wisconsin - Madison, Wis.

1. – Introduction.

L'étude expérimentale et phénoménologique de la recouvrance des verres nous a montré que leur viscosité de volume, et les temps de retard des mouvements moléculaires qui y contribuent, dépendent essentiellement du volume libre [1]. Il était tentant de vérifier cette proposition en étudiant les variations des paramètres viscoélastiques de cisaillement dans le domaine de la transition vitreuse. On pouvait prévoir, en effet, que ces paramètres dépendent, comme le volume, de l'histoire thermique de l'échantillon. Plusieurs auteurs [2-4] ont déjà signalé de tels phénomènes, mais aucune étude systématique n'a été entreprise, à notre connaissance, afin de relier les variations des paramètres rhéologiques des verres à celles de leur volume.

Nous rapporterons ici les premières conclusions d'une telle étude faite avec un échantillon de polyacétate de vinyle (PVA II), de masse moléculaire (moyenne en poids), $M_w = 2.0 \cdot 10^6$. Elle concerne la mesure dynamique de la partie réelle (G') et imaginaire (G'') du module de cisaillement au cours de l'évolution spontanée des verres, et à l'équilibre de volume, lorsque ce dernier pouvait être obtenu dans un temps raisonnable.

Ces mesures ont été effectuées à l'aide d'un pendule de torsion à oscillations libres, réalisé par PLAZEK et ses collaborateurs [5] que nous avons adapté à nos buts [6]. L'intervalle des fréquences circulaires (ω) couvert s'étend de 0.7 à 40 rad/s. Le module d'élasticité (G'), et la tangente de l'angle de perte

($\operatorname{tg} \delta = G''/G'$), ont été déterminés selon le procédé classique [7] à partir de la mesure de la fréquence, et du décrément logarithmique des oscillations, en tenant compte de diverses corrections [6].

2. – Résultats expérimentaux.

2·1. *Mesures à l'équilibre de volume.* – L'échantillon utilisé atteint son équilibre de volume à 30 °C au bout d'un mois seulement. Par contre, au dessus de 39 °C la technique de mesure devient inutilisable par suite de l'accroissement de tg δ, qui dépasse 0.4.

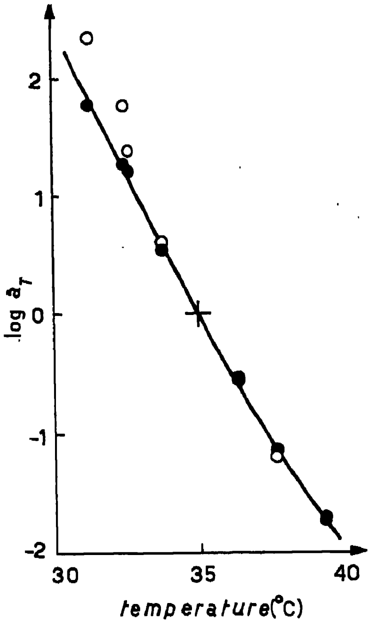

Fig. 1. – Log a_T en fonction de T, obtenu à partir de la superposition des isothermes de G' (cercles noirs), et de tg δ (cercles blancs). Courbe calculée à partir de la formule de WLF, avec $f_{35} = 0{,}0225$, et $\alpha = 5.3 \cdot 10^{-4}/°C$. Température de référence 35 °C.

En portant G' et tg δ en fonction de log ω nous avons obtenu 9 courbes isothermes pour ces deux paramètres entre 30 et 39 °C, dont certaines sont reproduites sur les (Fig. 6 et 7. Ces isothermes d'équilibre peuvent être superposées par translation le long de l'axe de log ω, aux erreurs près; on obtient ainsi une courbe composite.

La translation mesure le rapport de l'échelle des fréquences en fonction de la température T. Sur la Fig. 1 nous avons porté ces rapports, a_T, en adoptant comme référence l'isotherme obtenue à 35.0 °C.

Cette figure montre qu'au dessus de 33 °C, environ, les valeurs de log a_T déduites de la translation des isothermes de G', et de tg δ coïncident, aux erreurs près, mais elles divergent sensiblement au dessous de cette température, de sorte que la méthode de réduction des fréquences n'est plus applicable dans cette région de T.

Au dessus de 33 °C, la formule WLF [8]:

$$(1) \qquad \log a_T = - \frac{(1/2.303 f_{35})(T - 308{,}2)}{(f_{35}/\alpha_f) + T - 308.2},$$

où f_{35} est la *fraction libre du volume* à 35 °C (308.2 °K), et α_f son coefficient de dilatation, représente bien la variation de log α_T. Toutefois, il est impossible de préciser la valeur de ces deux paramètres simultanément, car l'intervalle de température est très petit; seulement le rapport f_{35}^2/α_f peut être connu, à partir de la tangente d log a_T/dT, à 35 °C, avec une précision suffisante. Nous avons trouvé pour ce dernier: $f_{35}^2/\alpha_f = (0.95 \pm 0.04)$ °C.

Lors de l'étude des isothermes de contraction de volume nous avons trouvé [1] pour les deux paramètres de la relation WLF: $f_{35}^2 = 0.0196$, et $\alpha_f = 4.2\cdot10^{-4}/°\mathrm{C}$, pour le même échantillon, de sorte que le rapport $f_{35}^2/\alpha_f = 0.92\,°\mathrm{C}$, valeur sensiblement égale à celle déduite de G' et $\mathrm{tg}\,\delta$ (Fig. 1). Ce résultat montre que les variations thermiques de la viscosité de volume, et celle de cisaillement sont sensiblement égales dans la zone de transition vitreuse, et que ces deux coefficients de viscosité obéissent à la formule (1), dérivée de la relation de Doolittle [9].

L'étude de la variation de G' et de $\mathrm{tg}\,\delta$ au cours de la contraction isotherme de l'échantillon trempé permet, cependant, comme nous le montrerons plus loin, de préciser le seul paramètre α_f, et nous avons trouvé ainsi: $\alpha_f = (5.3 \pm 0.2)\cdot10^{-4}/°\mathrm{C}$, d'où il résulte: $f_{35} = 0.0225$. Ce couple de valeurs est sensiblement supérieur à celui obtenu précédemment à partir des courbes de recouvrance de volume [1], et nous reviendrons sur les causes possibles de ce désaccord. Notons pourtant que la courbe de la Fig. 1, tracée à partir de la formule (1), et des dernières valeurs de f_{35} et α_f, ne diffère que d'une manière imperceptible de celle qu'on obtient avec $f_{35} = 0.0196$, et $\alpha_f = 4.2\cdot10^{-4}/°\mathrm{C}$. En fait, cette courbe calculée satisfait toutes les valeurs de $\log a_T$ déduites de G' et des isothermes de contraction (*).

En portant les valeurs de G' et G'' en fonction de la fréquence réduite à 35 °C, selon les valeurs de a_T calculées à partir de la formule (1), on obtient une courbe composite unique pour G' (Fig. 2). Cependant, pour G'' les branches de courbes correspondant à des températures inférieures à 33 °C se placent *parallèlement, mais au dessous* de la courbe composite. Notons que les valeurs absolues de G' et G'' correspondent bien aux mesures antérieures de WILLIAMS et FERRY [10], effectuées entre 45 et 90 °C à l'aide d'une technique différente, et sur un autre échantillon de PVA.

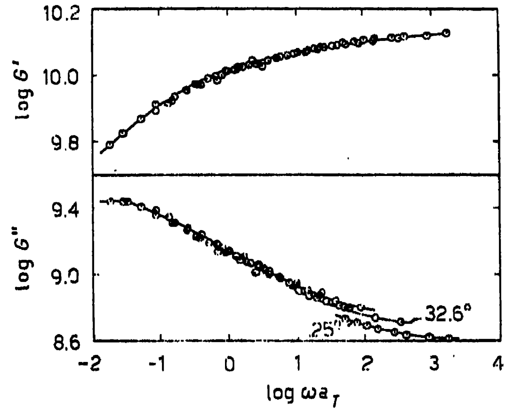

Fig. 2. – Courbes composites de G' et G'', réduites à 35 °C. L'orientation du rayon des cercles blancs indique la température; rayon vers le haut: 31.25°, et respectivement par rotation de 45° dans le sens des aiguilles d'une montre: 32.45°, 32.6, 33.8, 35.0, 35.05, 36.35, 37.6 et 39.2 °C.

On peut calculer à partir des courbes de la Fig. 2 la portion du spectre des temps de relaxation H [6], qui prolonge celui obtenu précédemment [10] de

---

(*) Réf. [1], Fig. 3 et 7.

quatre décades, vers les temps courts. Dans cette région le spectre atteint un plateau dont la hauteur s'abaisse par suite du dédoublement des courbes de G'' (Fig. 2) au dessous de 33 °C. Cette anomalie, nous le verrons, peut être associée aussi à un effet de la diminution du volume libre.

2'2. *Mesures pendant l'évolution isotherme du volume.* – La Fig. 3 montre la variation isotherme de tg δ en fonction du temps t, pour un échantillon trempé à partir de 45 °C (en équilibre), à différentes températures T, indiquées. La technique de la trempe est sensiblement différente dans ces expériences de celle utilisée en dilatométrie [1], car l'échantillon n'atteint son équilibre thermique dans l'appareil de torsion qu'au bout de 30 minutes environ. Aussi a-t-on procédé en deux étapes: trempe rapide de 45 °C à la température du laboratoire (~ 27 °C), puis installation de l'échantillon dans le pendule de torsion, préchauffé à T. Ces deux opérations durent environ 10 minutes; cependant, l'équilibre thermique n'est atteint que 30 minutes après l'installation.

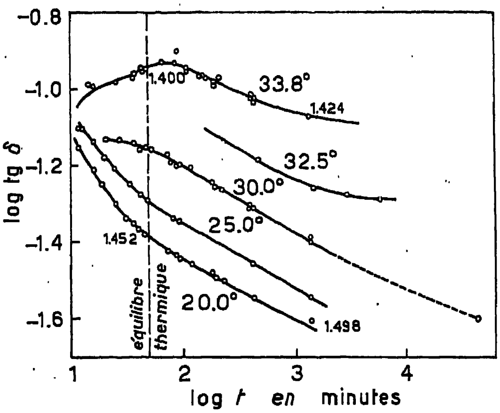

Fig. 3. – Variation de tg δ à différentes températures T, en fonction du temps, après la trempe de l'échantillon. Les chiffres de petite taille indiquent quelques valeurs de ω.

Ces courbes partent toutes des environs d'une même valeur de tg δ, montrant la reproductibilité du traitement, puis tendent vers leurs isothermes respectives au fur et à mesure que la température de l'échantillon s'approche de T. Des traitements similaires faits avec un dilatomètre montrent que des effets secondaires dûs au retard de l'établissement de l'équilibre thermique disparaissent au bout de 1 à 2 heures, et la contraction isotherme coïncide pratiquement avec celle observée après trempe brusque.

Dans ces régions de temps, les courbes deviennent sensiblement linéaires, et leur pente $(\partial \log \mathrm{tg}\, \delta / \partial \log t)_T$, peut être comparée aux pentes des tangentes d'inflexion $\bar{\beta} = -(\partial v/\partial \cdot v \log t)_T$ des isothermes de contraction (*).

La fréquence des oscillations pendant ces mesures n'étant pas rigoureusement constante ($1.38 < \omega < 1.5$), la Fig. 3 indique quelques valeurs individuelles. Ces variations de ω n'ont qu'une influence négligeable sur les valeurs de tg δ; elles correspondent à la variation de G' avec le temps, représentée sur la Fig. 4.

(*) Réf. [1], Fig. 3.

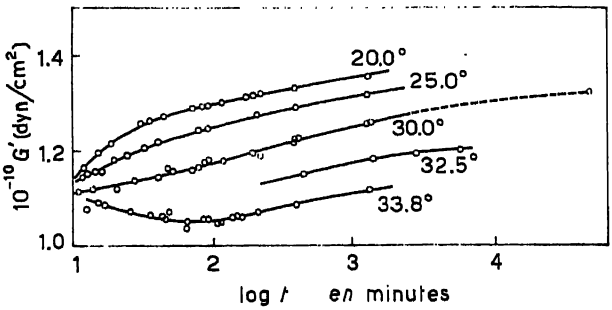

Fig. 4. – Variation isotherme de G' en fonction du temps (voir Fig. 3).

Les Fig. 3 et 4 montrent clairement que l'effet d'une prolongation du temps de séjour sur la variation isotherme de G' et tg δ, est équivalent à celui d'une diminution de la température, dans des conditions d'équilibre. Notons aussi que ces deux paramètres atteignent leurs valeurs limites, ($T \geq 32.5$), sensiblement en même temps que le volume atteint son équilibre (*).

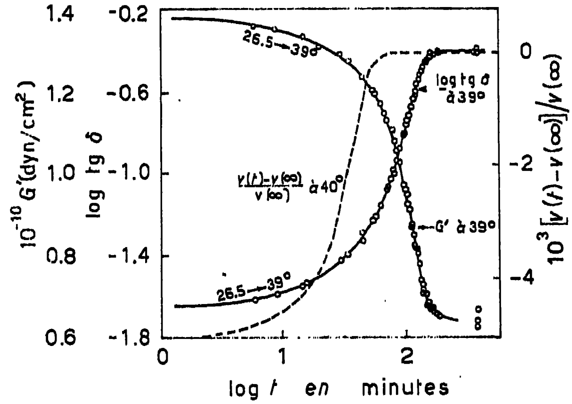

Fig. 5. – Variation de G', et de tg δ, pendant la dilatation isotherme à 39 °C, en fonction de log t. En pointillés: dilatation isotherme à 40 °C.

La Fig. 5 représente les variations de G', et tg δ, en fonction de log t, pour un échantillon qui a été maintenu à la température du laboratoire (27 ± 2 °C) pendant environ deux mois, et réchauffé après, à 39 °C, dans le pendule de torsion. Ici encore, l'équilibre thermique n'est atteint qu'au bout d'environ 40 minutes, mais l'on constate que les variations de G' et tg δ s'accélèrent et deviennent autocatalytiques *après* ce temps. La courbe en pointillé représente la dilatation isotherme du volume d'un échantillon similairement conditionné, et rapidement réchauffé à 40 °C (**).

(*) Ref. [1], Fig. 3.

(**) Cette courbe est comparable à celle de la Fig. 6 de la ref. [1] pour $t_1 \simeq 1500$ h.

Ces résultats montrent non seulement que les paramètres de cisaillement suivent une évolution parallèle au volume, mais aussi que c'est le volume libre qui contrôle essentiellement ces évolutions [1].

3. – Discussion des résultats.

Si l'on admet que les paramètres viscoélastiques dépendent des trois variables, T, ω et t, on a par exemple pour G':

$$\mathrm{d}G' = (\partial G'/\partial \log \omega)_{T,t}\, \mathrm{d} \log \omega + (\partial G'/\partial T)_{\omega,t}\, \mathrm{d}T + (\partial G'/\partial \log t)_{T,\omega}\, \mathrm{d} \log t\,. \tag{2}$$

On peut définir, à ω constant (ce qui correspond essentiellement aux conditions expérimentales des Fig. 3 et 4), une ***dérivée de corrélation***: $(\partial \log t/\partial T)_{G',\infty}$, qui compare les effets du temps à ceux de la température par:

$$(\partial \log t/\partial T)_{G',\infty} = -\,(\partial G'/\partial T)_{t=\infty}\big/(\partial G'/\partial \log t)_T \tag{3}$$

où les dérivées partielles du 2ème membre peuvent être évaluées à partir des expériences à l'équilibre: $(\partial G'/\partial T)_{t=\infty}$, et celles représentées par la Fig. 4 On obtient aussi d'une manière analogue: $(\partial \log t/\partial T)_{\mathrm{tg}\,\delta,\infty}$.

Si G', et $\mathrm{tg}\,\delta$ ne dépendent que du volume libre, on devrait avoir:

$$(\partial \log t/\partial T)_{G',\infty} = (\partial \log t/\partial T)_{\mathrm{tg}\,\delta,\infty} = (\partial \log t/\partial T)_{f,\infty} \tag{4}$$

où

$$(\partial \log t/\partial T)_{f,\infty} = -\,(\partial f/\partial T)_{t=\infty}\big/(\partial f/\partial \log t)_T = \alpha_f/\beta\,. \tag{5}$$

En comparant ces diverses valeurs déduites des expériences, et en considérant α_f comme inconnu, on obtient [6] pour ce dernier: $5.3\cdot10^{-4}$/°C. Cette valeur dépasse de $9\cdot10^{-5}$/°C *l'excès* du coefficient de dilatation, $\Delta\alpha = 4.4\cdot10^{-4}$/°C, du liquide surfondu par rapport à celui du verre, α_g, excès qui correspond phénoménologiquement au coefficient de dilatation du volume libre [1].

Parmi les diverses interprétations possibles de ce désaccord, nous ne mentionnerons ici que celle qui nous semble la plus plausible; elle revient à admettre que dans *l'effet total* de la température, seulement une partie est dûe à la variation du volume libre, la fraction résiduelle (environ 20 %) devant être attribuée à un effet pur de T, opérant à volume libre constant. On a ainsi pour G', par exemple,

$$\left(\frac{\partial G'}{\partial T}\right)_{t=\infty} = \left(\frac{\partial G'}{\partial T}\right)_f + \left(\frac{\partial G'}{\partial f}\right)_T \left(\frac{\partial f}{\partial T}\right)_{t=\infty}, \tag{6}$$

où évidemment ω est constant, et $t = \infty$ (équilibre). On peut écrire une expression similaire à (6) aussi pour $\operatorname{tg} \delta$ (ou G''), dans laquelle la contribution pure de la température n'a pas nécessairement la même importance que pour G'.

Il est peu probable que cette contribution résulte d'un processus activé, car l'énergie d'activation correspondante (~ 40 kcal/mole) serait nettement supérieure à celle trouvée précédemment [1]. Par contre, une variation de G', et de $\operatorname{tg} \delta$, peut résulter des modifications, provoquées par une variation de T, des mouvements vibratoires anharmoniques des particules élémentaires du verre, comme cela se produit aussi dans les milieux cristallins; la contribution de ces oscillations au coefficient de dilatation est mesurée par $\alpha_g \approx \alpha_{\text{crist.}}$ [1].

L'existence d'une telle contribution a été d'ailleurs mise en évidence par Litovitz et ses collaborateurs [11] pour les liquides organiques excités par des ultrasons. Ces auteurs ont montré, en effet, que l'élasticité dans le domaine vitreux est d'origine « énergétique », et non pas « entropique », (comme c'est le cas des caoutchoucs), et d'autre part, qu'il convient d'admettre un coefficient de température *négatif* de l'ordre de 10^8 dyne/cm$^2 \cdot$°C pour le module vitreux G_∞, mesuré aux très hautes fréquences.

Il semble qu'un tel coefficient serait susceptible de réduire la majeure partie du désaccord signalé à propos de α_f et $\Delta\alpha$, mais cette interprétation devrait être confirmée par de nouvelles mesures.

Quoi qu'il en soit, le couple de valeurs des paramètres $f_{35} = 0.0225$ et $\alpha_f = 5.3 \cdot 10^{-4}/°\text{C}$, permet de rendre compte de tous nos résultats, aux erreurs près, en attribuant une fraction ($\sim 1/5$) de ce dernier paramètre à une contribution pure de la température.

4. – Superposition des isothermes de non-équilibre.

En mesurant G' et $\operatorname{tg} \delta$ pour différentes fréquences ω, au cours de la contraction isotherme à 20, 25 et 30 °C, on peut porter les valeurs de ces paramètres, correspondant à *un même temps* t, après la trempe, en fonction de $\log \omega$. Les Fig. 6 et 7 représentent ces courbes à 20 et à 30 °C, pour des temps $t = 50$, 100, 200, 400 et $1360 \div 1380$ minutes. Ces isothermes de non-équilibre, mais correspondant au « même âge » de l'échantillon, forment une famille de courbes cohérentes, et sensiblement parallèles aux isothermes « d'équilibre » (en traits pleins) obtenues aux différentes températures indiquées.

Ce parallélisme suggère l'emploi de la « température fictive », proposée par Tool [12], comme variable de réduction. Par exemple, l'isotherme à 20 °C, pour $t = 200$ min, de la Fig. 6, a pour température fictive 30 °C. Phénoménologiquement cette variable de réduction est équivalente au volume libre, et conduit à des conclusions similaires. Nous préférons utiliser, cependant, ce dernier concept, de signification physique plus directe, et d'un emploi plus commode.

On peut définir, en effect un facteur de réduction $a_{T,t}$, comme mesurant le rapport d'un temps de relaxation quelconque, (à une température T, et au temps t), à la valeur qu'il a dans un état de référence. Pour ce dernier nous prendrons encore l'état d'équilibre à 35.0 °C. On peut écrire ainsi à partir de la relation de Doolittle [1, 9)]:

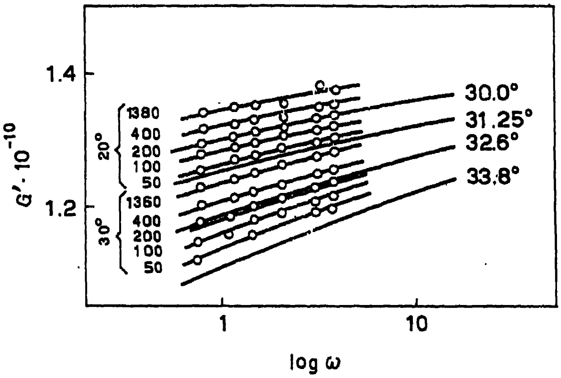

Fig. 6. – Variation de G' en fonction de $\log \omega$, à 20 et 30 °C, au cours de la contraction isotherme, aux temps indiqués après la trempe. Les traits pleins correspondent aux conditions d'équilibre de volume, à différentes températures indiquées.

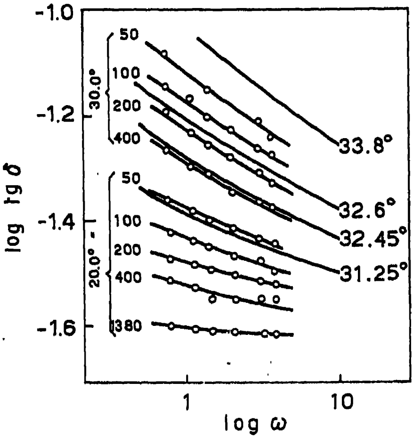

Fig. 7. – Variation de $\log \operatorname{tg} \delta$ en fonction de $\log \omega$ au cours de la contraction isotherme, comme sur la Fig. 6.

$$\log a_{T,t} = (1/2.303)(1/f_{T,t} - 1/f_{35,\infty}) \tag{7}$$

et

$$f_{T,t} = f_{35,\infty} + \alpha_f(T - 308.2) + [(v_t - v_\infty)/v_\infty]_T \tag{8}$$

où le dernier terme du second membre est *l'excès* (relatif) du volume du verre (à T, et au temps t) par rapport à sa valeur d'équilibre, que nous avons mesuré par dilatométrie [1].

La Fig. 8 montre les résultats de cette réduction pour G', à partir des valeurs de la Fig. 6, incluant aussi les mesures faites à 25 °C. Le facteur de réduction des fréquences $a_{T,t}$ a été calculé à partir des expressions (7) et (8) (en prenant $f_{35,8} = 0.0225$, et $\alpha_f = 5.3 \cdot 10^{-4}$/°C), et les résultats des expérien-

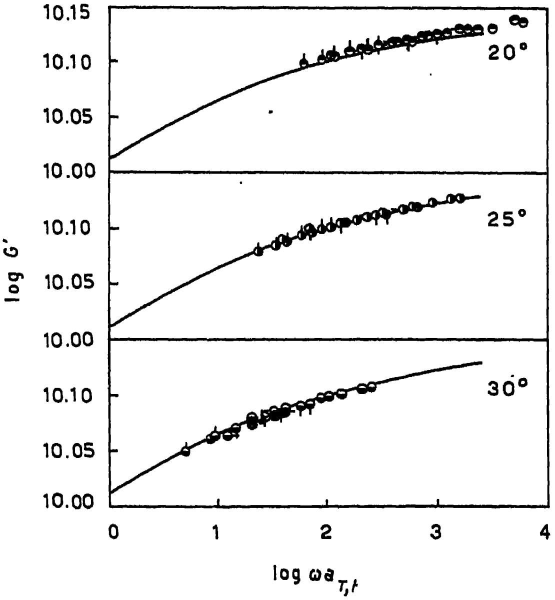

Fig. 8. – Valeurs de G' en fonction de la fréquence réduite calculée, pour des expériences de non-équilibre de la Fig. 6. Le trait plein représente la courbe composite de la Fig. 2.

ces dilatométriques (*). La courbe en trait plein reproduit chaque fois celle de la Fig. 2, obtenue dans des conditions d'équilibre de volume. On remarquera que les valeurs de G' coïncident, aux erreurs près, avec la courbe d'équilibre, quels que soient T et t; ce qui confirme la cohérence de la méthode de réduction, et les valeurs des paramètres utilisés.

En ce qui concerne G'' (Fig. 9) les divergences sont analogues à celles signalées précédemment pour des courbes d'équilibre aux températures infé-

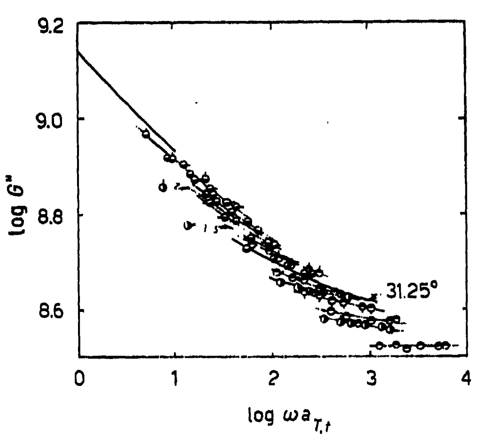

Fig. 9. – Valeurs de G'' en fonction de la fréquence réduite calculée pendant la contraction isotherme. Les courbes en gros traits correspondent aux conditions d'équilibre (Fig. 2).

(*) Réf. [1], Fig. 3.

rieurs à 33 °C (Fig. 2). Le dédoublement de ces courbes reflète la dépression progressive du plateau du spectre H pour des temps de relaxation courts [6]. La similarité de cette dépression dans les expériences d'équilibre, et de non-équilibre, suggère que cette anomalie est associée aussi à la variation du volume libre. En mesurant la séparation verticale, $\Delta \log G''$, par rapport à la courbe d'équilibre composite, obtenue au dessus de 33 °C (Fig. 2), on constate, en effet, que les valeurs de $\Delta \log G''$ se placent toutes sur une même courbe si on les porte en fonction de $f_{T,t}$ (éq. (8)), quels que soient T et t. Cependant, à l'heure actuelle, nous ne pouvons donner aucune interprétation à ce phénomène.

RÉFÉRENCES

[1] A. J. Kovacs: *Ce volume*, p. 401.
[2] G. S. Parks *et al.*: *Physics*, **5**, 193 (1934).
[3] J. R. McLoughlin et A. V. Tobolsky: *Journ. Polym. Sci.*, **7**, 658 (1951).
[4] M. Prod'homme: *Verres et Réfractaires*, **14**, 261 (1960).
[5] D. J. Plazek, M. N. Vrancken et J. W. Berge: *Trans. Soc. Rheol.*, **2**, 39 (1958).
[6] A. J. Kovacs, R. S. Stratton et J. D. Ferry: *Journ. Phys. Chem.*, **67**, 152 (1963).
[7] L. E. Nielsen: *Bull. Am. Soc. Testing Materials*, **165**, 48 (1950).
[8] J. D. Ferry: *Viscoelastic Properties of Polymers* (New York, 1961), Chap. 11, p. 225.
[9] A. K. Doolittle: *Journ. Appl. Phys.*, **22**, 1471 (1951).
[10] M. L. Williams et J. D. Ferry: *Journ. Coll. Sci.*, **9**, 479 (1954).
[11] R. Meister, C. J. Marhoeffer, R. Sciamanda, L. Cotter et T. Litovitz *Journ. Appl. Phys.*, **31**, 854 (1960).
[12] A. Q. Tool: *Journ. Res. Natl. Bur. Stand.*, **37**, 73 (1946).

Relaxation of Lattice Imperfections in Solids.

P. G. Bordoni

Facoltà di Ingegneria dell' Università - Roma

1. – Introduction.

The most striking property of solid bodies is the regularity of their lattice structure. This regularity is directly related to some well-known phenomena, such as the fixed value of the melting point and the diffraction of X-rays. When we go deeper into solid state physics we see that some aspects of the macroscopic behavior cannot be reconciled with the simple picture of a perfect geometrical lattice. For instance the shear stress required to break a crystal is some orders of magnitude smaller than the force computed according to such a model. Another instance is that of the electrical resistivity at low temperatures, which is very different from the resistivity computed for a perfect solid. Moreover a perfect crystal would not grow from the melt or from an electrolytic solution.

To reconcile these facts with the obvious evidence of a regular structure afforded by the X-ray experiments we must assume the existence of lattice imperfections. Their number cannot be large enough to cancel the regular character of the lattice, but must be sufficient to explain the substantial deviations between the observed values of some macroscopic properties and the values computed for an ideal crystal.

According to Seitz's classification the lattice imperfections which are presently known belong to six fundamental classes: i) phonons, ii) electrons and holes, iii) excitons, iv) vacant lattice sites and interstitial atoms, v) foreign atoms in either interstitial or substitutional positions, vi) dislocations. Some of them may eventually combine to form more complex imperfections such as for instance couples or clusters of vacancies or foreign atoms trapped by dislocations. From a purely geometrical standpoint lattice imperfections may also be classified as: *a*) point imperfections (interstitial, Schottky defect, Frenkel defect), *b*) line defects (edge or screw dislocation), *c*) plane defects (lineage boundary, grain boundary, stacking fault).

In ideal crystals elastic waves would propagate without energy loss. To say better no mechanism is presently known which could give rise to a dissipation of elastic energy in a perfect lactice. If a vibration mode of such a lattice were excited, the vibration amplitude would be constant in time, with no external force applied; the resonance coefficient Q would be infinitely large, and the corresponding logarithmic decrement $d = \pi \cdot Q^{-1}$ zero.

In real crystals with lattice imperfections (or in polycrystalline solids) the imperfections interact with elastic waves and subtract energy from them. This amounts to say that the phonons of the elastic waves collide with the imperfections and the collisions on the average are not perfectly elastic. After more or less complex processes the energy subtracted is converted into heat. An elastic wave is then attenuated during its propagation or, if a vibration mode is excited, energy must be continuously supplied by an esternal vibromotive force to keep the vibration amplitude constant. If this is not done the vibrations decay exponentially. It may be convenient to remember that the logarithmic decrement d gives the ratio between the energy ΔU dissipated in half a vibration period and the total vibration energy U.

$$d = \frac{\Delta U}{U} = \pi Q^{-1} . \tag{1}$$

The interaction between the lattice imperfections and the elastic waves, in addition to its own physical significance, is important because it gives us a very simple and efficient means to evaluate the number, the distribution and the basic properties of lattice imperfections. Moreover it is possible to follow the formation of lattice imperfections as a result of permanent strain, or their inactivation due to thermal treatments. According to the above remarks this may be done in two ways: measuring the attenuation coefficient of elastic waves or the decrement of the vibration modes. The first way, which is so convenient for liquids and gases, is less suitable for investigations in solid state, as in this case the optical methods can seldom be applied. The interaction between the lattice imperfections and the elastic vibrations is better evaluated by means of resonance methods, and the actual technique makes it possible to measure the resonance coefficient Q and/or the logarithmic decrement d over a wide range of temperatures and frequencies, even when the fraction of the energy dissipated in half a period does not exceed 10^{-5} of the total vibration energy. For this reason the inverse Q^{-1} of the resonance coefficient is usually taken as a measure of energy dissipation in solids and is often called dissipation coefficient. For comparison it may be useful to compute the attenuation coefficient α which measures the decrease of vibration amplitude with space; this may be done by means of the well-known formula

$$\alpha = \frac{d}{\lambda} = \frac{\pi Q^{-1}}{\lambda} , \tag{2}$$

where λ is the wavelength of vibrations and α is measured in $\mathrm{Np \cdot cm^{-1}}$.

In the following a diffusion theory will be outlined to explain the interaction between lattice imperfections and the elastic waves. This theory may be directly applied to some simple types of interactions such as those due to interstitials and to dislocations. Moreover it may be used as a starting point to explain more complex interactions, like those due to conduction electrons in metals. Some information will finally be given concerning the best-known types of interaction (interstitial, electron, and dislocation), and showing how the distribution and behavior of these imperfections can be evaluated by means of dissipation measurements.

2. – Diffusion of lattice imperfections.

When no external forces are applied to a crystal (or to a polycrystalline body) its macroscopic natural equilibrium state corresponds to a *natural statistic equilibrium* of the lattice and of its imperfections. This means that all the equally possible positions for a certain type of imperfection are occupied by this imperfection for nearly the same time. For instance if the equally possible positions of an interstitial impurity such as carbon are the octahedral positions of a bcc lattice like the iron lattice, each atom spends approximately the same fraction of its time in each of the possible positions. Another instance is that of a straight dislocation line lying along one of the crystallographic directions. When the solid is in natural equilibrium the dislocation line is trapped in its position by two potential barriers which have the same height for symmetry reasons. Under the influence of thermal agitation a segment of the dislocation line may eventually jump into one of the nearest crystallographic directions (Fig. 1). The time spent by the dislocation on each side of its equilibrium position is the same, owing to the symmetry, and therefore the thermal motion of dislocation segments does not produce, on the average, any macroscopic strain of the crystal.

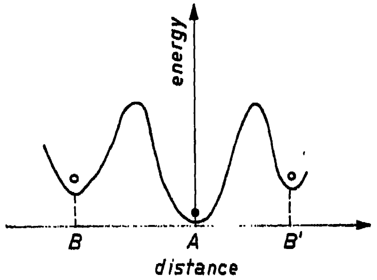

Fig. 1. – Motion of a dislocation segment from its equilibrium position A into the nearest crystallographic lines B, B'.

When an external force is applied to the crystal we must consider two basically different cases. If the force and the symmetry of the crystal are such that the atomic lattice changes its size without deformation (pure compression or pure expansion), the natural distribution of lattice imperfections is still in equilibrium with the crystal, as the distribution cannot depend upon the absolute values of the interatomic distances in the different directions, but only upon their ratios, that is upon the shape of the crystal lattice *Hence no effect due to the presence of lattice imperfections can be expected for a strain of this type.* This result is of fundamental importance for the theory of the interaction between imperfections and elastic waves.

The other case which must be considered is that of an external force giving rise to some deformation of the lattice. In this case the natural distribution of imperfections is no longer in equilibrium with the deformed crystal, as all the possible positions are no more equally possible. For instance when a bcc lattice is extended in one direction, some of the octahedral positions are more easily occupied by interstitial atoms. Hence, when the crystal is deformed, an interstitial impurity will spend more time in some of the octahedral positions than in the others. In the same way, if the external force gives rise to a shear stress different from zero in the glide plain of a dislocation line, the potential barriers have no longer the same height on both sides, and the dislocation line will obviously spend more time on the side in which the barrier is lower. This means that each forced macroscopic equilibrium state of a solid corresponds to a *forced statistical distribution* of imperfections different from the natural distribution.

Lets now consider what happens when a finite stress is suddenly applied at the time $t = 0$ to a solid. Neglecting inertia effects (this can always be done provided the solid is small enough), the stress produces an instantaneous elastic strain which may be represented, like the stress, by a step function for the time $t = 0$. Owing to this strain, the natural distribution of imperfections is no longer in equilibrium with the deformed lattice; hence this distribution changes until a forced statistical equilibrium is reached. In other words there is a *diffusion of imperfections* from the natural to the forced equilibrium state. A very significant classification of these processes may be made according to the *distance* over which the diffusion takes place. A typical case is that of a diffusion over a *macroscopic* distance. A diffusion of this type takes place for instance when a thin rod is bent by suddenly applied forces. After the instantaneous elastic strain, the imperfections (in this case the thermal phonons) have a larger density in the compressed fibers of the rod than in the extended ones. A diffusion of thermal phonons (that is an exchange of heat) takes then place in a direction orthogonal to the rod axis, and the average diffusion distance is of the same order as the thickness of the rod.

The opposite case is that of a diffusion taking place over a *microscopic* distance. This happens for instance when the imperfections are interstitial atoms or dislocations. In both cases the average diffusion distance is of the order of the interatomic distance. A third case is also worth of notice, that of a *semi-macroscopic* diffusion. If we consider a polycrystalline solid which undergoes a simple extension, the elastic strain of adjacent grains is slightly different, owing to their different orientation. This gives rise to slight differences of temperature, and to a diffusion of thermal phonons over a distance which is of the order of the average grain size.

All the above types of diffusion have the following common properties:

i) they give rise to *a macroscopic strain*;

ii) the strain produced is not *instantaneous*, like the elastic strain, but *tends asymptotically to its final value.*

The point i) is quite easily understood with reference to the case of dislocations. If all the dislocations in a plane spend more time on one side than on the other, owing to the shear stress which lowers one of the barriers with respect to the other, the total effect will be a *glide motion* of the half-crystal which is on one side of the plain with respect to the other half. The point ii) is also easy to understand with reference to the same case. The displacement of each atom due to the elastic strain is always very small in comparison with the interatomic distance, and vanishes with the strain. On the opposite a single imperfection must travel over a *finite distance*, which is at least of the order of the interatomic distance, to reach its forced equilibrium position, even when the strain is *infinitely small.* If we assume that imperfections travel with a speed of the same order as the velocity of the elastic waves (about 10^5 cm·s^{-1}) and we take 10^{-8} cm for the order of the interatomic distance, we see that the value of 10^{-13} s gives a *lower limit* for the diffusion time of lattice imperfections. It is also clear from the general principles of mechanics that, when a system tends towards an equilibrium state, this state cannot be reached in a finite time, but is approached asymptotically (*). Hence the macroscopic strain due to the diffusion of lattice imperfections must also tend asymptotically to a finite value. According to the accepted terminology a strain of this type is called anelastic (**) (Fig. 2).

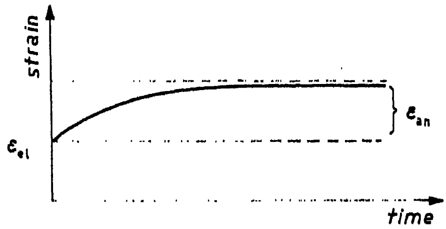

Fig. 2. — Anelastic strain due to a suddenly applied stress.

(*) A good instance of this is given by a rigid pendulum whose energy is barely sufficient to reach its unstable equilibrium position, with the center of gravity above the suspension axis. It is a familiar result that an infinite time is required to reach this position. It may also be shown that this is a special case of the general theorem quoted above.

(**) The creep is not an anelastic strain as it does not tend to a finite value. It has however been shown that it may be considered as a limiting case of an anelastic strain (P. G. Bordoni and M. Nuovo: *Colloque International sur les Ultrasons* (Bruxelles, 1951), p. 234).

From what has been said it is clear that the *anelastic deformations are linear*, and that *the superposition principle is valid for them* as for the elastic ones. From the mathematical standpoint a simple type of asymptotic motion is that represented by an exponential law. If this law is accepted for the diffusion of imperfections, then the anelastic strain is represented as a function of time by the function

$$\varepsilon_{\text{an}}(t) = \bar{\varepsilon}_{\text{an}}\left[1 - \exp\left[-\frac{t}{\tau_\sigma}\right]\right], \tag{3}$$

where $\bar{\varepsilon}_{\text{an}}$ is the limiting value of the anelastic strain for $t = \infty$, and τ_σ is the characteristic time associated with the strain which takes place under constant stress.

The theory outlined above makes it quite easy to predict what happens when a finite strain is suddenly imposed on the solid at the time $t = 0$. The instantaneous stress produced must be large enough to overcome the elastic forces and *to keep the imperfections in a distribution which is no longer an equilibrium one.* The latter part of the stress is gradually *relaxed* as time increases, and the lattice imperfections diffuse towards the forced equilibrium distribution. The limiting value of the stress is always smaller than the initial value, and corresponds to the static stress considered in Hooke's law. If we assume, as above, that the diffusion follows an exponential law, then the anelastic part of the stress produced by a sudden strain is represented by the function

$$\sigma_{\text{an}}(t) = \bar{\sigma}_{\text{an}} \cdot \exp\left[-\frac{t}{\tau_\varepsilon}\right], \tag{4}$$

where $\bar{\sigma}_{\text{an}}$ is the initial value of the anelastic stress, and τ_ε is the characteristic time associated with the stress produced by a constant strain. It is important to note that the characteristic times are always different, and that τ_σ is larger than τ_ε.

3. – Energy dissipation due to lattice imperfections.

According to the above theory, the diffusion of lattice imperfections could eventually be detected by applying to a solid a sudden stress, and by following the time-dependence of the anelastic part $\varepsilon_{\text{an}}(t)$ of the strain. It would also be possible to apply a sudden strain, and follow the time dependent part $\sigma_{\text{an}}(t)$ of the stress. This is however impossible with the present experimental technique as the ratios $\bar{\varepsilon}_{\text{an}}/\varepsilon_{\text{total}}$ and $\bar{\sigma}_{\text{an}}/\sigma_{\text{total}}$ seldom exceed the value 10^{-3}. A more sensitive way to detect the diffusion of imperfections is to apply to the solid a stress sinusoidally dependent upon time with angular frequency ω. This stress may be ideally decomposed in a sum of step functions corresponding to increasing values of the time t. For each step function the strain produced is the sum of an *instantaneous* (or elastic) part, and of *retarded* (anelastic) terms. If we integrate for all the step functions, we find that the *total strain* produced by a sinusoidal stress *is also a sinusoidal function of the time*, which has the same angular frequency ω, but *lags* slightly with respect to the stress (*). This means that the vibration velocity has a term which is in phase with the applied stress. The work done by this force is required to sustain the vibrations. If the force is removed the vibrations decay according to an exponential law. The same mathematical treatment employed for the relaxation effects occurring in liquids and gases shows that the dissipation coefficient Q^{-1} is a function of the angular frequency and of a relaxation time which is the geometrical average of the characteristic times τ_σ and τ_ε, according to the equation (Fig. 3)

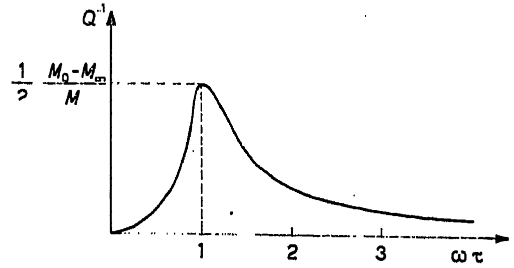

Fig. 3. – Dissipation coefficient Q^{-1} as a function of the angular frequency (Zener's curve).

(5)
$$Q^{-1}(\omega) = \frac{M_0 - M_\infty}{M} \cdot \frac{\omega\tau}{1 + \omega^2\tau^2}\,,$$

where M_0 is the instantaneous or unrelaxed modulus; M_∞ is the limiting value of the same modulus for $t = \infty$, and coincides with the modulus measured in static or relaxed experiments; M is the geometrical mean of the above values.

According to the above equation, Q^{-1} vanishes when $\omega = 0$ and when $\omega = \infty$. This is quite obvious from a physical standpoint. In the first case (very low frequencies) the vibration period $2\pi/\omega$ is large with respect to the relaxation time τ. Hence the retardation of the anelastic part of the strain with respect to the stress is hardly felt, and its contribution to the energy dissipation is negligible. In the second case (very high frequency) the vibration period is small in comparison with τ. The anelastic part of the strain has no time to build up, and its contribution to the dissipation is also negligible.

According to the above equation the energy dissipation is maximum when $\omega\tau = 1$. If the angular frequency of maximum dissipation is found by experiment we may compute a fundamental parameter of the interaction between

---

(*) The same result may be obtained by means of operational calculus. The mathematics involved is simpler but the treatment is not so evident from the physical standpoint (P. G. BORDONI: *Suppl. Nuovo Cimento*, **7**, 144 (1950)).

imperfections and elastic waves, that is the relaxation time τ. The same experiment gives another significant parameter of the same interaction, the relaxation strength $(M_0 - M_\infty)/M$ which equals twice the maximum dissipation coefficient. However in solids it is generally impossible to measure the dissipation coefficient as a function of frequency, as it is commonly done in liquids and gases. This is because with resonance methods, which are the most convenient ones for solids, to change the vibration frequency over a wide range we must either have a collection of specimens of the same material, having the same shape but different sizes, or we must use a single specimen, exciting its different vibration modes (for instance flexural vibrations for the lower frequencies and longitudinal vibrations for the higher frequencies). In both cases the experimental results are not self-consistent. If we use different specimens, it is impossible to obtain that all of them have the same density of lattice imperfections, and in any case this density cannot be easily controlled (*). On the other hand, if we excite the different vibration modes of a single specimen, the experimental values of Q^{-1} cannot be compared between them, as they depend upon the *type* of vibration as well as on frequency, as it has been shown in the previous section, and are larger for the vibrations which involve a larger deformation of the lattice, and smaller for the vibrations wich are nearer to pure dilatation.

This difficulty may be overcome in almost all the cases of physical interest, by observing that the diffusion of imperfections from the natural to the forced equilibrium state is *controlled* by the external forces applied to the solid, but is *essentially due to the thermal agitation.* As it has been pointed out, even in the natural equilibrium state, the imperfections move with respect to the lattice, and it is only their *statistical or average distribution which is constant.* The number of jumps made by a single imperfection in a given time is obviously larger when the thermal agitation is larger, that is at high temperatures. Hence it may be expected that the characteristic time associated with the diffusion of imperfections *decreases with increasing temperature.* It may be proved by means of statistical mechanics that for several imperfections (for instance interstitials and dislocations) the relaxation time introduced above depends upon the absolute temperature T according to an Arrhenius equation

$$\tau = \tau_0 \exp\left[\frac{W}{kT}\right] \tag{6}$$

(*) An important exception is that of the diffusion of thermal phonons between adjacent grains in a polycrystalline solid. In this case the physically significant parameter (the average grain size) is semi-macroscopic, and can be controlled optically. It has been therefore possible to C. ZENER to study this type of relaxations on several specimens of the same metal, having different and known grain sizes.

where τ_0 is the limiting value of the relaxation time for very high temperatures; W is the activation energy of the process, and k is the Boltzmann constant.

If the above value of τ is inserted in the equation which gives Q^{-1}, this parameter is obtained as a function of temperature, and is given by (Fig. 4)

$$Q^{-1}(T) = \frac{1}{2}\,\frac{M_0 - M_\infty}{M}\,\mathrm{sech}\,\left[W k^{-1}\,(T_m^{-1} - T^{-1})\right]. \tag{7}$$

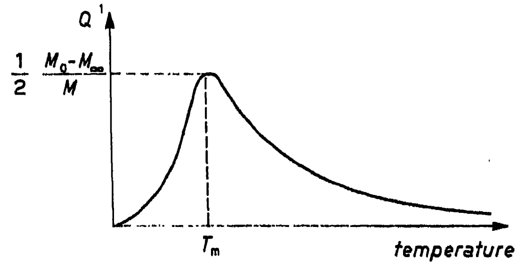

Fig. 4. – Dissipation coefficient Q^{-1} for a thermally activated effect as a function of the absolute temperature (hyperbolic secant).

where T_m is the temperature at which $\omega\tau = 1$.

The above equation is of fundamental importance for the study of the interaction between lattice imperfections and elastic waves. The function $Q^{-1}(T)$ represents a bell-shaped curve, which has a maximum for $T = T_m$ (Fig. 4), and the value of this maximum gives one half of the relaxation strength. When the relaxation of the imperfections is *thermally activated*, that is when the time is given by an Arrhenius equation, it is possible to measure the dissipation coefficient *on a single specimen and for a single mode of vibration by changing the temperature of the experiment*. A small difficulty arises from the fact that to compute τ, two parameters are needed for thermally activated effects: the activation energy W, and the limiting value τ_0 of the relaxation time. They are however easily obtained measuring the dissipation coefficient as a function of temperature *for two different vibration frequencies* (Fig. 5). The experimental curves obtained in this way have their peaks at different values of the temperature, say T'_m and T''_m (according to the equation which gives $Q^{-1}(T)$, the higher temperature corresponds to the higher vibration frequency). The experimental results may be summarized in a

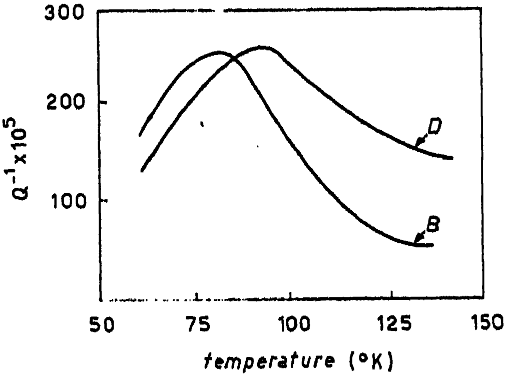

Fig. 5. – Relaxation peak due to the dislocations in silver. (Curve B) frequency 50 kHz^{-1}; curve D) frequency 820 MHz^{-1}. As the effect is thermally activated, the peak displaces toward the higher temperatures when the vibration frequency increases.

diagram in which the abscissae are the inverses of the peak temperatures, and the ordinates the logarithms of the vibration frequencies, multiplied by the Boltzmann constant k (Fig. 6). It is then easily seen that the slope of the straight line drawn through the points $[(T'_m)^{-1}, k\cdot\log f']$ and $[(T''_m)^{-1}, \log f'']$ gives the activation energy W, while the limiting time τ_0 may be computed from the intercept of the same line with the frequency axis. It may be added that no error is introduced in this way by the fact that the two vibration frequencies may correspond to different vibration modes. The above theory shows that the type of vibration affects *only the relaxation strength but not the value of the characteristic time.*

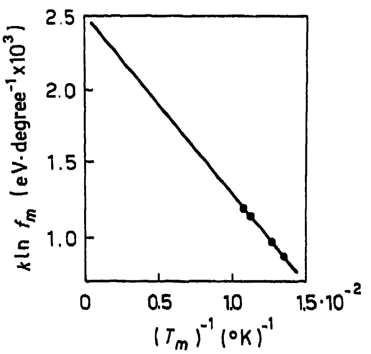

Fig. 6. – Frequency-dependence of the temperature T_m of maximum dissipation for silver. The slope of the straight line drawn trough the experimental points gives the activation energy; its intercept with the ordinate axis gives the limiting value of the characteristic time.

As in liquids and gases, relaxation effects involve not only energy dissipation but also changes in the elastic moduli. In parallel with the expressions of Q^{-1} as a function of frequency or temperature, equations may be derived which give the elastic moduli as functions of the same variables. These equations are not of primary interest, and may therefore be dropped in the present review, as *in solids dissipation is always a much more sensitive parameter for the study of lattice imperfections than the changes in elastic moduli.*

Two more theoretical remarks must however be made before going into a short review of the information on lattice imperfections collected by means of measurements on elastic vibrations. The first point to be considered is that the assumption made for the diffusion of lattice imperfections (simple exponential law, with a single characteristic time) gives a somewhat oversimplified picture of the physical truth. A satisfactory generalization can be obtained assuming that all the imperfections diffuse according to an exponential law, but with different values of the relaxation time. It is easy to prove that in this case the curves which give Q^{-1} as a function either of frequency or of temperature, must always be *broader than the simple curves (Zener's curves) associated with a single chraacteristic time.* Comparing the width of the experimental curves with that of the theoretical Zener's curve, it is possible to obtain some information on the *relaxation spectrum.*

The second point which must be considered is that for every type of relaxation due to lattice imperfections the characteristic time (or the relaxation spectrum) depends upon temperature, but this dependence is not always characterized by a simple Arrhenius equation. Important exceptions are the relaxation effects due to thermal phonons and to the conduction electrons in metals. In these cases the only way to determine the relaxation time is to measure the dissipation coefficient as a function of frequency, notwithstanding the experimental difficulties which we have pointed out in connection with this type of measurement. However, even in these cases, the temperature-dependence of Q^{-1} may give very useful information upon the behavior of the imperfections responsible for the effect.

4. – Experimental results.

The first relaxation effects investigated have been those in which the lattice imperfections diffuse over a macroscopic or a semi-macroscopic distance (diffusion of thermal phonons across a thin rod for flexural vibrations, and diffusion of phonons between adjacent grains in a polycrystalline solid). These are not thermally activated effects, but as it was explained no difficulty is found in this case in measuring the dissipation coefficient as a function of frequency. The physically significant parameters which can be obtained from these measurements as a function of temperature are: the thermal diffusion constant D and the difference between the specific heats at constant stress and at constant volume. Moreover from the measurements on intergrain thermal exchanges some information can be obtained on elastic anysotropy and on preferred orientation.

The early work in this field is due to C. ZENER; it was made with a somewhat inadequate experimental technique and was essentially intended as a proof of the theory of relaxation effects due to the same author. Very little work in this field has been done since then, notwithstanding the considerable refinement of the experimental methods. It would not be devoid of interest to evaluate the above parameters at low temperatures, that is in the region where the thermal energy has a nonclassical behavior. It could also be interesting to evaluate the same parameters for nickel and nickel alloys in the temperature region where the thermal expansion and the elastic moduli have an anomalous behaviour, or for some bcc metals whose technical applications became recently very important, like molibdenum, niobium and tantalum. To this purpose it must be considered that the measurements of the energy dissipation due to thermal exchanges are rather easy, as the most convenient vibration frequencies fall in the acoustic range; moreover the experimental work done in the last years on other relaxation effects has shown how to prepare specimens of metals almost entirely free of any other cause of energy dissipation.

For the last ten years the attention of the experimenters has been almost entirely focussed on those relaxation effects which are related to lattice imperfections diffusing over a microscopic range, as these imperfections have a basic interest in solid state physics. All the three types of imperfection listed under *a*), *b*), *c*) in Section 1 have been investigated. The first type considered was that of plane imperfections; T. **Kê** discovered that stress relaxation takes place at grain boundaries in polycrystalline solids. The effect is thermally activated, with an energy which equals the self-diffusion energy of atoms, and is therefore of the order of 10 eV or more. At room temperature for all the metals investigated the characteristic time is rather long, and it becomes of the order of 1 s when the temperature is raised to a few hundreds of centigrades. This makes the experimental work a little difficult because the measurements made for very low frequencies with the torsion pendulum are less easy and accurate than those for truly acoustic or ultrasonic frequencies, and because in the above temperature range other causes of energy dissipation are present, different from grain boundary relaxation. The peaks of the dissipation-temperature curves for this effect are therefore not very sharp (Fig. 7), and moreover the experimental curves are not easily reproduced, owing to irreversible changes which take place in grain boundaries at high temperatures. It has however been possible to show that the interaction between grain boundaries and elastic waves is much larger for those waves which involve a large amount of lattice deformation, like torsional waves, than for extensional waves, in which a considerable amount of energy is associated with lattice dilatation. The ratio between the experimental values of the relaxation strength for the two types of waves is in good agreement with that predicted by the theory of Section 2, according to the fundamental result that no effect due to lattice imperfections can be expected for a pure dilatation of the lattice. It was also checked that the relaxation effect due to grain boundaries is not found in single crystals of the same material.

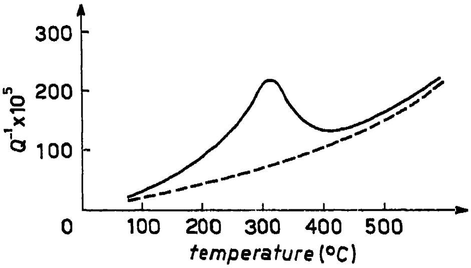

Fig. 7. – Typical relaxation peak due to grain boundaries. Heavy line, measured dissipation; dashed line, additional dissipation due to different physical causes.

The theoretical interpretation of the grain boundary relaxation has not much contributed to the knowledge of the structure of solids, partly because plane imperfections are very complex ones, and partly because **Kê** and **Zener** started from the wrong assumption that grain boundaries had a quasi-liquid behaviour. It would therefore be convenient to reconsider the experimental data available on this effect in the light of the present knowledge of the structure of grain boundaries considered as a row of dislocations. Some more experimental work would also be useful, provided a careful control of the impurity content were made, as these impurities collect at grain boundaries and may have a large influence on the relaxation effect.

Several instances of the opposite type of imperfections, the point imperfections, have also been considered in connection with relaxation effects. The best known type of these effects are those due to interstitial atoms of carbon and nitrogen in the iron lattice, which is a bcc lattice and has room enough for small interstitial impurity atoms. These effects are thermally activated: hence the dissipation can be measured as a function of temperature, and the effect is shown by a peak in the experimental curve, as it has been explained in Section 3. As with grain boundaries, the measurements on the carbon and nitrogen relaxation effect in iron are somewhat difficult owing to the fact that the relaxation time is rather long at room temperature, and at higher temperatures irreversible changes take place in the material. Effects of the same type but in a somewhat lower temperature range have also been observed in other bcc metals like molibdenum, niobium and tantalium. These effects are more stable that those observed in iron, and seem therefore to be worth of a more detailed investigation. The activation energies are not very significant from the standpoint of solid-state physics, as they are related not only to the type of lattice (which in every case is bcc) but also to the interstitial impurity considered. It would be interesting to compare the values of the activation energy for the same type of interstitial impurity inserted in different bcc metals. This requires more experimental work which could be started from the simplest type of interstitial impurity, that is from hydrogen, whose atoms may be easily introduced in bcc lattices at room temperature by means of an electrolytic charge.

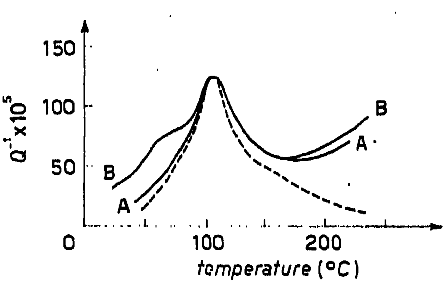

Fig. 8. – Typical relaxation peak due to interstitial impurities in iron. Dashed line, Zener's curve; curve *A*) peak due to a single type of impurity atoms; curve *B*) experimental curve for more than one type of atoms.

The peaks of the experimental dissipation-temperature curves for interstitial relaxation are almost as sharp as the theoretical Zener's curve (Fig. 8). According to the final remark of Section 3 this shows that the jumps of the impurity atoms from one equilibrium position to the other are all of the same type, every mutual influence or every effect of other lattice imperfections being negligible. It has also been shown that when more than one type of interstitial impurity is present in the same lattice, the peaks of the experimental curves become broader; small side-peaks or bumps may also be observed in this case. This shows the existence of more that one type of atomic jump, and sometimes also of complex jumps in which more than one impurity atom is interested. Hence the relaxation measurements make it possible to follow the detailed motion of the interstitial atoms.

Among the relaxation effects associated with point-like imperfections the most important for the knowledge of solid state is doubtless that due to the interaction between elastic waves and conduction electrons. This effect was discovered by H. Boemmel, and has been theoretically studied by Mason, Pippard and Morse. Many of the experimental facts may be accounted for, assuming that the elastic waves are damped by the viscous electron gas. As with common gases, the viscosity coefficient depends upon the mean free path of the electrons between their collisions with the lattice (collisions between electrons don't contribute to the energy dissipation). This mean free path, which is the same considered in the theory of electrical conductivity, increases when the temperature decreases, and the corresponding dissipation coefficient becomes larger (Fig. 9). This result agrees with those obtained by more refined quantum-mechanical computations, in which the electrons are treated as a Fermi gas, enclosed in a box subjected to periodical distortion. Theory predicts also that the attenuation coefficient α for the elastic waves is proportional to the square of frequency (*); hence to detect the electron-phonon interaction experiments must be made at high frequency (usually above 10 MHz^{-1}). The main parameters which characterize the effect is the ratio between the mean free path and the wavelength of the elastic waves. At room temperature the m.f.p. is of the order of 10^{-5} cm, while the wavelength is of the order of 10^{-2} cm. The measurements must therefore be made at low temperatures, generally in the liquid helium range; the specimens must be single crystals, to avoid the scattering of the elastic waves at the grain boun-

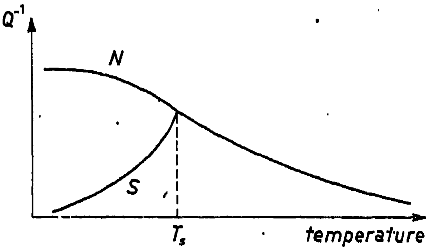

Fig. 9. – Typical dissipation-temperature curve due to electron-phonon interaction. Curve N) normal state of the metal; curve S) superconducting state.

(*) According to eq. (2) of Section 1 the logarithmic decrement d and the dissipation coefficient Q^{-1} for the same effect are less sensitive to frequency, being proportional to its first power. This may be of interest for future attempts to detect the electron-phonon interaction by means of resonance experiments. Until now all the measurements in this field have been made with progressive waves, by means of a pulse technique, which gives rise to a comparatively high additional dissipation owing to mismatching—and reflection—losses.

daries, and the impurity content must be very small, otherwise the conduction electrons are scattered by them, and it is impossible to obtain large values of the mean free path. The effect is not thermally activated; hence the relaxation time cannot be evaluated from the dissipation-temperature curves. However these curves are of great interest, as they characterize the temperature dependence of the mean free path of the electrons. By means of measurements made on single crystals with waves propagating in different directions, Morse and his group have been able to obtain experimental data on the shape of the Fermi surface. It has also been observed that when a magnetic field is applied to the solid in a direction normal to the vibration velocity, there are values of the field intensity for which the dissipation becomes larger. This is due to the fact that the motion of electrons follows curved lines, and this in some cases may give rise to a considerable increase of the phonon-electron interaction.

For metals having a superconducting transition the dissipation due to electrons decreases below the transition point when the metal is in the S-state, owing to the fact that the dissipation itself is proportional to the number of normal electrons (Fig. 8). In this way it has been possible to measure as a function of temperature the fraction of normal electrons, and to check different theories of the superconducting transition.

One more type of lattice imperfections must finally be considered in connection with relaxation effects: the line imperfections or dislocations. Presently this is the best known relaxation effect, owing to the fact that it is very stable, that the corresponding dissipation peaks are large in comparison with the room temperature dissipation and that for frequencies in the lower ultrasonic range the temperature of the peaks falls in a very convenient interval, being usually higher than the liquid nitrogen point (*). Moreover the effect is little influenced by grain boundaries and by impurities when their content does not exceed a few parts in 10^{-3} of the number of the atoms. Hence the experiments may eventually be made on polycrystalline metals of technical purity (Fig. 5 and Fig. 10).

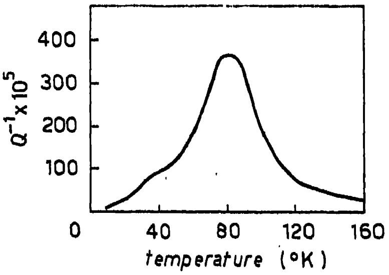

Fig. 10. – Relaxation peak due to the dislocations in a polycrystalline specimen of technically pure copper. Vibration frequency 14 kHz^{-1}. The small hump on the experimental curve at about 40 °K is due to a different type of dislocations.

The effect was first observed about ten years ago on some fcc metals (lead,

---

(*) The only known exception is lead, in which the peak's temperatures are somewhat lower.

copper, aluminum and silver). Since then it has been observed in several other metals having the same structure (gold, palladium and platinum) and more recently also in bcc metals (niobium, tantalum, tungsten and molibdenum). Iron is the only pure metal in which no trace of an effect of this type has been found until now. From these experiments and from the theoretical treatment due to MASON, WEERTMAN and SEEGER, a detailed knowledge has been obtained of the motion of dislocations near their equilibrium positions. We know that a dislocation segment does not jump over a potential barrier as a stiff rod, but first forms a couple of kinks very near to each other (Fig. 11); successively the distance between kinks may increase, extending the length of the dislocation segment which has overcome the potential barrier. When no external stress is applied to the solid, the formation of kinks and their motion is symmetrical on each side of the equilibrium position and no macroscopic strain is produced. If an external stress is present, the theory outlined in Section 2 shows that the kinks are more easily formed and more easily extended on one side of the dislocation line. A macroscopic anelastic strain is produced and the corresponding relaxation effect is thermally activated, as the energy required to overcome the potential barriers is supplied by the thermal agitation. The two basic parameters of the relaxation effect (the activation energy and the limiting time), have a very evident meaning for dislocations. The first gives the height of the potential barriers by which each dislocation segment is trapped, the second is of the order of the oscillation period of each dislocation segment in its potential well. According to this model the motion of dislocations near their equilibrium positions is a structure-characteristic phenomenon. This is in agreement with the experimental results, which show that the energy W has values near 0.16 eV for the fcc lattices and near to 0.26 eV for the bcc lattices. The limiting time is generally of the order of 10^{-12} s, being somewhat larger that the *characteristic Debye's time* of the solid. This is quite reasonable, as the vibration frequency of dislocation in their potential wells cannot exceed the highest frequency which can propagate through the lattice.

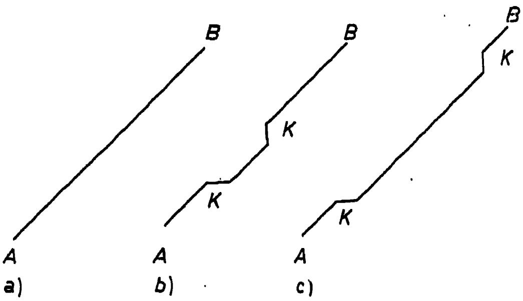

Fig. 11. – Motion of dislocations near their equilibrium positions: *a*) straight dislocation segment; *b*) formation of a couple of kinks K, K; *c*) increase of the distance between the kinks.

Owing to the length and to the number of dislocation segments, (which incidentally may be computed from the height of the relaxation peaks), it may be expected that an appreciable interaction takes place between different dislocations, even when they move near their equilibrium positions. This means that dislocation relaxation must be associated with *a spectrum of times rather then with a single time*. The experimental evidence proves that this is the case (Fig. 12); the measurements made on fcc metals have shown that the times associated with the relaxation effect may differ between them by a factor of 100 or even larger. In bcc metals recent experiments have shown that the spectrum is considerably narrower, so that even the *spectrum width is a structure-characteristic property*. However a structural interpretation of this fact is still wanted, as the present models of dislocation motion do not provide an explanation of the mutual interaction of dislocation segments.

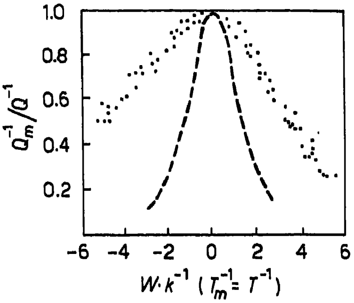

Fig. 12. – Evidence of a relaxation spectrum associated with the dislocations. Dashed line, theoretical Zener's curve for a single time; points, experimental values of the dissipation for copper, at different vibration frequencies.

The experiments on dislocation relaxation make it possible to follow the introduction of dislocation by means of permanent strain and their inactivation by means of thermal treatments. When the permanent strain is of simple type (extension, flexure) the distribution of dislocations is by no means isotropic. This is proved by comparing the height of the relaxation peaks for different types of vibrations on the same specimen. As a rule the dislocations interact more readily with the elastic vibrations associated with elastic strains of the same type as those employed in introducing the dislocations. For instance if a rod has been extended, the relaxation peak for extensional vibrations is comparatively higher than for torsional vibrations. This happens to be the case even when the specimen has a polycrystalline structure with random grain orientation. A significant result which has been recently obtained in this field is that a *permanent shear* of a thin plate of an fcc metal introduces imperfections a part of which must necessarily be dislocations but *which are not associated with a thermally activated relaxation effect*.

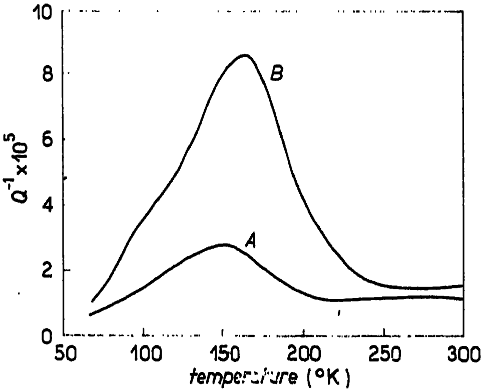

Fig. 13. – Evidence of a slight dependence of the temperature of the relaxation peak due to the dislocations upon the height of the peak. Measurements on the same niobium specimen; vibration frequency 19 kHz^{-1}; curve *A*) after an annealing treatment; curve *B*) after permanent strain.

The thermal treatments have a selective influence upon the dislocations responsible for the relaxation effect. The first dislocations which are inactivated by the thermal treatment at comparatively low temperatures are those associated with the lowest values of the relaxation time. This is shown by the fact that for a given specimen and for a given vibration frequency, the temperature of the relaxation peak decreases slightly after each thermal treatment (Fig. 13). This seems to indicate that the inactivation process is rather an *alteration* of the existing dislocations (for instancy by impurity trapping or by interlocking) than a *cancellation*. To remove every trace of the relaxation peak from the experimental curves the material must be treated at temperatures at which an appreciable recrystallization takes place, at least in the case of fcc lattice. For bcc metals recent experimental work suggests that the temperatures required to cancel the effect are considerably lower than the recrystallization temperatures.

The influence of impurity atoms upon dislocation relaxation has also been investigated in some special cases, as for instance the complete series of gold-silver alloys which are of the substitutional type and have an exceedingly favorable ratio of the atomic diameters. Even in this case, when the atomic content of one of the components approaches 50 % the relaxation peaks become exceedingly small. This shows that dislocation motion is very sensitive to lattice distortion. When the atomic ratio is less favorable, as for copper-gold alloys, much smaller amounts of one of the components are required to prevent the dislocation relaxation.

5. – Conclusions.

The investigations on the relaxation effects contribute in a substantial way to the structural knowledge of the condensed state of matter. In solids there is a wider variety of relaxation effects than in liquids or in gases, owing to the large number of imperfections which interact with elastic waves. All these effects may be explained by means of a single general theory which considers the diffusion of lattice imperfections from a natural to a forced statistical equilibrium distribution.

From comparatively simple experiments of the macroscopic type (measurements of the dissipation of the elastic waves) detailed information is obtained upon the structure and the behavior of the imperfections on the atomic scale. This is clearly shown by the results concerning the relaxation of interstitials, of the conduction electrons and of the dislocations.

Hints have been given of possible trends of future work in connection with the different relaxation effects which have been rewieved. Wider and more basic contributions may be expected from the investigation of other effects which are as yet almost unexplored, like the interaction between vacancies and elastic waves and the mechanical relaxation in non metallic solids.

6. – Suggestions for further reading.

A) *Lattice imperfections.*

H. G. VAN BUEREN: *Phil. Tech. Rev.*, **15**, 246 (1954).
A. H. COTTRELL: *Theoretical Structural Metallurgy* (New York, 1957).
A. H. COTTRELL: *Dislocations and Plastic Flow in Crystals* (London, 1956).
W. SHOCKLEY *et al.*: *Imperfections in nearly Perfect Crystals* (New York, 1952).
W. T. READ: *Dislocations in Crystals* (New York, 1953).
F. SEITZ and D. TURNBULL (eds.): *Solid State Physics*, vol. **3** (New York, 1956).
L. V. AZAROFF: *Introduction to Solids* (New York, 1960).

B) *Relaxation effects.*

C. ZENER: *Elasticity and Anelasticity of Metals* (Chicago, 1948).
P. G. BORDONI: *Suppl. Nuovo Cimento*, **7**, 144 (1950).
P. G. BORDONI: *Proc. of the Second I.C.A. Congress*, (1956), p. 101 (with a wide bibliography of original contributions up to 1956).
W. P. MASON: *Physical Acoustics and the Properties of Solids* (New York, 1958) (extensive rewiev of the different types of relaxation effects).
P. G. BORDONI: *Suppl. Nuovo Cimento*, **17**, 43 (1960), (with a complete bibliography for this type of relaxation up to 1960).
D. H. NIBLETT and J. WILKS: *Phil. Mag. Suppl.*, **9**, 1 (1960), (with a bibliography similar to that of the previous paper).
H. G. VAN BUEREN: *Imperfections in Crystals* (Amsterdam, 1960), (wide and up-to-date review of the different types of relaxation effects, like that given in Mason's book).

Tipografia Compositori - Bologna - Italy